

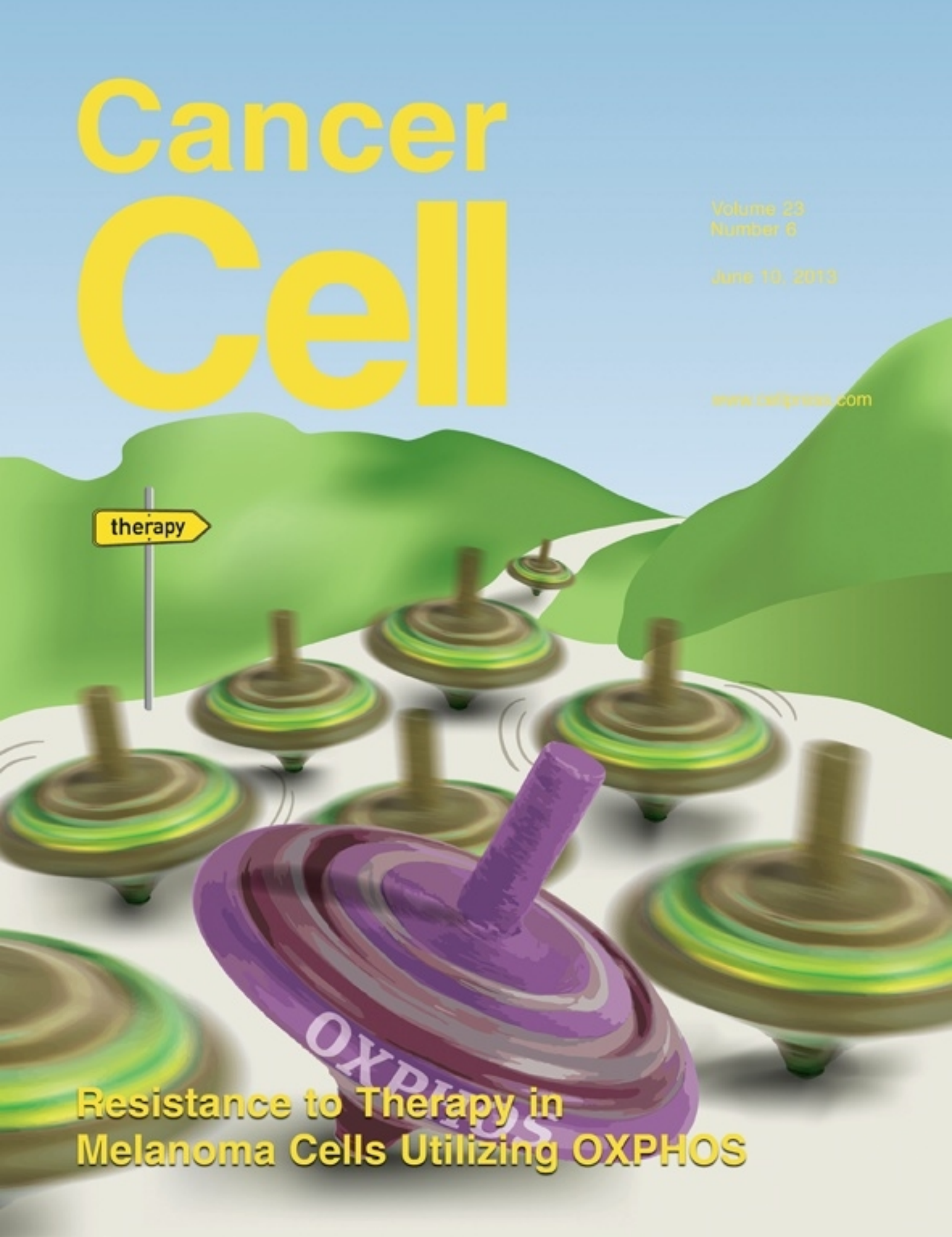
Cancer Cell

Volume 23
Number 6

June 10, 2013

www.cellpress.com

therapy



Resistance to Therapy in
Melanoma Cells Utilizing OXPHOS

Hopping between Differentiation States in Lung Adenocarcinoma

Hideo Watanabe^{1,2,3,*} and Matthew Meyerson^{1,2,3,4}

¹Department of Medical Oncology

²Center for Cancer Genome Discovery

Dana-Farber Cancer Institute, 450 Brookline Avenue, Boston, MA 02215, USA

³Cancer Program, Broad Institute of Harvard and MIT, 7 Cambridge Center, Cambridge, MA 02142, USA

⁴Department of Pathology, Harvard Medical School and Brigham and Women's Hospital, Boston, MA 02115, USA

*Correspondence: hideo_watanabe@dfci.harvard.edu

<http://dx.doi.org/10.1016/j.ccr.2013.05.013>

The work by Cheung and colleagues, in this issue of *Cancer Cell*, demonstrates another example of how lineage-specific transcriptional regulators of differentiation, GATA6 and HOPX, can control the fate of lung adenocarcinoma progression.

Lineage-specific transcriptional regulators govern differentiation status during normal lung development as well as in lung adenocarcinoma. Aberrant activation or inactivation of transcriptional regulators important for lineage commitment have been frequently observed in hematopoietic malignancies such as *PAX5* deletion and *TAL1* translocation in acute lymphocytic leukemia and *RUNX1* and *RARA* translocations in acute myelogenous leukemia. There has been emerging evidence that tissue-specific differentiation programs also become dysregulated during cancer evolution in solid tumors. *ETS* family members are frequently translocated in prostate cancer, and a lineage-restricted genomic amplification of developmental transcription factors occurs frequently in solid tumors, as exemplified by *MITF* in melanoma, *NKX2-1* in lung adenocarcinoma, and *SOX2* in lung and esophageal squamous cell carcinomas.

In the orderly development of tissues, temporally and spatially controlled mitogenic signaling directs cell lineages to proliferate and/or migrate. However, over the course of cancer evolution, cells accumulate genomic and/or epigenomic alterations to adapt their lineage identity to support persistent oncogenic signal activation. These adapted differentiation states often predict the fate of cancer progression. For example, poorly differentiated lung adenocarcinomas, the most divergent differentiation state from the normal respiratory unit, generally have the worst prognosis, whereas, for subtypes of lung adenocarcinoma that more

closely resemble normal progenitors, the prognosis varies among subtypes classified based on architectural patterns that resemble normal differentiation status (Yoshizawa et al., 2011) (Figure 1).

Studies using animal models of lung adenocarcinoma have shown that tumors with dysregulated developmental transcriptional regulators indeed present with differential biological properties. In the case of *NKX2-1*, the most well-characterized example of a transcriptional regulator of lung adenocarcinoma differentiation, stochastic loss of mouse *Nkx2-1* promotes de-differentiation and metastasis in a model of *Kras*-driven lung adenocarcinoma (Winslow et al., 2011), while discrete *Nkx2-1* deletion induces endodermal trans-differentiation and increases tumor initiation and progression (Maeda et al., 2012; Snyder et al., 2013). However, the consequences of an altered differentiation program are context-dependent, as shown by Maeda et al. (2012), where haplo-insufficiency of *Nkx2-1* conversely decreased the incidence and progression of *Egfr*-driven lung adenocarcinomas. These results are consistent with the heterogeneity of human lung adenocarcinomas where tumors with low *NKX2-1* expression have generally worse prognoses while oncogenic amplification of *NKX2-1* is also found in a subset of the disease.

Another developmental pathway, WNT/TCF signaling, has also been shown to mediate lung adenocarcinoma progression and metastasis. The TCF4 transcriptional signature is associated with human lung adenocarcinoma recurrence, and

maintenance of TCF4 activity through its downstream effectors, including *LEF1* and *HOXB9*, in metastatic derivatives of lung adenocarcinoma cell lines is required for metastatic potential in a xenograft model (Nguyen et al., 2009). In highly metastatic *Lkb1*-deficient *Kras*-driven lung tumors, progression to metastasis is associated with signatures of β -catenin activity, epithelial-mesenchymal transition (EMT), and focal adhesion (Carretero et al., 2010). In addition, in a transgenic mouse model, constitutively active β -catenin cooperates with oncogenic *Kras* to enhance tumor development and de-differentiation to an immature distal epithelial lineage through increased expression of *Id2* and *Sox9* and a decreased expression of *Hopx* (Pacheco-Pinedo et al., 2011). Thus, there seems to be interplay between WNT/TCF signaling and transcriptional regulators of differentiation in the lung.

The study by Cheung et al. (2013) in this issue of *Cancer Cell* describes an “alveolar” gene signature compiled from the published transcriptomic data of several experimental alveolar differentiation phenotypes, which further anti-correlates with an embryonic stem cell signature and can cluster lung adenocarcinomas into two subgroups: “alveolar-like” and “distal airway stem cell-like”. The “alveolar-like” subgroup represents histologically more differentiated lung adenocarcinomas with decreased incidence of metastasis. The alveolar-like subgroup was characterized by increased expression levels of *NKX2-1*, *GATA6*, and their known interactor *HOPX*, consistent with

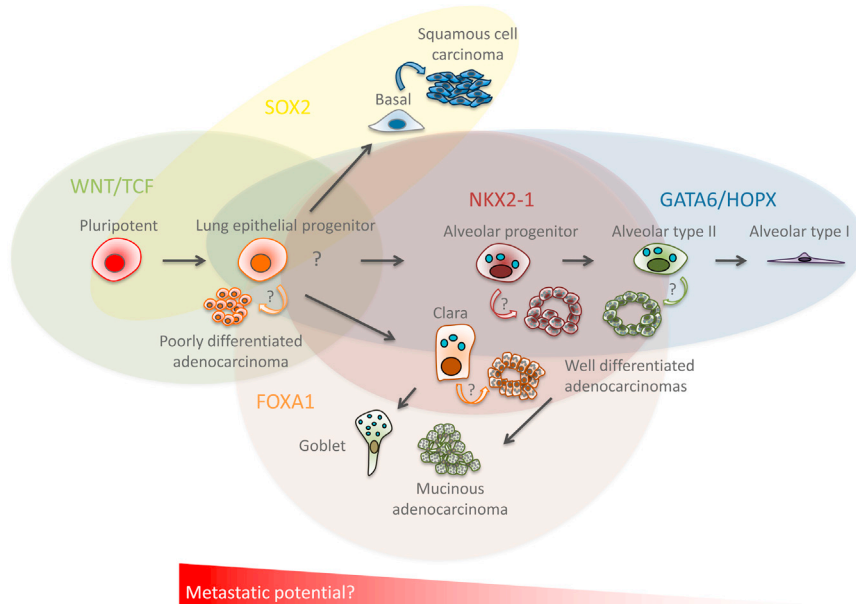


Figure 1. Metastatic Potential Varies among Subtypes of Lung Cancer Defined by Transcriptional Regulation of Cell Lineages

Transcriptional regulators active in different cell lineages are shaded in green (WNT/TCF), yellow (SOX2), orange (FOXA1), red (NKX2-1), and blue (GATA6/HOPX). Arrows indicate differentiation. Curved arrows indicate malignant transformation.

the findings in nonmetastatic primary murine *Kras*-driven lung adenocarcinomas (Winslow et al., 2011).

Cheung et al. (2013) further demonstrate that GATA6 and HOPX cooperatively suppress in vitro invasion and metastatic potential in xenograft models using human lung adenocarcinoma cell lines. GATA6, another key transcriptional regulator in lung morphogenesis, is essential for the maturation of alveolar type I epithelial cells. Furthermore, HOPX has been shown to regulate alveolar cell maturation in vivo by suppressing surfactant protein production downstream of NKX2-1 and GATA6 activity in the developing airway (Yin et al., 2006). Therefore, it is plausible that the cooperative function of GATA6 and HOPX is to direct a subpopulation of alveolar type II cells toward a more mature state, which will then terminally differentiate into alveolar type I cells. Furthermore, it suggests that the repression of this pro-differentiation function confers a more invasive and metastatic lung adenocarcinoma phenotype (Figure 1).

Interestingly, Cheung et al. (2013) found these effects were not mediated through β -catenin activity or EMT, but

rather by suppression of squamoid differentiation, the gene signature of which includes expression of *KRT6A* and *KRT6B*. While GATA6 has been shown to suppress expansion of bronchiolar epithelial cells through inhibition of the β -catenin pathway in developing and regenerating lungs, *Gata6* is not required for the earliest stages of lung branching, but is expressed throughout the developing foregut endoderm (Zhang et al., 2008). In the esophagus, where stratified squamous epithelium is native, GATA6 serves as an amplified lineage oncogene in metaplastic adenocarcinomas (Lin et al., 2012). Therefore, the role of GATA6 may generally be to suppress differentiation to the stratified squamous epithelial lineage.

Another interesting finding of the Cheung et al. (2013) study is that, unlike *Nkx2-1* in mouse models of lung cancer, the genotypes of the major driver oncogenes, *KRAS* and *EGFR*, in the two lung adenocarcinoma cell lines primarily used in this study did not have differential effects on metastatic phenotype. Consistent with this result, the “alveolar” subgroup is not associated with particular genotypes of *KRAS*, *EGFR*, *STK11*, and

TP53. However, the high level of genomic complexity in human cancer cell lines makes it difficult to interpret the influence of a single genotype, and it would be of interest to test whether these observations are genotype-specific within genetically defined autochthonous in vivo models.

The work by Cheung et al. (2013) provides mechanistic insight into how lineage factors play roles in maintaining cellular identity within tumors: in some cases deleterious for cancer fitness, invasion, and/or metastasis while advantageous in other cases. Cancer cells are typically characterized by reduced developmental plasticity or fixation at a particular developmental point within a lineage, which are ordinarily tightly regulated in tissue development in part through the accumulation of genomic alterations. Whereas studies of genomic alterations that lead to activation or inactivation of signaling molecules in lung adenocarcinoma have been fruitful, the molecular regulators of lung adenocarcinoma differentiation, and indeed of differentiation in normal lung alveolar epithelium, remain poorly understood. Therefore, further investigation of dysregulated transcriptional networks in solid tumors may provide clues to the stages of normal lung epithelial development as well as identify additional important tumor vulnerabilities.

REFERENCES

- Carretero, J., Shimamura, T., Rikova, K., Jackson, A.L., Wilkerson, M.D., Borgman, C.L., Buttarazzi, M.S., Sanofsky, B.A., McNamara, K.L., Brandstetter, K.A., et al. (2010). *Cancer Cell* 17, 547–559.
- Cheung, W.K.C., Zhao, M., Liu, Z., Stevens, L.E., Cao, P.D., Fang, J.E., Westbrook, T.F., and Nguyen, D.X. (2013). *Cancer Cell* 23, this issue, 725–738.
- Lin, L., Bass, A.J., Lockwood, W.W., Wang, Z., Silvers, A.L., Thomas, D.G., Chang, A.C., Lin, J., Orringer, M.B., Li, W., et al. (2012). *Proc. Natl. Acad. Sci. USA* 109, 4251–4256.
- Maeda, Y., Tsuchiya, T., Hao, H., Tompkins, D.H., Xu, Y., Mucenski, M.L., Du, L., Keiser, A.R., Fukazawa, T., Naomoto, Y., et al. (2012). *J. Clin. Invest.* 122, 4388–4400.
- Nguyen, D.X., Chiang, A.C., Zhang, X.H.-F., Kim, J.Y., Kris, M.G., Ladanyi, M., Gerald, W.L., and Massagué, J. (2009). *Cell* 138, 51–62.
- Pacheco-Pinedo, E.C., Durham, A.C., Stewart, K.M., Goss, A.M., Lu, M.M., Demayo, F.J., and Morrissey, E.E. (2011). *J. Clin. Invest.* 121, 1935–1945.

Snyder, E.L., Watanabe, H., Magendantz, M., Hoersch, S., Chen, T.A., Wang, D.G., Crowley, D., Whittaker, C.A., Meyerson, M., Kimura, S., and Jacks, T. (2013). *Mol. Cell* 50, 185–199.

Winslow, M.M., Dayton, T.L., Verhaak, R.G.W., Kim-Kiselak, C., Snyder, E.L., Feldser, D.M., Hub-

bard, D.D., DuPage, M.J., Whittaker, C.A., Hoersch, S., et al. (2011). *Nature* 473, 101–104.

Yin, Z., Gonzales, L., Kolla, V., Rath, N., Zhang, Y., Lu, M.M., Kimura, S., Ballard, P.L., Beers, M.F., Epstein, J.A., and Morrissey, E.E. (2006). *Am. J. Physiol. Lung Cell. Mol. Physiol.* 291, L191–L199.

Yoshizawa, A., Motoi, N., Riely, G.J., Sima, C.S., Gerald, W.L., Kris, M.G., Park, B.J., Rusch, V.W., and Travis, W.D. (2011). *Mod. Pathol.* 24, 653–664.

Zhang, Y., Goss, A.M., Cohen, E.D., Kadzik, R., Lepore, J.J., Muthukumaraswamy, K., Yang, J., DeMayo, F.J., Whitsett, J.A., Parmacek, M.S., and Morrissey, E.E. (2008). *Nat. Genet.* 40, 862–870.

Succinate: A New Epigenetic Hacker

Ming Yang¹ and Patrick J. Pollard^{1,*}

¹Cancer Biology and Metabolism Group, Nuffield Department of Medicine, Henry Wellcome Building for Molecular Physiology, University of Oxford, Oxford OX3 7BN, UK

*Correspondence: patrick.pollard@well.ox.ac.uk

<http://dx.doi.org/10.1016/j.ccr.2013.05.015>

Epigenetic reprogramming is a feature of many human cancers. In this issue of *Cancer Cell*, Letouzé and colleagues describe DNA hypermethylation in paragangliomas harboring mutations in succinate dehydrogenase genes. These tumors accumulate succinate, which inhibits 2-oxoglutarate-dependent histone and DNA demethylase enzymes, resulting in epigenetic silencing that affects neuroendocrine differentiation.

Metabolic rewiring has long been regarded as a consequence of malignant transformation driven by abnormal signal transduction mediated by oncogenes and tumor suppressors. The identification that the metabolite (R)-2-hydroxyglutarate [(R)-2HG] plays an oncogenic role in subsets of gliomas and acute myelogenous leukemia with mutations in isoforms of isocitrate dehydrogenase (IDH) has provided direct evidence linking altered metabolism and cancer and founded the notion of the “oncometabolite” (Ward et al., 2010). (R)-2HG is a product of the neomorphic activities of mutant IDH1/2 and accumulates to millimolar concentrations in IDH-associated gliomas (Dang et al., 2010). Due to the structural similarity to 2-oxoglutarate (2OG), (R)-2HG competitively inhibits the 2OG-utilizing Jumonji C (JmjC)-domain containing histone lysine demethylases and the TET family of 5-methylcytosine (5mC) hydroxylases, leading to DNA hypermethylation at CpG islands in promoter regions of genes involved in cell differentiation (Kim and DeBerardinis, 2013).

The Krebs cycle enzymes succinate dehydrogenase (SDH) and fumarate hydratase (FH) are tumor suppressors whose loss-of-function mutations predispose to familial cancer syndromes (Frezza

et al., 2011). SDH and FH inactivation results in a blockade of Krebs cycle, impaired respiration, and abnormal accumulation of their substrates succinate and fumarate, respectively. Both metabolites are also inhibitors of 2OG-dependent dioxygenases, particularly the hydroxylases for the transcription factor hypoxia-inducible factor (HIF), resulting in HIF-dependent activation of a “pseudo-hypoxic” response characterized by enhanced angiogenesis and increased anaerobic metabolism (Frezza et al., 2011). In the case of fumarate, the metabolite is also an endogenous electrophile and can chemically modify cysteine residues in Kelch-like ECH-associated protein 1, leading to constitutive (and potentially oncogenic) activation of transcription factor nuclear factor erythroid 2-related factor 2 (Adam et al., 2011; Ooi et al., 2011). Until recently, HIF activation by fumarate and succinate has been the only mechanistic link to oncogenesis that has been described in FH and SDH mutant cancer models (Pollard et al., 2007; Selak et al., 2005). However, at least in the context of FH-deficiency, a causal role for HIF in tumorigenesis is questionable (Adam et al., 2011), and the quest for other oncogenic drivers in SDH- and FH-associated malignancy continues. Recent re-

ports by Killian et al. (2013) and Letouzé et al. (2013; in this issue of *Cancer Cell*) both demonstrate that, similarly to (R)-2HG, succinate can also remodel the epigenome and alter gene expression.

SDH mutations occur frequently in paraganglioma (PGL), pheochromocytoma (PCC), gastrointestinal stromal tumor (GIST), as well as in renal carcinoma (Killian et al., 2013). GIST tumors can alternatively be driven by mutations in signal transduction kinases. Killian et al. (2013) compared the methylation profiles of GISTs with mutations in either SDH or KIT tyrosine kinase and uncovered marked global hypermethylation in the SDH versus KIT mutant subgroup. Further examination of a PGL/PCC cohort showed a similar hypermethylation phenotype in SDH mutant tumors compared to SDH-wild-type reference tissues. Bioinformatic analyses of methylomes from developmentally distinct tumors including GIST, PGL, PCC, and gliomas revealed comparable methylation signatures in those harboring SDH and IDH mutations (Killian et al., 2013).

Letouzé et al. (2013) classified a large PGL/PCC cohort based on DNA methylation and obtained three stable clusters. Strikingly, a distinct subgroup characterized by the presence of a

Snyder, E.L., Watanabe, H., Magendantz, M., Hoersch, S., Chen, T.A., Wang, D.G., Crowley, D., Whittaker, C.A., Meyerson, M., Kimura, S., and Jacks, T. (2013). *Mol. Cell* 50, 185–199.

Winslow, M.M., Dayton, T.L., Verhaak, R.G.W., Kim-Kiselak, C., Snyder, E.L., Feldser, D.M., Hub-

bard, D.D., DuPage, M.J., Whittaker, C.A., Hoersch, S., et al. (2011). *Nature* 473, 101–104.

Yin, Z., Gonzales, L., Kolla, V., Rath, N., Zhang, Y., Lu, M.M., Kimura, S., Ballard, P.L., Beers, M.F., Epstein, J.A., and Morrissey, E.E. (2006). *Am. J. Physiol. Lung Cell. Mol. Physiol.* 291, L191–L199.

Yoshizawa, A., Motoi, N., Riely, G.J., Sima, C.S., Gerald, W.L., Kris, M.G., Park, B.J., Rusch, V.W., and Travis, W.D. (2011). *Mod. Pathol.* 24, 653–664.

Zhang, Y., Goss, A.M., Cohen, E.D., Kadzik, R., Lepore, J.J., Muthukumaraswamy, K., Yang, J., DeMayo, F.J., Whitsett, J.A., Parmacek, M.S., and Morrissey, E.E. (2008). *Nat. Genet.* 40, 862–870.

Succinate: A New Epigenetic Hacker

Ming Yang¹ and Patrick J. Pollard^{1,*}

¹Cancer Biology and Metabolism Group, Nuffield Department of Medicine, Henry Wellcome Building for Molecular Physiology, University of Oxford, Oxford OX3 7BN, UK

*Correspondence: patrick.pollard@well.ox.ac.uk

<http://dx.doi.org/10.1016/j.ccr.2013.05.015>

Epigenetic reprogramming is a feature of many human cancers. In this issue of *Cancer Cell*, Letouzé and colleagues describe DNA hypermethylation in paragangliomas harboring mutations in succinate dehydrogenase genes. These tumors accumulate succinate, which inhibits 2-oxoglutarate-dependent histone and DNA demethylase enzymes, resulting in epigenetic silencing that affects neuroendocrine differentiation.

Metabolic rewiring has long been regarded as a consequence of malignant transformation driven by abnormal signal transduction mediated by oncogenes and tumor suppressors. The identification that the metabolite (R)-2-hydroxyglutarate [(R)-2HG] plays an oncogenic role in subsets of gliomas and acute myelogenous leukemia with mutations in isoforms of isocitrate dehydrogenase (IDH) has provided direct evidence linking altered metabolism and cancer and founded the notion of the “oncometabolite” (Ward et al., 2010). (R)-2HG is a product of the neomorphic activities of mutant IDH1/2 and accumulates to millimolar concentrations in IDH-associated gliomas (Dang et al., 2010). Due to the structural similarity to 2-oxoglutarate (2OG), (R)-2HG competitively inhibits the 2OG-utilizing Jumonji C (JmjC)-domain containing histone lysine demethylases and the TET family of 5-methylcytosine (5mC) hydroxylases, leading to DNA hypermethylation at CpG islands in promoter regions of genes involved in cell differentiation (Kim and DeBerardinis, 2013).

The Krebs cycle enzymes succinate dehydrogenase (SDH) and fumarate hydratase (FH) are tumor suppressors whose loss-of-function mutations predispose to familial cancer syndromes (Frezza

et al., 2011). SDH and FH inactivation results in a blockade of Krebs cycle, impaired respiration, and abnormal accumulation of their substrates succinate and fumarate, respectively. Both metabolites are also inhibitors of 2OG-dependent dioxygenases, particularly the hydroxylases for the transcription factor hypoxia-inducible factor (HIF), resulting in HIF-dependent activation of a “pseudo-hypoxic” response characterized by enhanced angiogenesis and increased anaerobic metabolism (Frezza et al., 2011). In the case of fumarate, the metabolite is also an endogenous electrophile and can chemically modify cysteine residues in Kelch-like ECH-associated protein 1, leading to constitutive (and potentially oncogenic) activation of transcription factor nuclear factor erythroid 2-related factor 2 (Adam et al., 2011; Ooi et al., 2011). Until recently, HIF activation by fumarate and succinate has been the only mechanistic link to oncogenesis that has been described in FH and SDH mutant cancer models (Pollard et al., 2007; Selak et al., 2005). However, at least in the context of FH-deficiency, a causal role for HIF in tumorigenesis is questionable (Adam et al., 2011), and the quest for other oncogenic drivers in SDH- and FH-associated malignancy continues. Recent re-

ports by Killian et al. (2013) and Letouzé et al. (2013; in this issue of *Cancer Cell*) both demonstrate that, similarly to (R)-2HG, succinate can also remodel the epigenome and alter gene expression.

SDH mutations occur frequently in paraganglioma (PGL), pheochromocytoma (PCC), gastrointestinal stromal tumor (GIST), as well as in renal carcinoma (Killian et al., 2013). GIST tumors can alternatively be driven by mutations in signal transduction kinases. Killian et al. (2013) compared the methylation profiles of GISTs with mutations in either SDH or KIT tyrosine kinase and uncovered marked global hypermethylation in the SDH versus KIT mutant subgroup. Further examination of a PGL/PCC cohort showed a similar hypermethylation phenotype in SDH mutant tumors compared to SDH-wild-type reference tissues. Bioinformatic analyses of methylomes from developmentally distinct tumors including GIST, PGL, PCC, and gliomas revealed comparable methylation signatures in those harboring SDH and IDH mutations (Killian et al., 2013).

Letouzé et al. (2013) classified a large PGL/PCC cohort based on DNA methylation and obtained three stable clusters. Strikingly, a distinct subgroup characterized by the presence of a

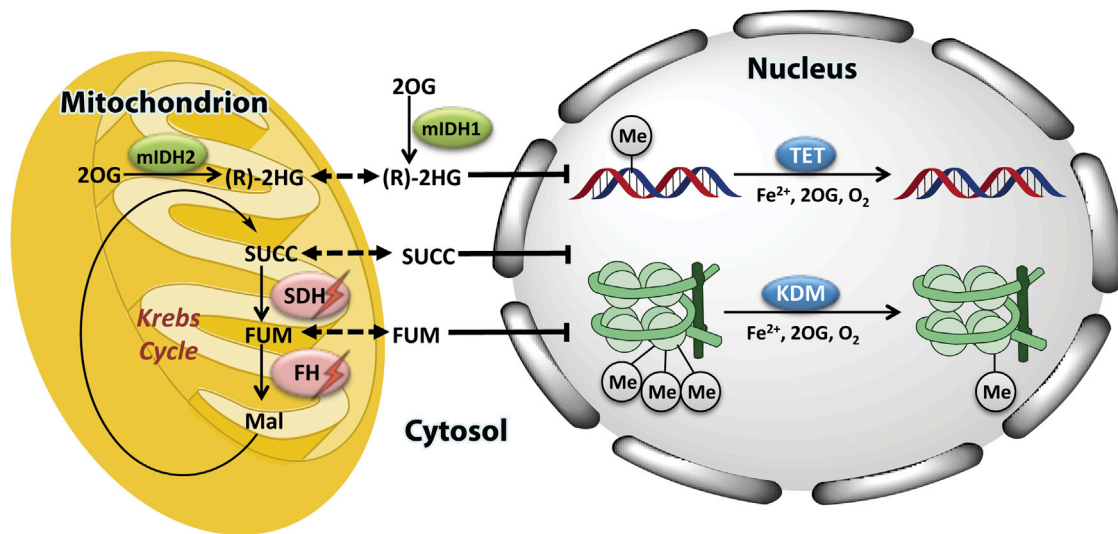


Figure 1. Epigenetic Reprogramming by Oncometabolites

Mutations in the metabolic enzymes isocitrate dehydrogenase (IDH)-1 and -2, succinate dehydrogenase (SDH), and fumarate hydratase (FH) lead to abnormal accumulation of (R)-2-hydroxyglutarate [(R)-2HG], succinate, and fumarate, respectively. Their accumulation inhibits the activities of 2-oxoglutarate (2OG)-dependent dioxygenases, including the TET family of DNA modifying enzymes and the JmjC domain-containing histone lysine demethylases (KDMs). Subsequent epigenetic alterations result in cell differentiation arrest and promote malignant transformation. Thus, epigenetic modification, through the action of oncometabolites, is a shared feature among IDH-, SDH-, and FH-associated cancers. SUCC, succinate; FUM, fumarate; Mal, malate; mIDH1/2, mutant IDH1/2; Me, methyl group.

hypermethylator phenotype contained 16 of 17 samples that harbor *SDH* mutations. The prevailing model is that accumulation of succinate in these tumors inhibits 2OG-dependent oxidative demethylation in a manner analogous to the action of (R)-2HG, giving rise to DNA hypermethylation. Integration of methylation and gene expression data revealed, whereas most hypermethylated CpG sites had no functional consequences, there were 191 genes that showed correlated levels of hypermethylation and downregulation (Letouzé et al., 2013).

SDH- and VHL-related tumors share some similar features in gene expression profiles, possibly due to activation of HIF-orchestrated hypoxia-related genes. Nonetheless, SDH- and VHL-associated PGL/PCC from the cohort studied were clustered as two distinct gene-expression subgroups, suggesting that epigenetic remodelling plays a major role in the transcriptional divergence of these two tumor subclasses. Intriguingly, the only tumor sample in the hypermethylated PGL/PCC subgroup without SDH mutations was shown to harbor germline inactivating FH mutations. This finding corroborates recent evidence demonstrating that fumarate-mediated inhibition of TET and KDM enzymes alters histone and DNA methylation pat-

terns (Xiao et al., 2012) and raises the necessity to test FH-associated neoplasms for epigenetic abnormalities in future studies.

Consistent with the findings by Killian et al. (2013), Letouzé et al. (2013) compared the CpG methylator phenotypes between SDH/FH mutant PGL/PCC and IDH mutant gliomas and identified significant overlap in hypermethylated CpG sites. Particularly, 17 genes were concordantly hypermethylated and downregulated in both tumor groups. The connection in methylation profiles between the SDH, FH, and IDH mutant tumors may reflect a similar inhibitory role for succinate, fumarate, and (R)-2HG (see Figure 1), whereas the differences may partly be attributed to the variable susceptibilities of the panoply of 2OG-dependent oxygenases to the three oncometabolites.

All of the SDH mutant PGL/PCC in this study exhibited low 5-hydroxymethylcytosine (5hmC) levels by immunohistochemistry analyses, and the majority also showed elevated histone methylation at H3K27, supporting the hypothesis that succinate inhibits TET- and KDM-mediated demethylations. Consistently, *Sdhb*^{-/-} mouse chromaffin cells displayed higher 5mC/5hmC ratios compared to wild-type cells, which could be

reversed by the addition of exogenous 2OG to the culture medium. Importantly, the hypermethylated genes detected in these cells significantly overlapped with those identified in SDH mutant PGL/PCC.

The SDH enzyme complex comprises four subunits (SDHA, SDHB, SDHC, and SDHD). Although mutations in all subunits occur in cancer, tumors harboring mutations in the catalytic subunit SDHB are particularly malignant and associated with a higher risk of metastasis (Frezza et al., 2011). Letouzé et al. (2013) showed that the mean methylation levels across all CpG sites are higher in SDHB-mutated PGL/PCC than other SDH mutant PGL/PCC. It is possible that the loss of SDHB function results in bona fide inactivation of the SDH complex, whereas reductions of enzyme activity through mutations in other subunits are not as complete. Consequently, there might be higher succinate accumulation and stronger inhibition of demethylation in *SDHB* mutant tumors. Although the differences in succinate levels could not be demonstrated from the SDH mutant PGL/PCC cohort, the heterogeneity of tumor samples may preclude accurate analyses and further investigations employing cell culture models could be more informative. Two of the most significantly silenced genes in the hypermethylated subgroup,

PNMT and *KRT19*, are respectively involved in neuroendocrine differentiation and epithelial-to-mesenchymal transition (EMT). Interestingly, despite exhibiting a decreased growth rate similar to the *Fh1*^{-/-} mouse embryonic fibroblasts, the *Sdhb*^{-/-} chromaffin cells showed markedly increased migratory capacities, potentially reflecting epigenetic deregulation of EMT genes and the aggressive nature of SDHB-related PCC/PGL.

Recently, inhibitors that specifically target mutant IDH1 and IDH2 have been reported. Such inhibitors could reverse (R)-2HG-mediated epigenetic deregulation, induce cell differentiation, and suppress the growth of IDH mutant tumor cells (Kim and DeBerardinis, 2013). Letouzé et al. (2013) showed that transient treatment with a DNA methyltransferase inhibitor repressed the migration capacities of *Sdhb*^{-/-} cells, implicating the possibility of epigenetic targeting in SDH-related tumors. However, succinate and fumarate accumulation exert various

nonepigenetic cellular impacts, and, to achieve therapeutic efficacy, a synergistic lethality approach is probably desired. Nonetheless, the emergence of epigenetically silenced gene sets may serve as useful biomarkers for early detection of cancers characterized by Krebs cycle defects.

REFERENCES

- Adam, J., Hatipoglu, E., O'Flaherty, L., Ternette, N., Sahgal, N., Lockstone, H., Baban, D., Nye, E., Stamp, G.W., Wolhuter, K., et al. (2011). *Cancer Cell* 20, 524–537.
- Dang, L., White, D.W., Gross, S., Bennett, B.D., Bittinger, M.A., Driggers, E.M., Fantin, V.R., Jang, H.G., Jin, S., Keenan, M.C., et al. (2010). *Nature* 465, 966.
- Frezza, C., Pollard, P.J., and Gottlieb, E. (2011). *J. Mol. Med.* 89, 213–220.
- Killian, J.K., Kim, S.Y., Miettinen, M., Smith, C., Merino, M., Tsokos, M., Quezado, M., Smith, W.I., Jr., Jahromi, M.S., Xekouki, P., et al. (2013). *Cancer Discov.* Published online May 21, 2013. <http://dx.doi.org/10.1158/2159-8290.CD-13-0092>.
- Kim, J., and DeBerardinis, R.J. (2013). *Science* 340, 558–559.
- Letouzé, E., Martinelli, C., Lorient, C., Burnichon, N., Abermil, N., Ottolenghi, C., Janin, M., Menara, M., Nguyen, A.T., Benit, P., et al. (2013). *Cancer Cell* 23, this issue, 739–752.
- Ooi, A., Wong, J.C., Petillo, D., Roossien, D., Perrier-Trudova, V., Whitten, D., Min, B.W., Tan, M.H., Zhang, Z., Yang, X.J., et al. (2011). *Cancer Cell* 20, 511–523.
- Pollard, P.J., Spencer-Dene, B., Shukla, D., Howarth, K., Nye, E., El-Bahrawy, M., Deheragoda, M., Joannou, M., McDonald, S., Martin, A., et al. (2007). *Cancer Cell* 17, 311–319.
- Selak, M.A., Armour, S.M., MacKenzie, E.D., Boulahbel, H., Watson, D.G., Mansfield, K.D., Pan, Y., Simon, M.C., Thompson, C.B., and Gottlieb, E. (2005). *Cancer Cell* 7, 77–85.
- Ward, P.S., Patel, J., Wise, D.R., Abdel-Wahab, O., Bennett, B.D., Coller, H.A., Cross, J.R., Fantin, V.R., Hedvat, C.V., Perl, A.E., et al. (2010). *Cancer Cell* 17, 225–234.
- Xiao, M., Yang, H., Xu, W., Ma, S., Lin, H., Zhu, H., Liu, L., Liu, Y., Yang, C., Xu, Y., et al. (2012). *Genes Dev.* 26, 1326–1338.

Cancer Stem Cells Activate STAT3 the EZ Way

Shaun D. Fouse¹ and Joseph F. Costello^{1,*}

¹Brain Tumor Research Center, Department of Neurosurgery, University of California, San Francisco, San Francisco, CA 94158, USA

*Correspondence: jcostello@cc.ucsf.edu

<http://dx.doi.org/10.1016/j.ccr.2013.05.016>

Activated STAT3 and increased expression of the histone methyltransferase EZH2 are independently associated with the most malignant subset of gliomas. In this issue of *Cancer Cell*, Kim and colleagues discover that EZH2 enhances STAT3 activation by trimethylating lysine180 in STAT3 and does so preferentially in glioma stem-like cells.

Presuming that cancer stem cells are responsible for therapeutic resistance in cancer patients, the discovery of the molecular differences that drive cancer stem cell phenotypes holds significant value for improving therapy. More valuable still would be the ability to selectively inhibit these molecular drivers of stemness. In this issue of *Cancer Cell*, Kim et al. (2013) employ cultures of glioma stem-like cells (GSCs) and their isogenic bulk tumor cells along with intracranial xenografts and come one step closer to achieving this ambitious goal.

Mutation or overexpression of enhancer of Zeste homolog 2 (EZH2) can drive the clonal expansion of leukemias and the growth of solid cancers, though individual EZH2 alterations follow divergent paths toward malignancy. EZH2 is most known as an enzymatically active component of the Polycomb repressive complex 2 (PRC2), which is responsible for depositing methyl groups onto lysine 27 (K27) of histone H3 (H3K27). EZH2 plays an important role in maintaining stem cell function. The most common EZH2 mutations in cancer occur within

the SET domain at Y641, which result in increased trimethylation activity, leading to an increase in global H3K27me3 levels in B cell lymphomas (Yap et al., 2011). In contrast, in breast cancer cells, AKT-mediated phosphorylation of S21 reduces EZH2 interaction with histone H3, leading to a decrease in global H3K27me3 levels (Cha et al., 2005). In addition, in pediatric brain tumors, recurrent somatic mutation of K27 on histone H3 variant *H3F3A* may deplete H3K27me3 on canonical H3 indirectly because of increased interaction between mutant *H3F3A* and EZH2.

PNMT and *KRT19*, are respectively involved in neuroendocrine differentiation and epithelial-to-mesenchymal transition (EMT). Interestingly, despite exhibiting a decreased growth rate similar to the *Fh1*^{-/-} mouse embryonic fibroblasts, the *Sdhb*^{-/-} chromaffin cells showed markedly increased migratory capacities, potentially reflecting epigenetic deregulation of EMT genes and the aggressive nature of SDHB-related PCC/PGL.

Recently, inhibitors that specifically target mutant IDH1 and IDH2 have been reported. Such inhibitors could reverse (R)-2HG-mediated epigenetic deregulation, induce cell differentiation, and suppress the growth of IDH mutant tumor cells (Kim and DeBerardinis, 2013). Letouzé et al. (2013) showed that transient treatment with a DNA methyltransferase inhibitor repressed the migration capacities of *Sdhb*^{-/-} cells, implicating the possibility of epigenetic targeting in SDH-related tumors. However, succinate and fumarate accumulation exert various

nonepigenetic cellular impacts, and, to achieve therapeutic efficacy, a synergistic lethality approach is probably desired. Nonetheless, the emergence of epigenetically silenced gene sets may serve as useful biomarkers for early detection of cancers characterized by Krebs cycle defects.

REFERENCES

Adam, J., Hatipoglu, E., O'Flaherty, L., Ternette, N., Sahgal, N., Lockstone, H., Baban, D., Nye, E., Stamp, G.W., Wolhuter, K., et al. (2011). *Cancer Cell* 20, 524–537.

Dang, L., White, D.W., Gross, S., Bennett, B.D., Bittinger, M.A., Driggers, E.M., Fantin, V.R., Jang, H.G., Jin, S., Keenan, M.C., et al. (2010). *Nature* 465, 966.

Frezza, C., Pollard, P.J., and Gottlieb, E. (2011). *J. Mol. Med.* 89, 213–220.

Killian, J.K., Kim, S.Y., Miettinen, M., Smith, C., Merino, M., Tsokos, M., Quezado, M., Smith, W.I., Jr., Jahromi, M.S., Xekouki, P., et al. (2013). *Cancer Discov.* Published online May 21, 2013. <http://dx.doi.org/10.1158/2159-8290.CD-13-0092>.

Kim, J., and DeBerardinis, R.J. (2013). *Science* 340, 558–559.

Letouzé, E., Martinelli, C., Lorient, C., Burnichon, N., Abermil, N., Ottolenghi, C., Janin, M., Menara, M., Nguyen, A.T., Benit, P., et al. (2013). *Cancer Cell* 23, this issue, 739–752.

Ooi, A., Wong, J.C., Petillo, D., Roossien, D., Perrier-Trudova, V., Whitten, D., Min, B.W., Tan, M.H., Zhang, Z., Yang, X.J., et al. (2011). *Cancer Cell* 20, 511–523.

Pollard, P.J., Spencer-Dene, B., Shukla, D., Howarth, K., Nye, E., El-Bahrawy, M., Deheragoda, M., Joannou, M., McDonald, S., Martin, A., et al. (2007). *Cancer Cell* 17, 311–319.

Selak, M.A., Armour, S.M., MacKenzie, E.D., Boulahbel, H., Watson, D.G., Mansfield, K.D., Pan, Y., Simon, M.C., Thompson, C.B., and Gottlieb, E. (2005). *Cancer Cell* 7, 77–85.

Ward, P.S., Patel, J., Wise, D.R., Abdel-Wahab, O., Bennett, B.D., Coller, H.A., Cross, J.R., Fantin, V.R., Hedvat, C.V., Perl, A.E., et al. (2010). *Cancer Cell* 17, 225–234.

Xiao, M., Yang, H., Xu, W., Ma, S., Lin, H., Zhu, H., Liu, L., Liu, Y., Yang, C., Xu, Y., et al. (2012). *Genes Dev.* 26, 1326–1338.

Cancer Stem Cells Activate STAT3 the EZ Way

Shaun D. Fouse¹ and Joseph F. Costello^{1,*}

¹Brain Tumor Research Center, Department of Neurosurgery, University of California, San Francisco, San Francisco, CA 94158, USA

*Correspondence: jcostello@cc.ucsf.edu

<http://dx.doi.org/10.1016/j.ccr.2013.05.016>

Activated STAT3 and increased expression of the histone methyltransferase EZH2 are independently associated with the most malignant subset of gliomas. In this issue of *Cancer Cell*, Kim and colleagues discover that EZH2 enhances STAT3 activation by trimethylating lysine180 in STAT3 and does so preferentially in glioma stem-like cells.

Presuming that cancer stem cells are responsible for therapeutic resistance in cancer patients, the discovery of the molecular differences that drive cancer stem cell phenotypes holds significant value for improving therapy. More valuable still would be the ability to selectively inhibit these molecular drivers of stemness. In this issue of *Cancer Cell*, Kim et al. (2013) employ cultures of glioma stem-like cells (GSCs) and their isogenic bulk tumor cells along with intracranial xenografts and come one step closer to achieving this ambitious goal.

Mutation or overexpression of enhancer of Zeste homolog 2 (EZH2) can drive the clonal expansion of leukemias and the growth of solid cancers, though individual EZH2 alterations follow divergent paths toward malignancy. EZH2 is most known as an enzymatically active component of the Polycomb repressive complex 2 (PRC2), which is responsible for depositing methyl groups onto lysine 27 (K27) of histone H3 (H3K27). EZH2 plays an important role in maintaining stem cell function. The most common EZH2 mutations in cancer occur within

the SET domain at Y641, which result in increased trimethylation activity, leading to an increase in global H3K27me3 levels in B cell lymphomas (Yap et al., 2011). In contrast, in breast cancer cells, AKT-mediated phosphorylation of S21 reduces EZH2 interaction with histone H3, leading to a decrease in global H3K27me3 levels (Cha et al., 2005). In addition, in pediatric brain tumors, recurrent somatic mutation of K27 on histone H3 variant *H3F3A* may deplete H3K27me3 on canonical H3 indirectly because of increased interaction between mutant H3F3A and EZH2.

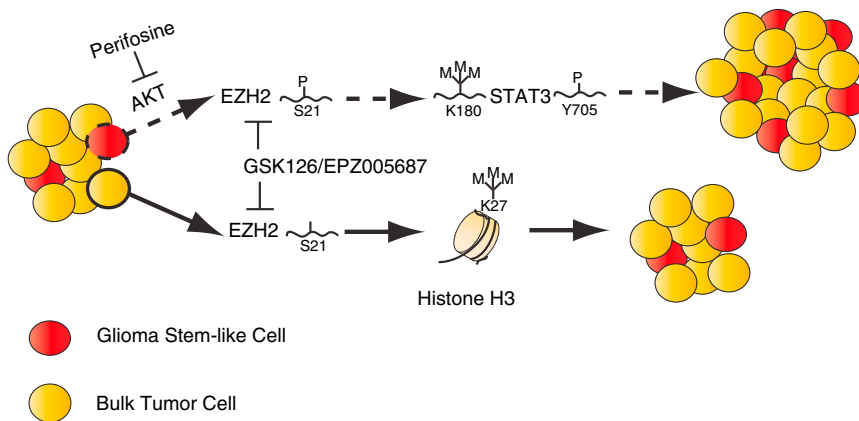


Figure 1. pS21-EZH2 Enhances STAT3 Activation through K180 Trimethylation in Glioma Stem-like Cells

In GSCs, AKT phosphorylates S21 on EZH2, switching its substrate preference from H3K27 to STAT3 and potentially other nonhistone proteins. K180 trimethylation of STAT3 results in increased STAT3 activation via increased phosphorylation of Y705 by JAKs, promoting tumor growth. In bulk tumor cells, AKT-mediated phosphorylation of EZH2 is diminished; EZH2 with unphosphorylated S21 preferentially binds and trimethylates H3K27. Inhibitors such as GSK126 or EPZ005687 selectively target the methyltransferase domain of EZH2 and, thus, can block both histone- and non-histone-mediated routes for GBM progression.

However, this occurs concurrently with increased H3K27me3 colocalized with EZH2 at specific genes associated with tumorigenesis (Chan et al., 2013; Lewis et al., 2013). These and other studies suggest altered EZH2 function contributes to tumor development by promoting aberrant expression of cellular oncogenes and tumor suppressor genes via cancer-associated changes in H3K27 methylation.

Although not appreciated until recently, EZH2 also methylates nonhistone proteins. EZH2 monomethylates transcription factors GATA4 and ROR α at lysines, resulting in a reduction in their ability to activate transcription (He et al., 2012; Lee et al., 2012). EZH2 also functions in a PRC2-independent manner as a transcriptional coactivator with androgen receptor in castration-resistant prostate cancer cells (Xu et al., 2012). This raises the important questions of whether EZH2 methylation of nonhistone proteins may contribute to tumorigenesis and how the balance of histone and nonhistone methylation activity is determined.

Kim et al. (2013) addressed these questions by first demonstrating that EZH2, along with multiple members of the PRC2 complex, interacts with STAT3. Importantly, this interaction exists preferentially in stem cells—specifically human neural progenitor cells and GSCs, but

neither in their differentiated isogenic progeny nor in established glioma cell lines grown in serum. STAT3 has a well characterized role in cancer progression, and its activation in glioblastoma multiforme (GBM) is associated with the aggressive mesenchymal subtype and poor overall survival (Carro et al., 2010). The activation of STAT3 is dependent on phosphorylation of Y705 by the Janus kinases (JAKs), but STAT3 can also be dimethylated at K140 by SET9, leading to a decrease in activated STAT3 (Yang et al., 2010). As with EZH2, STAT3 also plays an important role in the maintenance of GSCs. Therefore, the newly discovered interaction between EZH2 and STAT3 might underlie a shared function in the maintenance of GSC phenotypes. Inhibiting either of these proteins could potentially help eradicate the GSC pool within a GBM.

As a consequence of their interaction, EZH2 trimethylates STAT3 on K180, which Kim et al. (2013) found to be essential for STAT3 activation in GSCs and GBM xenografts. This is in contrast to EZH2-mediated methylation of ROR α or GATA4 or SET9-mediated STAT3 K140 dimethylation, because these methyl group modifications result in a decrease in transcriptional activity of the modified protein. The exact mechanism by which trimethylation at K180 contributes to STAT3 activation and how this might synergize with Y705

phosphorylation are not yet known. Methylation at K140 on STAT3 can be removed by LSD1 (Yang et al., 2010), but it is unknown at this point which, if any, protein(s) might be involved with the demethylation of K180. Temporal examination of the changing interaction and posttranslational modifications during differentiation of GSCs into non-stem cells could provide insight into the relative ordering of phosphorylation and methylation, the dynamics of EZH2-STAT3 interaction, and whether the loss of interaction is a driving force or a consequence of differentiation. It is also not yet clear if the EZH2-STAT3 interaction leads to robust STAT3 K180 methylation in normal neural progenitor cells and if this is important for neural progenitor function. It should be noted that GSCs are specifically enriched and maintained by culturing in EGF, which prior studies show is a potent inducer of STAT3 phosphorylation and activation.

Kim et al. (2013) show that AKT phosphorylates EZH2 at S21 in GSCs and, as shown for breast cancer cells, may enable EZH2 to bind substrates other than H3K27. In fact, approximately 90% of primary GBMs have AKT activation. In GSCs, AKT-induced phosphorylation of EZH2 increased activation of STAT3 via K180 trimethylation and decreased the survival of mice bearing xenografts of GSCs. These results underscore the importance of AKT activation in GBM and establish a pathway by which EZH2 can contribute to tumor growth independent of, or in addition to, gain or loss of H3K27me3 (Figure 1). However, in primary tumors, AKT is presumably active in both GSC and bulk tumor cell populations. Therefore, it will be important to determine why AKT-mediated S21 phosphorylation of EZH2 and subsequent K180 methylation on STAT3 occurs preferentially in GSCs.

Selective inhibition of STAT3 has been difficult to achieve in patients with cancer. The data from this new study suggested that it might be possible to decrease STAT3 activation by inhibiting EZH2. Emerging selective small molecule inhibitors of EZH2 (GSK126, GSK343, GSK503, and EPZ005687) suppress the growth of lymphoma cell lines and xenografts that have activating EZH2 mutations. Kim et al. (2013) found that GSK126 decreased levels

of phosphorylated STAT3 in GSCs. Substantial additional research is required to determine if this early experimental success will translate into notable clinical response.

The findings of Kim et al. (2013) are important, because they establish an H3K27-independent role for EZH2 in GBM through K180 trimethylation of STAT3, which appears to be involved in the aggressiveness of high-grade glioma (Figure 1). Furthermore, the results provide a new understanding of regulatory pathways that drive GSC phenotypes. If these findings are relevant to cancer stem cells in patients, STAT3 and/or EZH2 will become even more attractive targets for improving therapeutic response and patient survival.

REFERENCES

- Carro, M.S., Lim, W.K., Alvarez, M.J., Bollo, R.J., Zhao, X., Snyder, E.Y., Sulman, E.P., Anne, S.L., Doetsch, F., Colman, H., et al. (2010). *Nature* 463, 318–325.
- Cha, T.L., Zhou, B.P., Xia, W., Wu, Y., Yang, C.C., Chen, C.T., Ping, B., Otte, A.P., and Hung, M.C. (2005). *Science* 310, 306–310.
- Chan, K.M., Fang, D., Gan, H., Hashizume, R., Yu, C., Schroeder, M., Gupta, N., Mueller, S., James, C.D., Jenkins, R., et al. (2013). *Genes Dev.* 27, 985–990.
- He, A., Shen, X., Ma, Q., Cao, J., von Gise, A., Zhou, P., Wang, G., Marquez, V.E., Orkin, S.H., and Pu, W.T. (2012). *Genes Dev.* 26, 37–42.
- Kim, E., Kim, M., Woo, D.-H., Shin, Y., Shin, J., Chang, N., Oh, Y.T., Kim, H., Rhee, J., Nakano, I., et al. (2013). *Cancer Cell* 23, this issue, 839–852.
- Lee, J.M., Lee, J.S., Kim, H., Kim, K., Park, H., Kim, J.Y., Lee, S.H., Kim, I.S., Kim, J., Lee, M., et al. (2012). *Mol. Cell* 48, 572–586.
- Lewis, P.W., Müller, M.M., Koletsky, M.S., Cordero, F., Lin, S., Banaszynski, L.A., Garcia, B.A., Muir, T.W., Becher, O.J., and Allis, C.D. (2013). *Science* 340, 857–861.
- Xu, K., Wu, Z.J., Groner, A.C., He, H.H., Cai, C., Lis, R.T., Wu, X., Stack, E.C., Loda, M., Liu, T., et al. (2012). *Science* 338, 1465–1469.
- Yang, J., Huang, J., Dasgupta, M., Sears, N., Miyagi, M., Wang, B., Chance, M.R., Chen, X., Du, Y., Wang, Y., et al. (2010). *Proc. Natl. Acad. Sci. USA* 107, 21499–21504.
- Yap, D.B., Chu, J., Berg, T., Schapira, M., Cheng, S.W., Moradian, A., Morin, R.D., Mungall, A.J., Meissner, B., Boyle, M., et al. (2011). *Blood* 117, 2451–2459.

Adaptation to Starvation: Translating a Matter of Life or Death

Brendan D. Manning^{1,*}

¹Department of Genetics and Complex Diseases, Harvard School of Public Health, 665 Huntington Avenue, SPH2-117, Boston, MA 02115, USA

*Correspondence: bmanning@hsph.harvard.edu
<http://dx.doi.org/10.1016/j.ccr.2013.05.012>

There is much interest in defining the nutrient dependencies of cancer cells and their mechanisms of adaptation to nutrient depletion. In a recent issue of *Cell*, Lepruvier and colleagues demonstrate that eEF2K, which can inhibit translation elongation acutely during protein synthesis, is a critical switch in the survival versus death fate of starved cancer cells.

Cells and organisms have evolved exquisite mechanisms to acutely adapt to fluctuations in nutrient availability. Starvation impinges on highly conserved nutrient-sensing pathways, resulting in an integrated and adaptive response that includes an abrupt halt to anabolic processes that consume nutrients and energy. The mammalian target of rapamycin complex 1 (mTORC1), general amino acid control nonderepressible 2 (GCN2), and AMP-dependent protein kinase (AMPK) are the best characterized of these nutrient sensors (Yuan et al., 2013), all of which exert acute control over protein synthesis (Figure 1A), perhaps the most nutrient-

and energy-costly of cellular processes. It is now evident that cancer cells can drive anabolic processes that promote cell growth and proliferation in a manner largely independent of normal growth signals (Cantor and Sabatini, 2012). Importantly, oncogenic events that disconnect anabolic processes from normal control mechanisms are likely to render tumor cells more vulnerable to the loss of specific nutrients. In a recent study published in *Cell*, Lepruvier et al. (2013) find that the adaptation of tumor cells to nutrient deprivation is dependent on their ability to acutely block translation elongation during protein synthesis.

In an isogenic fibroblast model, Lepruvier et al. (2013) found that oncogene-transformed cells were much more sensitive to severe nutrient depletion in the form of complete removal of glucose, amino acids, and serum. Surprisingly, this susceptibility was not due to increased ATP consumption as, unlike nontransformed cells, the oncogene-expressing cells somehow sustained their ATP levels in the absence of nutrients. This difference was also reflected in a lack of activation of AMPK, which is normally stimulated in response to energy stress (defined as an increase in the ratio of cellular AMP or ADP to ATP) and plays a critical role in

of phosphorylated STAT3 in GSCs. Substantial additional research is required to determine if this early experimental success will translate into notable clinical response.

The findings of Kim et al. (2013) are important, because they establish an H3K27-independent role for EZH2 in GBM through K180 trimethylation of STAT3, which appears to be involved in the aggressiveness of high-grade glioma (Figure 1). Furthermore, the results provide a new understanding of regulatory pathways that drive GSC phenotypes. If these findings are relevant to cancer stem cells in patients, STAT3 and/or EZH2 will become even more attractive targets for improving therapeutic response and patient survival.

REFERENCES

- Carro, M.S., Lim, W.K., Alvarez, M.J., Bollo, R.J., Zhao, X., Snyder, E.Y., Sulman, E.P., Anne, S.L., Doetsch, F., Colman, H., et al. (2010). *Nature* 463, 318–325.
- Cha, T.L., Zhou, B.P., Xia, W., Wu, Y., Yang, C.C., Chen, C.T., Ping, B., Otte, A.P., and Hung, M.C. (2005). *Science* 310, 306–310.
- Chan, K.M., Fang, D., Gan, H., Hashizume, R., Yu, C., Schroeder, M., Gupta, N., Mueller, S., James, C.D., Jenkins, R., et al. (2013). *Genes Dev.* 27, 985–990.
- He, A., Shen, X., Ma, Q., Cao, J., von Gise, A., Zhou, P., Wang, G., Marquez, V.E., Orkin, S.H., and Pu, W.T. (2012). *Genes Dev.* 26, 37–42.
- Kim, E., Kim, M., Woo, D.-H., Shin, Y., Shin, J., Chang, N., Oh, Y.T., Kim, H., Rhee, J., Nakano, I., et al. (2013). *Cancer Cell* 23, this issue, 839–852.
- Lee, J.M., Lee, J.S., Kim, H., Kim, K., Park, H., Kim, J.Y., Lee, S.H., Kim, I.S., Kim, J., Lee, M., et al. (2012). *Mol. Cell* 48, 572–586.
- Lewis, P.W., Müller, M.M., Koletsky, M.S., Cordero, F., Lin, S., Banaszynski, L.A., Garcia, B.A., Muir, T.W., Becher, O.J., and Allis, C.D. (2013). *Science* 340, 857–861.
- Xu, K., Wu, Z.J., Groner, A.C., He, H.H., Cai, C., Lis, R.T., Wu, X., Stack, E.C., Loda, M., Liu, T., et al. (2012). *Science* 338, 1465–1469.
- Yang, J., Huang, J., Dasgupta, M., Sears, N., Miyagi, M., Wang, B., Chance, M.R., Chen, X., Du, Y., Wang, Y., et al. (2010). *Proc. Natl. Acad. Sci. USA* 107, 21499–21504.
- Yap, D.B., Chu, J., Berg, T., Schapira, M., Cheng, S.W., Moradian, A., Morin, R.D., Mungall, A.J., Meissner, B., Boyle, M., et al. (2011). *Blood* 117, 2451–2459.

Adaptation to Starvation: Translating a Matter of Life or Death

Brendan D. Manning^{1,*}

¹Department of Genetics and Complex Diseases, Harvard School of Public Health, 665 Huntington Avenue, SPH2-117, Boston, MA 02115, USA

*Correspondence: bmanning@hsph.harvard.edu
<http://dx.doi.org/10.1016/j.ccr.2013.05.012>

There is much interest in defining the nutrient dependencies of cancer cells and their mechanisms of adaptation to nutrient depletion. In a recent issue of *Cell*, Lepruvier and colleagues demonstrate that eEF2K, which can inhibit translation elongation acutely during protein synthesis, is a critical switch in the survival versus death fate of starved cancer cells.

Cells and organisms have evolved exquisite mechanisms to acutely adapt to fluctuations in nutrient availability. Starvation impinges on highly conserved nutrient-sensing pathways, resulting in an integrated and adaptive response that includes an abrupt halt to anabolic processes that consume nutrients and energy. The mammalian target of rapamycin complex 1 (mTORC1), general amino acid control nonderepressible 2 (GCN2), and AMP-dependent protein kinase (AMPK) are the best characterized of these nutrient sensors (Yuan et al., 2013), all of which exert acute control over protein synthesis (Figure 1A), perhaps the most nutrient-

and energy-costly of cellular processes. It is now evident that cancer cells can drive anabolic processes that promote cell growth and proliferation in a manner largely independent of normal growth signals (Cantor and Sabatini, 2012). Importantly, oncogenic events that disconnect anabolic processes from normal control mechanisms are likely to render tumor cells more vulnerable to the loss of specific nutrients. In a recent study published in *Cell*, Lepruvier et al. (2013) find that the adaptation of tumor cells to nutrient deprivation is dependent on their ability to acutely block translation elongation during protein synthesis.

In an isogenic fibroblast model, Lepruvier et al. (2013) found that oncogene-transformed cells were much more sensitive to severe nutrient depletion in the form of complete removal of glucose, amino acids, and serum. Surprisingly, this susceptibility was not due to increased ATP consumption as, unlike nontransformed cells, the oncogene-expressing cells somehow sustained their ATP levels in the absence of nutrients. This difference was also reflected in a lack of activation of AMPK, which is normally stimulated in response to energy stress (defined as an increase in the ratio of cellular AMP or ADP to ATP) and plays a critical role in

adaptation to nutrient depletion (Shackelford and Shaw, 2009). AMPK phosphorylates numerous targets aimed at alleviating energy stress by promoting catabolic processes and inhibiting anabolic processes. A major mechanism of AMPK-mediated inhibition of anabolic processes is to block mTORC1 signaling, which is also inhibited by starvation through AMPK-independent pathways (Yuan et al., 2013). mTORC1 stimulates protein synthesis, primarily at the level of translation initiation, and an inability to inhibit mTORC1 can sensitize cells to nutrient starvation (Choo et al., 2010). However, Lepruvier et al. (2013) found that mTORC1 signaling is properly attenuated under starvation in both normal and transformed cells in their system, reflected in blocked mRNA translation initiation and decreased global protein synthesis.

In contrast to mTORC1, another downstream target of AMPK that regulates mRNA translation the eukaryotic elongation factor 2 (eEF2) kinase (eEF2K) was found to be differentially regulated in normal and transformed cells (Lepruvier et al., 2013). AMPK is thought to activate eEF2K by direct phosphorylation of S398 (Browne et al., 2004), which lies within an atypical AMPK phosphorylation sequence (Shackelford and Shaw, 2009). Activated eEF2K phosphorylates eEF2 on T56 to inhibit its function in translation elongation (Figure 1A). Importantly, Lepruvier et al. (2013) found a pronounced difference in the inhibitory phosphorylation of eEF2-T56 in response to nutrient deprivation in the normal and transformed cells, with the latter displaying greatly reduced levels. Despite blocked translation initiation in both settings, loss of proper control over eEF2 in transformed cells resulted in continued elongation on

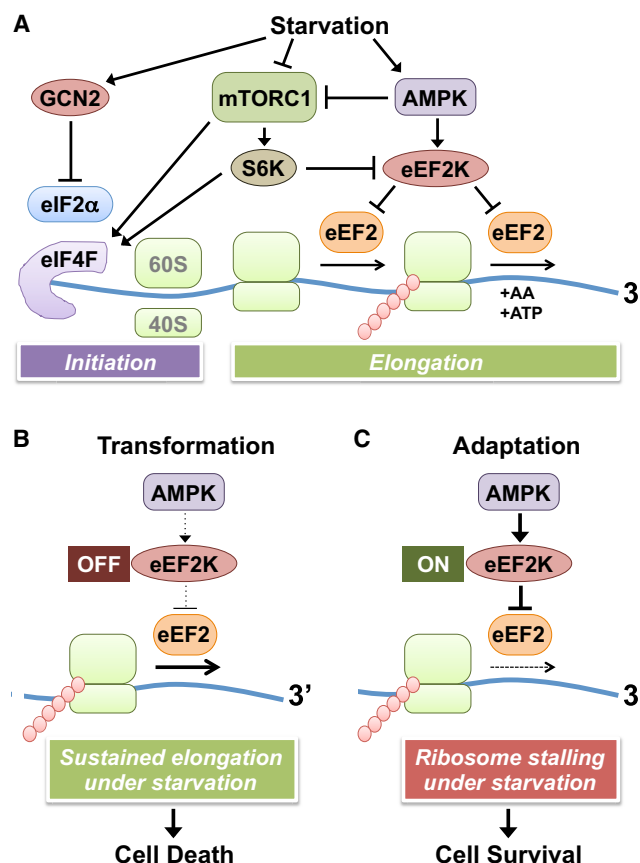


Figure 1. Model of the Adaptive Regulation of mRNA Translation in Response to Starvation in Normal and Transformed Cells

(A) Starvation regulates downstream kinases to acutely inhibit mRNA translation initiation and elongation. In response to starvation, GCN2 is activated to inhibit eIF2α, and mTORC1 and S6K are inhibited to block their promotion of translation initiation through downstream targets, including those that affect assembly of the eIF4F complex. Starvation also activates AMPK, which inhibits mTORC1 and activates eEF2K, which inhibits translation elongation by blocking the function of eEF2. Translation elongation consumes amino acids (AA) and ATP.

(B) Oncogenic transformation can attenuate AMPK activation or lead to other events, resulting in a defect in the proper activation of eEF2K in response to starvation. This defect results in sustained translation elongation under starvation conditions, which triggers cell death through an unknown mechanism.

(C) Restoring the response of eEF2K to starvation results in inhibition of eEF2, thereby stalling the translating ribosome and blocking elongation. This acute adaptive response protects cells from starvation-induced death.

mRNAs that had already initiated translation, with ribosomes ultimately running off of those transcripts (Figure 1B). In contrast, normal cells, and transformed cells adapted to starvation, display proper eEF2K activation and eEF2 inhibition, resulting in an acute block in translation elongation in response to starvation, reflected in stalled ribosomes on bound transcripts (Figure 1C).

Acute inhibition of translation elongation by AMPK-mediated eEF2K activation was found to be essential for the

survival of both normal and transformed cells in response to nutrient deprivation (Lepruvier et al., 2013). A defect in triggering this adaptive response appears to be a major mechanism by which some cancer cells display enhanced sensitivity to starvation (Figures 1B and 1C). Cancer cells with defects in AMPK activation will be particularly susceptible to nutrient deprivation. The most frequent genetic event in human cancers known to lead to strong attenuation of AMPK signaling is the loss of the tumor suppressor LKB1, which activates AMPK in response to energy stress (Shackelford and Shaw, 2009). Interestingly, LKB1-deficient tumors are sensitized to energy stress-inducing agents (e.g., phenformin) (Shackelford et al., 2013), suggesting that loss of control over eEF2K along with other established AMPK targets might underlie this susceptibility. In the study by Lepruvier et al. (2013), oncogene introduction yielded transformed cells where nutrient deprivation failed to cause the type of energy stress that normally activates AMPK. How ATP levels are sustained under starvation conditions in these transformed cells is a key question for understanding the nature of this adaptive response. Also, transforming events leading to aberrant

activation of mTORC1 or ERK signaling could chronically block eEF2K function independent of effects on AMPK, because the respective downstream kinases S6K and RSK can phosphorylate and inhibit eEF2K (Proud, 2007).

Upon starvation, eEF2K is transcriptionally upregulated in mammalian cells and *Caenorhabditis elegans*, and there is an evolutionarily conserved requirement for eEF2K for survival under such conditions (Lepruvier et al., 2013). Elevated eEF2K transcript levels correlated with

increased tumor grade and decreased patient survival in glioma, suggesting that increased eEF2K might promote tumor cell survival, perhaps by providing protection from nutrient deprivation. While still a poorly defined area of tumor biology, tumor cells are believed to experience intermittent availability of specific nutrients during the course of tumor progression due to insufficient or aberrant vasculature feeding the tumor. Therefore, the observed increase in eEF2K expression in glioma may be an adaptive response to fluctuating nutrients in the tumor microenvironment, especially in advanced tumors. Another question is whether the tumor microenvironment ever experiences extreme levels of nutrient starvation approaching those levels typically used in cell culture experiments. Interestingly, Leprivier et al. (2013) demonstrate that xenograft tumors from cells overexpressing eEF2K, while greatly reduced in size, are resistant to the growth inhibitory effects of calorie restriction. Reciprocally, eEF2K null tumors displayed increased necrosis and apoptosis under calorie restriction, whereas their growth was indistinguishable from wild-type tumors in mice fed a normal diet. Therefore, these findings provide another example whereby tumor cell-intrinsic

nutrient-sensing pathways act in concert with the nutritional status of the host to influence tumor growth (Kalaany and Sabatini, 2009). However, as circulating glucose levels are only marginally affected by calorie restriction, this response is likely to reflect changes in both local and systemic (insulin and IGF1) nutrient signals.

Other key questions remain. How does sustained translation elongation kill nutrient-deprived cells when translation initiation is appropriately inhibited? The signal stimulating cell death must emanate from a specific form of stress, or perhaps a selected class of proteins, produced by sustained translation elongation in the absence of exogenous nutrients. Would pharmacological inhibitors to eEF2K, alone or in combination with other compounds, be effective cancer treatments? Intriguingly, reducing eEF2K expression has been shown to sensitize glioma cells to the glucose analog 2-deoxyglucose (Wu et al., 2009). Whereas the dependence on eEF2K under nutrient-deplete conditions is not specific to tumor cells, it might be particularly important in the context of the tumor microenvironment. eEF2K joins a growing list of adaptive responses to starvation (including the regulation of AMPK,

mTORC1, and autophagy), which, due to defective control in tumor cells, could represent a vulnerability and a therapeutic opportunity.

REFERENCES

- Browne, G.J., Finn, S.G., and Proud, C.G. (2004). *J. Biol. Chem.* 279, 12220–12231.
- Cantor, J.R., and Sabatini, D.M. (2012). *Cancer Discov.* 2, 881–898.
- Choo, A.Y., Kim, S.G., Vander Heiden, M.G., Mahoney, S.J., Vu, H., Yoon, S.O., Cantley, L.C., and Blenis, J. (2010). *Mol. Cell* 38, 487–499.
- Kalaany, N.Y., and Sabatini, D.M. (2009). *Nature* 458, 725–731.
- Leprivier, G., Remke, M., Rotblat, B., Dubuc, A., Mateo, A.-R.F., Kool, M., Agnihotri, S., El-Naggar, A., Yu, B., Somasekharan, S.P., et al. (2013). *Cell* 153, 1064–1079.
- Proud, C.G. (2007). *Biochem. J.* 403, 217–234.
- Shackelford, D.B., and Shaw, R.J. (2009). *Nat. Rev. Cancer* 9, 563–575.
- Shackelford, D.B., Abt, E., Gerken, L., Vasquez, D.S., Seki, A., Leblanc, M., Wei, L., Fishbein, M.C., Czernin, J., Mischel, P.S., and Shaw, R.J. (2013). *Cancer Cell* 23, 143–158.
- Wu, H., Zhu, H., Liu, D.X., Niu, T.K., Ren, X., Patel, R., Hait, W.N., and Yang, J.M. (2009). *Cancer Res.* 69, 2453–2460.
- Yuan, H.X., Xiong, Y., and Guan, K.L. (2013). *Mol. Cell* 49, 379–387.

Mind the IQGAP

Berta Sanchez-Laorden,¹ Amaya Viros,¹ and Richard Marais^{1,*}

¹Molecular Oncology Group, The Paterson Institute for Cancer Research, Manchester M20 4, UK

*Correspondence: rmarais@picr.man.ac.uk
<http://dx.doi.org/10.1016/j.ccr.2013.05.017>

The scaffold protein IQGAP1 regulates cell signaling through the RAF/MEK/ERK pathway. Recent data show that cancer cells in which the RAF/MEK/ERK pathway is activated are particularly sensitive to the disruption of IQGAP1 function. IQGAP drugs may be particularly effective in tumors that develop resistance to existing pathway drugs.

The receptor tyrosine kinase (RTK)/RAS/RAF/MEK/ERK pathway drives proliferation, survival, invasion, and metastasis in human cancer. Antibodies that bind to the extracellular domains of RTKs or small molecule inhibitors that block RTK kinase activity are effective in a variety of cancers

if the patients are appropriately selected. More recently, it has been shown that drugs that target BRAF and MEK are effective in melanoma patients whose tumors carry BRAF mutations (Catalanotti et al., 2013; Chapman et al., 2011; Falchhook et al., 2012; Flaherty et al., 2010,

2012; Hauschild et al., 2012). Thus, this pathway is a validated therapeutic target in cancer, and its protein kinases, in particular, have been shown to be tractable therapeutic targets.

In contrast to kinases, the RAS small G-proteins appear to be intractable

increased tumor grade and decreased patient survival in glioma, suggesting that increased eEF2K might promote tumor cell survival, perhaps by providing protection from nutrient deprivation. While still a poorly defined area of tumor biology, tumor cells are believed to experience intermittent availability of specific nutrients during the course of tumor progression due to insufficient or aberrant vasculature feeding the tumor. Therefore, the observed increase in eEF2K expression in glioma may be an adaptive response to fluctuating nutrients in the tumor microenvironment, especially in advanced tumors. Another question is whether the tumor microenvironment ever experiences extreme levels of nutrient starvation approaching those levels typically used in cell culture experiments. Interestingly, [Leprivier et al. \(2013\)](#) demonstrate that xenograft tumors from cells overexpressing eEF2K, while greatly reduced in size, are resistant to the growth inhibitory effects of calorie restriction. Reciprocally, eEF2K null tumors displayed increased necrosis and apoptosis under calorie restriction, whereas their growth was indistinguishable from wild-type tumors in mice fed a normal diet. Therefore, these findings provide another example whereby tumor cell-intrinsic

nutrient-sensing pathways act in concert with the nutritional status of the host to influence tumor growth ([Kalaany and Sabatini, 2009](#)). However, as circulating glucose levels are only marginally affected by calorie restriction, this response is likely to reflect changes in both local and systemic (insulin and IGF1) nutrient signals.

Other key questions remain. How does sustained translation elongation kill nutrient-deprived cells when translation initiation is appropriately inhibited? The signal stimulating cell death must emanate from a specific form of stress, or perhaps a selected class of proteins, produced by sustained translation elongation in the absence of exogenous nutrients. Would pharmacological inhibitors to eEF2K, alone or in combination with other compounds, be effective cancer treatments? Intriguingly, reducing eEF2K expression has been shown to sensitize glioma cells to the glucose analog 2-deoxyglucose ([Wu et al., 2009](#)). Whereas the dependence on eEF2K under nutrient-deplete conditions is not specific to tumor cells, it might be particularly important in the context of the tumor microenvironment. eEF2K joins a growing list of adaptive responses to starvation (including the regulation of AMPK,

mTORC1, and autophagy), which, due to defective control in tumor cells, could represent a vulnerability and a therapeutic opportunity.

REFERENCES

- Browne, G.J., Finn, S.G., and Proud, C.G. (2004). *J. Biol. Chem.* 279, 12220–12231.
- Cantor, J.R., and Sabatini, D.M. (2012). *Cancer Discov.* 2, 881–898.
- Choo, A.Y., Kim, S.G., Vander Heiden, M.G., Mahoney, S.J., Vu, H., Yoon, S.O., Cantley, L.C., and Blenis, J. (2010). *Mol. Cell* 38, 487–499.
- Kalaany, N.Y., and Sabatini, D.M. (2009). *Nature* 458, 725–731.
- Leprivier, G., Remke, M., Rotblat, B., Dubuc, A., Mateo, A.-R.F., Kool, M., Agnihotri, S., El-Naggar, A., Yu, B., Somasekharan, S.P., et al. (2013). *Cell* 153, 1064–1079.
- Proud, C.G. (2007). *Biochem. J.* 403, 217–234.
- Shackelford, D.B., and Shaw, R.J. (2009). *Nat. Rev. Cancer* 9, 563–575.
- Shackelford, D.B., Abt, E., Gerken, L., Vasquez, D.S., Seki, A., Leblanc, M., Wei, L., Fishbein, M.C., Czernin, J., Mischel, P.S., and Shaw, R.J. (2013). *Cancer Cell* 23, 143–158.
- Wu, H., Zhu, H., Liu, D.X., Niu, T.K., Ren, X., Patel, R., Hait, W.N., and Yang, J.M. (2009). *Cancer Res.* 69, 2453–2460.
- Yuan, H.X., Xiong, Y., and Guan, K.L. (2013). *Mol. Cell* 49, 379–387.

Mind the IQGAP

Berta Sanchez-Laorden,¹ Amaya Viros,¹ and Richard Marais^{1,*}

¹Molecular Oncology Group, The Paterson Institute for Cancer Research, Manchester M20 4, UK

*Correspondence: rmarais@picr.man.ac.uk

<http://dx.doi.org/10.1016/j.ccr.2013.05.017>

The scaffold protein IQGAP1 regulates cell signaling through the RAF/MEK/ERK pathway. Recent data show that cancer cells in which the RAF/MEK/ERK pathway is activated are particularly sensitive to the disruption of IQGAP1 function. IQGAP drugs may be particularly effective in tumors that develop resistance to existing pathway drugs.

The receptor tyrosine kinase (RTK)/RAS/RAF/MEK/ERK pathway drives proliferation, survival, invasion, and metastasis in human cancer. Antibodies that bind to the extracellular domains of RTKs or small molecule inhibitors that block RTK kinase activity are effective in a variety of cancers

if the patients are appropriately selected. More recently, it has been shown that drugs that target BRAF and MEK are effective in melanoma patients whose tumors carry BRAF mutations ([Catalanotti et al., 2013](#); [Chapman et al., 2011](#); [Falcone et al., 2012](#); [Flaherty et al., 2010](#),

[2012](#); [Hauschild et al., 2012](#)). Thus, this pathway is a validated therapeutic target in cancer, and its protein kinases, in particular, have been shown to be tractable therapeutic targets.

In contrast to kinases, the RAS small G-proteins appear to be intractable

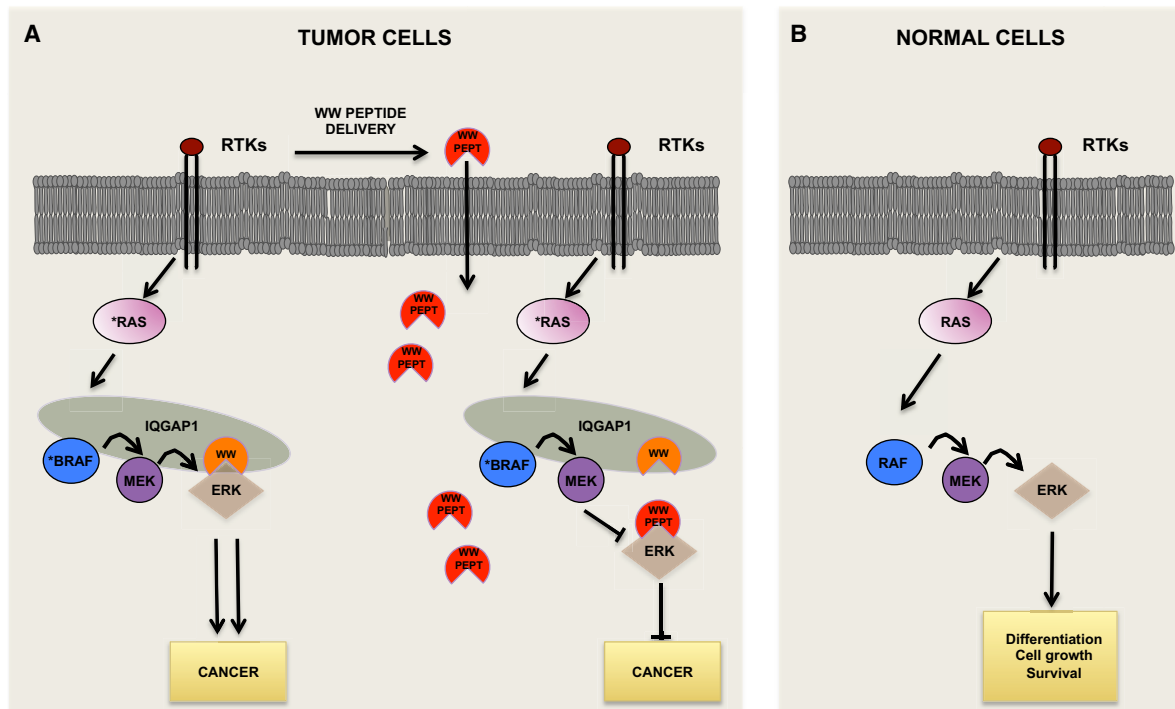


Figure 1. IQGAP1 Is a Therapeutic Target in ERK-Pathway-Driven Cancer Cells

(A) IQGAP1 forms a signaling complex with RAF, MEK, and ERK. Mutant RAS (*RAS) or BRAF (*BRAF) hyperactivates ERK signaling and promotes tumor cell proliferation and survival. Delivery of exogenous WW peptide (WW PEPT) prevents ERK binding to IQGAP1 through its WW domain (WW) and suppresses ERK activity, thereby blocking proliferation in cancer cells that are addicted to the ERK pathway.

(B) The scaffold function of IQGAP1 within the ERK pathway is dispensable in normal cell differentiation, growth, and survival.

therapeutic targets. This is frustrating, because collectively the *RAS* genes (*HRAS*, *KRAS*, and *NRAS*) are the most commonly mutated oncogenes in human cancer. Oncogenic RAS thus is an important but untapped therapeutic target. One way to resolve this problem is to target downstream kinases on the pathway, such as MEK and AKT. Recently, it was suggested that the scaffold protein IQGAP1 may be another Achilles' heel downstream of RAS that can also be targeted (Jameson et al., 2013).

Scaffold proteins regulate cell biology by binding to and organizing the components of a signaling pathway into complexes. This improves signaling efficiency by tethering proteins to each other to increase signal flux between them. It also improves fidelity by confining signaling to the proteins within the complexes. IQGAP1 is a multifunctional scaffold protein that binds to almost 100 other proteins. Although IQGAP1 has two closely related family proteins (IQGAP2 and IQGAP3) that serve distinct functions,

IQGAP1 is the more widely expressed protein and the only one reported as up-regulated in cancer. IQGAP1 is implicated in cytoskeletal reorganization and regulation of cell-cell adhesion, polarity, and migration (Johnson et al., 2009). IQGAP1 also binds to RAF and MEK through the IQ domain and to ERK through the proline-rich WW domain to regulate RAF/MEK/ERK signaling.

Starting with the premise that IQGAP regulates tumorigenesis through the RAF/MEK/ERK pathway, Jameson et al. (2013) demonstrated that *Iqgap* null mice were resistant to *Hras*-driven chemical carcinogenesis, depletion of IQGAP reduced in vitro invasion of RAS-driven cancer cells, and IQGAP1 is highly expressed in human cutaneous squamous cell carcinoma. They found that depletion of IQGAP suppressed ERK activity and that this could be rescued by IQGAP re-expression unless the WW domain was mutated to prevent ERK binding. Furthermore, expression of the WW domain using lentiviruses or introduction of the peptide into cells using cell-permeable

signals blocked ERK activity in EGFR and RAS-driven cancer cells. It also suppressed growth and invasion of these cells in vitro and inhibited the growth of tumor xenografts in immunocompromised mice. Notably, no such effects were seen in cells when the RAS/RAF/MEK/ERK pathway was not hyperactivated, demonstrating the specificity of this response. To assess the consequences of long-term WW peptide treatment, the authors used a transgenic pancreatic cancer model driven by oncogenic Ras and loss of Tp53. They found that the WW peptide extended the life of these animals with a notable lack of toxicity when compared to animals treated with gemcitabine.

Markedly, Jameson et al. (2013) examined the potency of WW peptides in BRAF drug-resistant melanoma cells. Unfortunately, although BRAF drugs can achieve impressive responses in BRAF mutant melanoma patients, after a few months of disease control, most patients fail on therapy, highlighting an urgent need to improve effectiveness of the existing

drugs or to develop second line treatments for relapsed patients. Resistance generally occurs through pathway reactivation brought about by a variety of mechanisms including upregulation of RTK signaling, acquisition of mutations in NRAS or MEK, amplification of the mutant *BRAF* gene, or expression of truncated forms of the *BRAF* oncoprotein. Jameson et al. (2013) showed that the WW peptide was effective against cell lines whose resistance was mediated by PDGFR or IGF1R upregulation, mutant NRAS, or overexpression of the MEK kinase COT.

Thus, the WW peptide suppressed ERK activity and blocked in vitro and in vivo growth of cells that were addicted to the ERK pathway (Figure 1A), establishing that the IQGAP1 scaffold function is essential in ERK-pathway-driven cancer cells and validating IQGAP1 as a therapeutic target. What is remarkable is that the WW peptide was relatively nontoxic. It is known that IQGAP1 function is not essential, because *iqgap* null mice are viable, fertile, and apparently normal, suggesting that the scaffold function of IQGAP within the ERK pathway is not required in normal cells (Figure 1B). It seems unlikely that IQGAP2 or IQGAP3 compensate for the loss of IQGAP1 scaffold function in normal cells in the presence of the WW peptide, because the WW domain is conserved, so all three isoforms are likely to be equally sensitive to disruption by the WW peptide. This suggests that ERK-driven cancer cells are particularly sensitive to both the levels and fidelity of ERK signaling and that IQGAP plays a key role in ensuring that signaling is maintained at optimal levels. Perhaps this is why these cells are so

sensitive to peptides that disrupt ERK binding, begging the question of whether these cells would be equally sensitive to peptides that disrupt RAF and/or MEK binding to the IQ domain.

An exciting aspect of this study is that the WW peptide also targets cells that are resistant to *BRAF* drugs. Unfortunately, the WW peptide did not synergize with *BRAF* drugs to suppress the growth of sensitive cells, but it would nevertheless be interesting to determine if it delayed the onset of resistance, as when *BRAF* and MEK inhibitors are combined. It would also be interesting to determine the mechanisms by which cells can develop resistance to IQGAP1 drugs. Scaffold proteins need to be expressed within a narrow concentration range; too little and productive signaling complexes cannot form, but too much and the pathway components are diluted into incomplete and unproductive complexes. Resistance may, therefore, arise by manipulating the expression of the pathway components or of IQGAP itself. To this end, it would be interesting to know how effective WW peptides are when *BRAF* drug resistance is mediated by the amplification of oncogenic *BRAF*, expression of truncated *BRAF* oncoproteins, or mutations in MEK. It would also be intriguing to know if IQGAP itself can mediate resistance to *BRAF* drugs, and it would be important to validate IQGAP as a therapeutic target in *BRAF* mutant colorectal cancer and thyroid carcinoma, which typically display intrinsic resistance to *BRAF* drugs (Corcoran et al., 2012; Montero-Conde et al., 2013).

This is an important study that validates IQGAP as a therapeutic target

for first- and second-line treatments in ERK-driven cancers. Now we need to determine if it will prove to be a tractable target like a kinase or a frustrating target like RAS.

REFERENCES

- Catalanotti, F., Solit, D.B., Pulitzer, M.P., Berger, M.F., Scott, S.N., Iyriboz, T., Lacouture, M.E., Panageas, K.S., Wolchok, J.D., Carvajal, R.D., et al. (2013). Clin. Cancer Res. 19, 2257–2264.
- Chapman, P.B., Hauschild, A., Robert, C., Haanen, J.B., Ascierto, P., Larkin, J., Dummer, R., Garbe, C., Testori, A., Maio, M., et al.; BRIM-3 Study Group. (2011). N. Engl. J. Med. 364, 2507–2516.
- Corcoran, R.B., Ebi, H., Turke, A.B., Coffee, E.M., Nishino, M., Cogdill, A.P., Brown, R.D., Della Pelle, P., Dias-Santagata, D., Hung, K.E., et al. (2012). Cancer Discov. 2, 227–235.
- Falchook, G.S., Lewis, K.D., Infante, J.R., Gordon, M.S., Vogelzang, N.J., DeMarini, D.J., Sun, P., Moy, C., Szabo, S.A., Roadcap, L.T., et al. (2012). Lancet Oncol. 13, 782–789.
- Flaherty, K.T., Puzanov, I., Kim, K.B., Ribas, A., McArthur, G.A., Sosman, J.A., O'Dwyer, P.J., Lee, R.J., Grippo, J.F., Nolop, K., and Chapman, P.B. (2010). N. Engl. J. Med. 363, 809–819.
- Flaherty, K.T., Infante, J.R., Daud, A., Gonzalez, R., Kefford, R.F., Sosman, J., Hamid, O., Schuchter, L., Cebon, J., Ibrahim, N., et al. (2012). N. Engl. J. Med. 367, 1694–1703.
- Hauschild, A., Grob, J.J., Demidov, L.V., Jouary, T., Gutzmer, R., Millward, M., Rutkowski, P., Blank, C.U., Miller, W.H., Jr., Kaempgen, E., et al. (2012). Lancet 380, 358–365.
- Jameson, K.L., Mazur, P.K., Zehnder, A.M., Zhang, J., Zarnegar, B., Sage, J., and Khavari, P.A. (2013). Nat. Med. 19, 626–630.
- Johnson, M., Sharma, M., and Henderson, B.R. (2009). Cell. Signal. 21, 1471–1478.
- Montero-Conde, C., Ruiz-Llorente, S., Dominguez, J.M., Knauf, J.A., Viale, A., Sherman, E.J., Ryder, M., Ghossein, R.A., Rosen, N., and Fagin, J.A. (2013). Cancer Discov. 3, 520–533.

NKX2-1/TTF-1: An Enigmatic Oncogene that Functions as a Double-Edged Sword for Cancer Cell Survival and Progression

Tomoya Yamaguchi,¹ Yasuyuki Hosono,¹ Kiyoshi Yanagisawa,¹ and Takashi Takahashi^{1,*}

¹Division of Molecular Carcinogenesis, Center for Neurological Diseases and Cancer, Nagoya University Graduate School of Medicine, Nagoya 466-8550, Japan

*Correspondence: tak@med.nagoya-u.ac.jp
<http://dx.doi.org/10.1016/j.ccr.2013.04.002>

Emerging evidence indicates that NKX2-1, a homeobox-containing transcription factor also known as TTF-1, plays a role as a “lineage-survival” oncogene in lung adenocarcinomas. In T cell acute lymphoblastic leukemia, gene rearrangements lead to aberrant expression of NKX2-1/TTF-1. Despite accumulating evidence supporting its oncogenic role, it has become apparent that NKX2-1/TTF-1 expression also has biological and clinical functions in the opposite direction that act against tumor progression. Herein, we review recent findings showing these enigmatic double-edged characteristics, with special attention given to the roles of NKX2-1/TTF-1 in lung development and carcinogenesis.

Oncogenic Involvement of NKX2-1/TTF-1

Emerging evidence suggests that “lineage-specific addiction” to survival mechanisms that are programmed for developmental roles in normal progenitor cells of particular lineages may exist in cancer cells. The transcription factor MITF in melanoma is considered to be an archetypal prototype (Garraway and Sellers, 2006), whereas survival of lung cancers with neuroendocrine (NE) features such as small-cell lung cancer (SCLC) is dependent on continued expression of ASH1, a transcription factor indispensable for pulmonary NE cell development (Nishikawa et al., 2011; Osada et al., 2005, 2008). Thyroid transcription factor 1 (TTF-1), also known as NKX2-1, is a homeobox-containing transcription factor essential for the development of the lung and thyroid as well as a restricted part of the brain (Stanfel et al., 2005), and a series of peripheral lung cells defined as the terminal respiratory unit (TRU) is under the control of this master regulator. About 70% of adenocarcinomas express NKX2-1/TTF-1 independent of disease stage and retain features of the TRU to a certain extent (Yatabe et al., 2002). These TRU-type adenocarcinomas exhibit a distinctively higher prevalence of EGFR mutations, disproportionately high occurrence in females and nonsmokers, and characteristic expression profiles; in fact, p53 and KRAS mutations are inversely associated with NKX2-1/TTF-1 expression (Takeuchi et al., 2006; Yatabe et al., 2005). We and others have previously found that NKX2-1/TTF-1-positive lung adenocarcinomas are dependent on sustained expression of NKX2-1/TTF-1 and sometimes even exhibit focal copy-number increases (Figure 1; Table 1) (Kendall et al., 2007; Kwei et al., 2008; Tanaka et al., 2007; Weir et al., 2007). Intriguingly, *Nkx2-1/Ttf-1* transgenic mice exhibit hyperplasia of type II alveolar cells (Wert et al., 2002). In addition, NKX2-1/TTF-1 is prominently expressed in lung epithelial cells undergoing regeneration (Stahlman et al., 1996). Furthermore, haploinsufficiency of *Nkx2-1/Ttf-1* was recently reported to reduce tumor formation in transgenic mice expressing mutant EGFR (Maeda et al., 2012).

Several lines of evidence suggest possible oncogenic involvement of NKX2-1/TTF-1 in other types of cancers. In addition to

the lung, the thyroid is another organ that expresses NKX2-1/TTF-1. A germline missense mutation of *NKX2-1/TTF-1* that results in a valine substitution for alanine at codon 339 has been identified in families affected by multinodular goiter and papillary thyroid carcinoma (Ngan et al., 2009). It is of note that the SNP rs944289, which maps close to *NKX2-1/TTF-1*, was shown to be significantly associated with increased risk of thyroid cancer (Gudmundsson et al., 2009), although the mechanistic link remains to be elucidated. Rearrangements of *NKX2-1/TTF-1* with T cell receptor or immunoglobulin heavy-chain loci were recently identified in T cell acute lymphoblastic leukemia (T-ALL), suggesting a role in the pathogenesis of hematopoietic malignancies (Homminga et al., 2011). Rearrangements and ectopic expression of *NKX2-2* and *NKX2-5*, both homeobox-containing transcription factors closely related to *NKX2-1/TTF-1*, have also been reported in a subset of T-ALL (Homminga et al., 2011; Nagel et al., 2003). These data strongly suggest an oncogenic role for NKX2-1/TTF-1 as well as other members of the NK2 family, not only in lung and thyroid cancers but also in hematopoietic malignancies. On the other hand, *NKX2-8*, residing in close proximity to *NKX2-1*, exhibits loss of heterozygosity and reduced expression in lung squamous cell carcinomas (Harris et al., 2011), suggesting distinct modes of involvement.

Enigma Surrounding NKX2-1/TTF-1 in Tumor Biology

Despite its role as a lineage-survival oncogene in lung adenocarcinomas, NKX2-1/TTF-1 expression is also known to be associated with favorable prognosis in affected patients (Anagnostou et al., 2009). Evidence to explain this paradox has recently emerged (Figure 2). For example, we found that MYBPH is directly transactivated by NKX2-1/TTF-1 and inhibits phosphorylation of the myosin regulatory light chain via direct interaction with ROCK1, which is a prerequisite process for acquisition of assembly competence (Hosono et al., 2012b). In addition, MYBPH directly binds to and inhibits assembly of nonmuscle myosin heavy chain IIA (Hosono et al., 2012a), thereby conferring

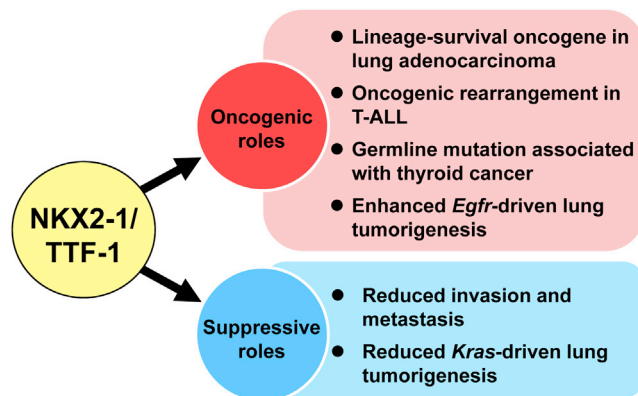


Figure 1. Double-Edged Characteristic of NKX2-1/TTF-1

NKX2-1/TTF-1 has shown both oncogenic and inhibitory activities in cancer development and progression.

firm inhibition of actomyosin assembly by two distinct mechanisms and consequently reducing cell motility, invasion, and metastasis. These apparently deleterious effects in lung adenocarcinoma progression appear to be negated by frequent promoter DNA methylation of *MYBPH*. The epithelial tight-junction protein OCLN as well as two other epithelial tight-junction proteins, CLDN1 and CLDN18, were also shown to be transcriptionally activated by NKX2-1/TTF-1 (Niimi et al., 2001; Runkle et al., 2012). These findings indicate that genes implicated in regulation of cytoskeletal and cell-cell organization are prime transcriptional targets of TTF-1, which negatively affects cell motility, invasion, and metastasis and is also conceivably involved in lung morphogenesis and regeneration after lung injury. In addition, downregulation of *Nkx2-1/Ttf-1* has been shown to lead to eventual derepression of *Hmga2* and acquisition of metastatic ability in a mouse model of lung adenocarcinoma with conditionally activated *Kras* and loss-of-function *p53* mutant alleles (Snyder et al., 2013; Winslow et al., 2011). Interestingly, haploinsufficiency or conditional knockout of *Nkx2-1/Ttf-1* was recently reported to enhance development of invasive *Kras*-driven mucinous lung adenocarcinoma (Maeda et al., 2012; Snyder et al., 2013), in contrast to suppressing *Egfr*-driven lung tumorigenesis (Maeda et al., 2012). Loss of *Nkx2-1/Ttf-1* appears to induce the mucin-producing phenotype through consequential release of *Foxa1/Foxa2*, transcription factors known to physically interact and cooperate with *Nkx2-1/Ttf-1*, onto de novo

binding sites near gastrointestinal differentiation-related genes including *Hnf4α*, which critically regulates the differentiation program (Snyder et al., 2013). Along this line, it is notable that human invasive mucinous adenocarcinomas of the lung almost invariably express HNF4α, and have exhibited a significant association with negative TTF-1 expression and positive KRAS mutation status (Kunii et al., 2011). Although epithelial-to-mesenchymal transition (EMT) is linked with cancer progression, NKX2-1/TTF-1 represses TGF-β-induced EMT by alleviating TGF-β-mediated induction of Snail and Slug, as well as by reducing TGF-β production (Saito et al., 2009). Conversely, TGF-β represses NKX2-1/TTF-1 by induction of miR-365 (Qi et al., 2012). Thus, accumulated evidence points to the notion that NKX2-1/TTF-1 plays a double-edged role in cancer.

NKX2-1/TTF-1-Mediated Lineage-Survival Signaling

Despite the requirement for sustained NKX2-1/TTF-1 expression in the survival of lung adenocarcinoma cells, NKX2-1/TTF-1 itself cannot be considered as a molecular target for treating this devastating cancer because of its indispensable roles in normal lung physiology, such as the production and secretion of surfactant proteins. Thus, elucidation of how NKX2-1/TTF-1 mediates survival signals has long been anticipated. In this regard, we recently found that NKX2-1/TTF-1 directly transactivates the receptor tyrosine kinase *ROR1*, which in turn sustains a favorable balance between prosurvival PI3K-AKT and proapoptotic p38 signaling, in part through ROR1 kinase-dependent c-Src activation as well as kinase activity-independent sustainment of EGFR-ERBB3 association, ERBB3 phosphorylation, and consequential PI3K activation (Yamaguchi et al., 2012). These findings may underlie the molecular basis for the functional interrelationship between NKX2-1/TTF-1 and EGFR. Consistently, NKX2-1/TTF-1 expression is significantly associated with *EGFR* mutations in lung cancer tissues (Takeuchi et al., 2006; Yatabe et al., 2005), and *Nkx2-1/Ttf-1* haploinsufficiency reduces mutant *Egfr*-driven lung tumorigenesis (Maeda et al., 2012). It is also of particular interest from a clinical point of view that ROR1 inhibition appears to be effective for treatment of lung adenocarcinomas carrying various gefitinib-resistance mechanisms, such as secondary EGFR mutations and HGF overexpression, because the existence of such diverse mechanisms makes it difficult to predict which should be targeted to prevent expansion of resistant clones. This molecule with possible druggability, namely a cell-surface receptor with a

Table 1. Alterations of the NK2 Family in Human Cancers

NK2 Family	Aberrations	Organ Sites	Cancer Types	References
NKX2-1	amplification	lung	adenocarcinoma	Tanaka et al., 2007
	amplification	lung	adenocarcinoma	Kendall et al., 2007
	amplification	lung	adenocarcinoma	Weir et al., 2007
	amplification	lung	adenocarcinoma	Kwei et al., 2008
	germline mutation	thyroid	multinodular goiter, papillary adenocarcinoma	Ngan et al., 2009
	rearrangement	hematopoietic	T cell acute lymphoblastic leukemia	Homminga et al., 2011
NKX2-2	rearrangement	hematopoietic	T cell acute lymphoblastic leukemia	Homminga et al., 2011
NKX2-5	rearrangement	hematopoietic	T cell acute lymphoblastic leukemia	Nagel et al., 2003
NKX2-8	loss of heterozygosity	lung	squamous cell carcinoma	Harris et al., 2011

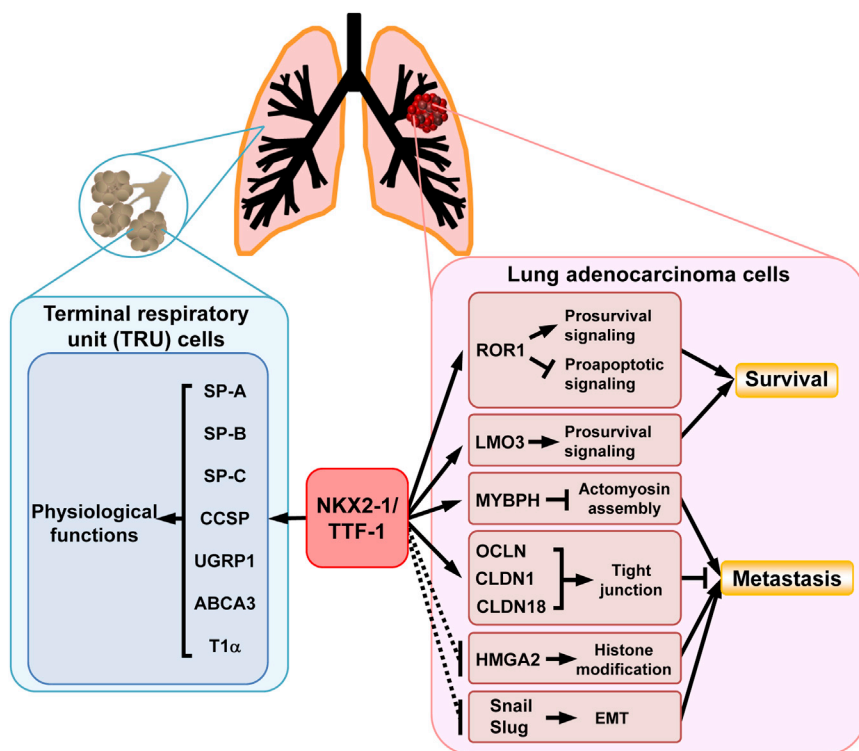


Figure 2. NKX2-1/TTF-1-Mediated Transcriptional Regulation and Consequences in Normal and Cancer Cells of the Lung

NKX2-1/TTF-1 is required for maintenance of physiological lung functions in addition to its developmental roles. The oncogene plays a role as a lineage-survival oncogene in lung adenocarcinomas, whereas it also inhibits invasion, metastasis, and progression, paradoxically conferring better prognosis. Solid and dashed lines represent direct and indirect regulation, respectively.

genesis (Yuan et al., 2000). NKX2-1/TTF-1 critically translates instructive morphogenic signals from the surrounding mesenchyme into transcriptional regulation of its targets, which are mediated by factors including fibroblast growth factors, Sonic hedgehog, and bone morphogenetic proteins. In humans, NKX2-1/TTF-1 haploinsufficiency confers the rare autosomal-dominant disorder benign hereditary chorea as well as brain-lung-thyroid syndrome, which is manifested by chorea, hypothyroidism, and infantile respiratory distress (Inzelberg et al., 2011). Human NKX2-1/TTF-1 haploinsufficiency might be associated

tyrosine kinase domain, may thus be considered to be an “Achilles’ heel” in lung adenocarcinomas, and future development of therapeutic means is greatly anticipated to reduce the intolerable death toll from currently “hard-to-cure” lung adenocarcinomas. In addition to *ROR1*, *LMO3*, a paralog of the *LMO1* and *LMO2* oncogenes in T-ALL, was recently identified as an additional direct transcriptional target for mediating survival signals (Watanabe et al., 2013). NKX2-1/TTF-1 appears to cooperatively transactivate *LMO3* together with FOXA1, whereas *LMO3* knockdown induced apoptosis in a lung adenocarcinoma cell line. However, ectopic overexpression of *LMO3* failed to overcome NKX2-1/TTF-1 knockdown-induced apoptosis, suggesting the existence of additional crucial targets for lineage-survival signaling in lung adenocarcinoma cells.

Developmental Roles of NKX2-1/TTF-1 in Relation to Cancer Biology

During embryonic lung development, temporal-spatial expression of NKX2-1/TTF-1 is tightly regulated. NKX2-1/TTF-1 expression is first detected in the ventral foregut endoderm during a very early stage and then becomes abundantly expressed in virtually all cells in the progenitor of the trachea arising from the lung primordium. As subsequent branching morphogenesis proceeds, NKX2-1/TTF-1 expression is progressively restricted to distal airway cells and finally confined to epithelial cells in the TRU (Stahlman et al., 1996; Yatabe et al., 2002). A lung rudiment in *Nkx2-1/Ttf-1* knockout mice exhibited proximal, albeit abnormal, airway characteristics, suggesting its dispensable nature in specification of the lung primordium and proximal lung morphogenesis (Minoo et al., 1999). In contrast, this oncogene was shown to be strictly required for distal lung morpho-

with lung tumorigenesis in context-dependent and subtype-specific manners, as reported in mice (Maeda et al., 2012; Snyder et al., 2013). Unfortunately, no comprehensive epidemiologic data on the predisposition to lung cancers in affected individuals have been presented.

In addition to lung adenocarcinoma, it is interesting to note that NKX2-1/TTF-1 is frequently detected in SCLCs, which usually arise in the proximal airway, a region that normally lacks NKX2-1/TTF-1 expression. Because NKX2-1/TTF-1 expression is seen in the lung primordium, this phenomenon may reflect an atavistic, yet committed, state of SCLCs, which is consistent with its lack of expression in small-cell carcinomas arising from other organs, despite the similar characteristics of small and round morphology and NE properties. Future study comparing NKX2-1/TTF-1 target gene regulation between adenocarcinomas and those in small-cell carcinomas of various organs, including the adult and developing fetal lungs, would likely shed light on both similarities and distinctions with regard to its functional roles.

Regulation of NKX2-1/TTF-1 and Context Dependence

The 42 kD major isoform is encoded by mRNAs harboring exons 2 and 3, whereas the 44 kD minor isoform is encoded by all three exons (Figure 3). The proximal major promoter contains a TATA-like element and binding sites for FOXA1 (also known as HNF-3α), FOXA2 (HNF-3β), and GATA6, all of which are known to be crucially involved in lung development (Costa et al., 2001). The minor distal promoter is regulated by SP1 and SP3. NKX2-1/TTF-1 directly transactivates multiple genes implicated to have physiological lung functions, including SP-A, SP-B, SP-C, CCSP (also known as CC10, uteroglobin, or secretoglobin),

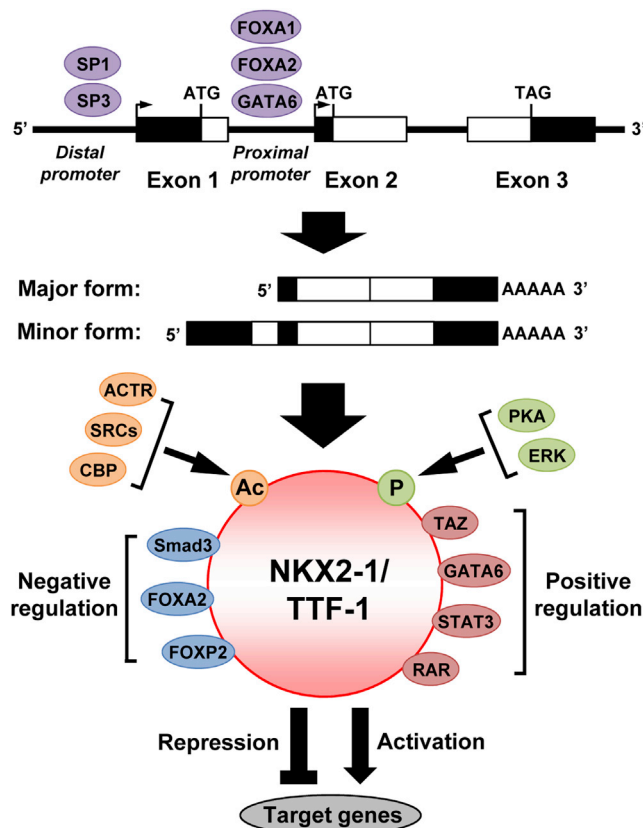


Figure 3. Regulatory Mechanisms of NKX2-1/TTF-1

NKX2-1/TTF-1 is transcribed from two distinct promoters under the influence of various transcription factors. Its transcriptional regulatory activities are modulated in a context-dependent manner, possibly by cooperating transcription factors as well as protein modifications. Ac, acetylation; P, phosphorylation.

UGRP1, and ABCA3. NKX2-1/TTF-1 also transactivates the functions of HOP, an HDAC-dependent negative regulator of NKX2-1/TTF-1 (Yin et al., 2006), as well as T1 α , a type I pneumocyte-specific marker (Ramirez et al., 1997). CLDN18 and OCLN tight-junction proteins MYBPH, LMO3, and ROR1 have recently been identified as targets for their roles in cancer, as discussed above. Transcription factors that interact and cooperate with NKX2-1/TTF-1 include FOXA2 (Minoo et al., 2007), FOXP2 (Zhou et al., 2008), GATA6 (Liu et al., 2002), STAT3 (Yan et al., 2002), and RAR (Yan et al., 2001). Furthermore, Smad3 and TAZ modulate the transcriptional activity of NKX2-1/TTF-1 via their binding in a negative and positive manner, respectively (Li et al., 2002; Park et al., 2004). Posttranslational modifications are also important as a regulatory mechanism of NKX2-1/TTF-1 functions. Multiple nuclear coactivators, including ACTR, p160 steroid receptor coactivators, and p300/CBP, acetylate NKX2-1/TTF-1 (Yang et al., 2004), whereas NKX2-1/TTF-1 is also regulated through its phosphorylation, positively by PKA (Yan and Whitsett, 1997) and negatively by ERK (Missero et al., 2000). In addition, Smad3 physically interacts with NKX2-1/TTF-1 and inhibits NKX2-1/TTF-1-mediated transcription from the *SP-B* promoter lacking a Smad binding site (Li et al., 2002).

Recent ChIP-seq and ChIP-chip analyses have revealed a large number of additional potential transcriptional targets of NKX2-1/TTF-1 (Maeda et al., 2012; Tagne et al., 2012; Watanabe et al., 2013), with experimental validation of the induction of LMO3, E2F3, and cyclins B1 and B2, as well as repression of MUC5A, FGFR1, and MET. It is notable that NKX2-1/TTF-1 appears to be associated with and affect promoters via not only its canonical binding sites but also by the AP-1, forkhead, and nuclear hormone receptor-binding motifs. Therefore, downstream targets appear to be regulated by NKX2-1/TTF-1 in a context-dependent manner, possibly reflecting the expression of its cofactors.

Accumulating evidence, as noted above, implicates opposing roles of NKX2-1/TTF-1 in lung cancer development, which may also be the case in thyroid tumors and hematopoietic malignancies. NKX2-1/TTF-1 expression is absolutely required for peripheral lung development and differentiation, whereas its level in lung adenocarcinoma is associated with but not deterministic of differentiated morphologies (Takeuchi et al., 2006; Yatabe et al., 2002). It would be interesting to investigate whether any similarities and/or distinctions exist in the regulation of downstream targets by this enigmatic oncogene in cancer cells as well as in normal development, with special attention given to context dependence.

Conclusions and Future Perspectives

NKX2-1/TTF-1 has long been a focus of research in the field of lung and thyroid physiology, whereas emerging evidence has called attention to its roles in cancer. This oncogene appears to function as a double-edged sword in the pathogenesis of lung adenocarcinoma and possibly in other tumors as well. A future rigorous search for additional downstream molecules is warranted to gain a more complete picture of NKX2-1/TTF-1-centered regulatory networks in order to take advantage of its Jekyll-and-Hyde characteristics. It should also be kept in mind that current understanding of the regulatory web surrounding this enigmatic transcription factor may be oversimplified, as the same architecture may not exist in normal and cancerous states, or even among individual tumors. For example, a sizable fraction of NKX2-1/TTF-1-positive human lung adenocarcinomas are negative for surfactant proteins, which are authentic targets for transcriptional activation in normal lungs, and/or positive for HMGA2, a target for transcriptional repression. Opposing effects of *Nkx2-1/Ttf-1* haploinsufficiency in transgenic mice carrying mutant *Kras* and *Egfr* also suggest its multifaceted nature. Thus, the NKX2-1/TTF-1 regulatory networks present in cells in both normal and cancerous conditions may well be quite complex and context dependent, and likely require a radically different approach to elucidate. Along this line, a cancer systems biology approach with the aid of ever-increasing computing power may help to reveal a path to resolve this challenge, ultimately allowing an opportunity to take advantage of the double-edged characteristics of NKX2-1/TTF-1 in patients affected by cancer.

ACKNOWLEDGMENTS

We thank all of the members of our research group for their invaluable contributions, including helpful discussions and critical comments. We also

apologize for the incompleteness of the referencing due to space constraints. Studies in our laboratory have been supported in part by grants from the Ministry of Education, Science, Sports and Culture, Japan, and the Ministry of Health, Labor and Welfare, Japan.

REFERENCES

- Anagnostou, V.K., Syrigos, K.N., Bepler, G., Homer, R.J., and Rimm, D.L. (2009). Thyroid transcription factor 1 is an independent prognostic factor for patients with stage I lung adenocarcinoma. *J. Clin. Oncol.* 27, 271–278.
- Costa, R.H., Kalinichenko, V.V., and Lim, L. (2001). Transcription factors in mouse lung development and function. *Am. J. Physiol. Lung Cell. Mol. Physiol.* 280, L823–L838.
- Garraway, L.A., and Sellers, W.R. (2006). Lineage dependency and lineage-survival oncogenes in human cancer. *Nat. Rev. Cancer* 6, 593–602.
- Gudmundsson, J., Sulem, P., Gudbjartsson, D.F., Jonasson, J.G., Sigurdsson, A., Bergthorsson, J.T., He, H., Blondal, T., Geller, F., Jakobsdottir, M., et al. (2009). Common variants on 9q22.33 and 14q13.3 predispose to thyroid cancer in European populations. *Nat. Genet.* 41, 460–464.
- Harris, T., Pan, Q., Sironi, J., Lutz, D., Tian, J., Sapkar, J., Perez-Soler, R., Keller, S., and Locker, J. (2011). Both gene amplification and allelic loss occur at 14q13.3 in lung cancer. *Clin. Cancer Res.* 17, 690–699.
- Homminga, I., Pieters, R., Langerak, A.W., de Rooij, J.J., Stubbs, A., Versteegen, M., Vuerhard, M., Buijs-Gladdines, J., Kooi, C., Klous, P., et al. (2011). Integrated transcript and genome analyses reveal NKX2-1 and MEF2C as potential oncogenes in T cell acute lymphoblastic leukemia. *Cancer Cell* 19, 484–497.
- Hosono, Y., Usukura, J., Yamaguchi, T., Yanagisawa, K., Suzuki, M., and Takahashi, T. (2012a). MYBPH inhibits NM IIA assembly via direct interaction with NMHC IIA and reduces cell motility. *Biochem. Biophys. Res. Commun.* 428, 173–178.
- Hosono, Y., Yamaguchi, T., Mizutani, E., Yanagisawa, K., Arima, C., Tomida, S., Shimada, Y., Hiraoka, M., Kato, S., Yokoi, K., et al. (2012b). MYBPH, a transcriptional target of TTF-1, inhibits ROCK1, and reduces cell motility and metastasis. *EMBO J.* 31, 481–493.
- Inzelberg, R., Weinberger, M., and Gak, E. (2011). Benign hereditary chorea: an update. *Parkinsonism Relat. Disord.* 17, 301–307.
- Kendall, J., Liu, Q., Bakleh, A., Krasnitz, A., Nguyen, K.C., Lakshmi, B., Gerald, W.L., Powers, S., and Mu, D. (2007). Oncogenic cooperation and coamplification of developmental transcription factor genes in lung cancer. *Proc. Natl. Acad. Sci. USA* 104, 16663–16668.
- Kunii, R., Jiang, S., Hasegawa, G., Yamamoto, T., Umez, H., Watanabe, T., Tsuchida, M., Hashimoto, T., Hamakubo, T., Kodama, T., et al. (2011). The predominant expression of hepatocyte nuclear factor 4 α (HNF4 α) in thyroid transcription factor-1 (TTF-1)-negative pulmonary adenocarcinoma. *Histopathology* 58, 467–476.
- Kwei, K.A., Kim, Y.H., Girard, L., Kao, J., Pacyna-Gengelbach, M., Salari, K., Lee, J., Choi, Y.L., Sato, M., Wang, P., et al. (2008). Genomic profiling identifies TTF1 as a lineage-specific oncogene amplified in lung cancer. *Oncogene* 27, 3635–3640.
- Li, C., Zhu, N.L., Tan, R.C., Ballard, P.L., Derynck, R., and Minoo, P. (2002). Transforming growth factor- β inhibits pulmonary surfactant protein B gene transcription through SMAD3 interactions with NKX2.1 and HNF-3 transcription factors. *J. Biol. Chem.* 277, 38399–38408.
- Liu, C., Glasser, S.W., Wan, H., and Whitsett, J.A. (2002). GATA-6 and thyroid transcription factor-1 directly interact and regulate surfactant protein-C gene expression. *J. Biol. Chem.* 277, 4519–4525.
- Maeda, Y., Tsuchiya, T., Hao, H., Tompkins, D.H., Xu, Y., Mucenski, M.L., Du, L., Keiser, A.R., Fukazawa, T., Naomoto, Y., et al. (2012). Kras(G12D) and Nkx2-1 haploinsufficiency induce mucinous adenocarcinoma of the lung. *J. Clin. Invest.* 122, 4388–4400.
- Minoo, P., Su, G., Drum, H., Bringas, P., and Kimura, S. (1999). Defects in tracheoesophageal and lung morphogenesis in Nkx2.1(–/–) mouse embryos. *Dev. Biol.* 209, 60–71.
- Minoo, P., Hu, L., Xing, Y., Zhu, N.L., Chen, H., Li, M., Borok, Z., and Li, C. (2007). Physical and functional interactions between homeodomain NKX2.1 and winged helix/forkhead FOXA1 in lung epithelial cells. *Mol. Cell. Biol.* 27, 2155–2165.
- Missero, C., Pirro, M.T., and Di Lauro, R. (2000). Multiple Ras downstream pathways mediate functional repression of the homeobox gene product TTF-1. *Mol. Cell. Biol.* 20, 2783–2793.
- Nagel, S., Kaufmann, M., Drexler, H.G., and MacLeod, R.A. (2003). The cardiac homeobox gene NKX2-5 is deregulated by juxtaposition with BCL11B in pediatric T-ALL cell lines via a novel t(5;14)(q35.1;q32.2). *Cancer Res.* 63, 5329–5334.
- Ngan, E.S., Lang, B.H., Liu, T., Shum, C.K., So, M.T., Lau, D.K., Leon, T.Y., Cherny, S.S., Tsai, S.Y., Lo, C.Y., et al. (2009). A germline mutation (A339V) in thyroid transcription factor-1 (TTF-1/NKX2.1) in patients with multinodular goiter and papillary thyroid carcinoma. *J. Natl. Cancer Inst.* 101, 162–175.
- Niimi, T., Nagashima, K., Ward, J.M., Minoo, P., Zimonjic, D.B., Popescu, N.C., and Kimura, S. (2001). claudin-18, a novel downstream target gene for the T/EBP/NKX2.1 homeodomain transcription factor, encodes lung- and stomach-specific isoforms through alternative splicing. *Mol. Cell. Biol.* 21, 7380–7390.
- Nishikawa, E., Osada, H., Okazaki, Y., Arima, C., Tomida, S., Tatematsu, Y., Taguchi, A., Shimada, Y., Yanagisawa, K., Yatabe, Y., et al. (2011). miR-375 is activated by ASH1 and inhibits YAP1 in a lineage-dependent manner in lung cancer. *Cancer Res.* 71, 6165–6173.
- Osada, H., Tatematsu, Y., Yatabe, Y., Horio, Y., and Takahashi, T. (2005). ASH1 gene is a specific therapeutic target for lung cancers with neuroendocrine features. *Cancer Res.* 65, 10680–10685.
- Osada, H., Tomida, S., Yatabe, Y., Tatematsu, Y., Takeuchi, T., Murakami, H., Kondo, Y., Sekido, Y., and Takahashi, T. (2008). Roles of achaete-scute homologue 1 in DKK1 and E-cadherin repression and neuroendocrine differentiation in lung cancer. *Cancer Res.* 68, 1647–1655.
- Park, K.S., Whitsett, J.A., Di Palma, T., Hong, J.H., Yaffe, M.B., and Zannini, M. (2004). TAZ interacts with TTF-1 and regulates expression of surfactant protein-C. *J. Biol. Chem.* 279, 17384–17390.
- Qi, J., Rice, S.J., Salzberg, A.C., Runkle, E.A., Liao, J., Zander, D.S., and Mu, D. (2012). MiR-365 regulates lung cancer and developmental gene thyroid transcription factor 1. *Cell Cycle* 11, 177–186.
- Ramirez, M.I., Rishi, A.K., Cao, Y.X., and Williams, M.C. (1997). TGT3, thyroid transcription factor I, and Sp1 elements regulate transcriptional activity of the 1.3-kilobase pair promoter of T1 α , a lung alveolar type I cell gene. *J. Biol. Chem.* 272, 26285–26294.
- Runkle, E.A., Rice, S.J., Qi, J., Masser, D., Antonetti, D.A., Winslow, M.M., and Mu, D. (2012). Occludin is a direct target of thyroid transcription factor-1 (TTF-1/NKX2-1). *J. Biol. Chem.* 287, 28790–28801.
- Saito, R.A., Watabe, T., Horiguchi, K., Kohyama, T., Saitoh, M., Nagase, T., and Miyazono, K. (2009). Thyroid transcription factor-1 inhibits transforming growth factor- β -mediated epithelial-to-mesenchymal transition in lung adenocarcinoma cells. *Cancer Res.* 69, 2783–2791.
- Snyder, E.L., Watanabe, H., Magendantz, M., Hoersch, S., Chen, T.A., Wang, D.G., Crowley, D., Whittaker, C.A., Meyerson, M., Kimura, S., and Jacks, T. (2013). Nkx2-1 represses a latent gastric differentiation program in lung adenocarcinoma. *Mol. Cell.* Published online March 19, 2013. <http://dx.doi.org/10.1016/j.molcel.2013.02.018>.
- Stahlman, M.T., Gray, M.E., and Whitsett, J.A. (1996). Expression of thyroid transcription factor-1 (TTF-1) in fetal and neonatal human lung. *J. Histochem. Cytochem.* 44, 673–678.
- Stanfel, M.N., Moses, K.A., Schwartz, R.J., and Zimmer, W.E. (2005). Regulation of organ development by the NKX-homeodomain factors: an NKX code. *Cell. Mol. Biol. (Noisy-le-grand) (Suppl 51)*, OL785–OL799.
- Tagne, J.B., Gupta, S., Gower, A.C., Shen, S.S., Varma, S., Lakshminarayanan, M., Cao, Y., Spira, A., Volkert, T.L., and Ramirez, M.I. (2012). Genome-wide analyses of Nkx2-1 binding to transcriptional target genes uncover novel regulatory patterns conserved in lung development and tumors. *PLoS One* 7, e29907.
- Takeuchi, T., Tomida, S., Yatabe, Y., Kosaka, T., Osada, H., Yanagisawa, K., Mitsudomi, T., and Takahashi, T. (2006). Expression profile-defined classification of lung adenocarcinoma shows close relationship with underlying major

genetic changes and clinicopathologic behaviors. *J. Clin. Oncol.* 24, 1679–1688.

Tanaka, H., Yanagisawa, K., Shinjo, K., Taguchi, A., Maeno, K., Tomida, S., Shimada, Y., Osada, H., Kosaka, T., Matsubara, H., et al. (2007). Lineage-specific dependency of lung adenocarcinomas on the lung development regulator TTF-1. *Cancer Res.* 67, 6007–6011.

Watanabe, H., Francis, J.M., Woo, M.S., Etemad, B., Lin, W., Fries, D.F., Peng, S., Snyder, E.L., Tata, P.R., Izzo, F., et al. (2013). Integrated cistronic and expression analysis of amplified NKX2-1 in lung adenocarcinoma identifies LMO3 as a functional transcriptional target. *Genes Dev.* 27, 197–210.

Weir, B.A., Woo, M.S., Getz, G., Perner, S., Ding, L., Beroukhi, R., Lin, W.M., Province, M.A., Kraja, A., Johnson, L.A., et al. (2007). Characterizing the cancer genome in lung adenocarcinoma. *Nature* 450, 893–898.

Wert, S.E., Dey, C.R., Blair, P.A., Kimura, S., and Whitsett, J.A. (2002). Increased expression of thyroid transcription factor-1 (TTF-1) in respiratory epithelial cells inhibits alveolarization and causes pulmonary inflammation. *Dev. Biol.* 242, 75–87.

Winslow, M.M., Dayton, T.L., Verhaak, R.G., Kim-Kiselak, C., Snyder, E.L., Feldser, D.M., Hubbard, D.D., DuPage, M.J., Whittaker, C.A., Hoersch, S., et al. (2011). Suppression of lung adenocarcinoma progression by Nkx2-1. *Nature* 473, 101–104.

Yamaguchi, T., Yanagisawa, K., Sugiyama, R., Hosono, Y., Shimada, Y., Arima, C., Kato, S., Tomida, S., Suzuki, M., Osada, H., and Takahashi, T. (2012). NKX2-1/TITF1/TTF-1-induced ROR1 is required to sustain EGFR survival signaling in lung adenocarcinoma. *Cancer Cell* 21, 348–361.

Yan, C., and Whitsett, J.A. (1997). Protein kinase A activation of the surfactant protein B gene is mediated by phosphorylation of thyroid transcription factor 1. *J. Biol. Chem.* 272, 17327–17332.

Yan, C., Naltner, A., Conkright, J., and Ghaffari, M. (2001). Protein-protein interaction of retinoic acid receptor α and thyroid transcription factor-1 in respiratory epithelial cells. *J. Biol. Chem.* 276, 21686–21691.

Yan, C., Naltner, A., Martin, M., Naltner, M., Fangman, J.M., and Gurel, O. (2002). Transcriptional stimulation of the surfactant protein B gene by STAT3 in respiratory epithelial cells. *J. Biol. Chem.* 277, 10967–10972.

Yang, L., Yan, D., Bruggeman, M., Du, H., and Yan, C. (2004). Mutation of a lysine residue in a homeodomain generates dominant negative thyroid transcription factor 1. *Biochemistry* 43, 12489–12497.

Yatabe, Y., Mitsudomi, T., and Takahashi, T. (2002). TTF-1 expression in pulmonary adenocarcinomas. *Am. J. Surg. Pathol.* 26, 767–773.

Yatabe, Y., Kosaka, T., Takahashi, T., and Mitsudomi, T. (2005). EGFR mutation is specific for terminal respiratory unit type adenocarcinoma. *Am. J. Surg. Pathol.* 29, 633–639.

Yin, Z., Gonzales, L., Kolla, V., Rath, N., Zhang, Y., Lu, M.M., Kimura, S., Ballard, P.L., Beers, M.F., Epstein, J.A., and Morrissey, E.E. (2006). Hop functions downstream of Nkx2.1 and GATA6 to mediate HDAC-dependent negative regulation of pulmonary gene expression. *Am. J. Physiol. Lung Cell. Mol. Physiol.* 291, L191–L199.

Yuan, B., Li, C., Kimura, S., Engelhardt, R.T., Smith, B.R., and Minoo, P. (2000). Inhibition of distal lung morphogenesis in Nkx2.1(–/–) embryos. *Dev. Dyn.* 217, 180–190.

Zhou, B., Zhong, Q., Minoo, P., Li, C., Ann, D.K., Frenkel, B., Morrissey, E.E., Crandall, E.D., and Borok, Z. (2008). Foxp2 inhibits Nkx2.1-mediated transcription of SP-C via interactions with the Nkx2.1 homeodomain. *Am. J. Respir. Cell Mol. Biol.* 38, 750–758.

Control of Alveolar Differentiation by the Lineage Transcription Factors GATA6 and HOPX Inhibits Lung Adenocarcinoma Metastasis

William K.C. Cheung,¹ Minghui Zhao,¹ Zongzhi Liu,¹ Laura E. Stevens,¹ Paul D. Cao,¹ Justin E. Fang,³ Thomas F. Westbrook,³ and Don X. Nguyen^{1,2,*}

¹Department of Pathology

²Yale Cancer Center

Yale University School of Medicine, New Haven, CT 06510, USA

³Department of Biochemistry, Baylor College of Medicine, Houston, TX 77030, USA

*Correspondence: don.nguyen@yale.edu

<http://dx.doi.org/10.1016/j.ccr.2013.04.009>

SUMMARY

Molecular programs that mediate normal cell differentiation are required for oncogenesis and tumor cell survival in certain cancers. How cell-lineage-restricted genes specifically influence metastasis is poorly defined. In lung cancers, we uncovered a transcriptional program that is preferentially associated with distal airway epithelial differentiation and lung adenocarcinoma (ADC) progression. This program is regulated in part by the lineage transcription factors GATA6 and HOPX. These factors can cooperatively limit the metastatic competence of ADC cells, by modulating overlapping alveolar differentiation and invasogenic target genes. Thus, GATA6 and HOPX are critical nodes in a lineage-selective pathway that directly links effectors of airway epithelial specification to the inhibition of metastasis in the lung ADC subtype.

INTRODUCTION

Aberrant activation of cell-lineage-restricted pathways is required for oncogenic transformation in certain malignancies (Garraway and Sellers, 2006). In contrast, the role of cell differentiation programs in constraining tumor progression and metastasis is poorly defined. Understanding how the molecular determinants of cell fate affect metastasis is particularly relevant in nonsmall cell lung cancers (NSCLC). NSCLC encompass therapeutically intractable and biologically diverse subtypes of tumors, including adenocarcinomas (ADC), squamous cell carcinomas (SCC), and large cell carcinomas (LCC) (Gabrielson, 2006). Each subtype harbors different genetic alterations, exhibits unique histological features, and contains epithelial cells of distinct lineages, portending major challenges in predicting their clinical outcome.

Multipotent cells from the primary lung buds differentiate into epithelial bronchiolar or alveolar progenitors of the proximal and distal airway, respectively (Morrissey and Hogan, 2010). In post-natal lungs, these cells may arise from regional stem cells in the trachea or distal airways. Bronchiolar lineages include ciliated and secretory cell types, whereas alveolar stem or progenitors specify into alveolar type I or type II pneumocytes that are required for proper gas exchange. Lung epithelial differentiation is coordinated by a complex network of transcription factors (TFs) whose expression and activity are lineage specific (Maeda et al., 2007). Significantly, SCC cells resemble proximal basal progenitors of the trachea and bronchi (Eramo et al., 2010). Conversely, ADCs form in the distal airways and can arise from alveolar progenitors, including alveolar type II (AT2) cells (Xu et al., 2012). The distinct pathways that maintain pulmonary epithelial lineages may therefore also influence the biology of lung cancers.

Significance

Lung adenocarcinoma (ADC) is a deadly and heterogeneous subtype of nonsmall cell lung cancer. During lung ADC progression, the emergence of alternate cell lineage traits in primary tumors correlates with poor outcome. The underlying mechanisms and biological consequences of these phenomena are poorly understood. Through an integrated approach, we identified two lineage transcription factors, GATA6 and HOPX, as inhibitors of metastatic progression. Downregulation of their expression in a subset of ADCs correlates with aberrant tumor differentiation and relapses. GATA6 and HOPX cooperatively restrict the metastatic potential of ADC cells, by modulating converging transcriptional programs of airway epithelial differentiation and malignant invasion. Our findings demonstrate that perturbation of intrinsic cell lineage pathways is a determinant of metastasis in specific lung cancers.

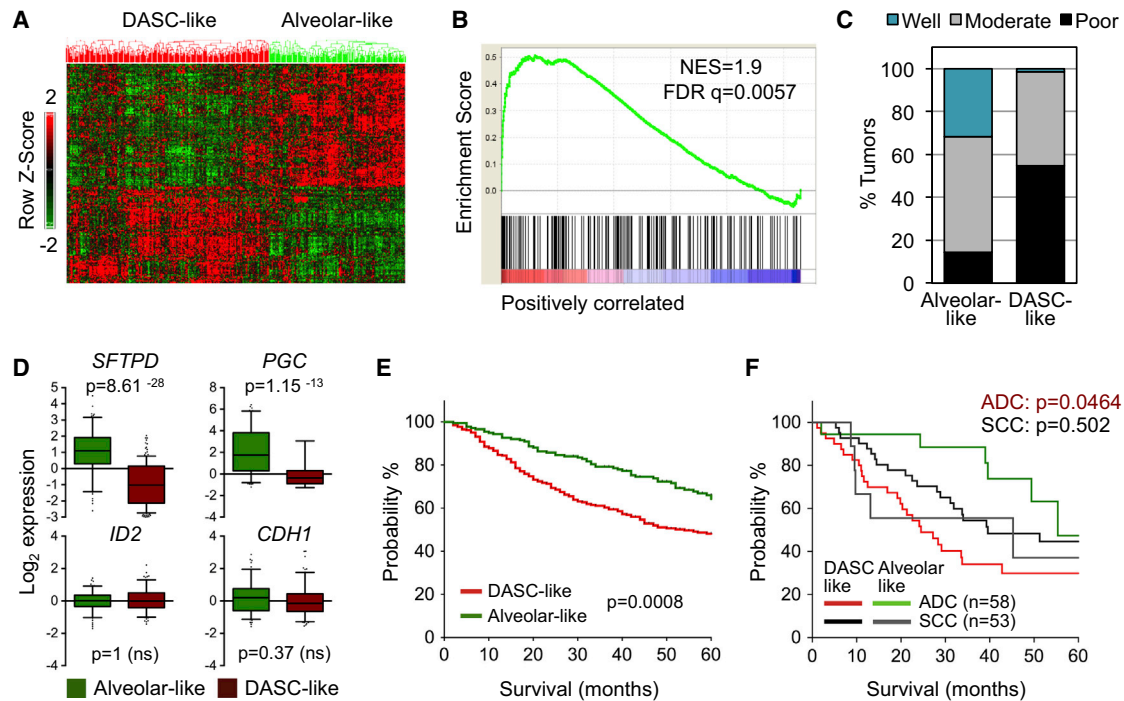


Figure 1. Expression of an Alveolar-like Gene Module Correlates with Lung ADC Patient Outcome

(A) Hierarchical clustering was performed on primary ADCs from the NCI Director's Challenge Cohort (DCC; $n = 442$) based on 249 genes that mark AT2 cell differentiation and airway homeostasis. The heatmap represents tumors clustered into "DASC-like" or "alveolar-like" subsets.

(B) Gene set enrichment analysis (GSEA) showing the similarities between activated genes in "DASC-like" tumors and distal airway stem cells. NES, normalized enrichment score.

(C) Frequency of poorly, moderately, or well-differentiated stage I tumors within the "alveolar-like" and "DASC-like" groups.

(D) Normalized \log_2 expression values of epithelial lineage markers in stage I ADCs in DCC tumors. Data presented as a Box-whisker plot (5%–95%). The p values were calculated by Student's t test with Bonferroni correction. ns, not significant.

(E) Kaplan-Meier curves for the overall survival of DCC patients classified as in (A). The p values were calculated by log rank test.

(F) NSCLCs from the Duke Medical Center were classified as in (A), and survival is plotted for patients with ADC (green and red curves) versus SCC (black and gray curves). The p values were calculated by log rank test.

See also Figure S1 and Table S1.

Lung ADC is the most frequently diagnosed thoracic malignancy with a high incidence of metastasis and death (Jemal et al., 2008). To date, many somatic mutations have been discovered in ADCs, with most being predicted oncogenes (Weir et al., 2007). Several of these mutations are required for the survival of well-differentiated cancer cells (Singh et al., 2009; Weir et al., 2007), which can maintain features of alveolar cells (Hecht et al., 2001). However, during its clinical course, ADC can also adopt mixed histological and molecular features of squamous (Wilkerson et al., 2012) and small cell lung cancers (Alam et al., 2010), which express markers of basal and neuroendocrine cells, respectively. The appearance of these alternate lineage traits in ADCs correlates with therapeutic resistance and poor prognosis, but their underlying causes and influence on metastasis are unknown.

Primary lung ADCs are biologically heterogeneous and can be classified by gene expression profiles (Bhattacharjee et al., 2001; Wilkerson et al., 2012). Given that ADCs arise in the peripheral lungs, we hypothesized that a comprehensive analysis of genes involved in airway and/or alveolar differentiation would reveal mechanisms of ADC heterogeneity and metastasis. In the present study, we examined the molecular relationship between

cell differentiation states, lung cancer subtypes, and clinical outcome, to discover a role for lineage-restricted genes in the pathogenesis of lung ADC.

RESULTS

Identification of an Alveolar-like Differentiation Gene Module that Correlates with Lung ADC Outcome

To stratify ADCs into biologically informative subsets, we first compiled transcriptomic alterations observed in activated embryonic stem cells (Ben-Porath et al., 2008; Wong et al., 2008), human AT2 cells differentiated from embryonic cells (Ballard et al., 2010; Gonzales et al., 2002), and mouse models of airway homeostasis (Xu et al., 2010). These gene expression patterns were analyzed across multiple cohorts of resected primary human ADCs (Figure S1A available online). From this, we identified a module of 249 airway and/or alveolar-like differentiation genes (Table S1) that stratifies two distinctive molecular classes of ADCs (Figure 1A). We refer to these groups here as the "distal airway stem cell (DASC)-like" subtype and the "alveolar-like" subtype, based on a number of observations.

First, according to the recent characterization of human airway stem or progenitor cells (Kumar et al., 2011), the molecular features of “DASC-like” tumors are more akin to undifferentiated distal airway stem cells (DASCs) as opposed to proximal tracheal airway stem cells (TASCs) (Figures 1B and S1B). Second, many poorly differentiated ADCs are grouped in the DASC-like subset, while most well-differentiated tumors classify as alveolar-like (Figure 1C). Notably, even within early-stage tumors, the expression of prototypical AT2 lineage markers were decreased in the DASC-like tumors, including surfactant proteins encoded by *SFTPB-D* (Morrissey and Hogan, 2010) and the protease that cleaves their immature form encoded by *PGC* (Gerson et al., 2008) (Figures 1D and S1C). These tumors also expressed lower levels of *SCGB1A1* (Figure S1C), which is expressed in cells of the proximal lung and bronchioalveolar junctions. However, the expression of the marker of multipotent lung progenitors *ID2* (Rawlins et al., 2009) and the epithelial marker *CDH1* (E-cadherin) were unchanged (Figure 1D). As such, the bulk of DASC-like tumors is partially dedifferentiated relative to known airway lineages but retains features of an epithelial cell type. In DASC-like tumors, the expression of WNT inhibitory factor 1 (*WIF1*), an antagonist of the canonical WNT pathway (Clevers, 2006), was suppressed (Figure S1C), consistent with hyperactive WNT/TCF signaling being a mediator of lung ADC progression and metastasis (Nguyen et al., 2009; Pacheco-Pinedo et al., 2011). Patients harboring DASC-like tumors tended to have decreased five-year survival rates and increased incidence of metastasis or recurrence (Figures 1E and 1F; Figures S1D and S1E, red versus green subsets). These observations were conserved across seven independent ADC data sets (664 tumors) and are significant based on random permutation tests ($p < 0.0001$). However, in two SCC cohorts, this gene module was not linked to outcome (Figures 1F and S1E, gray versus black subsets). The transcriptional control of alveolar differentiation in NSCLCs is therefore preferentially associated with ADC metastatic progression.

Expression of the Lineage Transcription Factors GATA6 and HOPX Is Linked to Metastatic Competence in Lung ADC

The transcriptome of DASC-like ADCs may reflect the activity of a molecular pathway linked to alveolar differentiation. Frequent ADC mutations include the mutants *EGFR*, *KRAS*, *STK11*, and *TP53*. However, the presence of these mutations by themselves did not correlate with the lineage classification (Figure S2A). To identify mediators of this putative metastasis program, we focused on TF expression and activity, because several classes of TFs are known to balance pluripotency and pulmonary cell fate (Morrissey and Hogan, 2010). Global TF activity can be inferred from the relative enrichment of known TF binding motifs within the promoters of a given gene set. We cross-validated two independent algorithms for TF *cis* motif analysis across four major ADC cohorts. Motifs for 57 TFs were enriched in the transcriptome of DASC-like ADCs (Figure 2A; Table S2). The over-represented motifs were mainly for E2F family members and MYC (Figure 2A; orange), consistent with previous reports showing activation of their target genes in aggressive cancers (Rhodes et al., 2005; Sinha et al., 2008). In contrast, the under-represented motifs were targets for less-well-characterized

TFs that are tissue specific. This included several conserved GATA family binding sites (Figure 2A; blue).

GATAs can either activate or repress transcription and have redundant or specific target genes depending on the biological context (Molkentin, 2000). Of the six known family members, GATA6 is essential for endodermal differentiation and distal airway homeostasis (Keijzer et al., 2001; Liu et al., 2002a; Yang et al., 2002). It maintains proper alveolar gene expression in cooperation with other known lineage TFs, including HOPX (Yin et al., 2006) and NKX2-1 (Liu et al., 2002b; Zhang et al., 2007). Interestingly, GATA6, HOPX, and NKX2-1 were part of the lineage signature (Table S1), and their expression was generally reduced in poor prognosis tumors (Figures 2B and S2B). The expression of other GATAs varied less across human ADCs (Figure S2B). HOPX lacks a DNA binding domain (Chen et al., 2002; Shin et al., 2002), explaining why it did not score in our *cis* motif analysis. NKX2-1 targets annotated in this analysis were not broadly over- or underrepresented. Based on recent ADC resequencing efforts, copy number variations and somatic mutations in GATA6 and HOPX were rare (Figure S2C), suggesting that perturbation of these TFs occurs at the level of their expression.

To further ascertain the correlation of these lineage TFs with metastasis, we compared their expression in several models of ADC metastatic progression. ADC metastasis can be generated via *in vivo* selection of metastatic cell subpopulations (BrM3 cells) from the human lung ADC cell lines H2030 and PC9, which carry *KRAS* and *EGFR* mutations, respectively. Following transplantation in mice, BrM3 cells have enhanced metastatic predilections when compared to their parental cells (Nguyen et al., 2009). Messenger RNA (mRNA) levels of GATA members were generally reduced in BrM3 cells (Figure S2D). Suppression of GATA6 and known HOPX isoforms was not entirely associated with DNA methylation (Figures S2E and S2F). Still, GATA6 expression was notably decreased in the metastatic H2030-BrM3 cells as compared to their indolent parental cells, whereas HOPX was undetectable in both H2030 populations (Figures 2C and 2D). GATA6 expression varied less in the PC9-BrM3 subpopulation, but these cells express significantly lower levels of HOPX (Figures 2C and 2D). Although NKX2-1 is a prognostic marker (Barletta et al., 2009), its inhibition may occur independently because its expression was already low to undetectable in these human cells and did not further correlate with their metastatic predilection (Figure S2G). Murine ADC cell lines have been isolated from genetically engineered mice with NSCLC initiated by *Kras* and *p53* mutations (Winslow et al., 2011). In this model, aggressive primary tumor cells (T_{Met}) with low *Nkx2-1* and their clonally derived metastatic cells (Met) also tend to express decreased levels of *Gata6* and *Hopx* as compared to cells from nonmetastatic ADCs (T_{nonMet}) (Figure 2E). Altogether, the suppression of alveolar lineage TFs in a subset of primary tumors is linked to the selection of metastatic ADCs. In particular, low levels of both GATA6 and HOPX in ADCs correlated with poor outcome, even when accounting for patient smoking status, sex, and tumor stage (Figure 2F).

GATA6 and HOPX Limit Multiorgan Metastasis

To test the functions of GATA6 and HOPX in human ADC cells, we reduced their levels via inducible small hairpin RNAs (shRNAs) in the less aggressive H2030 and PC9 parental cells.

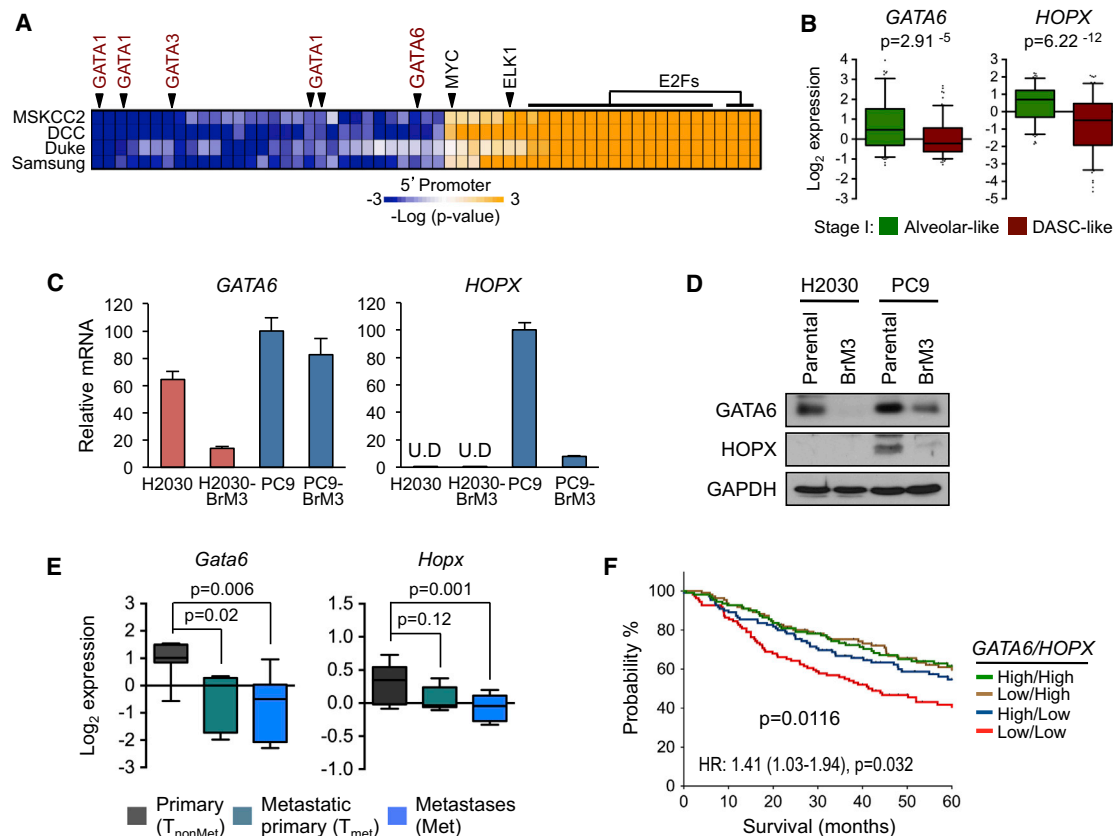


Figure 2. TF Activity and Expression in DASC-like Tumors and Metastatic ADC Cells

(A) Annotated *cis* TF motifs from TRANSFAC database were computed for enrichment in the transcriptome of ADC subsets. The heatmap depicts motifs that are significantly over- (orange) or underrepresented (blue) in “DASC-like” ADCs from four independent patient cohorts. Enrichment scores were reported based on $-\log_{10}(p \text{ value})$ from GSEA.

(B) Normalized \log_2 values for *GATA6* and *HOPX* expression in DCC. The *p* values were calculated by Student’s *t* test with Bonferroni correction.

(C) *GATA6* and *HOPX* were measured in the indicated cell lines via quantitative real-time PCR. U.D., undetected. Bar charts represent the mean \pm SEM.

(D) Western blot of *GATA6* and *HOPX* in the indicated cell lines.

(E) Normalized \log_2 values of *Gata6* and *Hopx* expression in nonmetastatic primary (T_{nonMet} ; $n = 7$), metastatic primary (T_{met} ; $n = 7$) and metastases (Met; $n = 9$) cell lines derived from a *Kras*^{LSL-G12D/+}; *p53*^{fllox/fllox} lung ADC mouse model. The *p* values were calculated by Student’s *t* test with Bonferroni correction.

(F) Survival of DCC patients based on the median expression of *GATA6* and *HOPX* in their primary tumors. The *p* values were calculated by log rank test. Hazard ratio (HR) and confidence interval were calculated using patient sex, smoking status, and tumor stage as covariates.

See also Figure S2 and Table S2.

We confirmed that doxycycline (DOX) treatment caused efficient and sustained induction of hairpin expression in disseminated tumor cells in an immunocompromised mouse model (Figure S3A). Our functional results were validated using independent hairpins (shRNAs a and b) and small interfering RNA (siRNAs) against each gene where indicated.

Based on the alveolar-like signature, H2030 cells were less differentiated than PC9 cells (data not shown) and already express low amounts of *HOPX* (see Figure 2D). Accordingly, we reduced *GATA6* in parental H2030 cells (Figure 3A) and injected them at different dilutions into the arterial circulation of mice that were either treated with DOX or control feed. Knockdown of *GATA6* in parental H2030 cells was sufficient to enhance their metastatic capabilities (Figure 3B) but had only a modest effect on subcutaneous tumorigenesis (Figure S3B). On the other hand, overexpression of *GATA6* and/or *HOPX* in the highly metastatic H2030-BrM3 cells, which express low

endogenous levels of both TFs (Figure S3C), inhibited their metastatic potential (Figure 3C). We then decreased the expression of *GATA6* and *HOPX* individually or in combination in the more differentiated PC9 cells, which express high levels of both TFs, and achieved 71% knockdown of *GATA6* and over 90% knockdown of *HOPX* (Figures 3D and S3D). Although *HOPX* is a downstream target of *GATA6* in AT2 cells (Yin et al., 2006), their expressions were not interdependent in PC9 cells (Figure 3D). Knockdown of *GATA6*, together with *HOPX*, enhanced the proportion of animals with high metastatic burden, which could be rescued by ectopic expression of shRNA-resistant complementary DNAs (cDNAs) (Figure 3E; Figures S3E and S3F). When injected into circulation at lower cell numbers, *GATA6* and *HOPX* knockdown increased the incidence of multiorgan metastasis (Figure 3F). Metastases were confirmed in brain, bone, and lungs (Figure 3G). *GATA6* and *HOPX* did not significantly alter the proportion of PC9 cells expressing CD133 (Figure S3G), a

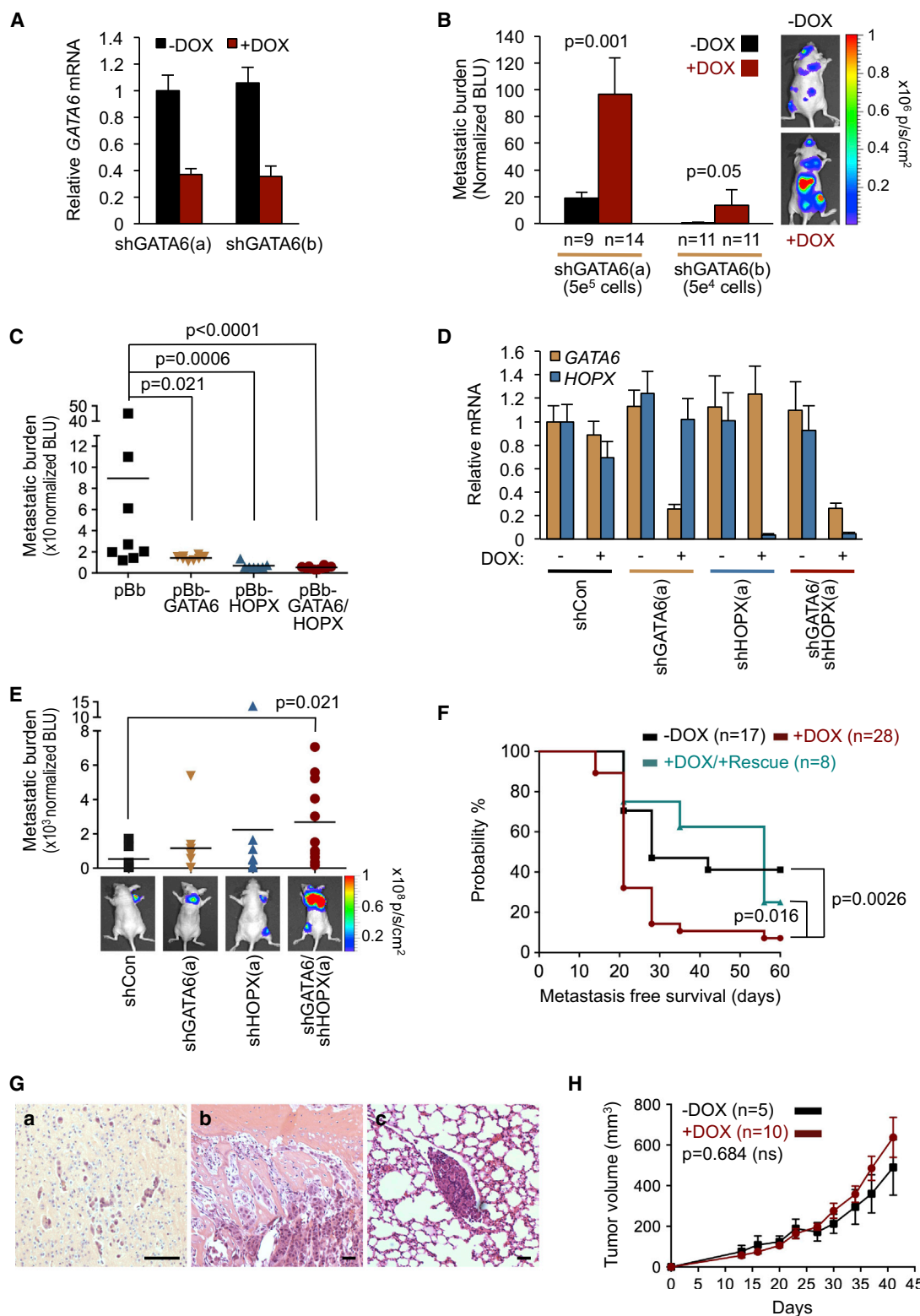


Figure 3. The Lineage TFs GATA6 and HOPX Limit Metastatic Colonization

(A) H2030 cells stably expressing two separate doxycycline (DOX)-inducible shRNAs, (a) or (b), against GATA6 were cultured in the absence or presence of DOX. GATA6 level was measured by quantitative real-time PCR.

(B) H2030 cells from (A) were injected at indicated cell numbers into the arterial circulation of mice fed with regular (–DOX) or DOX (+DOX) diet. Metastatic burden was measured by bioluminescent imaging. The bar chart shows the whole-body bioluminescent units (BLU) collected at day 36 [shGATA6(a)] or day 40 [shGATA6(b)] (legend continued on next page)

putative tumor-initiating cell marker, and did not affect tumorigenic potential (Figure 3H). We conclude that these TFs can cooperatively limit the metastatic competence of ADC cells independent of tumor growth.

GATA6 and HOPX Constrain Invasogenic Outgrowth

Given the metastasis inhibitory functions of GATA6 and HOPX in vivo, we ascertained the cell biological mechanism of their action. Under two-dimensional (2D) growing conditions, knockdown of GATA6 in H2030 cells did not affect cell survival even when deprived of growth factors, whereas *KRAS* knockdown caused a significant decrease in their viability (Figures 4A and S4A). In PC9 cells, loss of GATA6 and/or *HOPX* did not alter cell growth (Figure 4B), whereas reduction of GATA2 and *EGFR* inhibited cell viability as previously reported (Figure 4C; Figures S4B and S4C) (Kumar et al., 2012; Rothenberg et al., 2008). Thus, in these ADC cells, GATA6 and *HOPX* are not lineage survival genes.

To study metastatic cellular phenotypes in the more differentiated PC9 cells, we optimized a three-dimensional (3D) culture model for tumor organoid formation in extracellular matrix. Under these conditions, PC9 parental cells formed solid organoids (Figure 5A; inset). Suppression of *HOPX* caused an outgrowth of these organoids, and this effect was enhanced in combination with GATA6 knockdown (Figures 5A and 5B; Figures S5A and S5B). GATA6 and/or *HOPX* knockdown did not alter the overall number of organoids (Figure 5C, top), even when single cells were seeded (Figure S5C), but significantly changed the morphologies of these organoids. Extending on prior characterization (Kenny et al., 2007), we termed these mass, grape-like or expansive organoids. Mass organoids maintained spherical appearance, whereas grape-like and expansive organoids were disorganized. The expansive organoids were the largest multicellular structures, and they correlated with an increase in PC9 cell outgrowth. Knockdown of GATA6 or *HOPX* augmented the proportion of grape-like organoids (Figure 5C, teal). *HOPX* suppression also moderately increased the amount of expansive organoids (Figure 5C, red). Double GATA6 and *HOPX* knockdown greatly increased the proportion of expansive organoids (Figure 5C), which was prevented by rescue of GATA6 and *HOPX* expression (Figure S5D). Moreover, GATA6 and *HOPX* reinduction in pre-established organoids by DOX withdrawal delayed their expansion (Figure 5D).

The morphology of the grape-like and expansive organoids suggests that they are highly invasive. To test this directly, we dissociated cells from the organoids and compared their invasive

potential through Matrigel. Cells from the grape-like and/or expansive organoids were more invasive than those from the masses (Figure 5E). GATA6 and *HOPX* also cooperatively limit the invasion of PC9 cells cultured directly from monolayer (Figure 5F). The effect of double knockdown was consistent across four additional ADC cell lines that express high levels of these TFs and encompass different genetic backgrounds and tumor stages (Figures 5G and S5E). In contrast, invasion was not affected by knockdown in two high GATA6/*HOPX* expressing non-ADC cell lines (1 SCC and 1 LCC) that we tested (Figures S5F and S5G). GATA6 reduction was sufficient to promote invasion of the parental H2030 cells (Figure 5G, yellow), consistent with low levels of *HOPX* in these ADC cells. This effect was partially rescued by re-expression of *HOPX* (Figures S5H and S5I), confirming its cooperativity with GATA6. Restoration of GATA6 and *HOPX* in the metastatic H2030-BrM3 ADC subpopulation inhibited its invasion, whereas overexpression of these TFs in the low GATA6/*HOPX*-expressing SCC cell line H520 did not alter its modest baseline invasiveness (Figures S5J and S5K).

Activation of Specific Proinvasive Pathways following GATA6 and HOPX Reduction

Having defined a cellular function for GATA6 and *HOPX* in lung ADC cells, we examined if these TFs affect pathways reported to mediate lung cancer invasion (Carretero et al., 2010; Nguyen et al., 2009; Roman et al., 2010; Saito et al., 2009). We analyzed PC9 cells with GATA6 and/or *HOPX* knockdown because the greatest phenotypic alterations were observed in this model. Surprisingly, the levels of epithelial-mesenchymal transition (EMT) markers, ZEB1/2, TWIST1, E-cadherin, and vimentin, were not affected (Figures 6A and S6A). Activation of the canonical WNT pathway was only marginally regulated downstream of these TFs (Figures 6B and S6B). On the other hand, reduction of GATA6 and *HOPX* cooperatively increased Src activation but not focal adhesion kinase (FAK) (Figure 6C). Finally, we examined the steady-state levels of several integrin subunits and found that GATA6 and/or *HOPX* knockdown led to a marked increase in integrin $\alpha 5$ but did not consistently affect others (Figure 6C; data not shown). Thus, GATA6 and *HOPX* can repress Src activity and integrin $\alpha 5$ expression in poorly metastatic cells.

GATA6 and HOPX Regulate a Set of Common Genes Involved in Epithelial Differentiation and Metastasis

To comprehensively understand how GATA6 and *HOPX* link lineage fate to metastatic competence, we identified their downstream target genes using genome-wide RNA sequencing.

[shGATA6(b)] and normalized to day 0. Right: representative images of mice injected with H2030-shGATA6(a) cells on day 36. The p values were calculated using the Mann-Whitney test.

(C) H2030-BrM3 cells overexpressing GATA6, *HOPX*, or both were injected (5×10^4 cells/mouse) as in (B). The scatterplot shows the metastatic burden at day 42. The p values were calculated using the Mann-Whitney test.

(D) GATA6 and *HOPX* levels in PC9 cells expressing the indicated shRNAs. shCon, a control shRNA.

(E) PC9 cells expressing the indicated shRNAs were injected intracardially into DOX-treated mice (5×10^4 cells/mouse). The scatterplot shows the metastatic burden at day 48. Bottom: representative images of mice with metastases. The p values were calculated using the Mann-Whitney test.

(F) Kaplan-Meier curve showing the metastasis-free survival of mice inoculated with 2.5×10^4 PC9-shGATA6/shHOPX(b) cells as in (B) or injected with PC9-shGATA6/shHOPX(b) cells that coexpress GATA6 and *HOPX* cDNAs (+Rescue). The p values were calculated using the log rank test.

(G) Hematoxylin and eosin staining of metastases in the (a) brain, (b) bone, and (c) lung of mice harvested from (E). Scale bars, 100 μ m.

(H) Volumes of subcutaneous tumors formed by PC9-shGATA6/shHOPX(a) cells. Mean \pm SEM; the p values were calculated using the Student's t test. ns, not significant.

Bar charts represent the mean \pm SEM. See also Figure S3.

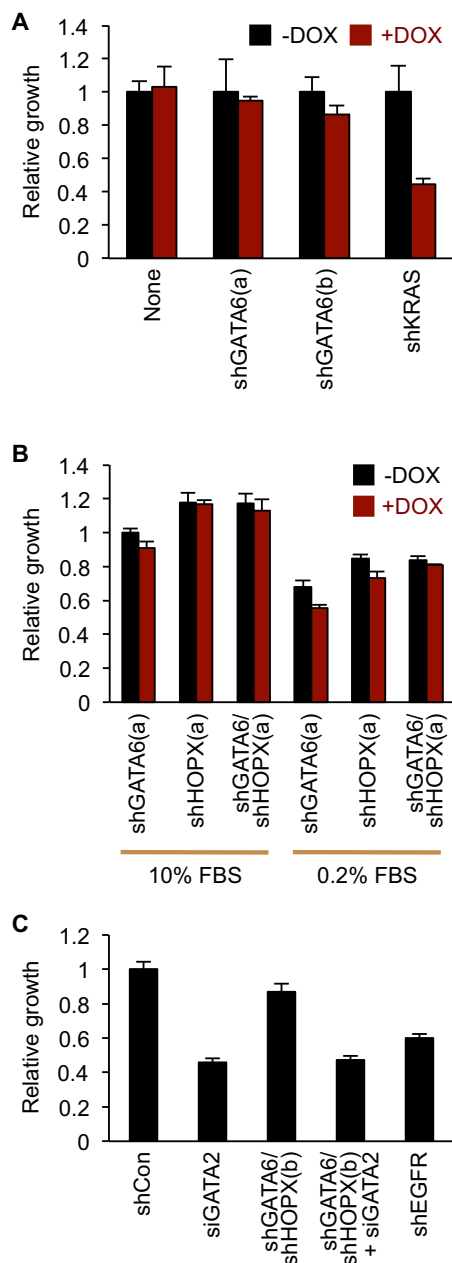


Figure 4. GATA6 and HOPX Do Not Affect Tumor Cell Survival

(A) H2030 cells with the indicated shRNAs were cultured in media containing 0.2% fetal bovine serum (FBS). Cell viability was measured at 72 hr after DOX treatment.

(B) The viability of PC9 cells with the indicated shRNAs was measured in media supplemented with 10% or 0.2% FBS as in (A).

(C) The indicated PC9 cell lines were transfected with siRNA targeting GATA2 (siGATA2). Cell viability was measured in 0.2% FBS at day 5 posttransfection. Bar charts represent the mean \pm SEM. See also Figure S4.

Knockdown of both TFs in PC9 cells caused transcriptomic alterations that resemble those of human DASC-like tumors (Figure 7A, orange labels). These changes also inversely correlate with the transcriptome of AT2 cells differentiated in vitro and broadly resemble those of DASCs, but not TASCs (Figure S7A). To determine if the perturbation of these TFs contributes to rele-

vant molecular and histopathological classes of human ADCs, we examined the relationship between GATA6/HOPX-regulated genes and three major ADC subgroups, including bronchioid, magnoid, and squamoid cancers (Wilkerson et al., 2012). The gene expression profiles of GATA6/HOPX knockdown cells correlated most with the squamoid subtype (Figure 7A, cyan labels), which includes highly invasive tumors with mixed adenosquamous features (Wilkerson et al., 2012).

By filtering the list of coding transcripts based on genes similarly expressed in human tumors, we identified 426 relevant mRNAs that were differentially regulated by GATA6/HOPX (Figure 7B; Table S3). We confirmed that many of these genes were redundantly or cooperatively modulated by GATA6 and HOPX (Figure 7B, gray and red rectangles), whereas an additional gene set was only altered by HOPX (Figure 7B, blue rectangles). The alveolar markers *SFTPD* and *PGC* were down-regulated after reduction of these TFs (Figures 7C and S7B). Surprisingly, the loss of AT2 identity in tumor cells was accompanied by an increase in the expression of cytokeratins 6A (*KRT6A*) and 6B (*KRT6B*) (Figures 7C and S7B), which are normally expressed in basal cells and putative DASCs (Kumar et al., 2011). The expression of secretogranin II (*SCG2*), a marker of neuroendocrine cells (Feldman and Eiden, 2003), was also activated. Consistent with an epithelial lineage switch controlled by these TFs, GATA6/HOPX expression significantly correlated with AT2 markers and inversely correlated with *KRT6A/B* levels in a proportion of resected human ADCs (Figure S7C).

We also identified a number of target genes that are known mediators of metastatic colonization (Figures 7D and S7B). For instance, reduction of GATA6 and/or HOPX led to increased expression of *IL1B*, *IL11*, and *EREG*, which encode for secreted factors associated with organotropic metastasis (Bos et al., 2009; Gupta et al., 2007; Kang et al., 2003). Vascular and ECM remodeling genes (*VEGFA* and *PLAU*) that promote metastatic progression (Blanco et al., 2012; Weis et al., 2004) were also activated. Some of the described transcriptional changes were observed in other ADC cell lines, with *KRT6A/B* induction being the most consistent response (Figures S7D and S7E). Consequently, inhibition of GATA6 and HOPX may activate a multigenic program that enhances dissemination as well as distant organ colonization.

GATA6 and HOPX Lineage Target Genes Control Malignant Cell Invasion

Given that GATA6/HOPX-regulated genes include markers of lung differentiation and metastasis, the repression of certain metastatic functions may be intrinsic to the lineage-specifying activity of these TFs. Moreover, we found that the formation of tumor organoids from 2D culture upregulates the expression of the alveolar-like genes *HOPX* and *PGC* but represses *KRT6A* expression (Figure 8A). Hence, this organoid system recapitulates extracellular conditions that enforce alveolar fate at the expense of other lineages. The expression pattern of these markers was reversed in the invasive organoids after GATA6/HOPX knockdown (Figure 8A), suggesting that this particular differentiation program may directly constrain tumor cell invasion.

To test this possibility, we focused on the function of putative epithelial lineage markers that were aberrantly activated upon GATA6 and HOPX repression, including *KRT6A*, *KRT6B* (Moll

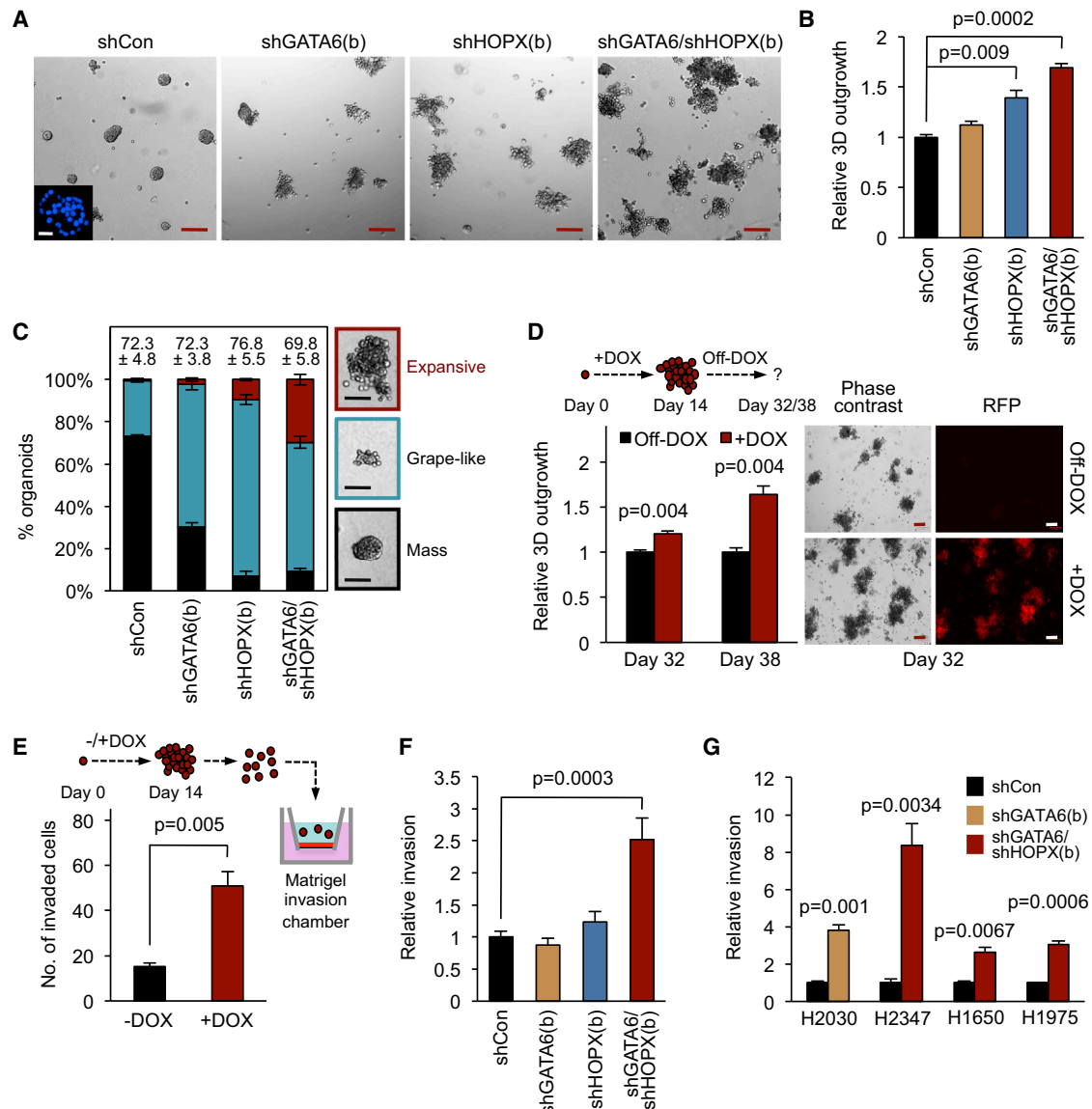


Figure 5. GATA6 and HOPX Constrain Cell Invasion

(A) PC9 cells expressing the indicated shRNAs were cultured in low attachment plates with media containing Matrigel and DOX. Phase contrast images were captured after 14 days of culture. The inset shows a cross-section of a DAPI-stained organoid. Scale bars, 200 μ m (25 μ m in insert).

(B) Organoids from (A) were harvested, and cell outgrowth was measured as a function of luciferase activity.

(C) The bar chart shows the percentage of mass (black), grape-like (teal), and expansive (red) organoids. The numbers at the top of graph show the overall numbers (\pm SEM) of tumor organoids formed at day 8. Representative images of indicated organoids are shown at right. Scale bars, 100 μ m.

(D) After 14 days of 3D culture in the presence of DOX, PC9-shGATA6/shHOPX(b) organoids were replated in Matrigel with (+DOX) or without DOX (off-DOX) for an additional 18–24 days. Tumor cell growth was measured at days 32 and 38 as in (B). Representative images at day 32 are shown. The red fluorescent protein (RFP) signal indicates shRNA expression. Scale bars, 200 μ m.

(E) At day 14, PC9-shGATA6/shHOPX(b) organoids formed in Matrigel in the presence or absence of DOX were disaggregated and subjected to invasion assay in Boyden chambers.

(F) PC9 cells expressing the indicated shRNAs were grown in monolayer with DOX for 5 days and then directly subjected to an invasion assay as in (E). Quantification was normalized to the invasion of cells expressing shCon.

(G) Invasion of additional ADC lines was determined as in (F).

Bar charts represent the mean \pm SEM; the p values were calculated using Student's t test. See also Figure S5.

et al., 1982), *STEAP1* (Gomes et al., 2012), and *GPR87* (Glatt et al., 2008) (Figure 8A). We successfully inhibited their activation by shRNA or siRNAs in double *GATA6/HOPX* knockdown cells (Figures 8B and S8A; data not shown). Surprisingly, reduction

of both *KRT6A* and *KRT6B* partially restored the expression of the alveolar marker *PGC* (Figure 8B). This partial alveogenic rescue diminished the induction of several prometastatic genes (Figure 8B) and integrin $\alpha 5$ expression (Figure 8C). Functionally,

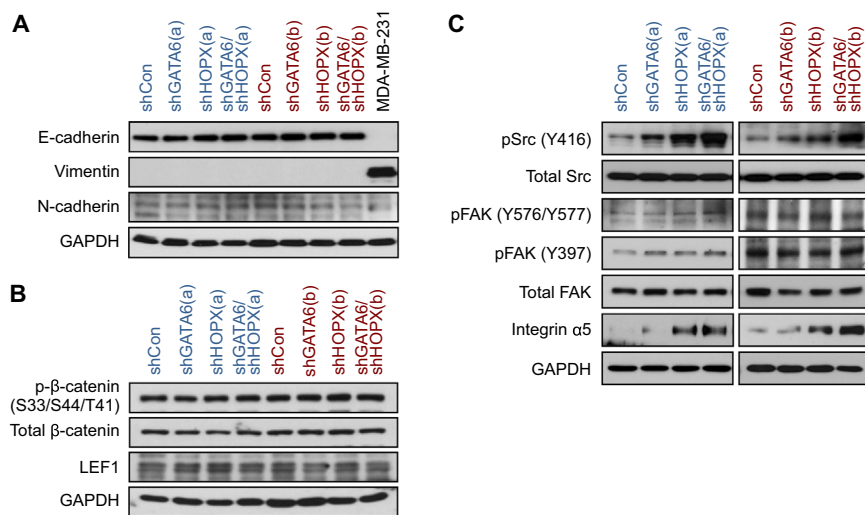


Figure 6. Src and Integrin $\alpha 5$ Are Suppressed by GATA6 and HOPX

(A–C) PC9 cells with the indicated shRNAs targeting GATA6 and/or HOPX were cultured in monolayer. After 5 days of DOX treatment, cells were harvested for western blot analysis for (A) epithelial (E-cadherin) and mesenchymal (vimentin and N-cadherin) markers, (B) canonical WNT signaling pathway components, β -catenin and LEF1, and (C) Src, FAK, and integrin $\alpha 5$. Lysate from MDA-MB-231 cells serves as a control for vimentin.

See also Figure S6.

GATA6 and HOPX as Inhibitors of Metastasis

We discovered that GATA6 and HOPX expression and activity are reduced in a

subset of high-grade ADCs and metastatic cells. Suppression of both TFs can enhance the invasion of lung ADC cell lines with different mutations, but this did not have the same effect in SCC cell lines tested here. Although GATA6 with HOPX preferentially limits ADC metastatic competence, it remains to be determined under which genetic/epigenetic context(s) this activity is enforced and whether these TFs have alternate roles in other NSCLCs with particular molecular aberrations or tumor stages. In various cancers, GATA members may promote (Belaguli et al., 2010; Collisson et al., 2011; Lin et al., 2012; Yang et al., 2011) or inhibit (Cai et al., 2009; Kouros-Mehr et al., 2008; Lindholm et al., 2009) cancer. This is analogous to another important TF in NSCLC, NKX2-1, which can function as an oncogene (Weir et al., 2007) or tumor suppressor (Maeda et al., 2012; Snyder et al., 2013; Winslow et al., 2011). HOPX levels inversely correlate with tumorigenesis (Chen et al., 2007; Ooki et al., 2010), but its mechanism of action has been unknown. The biological activity of such lineage factors likely depends on their integration within a TF network that is unique to particular cellular contexts.

DISCUSSION

Lineage Markers and ADC Progression

Although several genomic aberrations are associated with lung cancer progression, our understanding of the metastatic process remains incomplete. Emerging evidence indicates that the transcriptional pathways that are critical for lung morphogenesis can be disrupted or reused during chronic diseases of the airways (Whitsett et al., 2011). Differentiation and regeneration of the lung epithelium is dictated by many cooperating transcriptional effectors. Our integrated approach uncovered a transcriptional network that is preferentially active in committed airway epithelial cells and is inhibited in a subset of metastatic cancers arising from the distal lungs. Within this network, we found that the cooperative action of at least two TFs, GATA6 and HOPX, links the molecular determinants of alveologenesis to metastatic competence in the lung ADC subtype.

Lung ADCs can arise from AT2 cells, and expression of alveolar markers is employed to discriminate lung ADCs from other thoracic malignancies. However, epithelial transdifferentiation may occur in ADCs. Notably, some ADCs express markers of squamous (Wilkerson et al., 2012) or small cell lung cancers (Alam et al., 2010), and distinct histological subgroups correlate with relapse (Travis et al., 2011). These observations imply that the cellular composition and/or molecular determinants of airway specification vary during ADC progression and can influence clinical outcome. We found that a gene signature modulated in part by GATA6 and HOPX repression correlates with classifiers of poor prognosis. Importantly, this lineage classification is associated with metastasis in patients with ADC, but not SCC.

The lung buds are derived from the endoderm, which is specified by GATA6 (Morrissey and Hogan, 2010). GATA6 also restricts the expansion of progenitor cells in the adult airways, where it is abundantly expressed (Morrissey et al., 1996; Zhang et al., 2008). To maintain AT2 homeostasis, at least two other TFs, NKX2-1 and HOPX, can synergize with or are regulated by GATA6 (Liu et al., 2002b; Yin et al., 2006; Zhang et al., 2007). Our data, along with the aforementioned studies, support a model in which suppression of this TF node and divergent alveologenesis directly influence ADC progression. These findings further suggest that inhibition of HOPX together with GATA6 in transformed ADC cells is an important determinant of invasion and metastasis initiation. This does not inherently exclude the possibility that metastasis could also originate from progenitors with low GATA6 and HOPX activity. Although we found that GATA6 and HOPX could further limit ADC metastatic colonization, overt metastasis likely requires multiple physiological or molecular perturbations and other lineage genes may be involved. Additional insight into the diverse pathogenesis of NSCLCs will be uncovered by studying the timing, cellular context, and mechanisms by which combinations of lineage TFs are deregulated.

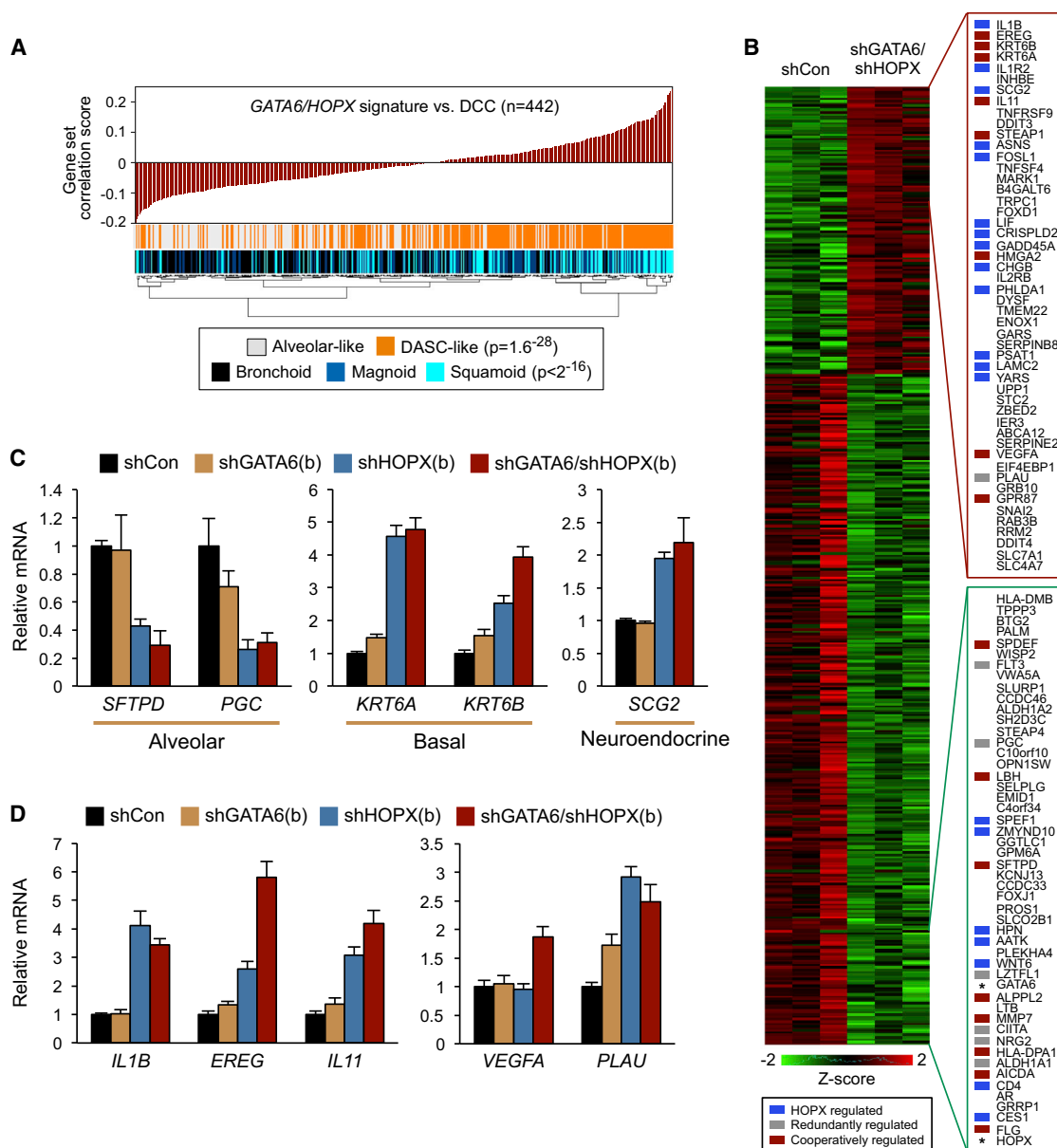


Figure 7. Common Regulation of Airway Differentiation and Metastasis Gene Sets

(A) Pearson correlation coefficients were calculated for each DCC tumor by comparing its mRNA transcriptome to the shGATA6/shHOPX knockdown signature generated by RNA sequencing of PC9 cells. DCC tumors were ordered from lowest to highest correlation with shGATA6/shHOPX knockdown cells (top). Histological and molecular subtypes are annotated in the middle and bottom rows for comparisons. DASC-like samples have a higher correlation with GATA6/HOPX knockdown cells than with alveolar-like tumors (middle row; p value by Student's t test). Squamoid and magnoid tumors have a higher correlation than bronchioid tumors (bottom row; p value by ANOVA).

(B) Left: the heatmap depicts 426 genes that are commonly upregulated (red) or downregulated (green) in shGATA6/shHOPX knockdown cells and DCC tumors. Right: top 50 up- and downregulated genes. Genes that were validated by quantitative real-time PCR are denoted with rectangles. Blue, controlled by HOPX; gray, redundantly controlled by GATA6 and HOPX; red, cooperatively controlled by GATA6 and HOPX; *, confirmation of HOPX and GATA6 knockdown.

(C) Quantitative real-time PCR measurement of alveolar (*SFTPD* and *PGC*), basal (*KRT6A* and *KRT6B*), and neuroendocrine (*SCG2*) marker expression in DOX-treated PC9 cells with the indicated shRNAs.

(D) Expression of known metastasis genes as in (C).

For quantitative real-time PCR data, expression was normalized to PC9-shCon cells and presented as the mean \pm SEM. See also Figure S7 and Table S3.

GATA6 and HOPX Directly Link Metastatic Invasion to Airway Cell Fate

GATA6 and HOPX modulated the transcription of overlapping genes, some of which were cooperatively activated or

repressed. Because HOPX lacks a DNA binding domain, it must interact with other sequence-specific TFs to account for its effects. Certain GATA6/HOPX-regulated genes encode for cellular functions that link airway epithelial differentiation

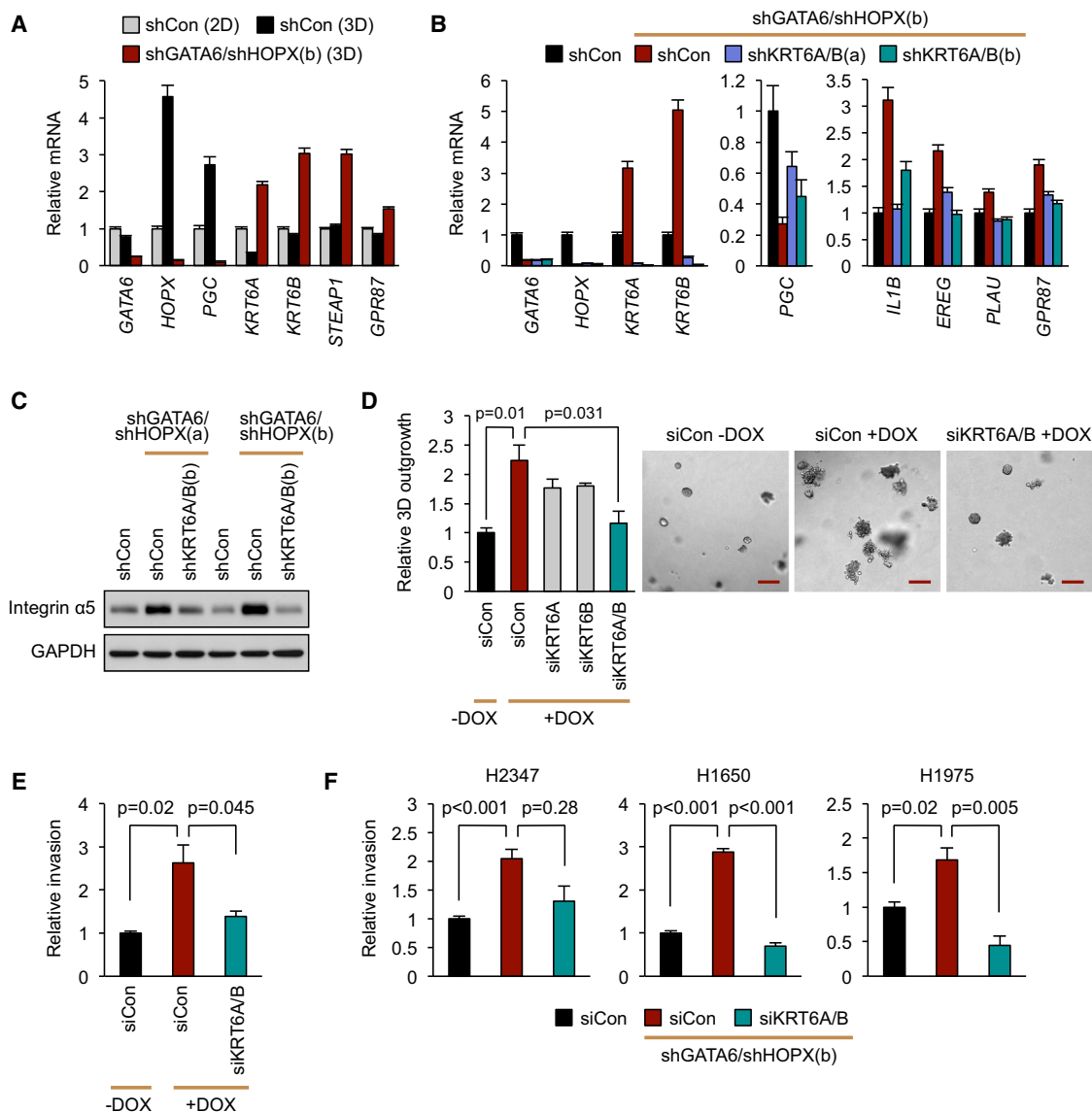


Figure 8. GATA6 and HOPX Link Epithelial Identity with Invasion through KRT6A and KRT6B

(A) PC9 cells with the indicated shRNAs were cultured in monolayer (2D) or Matrigel suspension (3D) for 5 days as in Figure 5. Expression of the indicated epithelial markers was detected by quantitative real-time PCR.

(B) PC9-shGATA6/shHOPX(b) knockdown cells were super-infected with lentiviruses encoding shCon or shRNAs against *KRT6A* and *KRT6B*. Expression of the indicated GATA6/HOPX target genes upon *KRT6A/B* suppression was detected as in (A).

(C) Western blot showing integrin $\alpha 5$ protein levels in the indicated cell lines.

(D) PC9-shGATA6/shHOPX(b) cells were transfected with the indicated siRNAs and cultured in 3D. Tumor cell outgrowth was quantified and representative images captured at day 10. Scale bar, 200 μ m.

(E) PC9-shGATA6/shHOPX(b) cells were transfected with a control siRNA (siCon) or siRNAs against *KRT6A* and *KRT6B*. At 48 hr posttransfection, cells were subjected to an invasion assay.

(F) Invasion assay was performed using indicated ADC lines with the indicated shRNAs/siRNAs.

Bar charts represent the mean \pm SEM; p values were calculated using Student's t test. See also Figure S8.

to metastasis. Indeed, suppression of these TFs in ADC cells decreased AT2 differentiation. This was not sufficient to induce EMT but caused transformed cells to display characteristics of basal epithelial cells, including *KRT6A/B* expression. Concomitantly, these TFs inhibited proinvasive pathways, such as Src activity and integrin $\alpha 5$ induction, while also

controlling known metastasis genes. Surprisingly, *KRT6A/B* themselves partially mediated alveolar gene expression and ADC cell invasion. *KRT6A/B* are activated in epithelial tissue during wound healing (Wojcik et al., 2000) and in putative stem cells of the distal lung following infections (Kumar et al., 2011). Hence, this switch in lineage markers may represent a

transdifferentiating or dedifferentiating event, enabling aggressive ADC cells to adopt traits normally required for airway regeneration.

Our study highlights the distinct mechanisms of metastatic competence in different types of lung cancers. In particular, we have demonstrated that the TFs, GATA6 and HOPX, can inhibit metastasis in the lung ADC subtype. These factors and their target genes directly link programs of airway specification to the pathogenesis of NSCLC. Consequently, certain facets of this lineage pathway may be explored to more effectively treat patients with metastatic lung cancers.

EXPERIMENTAL PROCEDURES

Additional details about the experimental procedures are provided in the [Supplemental Experimental Procedures](#).

Cell Culture, Viability, and Invasion Assays

Cell lines were cultured as recommended by the American Type Culture Collection (ATCC). Cell viability and invasion were assayed as previously mentioned (Nguyen et al., 2009). For 3D outgrowth, cells were grown in media with 5% Matrigel in ultra-low attachment plates (Corning, Tewksbury, MA, USA) at 37°C for 8–14 days. Organoids were categorized as previously described (Kenny et al., 2007). Expansive organoids are a subset of grape-like organoids with diameter >200 μ m. To quantify outgrowth, cells stably expressing *firefly luciferase* were harvested, and luciferase activity was measured by Dual-Luciferase Reporter Assay (Promega, Madison, WI).

Gene Knockdown, Quantitative Real-Time PCR, and Western Blot

shRNA sequences, inducible lentiviral vectors, primers, and antibodies are listed in the [Supplemental Experimental Procedures](#).

Animal Studies

Studies using athymic nu/nu male mice (NCI) aged between 5–7 weeks were conducted in compliance with U.S. guidelines for the care and use of laboratory animals and were approved by the Institutional Animal Care and Use Committee of Yale University. DOX was administered in chow (625 mg/kg). An IVIS Spectrum was used for bioluminescence imaging.

Microarray Data Analysis

Data sets for primary lung cancers, AT2/airway genes, and airway stem cells, as well as derivation of an “alveolar-like” signature, are listed in the [Supplemental Experimental Procedures](#) and [Table S1](#). Differential gene expression and hierarchical clustering were performed in Partek and R.

RNA Sequencing

RNA samples were sequenced on a HiSeq 2000 (Illumina, San Diego, CA, USA) and analyzed using Tophat and EdgeR.

Statistical Analysis

Experimental data are presented as mean \pm SEM. The p values for in vitro data and tumor volume are calculated by two-tailed Student's t test. Survival curves and metastatic burden were analyzed by log rank test and Mann-Whitney test, respectively.

ACCESSION NUMBERS

The GEO accession number for the RNA sequencing reported in this paper is GSE39121.

SUPPLEMENTAL INFORMATION

Supplemental Information includes eight figures, three tables, and Supplemental Experimental Procedures and can be found with this article online at <http://dx.doi.org/10.1016/j.ccr.2013.04.009>.

ACKNOWLEDGMENTS

We thank Mei Zhong for help with RNA sequencing and Katerina Politi for her review of the manuscript. This work was funded by grants from Uniting Against Lung Cancer, the National Lung Cancer Partnership, the American Cancer Society (IRG-58-012-52), and the National Cancer Institute (1R01CA166376) (to D.X.N.). T.F.W. is funded by the Cancer Prevention and Research Institute of Texas (RP120583) and the National Institutes of Health (P30 CA125123-06, CA058183, and CA149196). D.X.N. is a scholar of the V Foundation for Cancer Research, Yale Center for Clinical Investigation, and Young Investigator of the International Association for the Study of Lung Cancer.

Received: July 5, 2012

Revised: December 10, 2012

Accepted: April 8, 2013

Published: May 23, 2013

REFERENCES

- Alam, N., Gustafson, K.S., Ladanyi, M., Zakowski, M.F., Kapoor, A., Truskinovsky, A.M., and Dudek, A.Z. (2010). Small-cell carcinoma with an epidermal growth factor receptor mutation in a never-smoker with gefitinib-responsive adenocarcinoma of the lung. *Clin. Lung Cancer* 11, E1–E4.
- Ballard, P.L., Lee, J.W., Fang, X., Chapin, C., Allen, L., Segal, M.R., Fischer, H., Illek, B., Gonzales, L.W., Kolla, V., and Matthay, M.A. (2010). Regulated gene expression in cultured type II cells of adult human lung. *Am. J. Physiol. Lung Cell. Mol. Physiol.* 299, L36–L50.
- Barletta, J.A., Perner, S., Iafrate, A.J., Yeap, B.Y., Weir, B.A., Johnson, L.A., Johnson, B.E., Meyerson, M., Rubin, M.A., Travis, W.D., et al. (2009). Clinical significance of TTF-1 protein expression and TTF-1 gene amplification in lung adenocarcinoma. *J. Cell. Mol. Med.* 13(8B), 1977–1986.
- Belaguli, N.S., Aftab, M., Rigi, M., Zhang, M., Albo, D., and Berger, D.H. (2010). GATA6 promotes colon cancer cell invasion by regulating urokinase plasminogen activator gene expression. *Neoplasia* 12, 856–865.
- Ben-Porath, I., Thomson, M.W., Carey, V.J., Ge, R., Bell, G.W., Regev, A., and Weinberg, R.A. (2008). An embryonic stem cell-like gene expression signature in poorly differentiated aggressive human tumors. *Nat. Genet.* 40, 499–507.
- Bhattacharjee, A., Richards, W.G., Staunton, J., Li, C., Monti, S., Vasa, P., Ladd, C., Beheshti, J., Bueno, R., Gillette, M., et al. (2001). Classification of human lung carcinomas by mRNA expression profiling reveals distinct adenocarcinoma subclasses. *Proc. Natl. Acad. Sci. USA* 98, 13790–13795.
- Blanco, M.A., LeRoy, G., Khan, Z., Alečković, M., Zee, B.M., Garcia, B.A., and Kang, Y. (2012). Global secretome analysis identifies novel mediators of bone metastasis. *Cell Res.* 22, 1339–1355.
- Bos, P.D., Zhang, X.H., Nadal, C., Shu, W., Gomis, R.R., Nguyen, D.X., Minn, A.J., van de Vijver, M.J., Gerald, W.L., Foekens, J.A., and Massagué, J. (2009). Genes that mediate breast cancer metastasis to the brain. *Nature* 459, 1005–1009.
- Cai, K.Q., Caslini, C., Capo-chichi, C.D., Slater, C., Smith, E.R., Wu, H., Klein-Szanto, A.J., Godwin, A.K., and Xu, X.X. (2009). Loss of GATA4 and GATA6 expression specifies ovarian cancer histological subtypes and precedes neoplastic transformation of ovarian surface epithelia. *PLoS ONE* 4, e6454.
- Carretero, J., Shimamura, T., Rikova, K., Jackson, A.L., Wilkerson, M.D., Borgman, C.L., Buttarazzi, M.S., Sanofsky, B.A., McNamara, K.L., Brandstetter, K.A., et al. (2010). Integrative genomic and proteomic analyses identify targets for Lkb1-deficient metastatic lung tumors. *Cancer Cell* 17, 547–559.
- Chen, F., Kook, H., Milewski, R., Gitler, A.D., Lu, M.M., Li, J., Nazarian, R., Schnepf, R., Jen, K., Biben, C., et al. (2002). Hop is an unusual homeobox gene that modulates cardiac development. *Cell* 110, 713–723.
- Chen, Y., Pacyna-Gengelbach, M., Deutschmann, N., Niesporek, S., and Petersen, I. (2007). Homeobox gene HOP has a potential tumor suppressive activity in human lung cancer. *Int. J. Cancer* 121, 1021–1027.
- Clevers, H. (2006). Wnt/beta-catenin signaling in development and disease. *Cell* 127, 469–480.

- Collisson, E.A., Sadanandam, A., Olson, P., Gibb, W.J., Truitt, M., Gu, S., Cooc, J., Weinkle, J., Kim, G.E., Jakkula, L., et al. (2011). Subtypes of pancreatic ductal adenocarcinoma and their differing responses to therapy. *Nat. Med.* 17, 500–503.
- Eramo, A., Haas, T.L., and De Maria, R. (2010). Lung cancer stem cells: tools and targets to fight lung cancer. *Oncogene* 29, 4625–4635.
- Feldman, S.A., and Eiden, L.E. (2003). The chromogranins: their roles in secretion from neuroendocrine cells and as markers for neuroendocrine neoplasia. *Endocr. Pathol.* 14, 3–23.
- Gabrielson, E. (2006). Worldwide trends in lung cancer pathology. *Respirology* 11, 533–538.
- Garraway, L.A., and Sellers, W.R. (2006). Lineage dependency and lineage-survival oncogenes in human cancer. *Nat. Rev. Cancer* 6, 593–602.
- Gerson, K.D., Foster, C.D., Zhang, P., Zhang, Z., Rosenblatt, M.M., and Guttentag, S.H. (2008). Pepsinogen C proteolytic processing of surfactant protein B. *J. Biol. Chem.* 283, 10330–10338.
- Glatt, S., Halbauer, D., Heindl, S., Wernitznig, A., Kozina, D., Su, K.C., Puri, C., Garin-Chesa, P., and Sommergruber, W. (2008). hGPR87 contributes to viability of human tumor cells. *Int. J. Cancer* 122, 2008–2016.
- Gomes, I.M., Maia, C.J., and Santos, C.R. (2012). STEAP proteins: from structure to applications in cancer therapy. *Mol. Cancer Res.* 10, 573–587.
- Gonzales, L.W., Guttentag, S.H., Wade, K.C., Postle, A.D., and Ballard, P.L. (2002). Differentiation of human pulmonary type II cells in vitro by glucocorticoid plus cAMP. *Am. J. Physiol. Lung Cell. Mol. Physiol.* 283, L940–L951.
- Gupta, G.P., Nguyen, D.X., Chiang, A.C., Bos, P.D., Kim, J.Y., Nadal, C., Gomis, R.R., Manova-Todorova, K., and Massagué, J. (2007). Mediators of vascular remodelling co-opted for sequential steps in lung metastasis. *Nature* 446, 765–770.
- Hecht, J.L., Pinkus, J.L., Weinstein, L.J., and Pinkus, G.S. (2001). The value of thyroid transcription factor-1 in cytologic preparations as a marker for metastatic adenocarcinoma of lung origin. *Am. J. Clin. Pathol.* 116, 483–488.
- Jemal, A., Thun, M.J., Ries, L.A., Howe, H.L., Weir, H.K., Center, M.M., Ward, E., Wu, X.C., Ehemann, C., Anderson, R., et al. (2008). Annual report to the nation on the status of cancer, 1975–2005, featuring trends in lung cancer, tobacco use, and tobacco control. *J. Natl. Cancer Inst.* 100, 1672–1694.
- Kang, Y., Siegel, P.M., Shu, W., Drobniak, M., Kakonen, S.M., Cordon-Cardo, C., Guise, T.A., and Massagué, J. (2003). A multigenic program mediating breast cancer metastasis to bone. *Cancer Cell* 3, 537–549.
- Keijzer, R., van Tuyl, M., Meijers, C., Post, M., Tibboel, D., Grosveld, F., and Koutsourakis, M. (2001). The transcription factor GATA6 is essential for branching morphogenesis and epithelial cell differentiation during fetal pulmonary development. *Development* 128, 503–511.
- Kenny, P.A., Lee, G.Y., Myers, C.A., Neve, R.M., Semeiks, J.R., Spellman, P.T., Lorenz, K., Lee, E.H., Barcellos-Hoff, M.H., Petersen, O.W., et al. (2007). The morphologies of breast cancer cell lines in three-dimensional assays correlate with their profiles of gene expression. *Mol. Oncol.* 1, 84–96.
- Kouros-Mehr, H., Bechis, S.K., Slorach, E.M., Littlepage, L.E., Egeblad, M., Ewald, A.J., Pai, S.Y., Ho, I.C., and Werb, Z. (2008). GATA-3 links tumor differentiation and dissemination in a luminal breast cancer model. *Cancer Cell* 13, 141–152.
- Kumar, P.A., Hu, Y., Yamamoto, Y., Hoe, N.B., Wei, T.S., Mu, D., Sun, Y., Joo, L.S., Dagher, R., Zielonka, E.M., et al. (2011). Distal airway stem cells yield alveoli in vitro and during lung regeneration following H1N1 influenza infection. *Cell* 147, 525–538.
- Kumar, M.S., Hancock, D.C., Molina-Arcas, M., Steckel, M., East, P., Diefenbacher, M., Armenteros-Monterroso, E., Lassailly, F., Matthews, N., Nye, E., et al. (2012). The GATA2 transcriptional network is requisite for RAS oncogene-driven non-small cell lung cancer. *Cell* 149, 642–655.
- Lin, L., Bass, A.J., Lockwood, W.W., Wang, Z., Silvers, A.L., Thomas, D.G., Chang, A.C., Lin, J., Orringer, M.B., Li, W., et al. (2012). Activation of GATA binding protein 6 (GATA6) sustains oncogenic lineage-survival in esophageal adenocarcinoma. *Proc. Natl. Acad. Sci. USA* 109, 4251–4256.
- Lindholm, P.M., Soini, Y., Myllärmi, M., Knuutila, S., Heikinheimo, M., Kinnula, V.L., and Salmenkivi, K. (2009). Expression of GATA-6 transcription factor in pleural malignant mesothelioma and metastatic pulmonary adenocarcinoma. *J. Clin. Pathol.* 62, 339–344.
- Liu, C., Morrissey, E.E., and Whitsett, J.A. (2002a). GATA-6 is required for maturation of the lung in late gestation. *Am. J. Physiol. Lung Cell. Mol. Physiol.* 283, L468–L475.
- Liu, C., Glasser, S.W., Wan, H., and Whitsett, J.A. (2002b). GATA-6 and thyroid transcription factor-1 directly interact and regulate surfactant protein-C gene expression. *J. Biol. Chem.* 277, 4519–4525.
- Maeda, Y., Davé, V., and Whitsett, J.A. (2007). Transcriptional control of lung morphogenesis. *Physiol. Rev.* 87, 219–244.
- Maeda, Y., Tsuchiya, T., Hao, H., Tompkins, D.H., Xu, Y., Mucenski, M.L., Du, L., Keiser, A.R., Fukazawa, T., Naomoto, Y., et al. (2012). Kras(G12D) and Nkx2-1 haploinsufficiency induce mucinous adenocarcinoma of the lung. *J. Clin. Invest.* 122, 4388–4400.
- Molkentin, J.D. (2000). The zinc finger-containing transcription factors GATA-4, -5, and -6. Ubiquitously expressed regulators of tissue-specific gene expression. *J. Biol. Chem.* 275, 38949–38952.
- Moll, R., Franke, W.W., Schiller, D.L., Geiger, B., and Krepler, R. (1982). The catalog of human cytokeratins: patterns of expression in normal epithelia, tumors and cultured cells. *Cell* 31, 11–24.
- Morrissey, E.E., and Hogan, B.L. (2010). Preparing for the first breath: genetic and cellular mechanisms in lung development. *Dev. Cell* 18, 8–23.
- Morrissey, E.E., Ip, H.S., Lu, M.M., and Parmacek, M.S. (1996). GATA-6: a zinc finger transcription factor that is expressed in multiple cell lineages derived from lateral mesoderm. *Dev. Biol.* 177, 309–322.
- Nguyen, D.X., Chiang, A.C., Zhang, X.H., Kim, J.Y., Kris, M.G., Ladanyi, M., Gerald, W.L., and Massagué, J. (2009). WNT/TCF signaling through LEF1 and HOXB9 mediates lung adenocarcinoma metastasis. *Cell* 138, 51–62.
- Ooki, A., Yamashita, K., Kikuchi, S., Sakuramoto, S., Katada, N., Kokubo, K., Kobayashi, H., Kim, M.S., Sidransky, D., and Watanabe, M. (2010). Potential utility of HOP homeobox gene promoter methylation as a marker of tumor aggressiveness in gastric cancer. *Oncogene* 29, 3263–3275.
- Pacheco-Pinedo, E.C., Durham, A.C., Stewart, K.M., Goss, A.M., Lu, M.M., Demayo, F.J., and Morrissey, E.E. (2011). Wnt/ β -catenin signaling accelerates mouse lung tumorigenesis by imposing an embryonic distal progenitor phenotype on lung epithelium. *J. Clin. Invest.* 121, 1935–1945.
- Rawlins, E.L., Clark, C.P., Xue, Y., and Hogan, B.L. (2009). The Id2+ distal tip lung epithelium contains individual multipotent embryonic progenitor cells. *Development* 136, 3741–3745.
- Rhodes, D.R., Kalyana-Sundaram, S., Mahavisno, V., Barrette, T.R., Ghosh, D., and Chinnaiyan, A.M. (2005). Mining for regulatory programs in the cancer transcriptome. *Nat. Genet.* 37, 579–583.
- Roman, J., Ritzenthaler, J.D., Roser-Page, S., Sun, X., and Han, S. (2010). $\alpha 5 \beta 1$ -integrin expression is essential for tumor progression in experimental lung cancer. *Am. J. Respir. Cell Mol. Biol.* 43, 684–691.
- Rothenberg, S.M., Engelman, J.A., Le, S., Riese, D.J., 2nd, Haber, D.A., and Settleman, J. (2008). Modeling oncogene addiction using RNA interference. *Proc. Natl. Acad. Sci. USA* 105, 12480–12484.
- Saito, R.A., Watabe, T., Horiguchi, K., Kohyama, T., Saitoh, M., Nagase, T., and Miyazono, K. (2009). Thyroid transcription factor-1 inhibits transforming growth factor- β -mediated epithelial-to-mesenchymal transition in lung adenocarcinoma cells. *Cancer Res.* 69, 2783–2791.
- Shin, C.H., Liu, Z.P., Passier, R., Zhang, C.L., Wang, D.Z., Harris, T.M., Yamagishi, H., Richardson, J.A., Childs, G., and Olson, E.N. (2002). Modulation of cardiac growth and development by HOP, an unusual homeo-domain protein. *Cell* 110, 725–735.
- Singh, A., Greninger, P., Rhodes, D., Koopman, L., Violette, S., Bardeesy, N., and Settleman, J. (2009). A gene expression signature associated with “K-Ras addiction” reveals regulators of EMT and tumor cell survival. *Cancer Cell* 15, 489–500.
- Sinha, S., Adler, A.S., Field, Y., Chang, H.Y., and Segal, E. (2008). Systematic functional characterization of cis-regulatory motifs in human core promoters. *Genome Res.* 18, 477–488.

- Snyder, E.L., Watanabe, H., Magendantz, M., Hoersch, S., Chen, T.A., Wang, D.G., Crowley, D., Whittaker, C.A., Meyerson, M., Kimura, S., and Jacks, T. (2013). Nkx2-1 represses a latent gastric differentiation program in lung adenocarcinoma. *Mol. Cell*. Published online March 21, 2013. <http://dx.doi.org/10.1016/j.molcel.2013.02.018>.
- Travis, W.D., Brambilla, E., Noguchi, M., Nicholson, A.G., Geisinger, K.R., Yatabe, Y., Beer, D.G., Powell, C.A., Riely, G.J., Van Schil, P.E., et al. (2011). International association for the study of lung cancer/american thoracic society/european respiratory society international multidisciplinary classification of lung adenocarcinoma. *J. Thorac. Oncol.* 6, 244–285.
- Weir, B.A., Woo, M.S., Getz, G., Perner, S., Ding, L., Beroukhi, R., Lin, W.M., Province, M.A., Kraja, A., Johnson, L.A., et al. (2007). Characterizing the cancer genome in lung adenocarcinoma. *Nature* 450, 893–898.
- Weis, S., Cui, J., Barnes, L., and Cheres, D. (2004). Endothelial barrier disruption by VEGF-mediated Src activity potentiates tumor cell extravasation and metastasis. *J. Cell Biol.* 167, 223–229.
- Whitsett, J.A., Haitchi, H.M., and Maeda, Y. (2011). Intersections between pulmonary development and disease. *Am. J. Respir. Crit. Care Med.* 184, 401–406.
- Wilkerson, M.D., Yin, X., Walter, V., Zhao, N., Cabanski, C.R., Hayward, M.C., Miller, C.R., Socinski, M.A., Parsons, A.M., Thorne, L.B., et al. (2012). Differential pathogenesis of lung adenocarcinoma subtypes involving sequence mutations, copy number, chromosomal instability, and methylation. *PLoS ONE* 7, e36530.
- Winslow, M.M., Dayton, T.L., Verhaak, R.G., Kim-Kiselak, C., Snyder, E.L., Feldser, D.M., Hubbard, D.D., DuPage, M.J., Whittaker, C.A., Hoersch, S., et al. (2011). Suppression of lung adenocarcinoma progression by Nkx2-1. *Nature* 473, 101–104.
- Wojcik, S.M., Bundman, D.S., and Roop, D.R. (2000). Delayed wound healing in keratin 6a knockout mice. *Mol. Cell. Biol.* 20, 5248–5255.
- Wong, D.J., Liu, H., Ridky, T.W., Cassarino, D., Segal, E., and Chang, H.Y. (2008). Module map of stem cell genes guides creation of epithelial cancer stem cells. *Cell Stem Cell* 2, 333–344.
- Xu, Y., Zhang, M., Wang, Y., Kadambi, P., Dave, V., Lu, L.J., and Whitsett, J.A. (2010). A systems approach to mapping transcriptional networks controlling surfactant homeostasis. *BMC Genomics* 11, 451.
- Xu, X., Rock, J.R., Lu, Y., Futtner, C., Schwab, B., Guinney, J., Hogan, B.L., and Onaitis, M.W. (2012). Evidence for type II cells as cells of origin of K-Ras-induced distal lung adenocarcinoma. *Proc. Natl. Acad. Sci. USA* 109, 4910–4915.
- Yang, H., Lu, M.M., Zhang, L., Whitsett, J.A., and Morrissey, E.E. (2002). GATA6 regulates differentiation of distal lung epithelium. *Development* 129, 2233–2246.
- Yang, Y., Ahn, Y.H., Gibbons, D.L., Zang, Y., Lin, W., Thilaganathan, N., Alvarez, C.A., Moreira, D.C., Creighton, C.J., Gregory, P.A., et al. (2011). The Notch ligand Jagged2 promotes lung adenocarcinoma metastasis through a miR-200-dependent pathway in mice. *J. Clin. Invest.* 121, 1373–1385.
- Yin, Z., Gonzales, L., Kolla, V., Rath, N., Zhang, Y., Lu, M.M., Kimura, S., Ballard, P.L., Beers, M.F., Epstein, J.A., and Morrissey, E.E. (2006). Hop functions downstream of Nkx2.1 and GATA6 to mediate HDAC-dependent negative regulation of pulmonary gene expression. *Am. J. Physiol. Lung Cell. Mol. Physiol.* 291, L191–L199.
- Zhang, Y., Rath, N., Hannehalli, S., Wang, Z., Cappola, T., Kimura, S., Atochina-Vasserman, E., Lu, M.M., Beers, M.F., and Morrissey, E.E. (2007). GATA and Nkx factors synergistically regulate tissue-specific gene expression and development in vivo. *Development* 134, 189–198.
- Zhang, Y., Goss, A.M., Cohen, E.D., Kadzik, R., Lepore, J.J., Muthukumaraswamy, K., Yang, J., DeMayo, F.J., Whitsett, J.A., Parmacek, M.S., and Morrissey, E.E. (2008). A Gata6-Wnt pathway required for epithelial stem cell development and airway regeneration. *Nat. Genet.* 40, 862–870.

SDH Mutations Establish a Hypermethylator Phenotype in Paraganglioma

Eric Letouzé,^{1,13} Cosimo Martinelli,^{2,3,13} Céline Lorient,^{2,3} Nelly Burnichon,^{2,3,4} Nasséra Abermil,^{3,4} Chris Ottolenghi,^{3,6,7} Maxime Janin,^{6,7} Mélanie Menara,^{2,3} An Thach Nguyen,^{2,3} Paule Benit,⁸ Alexandre Buffet,^{2,3} Charles Marcaillou,⁹ Jérôme Bertherat,^{3,10,11,12} Laurence Amar,^{3,5,12} Pierre Rustin,⁸ Aurélien De Reyniès,¹ Anne-Paule Gimenez-Roqueplo,^{2,3,4,12,14} and Judith Favier^{2,3,14,*}

¹Programme Cartes d'Identité des Tumeurs, Ligue Nationale Contre Le Cancer, 75013 Paris, France

²INSERM, UMR970, Paris-Cardiovascular Research Center (PARCC), 75015 Paris, France

³Faculté de Médecine, Université Paris Descartes, 75006 Paris, France

⁴Service de Génétique

⁵Service d'Hypertension Artérielle

Assistance Publique-Hôpitaux de Paris (AP-HP), Hôpital Européen Georges Pompidou, 75015 Paris, France

⁶Service de Biochimie Métabolique, Assistance Publique-Hôpitaux de Paris, Hôpital Necker-Enfants Malades, 75015 Paris, France

⁷INSERM U747, 75015 Paris, France

⁸INSERM U676, Hôpital Robert Debré, 75019 Paris, France

⁹IntegraGen, 91030 Evry, France

¹⁰Service des Maladies Endocriniennes et Métaboliques, Assistance Publique-Hôpitaux de Paris (AP-HP), Hôpital Cochin, Centre de Référence Maladies Rares de la Surrénale, 75014 Paris, France

¹¹INSERM U1016, Institut Cochin, 75014 Paris, France

¹²Rare Adrenal Cancer Network-Cortico Médullosurrénale Tumeur Endocrine, Institut National du Cancer, 75014 Paris, France

¹³These authors contributed equally to this work

¹⁴These authors contributed equally to this work

*Correspondence: judith.favier@inserm.fr

<http://dx.doi.org/10.1016/j.ccr.2013.04.018>

SUMMARY

Paragangliomas are neuroendocrine tumors frequently associated with mutations in *RET*, *NF1*, *VHL*, and succinate dehydrogenase (*SDHx*) genes. Methylome analysis of a large paraganglioma cohort identified three stable clusters, associated with distinct clinical features and mutational status. *SDHx*-related tumors displayed a hypermethylator phenotype, associated with downregulation of key genes involved in neuroendocrine differentiation. Succinate accumulation in *SDH*-deficient mouse chromaffin cells led to DNA hypermethylation by inhibition of 2-OG-dependent histone and DNA demethylases and established a migratory phenotype reversed by decitabine treatment. Epigenetic silencing was particularly severe in *SDHB*-mutated tumors, potentially explaining their malignancy. Finally, inactivating *FH* mutations were identified in the only hypermethylated tumor without *SDHx* mutations. These findings emphasize the interplay between the Krebs cycle, epigenomic changes, and cancer.

INTRODUCTION

Paragangliomas (PGL) are neural crest-derived tumors that arise from parasympathetic ganglia of the head and neck region or

from sympathetic ganglia located in the thorax, abdomen, or pelvis. These tumors may develop in the adrenal medulla, in which case they are called pheochromocytomas (PCC) (Lenders et al., 2005). There has been extensive genetic characterization

Significance

Unexpected links between epigenetic and genetic alterations were recently identified with the demonstration that *IDH* mutations impair DNA demethylation in gliomas. Mutations affecting succinate dehydrogenase (*SDH*), another tricarboxylic acid cycle enzyme, have been identified in several cancers and are particularly frequent in paragangliomas. With this genome-wide analysis of DNA methylation changes in a large paraganglioma cohort, we demonstrate that *SDHx*, and particularly *SDHB*-related metastatic tumors, display a hypermethylator phenotype, associated with downregulation of key genes implicated in chromaffin cell differentiation. These findings explain the oncogenic effect of *SDH* inactivation and the invasiveness of *SDHB*-mutated tumors and raise the possibility of innovative epigenetic therapies involving DNA demethylating agents for these cancers.

of PGL/PCC. At least 30% of patients harbor a germline mutation in one of the ten identified susceptibility genes (Gimenez-Roqueplo et al., 2012): *RET*, *NF1*, *VHL*, *SDHAF2*, *TMEM127*, or *MAX*, and in genes encoding the four subunits of succinate dehydrogenase (*SDHA*, *SDHB*, *SDHC*, or *SDHD*, referred to as *SDHx* genes). Integrated genomic analysis of the largest available cohort of PGL/PCC, recruited by the French COMETE network, identified homogeneous molecular subgroups associated with susceptibility genes (Burnichon et al., 2011) and showed that a large proportion of sporadic PGL/PCC carry a somatic mutation in *VHL*, *RET*, *NF1*, *MAX*, or *HIF2A* genes (Burnichon et al., 2011, 2012a, 2012b; Favier et al., 2012). Overall, 60% of cases harbor a somatic or germline mutation in a known predisposing gene.

Various important issues remain to be unraveled, including the oncogenic role of *SDHx* mutations. Succinate dehydrogenase was the first mitochondrial enzyme to be identified as a tumor suppressor in familial PGL (Baysal et al., 2000). Its inactivation also predisposes to renal cell carcinoma (Ricketts et al., 2008) and gastrointestinal stromal tumors (Janeway et al., 2011). To date, the only mechanism linking SDH to cancer involves hypoxia-inducible factors (HIFs) (Dahia et al., 2005; Gimenez-Roqueplo et al., 2001). SDH dysfunction results in the accumulation of succinate (Pollard et al., 2005), its tricarboxylic acid cycle (TCA) substrate, which acts as a competitive inhibitor of the 2-oxoglutarate (2-OG)-dependent HIF prolyl-hydroxylases (Brière et al., 2005; Selak et al., 2005). This stabilizes HIF- α and activates genes that facilitate angiogenesis and anaerobic metabolism. However, the exact role of HIFs in oncogenesis remains unclear (Young and Simon, 2012). Understanding SDH-related tumorigenesis is crucial, because the presence of a germline mutation in the *SDHB* gene is a major risk factor of malignancy and of poor prognosis. Around 40% of all patients with a metastatic form of the disease harbor an *SDHB* mutation (Pasini and Stratakis, 2009). *SDHB*-mutation carriers have a 19-fold higher risk of developing a metastatic disease (Gimenez-Roqueplo et al., 2003) and shorter survival than patients with a malignant PGL/PCC but without *SDHB* mutations (Amar et al., 2007).

DNA methylation changes are hallmarks of human cancers (Hanahan and Weinberg, 2011). Cancer cells often display overall DNA hypomethylation and hypermethylation of promoter CpG islands, resulting in the transcriptional silencing of tumor suppressor genes (Jones and Baylin, 2007). Unlike genetic mutations, DNA methylation is a reversible process and is thus a promising target for drug development (Rodríguez-Paredes and Esteller, 2011). These epigenetic features are also useful as biomarkers for early detection of cancer in blood samples, for prognosis, or for prediction of response to treatment (Laird, 2003). Genome-scale DNA methylation profiling has allowed the identification of epigenetic subtypes in several cancers (Hinoue et al., 2012; Noushmehr et al., 2010). A CpG island methylator phenotype (CIMP), characterized by the concerted hypermethylation of a large number of genes, was initially described in colorectal cancer (Toyota et al., 1999) and was recently identified in glioma (G-CIMP; Noushmehr et al., 2010). In glioma, the G-CIMP phenotype is associated with gain-of-function mutations in *IDH1* and *IDH2* that confer to these enzymes a neomorphic capacity to convert α -ketoglutarate (α -KG, or 2-OG) into the oncometabolite 2-hydroxyglutarate (2-HG). 2-HG acts as a

competitive inhibitor of 2-OG-dependent dioxygenases, including histone demethylases and the TET family of 5-methylcytosine (5-mC) hydroxylases, leading to genome-wide DNA methylation alterations (Xu et al., 2011). Succinate also can inhibit these enzymes in vitro, suggesting that SDH-related tumorigenesis may involve epigenetic alterations (Xiao et al., 2012). However, DNA methylation changes of only a limited number of genes have been investigated so far in PGL/PCC (Geli et al., 2008) and have not been compared with expression data or mutational status.

Here, we report the genome-scale methylome and transcriptome profiling of the well-annotated COMETE cohort and investigate the relationship between *SDHx* mutations and DNA methylation changes in a mouse model of SDH-related paraganglioma.

RESULTS

DNA Methylation-Based Classification of Pheochromocytomas and Paragangliomas

We determined DNA methylation profiles of 145 pheochromocytomas and paragangliomas using the Illumina Infinium HM27 DNA methylation assay, which assesses the degree of methylation of 27,578 CpG sites in promoter regions of 14,495 protein-coding genes (Bibikova et al., 2009). Gene expression was previously characterized in most of these samples (Burnichon et al., 2011), and the mutation status of the main genes predisposing to PGL/PCC (*SDHx*, *VHL*, *NF1*, *RET*, *TMEM127*, and *MAX*) was analyzed (Table S1 available online). As previously described (Hinoue et al., 2012), we excluded probes that might be unreliable and probes designed for sequences on sex chromosomes. We selected the 10% most variant probes, according to the standard deviation of the beta values, and performed consensus clustering (Monti et al., 2003) to identify DNA methylation clusters. The optimal classification defined three tumor subgroups (Figure 1A; Figure S1). Tumors of the M1 cluster displayed concerted hypermethylation at a large number of loci (Figure 1B), reminiscent of the CpG island methylator phenotypes described in colorectal cancer and glioblastoma.

For comparison, we applied a second clustering approach, the recursively partitioned mixture model (RPMM; Houseman et al., 2008), to our data set. Cluster assignments using consensus clustering and RPMM were strongly correlated ($p = 9.7 \times 10^{-39}$), with the two methods agreeing on cluster membership for 90% (130/145) of the tumors (Figure S1F). In particular, the M1 cluster was similarly identified by the RPMM approach, with only 1/17 samples misclassified. We based our subsequent analyses on the consensus clusters, which showed better association with clinical criteria.

We next sought to characterize DNA methylation changes in each cluster. We analyzed probes located within and outside CpG islands separately (Takai and Jones, 2002). Most CpGs within CpG islands are demethylated in normal tissues and undergo hypermethylation in tumors (Jones and Baylin, 2007), whereas CpGs outside CpG islands are mostly highly methylated in normal tissues and undergo loss of DNA methylation in cancers (Feinberg and Vogelstein, 1983). Because of the difficulty in obtaining samples of normal adrenal medulla, only three normal controls were available, hence the comparison with tumor clusters had limited power. After FDR adjustment,

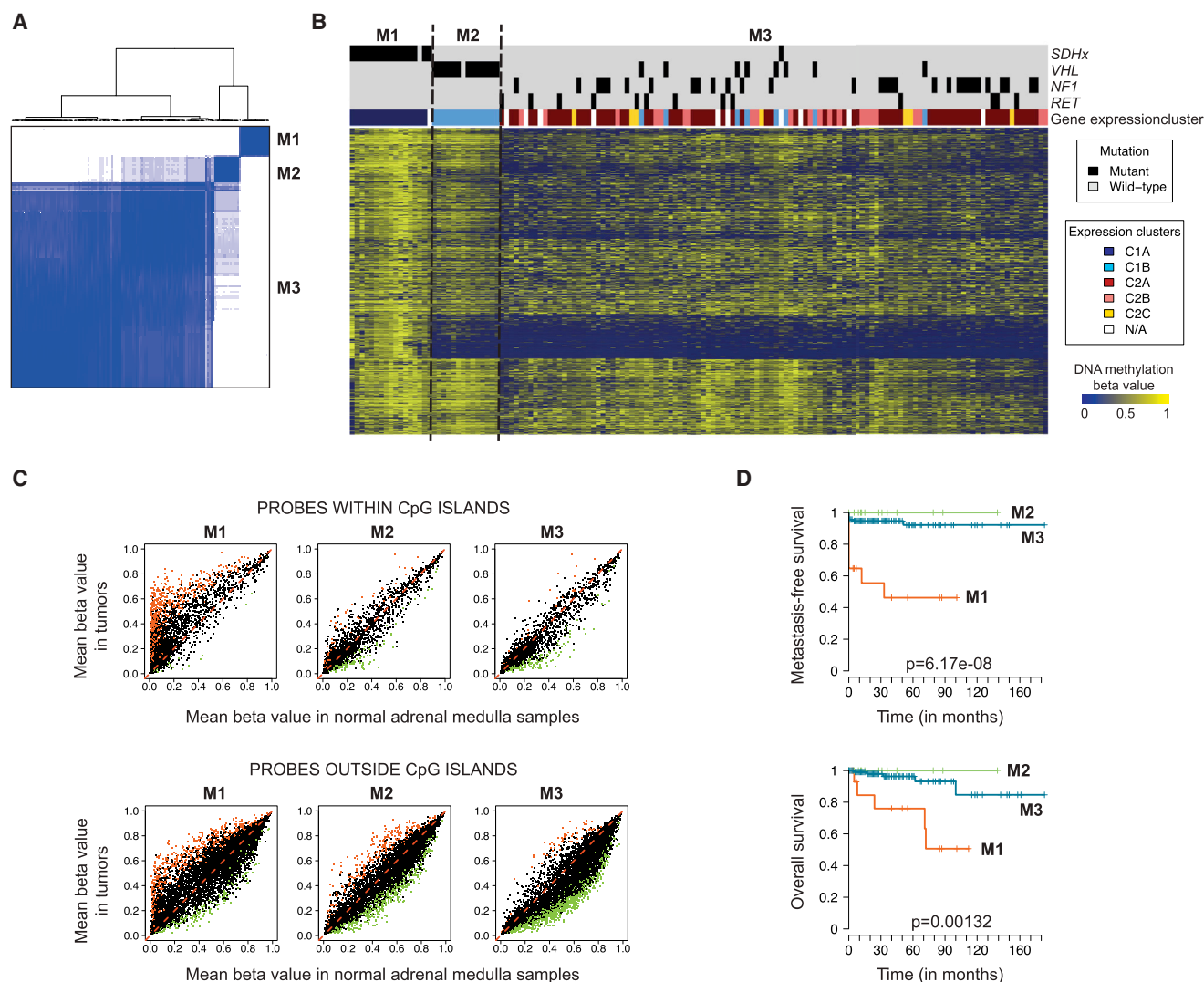


Figure 1. Genome-wide DNA Methylation Profiling of PGL/PCC Identifies a Hypermethylator Phenotype Associated with *SDHx* Mutations

(A) Unsupervised classification of 145 PGL/PCC samples (see Table S1) identifies three stable DNA methylation clusters. The consensus matrix represents the similarity between tumors. Consensus index values range from zero (highly dissimilar profiles, white) to one (highly similar profiles, dark blue). Samples are ordered on the x and y axes by the consensus clustering, which is depicted atop the heatmap. See also Figure S1.

(B) Heatmap representation of DNA methylation profiles. The degree of DNA methylation (beta value) for each probe (row) in each sample (column) is represented by a color scale (dark blue, nonmethylated; yellow, methylated). Tumors are ordered by methylation cluster. Probes are arranged by similarity, as assessed by hierarchical cluster analysis. The mutation status of the main genes predisposing to PGL/PCC (*SDHx*, *VHL*, *NF1*, and *RET*) is indicated above the heatmap, together with expression cluster memberships as determined in a previous study (Burnichon et al., 2011).

(C) Scatterplots comparing methylation levels between tumor subgroups and normal adrenal medulla controls are shown for probes located within (top) or outside (bottom) CpG islands (Takai-Jones definition [Takai and Jones, 2002]). Probes significantly hyper- or hypomethylated in tumors ($p < 0.01$) are indicated in red and green, respectively. See also Table S2.

(D) Kaplan-Meier curves for metastasis-free survival and overall survival.

significant methylation differences between tumors and normal controls were only detected in cluster M1 (1,015 probes with FDR-adjusted $p < 0.05$). However, the number of significant tests ($p < 0.01$) was substantially higher than expected by chance in each cluster (8.7%, 4.8%, and 6.4% in M1, M2, and M3, respectively). Cluster M1 tumors displayed a hypermethylation phenotype, characterized by high methylation levels at a large number of CpG sites, both within (7.2% of probes, $p < 0.01$; Figure 1C; Table S2) and outside (7.0%) CpG islands. Clusters M2 and

M3 did not display substantial hypermethylation within CpG islands, but a strong hypomethylation outside CpG islands was observed in both clusters, particularly in cluster M3 (5.9% of probes hypomethylated in M2, 9.6% in M3).

Association with Genomic and Clinical Features

DNA methylation clusters were highly associated with mutational status ($p = 3.3 \times 10^{-33}$) and gene expression clusters ($p = 1.3 \times 10^{-41}$) (Figure 1B; Table 1). In particular, the hypermethylation

Table 1. Clinical and Genomic Characteristics of DNA Methylation Consensus Clusters

	Overall (n = 145)	Cluster M1 (n = 17)	Cluster M2 (n = 14)	Cluster M3 (n = 114)	p Value
Gender					
Female	93 (64%)	11 (65%)	6 (43%)	76 (67%)	0.22
Male	52 (36%)	6 (35%)	8 (57%)	38 (33%)	
Age					
Median	44	32	25.5	47	1.80×10^{-7}
Range	7–82	10–63	10–49	7–82	
Histology ^a					
Paranglioma	15 (10%)	9 (56%)	1 (7%)	5 (4%)	1.51×10^{-9}
Pheochromocytoma	129 (90%)	7 (44%)	13 (93%)	109 (96%)	
Mutational Status					
<i>SDHx</i>	17 (12%)	16 (94%)	0	1 (1%)	3.32×10^{-33}
<i>VHL</i>	21 (14%)	0	13 (93%)	8 (7%)	
<i>NF1</i>	30 (21%)	0	0	30 (26%)	
<i>RET</i>	13 (9%)	0	0	13 (11%)	
Other	64 (44%)	1 (6%)	1 (7%)	62 (54%)	
Expression Cluster ^a					
C1A	16 (12%)	16 (100%)	0	0	1.33×10^{-41}
C1B	22 (16%)	0	14 (100%)	8 (8%)	
C2A	67 (50%)	0	0	67 (64%)	
C2B	22 (16%)	0	0	22 (21%)	
C2C	7 (5%)	0	0	7 (7%)	

Clinical and genomic features are indicated for each DNA methylation cluster, in absolute numbers and as a percentage of each group size. p values are obtained by chi-square tests for qualitative variables and ANOVA for age.

^aHistology could not be determined for one patient with both abdominal paraganglioma and adrenal pheochromocytoma at first presentation. Gene expression data were available for 134 samples.

phenotype was strongly associated with *SDHx* mutations. In cluster M1, 16/17 tumors were SDH-related (1 *SDHA*, 11 *SDHB*, 1 *SDHC*, and 3 *SDHD* germline mutations), and one was sporadic. Cluster M2 included 13/21 *VHL*-related tumors and one sporadic tumor. All *RET* and *NF1*-related samples were members of cluster M3, together with the remaining sporadic and *VHL*-mutated samples. Clusters M1 and M2 corresponded to the previously described C1A (*SDHx*-related) and C1B (*VHL*-related) expression clusters (Burnichon et al., 2011), and the M3 cluster comprised all tumors of the C2 (*RET/NF1*-related) expression cluster, plus eight tumors from the C1B group. Age at diagnosis and histology, which are known to be associated with mutational status (Amar et al., 2005; Neumann et al., 2002), differed significantly between DNA methylation clusters ($p = 1.8 \times 10^{-7}$ and $p = 1.5 \times 10^{-9}$, respectively). The median age at diagnosis was younger for clusters M1 (32 years) and M2 (25.5 years) than for cluster M3 (47 years), and cluster M1 was enriched in paragangliomas (56% versus $\leq 7\%$ in clusters M2 and M3). Note that only SDH-related paragangliomas displayed a hypermethylation phenotype. Hypermethylation is thus specifically associated with *SDHx* mutations, rather than a characteristic of extra-adrenal tumors. Methylation clusters were significantly associated with both metastasis-free survival (MFS, $p = 6.2 \times 10^{-8}$) and overall survival (OS, $p = 0.0013$), with the prognosis being much worse for M1 tumors than M2 and M3 tumors (Figure 1D). However, the presence of an *SDHB* mutation predicted prognosis more significantly than

methylation cluster membership in our series ($p = 8.9 \times 10^{-10}$ and $p = 8.2 \times 10^{-6}$ for MFS and OS, respectively).

Sdhb Knockout in Mouse Chromaffin Cells Establishes a Hypermethylator Phenotype and Promotes Cell Migration

To investigate the mechanisms linking SDH deficiency with methylation, we generated an immortalized mouse chromaffin cell (imCC) line harboring a complete defect in SDH. We created genetically modified mice in which the endogenous *Sdhb* exon 2 is flanked by LoxP sites, isolated chromaffin cells from their adrenal medulla, and deleted *Sdhb* by Cre-mediated recombination (Figure 2A). Suppression of exon 2 leads to a premature stop codon and to the predicted translation of a truncated 33 amino-acids protein, instead of the 283 amino-acids wild-type (WT) SDHB protein. Two independent *Sdhb*^{−/−} clones were studied (c6 and c8). As previously reported for human tumors (Favier et al., 2009; van Nederveen et al., 2009), *Sdhb*-deficient cells completely lost SDHB protein production but had normal SDHA levels (Figure S2A). They displayed a selective loss of SDH/succinate cytochrome c reductase (SCCR) activity (Figures 2B, S2B, and S2C), accompanied by large increases in both intracellular (Figure 2C) and secreted (Figure S2D) succinate levels and abnormally small amounts of the following organic acids (fumarate and malate) produced by the TCA cycle. Expression and nuclear translocation of HIF2 α were also higher than in controls (Figures S2E).

We used reduced representation bisulfite sequencing (RRBS) (Meissner et al., 2005) to examine base-pair resolution DNA methylation patterns in two samples of WT cells and in both *Sdhb*^{−/−} clones. We obtained more than 15 million high-quality aligned reads per sample, yielding quantitative DNA methylation data for 1,530,785 CpG dinucleotides (coverage ≥ 10 reads in each sample). Hierarchical clustering identified two clusters corresponding to WT and *Sdhb*^{−/−} cells (Figure 2D). Like SDHx-related tumors, *Sdhb*-deficient cells displayed a widespread hypermethylation both within and outside CpG islands (Figure 2E). We obtained DNA methylation rates with more than ten individual CpG measurements for 78% of CpG islands ($n = 12,503$). CpG island methylation rates were highly correlated between the two WT samples and between the two *Sdhb*^{−/−} clones (Figure S2F). By contrast, 3,357 CpG islands were significantly hypermethylated, and 242 were significantly hypomethylated in *Sdhb*^{−/−} clones as compared to WT cells (FDR-adjusted $p < 0.05$ and absolute methylation difference $> 5\%$) (Figure S2G). Genes hypermethylated in *Sdhb*-deficient imCCs significantly overlapped those hypermethylated in SDH-related PGL/PCC ($p = 3.2 \times 10^{-170}$), with 1,014 genes in common (Figure 2F; Table S3).

Although SDH-deficiency led to a mean 2-fold decrease in growth rate (Figure S2H), *Sdhb*^{−/−} cells had marked increased migration capacities as assessed in a wound healing scratch assay (Figure 2G). These characteristics are consistent with the known specificities of *SDHB*-related PGL/PCC, which are not associated with increased proliferation but are associated with invasiveness. To investigate the role of DNA methylation in this phenotype, we treated *Sdhb*^{−/−} cells for 72hr with low (10 nM) or higher (5 μ M) doses of 5-Aza-2'-deoxycytidine (decitabine or DAC), an epigenetic modifier that inhibits DNA methyltransferase activity. High doses induced cytotoxicity in all cell types (from 10% to 25% of cell death after 3 days), which was markedly reduced at low doses (cell death $< 8\%$). After drug withdrawal, the effect of DAC was assessed on cell proliferation and migration. We observed a dose-dependant blockade of cell growth in both WT and *Sdhb*^{−/−} cells (Figure S2H). In contrast, an inhibition of collective cell migration was specifically observed in SDH-deficient cells, but not in WT cells (Figure 2H).

SDH-Deficient Chromaffin Cells Display Increased 5-mC/5-hmC Ratio and Histone Methylation

Tet-mediated conversion of 5-mC to 5-hmC was evaluated by flow cytometry and immunofluorescence analyses: there was more 5-mC in *Sdhb*^{−/−} than the WT imCCs (Figures 3A and 3B). This effect was reversed by the addition of 2-OG to the culture medium, which also led to an increase in 5-hmC staining of *Sdhb*^{−/−} cells (Figure S3A). The methylation of lysines 9 and 27 of histone 3 was then assessed by western blotting. Loss of *Sdhb* increased H3K9me3, H3K27me2, and H3K27me3 levels (Figure 3C, quantified in Figure S3B). As both H3K9 and H3K27 methylation are closely linked with DNA methylation (Cedar and Bergman, 2009), these effects on histone methylation may contribute to the establishment of the hypermethylator phenotype.

To confirm the inhibition of oxidative demethylation by succinate in human PGL/PCC, we first measured succinate and fumarate concentrations in a subset of tumor samples and confirmed

a mean 100-fold increase in succinate levels in *SDHx*- versus non-*SDHx*-mutated PGL/PCC (Table S4). We next used immunohistochemistry to quantify 5-mC and 5-hmC, as well as H3K9me3 and H3K27me3, in 39 paraffin-embedded tumor samples with various genetic backgrounds. All (16/16) *SDHx*-mutated tumors had low 5-hmC levels, whereas 70% (16/23) of non-SDH samples had high levels of 5-hmC (Figure 3D; Table S5). Similarly, 81% of SDH-related PGL/PCC displayed abundant H3K27me3, whereas 43% of non-SDH tumors displayed low H3K27me3 levels (Figure 3E; Table S5). Succinate inhibition of oxidative demethylation by TET proteins and Jumonji domain-containing histone demethylases may thus be the mechanism responsible for the accumulation of DNA methylation in SDH-deficient tumors.

Transcriptional Changes Associated with the Hypermethylator Phenotype

To better understand the impact of DNA hypermethylation in tumors of the M1 cluster, we examined the relationship between methylation and expression changes in these tumors. Principal component analysis indicated that the transcriptome differed between the DNA methylation subgroups (Figure 4A), consistent with the strong association between methylation and expression clusters. Of the 7,136 CpG sites that were differently methylated in M1 and non-M1 tumors (FDR-adjusted $p < 0.05$), 6,850 (96%) were hypermethylated in M1 tumors, resulting in a highly asymmetric volcano plot (Figure 4B). The transcriptome data, available for 134/145 samples, revealed a similar asymmetry (Figure 4C), with 623 genes significantly downregulated (FDR-adjusted $p < 0.05$) and 356 genes significantly upregulated in cluster M1 (Table S6). Integrated transcriptome and methylome analysis revealed that 11.5% of genes with significant hypermethylation in M1 tumors (FDR-adjusted $p < 0.05$ and beta value difference > 0.1) also showed more than a 2-fold reduction in gene expression and that the mean shift in expression values correlated with the amplitude of the methylation difference (Figure 4D). To gain a more comprehensive view of DNA methylation changes in M1 tumors, we reanalyzed 22 tumors (ten M1, two M2, and ten M3) using the Illumina Infinium 450K assay, which assesses the methylation levels of more than 485,000 CpG sites. Using probes present on both the 27K and 450K arrays, we verified that the beta value differences between M1 and non-M1 tumors were consistent in the two data sets (mean absolute difference = 0.023). Overall, we identified 4,663 genes with significant hypermethylation of their promoter CpG islands (Table S7). The overlap between the lists of hypermethylated and downregulated genes was highly significant ($p = 1.5 \times 10^{-7}$), with 191 genes showing both significant CpG island hypermethylation and significant downregulation in M1 tumors (Table S8). Gene ontology analysis of this set of genes showed a significant enrichment in terms associated with neuroendocrine differentiation (Table S9). Several genes are associated with catecholamine metabolic process [*PNMT* (Figure S4), *DRD2*, and *SULT1A1*], transport (*SLC6A2*), or secretion (*NPY*); *RET* and *NRP2* are implicated in the differentiation of neural-crest cells. *RBP1* is a tumor suppressor known to be epigenetically silenced in several cancers (Esteller et al., 2002). Downregulation of *SPOCK2*, an inhibitor of matrix-metalloproteases, of *KRT19* (Figure S4), a key marker of the epithelial-to-mesenchymal transition

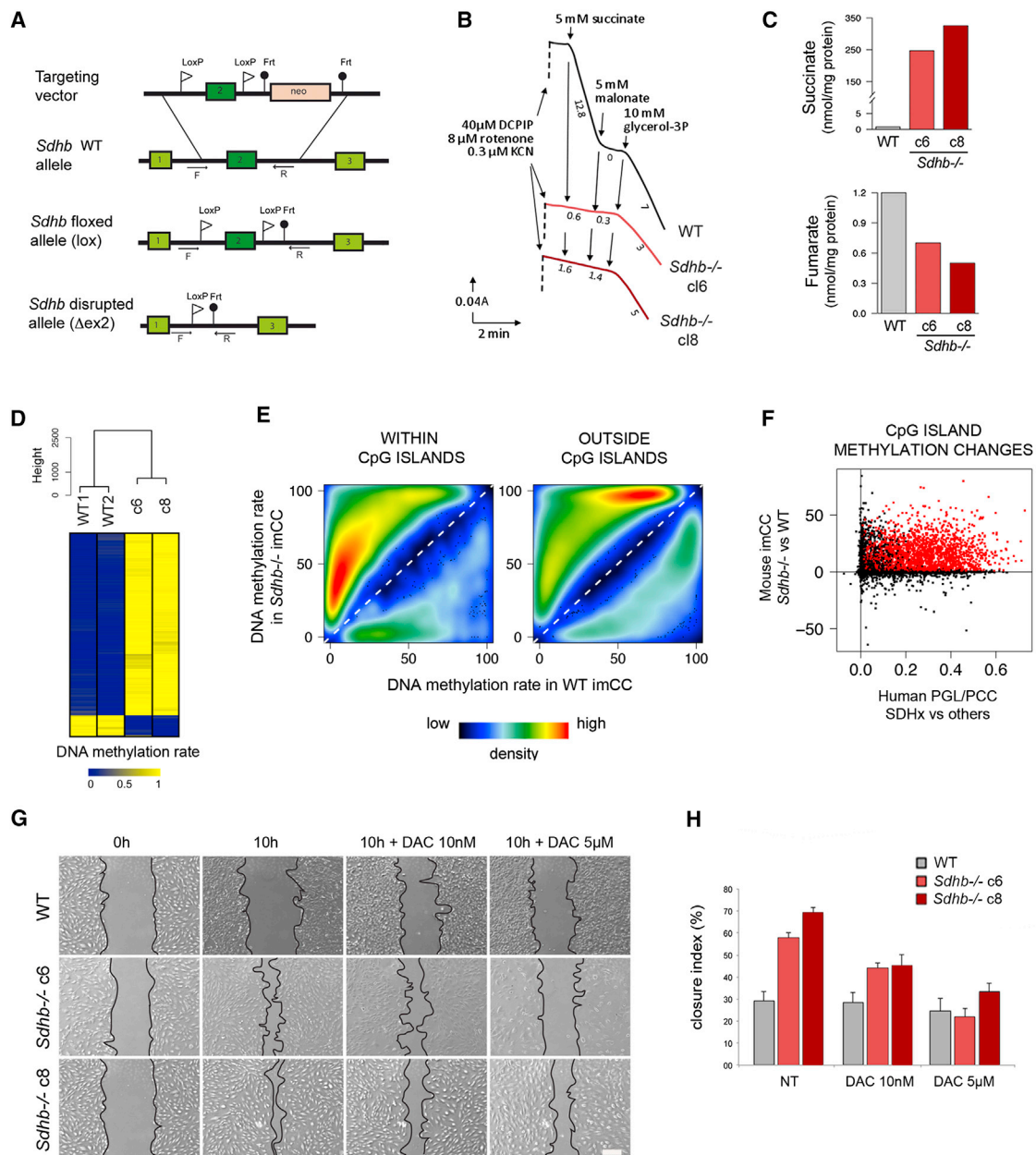


Figure 2. Generation and Characterization of *Sdhb*-Deficient Mouse Chromaffin Cells

(A) Strategy used for the generation of *Sdhb* knockout in mouse. The targeting vector comprises mouse *Sdhb* exon 2 locus flanked with LoxP sites and followed by a Neomycin (neo) resistance cassette flanked with Frt sites, which is removed after Flip-mediated recombination between the Frt sites. Primers for genotyping (arrows) are indicated below their target sequences.

(B) SDH activity in WT cells (black) measured by 2,6-dichlorophenol-indophenol reduction (in the presence of rotenone, inhibitor of complex I, and cyanide, inhibitor of complex IV) is triggered by succinate addition and subsequently inhibited by adding malonate, a specific SDH inhibitor. The subsequent addition of glycerol-3P triggers the activity of the mitochondrial glycerol-3P dehydrogenase in the same sample. Similar assays were carried out on *Sdhb*^{-/-} c6 (light red) and c8 (dark red) imCCs. Numbers along the traces are nmol/min per mg protein.

(C) Gas chromatography-mass spectrometry analysis of organic acids revealing a substantial accumulation of succinate and the depletion of fumarate in *Sdhb*^{-/-} cells relative to controls.

(D) Hierarchical clustering analysis of DNA methylation profiles from four mouse chromaffin cell samples, with (c6 and c8 clones) or without (WT1 and WT2) a knockout of *Sdhb* gene, analyzed by reduced representation bisulfite sequencing (RRBS). A heatmap indicates the degree of methylation of the 500 most variant CpG sites in each sample (dark blue, nonmethylated; yellow, methylated).

(E) Smoothed color density representation of the scatterplots representing DNA methylation changes between WT and *Sdhb*^{-/-} imCCs, within (left) and outside (right) CpG islands. Only CpG sites showing significantly different methylation rates between WT and *Sdhb*^{-/-} cells are represented.

(F) Comparison of DNA methylation changes in SDH-related human PGL/PCC and *Sdhb*^{-/-} imCCs. CpG island methylation rates were calculated for all mouse/human gene homologs represented in Illumina methylation arrays and RRBS data. Each point represents a gene, with the CpG island methylation difference (legend continued on next page)

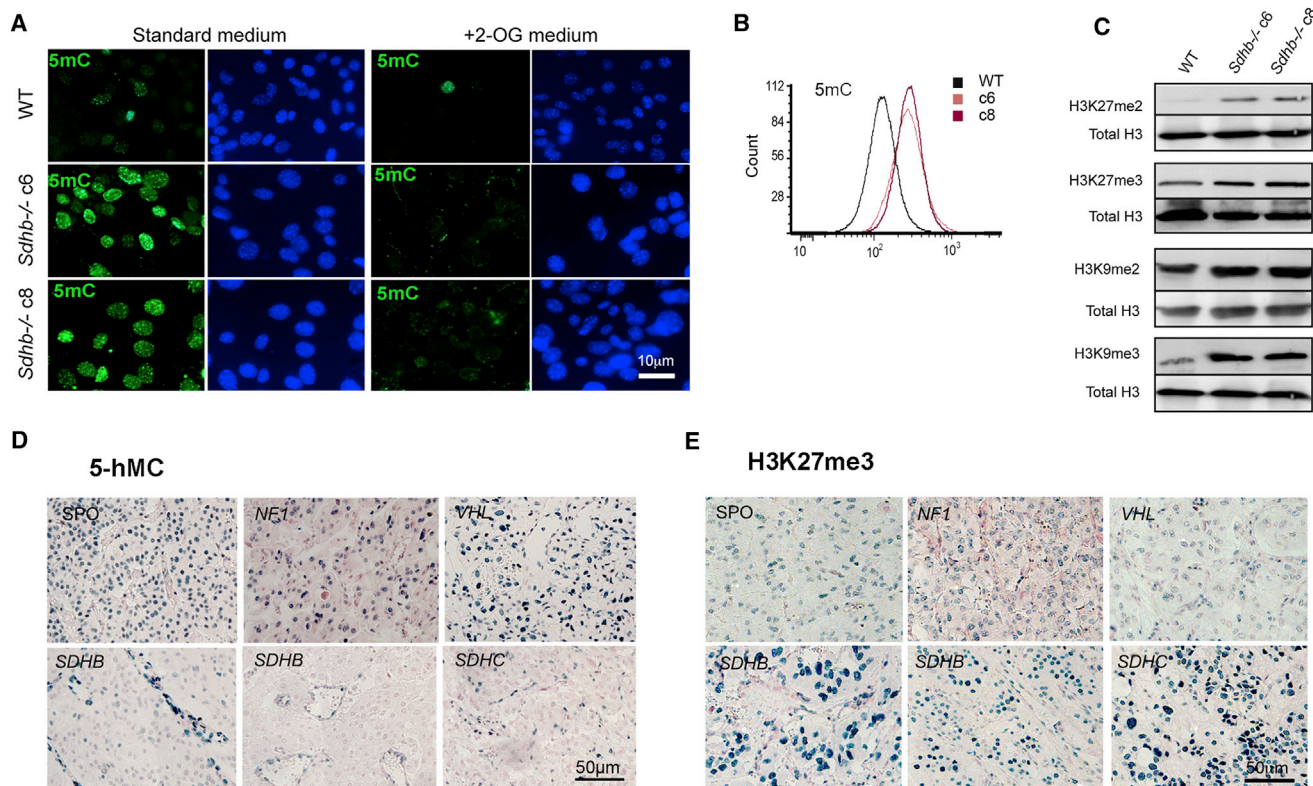


Figure 3. Functional Consequences of SDH Inactivation on Oxidative Demethylation

(A) Immunofluorescence showing a larger number of 5-mC-positive nuclei in *Sdhb*^{-/-} clones. Addition of 2-OG to the culture medium reversed this phenotype. Scale bar = 10 μm.

(B) Fluorescence-activated cell sorting (FACS) analysis also showed that *Sdhb* knockout leads to an increase in 5-mC in imCCs.

(C) Histone lysine methylation levels were assessed by western blotting with specific antibodies. Total H3 was used as a loading control.

(D) 5-hmC levels were studied on human PGL/PCC with various genetic backgrounds. Strong immunostaining of endothelial cell nuclei was observed in all tumor types, whereas the tumor cell staining was weaker in *SDHx*-mutated tumors. Scale bar = 50 μm.

(E) H3K27me3 levels are shown for tumors with various genetic backgrounds. Scale bar: 100 μm; SPO: sporadic tumor. See also Figure S3 and Tables S4 and S5. Scale bar = 50 μm.

(EMT) and of *DNAJA4*, recently shown to be a metastasis suppressor gene (Pancheva et al., 2012), may participate to the invasive phenotype of SDH-deficient cells. These findings indicate that methylome remodeling results in major transcriptional abnormalities in SDH-related tumors, directly associated with their phenotypic characteristics.

Exome Sequencing of the Only Hypermethylated Sample without *SDHx* Mutation Identified Inactivating Mutations in the *FH* Gene

A single tumor in our data set (HS_121) carried no *SDHx* mutation but displayed a hypermethylator phenotype (Figure 1B) as well as both low 5-hmC and high H3K9 and H3K27 methylation (Table S5). This tumor, which also belonged to the C1A (*SDH*-related) expression cluster was a local recurrence of an adrenal pheo-

chromocytoma resected from a 63-year-old female presenting a high level of urinary normetanephrines. To explain this “SDH-like” phenotype, we performed the whole-exome sequencing of tumor and matched blood DNA. We identified 21 nonsynonymous somatic mutations effecting exons or splice sites in this tumor, 16 of which were predicted to have functional consequences (Table S10). In particular, a somatic mutation was identified in exon 7 of the *fumarate hydratase* (*FH*) gene (c.1043G > C, p.Gly348Ala). This patient also carried a germline mutation in exon 3 of *FH* (c.349G > C, p.Ala117Pro). Both mutations were verified by Sanger sequencing (Figure 5A). The p.Ala117Pro mutation has been described previously in patients with multiple leiomyomatosis and/or renal cancer, displaying reduced *FH* activity. Interestingly, the patient’s clinical record revealed that she had benefited from a total hysterectomy at 35 years old for

between *Sdhb*^{-/-} and WT imCCs along the y axis and the CpG island methylation difference between *SDHx*-related PGL/PCC and other tumors along the x axis. Genes significantly hypermethylated in both human tumors and mouse chromaffin cells are indicated in red.

(G) Cell migration is shown in a wound scratch assay after 10 hr, in standard medium or following 72 hr of DAC treatment at 10 nM or 5 μM. Scale bar = 100 μm.

(H) Reversion of the migratory phenotype by decitabine treatment. Data are mean ± SEM.

See also Figure S2 and Table S3.

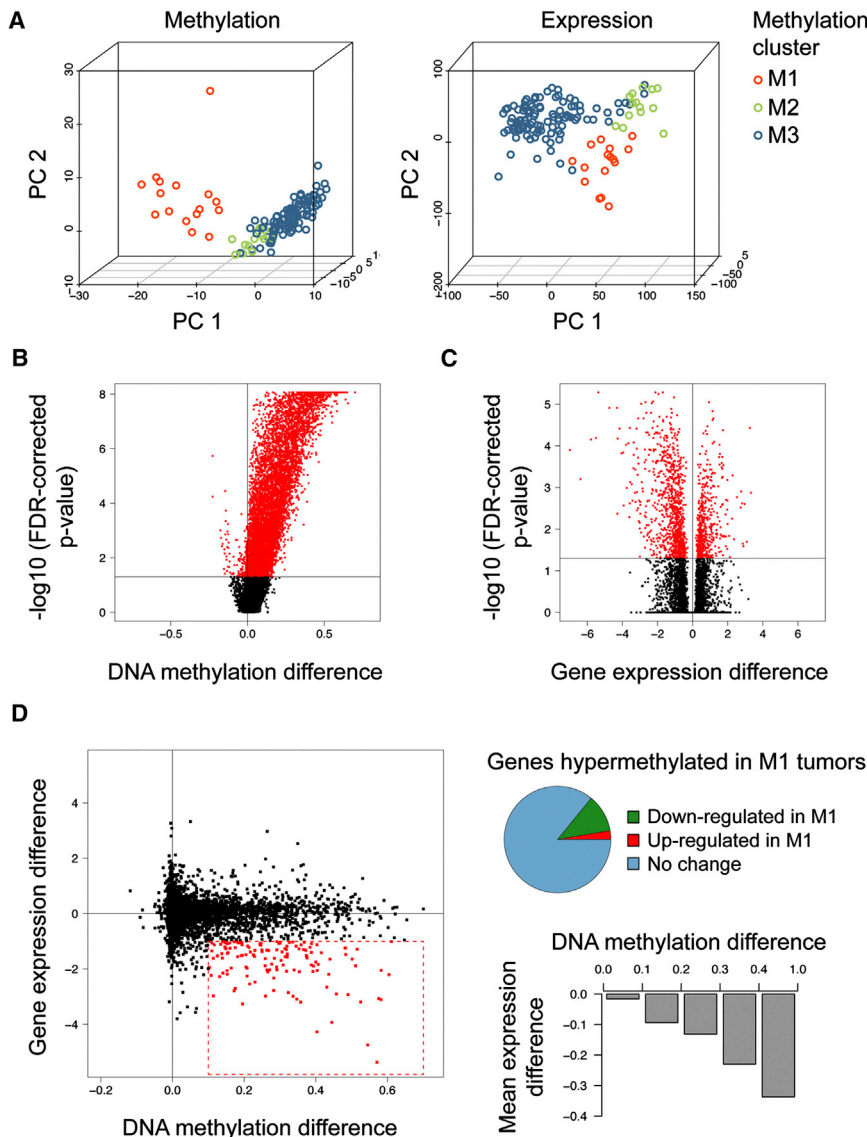


Figure 4. Transcriptional Changes Associated with the Hypermethylator Phenotype in SDH-Related PGL/PCC

(A) Principal component analysis of methylation (left) and expression (right) profiles of PGL/PCC. Tumor samples are plotted in three dimensions using their projections onto the first three principal components (PC). Methylation cluster membership is represented by a color code as described in the legend.

(B) Volcano plot analysis of differentially methylated CpG sites in tumors displaying a hyper-methylator phenotype (cluster M1). The beta value difference in DNA methylation between M1 and non-M1 tumors is plotted on the x axis, and the false-discovery rate (FDR)-adjusted significance is plotted on the y axis ($-\log_{10}$ scale). Red indicates probes differing significantly between groups.

(C) Volcano plot analysis of genes differentially expressed between M1 and non-M1 tumors.

(D) Integrated analysis of promoter DNA methylation and gene expression differences between M1 and non-M1 tumors. The starburst plot (left) represents the DNA methylation (x axis) and gene expression (y axis) differences between M1 and non-M1 tumors. Genes that are hypermethylated with a beta value difference >0.1 and have a more than 2-fold decrease in expression levels in M1 tumors are shown as red data points. The pie chart (top right) shows the proportion of hypermethylated genes (FDR adjusted $p < 0.05$ and beta value difference >0.1) that are significantly up- and downregulated in M1 tumors (gene expression difference >1 and <-1 , respectively). The histogram (bottom right) shows the mean difference in gene expression levels between M1 and non-M1 tumors as a function of the amplitude of DNA methylation beta value differences. See also Figure S4 and Tables S6, S7, S8, and S9.

hemorrhagic fibromas. The p.Gly348Ala mutation has not been described previously and was predicted to be “probably damaging” by Polyphen software. Tumor HS_121 displayed a selective loss of FH activity (Figure 5B), accompanied by an increase in fumarate concentrations (Figure 5C). Fumarate, like succinate, is a competitive inhibitor of 2-OG-dependent dioxygenases (Xiao et al., 2012), so these findings strongly suggest that FH inactivation causes PGL/PCC by establishing a hyper-methylator phenotype.

DNA Hypermethylation and Associated Gene Silencing Are Stronger in *SDHB*-Mutated Tumors

SDHB-mutated PGL/PCC tend to be more malignant than tumors harboring mutations in other SDH subunits (Amar et al., 2005; Pasini and Stratakis, 2009). To determine whether this aggressive behavior is associated with a more severe hyper-methylator phenotype, we calculated the mean methylation level across all the CpG sites significantly hypermethylated in

in M2 and M3 tumors (Figure 6A); but, *SDHB*-mutated tumors displayed stronger hypermethylation than other M1 tumors (1 *SDHA*-, 1 *SDHC*-, 3 *SDHD*-, and 1 *FH*-mutated tumors) ($p = 0.0071$). We examined the transcriptional consequences of these differences by calculating the mean expression level of the 191 genes significantly hypermethylated and downregulated in M1 tumors (Table S8). Although these genes were downregulated in all M1 tumors as compared to M2 and M3 tumors, their expression was significantly lower in *SDHB*-mutated tumors than in other M1 tumors ($p = 0.0055$, Figure 6B). The levels of hypermethylation and downregulation of target genes were highly correlated (Pearson's $r = -0.93$, $p = 7.0 \times 10^{-59}$; Figure 6C), suggesting that DNA methylation finely regulates the expression of these genes in PGL/PCC. These findings support the idea that a stronger hyper-methylator phenotype, associated with a stronger downregulation of target genes, may participate to the metastatic phenotype of *SDHB*-mutated tumors.

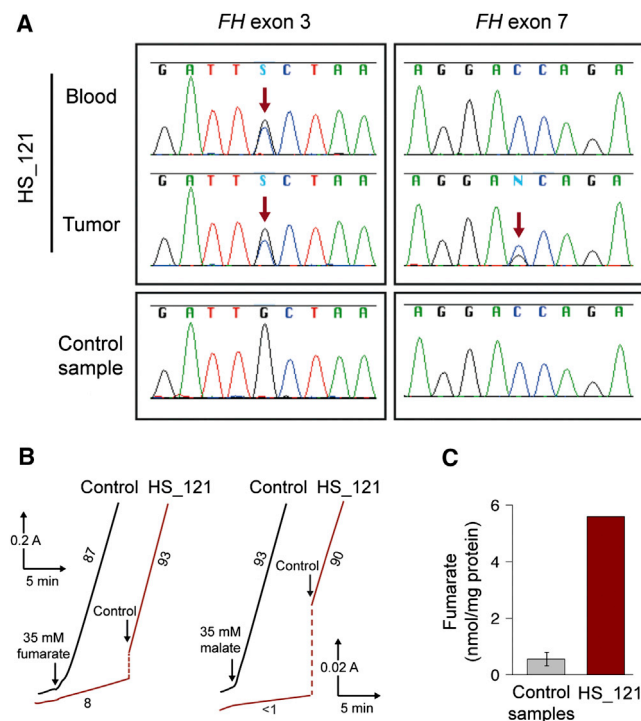


Figure 5. Inactivating *FH* Mutations in the Only Hypermethylated Tumor without *SDHx* Mutation

(A) Sanger sequencing of *FH* gene in DNA extracted from peripheral blood and frozen tumor from patient HS_121 identifies a heterozygous germline mutation (c.349G > C, p.Ala117Pro) in exon 3 and a heterozygous somatic mutation (c.1043G > C, p.Gly348Ala) in exon 7.

(B) Enzymatic activity, assayed spectrophotometrically for the forward (fumarate to malate, left traces) and backward (malate to fumarate, right traces) directions, reveals a severe fumarase deficiency in HS_121 (red) relative to control (black) PGL/PCC samples.

(C) Loss of fumarase activity is associated with a higher fumarate concentration in tumor HS_121 than that in control PGL/PCC (n = 6). For controls, data are mean \pm SEM. See also Table S10.

Comparison with the CpG Island Methylator Phenotypes Identified in Colorectal Cancer and Glioblastoma

We investigated whether the hypermethylator phenotype identified in PGL/PCC showed similarities with previously described CIMP phenotypes. We analyzed publicly available data concerning colorectal cancers (Hinoue et al., 2012) and glioblastomas (Noushmehr et al., 2010), obtained with the same Illumina Infinium HM27 methylation array used in this study. For each CpG site, we calculated the mean beta value difference between tumors with and without a hypermethylator phenotype (CIMP-high in colorectal cancer, G-CIMP in glioblastoma). Although we found a significant overlap between hypermethylated loci in the three cancers, the patterns of hypermethylation were particularly similar between PGL/PCC and G-CIMP glioblastomas (Figure 7A). Of 2,241 CpG sites hypermethylated in PGL/PCC of the M1 subgroup (mean beta value difference >0.2 as compared to non-M1 tumors), 847 (38%) were also hypermethylated in G-CIMP glioblastomas, whereas only 279 (12%) were hypermethylated in CIMP-high-colorectal tumors (Figure 7B). Gene set enrichment analysis (GSEA) confirmed that the set of genes hypermethylated in PGL/PCC was more significantly

enriched in genes hypermethylated in G-CIMP glioblastomas (enrichment score = 0.75) than genes hypermethylated in CIMP-high-colorectal cancers (enrichment score = 0.47) (Figure S5). Seventeen of the 191 genes epigenetically silenced in PGL/PCC were significantly hypermethylated and downregulated in glioblastoma (including *PNMT* and *RBP1*); 21 were hypermethylated but without significant downregulation (like *KRT19*); and 119, like *NPY*, were not found to be hypermethylated in glioblastoma (Table S8). The similarity between PGL/PCC and glioblastoma hypermethylator phenotypes may reflect the preferential activities of the 2-OG-dependent demethylases inhibited in these two cancers.

DISCUSSION

Metabolic reprogramming in cancer has long been regarded as an indirect response to cell proliferation, but recent evidence has shown that metabolites themselves can be oncogenic by altering several cellular processes (Ward and Thompson, 2012). The oncometabolite 2-HG, produced by mutated IDH enzymes, establishes the G-CIMP phenotype in glioma by inhibiting DNA and histone demethylases (Xu et al., 2011). Succinate and fumarate can activate the oncogenic HIF pathway by inhibiting HIF prolyl-hydroxylases (Brière et al., 2005; Selak et al., 2005). Here, we demonstrate that succinate accumulation in SDH-deficient PGL/PCC establishes a hypermethylator phenotype, by inhibiting 2-OG-dependent oxidative demethylation. Besides, we describe a specific model of SDH-related PGL/PCC, generated by knocking out *Sdhb* gene in chromaffin cells. In the past, the lack of an appropriate cellular model has opposed severe limitations to the understanding of SDH-related oncogenesis. Our model displays a complete inactivation of SDH activity, which cannot be achieved by siRNA-mediated gene silencing, and will be a crucial tool for deciphering the consequences of SDH inactivation in these cells. Our study also led to the identification of a case of *FH* germline mutation in an apparently sporadic PCC displaying a hypermethylator phenotype. *FH* mutations are known to predispose to hereditary leiomyomatosis and renal cell cancer (Tomlinson et al., 2002) but have never been described in PGL/PCC. Altogether, these findings shed light on a novel pathway explaining the tumor-suppressive role of SDH and FH and, echoing the role of *IDH* mutation in glioma, emphasize the link between TCA cycle dysfunction and epigenomic alterations in cancer. Gastrointestinal stromal tumors, renal cancer, and leiomyomas harboring *SDH* or *FH* mutations may also display epigenetic reprogramming, which should be assessed in future DNA methylation studies.

Many cancer-specific hypermethylation events occur in promoter regions of genes that are not normally expressed and are therefore not affected by DNA methylation changes (Widschwendter et al., 2007). To distinguish DNA methylation events of potential functional significance (“driver events”) from these “passenger events”, we integrated the DNA methylation data with gene expression profiles of the same tumors. Only 11.5% of genes with significant promoter hypermethylation in PGL/PCC of the M1 subgroup were underexpressed in these tumors. This is consistent with previous reports in colorectal cancer (7.3%; Hinoue et al., 2012) and glioblastoma (17%; Noushmehr

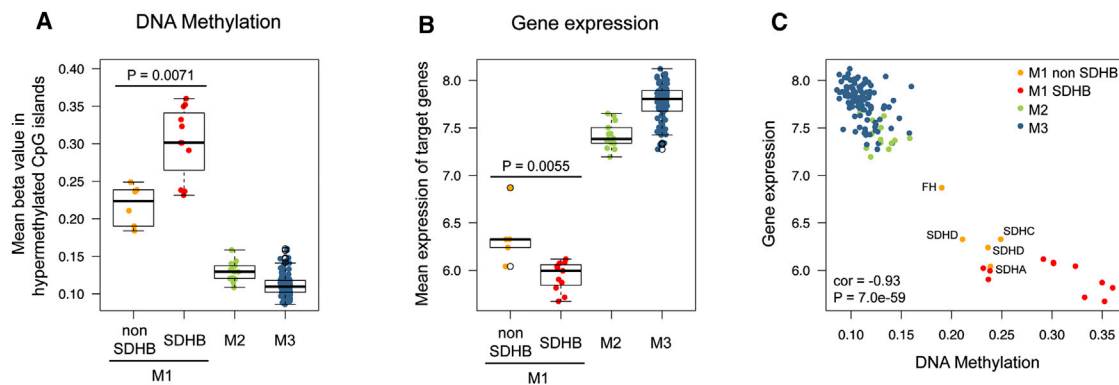


Figure 6. The Hypermethylator Phenotype Is Particularly Severe in *SDHB*-Mutated Tumors

(A) Mean methylation of all CpG island probes significantly hypermethylated in M1 tumors, according to tumor subgroup. Box-and-whisker plots show the distribution of mean beta values relative to each DNA methylation subgroup. M1 tumors are separated into *SDHB*-mutated and *SDHB*-wild-type tumors. The middle bar, median; box, interquartile range; bars extend to 1.5 times the interquartile range.

(B) Mean expression of genes significantly hypermethylated and downregulated in M1 tumors, according to tumor subgroup.

(C) Distribution of mean expression levels of target genes relative to the mean methylation levels of CpG sites hypermethylated in M1 tumors. Tumor subgroups are represented with a color code, and the mutations of non-*SDHB*-mutated M1 tumors are indicated next to each dot.

et al., 2010). Thus, most hypermethylated CpG sites appear to be silent consequences of the inhibition of DNA demethylases, with no evident functional impact. We were however able to show an overall correlation between the level of hypermethylation and downregulation of gene expression. In particular, we identified 191 genes that showed significant hypermethylation and downregulation in M1 tumors and whose expression was closely correlated with the degree of DNA methylation.

Two of the genes showing the strongest evidence for epigenetic silencing in hypermethylated PGL/PCC are, respectively, involved in the differentiation of chromaffin cells (*PNMT*; Eisenhofer et al., 2011) and the epithelial-to-mesenchymal transition (*KRT19*; Moreno-Bueno et al., 2006), which was recently identified as the first mechanistic clue to explain the particularly invasive phenotype of *SDHB*-related tumors (Loriot et al., 2012). The *PNMT* gene encodes the phenyl-ethanolamine-N-methyltransferase, a key enzyme of chromaffin cell metabolism, which catalyzes the conversion of noradrenaline to adrenaline. Reduced *PNMT* expression has been reported in SDH-related tumors, leading to an immature catecholamine secretory profile with predominant secretion of noradrenaline or dopamine (Burnichon et al., 2012b; Eisenhofer et al., 2001). Our findings reveal that *PNMT* is hypermethylated in SDH-related tumors, together with four other genes implicated in catecholamine metabolism (*DRD2*, *SULT1A1*, *SLC6A2*, and *NPY*). Epigenetic regulation is thus a previously unsuspected mechanism explaining the dedifferentiated phenotype of this subgroup of PGL/PCC. Another target of the PGL/PCC hypermethylator phenotype, *RBP1*, is also epigenetically silenced in G-CIMP gliomas (Noushmehr et al., 2010) and several cancer cell lines and primary tumors (Esteller et al., 2002). *RBP1* is involved in retinoic acid signaling, leading to loss of cell differentiation and tumor progression (Farias et al., 2005) and may thus have a tumor-suppressive role in PGL/PCC. Studies aimed at elucidating the functional consequences of epigenetic gene silencing will undoubtedly improve our understanding of the role of DNA hypermethylation in PGL/PCC tumorigenesis.

SDH- and VHL-related tumors were previously shown to have similar gene expression features, like the activation of hypoxia-related genes (Dahia et al., 2005). In the COMETE cohort, we showed that, although close, these tumors were classified in two separate gene expression clusters (C1A and C1B) (Burnichon et al., 2011). Here, we found that 150 out of 344 genes (44%) significantly downregulated in SDH- as compared to VHL-tumors were hypermethylated (data not shown). Epigenetic remodeling thus explains a significant part of transcriptional differences between SDH- and VHL-related tumors.

SDHB mutations confer a much worse prognosis than mutations in other *SDHx* genes (Amar et al., 2007). No mechanism has been proposed to explain these differences. We found that although all *SDHx*-mutated tumors displayed a hypermethylator phenotype, the level of hypermethylation was significantly higher, and the expression of target genes was significantly lower in *SDHB*-mutated tumors. As target genes include genes implicated in neuroendocrine differentiation and epithelial-to-mesenchymal transition (EMT), this may explain the particular malignancy of *SDHB*-mutated tumors. *SDHB* encodes a catalytic subunit of SDH (Rutter et al., 2010). We hypothesize that SDH inactivation may be more complete in *SDHB*-mutated tumors than in tumors harboring mutations in other subunits, leading to a higher succinate accumulation and hence to a stronger inhibition of 2-OG-dependent demethylation. However, we were not able to detect significant differences in succinate concentrations between *SDHB*-mutated and other SDH-related tumors. Future studies will be needed to dissect the functional impact of mutations affecting different SDH subunits.

There have recently been several promising findings for epigenetic cancer therapy. Notably, Tsai et al. (2012) demonstrated that low doses of the DNA demethylating agents, DAC and azacitidine, had durable antitumor effects on hematological and epithelial tumor cells. Thus, low doses may help avoid the extreme toxicities of these agents at high dose that have prevented the investigation of the true clinical responses. We show

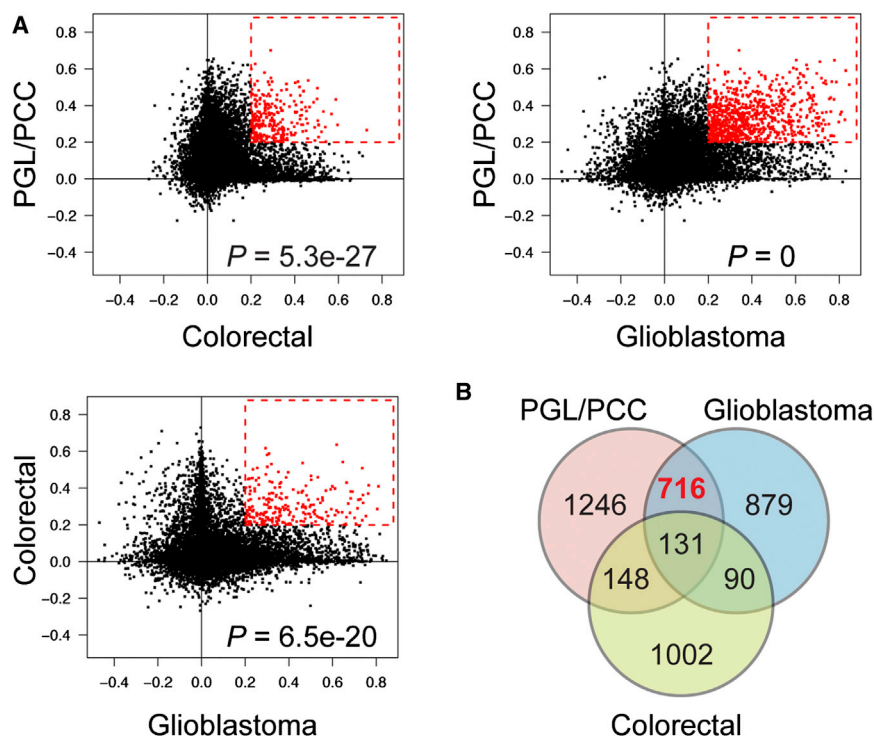


Figure 7. Comparison of Hypermethylator Phenotypes in PGL/PCC, Colorectal Cancer, and Glioblastoma

(A) Correlation between CIMP-specific hypermethylation patterns in the three cancers. The mean beta value difference between CIMP and non-CIMP tumors was calculated for all CpG sites in each cancer type. Each scatterplot represents the correlation of beta value differences between two cancers. Red dots indicate CpG sites hypermethylated in the CIMP subgroups of both cancers (beta value difference >0.2 between CIMP and non-CIMP tumors).

(B) Venn diagram showing hypermethylated loci shared by the PGL/PCC hypermethylator phenotype, the colorectal cancer CIMP-high phenotype, and the glioblastoma G-CIMP phenotype. See also Figure S5.

that the increased migratory capacities of *Sdhb*^{-/-} mouse chromaffin cells are repressed by transient DAC treatment, even at a 10 nM concentration, which led to minor cytotoxicity. The precise molecular changes associated with these treatments will have to be deciphered in future studies, both in vitro and in vivo. In view of these findings, the reversal of promoter DNA hypermethylation and associated gene silencing may rise as an attractive alternative approach to surgery for *SDHx*- and *FH*-mutated PGL/PCC. NPY, which shows the strongest transcriptional silencing in M1 tumors, may be a good marker. NPY levels were shown to be increased in the plasma and tumors of patients with PCC and to be significantly lower in extra-adrenal tumors (deS Senanayake et al., 1995). A comprehensive study of candidate markers in a large independent cohort will be useful to determine the best marker of this aggressive subgroup.

In summary, our analysis indicates that PGL/PCC can be classified into three distinct subgroups according to genome-scale DNA methylation changes. The identification of a hypermethylator phenotype in *SDHx*- and *FH*-mutated tumors helps in explaining both the tumor-suppressive role of these genes and some of the phenotypic characteristics of these tumors. The malignancy of *SDHB*-mutated PGL/PCC may be due to a severe epigenetic silencing of genes involved in cell differentiation and EMT. These findings have clinical implications for PGL/PCC diagnosis and may lead to targeted epigenetic treatment for patients with TCA cycle alterations.

EXPERIMENTAL PROCEDURES

Collection and Processing of PGL/PCC and Normal Tissue Samples

A total of 145 tumor samples from 145 different patients recruited in the COMETE network from 1993 to 2008 were included in the study. Ethical approval for the study was obtained from the institutional review board

QIAamp DNA Mini Kit or an AllPrep Kit (QIAGEN, Hilden, Germany). For details, see the Supplemental Experimental Procedures.

DNA Methylation Arrays

Whole-genome DNA methylation was analyzed in 145 PGL or PCC and three normal adrenal medulla samples using the Illumina Infinium HumanMethylation27 assay (Bibikova et al., 2009). Twenty-four samples were later reanalyzed using the more comprehensive Illumina Infinium HumanMethylation450 Beadchips. Microarray experiments were performed by Integrigen SA (Evry, France). In brief, genomic DNA was bisulfite-converted using the EZ-96 DNA Methylation Kit (Zymo Research, Irvine, CA, USA), whole-genome amplified, enzymatically fragmented, and hybridized to the BeadChip arrays in accordance with the manufacturer's instructions. The beta value DNA methylation scores for each locus were extracted together with detection p values from Illumina GenomeStudio software. As described elsewhere (Hinoue et al., 2012), we replaced data points with a detection p value >0.05 by "NA" values, and we masked data points as "NA" for 4,484 probes that contain single-nucleotide polymorphisms or overlap with a repetitive element that are not uniquely aligned to the human genome (NCBI build 36/Hg18) or that overlap with regions of insertions and deletions in the human genome. Probes were considered to be in a promoter CpG island if they were located within a CpG island (UCSC database) and less than 1,500 bp away from a transcription start site.

DNA Methylation-Based Classification of Pheochromocytomas and Paragangliomas

We used consensus clustering (Monti et al., 2003) to identify PGL/PCC subgroups on the basis of their DNA methylation profiles. We selected the 10% most variant probes ($n = 2,152$) among those that did not contain any «NA»-masked data point. We then established consensus partitions of the data set in K clusters (for $K = 2, 3, \dots, 8$), based on 1,000 resampling iterations of hierarchical clustering, with Pearson's dissimilarity as the distance metric and Ward's method for linkage analysis. We used the cumulative distribution functions (CDF) of the consensus matrices to determine the optimal number of clusters, considering both the shape of the functions and the area under the CDF curves (Figure S1). The Bioconductor ConsensusClusterPlus package was used for consensus clustering analysis.

Reduced Representation Bisulphite Sequencing Analysis of Mouse Chromaffin Cells

RRBS was performed by Integragen SA (Evry, France), as described elsewhere (Gu et al., 2011; Smallwood and Kelsey, 2012). In brief, 300 ng of mouse genomic DNA were digested with 14 units of MspI (NEB). After end-repair, A-tailing, and ligation to methylated Illumina adapters, the library fragments of 40–220 bp were gel isolated, subjected to a double bisulfite conversion with the EpiTect Bisulfite kit from QIAGEN, PCR amplified, and sequenced on an Illumina HiSeq2000 sequencer as paired-end 75 bp reads. We used Trim Galore! (http://www.bioinformatics.babraham.ac.uk/projects/trim_galore) to filter out the adaptor sequences. Bisulfite mapping and methylation calling were performed in a single step using the bismark software (Krueger and Andrews, 2011). Only reads uniquely aligned to the mm9 assembly of the mouse genome were retained, and we required a coverage of at least ten reads to call methylation score for a CpG site. We downloaded the list of Mouse CpG islands from the UCSC genome browser, and we inferred a DNA methylation rate to each CpG island with more than ten individual CpG measurements and more than 100 total reads. To identify differentially methylated CpG sites or CpG islands, we compared the number of methylated and unmethylated observations in WT and *Sdhb*^{−/−} cells using Fisher's exact test. CpG islands with an FDR-adjusted p value <0.05 and absolute methylation difference >5% were considered differentially methylated. Human and mouse orthologs were downloaded from the Mouse Genome Database (Eppig et al., 2012).

Generation of *Sdhb*^{−/−} Immortalized Mouse Chromaffin Cells

Sdhb-floxed mice were generated at the Mouse Clinical Institute (Illkirch, France). A targeting vector containing *Sdhb* exon 2 flanked by LoxP sites followed by a neomycin (neo) selection cassette flanked by Frt sites (Figure 2A) was introduced into P1 (129 S2/SvPas) ES cells by electroporation. Two positive embryonic stem clones were injected into C57BL/6J blastocysts, and the resulting male chimeras gave germline transmission. These mice were mated to Flipase-expressing mice to delete the *Neo* cassette. *Sdhb*^{+/lox} mice were intercrossed to obtain *Sdhb*^{lox/lox} mice, and mouse chromaffin cells (mCCs) were isolated from the adrenal medulla of these *Sdhb*^{lox/lox} as described elsewhere (Kolski-Andreaco et al., 2007). All studies were performed in accordance with the relevant guidelines of the French Ministry of Agriculture (Authorization Executive Order A751532) for scientific experimentation on animals, European Communities Council Directive, and international ethical standards. Cells were cultured at 37°C, under 5% CO₂ in a standard medium containing Dulbecco's modified Eagle's medium with glutamine and a high glucose concentration (DMEM glutaMAX, GIBCO, Life Technologies, Saint Aubin, France) supplemented with 10% fetal bovine serum (GIBCO) and 1% penicillin-streptomycin (GIBCO). The cultures remained quiescent for 6 months, after which some started to grow spontaneously from mCCs clusters. These immortalized cells were isolated and infected with 10⁷ plaque-forming units (pfu)/ml of an adenovirus expressing Cre-recombinase (Ad5CMV-Cre, Cell BioLabs, San Diego). A clonal approach by limiting dilution cloning assay was used to obtain homogeneous *Sdhb*^{−/−} immortalized mCCs clones (imCC clones 6 and 8). *Sdhb*^{−/−} and *Sdhb*^{lox/lox} (referred to as WT) imCCs were maintained in standard medium with or without 2.5 mM dimethyl 2-oxoglutarate (Sigma-Aldrich, St. Louis).

ACCESSION NUMBERS

Methylation array data from the 148 human samples and RRBS data from the four mouse cell lines analyzed in this study have been deposited in NCBI's Gene Expression Omnibus (<http://www.ncbi.nlm.nih.gov/geo>) and are accessible through the GEO series accession number GSE43298.

SUPPLEMENTAL INFORMATION

Supplemental Information includes ten tables, five figures, and Supplemental Experimental Procedures and can be found with this article online at <http://dx.doi.org/10.1016/j.ccr.2013.04.018>.

ACKNOWLEDGMENTS

This work is part of the "Cartes d'Identité des Tumeurs (CIT) program" funded and developed by the "Ligue Nationale contre le Cancer" (<http://cit.ligue-cancer.net>).

We express our gratitude to Profs. Pierre-François Plouin and Xavier Bertagna for making this work possible by creating the COMETE Network 20 years ago. We are grateful to Prof. X. Jeunemaitre for helpful discussions and continual support. We thank Dr. Juliette Hadchouel for her technical advice and the Mouse Clinical Institute for generating the *Sdhb*^{+/lox} mouse. We thank Jacqueline Godet and Jacqueline Metral for their strong support within the CIT program. We also thank Nabila Elarouci, Dr. Rossella Libé, Prof. Cécile Badoual, and Dr. Frédérique Tissier for their help, all members of the HEGP Genetics department, and Catherine Tritscher for technical assistance. We also thank Mélanie Letexier and Maud Vandpeene from IntegraGen for their efficacy in generating methylation data. The text was edited by Alex Edelman and associates. The work leading to these results has received funding from the Agence Nationale de la Recherche (ANR 08 GENOPATH 029 MitOxy and ANR-2011-JCJC-00701 MODEOMAPP), the GtS-Institut des Maladies Rares, and the Programme Hospitalier de Recherche Clinique grant COMETE 3 (AOM 06 179). The work leading to these results has received funding from the European Union Seventh Framework Programme (FP7/2007-2013) under grant agreement number 259735.

Received: October 13, 2012

Revised: January 29, 2013

Accepted: April 20, 2013

Published: May 23, 2013

REFERENCES

- Amar, L., Bertherat, J., Baudin, E., Aizenberg, C., Bressac-de Paillerets, B., Chabre, O., Chamontin, B., Delemer, B., Giraud, S., Murat, A., et al. (2005). Genetic testing in pheochromocytoma or functional paraganglioma. *J. Clin. Oncol.* 23, 8812–8818.
- Amar, L., Baudin, E., Burnichon, N., Peyrard, S., Silvera, S., Bertherat, J., Bertagna, X., Schlumberger, M., Jeunemaitre, X., Gimenez-Roqueplo, A.P., and Plouin, P.F. (2007). Succinate dehydrogenase B gene mutations predict survival in patients with malignant pheochromocytomas or paragangliomas. *J. Clin. Endocrinol. Metab.* 92, 3822–3828.
- Baysal, B.E., Ferrell, R.E., Willett-Brozick, J.E., Lawrence, E.C., Myssiorek, D., Bosch, A., van der Mey, A., Taschner, P.E., Rubinstein, W.S., Myers, E.N., et al. (2000). Mutations in SDHD, a mitochondrial complex II gene, in hereditary paraganglioma. *Science* 287, 848–851.
- Bibikova, M., Le, J., Barnes, B., Saedinia-Melnyk, S., Zhou, L., Shen, R., and Gunderson, K.L. (2009). Genome-wide DNA methylation profiling using Infinium® assay. *Epigenomics* 1, 177–200.
- Brière, J.J., Favier, J., Bénit, P., El Ghouzzi, V., Lorenzato, A., Rabier, D., Di Renzo, M.F., Gimenez-Roqueplo, A.P., and Rustin, P. (2005). Mitochondrial succinate is instrumental for HIF1α nuclear translocation in SDHA-mutant fibroblasts under normoxic conditions. *Hum. Mol. Genet.* 14, 3263–3269.
- Burnichon, N., Vescovo, L., Amar, L., Libé, R., de Reynies, A., Venisse, A., Jouanno, E., Laurendeau, I., Parfait, B., Bertherat, J., et al. (2011). Integrative genomic analysis reveals somatic mutations in pheochromocytoma and paraganglioma. *Hum. Mol. Genet.* 20, 3974–3985.
- Burnichon, N., Buffet, A., Parfait, B., Letouzé, E., Laurendeau, I., Lorient, C., Pasmant, E., Abermil, N., Valeyrie-Allanore, L., Bertherat, J., et al. (2012a). Somatic NF1 inactivation is a frequent event in sporadic pheochromocytoma. *Hum. Mol. Genet.* 27, 5397–5405.
- Burnichon, N., Cascón, A., Schiavi, F., Morales, N.P., Comino-Méndez, I., Abermil, N., Inglada-Pérez, L., de Cubas, A.A., Amar, L., Barontini, M., et al. (2012b). MAX mutations cause hereditary and sporadic pheochromocytoma and paraganglioma. *Clin. Cancer Res.* 18, 2828–2837.
- Cedar, H., and Bergman, Y. (2009). Linking DNA methylation and histone modification: patterns and paradigms. *Nat. Rev. Genet.* 10, 295–304.

- Dahia, P.L., Ross, K.N., Wright, M.E., Hayashida, C.Y., Santagata, S., Barontini, M., Kung, A.L., Sanso, G., Powers, J.F., Tischler, A.S., et al. (2005). A HIF1 α regulatory loop links hypoxia and mitochondrial signals in pheochromocytomas. *PLoS Genet.* 1, 72–80.
- deS Senanayake, P., Denker, J., Bravo, E.L., and Graham, R.M. (1995). Production, characterization, and expression of neuropeptide Y by human pheochromocytoma. *J. Clin. Invest.* 96, 2503–2509.
- Eisenhofer, G., Walthers, M.M., Huynh, T.T., Li, S.T., Bornstein, S.R., Vortmeyer, A., Mannelli, M., Goldstein, D.S., Linehan, W.M., Lenders, J.W., and Pacak, K. (2001). Pheochromocytomas in von Hippel-Lindau syndrome and multiple endocrine neoplasia type 2 display distinct biochemical and clinical phenotypes. *J. Clin. Endocrinol. Metab.* 86, 1999–2008.
- Eisenhofer, G., Pacak, K., Huynh, T.T., Qin, N., Bratslavsky, G., Linehan, W.M., Mannelli, M., Friberg, P., Grebe, S.K., Timmers, H.J., et al. (2011). Catecholamine metabolomic and secretory phenotypes in pheochromocytoma. *Endocr. Relat. Cancer* 18, 97–111.
- Eppig, J.T., Blake, J.A., Bult, C.J., Kadin, J.A., and Richardson, J.E.; Mouse Genome Database Group. (2012). The Mouse Genome Database (MGD): comprehensive resource for genetics and genomics of the laboratory mouse. *Nucleic Acids Res.* 40(Database issue), D881–D886.
- Esteller, M., Guo, M., Moreno, V., Peinado, M.A., Capella, G., Galm, O., Baylin, S.B., and Herman, J.G. (2002). Hypermethylation-associated inactivation of the cellular retinol-binding-protein 1 gene in human cancer. *Cancer Res.* 62, 5902–5905.
- Farias, E.F., Ong, D.E., Ghyselinck, N.B., Nakajo, S., Kuppumbatti, Y.S., and Mira y Lopez, R. (2005). Cellular retinol-binding protein I, a regulator of breast epithelial retinoic acid receptor activity, cell differentiation, and tumorigenicity. *J. Natl. Cancer Inst.* 97, 21–29.
- Favier, J., Brière, J.J., Burnichon, N., Rivière, J., Vescovo, L., Benit, P., Giscos-Douriez, I., De Reyniès, A., Bertherat, J., Badoual, C., et al. (2009). The Warburg effect is genetically determined in inherited pheochromocytomas. *PLoS ONE* 4, e7094.
- Favier, J., Buffet, A., and Gimenez-Roqueplo, A.P. (2012). HIF2A mutations in paraganglioma with polycythemia. *N. Engl. J. Med.* 367, 2161, author reply 2161–2162.
- Feinberg, A.P., and Vogelstein, B. (1983). Hypomethylation distinguishes genes of some human cancers from their normal counterparts. *Nature* 307, 89–92.
- Geli, J., Kiss, N., Karimi, M., Lee, J.J., Bäckdahl, M., Ekström, T.J., and Larsson, C. (2008). Global and regional CpG methylation in pheochromocytomas and abdominal paragangliomas: association to malignant behavior. *Clin. Cancer Res.* 14, 2551–2559.
- Gimenez-Roqueplo, A.P., Dahia, P.L., and Robledo, M. (2012). An update on the genetics of paraganglioma, pheochromocytoma, and associated hereditary syndromes. *Horm. Metab. Res.* 44, 328–333.
- Gimenez-Roqueplo, A.P., Favier, J., Rustin, P., Mourad, J.J., Plouin, P.F., Corvol, P., Rötig, A., and Jeunemaitre, X. (2001). The R22X mutation of the SDHD gene in hereditary paraganglioma abolishes the enzymatic activity of complex II in the mitochondrial respiratory chain and activates the hypoxia pathway. *Am. J. Hum. Genet.* 69, 1186–1197.
- Gimenez-Roqueplo, A.P., Favier, J., Rustin, P., Rieubland, C., Crespin, M., Nau, V., Khau Van Kien, P., Corvol, P., Plouin, P.F., and Jeunemaitre, X.; COMETE Network. (2003). Mutations in the SDHB gene are associated with extra-adrenal and/or malignant pheochromocytomas. *Cancer Res.* 63, 5615–5621.
- Gu, H., Smith, Z.D., Bock, C., Boyle, P., Gnirke, A., and Meissner, A. (2011). Preparation of reduced representation bisulfite sequencing libraries for genome-scale DNA methylation profiling. *Nat. Protoc.* 6, 468–481.
- Hanahan, D., and Weinberg, R.A. (2011). Hallmarks of cancer: the next generation. *Cell* 144, 646–674.
- Hinoue, T., Weisenberger, D.J., Lange, C.P., Shen, H., Byun, H.M., Van Den Berg, D., Malik, S., Pan, F., Noushmehr, H., van Dijk, C.M., et al. (2012). Genome-scale analysis of aberrant DNA methylation in colorectal cancer. *Genome Res.* 22, 271–282.
- Houseman, E.A., Christensen, B.C., Yeh, R.F., Marsit, C.J., Karagas, M.R., Wrensch, M., Nelson, H.H., Wiemels, J., Zheng, S., Wiencke, J.K., and Kelsey, K.T. (2008). Model-based clustering of DNA methylation array data: a recursive-partitioning algorithm for high-dimensional data arising as a mixture of beta distributions. *BMC Bioinformatics* 9, 365.
- Janeway, K.A., Kim, S.Y., Lodish, M., Nosé, J., Rustin, P., Gaal, J., Dahia, P.L., Liegl, B., Ball, E.R., Raygada, M., et al.; NIH Pediatric and Wild-Type GIST Clinic. (2011). Defects in succinate dehydrogenase in gastrointestinal stromal tumors lacking KIT and PDGFRA mutations. *Proc. Natl. Acad. Sci. USA* 108, 314–318.
- Jones, P.A., and Baylin, S.B. (2007). The epigenomics of cancer. *Cell* 128, 683–692.
- Kolski-Andreaco, A., Cai, H., Currie, D.S., Chandy, K.G., and Chow, R.H. (2007). Mouse adrenal chromaffin cell isolation. *J. Vis. Exp.* 2007 Jan 5, 129.
- Krueger, F., and Andrews, S.R. (2011). Bismark: a flexible aligner and methylation caller for Bisulfite-Seq applications. *Bioinformatics* 27, 1571–1572.
- Laird, P.W. (2003). The power and the promise of DNA methylation markers. *Nat. Rev. Cancer* 3, 253–266.
- Lenders, J.W., Eisenhofer, G., Mannelli, M., and Pacak, K. (2005). Pheochromocytoma. *Lancet* 366, 665–675.
- Loriot, C., Burnichon, N., Gadessaud, N., Vescovo, L., Amar, L., Libé, R., Bertherat, J., Plouin, P.F., Jeunemaitre, X., Gimenez-Roqueplo, A.P., and Favier, J. (2012). Epithelial to mesenchymal transition is activated in metastatic pheochromocytomas and paragangliomas caused by SDHB gene mutations. *J. Clin. Endocrinol. Metab.* 97, E954–E962.
- Meissner, A., Gnirke, A., Bell, G.W., Ramsahoye, B., Lander, E.S., and Jaenisch, R. (2005). Reduced representation bisulfite sequencing for comparative high-resolution DNA methylation analysis. *Nucleic Acids Res.* 33, 5868–5877.
- Monti, S., Tamayo, P., Mesirov, J.P., and Golub, T.R. (2003). Consensus clustering. A resampling-based method for class discovery and visualization of gene-expression microarray data. *Mach. Learn.* 52, 91–118.
- Moreno-Bueno, G., Cubillo, E., Sarrió, D., Peinado, H., Rodríguez-Pinilla, S.M., Villa, S., Bolós, V., Jordá, M., Fabra, A., Portillo, F., et al. (2006). Genetic profiling of epithelial cells expressing E-cadherin repressors reveals a distinct role for Snail, Slug, and E47 factors in epithelial-mesenchymal transition. *Cancer Res.* 66, 9543–9556.
- Neumann, H.P., Bausch, B., McWhinney, S.R., Bender, B.U., Gimm, O., Franke, G., Schipper, J., Klisch, J., Althoefer, C., Zerres, K., et al.; Freiburg-Warsaw-Columbus Pheochromocytoma Study Group. (2002). Germ-line mutations in nonsyndromic pheochromocytoma. *N. Engl. J. Med.* 346, 1459–1466.
- Noushmehr, H., Weisenberger, D.J., Diefes, K., Phillips, H.S., Pujara, K., Berman, B.P., Pan, F., Pelloski, C.E., Sulman, E.P., Bhat, K.P., et al.; Cancer Genome Atlas Research Network. (2010). Identification of a CpG island methylator phenotype that defines a distinct subgroup of glioma. *Cancer Cell* 17, 510–522.
- Pasini, B., and Stratakis, C.A. (2009). SDH mutations in tumorigenesis and inherited endocrine tumours: lesson from the pheochromocytoma-paraganglioma syndromes. *J. Intern. Med.* 266, 19–42.
- Pencheva, N., Tran, H., Buss, C., Huh, D., Drobnjak, M., Busam, K., and Tavazoie, S.F. (2012). Convergent multi-miRNA targeting of ApoE drives LRP1/LRP8-dependent melanoma metastasis and angiogenesis. *Cell* 151, 1068–1082.
- Pollard, P.J., Brière, J.J., Alam, N.A., Barwell, J., Barclay, E., Wortham, N.C., Hunt, T., Mitchell, M., Olpin, S., Moat, S.J., et al. (2005). Accumulation of Krebs cycle intermediates and over-expression of HIF1 α in tumours which result from germline FH and SDH mutations. *Hum. Mol. Genet.* 14, 2231–2239.
- Ricketts, C., Woodward, E.R., Killick, P., Morris, M.R., Astuti, D., Latif, F., and Maher, E.R. (2008). Germline SDHB mutations and familial renal cell carcinoma. *J. Natl. Cancer Inst.* 100, 1260–1262.
- Rodríguez-Paredes, M., and Esteller, M. (2011). Cancer epigenetics reaches mainstream oncology. *Nat. Med.* 17, 330–339.

- Rutter, J., Winge, D.R., and Schiffman, J.D. (2010). Succinate dehydrogenase - assembly, regulation and role in human disease. *Mitochondrion* 10, 393–401.
- Selak, M.A., Armour, S.M., MacKenzie, E.D., Boulahbel, H., Watson, D.G., Mansfield, K.D., Pan, Y., Simon, M.C., Thompson, C.B., and Gottlieb, E. (2005). Succinate links TCA cycle dysfunction to oncogenesis by inhibiting HIF- α prolyl hydroxylase. *Cancer Cell* 7, 77–85.
- Takai, D., and Jones, P.A. (2002). Comprehensive analysis of CpG islands in human chromosomes 21 and 22. *Proc. Natl. Acad. Sci. USA* 99, 3740–3745.
- Tomlinson, I.P., Alam, N.A., Rowan, A.J., Barclay, E., Jaeger, E.E., Kelsell, D., Leigh, I., Gorman, P., Lamlum, H., Rahman, S., et al.; Multiple Leiomyoma Consortium. (2002). Germline mutations in FH predispose to dominantly inherited uterine fibroids, skin leiomyomata and papillary renal cell cancer. *Nat. Genet.* 30, 406–410.
- Toyota, M., Ahuja, N., Ohe-Toyota, M., Herman, J.G., Baylin, S.B., and Issa, J.P. (1999). CpG island methylator phenotype in colorectal cancer. *Proc. Natl. Acad. Sci. USA* 96, 8681–8686.
- Tsai, H.C., Li, H., Van Neste, L., Cai, Y., Robert, C., Rassool, F.V., Shin, J.J., Harbom, K.M., Beaty, R., Pappou, E., et al. (2012). Transient low doses of DNA-demethylating agents exert durable antitumor effects on hematological and epithelial tumor cells. *Cancer Cell* 21, 430–446.
- van Nederveen, F.H., Gaal, J., Favier, J., Korpershoek, E., Oldenburg, R.A., de Bruyn, E.M., Sleddens, H.F., Derkx, P., Rivière, J., Dannenberg, H., et al. (2009). An immunohistochemical procedure to detect patients with paraganglioma and pheochromocytoma with germline SDHB, SDHC, or SDHD gene mutations: a retrospective and prospective analysis. *Lancet Oncol.* 10, 764–771.
- Smallwood, S.A., and Kelsey, G. (2012). Genome-wide analysis of DNA methylation in low cell numbers by reduced representation bisulfite sequencing. *Methods Mol. Biol.* 925, 187–197.
- Ward, P.S., and Thompson, C.B. (2012). Metabolic reprogramming: a cancer hallmark even warburg did not anticipate. *Cancer Cell* 21, 297–308.
- Widschwendter, M., Fiegl, H., Egle, D., Mueller-Holzner, E., Spizzo, G., Marth, C., Weisenberger, D.J., Campan, M., Young, J., Jacobs, I., and Laird, P.W. (2007). Epigenetic stem cell signature in cancer. *Nat. Genet.* 39, 157–158.
- Xiao, M., Yang, H., Xu, W., Ma, S., Lin, H., Zhu, H., Liu, L., Liu, Y., Yang, C., Xu, Y., et al. (2012). Inhibition of α -KG-dependent histone and DNA demethylases by fumarate and succinate that are accumulated in mutations of FH and SDH tumor suppressors. *Genes Dev.* 26, 1326–1338.
- Xu, W., Yang, H., Liu, Y., Yang, Y., Wang, P., Kim, S.H., Ito, S., Yang, C., Wang, P., Xiao, M.T., et al. (2011). Oncometabolite 2-hydroxyglutarate is a competitive inhibitor of α -ketoglutarate-dependent dioxygenases. *Cancer Cell* 19, 17–30.
- Young, R.M., and Simon, M.C. (2012). Untuning the tumor metabolic machine: HIF- α : pro- and antitumorigenic? *Nat. Med.* 18, 1024–1025.

PDEF Promotes Luminal Differentiation and Acts as a Survival Factor for ER-Positive Breast Cancer Cells

Gilles Buchwalter,^{1,4} Michele M. Hickey,^{2,4} Anne Cromer,² Laura M. Selfors,² Ruwanthi N. Gunawardane,² Jason Frishman,¹ Rinath Jeselsohn,¹ Elgene Lim,¹ David Chi,¹ Xiaoyong Fu,³ Rachel Schiff,³ Myles Brown,^{1,*} and Joan S. Brugge^{2,*}

¹Division of Molecular and Cellular Oncology, Department of Medical Oncology, and Center for Functional Cancer Epigenetics, Dana-Farber Cancer Institute and Harvard Medical School, Boston, MA 02215, USA

²Department of Cell Biology, Harvard Medical School, Boston, MA 02115, USA

³Department of Molecular and Cellular Biology, Baylor College of Medicine, Houston, TX 77054, USA

⁴These authors contributed equally to this work

*Correspondence: myles_brown@dfci.harvard.edu (M.B.), joan_brugge@hms.harvard.edu (J.S.B.)

<http://dx.doi.org/10.1016/j.ccr.2013.04.026>

SUMMARY

Breast cancer is a heterogeneous disease and can be classified based on gene expression profiles that reflect distinct epithelial subtypes. We identify prostate-derived ETS factor (PDEF) as a mediator of mammary luminal epithelial lineage-specific gene expression and as a factor required for tumorigenesis in a subset of breast cancers. PDEF levels strongly correlate with estrogen receptor (ER)-positive luminal breast cancer, and *PDEF* transcription is inversely regulated by ER and GATA3. Furthermore, PDEF is essential for luminal breast cancer cell survival and is required in models of endocrine resistance. These results offer insights into the function of this ETS factor that are clinically relevant and may be of therapeutic value for patients with breast cancer treated with endocrine therapy.

INTRODUCTION

Human breast cancer can be clustered into subtypes including basal, luminal, and ERBB2⁺ tumors (among others) based on gene expression profiling (Sørlie et al., 2001). Basal-like breast cancer is characterized by the absence of estrogen receptor (ER), progesterone receptor (PR), and ERBB2/HER2 and is commonly more aggressive and invasive, whereas luminal breast cancer is typically ER⁺ and is generally associated with a better prognosis. ER regulates gene expression in cooperation with coactivator or corepressor proteins and drives breast cancer cell survival and growth. This dependence is the basis for the treatment of ER⁺ luminal tumors with endocrine therapies including aromatase inhibitors that reduce estrogen levels and direct ER antagonists such as tamoxifen and fulvestrant (Osborne and Schiff, 2011). However, the long-term efficacy of

these treatments is diminished by recurrence of resistant tumors that have lost dependence on estrogen for growth. Although some of the mechanisms underlying this acquired resistance have been identified, including altered ER regulation and increased HER2 activity, identification of other pathways is essential to inform the design of additional therapies for these patients.

The gene expression differences between basal and luminal breast cancers represent distinctions in the expression of lineage markers identified in the two types of normal mammary epithelial cells: basal myoepithelial cells surrounding the branching ductal structures, and ductal luminal epithelial cells that generate milk-producing alveolar cells during pregnancy. These cells arise from a common multipotent stem/progenitor cell through a process of lineage commitment (Stingl et al., 2005). Altered regulation of developmental pathways has been

Significance

ER is the defining transcription factor of luminal breast tumors, and endocrine agents that target ER are well-established standards of care in breast cancer. However, intrinsic and acquired resistance limit the success of this therapeutic strategy, highlighting the need to identify additional pathways critical for luminal tumor growth and recurrence. Our findings provide evidence that prostate-derived ETS factor (PDEF) can drive luminal differentiation of basal mammary epithelial cells, regulate the survival of luminal tumor cells, and contribute to endocrine resistance. These findings suggest that increased PDEF expression may play a role in tumor recurrence following endocrine therapy and may be a clinically useful target for the treatment of patients with luminal breast cancer.

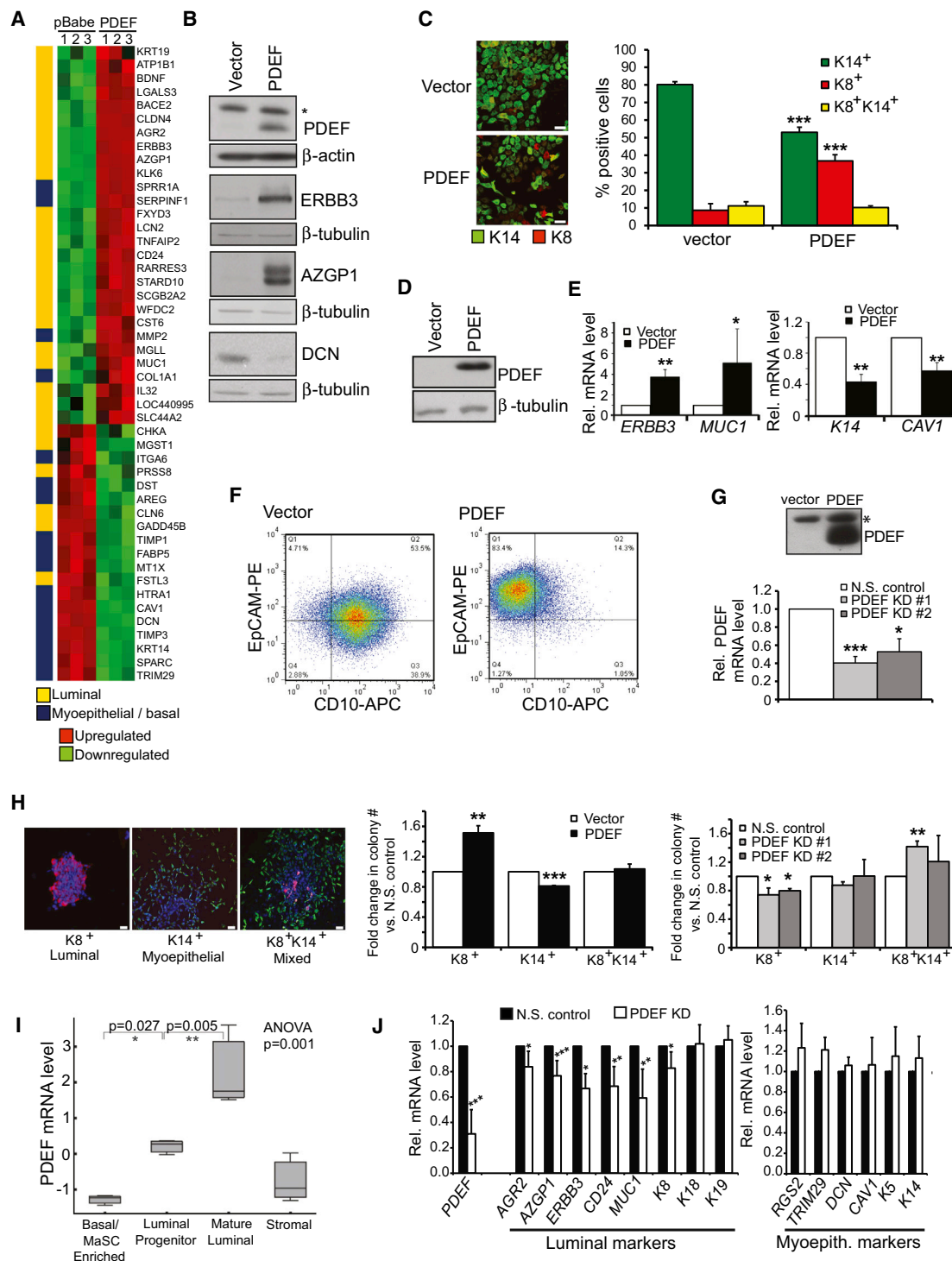


Figure 1. PDEF Induces a Luminal Lineage-Specific Gene Expression Profile in Non-Transformed Mammary Epithelial Cells

(A) Heatmap generated from microarray analysis of triplicate samples of MCF-10A cells expressing either vector control (pBabe) or PDEF. Differentially expressed mammary epithelial marker genes are shown. These expression changes were statistically significant ($p = 4.14 \times 10^{-14}$ by Fisher's exact test).

(B) Western blot analysis of vector control or PDEF-expressing MCF-10A cells (*NS band).

(C) Immunofluorescent staining for keratins 8 and 14 in MCF-10A cells. Representative images of vector control and PDEF-expressing cells are shown. Scale bars represent 100 μ M. Quantitation is shown in graph. Data represent mean \pm SEM (*** p < 0.0007).

(D) Western blot confirming PDEF overexpression in HMECs.

(E) Real-time PCR analysis of luminal (left) and basal (right) marker gene expression in HMECs overexpressing PDEF. Results were normalized to the housekeeping gene *RPLP0* and are presented as mean fold change \pm SD (* p < 0.05, ** p < 0.008).

(legend continued on next page)

proposed to play an important role in tumorigenesis and to contribute to the observed heterogeneity in breast cancer (Dontu et al., 2003). Identification of other factors that regulate mammary gland differentiation is important for understanding the mechanisms of breast cancer initiation and progression and for developing targeted treatments for each tumor subtype. Several transcription factors involved in both mammary development and breast cancer progression have been identified, including GATA3, which promotes luminal epithelial differentiation and exerts a tumor-suppressive function by sustaining differentiation and inhibiting metastasis (Asselin-Labat et al., 2007; Kourou-Mehr et al., 2008).

Members of the ETS family, such as ELF3, ELF5, and ETV4, have also been implicated in mammary development (Shepherd and Hassell, 2001) and are overexpressed in breast cancer, supporting a role in epithelial tumorigenesis (Galang et al., 2004; Kalyuga et al., 2012). Unlike most ETS proteins, the expression of prostate-derived ETS factor (PDEF/SPDEF), which was first identified as an activator of prostate specific antigen, (Oettgen et al., 2000) is largely restricted to epithelial tissues including the lung, stomach, colon, and hormone-regulated epithelia such as the prostate, breast, and ovary. In these tissues, PDEF mediates epithelial cell fate decisions and secretory cell differentiation (Gregorieff et al., 2009; Park et al., 2007); however, it is unclear whether PDEF functions similarly in the mammary gland. There is also little known about the regulation of PDEF expression apart from miRNA-mediated suppression in basal breast cancer cell lines (Findlay et al., 2008).

PDEF also appears to play a role in regulating tumor growth and loss of PDEF is associated with a more aggressive phenotype in prostate and colon cancer (Gu et al., 2007; Moussa et al., 2009). However, the role of PDEF in breast cancer is controversial, as several studies have demonstrated that PDEF expression is lost in invasive basal breast cancer cell lines, and that its re-expression inhibits the growth and migration of these cells, supporting a tumor-suppressive function (Feldman et al., 2003; Turner et al., 2007). In contrast, PDEF cooperates with known oncogenes to stimulate MCF-10A cell transformation (Gunawardane et al., 2005) and is one of the most highly overexpressed genes in human and mouse mammary tumors and in lymph node metastases (Galang et al., 2004; Ghadersohi and Sood, 2001). Furthermore, PDEF expression is enriched in luminal tumors and correlates with poor overall survival in ER⁺ breast cancer patients, suggesting instead a

possible oncogenic role (Sood et al., 2007, 2009; Gunawardane et al., 2005).

In this study we sought to investigate and clarify the role of PDEF in both normal mammary gland development and breast cancer. We hypothesize that PDEF may be important for the differentiation of normal mammary luminal cells and that this transcription factor may function differentially in luminal versus basal breast tumors.

RESULTS

PDEF Induces a Luminal Epithelial Gene Expression Program in Mammary Epithelial Cells

To investigate PDEF function in the mammary gland, we examined the effect of this transcription factor on gene expression using microarray-based profiling of MCF-10A cells. These cells are nontransformed mammary epithelial cells that express protein and gene expression programs of basal epithelial cells (Neve et al., 2006) and undetectable levels of endogenous PDEF (Gunawardane et al., 2005). Bioinformatics analysis of the genes induced or repressed by PDEF overexpression in MCF-10A cells revealed a striking effect on expression of luminal and myoepithelial cell markers. The heat map in Figure 1A shows the effects of PDEF overexpression on genes previously identified to be most specifically expressed in purified populations of primary luminal (left column, yellow) or myoepithelial cells (left column, blue) (Allinen et al., 2004; Jones et al., 2004). PDEF overexpression induced a switch in gene expression, resulting in the induction of luminal markers such as *ERBB3*, *MUC1*, and *AZGP1* and the concomitant suppression of myoepithelial marker genes, including *KRT14*, *CAV1*, and *DCN*. A complete list of the significantly regulated genes from the microarray is shown in Table S1 (available online).

These results were validated in MCF-10A cells at the mRNA level using quantitative real-time PCR (Figures S1A and S1B) and at the protein level by western blot (Figure 1B). Expression of PDEF also resulted in a shift to a luminal, EpCAM⁺CD10⁻ phenotype (76.5% versus 45.9% in vector control cells) as determined by flow cytometry surface marker analysis (Figure S1C), as well as a significant increase in luminal keratin-8⁺ (K8) cells with a simultaneous decrease in the percentage of myoepithelial keratin-14⁺ (K14) cells (Figure 1C). In addition, PDEF expression in a second, independent cell line, non-transformed human mammary epithelial cells (HMECs) (Figure 1D), also resulted in

(F) Flow cytometry surface marker analysis of HMECs using antibodies for the luminal gene EpCAM and the myoepithelial gene CD10. A representative experiment is shown; similar results were obtained in two independent experiments.

(G) PDEF overexpression in COMMA-1D murine mammary epithelial cells was detected by western blot (top). PDEF downregulation was detected by real-time PCR (bottom); two independent shRNAs (PDEF KD: KnockDown #1 and #2) were used and compared to a NS shRNA control. Results were normalized to the housekeeping gene *RPLP0* and are presented as mean fold change \pm SEM (* p < 0.02, *** p < 0.0005).

(H) COMMA-1D cells infected with lentivirus to modulate PDEF expression were plated on a layer of irradiated fibroblast feeder cells for colony formation assays. Colonies were scored based on K8 (red) and K14 (green) staining and categorized into three types of colonies: K8⁺ luminal, K14⁺ myoepithelial, or K8⁺K14⁺ mixed colonies. Representative images of each type of colony are shown (left), scale bars represent 100 μ M. Quantitation of PDEF-overexpressing cells (middle, \pm SEM) and PDEF-downregulated cells (right, \pm SD) are shown as the average fold change in colony number across three experiments compared to vector or NS control cells (* p < 0.05, ** p < 0.006, *** p < 0.0001).

(I) Box plot displaying PDEF mRNA levels in MaSC, luminal progenitors, mature luminal cells, and stromal cells derived from gene expression analysis of purified human mammary epithelial subpopulations (Lim et al., 2009).

(J) Relative mRNA expression levels of luminal (left) and myoepithelial (right) markers in luminal progenitor cells transduced with PDEF-targeting shRNA (KD) or NS shRNA. Cells were harvested 5 days after infection. Bars represent fold change \pm SD of two independent experiments (* p < 0.05, ** p < 0.01, *** p < 0.001).

See also Figure S1 and Table S1.

induction of luminal gene expression and inhibition of myoepithelial marker genes (Figure 1E) and a shift to a luminal, EpCAM⁺ CD10⁻ phenotype (83.4% versus 4.71% in vector control cells) (Figure 1F).

To further validate the possibility that PDEF regulates luminal differentiation, we examined the effect of modulating PDEF expression in a murine mammary epithelial cell line, COMMA-1D cells. These cells are derived from a mid-pregnant mouse and contain a population of stem/progenitor cells that are capable of both in vitro differentiation and mammary gland repopulation in transplantation assays (Danielson et al., 1984). Endogenous PDEF levels in these cells are low but can be detected using real-time PCR (Figure 1G). COMMA-1D cells were infected with lentiviral vectors expressing either PDEF cDNA or shRNAs targeting PDEF and then assayed for colony formation and scored for K8 and K14 staining (Figure 1H, left). PDEF mRNA was efficiently downregulated with each of two independent shRNAs (PDEF KnockDown #1 and #2) compared to a nonspecific (NS) shRNA control. Similar to the effects of PDEF on keratin expression in MCF-10A cells, PDEF overexpression in COMMA-1D cells led to enhanced formation of K8⁺ luminal colonies and a reduction in K14⁺ colonies (Figure 1H, middle). In contrast, downregulation of PDEF expression decreased the formation of K8⁺ luminal colonies and resulted in an increased proportion of K8⁺K14⁺ mixed colonies (Figure 1H, right), suggesting a block in luminal differentiation and the accumulation of bipotent double-positive colonies in the absence of PDEF.

In addition, gene expression analysis of FACS-sorted primary human breast epithelial subpopulations (Lim et al., 2009) revealed that PDEF mRNA levels are enriched in the CD49f⁺ EpCAM⁺ luminal progenitor cell population and are further enriched in CD49f⁺ EpCAM⁺ mature luminal cells, as compared to the basal/mammary stem cell-enriched (Basal/MaSC) and stromal fibroblast populations (Figure 1I). To determine whether PDEF regulates the expression of luminal and myoepithelial differentiation markers, we used this same FACS-sorting approach to purify mammary epithelial subpopulations from a reduction mastectomy specimen (Figures S1D and S1E). Although sorted mature luminal cells could not be cultured, we were able to successfully grow luminal progenitor cells in vitro and evaluated the expression of several luminal and myoepithelial markers after PDEF silencing in these cells (Figure 1J). Interestingly, PDEF knockdown significantly decreased the expression of multiple luminal markers, whereas myoepithelial marker expression was not significantly affected. These results further support a role for PDEF in driving the expression of luminal-specific genes and promoting the differentiation of this subset of mammary epithelial cells.

PDEF Is Co-Expressed with ER and Is Regulated by ER-Cooperating Factors GATA3 and FOXA1

PDEF mRNA is significantly overexpressed in ERBB2⁺ and luminal A and B tumors in two independent data sets, as compared to basal-like tumors (Figure 2A). This correlation with the luminal subtype was also confirmed in breast cancer cell lines (Figure 2B). Because ER expression is the major molecular determinant of luminal tumors (Perou et al., 2000), PDEF is significantly overexpressed in ER⁺ tumors (Figure 2C). Interestingly, PDEF is the only ETS transcription factor displaying a

positive correlation with ER expression among the 28 members of the family (Figure 2D). This correlation suggests that ER may regulate PDEF transcription.

To determine if ER regulates PDEF expression, we analyzed a previously established ER cistrome data set (Carroll et al., 2006) and found three ER-binding regions located in the PDEF gene locus (Figure 3A). Two enhancers (1 and 2) are located within the first intron of the gene and the third one (3) is located after the 3'-end of the gene. Direct ER chromatin immunoprecipitation (ChIP) in MCF7 cells showed an estradiol (E2)-induced recruitment of ER at these three enhancers, thus confirming PDEF as a direct ER target.

However, a time course analysis of MCF7 cells treated with increasing E2 doses did not reveal PDEF mRNA induction, in contrast with the strong increase of PR mRNA, a known direct ER target (Figure 3B). Direct RNA polymerase II (Pol2) ChIP corroborated the absence of PDEF induction by E2. Pol2 recruitment at the PDEF promoter was not increased after E2 treatment, whereas its recruitment at the PR promoter was strongly induced (Figure 3C). We investigated whether the three enhancers could be responsible for the activation of the genes adjacent to PDEF (PAC1N1 and c6orf106, Figure S2A). However, neither of these neighboring genes demonstrated a correlation with ER expression in breast carcinomas (Figure S2B), and E2 stimulation did not induce their expression (Figure S2C). The absence of PDEF mRNA induction by E2 was further validated in another ER⁺ breast cancer cell line (T47D, Figure S2D). In addition, ER downregulation in MCF7 cells did not affect PDEF mRNA levels (Figure 3D), further confirming the absence of regulatory activity, despite direct ER recruitment at the PDEF gene locus in an E2-dependent manner.

These results suggested that a potential repressor prevents transactivation of the PDEF gene by ER. Therefore, we examined the roles of the known ER-cooperating factors FOXA1 (Lupien et al., 2008) and GATA3 (Theodorou et al., 2013) as potential regulators of PDEF expression. FOXA1 downregulation in MCF7 cells led to a decrease in PDEF mRNA and protein levels, indicating a positive role of FOXA1 in the regulation of PDEF expression (Figure 3D). FOXA1 downregulation in another luminal cell line (SKBR3) also decreased PDEF mRNA levels (Figure S2E). In contrast, GATA3 downregulation in MCF7 cells triggered an increase of PDEF mRNA and protein levels (Figure 3D), demonstrating a negative role of GATA3 in the regulation of PDEF expression. Additionally, GATA3 overexpression in two luminal cell lines expressing low endogenous GATA3 levels resulted in decreased PDEF expression (Figure S2F). These regulatory effects occur through direct recruitment of FOXA1 and GATA3 at the PDEF locus in MCF7 cells because direct ChIP-qPCR revealed FOXA1 recruitment at the PDEF promoter and enhancer 3, whereas GATA3 was recruited at the most proximal enhancer (Figure 3E). These data suggest that PDEF is a downstream target of ER, FOXA1, and GATA3. As a control, we verified that PDEF downregulation did not affect the expression of ER, FOXA1, or GATA3, indicating that there is no reciprocal regulatory loop between these genes (Figure S2G).

GATA3 Prevents ER-Mediated Induction of PDEF

As a direct PDEF repressor, GATA3 could be responsible for the absence of E2-mediated induction of PDEF mRNA. To test this

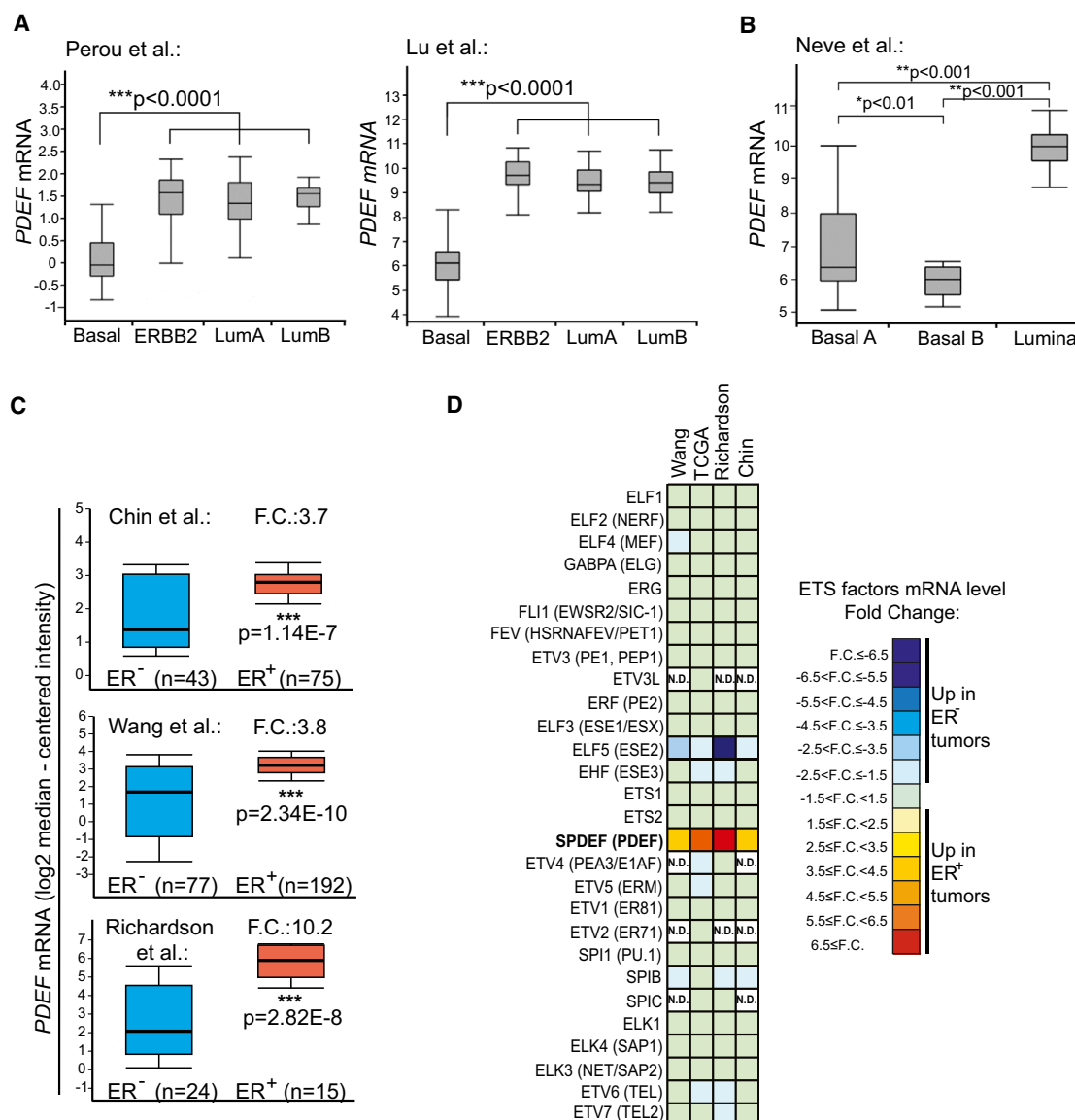


Figure 2. PDEF Is Enriched in Luminal Tumors and Strongly Correlates with ER Expression

(A and B) Box plots displaying *PDEF* mRNA levels between Basal-like, ERBB2⁺, and Luminal (Lum) subtypes of breast cancer (A) and breast cancer cell lines (B) using published microarray data sets (Lu et al., 2008; Perou et al., 2000; Neve et al., 2006).

(C) Box plots displaying *PDEF* mRNA levels between ER⁻ and ER⁺ breast carcinoma (F.C., fold change) in published microarray data sets (Chin et al., 2006; Richardson et al., 2006; Wang et al., 2005).

(D) Heatmap displaying the relative expression levels of the 28 ETS transcription factors in ER⁻ and ER⁺ breast cancer subtypes (Wang et al., 2005; Richardson et al., 2006; Chin et al., 2006) (N.D., not determined).

hypothesis, we compared the effect of E2 treatment in the presence or absence of GATA3 expression (Figure 4A). As expected, *PDEF* mRNA levels were unchanged in MCF7 cells transfected with a non-specific siRNA (NS). In contrast, GATA3 knockdown enabled the induction of *PDEF* mRNA (Figure 4A) and protein (Figure 4B) by E2 treatment. We then examined whether modulation of GATA3 expression affected the recruitment of various transcriptional regulators to the *PDEF* promoter and enhancer regions using ChIP in E2-treated MCF7 cells (Figure 4C). Indeed, Pol2 displayed a higher recruitment level at the *PDEF* promoter in GATA3-knockdown conditions, whereas the promoter of the ER

target gene *MYC* did not show differential Pol2 recruitment. ER recruitment to the three enhancers was also increased upon GATA3 depletion, with a more pronounced increase at enhancer 1, in contrast to the ER-recruiting enhancer located upstream of the *MYC* gene, which did not show differential ER recruitment. In the absence of estrogen stimulation (vehicle condition), ER recruitment at the *PDEF* enhancers was close to background level, and modulation of GATA3 expression did not affect ER recruitment (Figure S3). Furthermore, the transcriptional coactivator p300, known to associate with ligand-bound ER and to augment ligand-dependent activation by ER (Hanstein et al.,

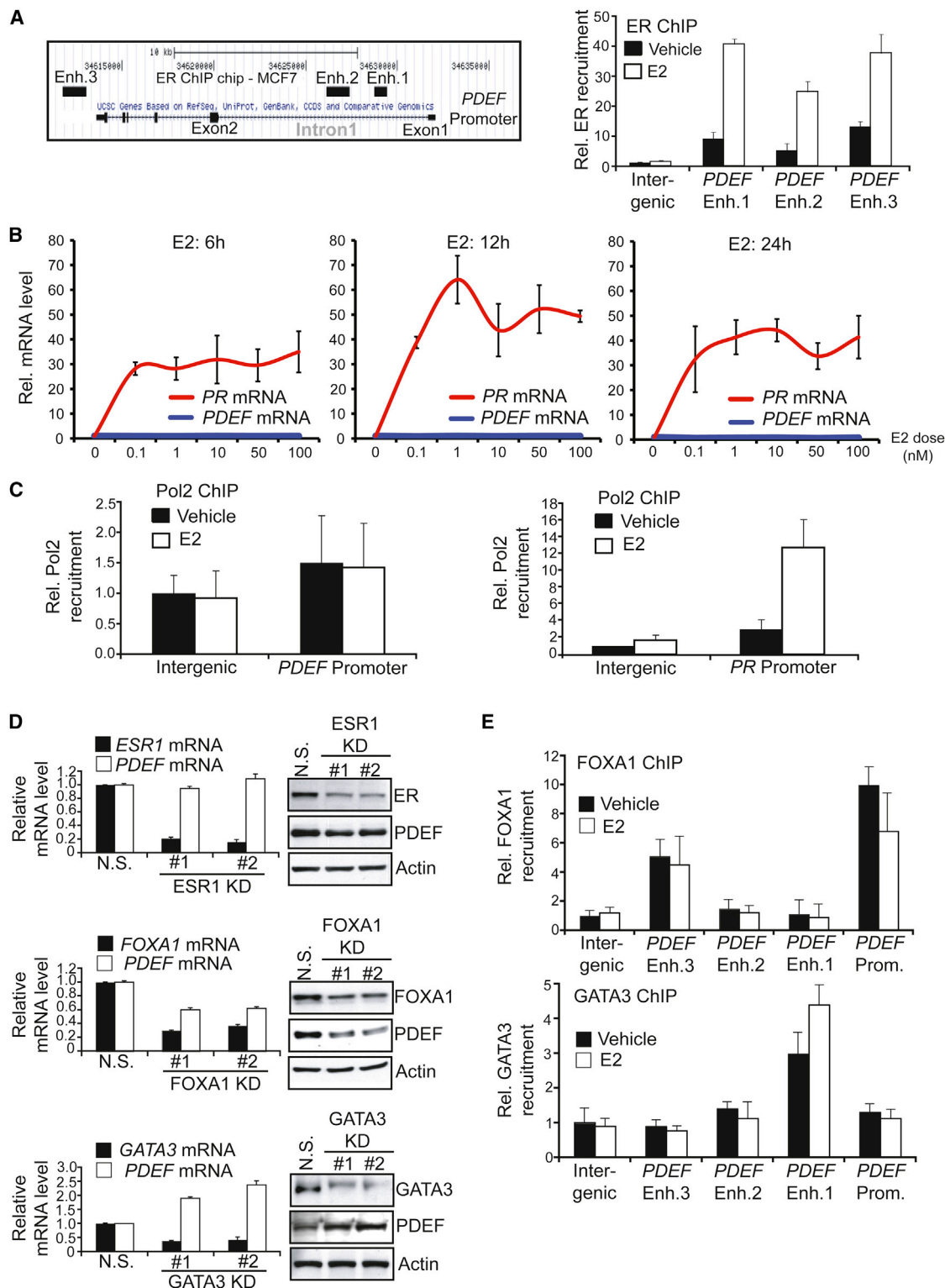


Figure 3. PDEF Is Not Directly Regulated by ER, but Is Activated by FOXA1 and Repressed by GATA3

(A) Left: Schematic diagram of the ER-binding regions within the *PDEF* gene locus as defined by ER ChIP on chip in MCF7 cells (Carroll et al., 2006). Enh., enhancer. Right: direct ER chromatin immunoprecipitation (ChIP) followed by qPCR after treatment of MCF7 cells with vehicle (black bars) or 10 nM estradiol (E2, white bars). Data represent means \pm SD.

(B) *PDEF* and *PR* mRNA levels were determined by real-time PCR after MCF7 cells were treated with increasing E2 doses for 6 hr (left), 12 hr (middle), and 24 hr (right). mRNA levels are presented as means \pm SD and normalized to the housekeeping gene *GAPDH*.

(legend continued on next page)

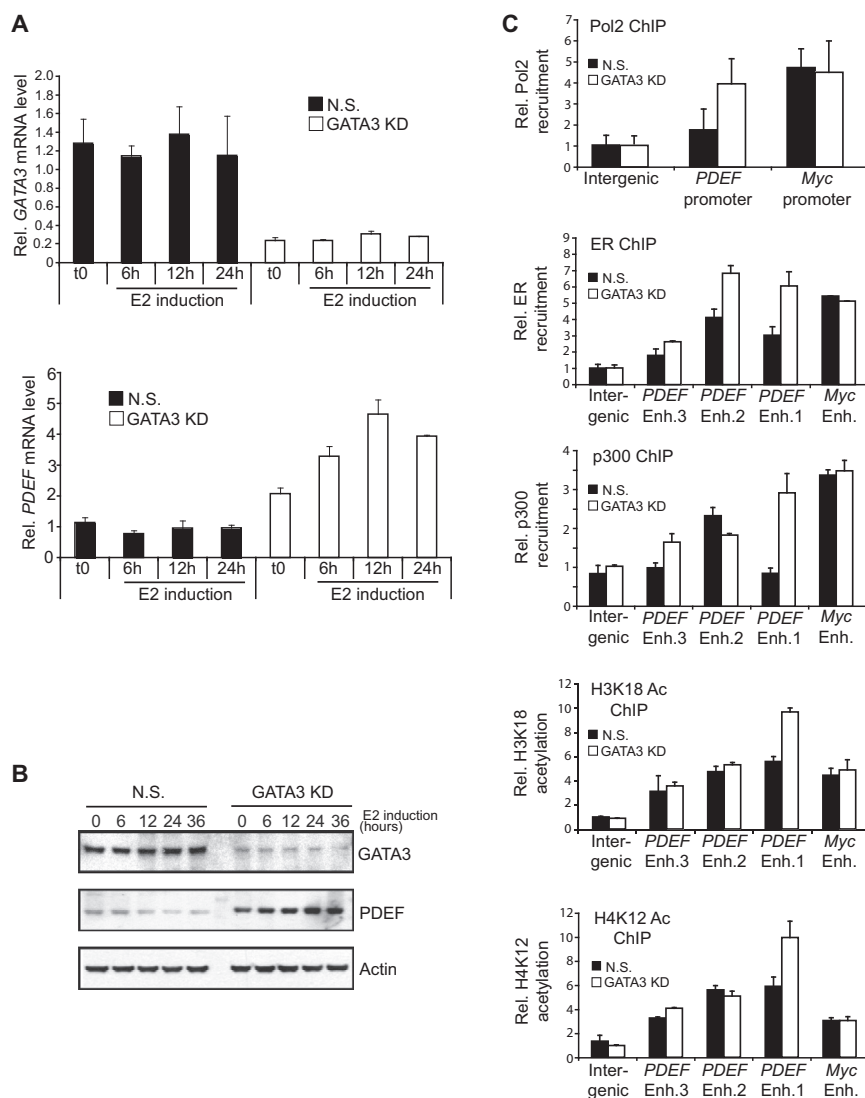


Figure 4. GATA3 Prevents PDEF Induction by ER

(A) GATA3 (upper) and PDEF (lower) mRNA levels were determined by RT-qPCR after MCF7 cells were transfected with a NS or GATA3-targeting (KD, KnockDown) siRNAs and challenged with 10 nM estradiol (E2). Data represent means \pm SD. (B) Western blot lysates from MCF7 cells transfected with NS or GATA3-targeting (KD) siRNAs, and challenged with 10 nM estradiol.

(C) Direct RNA polymerase II (Pol2), ER, p300, acetylated histone H3K18, and H4K12 ChIPs followed by real-time PCR after MCF7 cells were transfected with NS or GATA3-targeting (KD) siRNAs, and challenged with 10 nM E2. Data represent means \pm SD. Enh., enhancer. See also Figure S3.

analysis showed a statistically significant inverse correlation between PDEF and GATA3. Conversely, PDEF and FOXA1 levels were positively correlated, further confirming the positive regulation of PDEF expression by FOXA1. Validation of the negative correlation between PDEF and GATA3 expression was also performed in four ER⁺ breast cancer cell lines (Figure 5B).

PDEF Is Required for the Growth of ER⁺ Breast Cancers

To investigate the role of PDEF in breast cancer progression, we first analyzed gene expression profiling and clinical outcome data from published studies for correlations between PDEF/GATA3 expression levels and overall survival (Figure 5C). Due to the strong association between PDEF and ER expression, only

1996), also displayed a stronger recruitment in GATA3-knock-down conditions, specifically at enhancer 1. Consistent with the histone acetyltransferase activity of p300 (McManus and Hendzel, 2003), we found higher levels of the active histone marks acetylated-H3K18 and -H4K12 at PDEF enhancer 1. Collectively, these data demonstrate that the loss of GATA3 allows for ER-mediated PDEF induction.

To evaluate the repressive effect of GATA3 on PDEF expression in other cell lines, we examined the mRNA levels of these transcription factors in a subset of ER⁺ breast cancer cell lines (Neve et al., 2006). Clustering analysis revealed a clear distinction between [GATA3]^{high} [PDEF, FOXA1]^{low} and [GATA3]^{low} [PDEF, FOXA1]^{high} cell lines (Figure 5A). Pairwise correlation

ER⁺ breast tumors were included in this analysis. Patients were divided into two equal groups, high and low, based on the median PDEF expression level. Kaplan-Meier survival analyses in three independent data sets demonstrated that high PDEF expression is associated with worse overall survival for patients with ER⁺ breast cancer. We found that PDEF is a significant predictor of survival when treated as a continuous variable in Cox regression models (Chin $p = 0.0102$, Ivshina $p = 3.74 \times 10^{-3}$, Desmedt $p = 0.0476$), consistent with a previous report (Sood et al., 2009). In contrast, GATA3 is not a significant predictor of survival in the ER⁺ breast samples in these three studies when tumors are classified based on the median GATA3 expression or when GATA3 expression is treated as a continuous variable

(C) Direct RNA polymerase II (Pol2) ChIP followed by qPCR after treatment of MCF7 cells with vehicle or 10 nM E2 using primers flanking the PDEF promoter (left) and PR promoter (right). Data represent means \pm SD.

(D) PDEF, ESR1, FOXA1, and GATA3 mRNA and protein levels were determined by RT-qPCR (left panels) or western blot (right panels) after MCF7 cells were transfected with a NS or two independent siRNAs targeting ESR1/FOXA1/GATA3 (KD, KnockDown). Data represent means \pm SD.

(E) Direct FOXA1 (upper) and GATA3 (lower) ChIPs followed by qPCR after treatment of MCF7 cells with vehicle or 10 nM E2. Enh., enhancer; Prom., promoter. Data represent means \pm SD.

See also Figure S2.

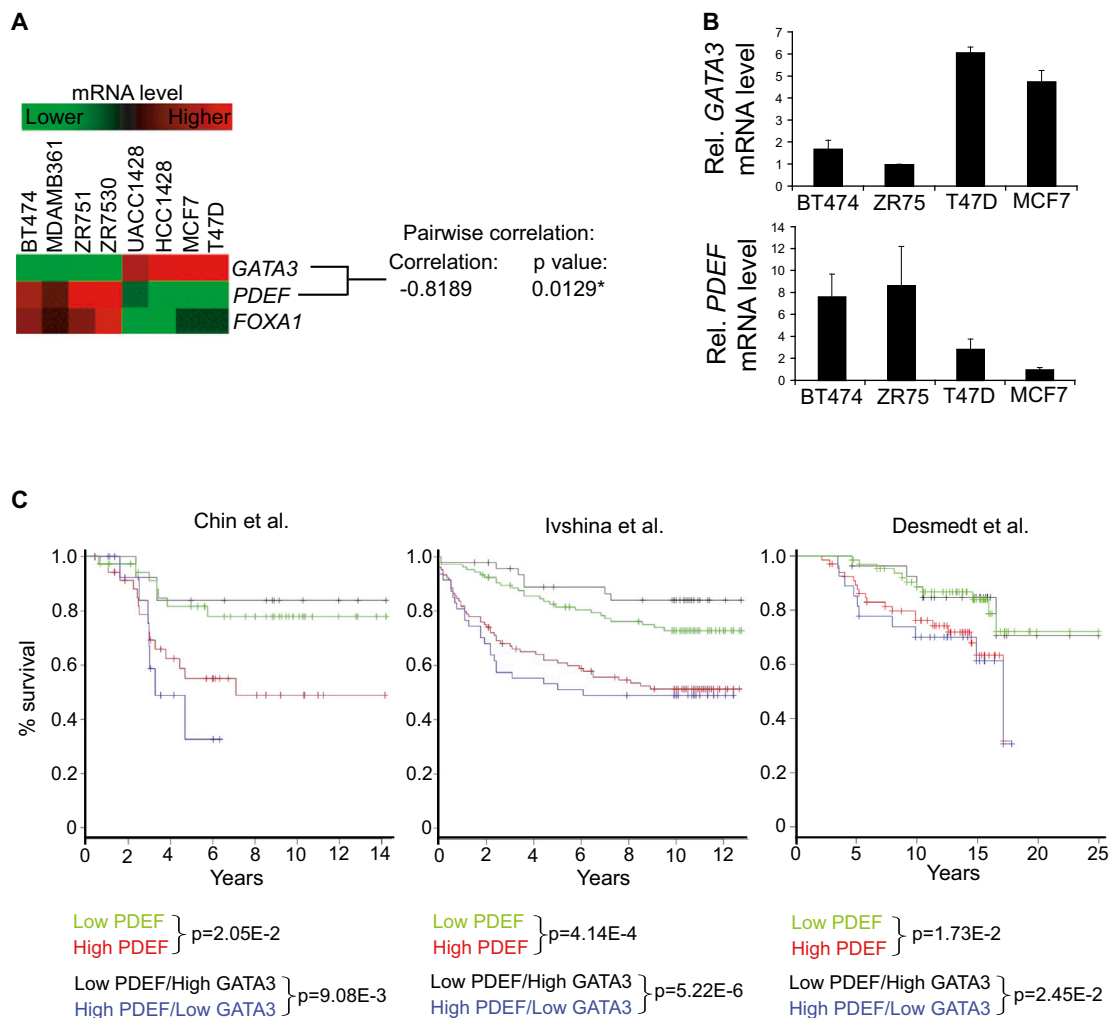


Figure 5. PDEF and GATA3 Are Inversely Correlated in ER⁺ Luminal Tumor Cell Lines, and Their Expression Levels Are of Prognostic Value for ER⁺ Breast Carcinoma Patient Survival

(A) Heatmap displaying GATA3, PDEF, and FOXA1 mRNA levels in eight ER⁺ breast cancer cell lines (Neve et al., 2006) with pairwise correlation analysis. Scale: +1, perfect positive correlation; 0, no correlation; -1: perfect inverse correlation.

(B) GATA3 (upper) and PDEF (lower) mRNA levels were determined by real-time PCR in four ER⁺ breast cancer cell lines. Data represent means \pm SD.

(C) Kaplan-Meier survival analysis of patients with ER⁺ breast carcinoma (Chin et al., 2006; Ivshina et al., 2006; Desmedt et al., 2007). Patients were stratified on the median value for each marker. The log-rank test p values are shown.

(data not shown). Interestingly, further stratification of patient groups based on inverse GATA3/PDEF expression improves the predictive capability of PDEF (Figure 5C). The significant correlation between high PDEF expression and poor overall survival strongly supports a potential role for PDEF in ER⁺ breast tumorigenesis.

To assess this hypothesis, we next investigated the biologic effects of PDEF knockdown on luminal breast cancer cell growth. PDEF downregulation by transient transfection with two independent siRNAs (Figure 6A) triggered a growth defect in MCF7 cells subjected to hormone starvation prior to E2 stimulation (Figure 6B). This growth defect was rescued by the expression of a mutant PDEF protein harboring a silent mutation preventing siRNA-mediated downregulation (Figures S4A and S4B). Stable PDEF knockdown by transduction of MCF7 cells

with lentiviral PDEF-targeting shRNAs also induced a growth defect in conditions of hormone depletion followed by E2 stimulation (Figures S4C and S4D).

Flow cytometry analysis did not reveal any obvious cell-cycle progression defect in PDEF knockdown cells subjected to hormone starvation and E2 induction. However, PDEF knockdown followed by treatment with nocodazole prevented a significant proportion of cells from entering mitotic arrest, suggesting that PDEF silencing does induce a subtle G0/G1 arrest (Figure S4E). In addition, PDEF knockdown cells subjected to hormone depletion displayed decreased viability with a statistically significant increase in apoptotic cells (Figure 6C). Based on this finding, we examined the effect of the ER antagonists tamoxifen and fulvestrant in cells expressing PDEF siRNA (Figure 6D). Increasing doses of anti-estrogens resulted in more pronounced

cytotoxicity in PDEF knockdown conditions. In addition, caspase 8 activity was also increased in MCF7 cells expressing PDEF-targeting shRNAs and subjected to hormone depletion or fulvestrant treatment (Figure S4F), further confirming a role for PDEF in mediating luminal tumor cell survival in response to hormone-related stress.

We also examined the effect of PDEF loss on luminal tumor cell survival in anchorage-independent conditions. Soft agar colony formation was markedly decreased in MCF7 cells expressing PDEF shRNA, suggesting that this ETS factor is essential for the transformation of luminal tumor cells (Figure 6E). Consistent with this notion, PDEF downregulation in three other luminal cancer cell lines, T47D, BT474, and SKBR3 (Figure S4G), resulted in similar decreases in cell growth (Figures S4H–S4J) and significantly impaired colony formation in soft agar assays (Figures S4K and S4L). As a control, we demonstrated that re-introduction of PDEF in the basal tumor cell line SUM159, which lacks endogenous PDEF expression, inhibited anchorage-independent growth and survival (Figure S4M), confirming the reported role of PDEF as a tumor suppressor in basal-like breast cancer (Feldman et al., 2003; Turner et al., 2007). To further test the role of PDEF in luminal tumor formation, NS control or PDEF knockdown MCF7 cells were injected in the inguinal mammary fat pads of NOD-SCID mice that had previously been implanted with an estrogen pellet (Figure 6F). In line with the observed in vitro growth defect, PDEF downregulation reduced tumor growth, with a 40% decrease in final tumor weight compared to tumors formed by control MCF7 cells. Interestingly, histological sections of PDEF knockdown tumors displayed a fragmented appearance and decreased cellularity, in contrast to the suppressive role of PDEF in basal SUM159 cells, because expression of PDEF in these cells diminished tumor formation in vivo (Figure S4N). Western blot analysis of lysates from PDEF knockdown tumors revealed increased detection of cleaved caspase 8, whereas the proliferation marker PCNA was not differentially expressed (Figure 6G), indicating that the reduced tumor size of PDEF knockdown xenograft tumors is predominantly due to increased apoptosis rather than a proliferation defect. TUNEL cell death detection in tumor sections also clearly showed increased cell death in PDEF knockdown tumors (Figure 6H). Collectively, these data support a critical prosurvival role of PDEF in ER⁺ breast cancer cells. Conversely, we confirmed a tumor-suppressive function for GATA3 (Asselin-Labat et al., 2007; Kouros-Mehr et al., 2008), because GATA3 silencing promoted soft agar colony formation in MCF7 cells (Figures S4O and S4P).

PDEF Is Involved in Endocrine Resistance

To better understand the mechanisms underlying acquired endocrine resistance, in vitro models of hormone-independent growth were previously developed through long-term culture of MCF7 cells in media devoid of any estrogens or in the presence of tamoxifen (Ariazi et al., 2011). We hypothesized that PDEF might play a functional role in this hormone-refractory phenotype based on our finding that PDEF downregulation sensitized MCF7 cells to hormone depletion and anti-estrogens. To evaluate this hypothesis, we analyzed two long-term estrogen-deprived clones (MCF7 2A and 5C) (Ariazi et al., 2011) and tamoxifen-resistant cells (TAM-R) isolated from parental MCF7 cells.

PDEF mRNA levels were higher in estrogen-deprived 2A and 5C cells relative to the parental controls (WS8), whereas the levels of GATA3 mRNA were lower (Figure 7A). The inverse correlation between PDEF and GATA3 was confirmed in this model at the protein level (Figure 7B). Similarly, TAM-R cells also displayed higher PDEF levels, concomitant with undetectable levels of GATA3 mRNA and protein (Figures 7A and 7B). To determine whether the higher PDEF expression observed in these models was functionally relevant, we assessed the survival of MCF7 5C cells after PDEF downregulation. PDEF knockdown induced increased cell death and a reduction in soft agar colony formation, suggesting that hormone-refractory cells are partially dependent on PDEF for survival (Figure 7C). In addition, PDEF downregulation in MCF7 TAM-R cells triggered a dramatic decrease in soft agar colony formation (Figure 7D). Interestingly, tamoxifen significantly increased colony numbers of TAM-R cells transduced with a NS shRNA (compare white bars), indicating that tamoxifen functions in TAM-R cells as an agonist to promote anchorage-independent cell growth. In fact, PDEF silencing resulted in a greater fold-reduction in colony formation in the presence of tamoxifen compared to the vehicle condition. These results support the conclusion that PDEF plays an important role in endocrine resistance.

PDEF Gene Expression Signature Reflects a Prosurvival Role and Identifies Cell Death Receptor FAS as an Important Target

Microarray gene expression analysis was performed in MCF7 cells transduced with NS or PDEF-targeting shRNAs after subjection to hormone depletion for 48 hr. Analyses of differentially expressed genes combined with gene ontology revealed a downregulation of cell cycle-related genes and an upregulation of apoptosis-related genes in PDEF knockdown cells (Figure 8A). A complete list of PDEF-regulated genes from this microarray analysis is shown in Table S2. These target genes constitute potential effectors of the prosurvival role of PDEF.

We next examined whether PDEF-regulated genes have prognostic value for survival of patients with ER⁺ breast carcinoma (Figure 8B). A semisupervised principal component method was implemented using the PDEF-regulated genes in MCF7 cells; we did not include the PDEF probe because it is prognostic as a single predictor. Using this approach, a 130-probe PDEF signature that is able to predict patient outcome in the Ivshina data set was identified (Figure 8B; Table S3). Importantly, this signature is also significant when applied to independent cohorts of ER⁺ tumors (Figure S5A). Because increased expression of cell cycle genes is a hallmark of cancer, it was necessary to define whether cell cycle genes solely contribute to the prognostic value of the PDEF signature. Survival analysis using a PDEF signature where cell cycle-associated genes were eliminated revealed that non-cell cycle PDEF-regulated genes are prognostic (Figure S5B, left panel). A PDEF signature restricted to genes implicated in response to stress and apoptosis is also prognostic (Figure S5B, right panel).

To further define the clinical relevance of PDEF target genes, we analyzed the overlap between the PDEF signature and existing breast carcinoma gene expression data sets. A large proportion of genes upregulated in PDEF knockdown MCF7 cells were significantly downregulated in tumors versus normal

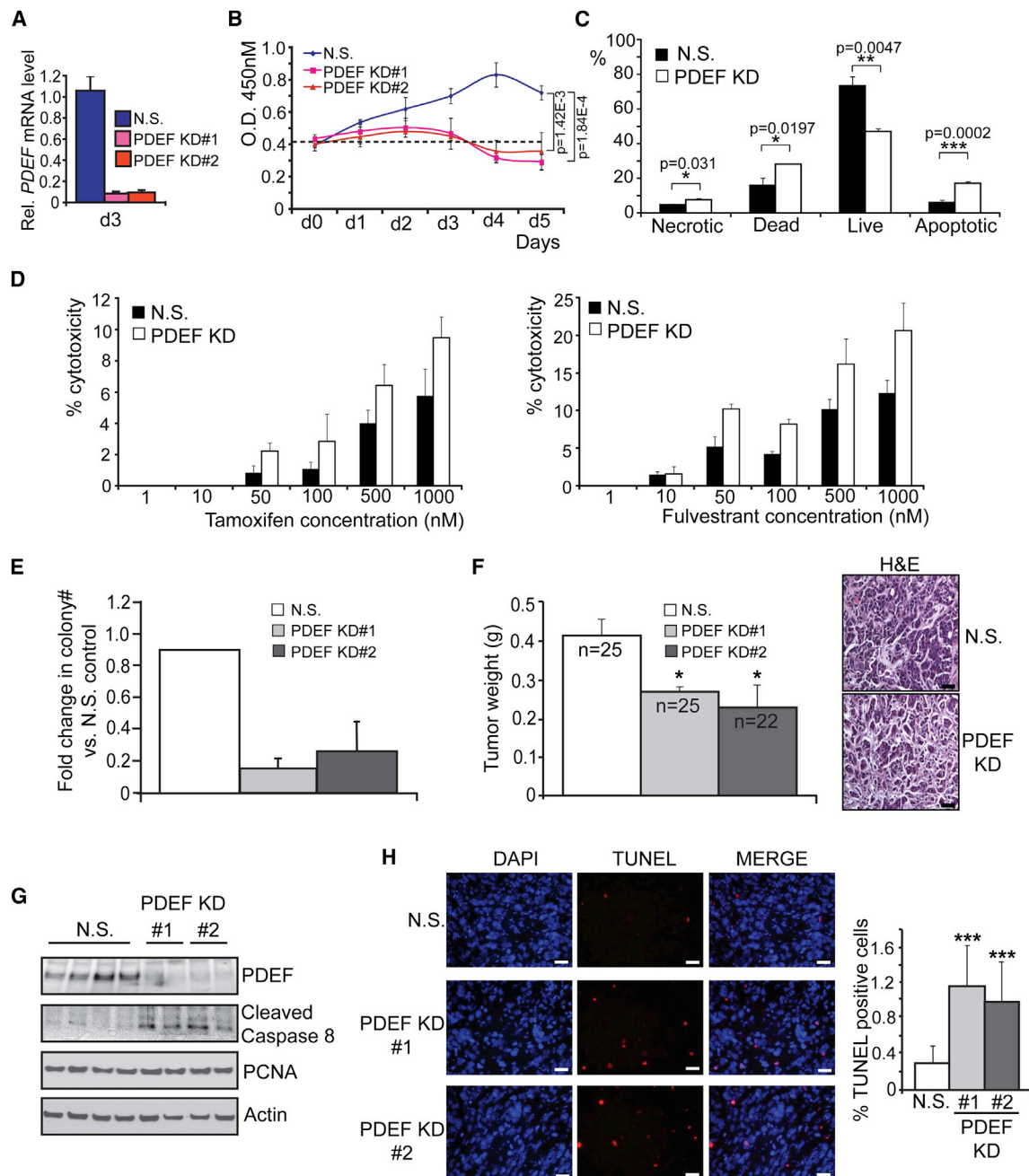


Figure 6. PDEF Knockdown Sensitizes MCF7 Cells to Hormone-Related Stress and Decreases Their Tumorigenic Properties

(A) PDEF mRNA levels were determined by real-time PCR in MCF7 cells transfected with NS or two independent PDEF-targeting (PDEF KD, KnockDown) siRNAs, and then grown for 3 days in hormone-depleted medium with 10 nM E2. Data represent means \pm SD.

(B) Growth curves of MCF7 cells transfected with NS or PDEF-targeting (KD) siRNAs in hormone-depleted medium with 10 nM E2. Data represent means \pm SD.

(C) AnnexinV/Propidium Iodide cell viability measurement of MCF7 cells transfected with NS or PDEF-targeting (KD) siRNAs, then grown for 24 hr in hormone-depleted medium. Data represent means \pm SD.

(D) Measurement of cytotoxicity after transfection of MCF7 cells with NS or PDEF-targeting (KD) siRNAs, followed by treatment for 48 hr with increasing doses of tamoxifen (left) or fulvestrant (right). Data represent means \pm SD.

(E) Soft agar colony formation assay of MCF7 cells infected with NS or PDEF-targeting (KD) shRNAs. The average fold change \pm SEM in colony number compared to control NS cells across three independent experiments is shown (* $p < 0.02$, *** $p < 0.0001$).

(F) Measurement of MCF7 xenograft tumor weight. Mammary fat pads of NOD/SCID mice were injected with NS or PDEF-targeting shRNA (KD #1 and #2) MCF7 cells. Estradiol release pellets were implanted subcutaneously 2–3 days prior to surgery. Tumors were harvested and weighed after 8 weeks of growth. Data represent mean \pm SEM, * $p < 0.04$. Tumor sections were analyzed with hematoxylin and eosin staining. Scale bars represent 50 μ m.

(G) Western blots of MCF7 xenograft tumor lysates. Tumors expressing either NS or PDEF-targeting (KD) shRNAs were analyzed.

(legend continued on next page)

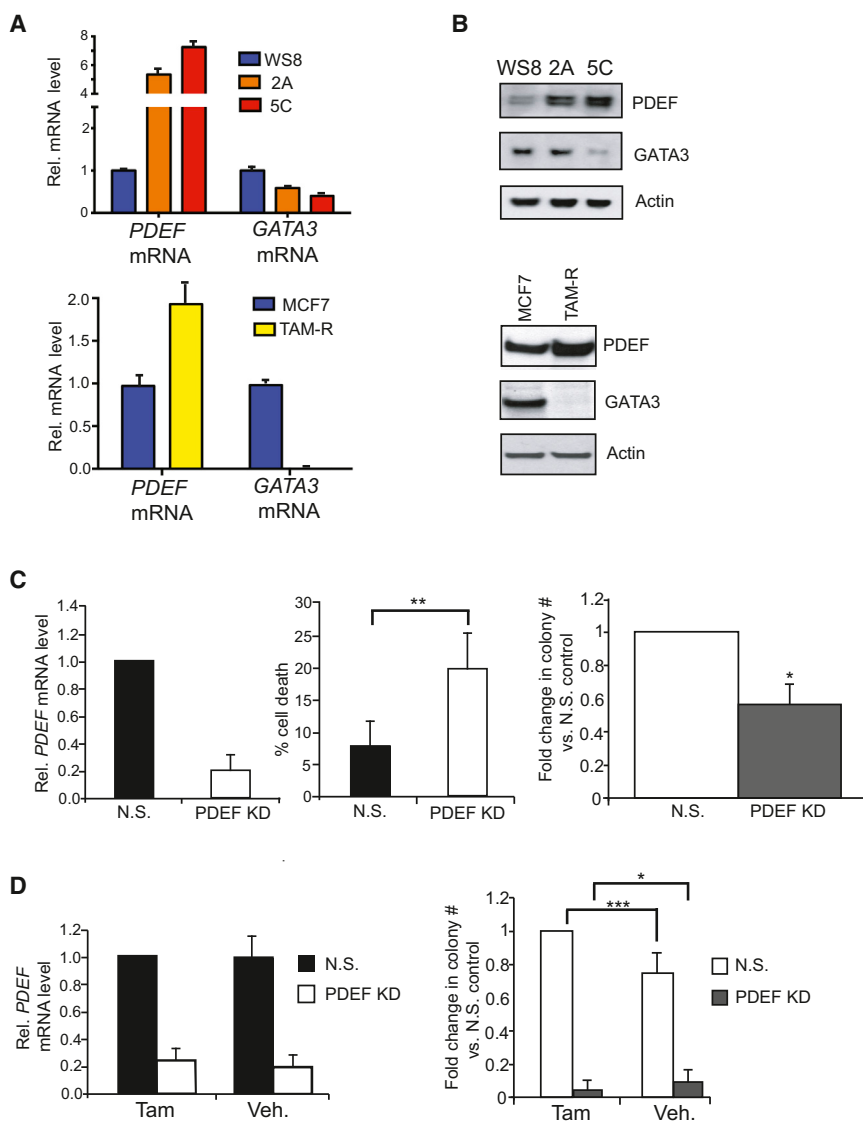


Figure 7. PDEF Expression Is Increased in Long-Term Estrogen-Deprived Cells and Tamoxifen-Resistant Cells Derived from MCF7 Cells

(A and B) PDEF and GATA3 mRNA and protein levels were determined by real-time PCR (A) or western blot (B) in parental MCF7 cells (WS8), clones 2A and 5C (upper panels), and tamoxifen-resistant (TAM-R) cells (lower panels). mRNA levels are presented as means \pm SD and normalized to the housekeeping gene *GAPDH*.

(C) Left: *PDEF* mRNA levels were determined in MCF7 5C cells by real-time PCR after transfection of NS or *PDEF*-targeting (*PDEF* KD, KnockDown) siRNAs. Middle: measurement of MCF7 5C cell mortality (** $p < 0.005$, data represent mean \pm SD). Right: soft agar colony formation assay of MCF7 5C cells infected with NS or *PDEF*-targeting (KD) shRNAs. Data represent the average fold change \pm SEM in colony number compared to control NS cells, * $p < 0.02$.

(D) Left: *PDEF* mRNA levels were determined in MCF7 TAM-R cells by real-time PCR 7 days after transduction of NS or *PDEF*-targeting (KD) shRNAs in the presence of 10^{-7} M tamoxifen or vehicle (EtOH). Right: soft agar colony formation assay of MCF7 TAM-R cells infected with NS control shRNA or *PDEF*-targeting shRNA (KD) in the presence of 10^{-7} M tamoxifen or vehicle (EtOH) (** $p < 0.001$, * $p < 0.05$). Data represent means \pm SD.

samples, whereas the genes downregulated in *PDEF* knockdown MCF7 cells were overexpressed in tumors compared to normal samples (Figure S5C). These findings demonstrate that *PDEF* knockdown triggers a gene expression program that switches cells toward a less tumorigenic phenotype.

In addition, we further analyzed these microarray results to identify potential mediators of the pro-apoptotic phenotype induced by *PDEF* loss. The cell death receptor *FAS* was selected as a candidate effector because *FAS* mRNA was overexpressed in MCF7 cells with *PDEF* knockdown under hormone-depleted conditions (Figures 8C and 8D), suggesting that *PDEF* acts as a repressor of *FAS* expression. Furthermore, analysis of a previously published *PDEF* cistrome established in VCaP prostate cancer cells (Wei et al., 2010) revealed the presence of a *PDEF*

binding region located upstream of the *FAS* gene locus. Direct *PDEF* ChIP in MCF7 cells confirmed *PDEF* recruitment to this binding region (Figure 8E). This result indicates that *PDEF* directly represses *FAS* expression and that this inhibition may promote the survival of MCF7 cells in hormone-depleted media. Interestingly, an inverse correlation between *FAS* and *PDEF* mRNA levels was observed in multiple ER⁺ breast carcinoma data sets (Figure S5D), thus confirming that *PDEF*-mediated repression of *FAS* expression is also relevant clinically.

To determine if *FAS* plays a functional role in the pro-apoptotic phenotype, we treated *PDEF* knockdown MCF7 cells with an anti-*FAS* Ligand (FasL) neutralizing antibody under hormone-depleted conditions (Figure 8F). FasL neutralizing antibody was sufficient to partially rescue the apoptotic phenotype in *PDEF* knockdown cells as compared to a negative control NS antibody. Moreover, *FAS* mRNA and protein expression were enhanced in both MCF7 2A and 5C clones upon *PDEF* downregulation (Figures 8G and 8H). Based on these findings, we hypothesize that increased *PDEF* levels promote the acquired endocrine resistance of estrogen-deprived

(H) Tumor sections were subjected to TUNEL cell death staining (red). Nuclei were stained with DAPI (blue). Three different tumors were stained for each shRNA (NS, *PDEF* KD#1 and #2) and five fields were photographed for each section. Representative images for each tumor type are shown. Scale bars represent 20 μ m. The ratio of TUNEL signal to the total number of nuclei is shown in the histogram. Data represent means \pm SD (** $p < 0.001$).

See also Figure S4.

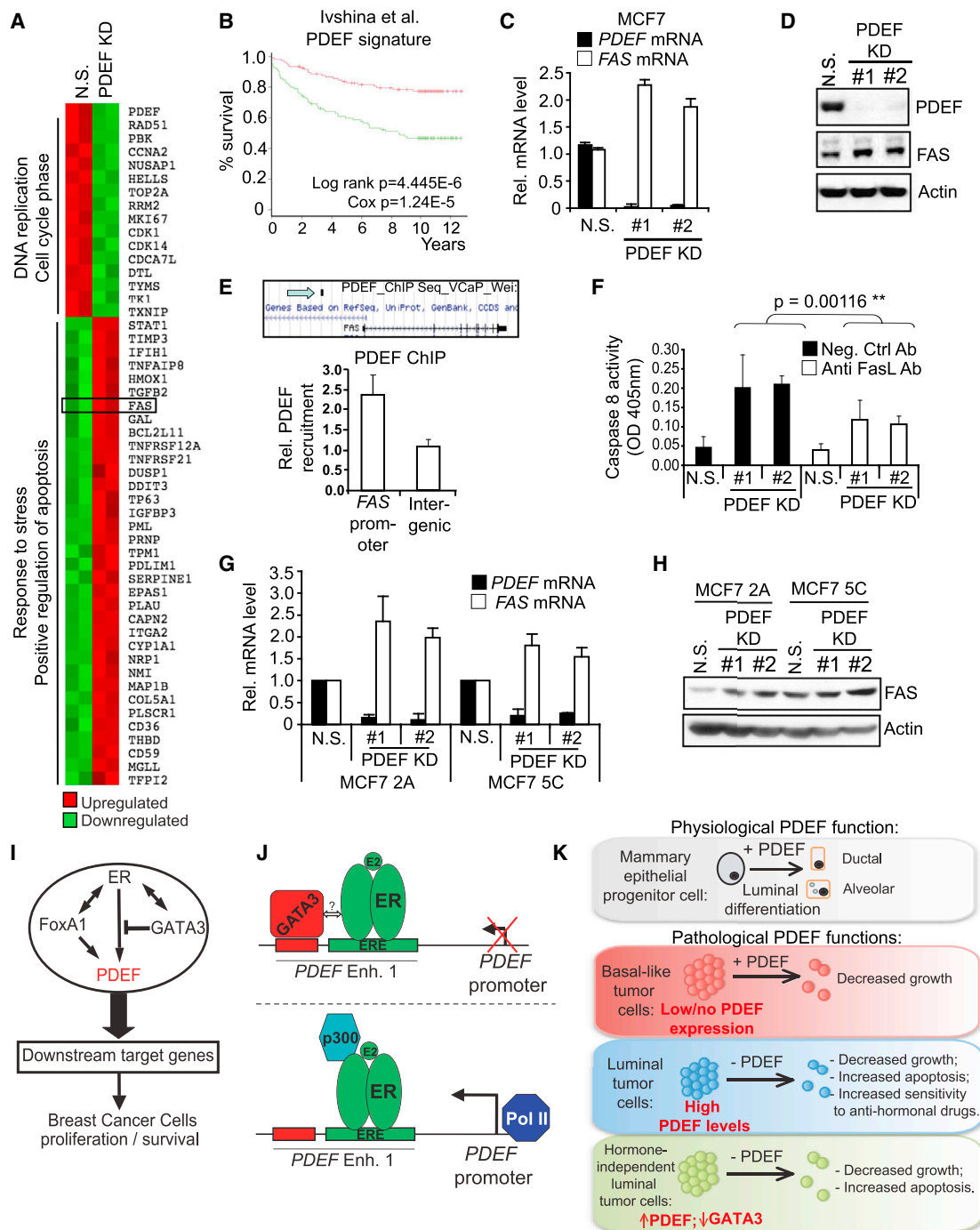


Figure 8. PDEF Promotes a Pro-Survival Gene Expression Program in Hormone-Depleted Conditions and Represses Pro-Apoptotic Death Domain FAS Receptor Expression

(A) Heatmap of a selection of differentially expressed genes generated from microarray analysis of MCF7 cells infected with NS or PDEF-targeting (PDEF KD, KnockDown) shRNAs, then subjected to hormone depletion for 48 hr. These expression changes were statistically significant.

(B) Kaplan-Meier survival analysis of the relationship between survival time and the PDEF signature. The PDEF signature was trained and tested on the Ivshina data set (Ivshina et al., 2006). The log-rank p-value is an indicator of significant differences in patient outcome when patients are dichotomized at the median of the predictor. The Cox p value treats the predictor as a continuous variable.

(C and D) PDEF and FAS mRNA and protein levels were determined by real-time PCR (C) or western blot (D) in MCF7 cells infected with NS or PDEF-targeting (KD) shRNAs, and grown for 48 hr (C) or 72 hr (D) in hormone-depleted medium. mRNA levels are presented as means \pm SD and normalized to the housekeeping gene GAPDH.

(E) Upper: schematic diagram of the PDEF binding region (indicated by arrow) upstream of the FAS gene locus as defined by PDEF ChIP sequencing in VCaP cells (Wei et al., 2010). Lower: direct PDEF ChIP followed by qPCR after culture of MCF7 cells in hormone-depleted medium for 48 hr. Data represent means \pm SD.

(legend continued on next page)

cells by inhibiting the expression of pro-apoptotic genes including *FAS*.

DISCUSSION

In this study, we demonstrated that PDEF is a downstream target of the ER/FOXA1/GATA3 network. In addition to its critical function as a lineage-specific regulator of ER⁺ breast cancer cell survival, PDEF also induces luminal differentiation of nontransformed basal epithelial cells (summarized in [Figures 8I–8K](#)).

Gene expression analyses revealed distinct PDEF signatures in two different contexts. PDEF overexpression in nontransformed MCF-10A mammary basal epithelial cells induced a striking luminal differentiation program, whereas PDEF knockdown in transformed luminal MCF7 cells subjected to hormone depletion induced a growth arrest and cell death program. The lack of significant overlap in these signatures suggests distinct roles for PDEF in the context of normal morphogenesis and tumorigenesis. Defining PDEF binding sites in the genome in these two contexts may reveal differential sets of direct target genes and cooperating factors. However, the role of PDEF in promoting survival is likely more important than its role in regulating differentiation in transformed cells because preliminary data suggest that PDEF knockdown induces changes in a subset of differentiation markers in luminal breast cancer cells, but does not appear to result in the generation of bipotent cells as observed in nontransformed COMMA-1D cells.

The dichotomous functions of PDEF in the context of normal and tumor cells distinguish it from other prodifferentiation factors that function as tumor suppressors. For example, GATA3 is required for luminal cell differentiation ([Asselin-Labat et al., 2007](#)); however, GATA3 downregulation enhances invasive activity and tumor cell dissemination to the lung, whereas GATA3 overexpression suppresses metastasis ([Kouros-Mehr et al., 2008](#)). In addition, GATA3 is mutated in 17.7% of ER⁺ breast carcinoma samples ([Stephens et al., 2012](#)). Interestingly, GATA3 silencing increased ER-binding intensity in a high proportion of recruiting regions ([Theodorou et al., 2013](#)). We hypothesize that PDEF could be an important target of the tumor-suppressive action of GATA3. The analysis of estrogen-deprived or tamoxifen-resistant cells provides supportive evidence for an inverse correlation between PDEF and GATA3, which may represent a marker of hormone-refractory breast cancers.

Studies of PDEF function in different cancers, including prostate and ovarian tumors, suggests a context-dependent role in tumorigenesis ([Johnson et al., 2010](#); [Sood et al., 2007](#); [Ghader-sohi et al., 2008](#); [Rodabaugh et al., 2007](#)). In breast cancer, PDEF cooperates with the oncogenes *ERBB2* and *CSF1R* to promote cell motility, invasion, and anchorage-independent growth of mammary epithelial cells ([Gunawardane et al., 2005](#)). In contrast,

other studies showed that ectopic expression of PDEF in highly malignant, ER[−], basal-like breast tumor cell lines ([Feldman et al., 2003](#); [Turner et al., 2007](#)) resulted in reduced proliferation, motility, and invasiveness, suggestive of a tumor suppressor role. However, the relevance of ectopic expression in tumor cell lineages in which PDEF is not normally expressed is difficult to interpret. Exogenous expression of ER in ER[−] cells led to similar paradoxical results, in which ER appeared to function as a tumor suppressor ([Levenson and Jordan, 1994](#)). Luminal epithelial-specific transcription factors, such as ER and PDEF, may reduce the mesenchymal properties of these cell lines, rendering them less invasive and migratory. Thus, loss of expression studies in ER⁺ cells represents a more appropriate context to examine the role of PDEF in tumorigenesis. Our data support a role for PDEF in breast cancer progression, at least in part by maintaining a proliferative state and enabling a prosurvival gene expression program.

Our results identify the FAS receptor, a member of the tumor necrosis family involved in the extrinsic apoptosis pathway ([Peter and Krammer, 2003](#)), as a direct PDEF transcriptional target. Nontransformed mammary epithelial cell lines express high levels of FAS, and its expression is decreased in several breast cancer cell lines ([Keane et al., 1996](#)). In addition, disease-free survival was significantly longer in patients with FAS-positive breast tumors compared to those with FAS-negative tumors ([Mottolese et al., 2000](#)). PDEF represses FAS gene expression, specifically under stress conditions such as hormone depletion. Several other ETS factors also display transcriptional-repressive activities, including Net, Yan, ERF, and Tel ([Mavrothalassitis and Ghysdael, 2000](#)). The mechanism of PDEF-mediated repression is not yet elucidated, and the identification of potential coregulators will provide new insights into its transcriptional activity.

Taken together, this study identifies PDEF not only as an essential factor within the ER-associated transcriptional network, but also as a potential therapeutic target for patients with ER⁺ breast carcinoma.

EXPERIMENTAL PROCEDURES

Reagents, Cells, and Tissue Culture Conditions

The antibodies, siRNAs, primers, and cells and tissue culture conditions are listed in the [Supplemental Experimental Procedures](#). Reduction mastectomy tissues were collected from patients who have provided informed consent under the DFCI IRB approved protocol 93-085. See the [Supplemental Experimental Procedures](#) for more details.

Gene Expression Microarray Analysis

Total RNA was isolated either from MCF-10A cells expressing pBabe/pBabe-PDEF or from MCF7 expressing NS/PDEF-targeting shRNA and subjected to reverse transcription, labeling, and hybridization to hgu133plus2 gene chip arrays (Affymetrix). See the [Supplemental Experimental Procedures](#) for more details.

(F) Measurement of caspase 8 activity in MCF7 cells transfected with NS or PDEF-targeting (KD) siRNAs, then subjected to hormone depletion (48 hr) in the presence of a negative control antibody or anti-Fas Ligand antibody (FasL, 5 ng/ml). Data represent means \pm SD.

(G and H) PDEF and FAS mRNA and protein levels were determined by real-time PCR (G) or western blot (H) in MCF7 2A and 5C clones infected with NS or PDEF-targeting (KD) shRNAs. mRNA levels are presented as means \pm SD and normalized to the housekeeping gene *GAPDH*.

(I) PDEF belongs to a network of ER-associated factors and is positively regulated by ER and FOXA1, whereas GATA3 acts as a repressor of PDEF expression.

(J) Mechanism of GATA3-mediated repression of PDEF.

(K) Physiologic and pathologic functions of PDEF.

See also [Figure S5](#) and [Tables S2](#) and [S3](#).

Lentiviral Infection and siRNA Transfection

Lentivirus was produced in 293T cells and retrovirus in 293GPG cells. For luminal progenitor cells, PDEF-targeting lentiviral particles were obtained from Santa Cruz Biotechnology (sc-45845-V). For PDEF overexpression, either the retroviral pBabe or lentiviral pBob vectors containing human or murine PDEF cDNA were used. See the [Supplemental Experimental Procedures](#) for more details.

Chromatin Immunoprecipitation

ChIP was performed as previously described (Carroll et al., 2006). See [Supplemental Experimental Procedures](#) for more details.

Growth Curves and Cytotoxicity Assay

Growth of MCF7 cells and cytotoxicity of tamoxifen and fulvestrant were measured using the cell proliferation WST-1 assay (Roche). See the [Supplemental Experimental Procedures](#) for more details.

Annexin V Analysis of Apoptosis and Caspase 8 Activity Assay

The Vybrant annexin V Kit #3 and the ApoTarget Caspase 8 colorimetric assay (Invitrogen) were used. See the [Supplemental Experimental Procedures](#) for more details.

Immunofluorescence

MCF-10A cells were stained with antibodies against cytokeratin-8 (Covance HK-8) and keratin-14 (Covance AF64). COMMA-1D colony assays were stained with antibodies against murine cytokeratin-8 (DSHB, University of Iowa; TROMA-1) and keratin-14 (Covance AF641). See the [Supplemental Experimental Procedures](#) for more details.

Flow Cytometry Analyses

MCF-10A and HMEC cells were trypsinized and resuspended in flow buffer (PBS containing 1% BSA, 2 mM EDTA, and 5% FBS) for 10 min. Cells were stained for 30 min with antibodies for PE-conjugated EpCAM and APC-conjugated CD10 (both eBioscience). Analysis was performed on a FACS Calibur machine (BD).

Soft Agar Assays

Six-well plates were coated with an underlay of 0.5% agarose (Sigma, type VII low melting). Cells were then plated in 0.35% agarose. Colonies were allowed to form for approximately 2 weeks. See the [Supplemental Experimental Procedures](#) for more details.

Fat Pad Tumor Assays

All animal studies were performed with the approval of the IACUC of Harvard Medical School. Eight-week-old female NOD/SCID mice were implanted with estrogen pellets (Innovative Research of America; 0.72 mg, 60 day release) prior to injection to support tumor growth; 2×10^6 MCF7 cells (expressing control or PDEF-targeting shRNAs, resuspended in Matrigel) were injected into the number 4 fat pad. Tumors were harvested after 8 weeks of growth. See the [Supplemental Experimental Procedures](#) for more details.

Survival Analysis

Breast tumor data sets were downloaded from <http://www.ncbi.nlm.nih.gov/geo> (lvhsina; GSE4922), (Desmedt; GSE7390) and <http://www.ebi.ac.uk/arrayexpress> (Chin; E-TABM-158). See the [Supplemental Experimental Procedures](#) for more details.

ACCESSION NUMBERS

The GEO accession number for the raw and processed microarray data presented in this paper is GSE40987.

SUPPLEMENTAL INFORMATION

Supplemental information includes Supplemental Experimental Procedures, five figures, and three tables and can be found with this article online at <http://dx.doi.org/10.1016/j.ccr.2013.04.026>.

ACKNOWLEDGMENTS

We are grateful to Housheng Hansen He for help with gene expression analysis and the Nikon Imaging Center at Harvard Medical School, the DF/HCC Rodent Histopathology Core, the Developmental Studies Hybridoma Bank at the University of Iowa, and members of the Brugge and Brown laboratories for technical assistance and helpful discussions. This work was supported by a DOD Breast Cancer Research Program Postdoctoral Fellowship (W81XWH-10-1-0029 to M.M.H.), fellowships from the Association pour la Recherche contre le Cancer (to G.B.) and Susan G. Komen for the Cure (KG080737 to G.B.), and grants from the Breast Cancer Research Foundation (to J.S.B.), the NCI (P01 CA080111 to M.B.), and NIDDK (R01 DK074967 to M.B.).

Received: September 21, 2012

Revised: February 19, 2013

Accepted: April 23, 2013

Published: June 10, 2013

REFERENCES

- Allinen, M., Beroukhi, R., Cai, L., Brennan, C., Lahti-Domenici, J., Huang, H., Porter, D., Hu, M., Chin, L., Richardson, A., et al. (2004). Molecular characterization of the tumor microenvironment in breast cancer. *Cancer Cell* 6, 17–32.
- Ariazi, E.A., Cunliffe, H.E., Lewis-Wambi, J.S., Slifker, M.J., Willis, A.L., Ramos, P., Tapia, C., Kim, H.R., Yerrum, S., Sharma, C.G., et al. (2011). Estrogen induces apoptosis in estrogen deprivation-resistant breast cancer through stress responses as identified by global gene expression across time. *Proc. Natl. Acad. Sci. USA* 108, 18879–18886.
- Asselin-Labat, M.L., Sutherland, K.D., Barker, H., Thomas, R., Shackleton, M., Forrest, N.C., Hartley, L., Robb, L., Grosveld, F.G., van der Wees, J., et al. (2007). Gata-3 is an essential regulator of mammary-gland morphogenesis and luminal-cell differentiation. *Nat. Cell Biol.* 9, 201–209.
- Carroll, J.S., Meyer, C.A., Song, J., Li, W., Geistlinger, T.R., Eeckhoutte, J., Brodsky, A.S., Keeton, E.K., Fertuck, K.C., Hall, G.F., et al. (2006). Genome-wide analysis of estrogen receptor binding sites. *Nat. Genet.* 38, 1289–1297.
- Chin, K., DeVries, S., Fridlyand, J., Spellman, P.T., Roydasgupta, R., Kuo, W.L., Lapuk, A., Neve, R.M., Qian, Z., Ryder, T., et al. (2006). Genomic and transcriptional aberrations linked to breast cancer pathophysiology. *Cancer Cell* 10, 529–541.
- Danielson, K.G., Oborn, C.J., Durban, E.M., Butel, J.S., and Medina, D. (1984). Epithelial mouse mammary cell line exhibiting normal morphogenesis in vivo and functional differentiation in vitro. *Proc. Natl. Acad. Sci. USA* 81, 3756–3760.
- Desmedt, C., Piette, F., Loi, S., Wang, Y., Lallemand, F., Haibe-Kains, B., Viale, G., Delorenzi, M., Zhang, Y., d'Assignies, M.S., et al.; TRANSBIG Consortium. (2007). Strong time dependence of the 76-gene prognostic signature for node-negative breast cancer patients in the TRANSBIG multicenter independent validation series. *Clin. Cancer Res.* 13, 3207–3214.
- Dontu, G., Al-Hajj, M., Abdallah, W.M., Clarke, M.F., and Wicha, M.S. (2003). Stem cells in normal breast development and breast cancer. *Cell Prolif.* 36 (Suppl 1), 59–72.
- Feldman, R.J., Sementchenko, V.I., Gayed, M., Fraig, M.M., and Watson, D.K. (2003). Pdef expression in human breast cancer is correlated with invasive potential and altered gene expression. *Cancer Res.* 63, 4626–4631.
- Findlay, V.J., Turner, D.P., Moussa, O., and Watson, D.K. (2008). MicroRNA-mediated inhibition of prostate-derived Ets factor messenger RNA translation affects prostate-derived Ets factor regulatory networks in human breast cancer. *Cancer Res.* 68, 8499–8506.
- Galang, C.K., Muller, W.J., Foos, G., Oshima, R.G., and Hauser, C.A. (2004). Changes in the expression of many Ets family transcription factors and of potential target genes in normal mammary tissue and tumors. *J. Biol. Chem.* 279, 11281–11292.
- Ghadersohi, A., and Sood, A.K. (2001). Prostate epithelium-derived Ets transcription factor mRNA is overexpressed in human breast tumors and is a candidate breast tumor marker and a breast tumor antigen. *Clin. Cancer Res.* 7, 2731–2738.

- Ghadarsohi, A., Odunsi, K., Zhang, S., Azrak, R.G., Bundy, B.N., Manjili, M.H., and Li, F. (2008). Prostate-derived Ets transcription factor as a favorable prognostic marker in ovarian cancer patients. *Int. J. Cancer* 123, 1376–1384.
- Gregorieff, A., Stange, D.E., Kujala, P., Begthel, H., van den Born, M., Korving, J., Peters, P.J., and Clevers, H. (2009). The ets-domain transcription factor Spdef promotes maturation of goblet and paneth cells in the intestinal epithelium. *Gastroenterology* 137, 1333–1345.
- Gu, X., Zerbini, L.F., Otu, H.H., Bhasin, M., Yang, Q., Joseph, M.G., Grall, F., Onatunde, T., Correa, R.G., and Libermann, T.A. (2007). Reduced PDEF expression increases invasion and expression of mesenchymal genes in prostate cancer cells. *Cancer Res.* 67, 4219–4226.
- Gunawardane, R.N., Sgroi, D.C., Wrobel, C.N., Koh, E., Daley, G.Q., and Brugge, J.S. (2005). Novel role for PDEF in epithelial cell migration and invasion. *Cancer Res.* 65, 11572–11580.
- Hanstein, B., Eckner, R., DiRenzo, J., Halachmi, S., Liu, H., Searcy, B., Kurokawa, R., and Brown, M. (1996). p300 is a component of an estrogen receptor coactivator complex. *Proc. Natl. Acad. Sci. USA* 93, 11540–11545.
- Ivshina, A.V., George, J., Senko, O., Mow, B., Putti, T.C., Smeds, J., Lindahl, T., Pawitan, Y., Hall, P., Nordgren, H., et al. (2006). Genetic reclassification of histologic grade delineates new clinical subtypes of breast cancer. *Cancer Res.* 66, 10292–10301.
- Johnson, T.R., Koul, S., Kumar, B., Khandrika, L., Venezia, S., Maroni, P.D., Meacham, R.B., and Koul, H.K. (2010). Loss of PDEF, a prostate-derived Ets factor is associated with aggressive phenotype of prostate cancer: regulation of MMP 9 by PDEF. *Mol. Cancer* 9, 148.
- Jones, C., Mackay, A., Grigoriadis, A., Cossu, A., Reis-Filho, J.S., Fulford, L., Dexter, T., Davies, S., Bulmer, K., Ford, E., et al. (2004). Expression profiling of purified normal human luminal and myoepithelial breast cells: identification of novel prognostic markers for breast cancer. *Cancer Res.* 64, 3037–3045.
- Kalyuga, M., Gallego-Ortega, D., Lee, H.J., Roden, D.L., Cowley, M.J., Caldon, C.E., Stone, A., Allerdice, S.L., Valdes-Mora, F., Launchbury, R., et al. (2012). ELF5 suppresses estrogen sensitivity and underpins the acquisition of anti-estrogen resistance in luminal breast cancer. *PLoS Biol.* 10, e1001461.
- Keane, M.M., Ettenberg, S.A., Lowrey, G.A., Russell, E.K., and Lipkowitz, S. (1996). Fas expression and function in normal and malignant breast cell lines. *Cancer Res.* 56, 4791–4798.
- Kouros-Mehr, H., Bechis, S.K., Slorach, E.M., Littlepage, L.E., Egeblad, M., Ewald, A.J., Pai, S.Y., Ho, I.C., and Werb, Z. (2008). GATA-3 links tumor differentiation and dissemination in a luminal breast cancer model. *Cancer Cell* 13, 141–152.
- Levenson, A.S., and Jordan, V.C. (1994). Transfection of human estrogen receptor (ER) cDNA into ER-negative mammalian cell lines. *J. Steroid Biochem. Mol. Biol.* 51, 229–239.
- Lim, E., Vaillant, F., Wu, D., Forrest, N.C., Pal, B., Hart, A.H., Asselin-Labat, M.L., Gyorki, D.E., Ward, T., Partanen, A., et al.; kConFab. (2009). Aberrant luminal progenitors as the candidate target population for basal tumor development in BRCA1 mutation carriers. *Nat. Med.* 15, 907–913.
- Lu, X., Lu, X., Wang, Z.C., Iglehart, J.D., Zhang, X., and Richardson, A.L. (2008). Predicting features of breast cancer with gene expression patterns. *Breast Cancer Res. Treat.* 108, 191–201.
- Lupien, M., Eeckhoutte, J., Meyer, C.A., Wang, Q., Zhang, Y., Li, W., Carroll, J.S., Liu, X.S., and Brown, M. (2008). FoxA1 translates epigenetic signatures into enhancer-driven lineage-specific transcription. *Cell* 132, 958–970.
- Mavrothalassitis, G., and Ghysdael, J. (2000). Proteins of the ETS family with transcriptional repressor activity. *Oncogene* 19, 6524–6532.
- McManus, K.J., and Hendzel, M.J. (2003). Quantitative analysis of CBP- and P300-induced histone acetylations in vivo using native chromatin. *Mol. Cell Biol.* 23, 7611–7627.
- Mottollese, M., Buglioni, S., Bracalenti, C., Cardarelli, M.A., Ciabocco, L., Giannarelli, D., Botti, C., Natali, P.G., Concetti, A., and Venanzi, F.M. (2000). Prognostic relevance of altered Fas (CD95)-system in human breast cancer. *Int. J. Cancer* 89, 127–132.
- Moussa, O., Turner, D.P., Feldman, R.J., Sementchenko, V.I., McCarragher, B.D., Desouki, M.M., Fraig, M., and Watson, D.K. (2009). PDEF is a negative regulator of colon cancer cell growth and migration. *J. Cell. Biochem.* 108, 1389–1398.
- Neve, R.M., Chin, K., Fridlyand, J., Yeh, J., Baehner, F.L., Fevr, T., Clark, L., Bayani, N., Coppe, J.P., Tong, F., et al. (2006). A collection of breast cancer cell lines for the study of functionally distinct cancer subtypes. *Cancer Cell* 10, 515–527.
- Oettgen, P., Finger, E., Sun, Z., Akbarali, Y., Thamrongsak, U., Boltax, J., Grall, F., Dube, A., Weiss, A., Brown, L., et al. (2000). PDEF, a novel prostate epithelium-specific ets transcription factor, interacts with the androgen receptor and activates prostate-specific antigen gene expression. *J. Biol. Chem.* 275, 1216–1225.
- Osborne, C.K., and Schiff, R. (2011). Mechanisms of endocrine resistance in breast cancer. *Annu. Rev. Med.* 62, 233–247.
- Park, K.S., Korfhagen, T.R., Bruno, M.D., Kitzmiller, J.A., Wan, H., Wert, S.E., Khurana Hershey, G.K., Chen, G., and Whitsett, J.A. (2007). SPDEF regulates goblet cell hyperplasia in the airway epithelium. *J. Clin. Invest.* 117, 978–988.
- Perou, C.M., Sørlie, T., Eisen, M.B., van de Rijn, M., Jeffrey, S.S., Rees, C.A., Pollack, J.R., Ross, D.T., Johnsen, H., Akslen, L.A., et al. (2000). Molecular portraits of human breast tumours. *Nature* 406, 747–752.
- Peter, M.E., and Krammer, P.H. (2003). The CD95(APO-1/Fas) DISC and beyond. *Cell Death Differ.* 10, 26–35.
- Richardson, A.L., Wang, Z.C., De Nicolò, A., Lu, X., Brown, M., Miron, A., Liao, X., Iglehart, J.D., Livingston, D.M., and Ganesan, S. (2006). X chromosomal abnormalities in basal-like human breast cancer. *Cancer Cell* 9, 121–132.
- Rodabaugh, K.J., Mhawech-Fauceglia, P., Groth, J., Lele, S., and Sood, A.K. (2007). Prostate-derived Ets factor is overexpressed in serous epithelial ovarian tumors. *Int. J. Gynecol. Pathol.* 26, 10–15.
- Shepherd, T., and Hassell, J.A. (2001). Role of Ets transcription factors in mammary gland development and oncogenesis. *J. Mammary Gland Biol. Neoplasia* 6, 129–140.
- Sood, A.K., Saxena, R., Groth, J., Desouki, M.M., Cheewakiangkrai, C., Rodabaugh, K.J., Kasyapa, C.S., and Geradts, J. (2007). Expression characteristics of prostate-derived Ets factor support a role in breast and prostate cancer progression. *Hum. Pathol.* 38, 1628–1638.
- Sood, A.K., Wang, J., Mhawech-Fauceglia, P., Jana, B., Liang, P., and Geradts, J. (2009). Sam-pointed domain containing Ets transcription factor in luminal breast cancer pathogenesis. *Cancer Epidemiol. Biomarkers Prev.* 18, 1899–1903.
- Sørlie, T., Perou, C.M., Tibshirani, R., Aas, T., Geisler, S., Johnsen, H., Hastie, T., Eisen, M.B., van de Rijn, M., Jeffrey, S.S., et al. (2001). Gene expression patterns of breast carcinomas distinguish tumor subclasses with clinical implications. *Proc. Natl. Acad. Sci. USA* 98, 10869–10874.
- Stephens, P.J., Tarpey, P.S., Davies, H., Van Loo, P., Greenman, C., Wedge, D.C., Nik-Zainal, S., Martin, S., Varela, I., Bignell, G.R., et al.; Oslo Breast Cancer Consortium (OSBREAC). (2012). The landscape of cancer genes and mutational processes in breast cancer. *Nature* 486, 400–404.
- Stingl, J., Raouf, A., Emerman, J.T., and Eaves, C.J. (2005). Epithelial progenitors in the normal human mammary gland. *J. Mammary Gland Biol. Neoplasia* 10, 49–59.
- Theodorou, V., Stark, R., Menon, S., and Carroll, J.S. (2013). GATA3 acts upstream of FOXA1 in mediating ESR1 binding by shaping enhancer accessibility. *Genome Res.* 23, 12–22.
- Turner, D.P., Moussa, O., Sauane, M., Fisher, P.B., and Watson, D.K. (2007). Prostate-derived ETS factor is a mediator of metastatic potential through the inhibition of migration and invasion in breast cancer. *Cancer Res.* 67, 1618–1625.
- Wang, Y., Klijn, J.G., Zhang, Y., Sieuwerts, A.M., Look, M.P., Yang, F., Talantov, D., Timmermans, M., Meijer-van Gelder, M.E., Yu, J., et al. (2005). Gene-expression profiles to predict distant metastasis of lymph-node-negative primary breast cancer. *Lancet* 365, 671–679.
- Wei, G.H., Badis, G., Berger, M.F., Kivioja, T., Palin, K., Enge, M., Bonke, M., Jolma, A., Varjosalo, M., Gehrke, A.R., et al. (2010). Genome-wide analysis of ETS-family DNA-binding in vitro and in vivo. *EMBO J.* 29, 2147–2160.

Sox4 Is a Master Regulator of Epithelial-Mesenchymal Transition by Controlling Ezh2 Expression and Epigenetic Reprogramming

Neha Tiwari,^{1,4} Vijay K. Tiwari,^{2,5} Lorenz Waldmeier,¹ Piotr J. Balwierz,³ Phil Arnold,³ Mikhail Pachkov,³ Nathalie Meyer-Schaller,¹ Dirk Schübeler,² Erik van Nimwegen,³ and Gerhard Christofori^{1,*}

¹Department of Biomedicine, University of Basel, 4058 Basel, Switzerland

²Friedrich Miescher Institute for Biomedical Research, 4058 Basel, Switzerland

³Biozentrum, University of Basel, and Swiss Institute of Bioinformatics, 4056 Basel, Switzerland

⁴Present address: Institute of Physiological Chemistry, University Medical Center, Johannes Gutenberg University Mainz, 55131 Mainz, Germany

⁵Present address: Institute for Molecular Biology gGmbH (IMB), 55128 Mainz, Germany

*Correspondence: gerhard.christofori@unibas.ch

<http://dx.doi.org/10.1016/j.ccr.2013.04.020>

SUMMARY

Gene expression profiling has uncovered the transcription factor Sox4 with upregulated activity during TGF- β -induced epithelial-mesenchymal transition (EMT) in normal and cancerous breast epithelial cells. Sox4 is indispensable for EMT and cell survival in vitro and for primary tumor growth and metastasis in vivo. Among several EMT-relevant genes, Sox4 directly regulates the expression of *Ezh2*, encoding the Polycomb group histone methyltransferase that trimethylates histone 3 lysine 27 (H3K27me3) for gene repression. Ablation of *Ezh2* expression prevents EMT, whereas forced expression of *Ezh2* restores EMT in Sox4-deficient cells. *Ezh2*-mediated H3K27me3 marks associate with key EMT genes, representing an epigenetic EMT signature that predicts patient survival. Our results identify Sox4 as a master regulator of EMT by governing the expression of the epigenetic modifier *Ezh2*.

INTRODUCTION

Epithelial-mesenchymal transition (EMT) is a cellular mechanism known to constitute the core of normal embryonic development (Hanahan and Weinberg, 2011; Kalluri, 2009; Kalluri and Weinberg, 2009; Nieto, 2010; Polyak and Weinberg, 2009; Thiery and Sleeman, 2006). Similar, yet pathophysiological transitions occur during the progression of epithelial tumors, endowing cancer cells with increased motility and invasiveness to seed metastasis and, sometimes, after metastatic dissemination to redifferentiate into epithelial structures by mesenchymal-epithelial transition (Kang and Massagué, 2004; Thiery and Morgan, 2004). Multiple oncogenic events and signaling pathways, mediated, for example, by transforming growth factor β (TGF- β), hepatocyte growth factor (HGF), Wnt and Notch signaling, or

oncogenic Src or Ras activation, are implicated in the induction of EMT (Hanahan and Weinberg, 2011; Kalluri, 2009; Kalluri and Weinberg, 2009; Nieto, 2010; Polyak and Weinberg, 2009; Thiery and Sleeman, 2006).

Sox4 is a member of the Sox (SRY-related HMG-box) family of transcription factors with a critical role in embryonic development and in cell-fate determination during organogenesis of the heart (Restivo et al., 2006; Schilham et al., 1996), pancreas (Lioubinski et al., 2003; Wilson et al., 2005), and brain (Cheung et al., 2000; Hong and Saint-Jeannet, 2005), and in B and T lymphocyte differentiation (Cheung et al., 2000; Hong and Saint-Jeannet, 2005; Lioubinski et al., 2003; Schilham et al., 1996, 1997; van de Wetering et al., 1993; Wilson et al., 2005). Sox4 gene expression is upregulated in many cancer types, and increased Sox4 activity contributes to cellular transformation (Liu et al., 2006; Shin

Significance

An epithelial-mesenchymal transition (EMT) is a key process during organismal development and the progression of epithelial tumors to metastatic cancers. Here, we identify the transcription factor Sox4 as a master regulator of EMT. Sox4 appears to act highly upstream in the epistatic hierarchy of EMT regulation. It controls a number of EMT-relevant genes in addition to *Ezh2*. Conversely, *Ezh2* is able to functionally replace Sox4 during EMT and regulates the expression of a number of EMT-associated genes. *Ezh2* thus represents one critical Sox4 target gene during EMT. The results exemplify an important interplay between transcriptional and epigenetic control during EMT and suggest that the inhibition of *Ezh2* could be an attractive avenue for the therapeutic intervention of malignant tumor progression.

et al., 2004), cell survival (Aaboe et al., 2006; Ahn et al., 2002; Liu et al., 2006; Pramoonjago et al., 2006), and metastasis (Liao et al., 2008; Tavazoie et al., 2008). For example, restoration of miR-335 expression suppresses lung and bone metastasis in human cancer cells by interfering with the expression of Sox4 (Tavazoie et al., 2008). Interestingly, Sox4 also directly modulates key cellular regulators, including the genes encoding for epidermal growth factor receptor (EGFR), tenascin-C, heat shock protein 70 (Hsp70), frizzled homolog 5 (Fzd5), Delta-like 1 (Dll1), and Patched-1 (Ptc1), the transcriptional regulators Mll, Foxa1, Znf281, and Nkx3-1, and components of the RNAi machinery, including Dicer, Argonaute 1, and RNA helicase A (Scharer et al., 2009). Finally, Sox4 regulates Wnt signaling by directly binding to β -catenin and Tcf family members (Sinner et al., 2007). Most recently, Sox4 has been reported to induce EMT and to cooperate with oncogenic Ras in breast cancer progression (Zhang et al., 2012); however, its direct transcriptional target genes during EMT have remained elusive. Here, we demonstrate a central role of Sox4 in EMT as well as in primary tumor growth and metastasis by directly regulating the expression of a number of genes with critical functions in EMT, including *Ezh2*.

The histone methyltransferase Ezh2 (Enhancer of Zeste homolog 2) is a component of the Polycomb (PcG) repressive complex 2 (PRC2), which epigenetically regulates genes involved in cell fate decisions. Ezh2 specifically trimethylates nucleosomal histone H3 at lysine 27 (H3K27me3), an epigenetic modification associated with gene silencing (Sparmann and van Lohuizen, 2006). A conditional knockout of the *Ezh2* gene in basal keratinocytes leads a precocious acquisition of an epidermal barrier function in the embryo (Ezhkova et al., 2009), while a conditional knockout of *Ezh2* in B-lymphocytes results in improper IgH rearrangements (Su et al., 2003), suggesting a role for Ezh2 methyltransferase in cell differentiation and maturation. Ezh2 is found to be highly expressed in a variety of cancer types where the genomic loss of miR-101 leads to increased expression of Ezh2 and concomitant deregulation of epigenetic pathways, altogether resulting in cancer progression (Varambally et al., 2008). Furthermore, Ezh2 can induce EMT and increase the metastatic potential of prostate cancer cells by downregulation of DAB2IP, a tumor-suppressive Ras GTPase-activating protein (RasGAP) (Chen et al., 2005; Min et al., 2010). Finally, low Ezh2 expression levels correlate with metastasis-free survival in breast cancer (Cao et al., 2008; Kleer et al., 2003). However, whether and how Ezh2-mediated epigenetic mechanisms contribute to the transcriptional reprogramming that accompanies EMT is still poorly understood.

RESULTS

Sox4 Is Required for EMT

To identify critical genes underlying early, intermediate, and late stages of EMT, we induced EMT in the untransformed normal murine mammary gland (NMuMG) cell line by treatment with TGF- β for 0, 1, 4, 7, 10, and 20 days (data not shown). During this time course, the cells underwent progressive EMT and acquired a complete mesenchymal morphology (Lehembre et al., 2008). Motif activity response analysis (MARA) (Suzuki et al., 2009) of gene expression data derived from the EMT time course predicted several transcription factor binding motifs

to be important regulators of the EMT expression dynamics, including a motif bound by Sox transcription factors (Figure S1A available online). Gene expression profiling and quantitative RT-PCR experiments revealed that Sox4 and Sox9 were the only Sox family members significantly upregulated in their expression during TGF- β -induced EMT in NMuMG cells (Figures S1B–S1D). Sox4 expression was also robustly induced during EMT in a number of other cellular EMT systems, including TGF- β -induced EMT in Py2T murine breast cancer cells derived from a tumor of MMTV-PyMT transgenic mice (Waldmeier et al., 2012), in MCF10A human breast epithelial cells, in EpRas murine mammary epithelial cells (Figures S1D–S1G), and in human mammary epithelial cells (Kloeker et al., 2004). Sox4 expression was also increased in MCF7 human breast cancer cells that exert full EMT upon shRNA-mediated knockdown of E-cadherin expression (Lehembre et al., 2008; Figure S1H).

To directly assess the role of Sox4 and Sox9 in EMT, NMuMG cells were transfected with a pool of two different siRNAs against Sox4 (siSox4) and Sox9 (siSox9), as well as siSox4 and siSox9 together, to transiently ablate the expression of Sox4 and Sox9 in the absence and presence of TGF- β , resulting in an efficient repression of Sox4 and Sox9 expression (Figures 1A; Figures S1I and S1J). As reported recently (Zhang et al., 2012), Sox4-ablated NMuMG cells were not able to undergo EMT and largely retained their epithelial morphology during TGF- β treatment, whereas cells transfected with control-siRNA (siControl) changed to a mesenchymal, fibroblastoid phenotype (Figure 1B). In contrast, the single ablation of Sox9 did not have any effect on TGF- β -induced EMT, while the concomitant ablation of Sox4 and Sox9 mimicked the single ablation of Sox4 (Figures S1K and S1L). Immunofluorescence staining revealed that Sox4 depletion in the absence of TGF- β did not substantially affect the epithelial morphology of NMuMG cells (Figure 1C). In the presence of TGF- β , Sox4-depleted cells maintained the epithelial markers E-cadherin and ZO-1 at the cell membrane, and the expression of the mesenchymal marker N-cadherin was decreased compared to that observed for TGF- β -treated siControl cells (Figure 1C). Moreover, TGF- β -mediated remodeling of the cytoskeleton from cortical actin to stress fibers, as determined by phalloidin staining, and focal adhesion formation, as determined by paxillin staining, were significantly reduced in siSox4 cells (Figure 1C; Figure S1M). The failure to lose epithelial and gain mesenchymal marker expression in TGF- β -treated, Sox4-depleted cells was further confirmed by immunoblotting analysis (Figure 1D). Notably, Sox4 depletion in NMuMG cells treated previously with TGF- β for 15 days caused these mesenchymal cells to revert to an epithelial phenotype (Figure 1E). Similar to NMuMG cells, shRNA-mediated stable knockdown of Sox4 in Py2T cells markedly delayed TGF- β -induced EMT (Figures S1N–S1P). Together, these results demonstrate that Sox4, but not Sox9, is required for the induction and maintenance of TGF- β -induced EMT in murine mammary epithelial cells.

Sox4 Is Required and Sufficient for Cell Survival and Cell Migration

Sox4 has been implicated in cell survival in a variety of cancers (Hur et al., 2010; Pramoonjago et al., 2006; Shen et al., 2010). Indeed, Sox4-depleted NMuMG and Py2T cells also showed a

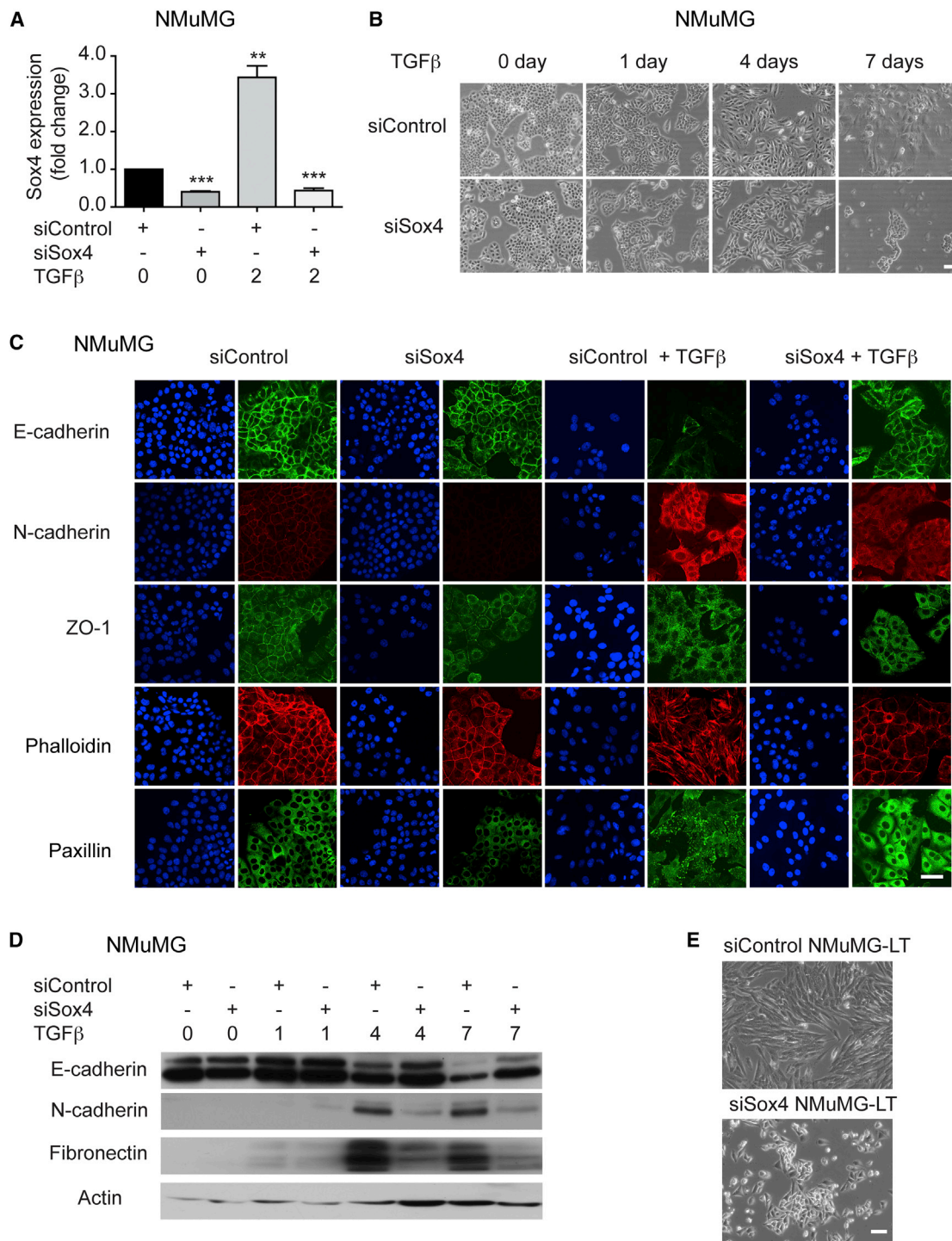


Figure 1. Sox4 Is Required for EMT

(A) Sox4 mRNA levels were determined by quantitative RT-PCR in NMuMG cells transfected with either control siRNA (siControl) or with siRNA against Sox4 (siSox4) in the absence or presence of TGF-β for 2 days. Fold changes are relative to those of cells transfected with control siRNA in the absence of TGF-β.

(B) NMuMG cells transfected with either siControl or siSox4 were treated with TGF-β for the number of days indicated, and their morphology was evaluated by phase-contrast microscopy. Scale bar, 100 μm.

(C) Immunofluorescence microscopy analysis of changes in the localization and expression levels of marker proteins during EMT. NMuMG cells transfected with either siControl or siSox4 were left untreated or treated with TGF-β for 2 days and were stained with antibodies against the epithelial markers E-cadherin and ZO-1, against the mesenchymal marker N-cadherin, against paxillin to detect focal adhesion plaques, and with phalloidin to visualize the actin cytoskeleton. Scale bar, 50 μm.

(legend continued on next page)

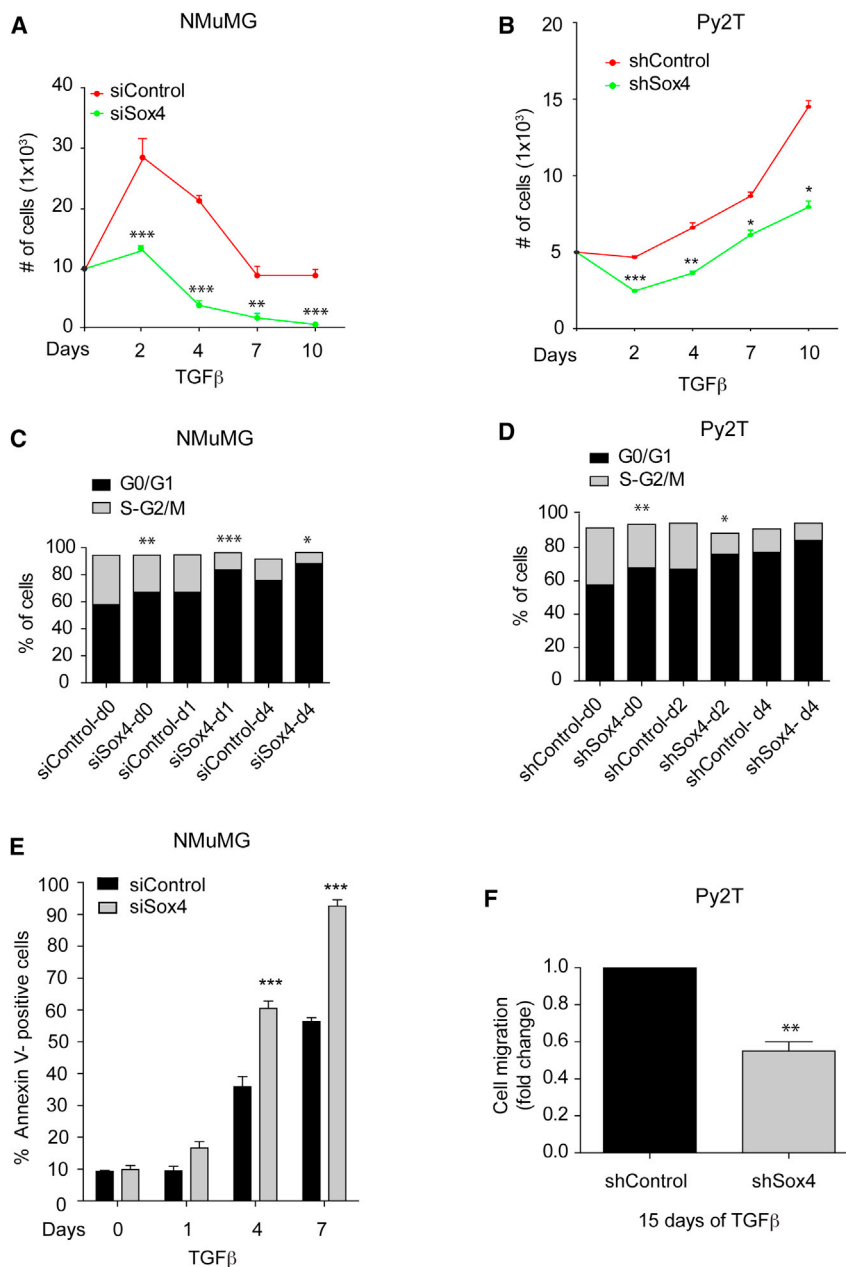


Figure 2. Sox4 Is Required for Cell Survival and Cell Migration during TGF- β -Induced EMT

(A and B) siRNA or shRNA-mediated ablation of Sox4 expression (siSox4 and shSox4, respectively) during TGF- β treatment of NMuMG (A) and Py2T (B) cells results in a significant decrease in cell numbers compared to transfection with control siRNA or shRNA (siControl and shControl, respectively).

(C and D) NMuMG cells (C) or Py2T cells (D) transfected with either siControl and shControl or siSox4 and shSox4 were treated with TGF- β for the days indicated (d0 to d4). Cells were stained with propidium iodide (PI), and the percentages of cells in G0/G1 and S-G2/M phases of the cell cycle were determined by flow cytometry.

(E) NMuMG cells transfected with either siControl or siSox4 were treated with TGF- β for the days indicated, and the rates of apoptosis were determined by Annexin-V staining and flow cytometry.

(F) shSox4-expressing and shControl-expressing Py2T murine breast cancer cells were treated for 15 days with TGF- β , and cell migration was determined in a modified Boyden chamber migration assay 20 hr after seeding and using 20% FBS as a chemoattractant.

Statistical values were calculated using an unpaired, two-tailed t test. *p < 0.05; **p < 0.01; ***p < 0.001. Error bars indicate the mean \pm SD.

significant reduction in cell growth in comparison to control cells and displayed a discernable sensitivity toward TGF- β -mediated growth inhibition (Figures 2A and 2B). Propidium iodide staining followed by flow-cytometry-based cell cycle analysis revealed a G0/G1 cell cycle arrest after Sox4 depletion (Figures 2C and 2D). Annexin-V staining demonstrated a marked increase in the levels of apoptosis in siSox4-transfected NMuMG cells (Figure 2E), but

not in Py2T cells (data not shown). These results indicate that Sox4 is required for cell survival and proliferation during TGF- β -induced EMT and that the prosurvival function of Sox4 only becomes critical in nontransformed cells. Cell migration is a characteristic feature of EMT and metastasis (Brabletz et al., 2005; Christofori, 2006; Grünert et al., 2003; Huber et al., 2005; Thiery and Sleeman, 2006). Transwell migration assays with the apoptosis-resistant Py2T breast cancer cells revealed that shSox4 Py2T cells migrated significantly less than shControl cells after long-term treatment with TGF- β (Figure 2F).

We next asked whether Sox4 was sufficient to induce EMT. Transient expression of HA-tagged Sox4 in NMuMG cells at the levels observed during TGF- β -induced EMT increased filopodia formation and cell scattering (Figure 3A) accompanied by the gain of the mesenchymal markers N-cadherin and fibronectin (Figures 3B and 3C). Although its mRNA and protein levels were not apparently affected, E-cadherin was displaced at the cell junctions of HA-Sox4-expressing cells (Figure 3D). Stable expression of

(D) Expression of E-cadherin, N-cadherin, and fibronectin was determined by immunoblotting during TGF- β -induced EMT in NMuMG cells transfected with either siSox4 or siControl. Immunoblotting for actin was used as a loading control.

(E) Morphology of long-term TGF- β -treated NMuMG (NMuMG-LT) cells transfected with either siControl or siSox4, as evaluated by phase-contrast microscopy. Scale bar, 100 μ m.

Statistical values were calculated using a paired, two-tailed t test. **p < 0.01; ***p < 0.001. Error bars indicate the mean \pm SD.

See also Figure S1.

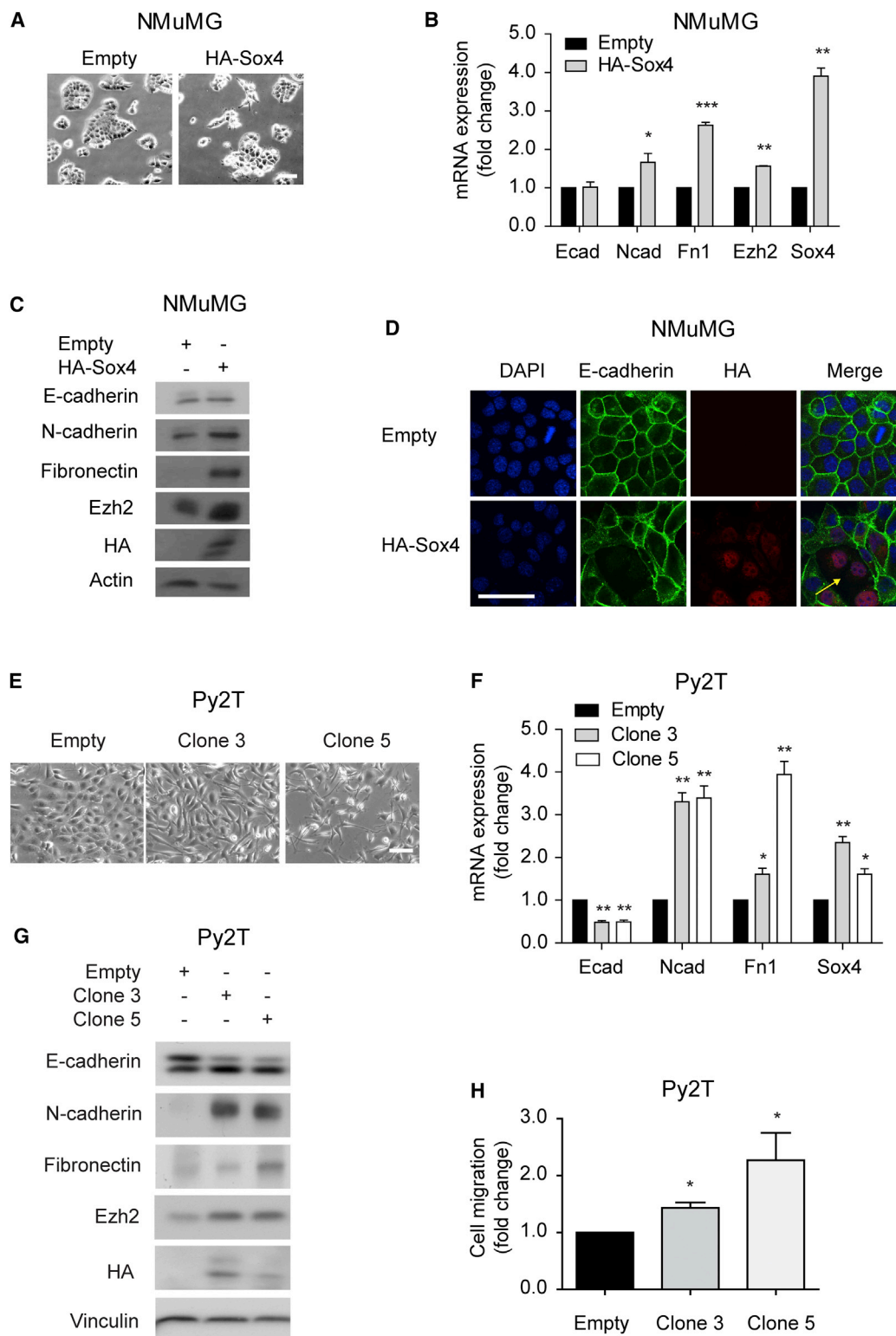


Figure 3. Ectopic Expression of Sox4 Promotes EMT and Cell Migration

(A) NMuMG cells were transiently transfected with pcDNA3-HA and pcDNA3-HA-Sox4 constructs, and cellular morphology was evaluated. Note the formation of filopodia and the cell dispersal upon Sox4 expression (HA-Sox4) as compared to empty vector control (Empty). Scale bar, 100 μ m.

(B) The expression of E-cadherin (Ecad), N-cadherin (Ncad), fibronectin (Fn1), Ezh2, and Sox4 was determined by quantitative RT-PCR in NMuMG cells transiently transfected with HA-Sox4 or with empty vector (Empty) in the absence of TGF- β . Fold changes are relative to those in cells transfected with empty vector.

(legend continued on next page)

HA-tagged Sox4 in Py2T cells also induced mesenchymal cell morphology in the absence of TGF- β , with a moderate loss of E-cadherin expression but a marked gain in N-cadherin and fibronectin expression (Figures 3E–3G). Furthermore, the forced expression of Sox4 promoted Py2T cell migration (Figure 3H). These results suggest that Sox4 is not only required but also sufficient for the induction of an EMT.

Sox4 Is Required for Tumorigenesis and Metastatic Spread

The critical role of Sox4 in EMT raised the question of whether Sox4 contributes to malignant tumor progression and metastasis. First, computational analysis revealed a significant correlation between high Sox4 expression and poor metastasis-free survival in the “Schmidt” database of 200 early-stage, lymph-node-negative breast cancer patients (Schmidt et al., 2008) (Figure 4A). The analysis of databases assembled of late-stage breast cancer patient data did not reveal a significant prognostic value for Sox4 expression (data not shown), suggesting that Sox4 may play a critical role in the early stages of the malignant progression of breast cancer.

Next, we investigated the functional contribution of Sox4 to primary tumor growth and metastasis formation in vivo. Py2T cells stably expressing an shRNA against Sox4 (shSox4) and control-transfected cells (shControl), both expressing the firefly luciferase gene, were orthotopically implanted into mammary fat pads of nude mice, and tumor growth and metastasis in lymph nodes, lungs, and livers were quantified. Quantitative RT-PCR (Figure S2A) and immunostaining of histological tumor sections (Figure 4B) documented an efficient depletion of Sox4 expression in the cultured cell line before implantation and in primary tumors, respectively. Ablation of Sox4 expression in Py2T cells lead to a significant reduction in primary tumor growth (Figure 4C). Luciferase activity levels representing the presence of tumor cells in distant organs were found to be decreased in axillary and inguinal lymph nodes and in lungs and livers of mice transplanted with shSox4 Py2T cells as compared to shControl Py2T cells (Figure S2B), even when the luciferase activities were normalized to the decreased primary tumor sizes observed with shSox4 Py2T cells (metastatic index; Figure 4D). The reduced ability of shSox4 Py2T cells to grow as primary tumors was also observed upon subcutaneous implantation into nude mice (Figure 4E).

We next addressed whether Sox4 is required for metastasis formation in other cancer types. Similar to NMuMG cells, in B16-F10 melanoma cells Sox4 expression was increased upon

TGF- β treatment (Figure S2C). Sox4 expression was then ablated in B16-F10 melanoma cells by stable expression of shRNA targeting Sox4 (shSox4; Figure S2D), and the cells were injected into the tail vein of C57Bl/6 mice. Quantification of lung metastasis showed that Sox4-depleted B16-F10 cells were significantly impaired in lung colonization as compared to shControl-expressing B16-F10 cells (Figures S2E and S2F). Taken together, these results indicate that the transcription factor Sox4 exerts a critical function in primary tumor growth and metastasis formation.

Ezh2 Is a Direct Transcriptional Target of Sox4

The critical role of Sox4 in EMT and tumor progression motivated us to identify the genes that were directly regulated by Sox4. We first compared the genome-wide gene expression profiles of siControl and siSox4 NMuMG cells in the absence and presence of TGF- β . Genes found to be differentially expressed in dependence on Sox4 function were further analyzed for Sox4 binding motifs within one kilobase of their transcription start sites (Figure S1A). Of the 189 genes fulfilling these criteria (Table S1), 106 also changed in their expression levels during TGF- β -induced EMT. Gene ontology analysis revealed that 32 of these genes have been previously implicated in processes relevant to tumor progression (Table S2). In order to identify the genes directly regulated by Sox4, we assessed the occupancy of Sox4 at the promoters of these 32 genes. NMuMG cells transiently expressing an HA-tagged version of Sox4 (HA-Sox4) were subjected to chromatin immunoprecipitation (ChIP) with HA-specific antibodies followed by quantitative PCR using primers specific for the region spanning the Sox4 motif found in the promoter of these genes. Of the 32 genes analyzed, the promoters of 28 genes—16 in NMuMG cells and 12 in Py2T cells—were directly bound by Sox4, including the key EMT genes *Spred1*, *Edn1*, *Palld*, *Cyr61*, *Ereg*, and *Areg* (Figures S3A–S3H; data not shown). Genes that were not immunoprecipitated by HA-antibody, as well as an intergenic region, served as negative controls (Figure S3I).

Snail, Zeb, and Twist family transcriptional repressors of E-cadherin gene expression are known to play critical roles in the induction of EMT. Hence, we assessed whether Sox4 is epistatic to the expression of these EMT inducers or whether they are regulating Sox4 expression during EMT. Ablation of Sox4 expression in NMuMG cells resulted in the reduced expression of Snail2, Zeb2, and Twist1, but not Snail1 and Zeb1, whereas in Py2T cells the expression of all five repressors was

(C) The expression of E-cadherin, N-cadherin, fibronectin, Ezh2, and HA-tagged Sox4 was determined by immunoblotting of NMuMG cells transiently transfected with empty vector or with HA-Sox4. Actin was used as the loading control.

(D) The localization of E-cadherin was determined by immunofluorescence staining in NMuMG cells transiently transfected with empty-vector control or HA-Sox4. The cells marked with an arrow express Sox4 (HA) and have lost E-cadherin at their cell membranes. Scale bar, 50 μ m.

(E) Cell scattering and mesenchymal morphology are observed even in the absence of TGF- β in Py2T cell clones stably expressing HA-Sox4 (Clones 3 and 5), as compared to empty-vector-transfected control cells (Empty). Scale bar, 100 μ m.

(F) The expression of E-cadherin (Ecad), N-cadherin (Ncad), fibronectin (Fn1), and Sox4 was determined by quantitative RT-PCR in Py2T cell clones stably transfected with either HA-Sox4 (Clones 3 and 5) or control vector (Empty) in the absence of TGF- β . Fold changes are relative to those of cells transfected with the control vector.

(G) Immunoblotting analysis of E-cadherin, N-cadherin, fibronectin, Ezh2, and HA-Sox4 (HA) during TGF- β -induced EMT in Py2T cell clones either stably transfected with HA-Sox4 (Clones 3 and 5) or with empty control vector (Empty) in the absence of TGF- β . Vinculin was used as loading control.

(H) Cell migration of Py2T cell clones stably transfected with HA-Sox4 (Clones 3 and 5) or transfected with control vector (Empty) was analyzed in a transwell migration assay in the absence of TGF- β after 20 hr of cell seeding with 20% FBS as a chemoattractant.

Statistical values were calculated using an unpaired, two-tailed t test. * $p \leq 0.05$; ** $p \leq 0.01$; *** $p \leq 0.001$. Error bars indicate the mean \pm SD.

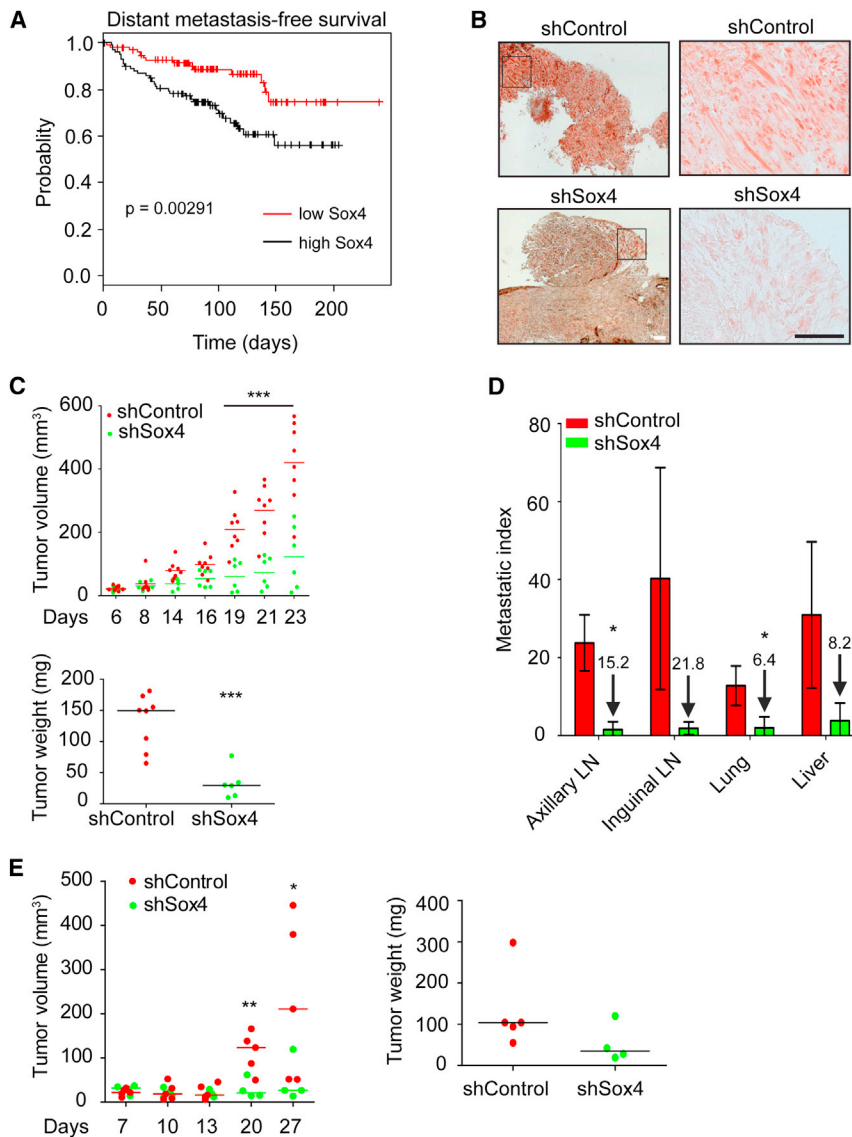


Figure 4. Sox4 Is Critical for Breast Carcinogenesis and Metastasis

(A) Correlation of the levels of Sox4 expression and prognosis in the “Schmidt” array data set of lymph-node-negative breast cancers (Schmidt et al., 2008). Shown is a Kaplan-Meier plot with survival curves for patient samples classified as having high Sox4 expression and those classified as having low Sox4 expression to assess metastasis-free survival.

(B) shSox4-expressing and shControl-expressing Py2T murine breast cancer cells were injected into the mammary fat pads of nude mice, and the resulting tumors were analyzed by immunohistochemistry for Sox4 expression. High magnification, as indicated by boxed areas, shows that shControl-transfected cells localize Sox4 primarily in the nucleus and exhibit spindle-like cell morphology, whereas shSox4-expressing cells lack significant Sox4 expression and exhibit a more differentiated morphology.

(C) shSox4-expressing and shControl-expressing Py2T cells were injected into the mammary fat pads of nude mice, and tumor growth in individual mice was measured over time (top). Tumor weight (bottom) was assessed after sacrificing the tumor-bearing mice 23 days after injection.

(D) Metastatic spread of firefly luciferase-expressing Py2T cells from the primary tumors analyzed in (C) was determined by measuring luciferase activity in extracts of lymph nodes (LN), lungs, and livers of transplanted mice. Luciferase activity levels in the various organs were divided by the primary tumor weights within the same mice to establish the metastatic index. Numbers indicate the fold differences between Sox4-expressing (shControl) and Sox4-depleted (shSox4) Py2T cells. Error bars indicate the mean \pm SE.

(E) Primary tumor growth of shControl and shSox4 Py2T cells upon subcutaneous injection into nude mice (left). Tumor weight was assessed 27 days after implantation (right).

Statistical values were calculated using an unpaired, two-tailed t test. * $p \leq 0.05$; ** $p \leq 0.01$; *** $p \leq 0.001$. Error bars indicate the mean \pm SEM. See also Figure S2.

reduced upon Sox4 depletion (Figures S3J–S3N and S3P–S3T). Conversely, when the five repressors were transiently expressed in NMuMG and Py2T cells, the levels of Sox4 mRNA were not affected (Figures S3O and S3U). Together, the data indicate that Sox4 acts upstream of the EMT inducers during EMT, most likely in an indirect manner, since none of the EMT inducers have been detected as a direct transcriptional target of Sox4.

Interestingly, the Sox4-dependent gene expression profiling and ChIP experiments also revealed the promoter of the *Ezh2* gene to be directly bound and regulated by Sox4 in NMuMG and Py2T cells (Figures 5A and 5B). Quantitative RT-PCR and immunoblotting showed that Sox4 depletion led to significantly reduced *Ezh2* expression and a global reduction in H3K27me3 levels in the presence of TGF- β in NMuMG and Py2T cells (Figure 5C). Moreover, the forced expression of Sox4 moderately increased *Ezh2* mRNA and protein levels (Figures 3B, 3C, and 3G). Finally, *Ezh2* promoter activity was reduced upon Sox4 depletion in NMuMG cells in the presence of TGF- β , as deter-

mined by *Ezh2* promoter luciferase reporter assay (Figure 5D). These results indicate that Sox4 is required for *Ezh2* expression during EMT. However, it should be noted that *Ezh2* expression levels were already substantial in epithelial cells, where Sox4 expression was low and did not markedly change with the increasing levels of Sox4 during TGF- β -induced EMT (Figures 5E, 5F, and 6B). Hence, Sox4 is required for the efficient expression of *Ezh2* during TGF- β -induced EMT, but not in epithelial cells in the absence of TGF- β , suggesting that factors other than Sox4 are critical for *Ezh2* gene expression in the epithelial state of the cells. Consistent with this notion, the dependence of *Ezh2* expression on Sox4 became already apparent between 2 and 8 hr of TGF- β stimulation in NMuMG and Py2T cells (Figures 5E and 5F).

Loss of *Ezh2* Function Impairs EMT and Metastasis

Based on the pleiotropic functions of *Ezh2* in mediating the H3K27me3 repressive mark, we speculated whether a major

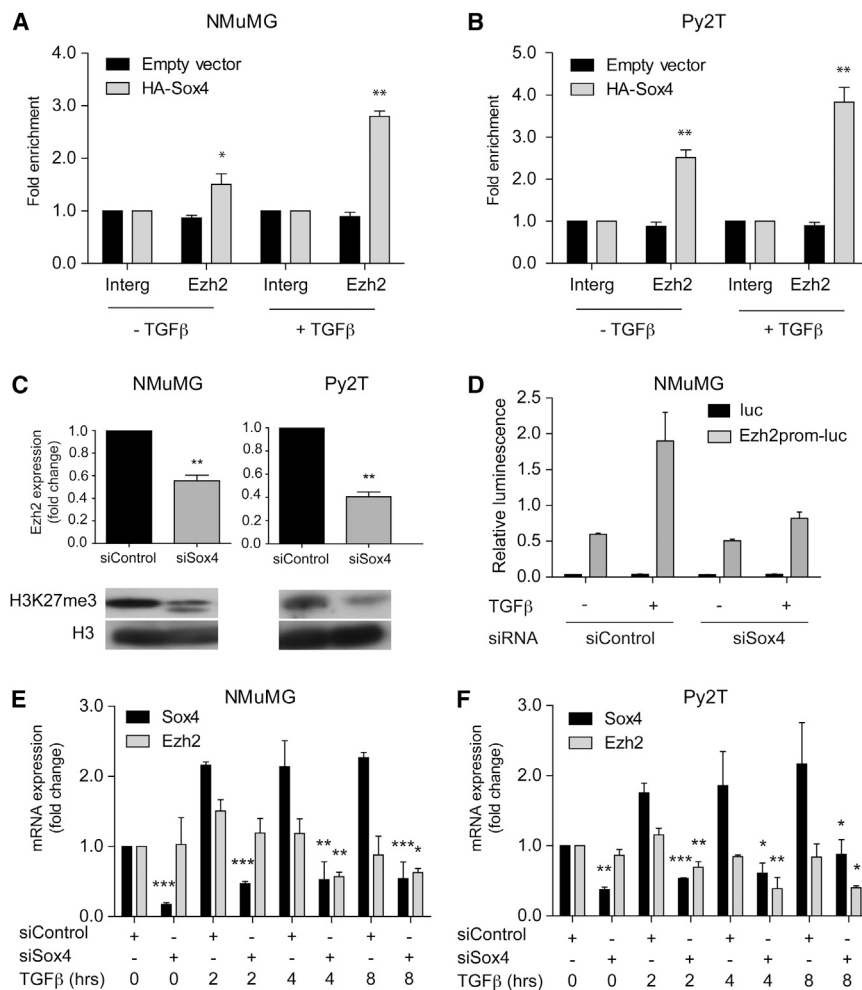


Figure 5. Sox4 Directly Regulates Ezh2 Gene Expression

(A and B) NMuMG cells (A) and Py2T cells (B) were transiently transfected with a construct encoding HA-Sox4 or empty vector and used for ChIP in the absence and presence of TGF-β for 2 days using HA-specific antibodies. Precipitated DNA fragments corresponding to Ezh2 promoter sequences were detected by quantitative PCR to assess Sox4 occupancy at this region. Fold changes are relative to those observed for a PCR reaction with primers specific for an intergenic region.

(C) Levels of Ezh2 mRNA were determined by quantitative RT-PCR in NMuMG cells or Py2T cells transfected with control siRNA (siControl) or siRNA against Sox4 (siSox4) in the presence of TGF-β for 2 days. Fold changes are relative to those in siControl-transfected cells (top). Global H3K27me3 levels were determined by immunoblotting in NMuMG cells or Py2T cells transfected with siControl or siSox4 and treated with TGF-β for 2 days. Total histone H3 was used as a loading control (bottom).

(D) Sox4 regulates Ezh2 promoter activity. NMuMG cells were transiently transfected with siControl or siSox4 and with a pGL3 luciferase reporter plasmid containing a 1.9 kb fragment of the Ezh2 promoter controlling the expression of firefly luciferase and then treated with or without TGF-β for 2 days. Firefly luciferase activity was normalized to cotransfected renilla luciferase activity (relative luminescence).

(E and F) Sox4 and Ezh2 expression levels were determined by quantitative RT-PCR after transient transfection of NMuMG (E) and Py2T cells (F) with siControl or siSox4 during the first hours of TGF-β treatment (0, 2, 4, and 8 hr).

Statistical values were calculated using a paired, two-tailed t test. *p ≤ 0.05; **p ≤ 0.01; ***p ≤ 0.001. Error bars indicate the mean ± SD. See also Figure S3 and Tables S1 and S2.

aspect of EMT regulation by Sox4 was dependent on its regulation of Ezh2 gene expression. Indeed, similar to the ablation of Sox4, siRNA-mediated knockdown of Ezh2 (siEzh2) in NMuMG cells led to an efficient downregulation of Ezh2 and retention of the epithelial phenotype of NMuMG cells upon TGF-β stimulation (Figure 6A; Figure S4A). Immunoblotting and immunofluorescence microscopy analysis demonstrated a failure to lose E-cadherin and ZO-1 expression as well as a reduced gain in the expression of fibronectin and impaired formation of actin stress fibers and focal adhesions in Ezh2-depleted cells compared to siControl-treated cells (Figures 6B and 6C). These effects became even more apparent in NMuMG cells when both methyltransferases, Ezh1 and Ezh2, were concomitantly depleted (Figures 6A and 6C; Figures S4B–S4F). Similar to NMuMG cells, shRNA-mediated stable codepletion of Ezh1 and Ezh2 in Py2T cells also delayed EMT (Figures S4G–S4I). Comparable to the ablation of Sox4 expression, Ezh2-depleted NMuMG cells showed significantly increased apoptosis, a block in G0/G1, and a substantial attenuation in their proliferation during TGF-β-induced EMT (Figures 6D–6F). Finally, similar to the depletion of Sox4 in B16-F10 melanoma cells, shRNA-mediated ablation of Ezh2 or Ezh1/2 together resulted in a significantly

reduced ability of these cells to form lung metastasis upon intravenous injection (Figure S4J). Notably, the concomitant high expression of Ezh2 and Sox4 significantly correlated with poor metastasis-free survival of early-stage, lymph-node-negative breast cancer patients (Schmidt et al., 2008; Figure 6G).

To directly assess whether Ezh2 is the major transcriptional target of Sox4 required for its EMT-inducing function, we transiently ablated Sox4 in NMuMG and Py2T cells and concomitantly expressed Ezh2 by transient transfection of an Ezh2 expression plasmid. Notably, the forced expression of Ezh2 overcame the reduced expression of endogenous Ezh2 upon Sox4 depletion and restored TGF-β-induced EMT and changes in marker expression that otherwise were repressed by Sox4 ablation in NMuMG and in Py2T cells (Figures 7A–7C; Figures S5A and S5B). These results indicate that Ezh2 is one critical target of Sox4 transcriptional regulation during EMT and metastasis formation.

Ezh2 Regulates EMT Genes via H3K27me3 Modification of Their Promoters

To identify the target genes that are modified by Ezh2-mediated H3K27me3 epigenetic imprint and regulated in their expression

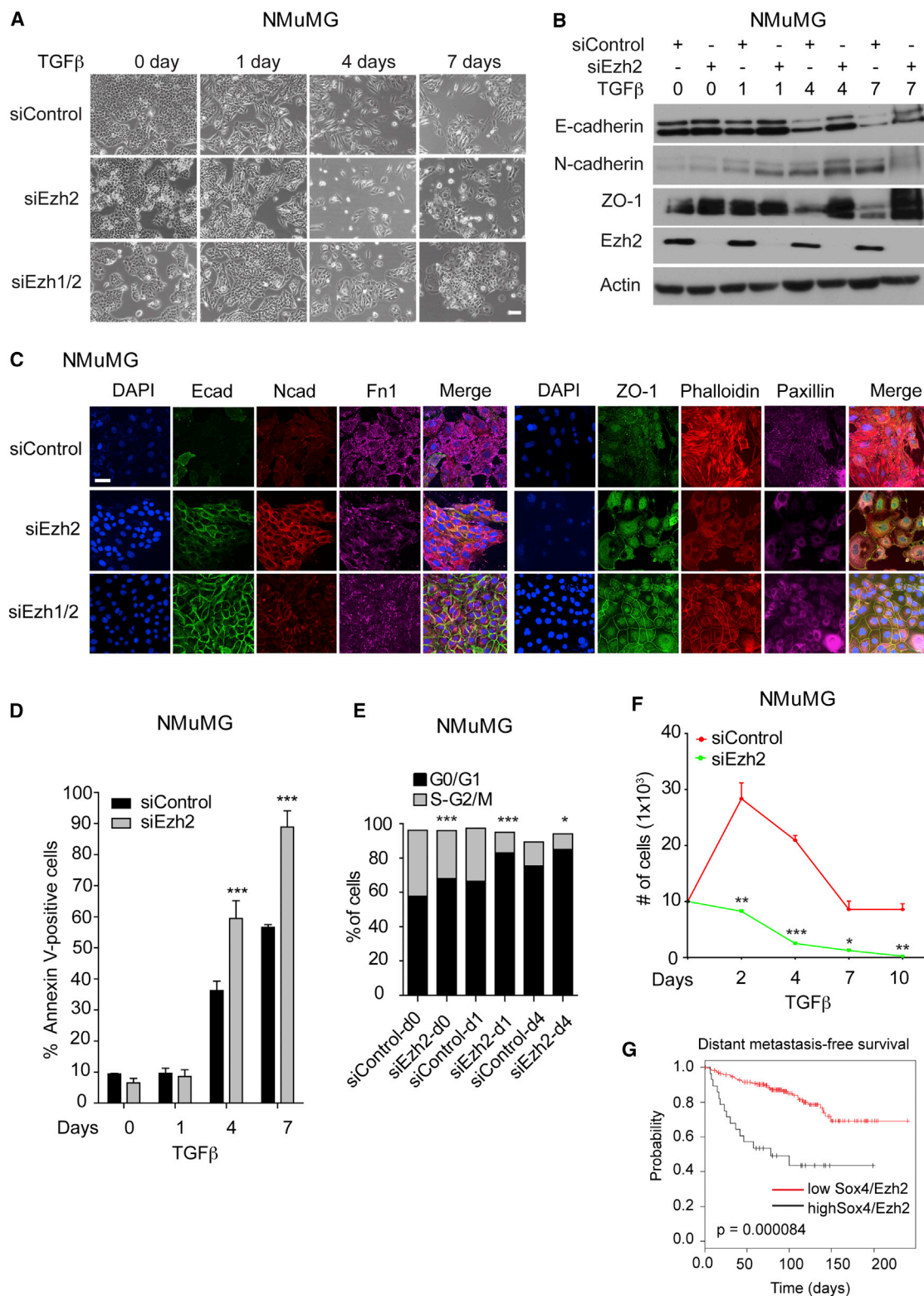


Figure 6. Depletion of Ezh2 Phenocopies the Ablation of Sox4 during TGF- β -Induced EMT

(A) NMuMG cells transfected with either control siRNA (siControl) or with siRNAs against Ezh2 or Ezh1 and Ezh2 together (siEzh1/2) were treated with TGF- β for the days indicated, and their morphology was evaluated by phase-contrast microscopy. Scale bar, 100 μ m.

(B) Expression of E-cadherin, N-cadherin, ZO-1, and Ezh2 was determined by immunoblotting analysis during TGF- β -induced EMT in NMuMG cells transfected either with siEzh2 or siControl. Immunoblotting for actin was used as a loading control.

(legend continued on next page)

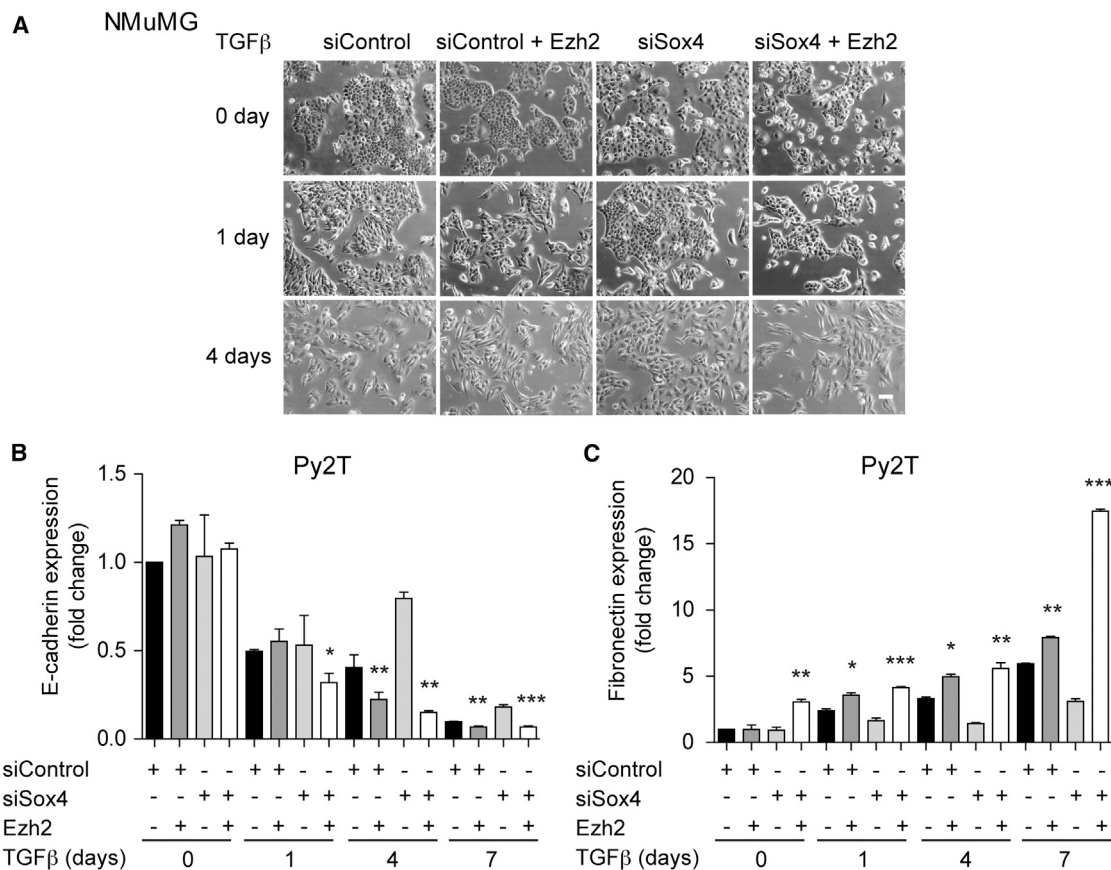


Figure 7. Forced Expression of Ezh2 Overcomes the Lack of Sox4 and Restores TGF-β-Induced EMT

(A) Although ablation of Sox4 expression (siSox4) repressed the TGF-β-induced mesenchymal morphology of NMuMG cells observed in siControl-transfected cells, transient expression of Ezh2 in Sox4-ablated cells (siSox4 + Ezh2) restored EMT and mesenchymal cell morphology. Cells were treated with TGF-β for the indicated times. Scale bar, 100 μm.

(B and C) mRNA expression levels of E-cadherin (B) and fibronectin (C) were determined after Ezh2 overexpression (+Ezh2) in control (shControl) and Sox4-ablated (shSox4) Py2T cells.

Statistical values were calculated using an unpaired, two-tailed t test. *p ≤ 0.05; **p ≤ 0.01; ***p ≤ 0.001.

See also Figure S5.

during EMT, we performed chromatin immunoprecipitation using an H3K27me3-specific antibody upon TGF-β treatment in NMuMG cells for 0, 1, 4, 7, 10, and 20 days followed by next-generation sequencing (ChIP-Seq) in combination with gene expression profiling. Whole-genome scanning revealed 970 regions corresponding to 301 genes with high variance in H3K27me3 levels during EMT and high reproducibility in the biological replicates (Figure 8A). Among the 301 genes,

genome-wide gene expression analysis identified 46 genes that were transcriptionally upregulated during EMT and lost their H3K27me3 marks and three genes that were transcriptionally downregulated during EMT and gained H3K27me3 marks (Figure S6A). We validated the changes in H3K27me3 levels at target gene promoters such as *Mcam*, *Pdgfrb*, *Itga5*, *Col4a1*, and *St6galnac4* in NMuMG and Py2T cells (Figures 8B and 8C; Figure S6B) by ChIP followed by quantitative PCR for the promoter

(C) Immunofluorescence microscopy analysis of NMuMG cells transfected with either siControl or with siEzh2 or siEzh1/2. Cells were treated with TGF-β for 7 days and stained with antibodies against E-cadherin, ZO-1, and fibronectin, and with phalloidin to visualize the actin cytoskeleton. Scale bar, 50 μm.

(D) NMuMG cells transfected with either siControl or siEzh2 were treated with TGF-β for the days indicated, and the rates of apoptosis were determined by Annexin-V staining and flow cytometry.

(E) siControl- and siEzh2-transfected NMuMG cells were treated with TGF-β for the days indicated. Cells were stained with propidium iodide (PI), and the percentages of cells in G0/G1 and S-G2/M phases of the cell cycle were determined by flow cytometry.

(F) siRNA-mediated ablation of Ezh2 expression during TGF-β treatment of NMuMG cells results in a significant decrease in cell numbers compared to transfection with control siRNA.

(G) Kaplan-Meier survival curve for patient samples of the “Schmidt” data set of lymph-node-negative breast cancers (Schmidt et al., 2008) classified as having concomitant low Sox4 and Ezh2 expression and high Sox4 and Ezh2 expression, to assess metastasis-free survival.

Statistical values were calculated using an unpaired, two-tailed t test. *p ≤ 0.05; **p ≤ 0.01; ***p ≤ 0.001. Error bars indicate the mean ± SD.

See also Figure S4.

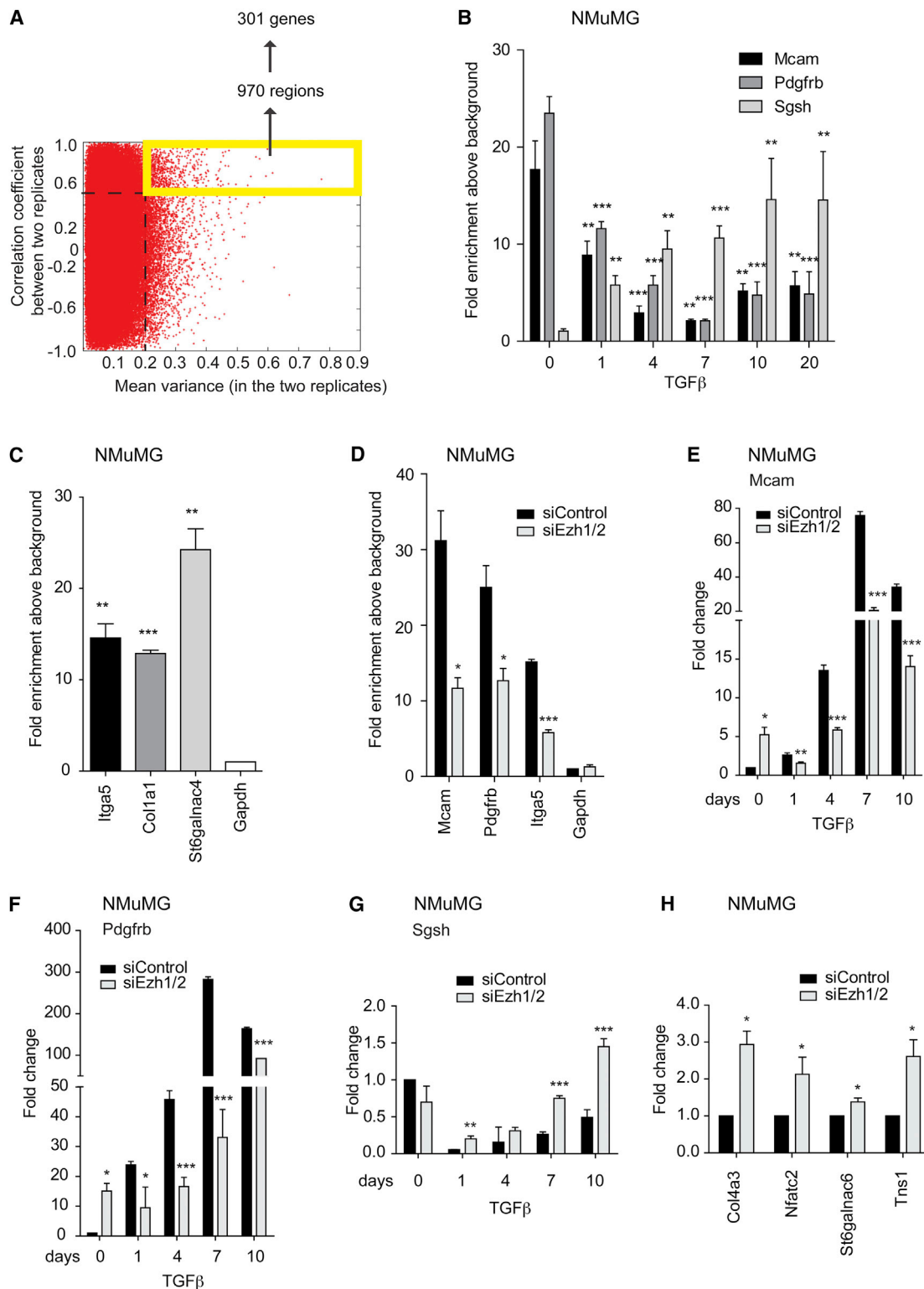


Figure 8. TGF- β -Induced EMT Accompanies Genome-wide Reprogramming of the Polycomb-Associated Mark H3K27me3

(A) TGF- β -induced EMT accompanies genome-wide reprogramming of the Polycomb-associated mark H3K27me3. Genome-wide H3K27me3 enrichment above background was calculated for 2-kb-wide windows overlapping by 1 kb. To extract those H3K27me3-regions that are most relevant for EMT dynamics, for each region both the variance in H3K27me3 levels during the progressive stages of EMT (horizontal axis) and the reproducibility of the H3K27me3 dynamics across biological replicates (vertical axis) were calculated, and 970 genes with high variance and high reproducibility were selected. Comparison of these regions with RefSeq transcripts show that they fall within 1 kb upstream and downstream of 301 distinct target genes.

(legend continued on next page)

regions of the genes. The expression of these target genes appeared highly dependent on the presence of Ezh1/2 and the H3K27me3 repressive imprint. For example, the promoters of the *Mcam*, *Pdgfrb*, and *Itga5* genes were found to be highly enriched in H3K27me3 marks in untreated NMuMG cells. Depletion of Ezh1/2 led to a loss of global H3K27me3 levels (Figure S6C) and of H3K27me3 at the promoters of the *Mcam*, *Pdgfrb*, and *Itga5* genes (Figure 8D; Figure S6D), with a concomitant increase in the expression of these genes (Figures 8E and 8F; Figures S6E and S6F) in NMuMG and Py2T cells. Conversely, the *Sgsh* gene gained H3K27me3 at its promoter during TGF- β -induced EMT, with a concomitant repression of its expression, and upon Ezh1/2 depletion, the lack of H3K27me3 marks on the *Sgsh* promoter during TGF- β -treatment resulted in increased *Sgsh* gene expression (Figure 8G). In addition, we validated a subset of other H3K27me3-enriched genes that changed in their expression profile upon depletion of Ezh1/2 (Figure 8H). Gene ontology analysis revealed a prominent enrichment for gene functions implicated in EMT, malignant tumor progression, and metastasis (Figure S6G). Furthermore, analysis of the “Minn” database of breast cancer (Minn et al., 2005) revealed that the 49 genes signature correlated with reduced bone-metastasis-free survival of patients in highly malignant breast cancers lacking estrogen receptor expression (ER $^-$) or lacking estrogen receptor, progesterone receptor, and ErbB2 expression (triple-negative [TN]; Figures S6H–S6K). Moreover, in the “Schmidt” database of early-stage breast cancer (Schmidt et al., 2008), the 49 genes signature correlated with the probability to develop distant metastasis (Figure S6L). In line with these findings, transwell migration assays revealed significantly lower chemotactic migration of NMuMG and Py2T cells depleted of both Ezh1 and Ezh2 (Ezh1/2) as compared to siControl-transfected cells upon treatment with TGF- β (Figure S6M). Together, these data indicate that Sox4 regulates *Ezh2* gene expression, that Ezh2-mediated H3K27me3 marks are critically involved in the transcriptomic reprogramming of cells undergoing EMT, and that an epigenetic EMT gene signature correlates with survival in breast cancer patients.

DISCUSSION

EMT is accompanied by massive changes in cell morphology and behavior, and transcription factors play a pivotal role in controlling the various cellular functions during EMT, such as cell proliferation, cell survival, cell differentiation, cell migration,

and cell adhesion. (Hanahan and Weinberg, 2011; Kalluri, 2009; Kalluri and Weinberg, 2009; Nieto, 2010; Polyak and Weinberg, 2009; Thiery and Sleeman, 2006). In this study, the transcription factor Sox4 was found to be upregulated in its expression and transcriptional activity during EMT in a number of murine and human nontransformed mammary gland epithelial cells and breast cancer cells. The upregulated expression of Sox4 during TGF- β -induced EMT in NMuMG cells was independent of canonical TGF- β signaling, since shRNA-mediated ablation of Smad4 did not substantially affect Sox4 expression (data not shown). Moreover, treatment of NMuMG and Py2T cells with inhibitors against various signaling pathways revealed that the inhibition of TGF- β receptor and Notch signaling and the activation of Wnt signaling interfered with TGF- β -induced Sox4 expression, whereas the inhibition of EGF receptor increased Sox4 mRNA levels (data not shown). These observations suggest a complex gene regulatory network that drives the increased expression of Sox4 during the early phases of TGF- β -induced EMT, perspectives that warrant further investigation.

We show that Sox4 is required not only for the initiation of EMT but also for its maintenance. Furthermore, Sox4 is crucial for primary tumor growth and metastatic spread of Py2T breast cancer and B16-F10 melanoma cells. Finally, we find a significant positive correlation between increased Sox4 expression and the metastatic potential of early-stage, lymph-node-negative breast cancer in patients. These results are consistent with a recent report demonstrating that Sox4 is critical for EMT and tumor growth of human breast cancer cells and that Sox4 correlates with poor prognosis in cancer patients (Zhang et al., 2012).

Despite the recent implications of Sox4 in EMT, its direct transcriptional target genes have remained elusive. Here, we show that Sox4 exerts its central function in EMT and tumor progression by directly regulating the expression of a number of genes implicated in EMT, cell cycle regulation, cell survival, and cell migration. Notably, one of the direct targets of Sox4 transcriptional control is *Ezh2*, and ablation of *Ezh2* function phenocopies the loss of Sox4 during TGF- β -induced EMT. Moreover, the forced expression of *Ezh2* overcomes the failure of Sox4-deficient cells to undergo EMT. These results indicate that *Ezh2* is a critical downstream effector of Sox4 and that Sox4 mediates epigenetic reprogramming by regulating the expression of epigenetic modulators during EMT. Consistent with this notion, the concomitant high expression of Sox4 and *Ezh2* correlates with poor prognosis in a subset of breast cancer patients. These findings are indeed highly relevant, since they unravel a combinatorial

(B and C) ChIP was performed using an H3K27me3-specific antibody in NMuMG cells and the enrichment of H3K27me3 was determined by quantitative PCR at the promoters of the *Mcam*, *Pdgfrb*, and *Sgsh* genes during TGF- β -induced EMT (B) and at the promoters of the *Itga5*, *Col1a1*, and *St6galnac4* genes in the absence of TGF- β (C). Average enrichments from independent assays are plotted on the y axis as the ratio of precipitated DNA relative to the total input DNA and further normalized to the *Gapdh* housekeeping gene promoter.

(D) ChIP was performed using an H3K27me3-specific antibody in NMuMG cells transiently transfected with control siRNA (siControl) or siRNA against Ezh1/2 (siEzh1/2), and quantitative PCR was performed using promoter-specific primers as indicated to determine enrichment of H3K27me3 at the *Mcam*, *Pdgfrb*, and *Itga5* promoters and normalized to the *Gapdh* housekeeping gene promoter.

(E–G) NMuMG cells transiently transfected with control siRNA (siControl) or siRNA against Ezh1/2 (siEzh1/2) were analyzed by quantitative RT-PCR analysis for the mRNA expression levels of *Mcam* (E) and *Pdgfrb* (F), which already carry high H3K27me3 marks in untreated NMuMG cells and lose this mark during EMT, and of *Sgsh* (G), which gains this mark upon TGF- β treatment for 1, 4, 7, and 10 days.

(H) Validation of selected genes enriched in H3K27me3 marks and their transcriptional derepression after Ezh1/2 ablation in NMuMG cells in the absence of TGF- β .

Statistical values were calculated using a paired, two-tailed t test. * $p \leq 0.05$; ** $p \leq 0.01$; *** $p \leq 0.001$. Error bars indicate the mean \pm SD.

See also Figure S6 and Tables S1 and S2.

action of key transcription factors and epigenetic regulators in driving the transcriptional reprogramming underlying cell-fate changes during morphogenic processes such as EMT.

The methyltransferase Ezh2 is the best-studied component of the Polycomb repressor complex 2 (PRC2). Increased expression or activity of Ezh2 is a marker of advanced and metastatic disease in many solid tumors, including prostate and breast cancer (Chase and Cross, 2011). Our genome-wide study of Ezh2-associated H3K27me3 marks during EMT revealed dynamic changes at a number of genes, of which a subset also show corresponding changes in transcriptional state. We further show that Ezh1 and Ezh2 together determine global as well as promoter-specific H3K27me3 levels. This activity modulates the transcriptional state of target genes, including a number of EMT-relevant genes, and it is a prerequisite for EMT. Notably, this epigenetic EMT signature significantly correlates with poor clinical outcome in patients with highly aggressive and metastatic ER- and triple-negative breast cancer. Thus, Polycomb-mediated transcriptional regulation is a critical contributor to the maintenance of epithelial differentiation and to transcriptional reprogramming during EMT.

Previously, single-gene studies have suggested a role for Ezh2 in EMT regulation. For example, the PRC2 complex is recruited to the promoter of the *Cdh1* gene for its repression (Cao et al., 2008; Rhodes et al., 2003), and Snail1-mediated repression of *Cdh1* during stem cell differentiation is PRC2-dependent (Herranz et al., 2008). Notably, Ezh2 forms a corepressor complex with HDAC1, HDAC2, and Snail to repress *Cdh1* expression and to promote nasopharyngeal carcinoma malignancy (Tong et al., 2012). Moreover, the loss of integrin $\beta 4$ expression during EMT correlates with a decrease in the activating histone modifications H3K9Ac and H3K4me3 and an increase in the repressive histone modification H3K27me3 at its promoter (Yang et al., 2009). Thus, previous single-gene studies have clearly demonstrated a role of PcG-mediated mechanisms in carcinogenesis (Mills, 2010; Sauvageau and Sauvageau, 2010; Sparmann and van Lohuizen, 2006). By identifying genome-wide targets of the PcG machinery during the stepwise progression of EMT and showing a direct role of Ezh1 and Ezh2 in the transcriptional regulation of key EMT genes, our study establishes a widespread and crucial role for PcG in EMT. We show that the transcription factor Sox4 acts upstream of epigenetic reprogramming events during EMT by directly regulating expression of the chromatin regulator Ezh2. Once expressed, Ezh2 and its accompanying chromatin regulators need to be recruited to specific target genes during EMT. It is surprising that we have not identified the EMT inducers Snail1/2, Twist1/2, and Zeb1/2 as direct targets of PcG-mediated regulation or Sox4 transcriptional control. Yet, given the critical role of Snail1/2, Twist1/2, and Zeb1/2 in regulating EMT and in associating with chromatin regulators, it will be important to further delineate the crosstalk of these proteins with the epigenetic machinery and to assess whether and how they are targeting epigenetic regulators to specific target genes.

Sox4 has been linked to the etiology of certain cancer types (Penzo-Méndez, 2010). Interestingly, the closely related family member Sox2 is one of the transcriptional factors required to reprogram somatic cells into induced pluripotent stem (iPS) cells (Takahashi and Yamanaka, 2006). In glioma-initiating cells, a

crosstalk between Sox4 and Sox2 has been implicated in maintaining the tumorigenicity of the cells by Sox4 binding to the Sox2 gene enhancer region (Ikushima et al., 2009). Together with previous reports that EMT increases the tumor-initiating (cancer stem cell) potential of cancer cells (Mani et al., 2008; Morel et al., 2008), our observation that Sox4 is required for EMT and for metastasis make Sox4 an exciting target for further investigation. Our experimental results indicate that Sox4 exerts its critical regulatory functions upstream of the Snail, Zeb, and Twist family transcriptional inducers of EMT, but without directly affecting their expression. The promoters of the known EMT regulators such as Snail1/2, Zeb1/2, or Twist1/2 also did not show any changes in H3K27me3 levels during EMT and were not affected following Ezh1/2 depletion (data not shown), suggesting that different regulatory pathways may underlie their expression dynamics during EMT. This suggests that independent regulatory pathways converge to control genes that drive EMT. These findings support our efforts to comprehensively understand the gene regulatory networks that underlie EMT. A recent report demonstrated that Sox9 cooperates with Snail2 to determine mammary stem cells and to promote malignant tumor progression (Guo et al., 2012), yet our study did not find a requirement of Sox9 for TGF- β -induced EMT in NMuMG and Py2T cells. In contrast, another Sox family member, Sox3, was shown to counteract the expression of the EMT-inducer Snail1, and conversely, Snail1 represses Sox3 gene expression during gastrulation and in human breast cancer cells (Acloque et al., 2011). We can only speculate that the differences between these findings may be based on the functional variety of Sox family members, which are classified into subgroups by the differences in their protein moieties outside of the HMG DNA binding domains and their varying biological functions (Chew and Gallo, 2009).

In summary, the data presented here provide critical insights into the regulatory networks by which one transcription factor, Sox4, regulates an important cell-fate determination event, namely, EMT. Notably, the observation that Sox4 regulates a number of EMT-relevant genes and *Ezh2*, and that Ezh2 modifies the expression of a number of genes known to be critical for EMT, exemplifies a critical interplay between transcriptional and epigenetic control during EMT. Our data suggest that the inhibition of Ezh2 function could be an attractive alternative for therapeutic intervention during malignant tumor progression. Indeed, early results with the Ezh2 inhibitor 3-deazaneplanocin (DZNep) are encouraging (Crea et al., 2011), and first results from clinical trials are impatiently awaited.

EXPERIMENTAL PROCEDURES

For more details see [Supplemental Information](#).

Cell Lines

A subclone of NMuMG cells (NMuMG/E9, hereafter NMuMG) and MCF7-shControl and MCF7-shEcad have been described previously (Lehembre et al., 2008; Maeda et al., 2005). B16-F10 melanoma cells, EpRas, and MCF10A cells were commercially available. Py2T cells were derived from a breast tumor of MMTV-PyMT transgenic mice (Waldmeier et al., 2012).

Chromatin Immunoprecipitation

ChIP experiments were performed as previously described (Weber et al., 2005). In brief, crosslinked chromatin was sonicated to achieve an average fragment size of 500 bp. Starting with 100 μ g of chromatin and 5 μ g

of anti-HA antibody or anti-H3K27me3 antibody, 1 μ l of ChIP material and 1 μ l of input material were used for quantitative real-time PCR using specific primers covering the motif of Sox4 in the promoter of target genes or covering the 1000 bp promoter region from the transcription start site. Primers covering an intergenic region were used as a control. The efficiencies of PCR amplification were normalized to the PCR product of the intergenic region. Primer sequences are listed in the [Supplemental Information](#).

Next-Generation Sequencing Analysis

The reads were mapped to the mouse genome assembly NCBI37/mm9 using the bowtie algorithm (Langmead et al., 2009), which allows up to two mismatches within the 36-bp-long sequence. Reads that mapped to more than 100 loci were discarded from the subsequent analysis. In total, 24–34 million reads were mapped to the genome in the first replicate and 95–106 million reads to the genome in the second replicate. The mean DNA fragment size was estimated from the mapping profile on both chromosome strands, and the reads were shifted by the half of the size toward the middle of the fragment. These data were exported to wiggle tracks for manual inspection in the UCSC genome browser and served as an input for the enrichment analysis. The genome was tiled with 2 kb windows overlapping by 1 kb, and each window was summarized by the numbers of reads in both replicates at every stage and the number of reads in the input DNA. The H3K27me3-enrichment was calculated assuming binomial statistics of the read counts,

$$z = \frac{\sum_{i=1}^S f_i - f_b}{\sqrt{\frac{\sum_{i=1}^S f_i \times (1 - f_i)}{S^2 N_i} + \frac{f_b \times (1 - f_b)}{N_b}}}$$

where $f_i = n_i/N_i$ is the frequency in the 2 kb window calculated from the number of reads in the window, n_i , and the total number of reads, N_i , in sample i , and $S = 12$ is the number of samples in both replicates. The background frequencies, f_b , are calculated analogously. Neighboring windows with $z \geq 5$ and $n_b \leq 50$ were merged and intersected with RefSeq loci extended by 1 kb upstream and 1 kb downstream. From the list of 96,224 such enriched regions a subset was selected by requiring dynamic (mean variance log-frequencies >0.2) and consistent (Pearson correlation coefficient of log frequencies >0.5) methylation changes. The resulting 970 regions lie within 1 kb of the loci of 301 genes.

Animal Experimentation

All studies involving mice have been approved by the Swiss Federal Veterinary Office (SFVO) and the regulations of the Cantonal Veterinary Office of Basel Stadt (licenses 1878, 1907, and 1908).

Statistical Analysis

Statistical analysis and graphs were generated using the GraphPad Prism software (GraphPad Software, San Diego, CA). All statistical analysis was done by unpaired/paired, two-sided t test.

ACCESSION NUMBERS

Gene expression data for Sox4 knockdown cells in the presence and absence of TGF- β in NMuMG cells and ChIP-seq data of H3K27me3 imprints during TGF- β -induced EMT in NMuMG cells are deposited in the Gene Expression Omnibus (GSE44050 and GSE45579, respectively).

SUPPLEMENTAL INFORMATION

Supplemental Information includes six figures, two tables, and Supplemental Experimental Procedures can be found with this article online at <http://dx.doi.org/10.1016/j.ccr.2013.04.020>.

ACKNOWLEDGMENTS

We are grateful to H. Antoniadis, I. Galm, and P. Schmidt for technical support and A. Fantozzi for critical comments. We thank I. Nissen (Laboratory of Quantitative Genomics at D-BSSE, ETH Zürich) and S. Dessus-Babus (FMI, Basel)

for Illumina sequencing. We thank A.P. Tsou (National Yang-Ming University, Taipei), A.H. Peters (FMI, Basel), N. Goldfinger and V. Rotter (Weizmann Institute, Rehovot), and G. Berx (VIB, Ghent) for providing important reagents and P. Demougin for gene expression profiling. This research has been supported by the Swiss National Science Foundation, the Swiss Initiative for Systems Biology (RTD Cellplasticity), the EU-FP7 framework program TuMIC 2008-201662, and the Swiss Cancer League. Research in the laboratory of V.K.T. is supported by Deutsche Forschungsgemeinschaft (DFG) grant TI 799/1-1, EpiGeneSys RISE1 program, Marie Curie CIG 322210, and Wilhelm Sander Stiftung 2012.009.1. Research in the laboratory of D.S. is supported by the Novartis Research Foundation, the European Union (NoE “EpiGeneSys” FP7-HEALTH-2010-257082 and the “Blueprint” consortium FP7-282510), the European Research Council (EpiGePlas), and the SNF Sinergia program.

Received: January 2, 2012

Revised: August 20, 2012

Accepted: April 22, 2013

Published: June 10, 2013

REFERENCES

- Aaboe, M., Birkenkamp-Demtroder, K., Wiuf, C., Sørensen, F.B., Thykjaer, T., Sauter, G., Jensen, K.M., Dyrskjot, L., and Ørntoft, T. (2006). SOX4 expression in bladder carcinoma: clinical aspects and in vitro functional characterization. *Cancer Res.* 66, 3434–3442.
- Acloque, H., Ocaña, O.H., Matheu, A., Rizzoti, K., Wise, C., Lovell-Badge, R., and Nieto, M.A. (2011). Reciprocal repression between Sox3 and snail transcription factors defines embryonic territories at gastrulation. *Dev. Cell* 21, 546–558.
- Ahn, S.G., Kim, H.S., Jeong, S.W., Kim, B.E., Rhim, H., Shim, J.Y., Kim, J.W., Lee, J.H., and Kim, I.K. (2002). Sox-4 is a positive regulator of Hep3B and HepG2 cells' apoptosis induced by prostaglandin (PG)A(2) and Δ 12-PGJ(2). *Exp. Mol. Med.* 34, 243–249.
- Brabletz, T., Jung, A., Spaderna, S., Hlubek, F., and Kirchner, T. (2005). Opinion: migrating cancer stem cells—an integrated concept of malignant tumour progression. *Nat. Rev. Cancer* 5, 744–749.
- Cao, Q., Yu, J., Dhanasekaran, S.M., Kim, J.H., Mani, R.S., Tomlins, S.A., Mehra, R., Laxman, B., Cao, X., Yu, J., et al. (2008). Repression of E-cadherin by the polycomb group protein EZH2 in cancer. *Oncogene* 27, 7274–7284.
- Chase, A., and Cross, N.C. (2011). Aberrations of EZH2 in cancer. *Clin. Cancer Res.* 17, 2613–2618.
- Chen, H., Tu, S.W., and Hsieh, J.T. (2005). Down-regulation of human DAB2IP gene expression mediated by polycomb Ezh2 complex and histone deacetylase in prostate cancer. *J. Biol. Chem.* 280, 22437–22444.
- Cheung, M., Abu-Elmagd, M., Clevers, H., and Scotting, P.J. (2000). Roles of Sox4 in central nervous system development. *Brain Res. Mol. Brain Res.* 79, 180–191.
- Chew, L.J., and Gallo, V. (2009). The Yin and Yang of Sox proteins: Activation and repression in development and disease. *J. Neurosci. Res.* 87, 3277–3287.
- Christofori, G. (2006). New signals from the invasive front. *Nature* 441, 444–450.
- Crea, F., Hurt, E.M., Mathews, L.A., Cabarcas, S.M., Sun, L., Marquez, V.E., Danesi, R., and Farrar, W.L. (2011). Pharmacologic disruption of Polycomb Repressive Complex 2 inhibits tumorigenicity and tumor progression in prostate cancer. *Mol. Cancer* 10, 40.
- Ezhkova, E., Pasolli, H.A., Parker, J.S., Stokes, N., Su, I.H., Hannon, G., Tarakhovskiy, A., and Fuchs, E. (2009). Ezh2 orchestrates gene expression for the stepwise differentiation of tissue-specific stem cells. *Cell* 136, 1122–1135.
- Grünert, S., Jechlinger, M., and Beug, H. (2003). Diverse cellular and molecular mechanisms contribute to epithelial plasticity and metastasis. *Nat. Rev. Mol. Cell Biol.* 4, 657–665.
- Guo, W., Keckesova, Z., Donaher, J.L., Shibue, T., Tischler, V., Reinhardt, F., Itzkovitz, S., Noske, A., Zürcher-Härdi, U., Bell, G., et al. (2012). Slug and Sox9 cooperatively determine the mammary stem cell state. *Cell* 148, 1015–1028.

- Hanahan, D., and Weinberg, R.A. (2011). Hallmarks of cancer: the next generation. *Cell* 144, 646–674.
- Herranz, N., Pasini, D., Díaz, V.M., Francí, C., Gutierrez, A., Dave, N., Escrivá, M., Hernandez-Muñoz, I., Di Croce, L., Helin, K., et al. (2008). Polycomb complex 2 is required for E-cadherin repression by the Snail1 transcription factor. *Mol. Cell. Biol.* 28, 4772–4781.
- Hong, C.S., and Saint-Jeannet, J.P. (2005). Sox proteins and neural crest development. *Semin. Cell Dev. Biol.* 16, 694–703.
- Huber, M.A., Kraut, N., and Beug, H. (2005). Molecular requirements for epithelial-mesenchymal transition during tumor progression. *Curr. Opin. Cell Biol.* 17, 548–558.
- Hur, W., Rhim, H., Jung, C.K., Kim, J.D., Bae, S.H., Jang, J.W., Yang, J.M., Oh, S.T., Kim, D.G., Wang, H.J., et al. (2010). SOX4 overexpression regulates the p53-mediated apoptosis in hepatocellular carcinoma: clinical implication and functional analysis in vitro. *Carcinogenesis* 31, 1298–1307.
- Ikushima, H., Todo, T., Ino, Y., Takahashi, M., Miyazawa, K., and Miyazono, K. (2009). Autocrine TGF- β signaling maintains tumorigenicity of glioma-initiating cells through Sry-related HMG-box factors. *Cell Stem Cell* 5, 504–514.
- Kalluri, R. (2009). EMT: when epithelial cells decide to become mesenchymal-like cells. *J. Clin. Invest.* 119, 1417–1419.
- Kalluri, R., and Weinberg, R.A. (2009). The basics of epithelial-mesenchymal transition. *J. Clin. Invest.* 119, 1420–1428.
- Kang, Y., and Massagué, J. (2004). Epithelial-mesenchymal transitions: twist in development and metastasis. *Cell* 118, 277–279.
- Kleer, C.G., Cao, Q., Varambally, S., Shen, R., Ota, I., Tomlins, S.A., Ghosh, D., Sewalt, R.G., Otte, A.P., Hayes, D.F., et al. (2003). EZH2 is a marker of aggressive breast cancer and promotes neoplastic transformation of breast epithelial cells. *Proc. Natl. Acad. Sci. USA* 100, 11606–11611.
- Kloeker, S., Major, M.B., Calderwood, D.A., Ginsberg, M.H., Jones, D.A., and Beckerle, M.C. (2004). The Kindler syndrome protein is regulated by transforming growth factor- β and involved in integrin-mediated adhesion. *J. Biol. Chem.* 279, 6824–6833.
- Langmead, B., Trapnell, C., Pop, M., and Salzberg, S.L. (2009). Ultrafast and memory-efficient alignment of short DNA sequences to the human genome. *Genome Biol.* 10, R25.
- Lehembre, F., Yilmaz, M., Wicki, A., Schomber, T., Strittmatter, K., Ziegler, D., Kren, A., Went, P., Derksen, P.W., Berns, A., et al. (2008). NCAM-induced focal adhesion assembly: a functional switch upon loss of E-cadherin. *EMBO J.* 27, 2603–2615.
- Liao, Y.L., Sun, Y.M., Chau, G.Y., Chau, Y.P., Lai, T.C., Wang, J.L., Horng, J.T., Hsiao, M., and Tsou, A.P. (2008). Identification of SOX4 target genes using phylogenetic footprinting-based prediction from expression microarrays suggests that overexpression of SOX4 potentiates metastasis in hepatocellular carcinoma. *Oncogene* 27, 5578–5589.
- Lioubinski, O., Müller, M., Wegner, M., and Sander, M. (2003). Expression of Sox transcription factors in the developing mouse pancreas. *Dev. Dyn.* 227, 402–408.
- Liu, P., Ramachandran, S., Ali Seyed, M., Schärer, C.D., Laycock, N., Dalton, W.B., Williams, H., Karanam, S., Datta, M.W., Jaye, D.L., and Moreno, C.S. (2006). Sex-determining region Y box 4 is a transforming oncogene in human prostate cancer cells. *Cancer Res.* 66, 4011–4019.
- Maeda, M., Johnson, K.R., and Wheelock, M.J. (2005). Cadherin switching: essential for behavioral but not morphological changes during an epithelium-to-mesenchyme transition. *J. Cell Sci.* 118, 873–887.
- Mani, S.A., Guo, W., Liao, M.J., Eaton, E.N., Ayyanan, A., Zhou, A.Y., Brooks, M., Reinhard, F., Zhang, C.C., Shipitsin, M., et al. (2008). The epithelial-mesenchymal transition generates cells with properties of stem cells. *Cell* 133, 704–715.
- Mills, A.A. (2010). Throwing the cancer switch: reciprocal roles of polycomb and trithorax proteins. *Nat. Rev. Cancer* 10, 669–682.
- Min, J., Zaslavsky, A., Fedele, G., McLaughlin, S.K., Reczek, E.E., De Raedt, T., Guney, I., Strohlic, D.E., Macconail, L.E., Beroukhi, R., et al. (2010). An oncogene-tumor suppressor cascade drives metastatic prostate cancer by coordinately activating Ras and nuclear factor- κ B. *Nat. Med.* 16, 286–294.
- Minn, A.J., Gupta, G.P., Siegel, P.M., Bos, P.D., Shu, W., Giri, D.D., Viale, A., Olshen, A.B., Gerald, W.L., and Massagué, J. (2005). Genes that mediate breast cancer metastasis to lung. *Nature* 436, 518–524.
- Morel, A.P., Lièvre, M., Thomas, C., Hinkal, G., Ansieau, S., and Puisieux, A. (2008). Generation of breast cancer stem cells through epithelial-mesenchymal transition. *PLoS ONE* 3, e2888.
- Nieto, M.A. (2010). The ins and outs of the epithelial to mesenchymal transition in health and disease. *Annu. Rev. Cell Dev. Biol.* 27, 347–376.
- Penzo-Méndez, A.I. (2010). Critical roles for SoxC transcription factors in development and cancer. *Int. J. Biochem. Cell Biol.* 42, 425–428.
- Polyak, K., and Weinberg, R.A. (2009). Transitions between epithelial and mesenchymal states: acquisition of malignant and stem cell traits. *Nat. Rev. Cancer* 9, 265–273.
- Pramoonjago, P., Baras, A.S., and Moskaluk, C.A. (2006). Knockdown of Sox4 expression by RNAi induces apoptosis in ACC3 cells. *Oncogene* 25, 5626–5639.
- Restivo, A., Piacentini, G., Placidi, S., Saffirio, C., and Marino, B. (2006). Cardiac outflow tract: a review of some embryogenetic aspects of the conotruncal region of the heart. *Anat. Rec. A Discov. Mol. Cell. Evol. Biol.* 288, 936–943.
- Rhodes, D.R., Sanda, M.G., Otte, A.P., Chinnaiyan, A.M., and Rubin, M.A. (2003). Multiplex biomarker approach for determining risk of prostate-specific antigen-defined recurrence of prostate cancer. *J. Natl. Cancer Inst.* 95, 661–668.
- Sauvageau, M., and Sauvageau, G. (2010). Polycomb group proteins: multifaceted regulators of somatic stem cells and cancer. *Cell Stem Cell* 7, 299–313.
- Scharer, C.D., McCabe, C.D., Ali-Seyed, M., Berger, M.F., Bulyk, M.L., and Moreno, C.S. (2009). Genome-wide promoter analysis of the SOX4 transcriptional network in prostate cancer cells. *Cancer Res.* 69, 709–717.
- Schilham, M.W., Oosterwegel, M.A., Moerer, P., Ya, J., de Boer, P.A., van de Wetering, M., Verbeek, S., Lamers, W.H., Kruisbeek, A.M., Cumano, A., and Clevers, H. (1996). Defects in cardiac outflow tract formation and pro-B lymphocyte expansion in mice lacking Sox-4. *Nature* 380, 711–714.
- Schilham, M.W., Moerer, P., Cumano, A., and Clevers, H.C. (1997). Sox-4 facilitates thymocyte differentiation. *Eur. J. Immunol.* 27, 1292–1295.
- Schmidt, M., Böhm, D., von Törne, C., Steiner, E., Puhl, H., Pilch, H., Lehr, H.A., Hengstler, J.G., Kölbl, H., and Gehrmann, M. (2008). The humoral immune system has a key prognostic impact in node-negative breast cancer. *Cancer Res.* 68, 5405–5413.
- Shen, R., Pan, S., Qi, S., Lin, X., and Cheng, S. (2010). Epigenetic repression of microRNA-129-2 leads to overexpression of SOX4 in gastric cancer. *Biochem. Biophys. Res. Commun.* 394, 1047–1052.
- Shin, M.S., Fredrickson, T.N., Hartley, J.W., Suzuki, T., Akagi, K., and Morse, H.C., 3rd. (2004). High-throughput retroviral tagging for identification of genes involved in initiation and progression of mouse splenic marginal zone lymphomas. *Cancer Res.* 64, 4419–4427.
- Sinner, D., Kordich, J.J., Spence, J.R., Opoka, R., Rankin, S., Lin, S.C., Jonatan, D., Zorn, A.M., and Wells, J.M. (2007). Sox17 and Sox4 differentially regulate β -catenin/T-cell factor activity and proliferation of colon carcinoma cells. *Mol. Cell. Biol.* 27, 7802–7815.
- Sparmann, A., and van Lohuizen, M. (2006). Polycomb silencers control cell fate, development and cancer. *Nat. Rev. Cancer* 6, 846–856.
- Su, I.H., Basavaraj, A., Krutchinsky, A.N., Hobert, O., Ullrich, A., Chait, B.T., and Tarakhovskiy, A. (2003). Ezh2 controls B cell development through histone H3 methylation and IgH rearrangement. *Nat. Immunol.* 4, 124–131.
- Suzuki, H., Forrest, A.R., van Nimwegen, E., Daub, C.O., Balwier, P.J., Irvine, K.M., Lassmann, T., Ravasi, T., Hasegawa, Y., de Hoon, M.J., et al.; FANTOM Consortium; Riken Omics Science Center. (2009). The transcriptional network that controls growth arrest and differentiation in a human myeloid leukemia cell line. *Nat. Genet.* 41, 553–562.
- Takahashi, K., and Yamanaka, S. (2006). Induction of pluripotent stem cells from mouse embryonic and adult fibroblast cultures by defined factors. *Cell* 126, 663–676.

- Tavazoie, S.F., Alarcón, C., Oskarsson, T., Padua, D., Wang, Q., Bos, P.D., Gerald, W.L., and Massagué, J. (2008). Endogenous human microRNAs that suppress breast cancer metastasis. *Nature* 451, 147–152.
- Thiery, J.P., and Morgan, M. (2004). Breast cancer progression with a Twist. *Nat. Med.* 10, 777–778.
- Thiery, J.P., and Sleeman, J.P. (2006). Complex networks orchestrate epithelial-mesenchymal transitions. *Nat. Rev. Mol. Cell Biol.* 7, 131–142.
- Tong, Z.T., Cai, M.Y., Wang, X.G., Kong, L.L., Mai, S.J., Liu, Y.H., Zhang, H.B., Liao, Y.J., Zheng, F., Zhu, W., et al. (2012). EZH2 supports nasopharyngeal carcinoma cell aggressiveness by forming a co-repressor complex with HDAC1/HDAC2 and Snail to inhibit E-cadherin. *Oncogene* 31, 583–594.
- van de Wetering, M., Oosterwegel, M., van Norren, K., and Clevers, H. (1993). Sox-4, an Sry-like HMG box protein, is a transcriptional activator in lymphocytes. *EMBO J.* 12, 3847–3854.
- Varambally, S., Cao, Q., Mani, R.S., Shankar, S., Wang, X., Ateeq, B., Laxman, B., Cao, X., Jing, X., Ramnarayanan, K., et al. (2008). Genomic loss of microRNA-101 leads to overexpression of histone methyltransferase EZH2 in cancer. *Science* 322, 1695–1699.
- Waldmeier, L., Meyer-Schaller, N., Diepenbruck, M., and Christofori, G. (2012). Py2T murine breast cancer cells, a versatile model of TGF β -induced EMT in vitro and in vivo. *PLoS ONE* 7, e48651.
- Weber, M., Davies, J.J., Wittig, D., Oakeley, E.J., Haase, M., Lam, W.L., and Schübeler, D. (2005). Chromosome-wide and promoter-specific analyses identify sites of differential DNA methylation in normal and transformed human cells. *Nat. Genet.* 37, 853–862.
- Wilson, M.E., Yang, K.Y., Kalousova, A., Lau, J., Kosaka, Y., Lynn, F.C., Wang, J., Mrejen, C., Episkopou, V., Clevers, H.C., and German, M.S. (2005). The HMG box transcription factor Sox4 contributes to the development of the endocrine pancreas. *Diabetes* 54, 3402–3409.
- Yang, X., Pursell, B., Lu, S., Chang, T.K., and Mercurio, A.M. (2009). Regulation of β 4-integrin expression by epigenetic modifications in the mammary gland and during the epithelial-to-mesenchymal transition. *J. Cell Sci.* 122, 2473–2480.
- Zhang, J., Liang, Q., Lei, Y., Yao, M., Li, L., Gao, X., Feng, J., Zhang, Y., Gao, H., Liu, D.X., et al. (2012). SOX4 induces epithelial-mesenchymal transition and contributes to breast cancer progression. *Cancer Res.* 72, 4597–4608.

A Critical Role for Notch Signaling in the Formation of Cholangiocellular Carcinomas

Steffen Zender,^{2,8} Irina Nিকেলেই,^{3,8} Torsten Wuestefeld,^{1,8} Inga Sørensen,⁵ Daniel Dauch,¹ Przemyslaw Bozko,¹ Mona El-Khatib,¹ Robert Geffers,⁶ Hueseyin Bektas,⁴ Michael P. Manns,² Achim Gossler,³ Ludwig Wilkens,⁷ Ruben Plentz,¹ Lars Zender,¹ and Nisar P. Malek^{1,*}

¹Department of Internal Medicine I, Eberhard Karls University Tübingen, Otfried-Müller-Straße 10, 72076, Tübingen, Germany

²Department of Gastroenterology, Hepatology and Endocrinology

³Institute for Molecular Biology

⁴Department of Visceral and Transplantation Surgery

⁵Department of Nephrology and Hypertension

Hannover Medical School, Carl Neuberg Strasse 1, 30625 Hannover, Germany

⁶Helmholtz Centre for Infection Research, Inhoffenstraße 7 38124 Braunschweig, Germany

⁷Institute of Pathology, Nordstadt Krankenhaus, Haltenhoffstr. 41, 30167 Hannover, Germany

⁸These authors contributed equally to this work

*Correspondence: nisar.malek@med.uni-tuebingen.de

<http://dx.doi.org/10.1016/j.ccr.2013.04.019>

SUMMARY

The incidence of cholangiocellular carcinoma (CCC) is increasing worldwide. Using a transgenic mouse model, we found that expression of the intracellular domain of Notch 1 (NICD) in mouse livers results in the formation of intrahepatic CCCs. These tumors display features of bipotential hepatic progenitor cells, indicating that intrahepatic CCC can originate from this cell type. We show that human and mouse CCCs are characterized by high expression of the cyclin E protein and identified the cyclin E gene as a direct transcriptional target of the Notch signaling pathway. Intriguingly, blocking γ -secretase activity in human CCC xenotransplants results in downregulation of cyclin E expression, induction of apoptosis, and tumor remission in vivo.

INTRODUCTION

Cholangiocellular carcinoma (CCC) is a primary liver cancer with biliary differentiation (Patel, 2006). Several recent studies describe a significant increase in the incidence of this tumor in Europe and the United States; the reasons for this increase are not understood (El-Serag et al., 2009; von Hahn et al., 2011; West et al., 2006). Even though CCC accounts for up to 15% of all liver cancers, the molecular alterations that lead to this disease are mostly unknown. Predisposing conditions such as primary sclerosing cholangitis, chronic infection with liver flukes, or biliary stones led to the hypothesis that chronic inflammation of the biliary epithelium might be a prerequisite for the formation of CCC. However, no uniform genetic alteration has been identified that is responsible for the formation of CCC. In addition, only very few mouse models of CCC are currently available. Recently Xu and colleagues showed that liver-specific disruption of the *SMAD4* and *PTEN* genes leads to the formation of CCC (Xu et al., 2006). NF2 knockout mice were shown to develop hepato-

cellular carcinomas and CCCs from a common progenitor cell (Benhamouche et al., 2010), supporting the hypothesis that CCC may arise from undifferentiated hepatic precursor cells.

A number of studies showed that the Notch signaling pathway is of central importance for embryonic development of the biliary tree. For example, loss of the Notch ligand *jagged1* or the Notch 2 gene results in congenital hypoplasia of the biliary system, called the Alagille syndrome (Geisler et al., 2008; Lorent et al., 2004; Ryan et al., 2008). Analysis of mice after liver-specific inactivation of RBP-J κ , a common transcriptional mediator of Notch signaling, revealed a reduced number of biliary cells differentiating from hepatoblasts (Zong et al., 2009). Notch levels are regulated by ubiquitylation-dependent protein turnover, which is controlled by the SCF^{Fbw7} E3-ubiquitin ligase (Welcker and Clurman, 2008). The F-Box component of this E3-ligase, the Fbw7 protein, was found to be frequently mutated in human CCC (Akhoondi et al., 2007). However, it is unknown whether Notch dysregulation is involved in the initiation and progression of CCC.

Significance

Overactivation of the Notch signaling pathway leads to a dysregulation of the oncogene cyclin E, resulting in the formation of CCC. Inhibition of Notch activity in CCC blocks tumor cell proliferation and induces apoptosis in vitro and in vivo. Our results shed light on the pathogenesis of CCC and pinpoint Notch inhibition as a promising treatment option.

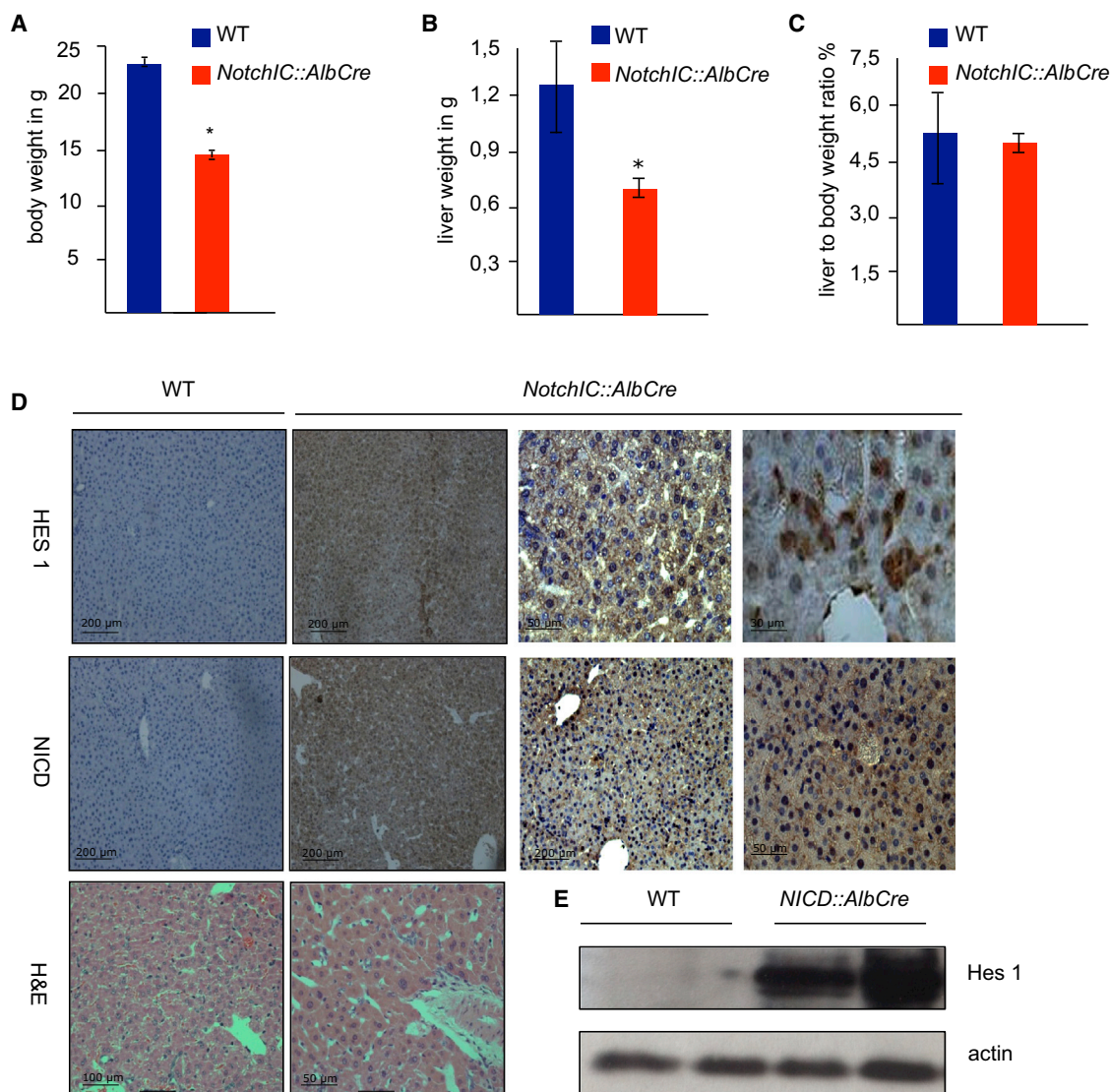


Figure 1. *Notch1C::AlbCre* Mice Show Reduced Body and Liver Weights

(A–C) Analysis of liver and body weight and liver-to-body weight ratio of the *Notch1C::AlbCre* mice compared to littermates (A and B: 10 weeks of age; C: 6 weeks of age).

(D) Hematoxylin and eosin (H&E) stained liver sections of *Notch1C::AlbCre* mice. Immunohistochemical staining of *Notch1C::AlbCre* livers using antibodies against Hes1 (10× and 60× magnification) and NICD in 6-week-old mice.

(E) Western blot analysis of liver tissue from two *Notch1C::AlbCre* mice and two wild-type littermates using an antibody against HES1, a downstream target of the Notch pathway in 6-week-old mice. Scale bars represent mean values ± SEM. **p* < 0.05; ***p* < 0.001.

See also Figure S1.

In this study, we set out to explore the function of Notch signaling in the formation of liver cancers. We used a transgenic mouse line that allows the liver-specific expression of the intracellular domain of Notch receptor 1 (NICD).

RESULTS

Expression of Notch ICD in Mouse Liver Interferes with Hepatocyte Proliferation

To directly test the consequences of constitutive Notch expression in liver tissue, we crossed a transgenic mouse line that allows for tissue-specific overexpression of the intracellular

domain of Notch 1 (*Rosa26Notch1IC*) (Murtaugh et al., 2003) to a mouse line that expresses cre-recombinase under the control of the albumin regulatory elements and the alpha-fetoprotein enhancers (*AlbCre*) (Kellendonk et al., 2000). Use of this cre-line results in the expression of NICD in the vast majority of all hepatocytes and biliary epithelial cells during the formation of the second ductal layer (E16.5) (Zong et al., 2009). *Notch1C::AlbCre* mice were born at normal Mendelian ratios, but showed proportionally reduced body and liver weights (Figures 1A–1C) and up to 25% reduced body size (Figure S1A [age, 7 months] available online) compared to wild-type control littermates. To show liver-specific activation of the NICD transgene,

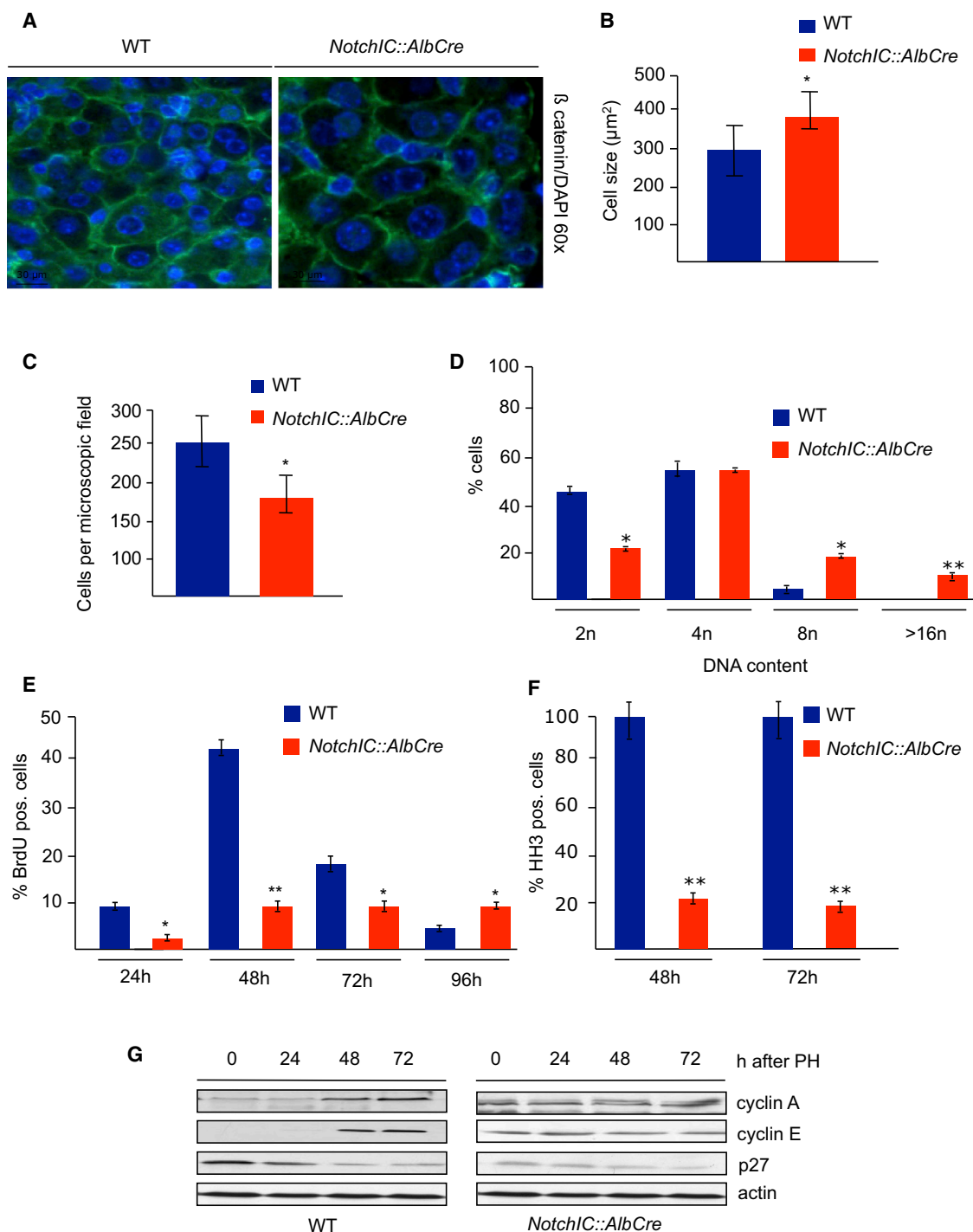


Figure 2. Notch Signaling Leads to Dysregulated Expression of Cyclin E and Genetic Instability

(A) β -catenin staining (for the detection of cell size) was performed on liver sections from wild-type and *Notch1C::AlbCre* mice at 12 weeks of age.

(B) Quantification of cell size in the indicated mouse strains was done after β -catenin staining to visualize the cell surface at 12 weeks of age. Five hundred cells on average were analyzed using a photometric system.

(C) Three hundred visual fields were counted on average to determine the number of hepatocytes in the livers of the indicated mouse strains at the age of 12 weeks.

(D) The DNA content of hepatocytes of the indicated mouse strains was determined by microphotometry analysis of Feulgen-stained liver sections at the age of 11 weeks.

(E and F) Quantification of the number of BrdU and phospho-Histone-H3-positive hepatocytes after induction of liver regeneration in wild-type and *Notch1C::AlbCre* double transgenic mice at the age of 10 weeks. For BrdU staining, an average of 900–2000 cells, and for HH3 staining at least 700 cells from up to (legend continued on next page)

we prepared extracts from different mouse tissues and determined the expression of the green fluorescent (GFP) protein, which is co-expressed with the NICD transgene after cre-recombinase-mediated activation of transcription. As shown in [Figure S1B](#), only the liver expressed detectable amounts of GFP, while in all other tested organs the transgene was not activated. To ensure expression and activity of the intracellular domain of Notch in cholangiocytes and hepatocytes, we performed immunostainings on mouse liver tissue from *Notch1C::AlbCre* mice and wild-type controls, using antibodies specific for the cleaved form of Notch. As shown in [Figure 1D](#), NICD expression was detected in both cell types in the transgenic animals but not in wild-type liver controls. In line with a constitutive activation of Notch signaling, we also detected strong expression of HES1, a transcriptional target of the Notch pathway in *Notch1C::AlbCre* livers ([Figure 1D](#)) and in liver lysates ([Figure 1E](#)).

Given the expression of Notch ICD in hepatocytes and the biliary compartments of the liver, we first set out to analyze the functional consequences of Notch expression in hepatocytes. Upon histologic examination of the *Notch1C::AlbCre* liver tissues, we detected a significant increase in the cell size of the NICD-positive hepatocytes as well as variations in nuclear size in transgenic livers compared to wild-type controls ([Figure 2A](#)). Serum transaminases and different liver metabolites were also changed in *Notch1C::AlbCre* mice compared to wild-type controls ([Figure S1C](#)). To measure the size of individual hepatocytes, we stained liver sections with a specific antibody against beta catenin ([Kossatz et al., 2004](#)) and quantified the differences between *Notch1C::AlbCre* and wild-type controls ([Figures 2A](#) and [2B](#)). In accordance with an increase in cell size, we also noticed a reduction in the number of hepatocytes per visual field in the *Notch1C::AlbCre* compared to wild-type livers ([Figure 2C](#)). Because an increase in hepatocyte size can be the result of a change in the nuclear-to-cytoplasmic ratio, we determined nuclear sizes and DNA content in *Notch1C::AlbCre* mice and wild-type control mice. As shown in [Figure 2A](#), the nuclei of hepatocytes in *Notch1C::AlbCre* mice are significantly larger than those in control mice. To analyze if these changes were paralleled by an increase in the amount of nuclear DNA, we performed Feulgen staining and measured the DNA content of single nuclei by cytometry. As shown in [Figure 2D](#), we found that the nuclei of hepatocytes in the *Notch1C::AlbCre* mice are not only enlarged but also contain significantly more DNA than the nuclei of nontransgenic control livers. Nuclear enlargement and an increase in DNA content are often the result of endoreduplication cycles in which the cell undergoes continuous rounds of DNA replication without cytokinesis ([Kossatz et al., 2004](#)). To test whether the *Notch1C::AlbCre* livers also display alterations with regard to cellular proliferation, we performed partial (two-thirds) hepatectomies in *Notch1C::AlbCre* transgenic animals and compared their regenerative potential with that of wild-type organs. As shown in [Figure 2E](#), expression of *Notch1C::AlbCre* leads to an almost complete loss of regeneration potential in

transgenic livers of 10-week-old mice as shown by a reduction of BrdU uptake after partial hepatectomy and a concomitant reduction in cells entering mitosis as measured by histone H3 phosphorylation ([Figure 2F](#)). This lack of proliferation was accompanied by a significant increase in hepatocyte cell size and a reduction in cell number after partial hepatectomy, thereby indicating that the *Notch1C::AlbCre* mice regenerated their liver mass through cellular hypertrophy of the remaining hepatocytes ([Figure S1D](#)). At the molecular level we found that wild-type livers downregulate the cyclin kinase inhibitor p27kip1 and started to express S phase cyclins E and A after induction of cell cycle progression by partial hepatectomy ([Figure 2G](#)). Importantly and in contrast to wild-type livers, we detected elevated levels of cyclin E and cyclin A even before partial hepatectomies were performed in *Notch1C::AlbCre* expressing livers. Together these results suggest that the expression of the intracellular domain of Notch in hepatocytes results in the induction of endoreduplication cycles and a severe impairment of cellular proliferation.

Expression of Notch ICD in Mouse Livers Leads to the Formation of Progenitor Cell Derived Cholangiocellular Carcinomas

To understand the long-term consequences of NICD overexpression, we followed a cohort of mice for up to 15 months. In 7-month-old mouse livers, we observed areas with clusters of small cells with an epithelial appearance ([Figure 3A](#)) that also formed gland-like structures. To determine the origin of these cells, we stained liver sections with antibodies specific for the biliary tract (CK7, CK17, and CK19), hepatocytic markers (CK8/18), and the stem cell marker CD34. As shown in [Figure 3A](#), the small epithelial cells stained positive for biliary-hepatocytic as well as stem cell markers, a finding which is typical for cells that show characteristics of hepatocytic and cholangiocytic differentiation. Such cells often arise through the transformation of bipotential hepatic progenitor cells ([Kim et al., 2004](#)), which are located in the canals of Hering.

Importantly, as early as 8 months after birth we started to observe changes in nuclear morphology in primary liver tissues from *Notch1C::AlbCre* mice. To test whether the observed cells were indeed tumor cells, we transplanted primary tissue from *Notch1C::AlbCre* mouse livers subcutaneously on the flanks of immunodeficient mice. All implantations resulted in the formation of tumors. [Figure 3B](#) shows the growth curve of the subcutaneous tumors that arose after cell transplantation. Histopathologic analysis revealed that these tumors show many features of human CCCs ([Figure 3C](#)), including the expression of CK7 and CK17 and a typical desmoid reaction of the surrounding tissue. Liver tissue from *Alb-Cre* mice was used as a control and did not give rise to tumors ([Figure S2G](#)). These results suggested that intrahepatic expression of NICD in hepatic progenitor cells can induce differentiation of these cells toward the biliary lineage and that, over time, NICD expression induces malignant transformation of these cells. To directly test this hypothesis, we

six mice per time point were counted. The average number of HH3-positive cells in the wild-type mouse was set as 100%. The number of HH3-positive cells in *Notch1C::AlbCre* mice is displayed relative to the number of HH3-positive cells in the wild-type mice.

(G) Analysis of the expression levels of cyclin A, cyclin E, p27, and actin in liver tissue lysates at the indicated time points after induction of liver regeneration in the indicated mouse strains at the age of 10 weeks.

Scale bars represent mean values \pm SEM. * $p < 0.05$; ** $p < 0.001$.

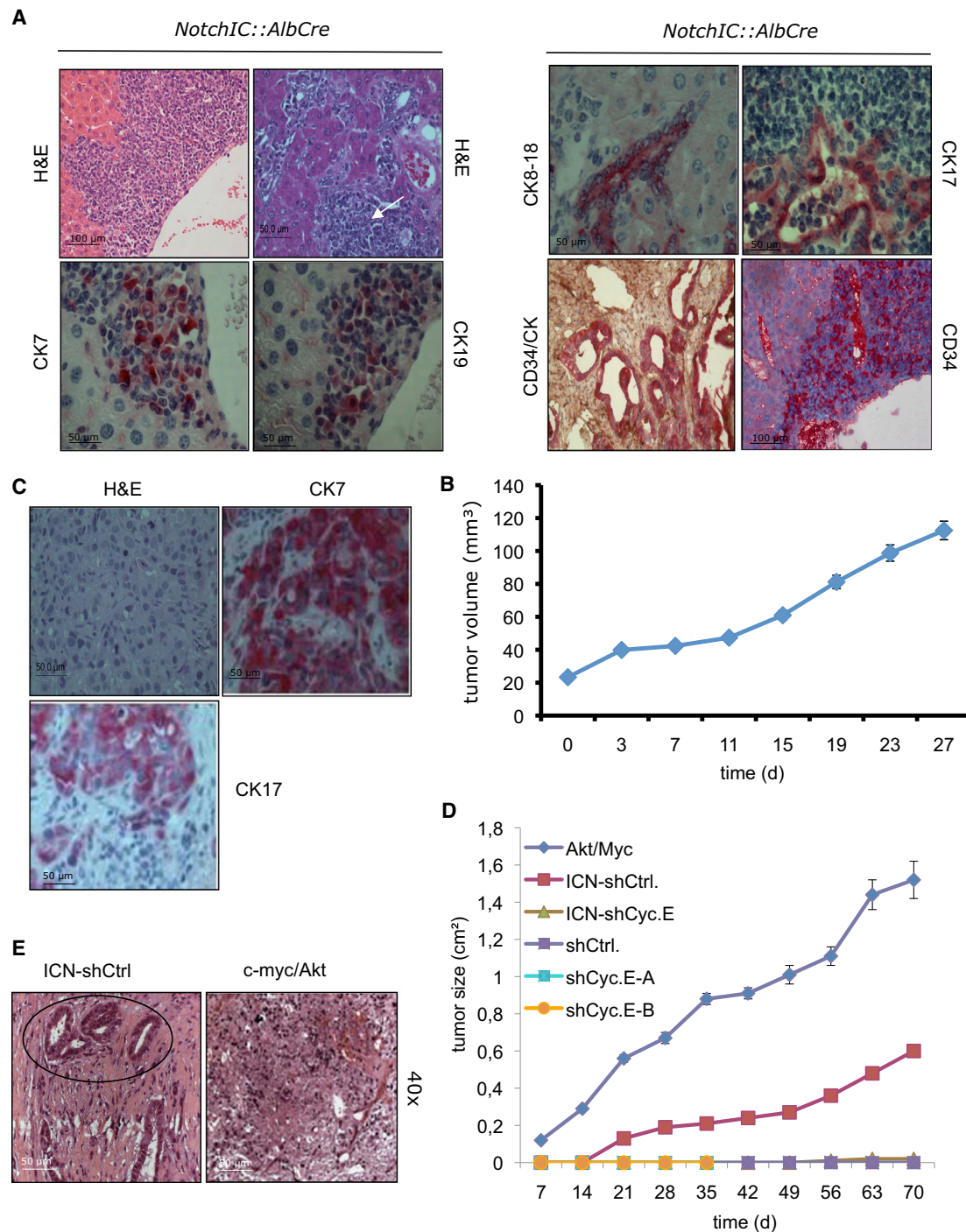


Figure 3. Expression of Notch ICD in Mouse Liver Leads to Formation of Progenitor Cell Derived Cholangiocellular Carcinomas

(A) H&E stained liver sections of *NotchIC::AlbCre* mice. Immunohistochemical staining of *NotchIC::AlbCre* livers at the age of nine months using antibodies against CK7, CK19, CK17, CK8-18, CD34, and CD34/Cytokeratin double staining.

(B) *NotchIC::Alb Cre* livers at the age of 9 months were minced and injected subcutaneously into nude mice. The growth of the resulting tumors was monitored.

(C) H&E and immunohistochemical analysis of the explanted tumor tissue using CK7 and CK17 antibodies 3 weeks after implantation of tumor cells.

(D) Growth curves of tumors after s.c. injection of progenitor cells of the indicated genotypes: progenitor cells expressing c-Myc and Akt, progenitor cells expressing the intracellular domain of notch and a control shRNA (ICN-shCtrl), progenitor cells expressing ICN together with a shRNA targeting cyclin E (ICN-shCyc.E), progenitors that only express shRNA control (shCtrl), and progenitor cells expressing only shRNAs that target cyclin E (shCyc.E-A/B).

(E) H&E stained tissue derived from subcutaneously growing tumors that originated from NICD expressing bipotential progenitors either transduced with ICN (ICN) and a shRNA control (ICN-shCtrl) or with Myc/Akt. The circle indicates atypical fused glands with hyperchromatic and irregular nuclei growing in a desmoplastic stroma. See also Figure S2.

infected previously described mouse bipotential liver progenitor cells (Zender et al., 2006) with retroviral vectors to stably overexpress the intracellular domain of Notch. Vector-infected cells served as controls. Figure S2A shows the expression levels of NICD in such cells compared to empty vector-infected cells. Cells stably expressing NICD were subcutaneously injected into nude mice and tumor growth was analyzed over time. While control vector-transduced cells did not give rise to tumors, NICD-overexpressing cells formed subcutaneous tumors (Figure 3D) in all transplantation experiments. These tumors showed all features of CCCs (Figure 3E). Interestingly, tumors arising from progenitor cells stably transduced with c-Myc and a constitutive active form of Akt showed a different histopathology and were classified as undifferentiated hepatocellular carcinomas/hepatoblastomas (Figure 3E). These results indicate that expression of the intracellular domain of Notch leads to tumor formation in all transgenic mice and can transform hepatic progenitor cells thereby leading to the development of CCCs.

Notch Signaling Leads to Dysregulated Expression of Cyclin E and Genetic Instability

To understand the molecular pathogenesis of Notch-dependent CCC formation, we focused our analysis on the function of the cyclin E protein. As shown in Figure 2G, cyclin E is highly expressed in *Notch1^{Cre}::AlbCre*-derived liver tissue even before the onset of liver regeneration (time point 0). In line with this finding, we detected high levels of cyclin E protein within the CCCs derived from *Notch1^{Cre}::AlbCre* mice (Figure 4A). Previous studies on the oncogenic function of cyclin E suggested that cyclin E induces DNA damage, thus resulting in genetic instability and contributing to the formation of malignant tumors (Spruck et al., 1999). We therefore tested if cyclin E-overexpressing cholangiocellular tumors might show signs of DNA damage by staining primary mouse CCC tissues derived from *Notch1^{Cre}::AlbCre* mice with antibodies specific for the phosphorylated form of Ser-139 of histone H2AX (γ H2AX), a marker for DNA double-strand breaks. As shown in Figure 4B, we found that more than 70% of all cells in these CCCs show signs of DNA damage as compared to wild-type liver tissue. Similarly, tumor tissues derived from nude mice transplanted with primary tumor cells from *Notch1^{Cre}::AlbCre* also showed high levels of cyclin E expression and stained positive for γ H2AX (Figure 4C). Mice expressing only cre-recombinase do not show any signs of genetic instability as measured by γ H2AX staining (Kossatz et al., 2010). We then determined whether a reduction in cyclin E expression would reduce the number of γ H2AX-positive cells. Figure 4D shows that transfection of human MzChA1 cholangiocarcinoma cells with siRNAs against cyclins E1 and E2 (Figure S2B) led to a significant reduction in the number of γ H2AX-positive cells.

Based on these results, we speculated that Notch signaling might be directly involved in the regulation of the cyclin E promoter and thus in the induction of genetic instability and CCC initiation and progression. Interestingly, the cyclin E1 promoter contains several Rbpjk binding sites that could be involved in the regulation of the promoter by NICD signaling. We used a previously described cyclin E1 promoter luciferase reporter construct (Geng et al., 1996) to measure promoter activity in the CCC cell with or without NICD overexpression. To determine the activity of the cyclin E gene, we transfected the CycE-Luc

promoter construct into CCC cells (MzChA1, TFK1) and measured luciferase expression in these cells as compared to that in hepatocellular carcinoma cell lines (Hep3B, HepG2). As shown in Figure 4E, we found higher basal levels of cyclin E promoter activity in the CCC cell lines as compared to levels in liver cancer cells (Hep3B) or hepatoblastoma cells (HepG2). Next, we determined whether NICD was able to induce the activation of the cyclin E promoter. Cotransfection of NICD with the CycE-Luc reporter construct resulted in a more than 10-fold induction of the cyclin E promoter (Figure 4E). Moreover, cotransfection of NICD with an expression plasmid for the dominant-negative co-activator Mastermind prevented the activation of the cyclin E promoter by NICD, indicating that the activation of the cyclin E promoter was a direct consequence of NICD activity.

Given the importance of cyclin E expression for the generation of genetically unstable CCC cells, we next tested whether the induction of cyclin E is required for the observed oncogenic transformation of bipotential hepatic progenitors. For this purpose, we transduced NICD-expressing liver progenitor cells with retroviruses for stable expression of two different shRNAs against cyclin E. After selection, we measured the knockdown level of cyclin E in these cell populations (Figures S2C and S2D) and transplanted these cells subcutaneously into immunodeficient mice. As shown in Figure 3D, compared to ICN-expressing cells that were transduced with control shRNAs, there was a strong inhibition of tumor development from cells with stable expression of cyclin E shRNAs together with ICN. Overall, only one mouse developed tumors (mouse 1a,1b). Western blot analysis of the tumor tissue showed profound cyclin E protein expression (Figure S2E), indicating a selection against RNAi-mediated cyclin E knockdown in these particular tumors. Our results suggest that expression of NICD results in the activation of the cyclin E promoter and increased cyclin E expression which, through the induction of genetic instability, leads to the formation of CCCs.

Notch 1 and 3 Are Overexpressed in Human Cholangiocellular Carcinoma

Prompted by these results, we next tested whether the Notch pathway is also active in human CCC cells and tissues. We first determined the expression and activity of the Notch signaling pathway in three established human CCC cell lines (TFK1, MzChA1, and Egl1) and also in a primary cell line that we derived from a CCC tumor specimen (SZ1). As shown in Figure 5A, all CCC cell lines expressed the Notch1 receptor as well as the Notch ligand jagged while hepatocellular or colon carcinoma cell lines did not show an activation of this pathway (Figure S2F). To determine whether the Notch signaling pathway is active in CCC cells, we used an antibody that recognizes the cleaved form of Notch 1 (Notch val 1744) and the downstream target gene *Hes1*. As shown in Figure 5A, all CCC cell lines expressed the activated form of the Notch receptor and the HES1 protein, indicating that the Notch signaling pathway is active in these tumor cells but not in HeLa cells, which we used as a control. To ensure that the NICD transgenic mouse line is an adequate model system, we compared the expression levels of NICD in the CCCs that arose in our transgenic animals to the levels expressed in the human CCC cell lines. As shown in Figure 5B, mouse tissue and human CCC lines express comparable levels of cleaved Notch and HES1 protein. Finally, we tested whether

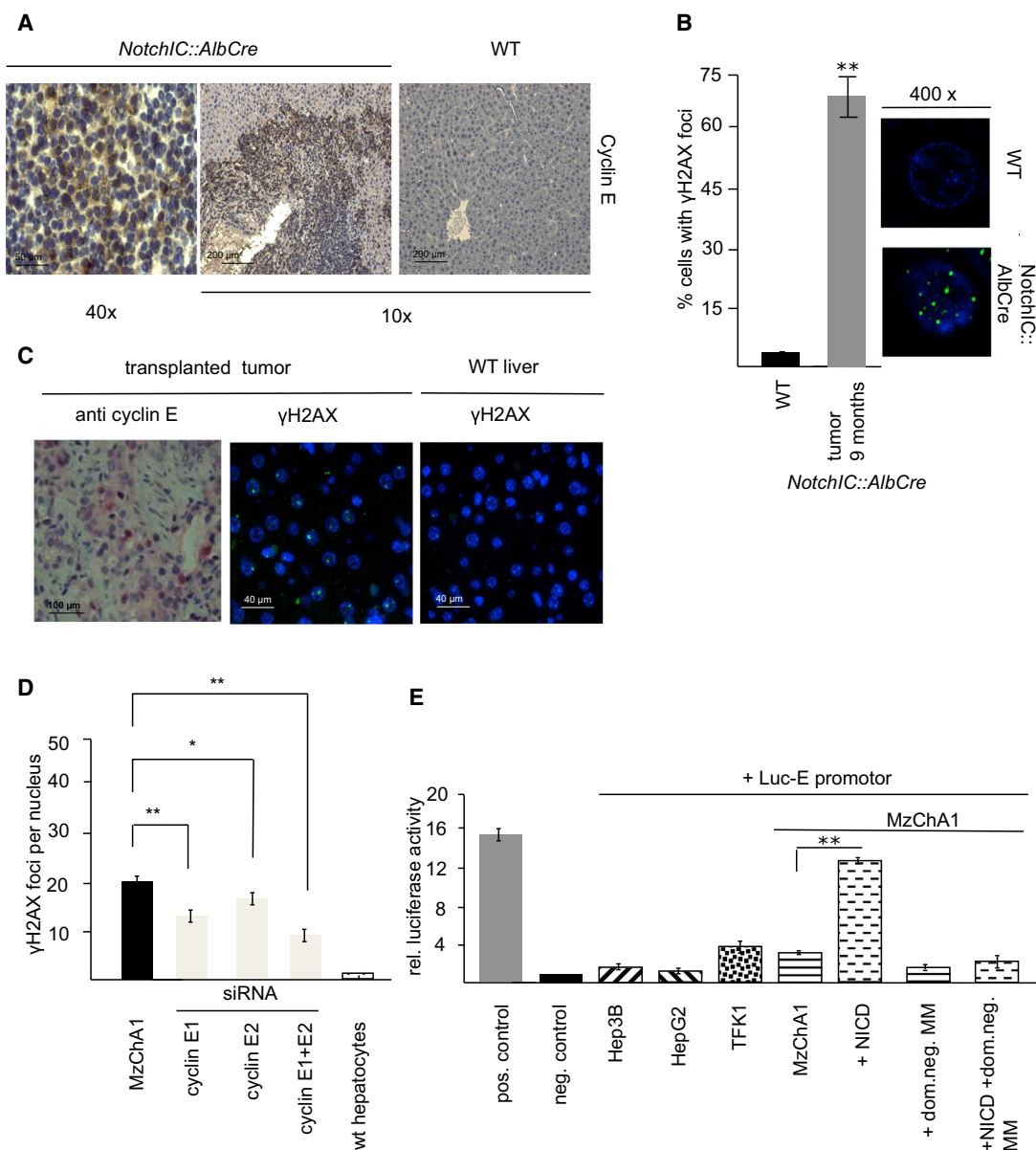


Figure 4. Notch Signaling Leads to the Transformation of Bipotential Hepatic Progenitors through Dysregulation of Cyclin E Expression

(A) Immunohistochemical staining of wild-type and *Notch1C::AlbCre* livers at the age of 9 months using a cyclin E antibody.

(B) Livers from wild-type controls or tumor tissue derived from 9-month-old *Notch1C::AlbCre* mice were stained with a γ H2AX antibody to determine the number of nuclei that showed signs of DNA damage. The plot shows the staining results of at least 300 cells per mouse strain. An example of *Notch1C::AlbCre* and wild-type nuclei is shown in a 400 \times magnification on the right side.

(C) Representative examples of γ H2AX and cyclin E stained transplanted mouse CCCs and wild-type liver control.

(D) Statistical analysis of γ H2AX foci in MzChA1 cells and after depletion of cyclin E expression through siRNA-mediated knockdown of cyclin E1, cyclin E2, or both.

(E) MzChA1, TFK1, Hep3B, and HepG2 cells were transfected with the indicated plasmids and relative luciferase activity was measured after 48 hr. Scale bars represent mean values \pm SEM. * $p < 0.05$; ** $p < 0.001$.

the activation of the Notch pathway is involved in the pathogenesis of human CCC. We determined the expression levels of the Notch receptors (Notch 1, 2, 3, and 4) in 56 primary CCC tumor tissues (see Table S1 for details) with immunohistochemical staining. As shown in Figure 5C and in the diagram in Figure 5D, we found that the majority of all CCCs overexpress the Notch 1 receptor. Additionally, we found a strong overexpression of the

Notch 3 receptor in primary tumor tissue as compared to that in wild-type liver tissue. For both types of receptors, we detected a predominant nuclear staining, whereas normal liver tissue did not stain positive for either receptor (Figures S3A and S3B). Finally, we tested the expression of the cyclin E protein in our collection of primary human CCC tissues. As shown in Figures 5E and S3C, we found a strong or very strong expression of the

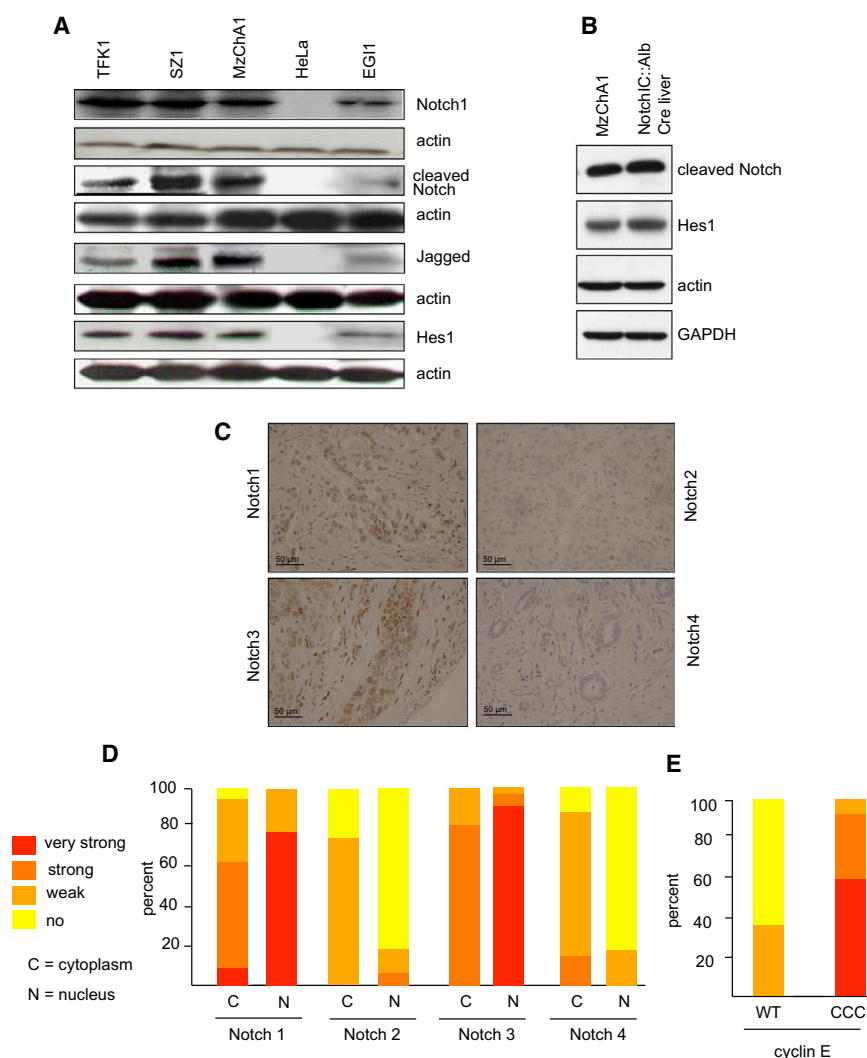


Figure 5. The Notch Signaling Pathway Is Activated in Human CCC

(A) TFK1, MzChA1, EGI1 cells, a CCC primary culture (SZ1), and HeLa cells were lysed and the expression levels of Notch 1, cleaved Notch, Jagged 1 and HES1 were analyzed by western blotting.

(B) Comparison of cleaved Notch and HES1 levels in human CCC cell lines and tumor tissue derived from *Notch1C::AlbCre* mice. Actin and GAPDH were used as loading controls.

(C) Fifty-six different human CCCs were screened for Notch 1, 2, 3, or 4 expression using a tissue microarray.

(D) Analysis of the staining intensities of the tissue microarray displayed is the percentage of tumors that express the Notch receptors 1–4 in the cytoplasm as well as in the nucleus in the 56 CCC samples tested.

(E) Immunohistochemical analysis of 56 human CCCs shows a strong expression of cyclin E1 compared to wild-type livers.

See also Figure S3 and Table S1.

after the transfection of Notch 1 siRNA, approximately 50% of all MzChA1 cells had undergone apoptosis (Figure 6B). Combined ablation of Notch 1 and 3 by siRNA led to an even more pronounced effect, indicating that signaling through both receptors is required for CCC maintenance (Figures S4A and S4B).

Notch signaling depends on γ -secretase-mediated generation of NICD, which translocates to the nucleus to induce a cell type-specific transcriptional program. To test whether γ -secretase inhibition of Notch signaling might constitute a treatment option against CCC, we treated

these cells with the γ -secretase inhibitor N-[N-(3,5-difluorophenacetyl)-L-alanyl]-S-phenylglycine t-butyl ester (DAPT). As shown in Figure 6C, DAPT treatment resulted in a time-dependent decrease in the expression of the cleaved form of the Notch receptor and the Notch target gene *Hes1*. Similar results were obtained with other CCC cell lines (Figure S4C). In line with our observation that Notch controls cyclin E transcription, DAPT treatment also led to a decrease in cyclin E expression in MzChA1 cells as determined by RT-PCR (Figure S4D). To determine the functional consequences of Notch inhibition, we determined the number of apoptotic MzChA1 cells after treatment with DAPT. As shown in Figure 6D, DAPT treatment of MzChA1 cells resulted in a significant increase in the number of apoptotic cells as measured by the activation of caspases 3 and 7. This decrease in viability was accompanied by a significant reduction of BrdU uptake (Figure S4E) and a strong increase in the expression levels of the cyclin kinase inhibitors p21 and p27 as well as the tumor suppressor protein p53 (Figure S4F). Similar results were found in the other CCC lines (EGI-1, TFK-1) (data not shown).

Notch Signaling as a Therapeutic Target in CCC

Our analysis of primary CCC tissues and the observation that NICD transgenic mice develop CCCs point toward a central role of the Notch signaling pathway in the formation of these tumors. To test whether the expression of Notch was also required for CCC maintenance, we transfected the cells with siRNAs specific for Notch 1. As shown in Figure 6A, loss of Notch 1 expression led to a reduction in HES1 and cyclin E expression while p53, p27, and p21 were strongly induced. Forty-eight hours

these cells with the γ -secretase inhibitor N-[N-(3,5-difluorophenacetyl)-L-alanyl]-S-phenylglycine t-butyl ester (DAPT). As shown in Figure 6C, DAPT treatment resulted in a time-dependent decrease in the expression of the cleaved form of the Notch receptor and the Notch target gene *Hes1*. Similar results were obtained with other CCC cell lines (Figure S4C). In line with our observation that Notch controls cyclin E transcription, DAPT treatment also led to a decrease in cyclin E expression in MzChA1 cells as determined by RT-PCR (Figure S4D). To determine the functional consequences of Notch inhibition, we determined the number of apoptotic MzChA1 cells after treatment with DAPT. As shown in Figure 6D, DAPT treatment of MzChA1 cells resulted in a significant increase in the number of apoptotic cells as measured by the activation of caspases 3 and 7. This decrease in viability was accompanied by a significant reduction of BrdU uptake (Figure S4E) and a strong increase in the expression levels of the cyclin kinase inhibitors p21 and p27 as well as the tumor suppressor protein p53 (Figure S4F). Similar results were found in the other CCC lines (EGI-1, TFK-1) (data not shown).

Finally, we tested whether inhibition of Notch signaling would also affect the growth of xenotransplanted human CCCs. To this

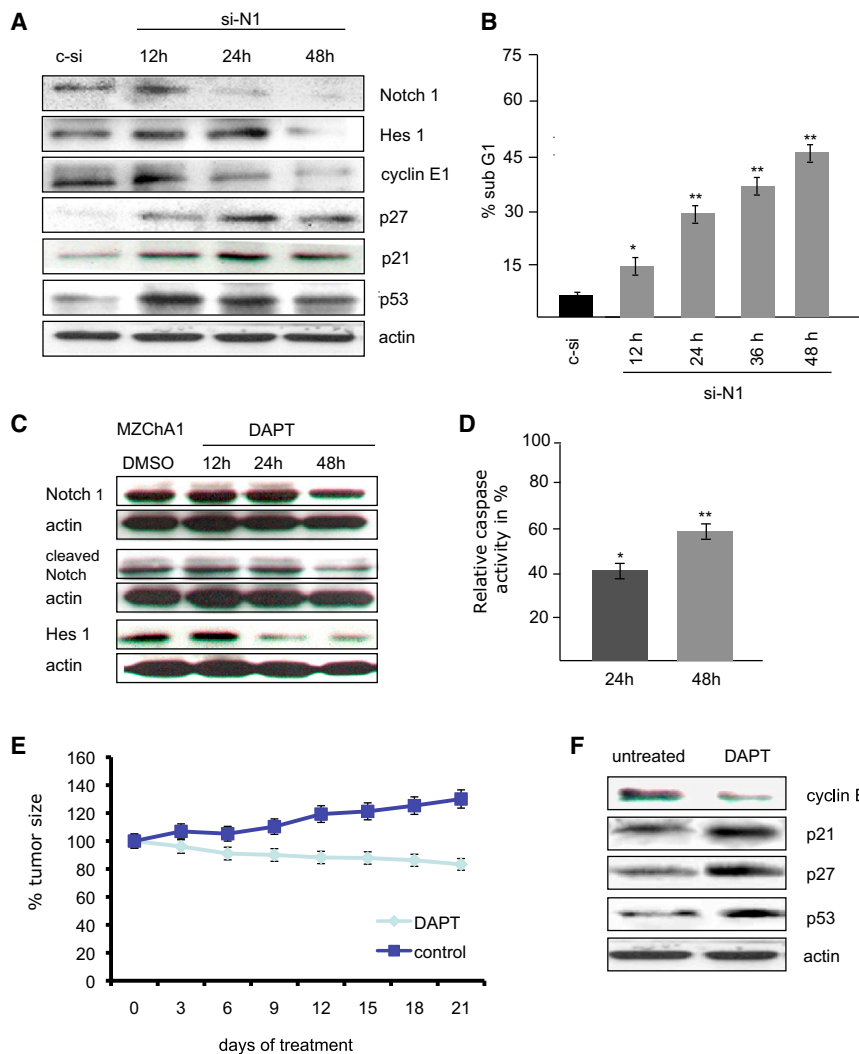


Figure 6. Notch Signaling as a Therapeutic Target in CCC

(A) Western blot expression analysis of Notch 1, HES1, cyclin E, p21, p53, and p27 after siRNA-mediated knockdown of Notch 1 in MzChA1 cells. (B) Determination of cell death (sub G1 fraction) by FACS scan analysis in MzChA1 cells in which Notch1 expression was reduced through siRNA-mediated knockdown.

(C) MzChA1 cells were treated with DAPT (10 μ M) for the indicated periods of time. At different time points cells were lysed and the expression levels of Notch 1, cleaved Notch 1, and HES1 were analyzed by western blotting.

(D) Caspase 3/7 activity in DAPT-treated MzChA1 cells at the indicated time points. The y-axis describes the relative caspase activity in percentages as compared to the DMSO control treated cells.

(E) Primary human CCC cells (SZ1) were transplanted under the skin of nu/nu mice (ten mice for each group). When the tumors reached a size of approximately 150–200 mm³, mice were treated with DAPT at a concentration of 50 mg/kg every 72 hr or with DMSO, which was used to dissolve DAPT (control).

(F) Western blot analysis of the expression levels of cyclin E1, p21, p27, p53, and actin in tumor tissue lysates from DAPT treated or untreated mice. Scale bars represent mean values \pm SEM.

See also Figure S4.

end, we established primary CCC cell lines from human CCCs that were resected at our institution. Cells derived from cell line SZ1 were mixed with Matrigel and injected subcutaneously into immunodeficient mice. When the tumors reached a size of approximately 150–200 mm³, mice were treated with DAPT at a concentration of 50 mg/kg every 72 hr. As shown in Figure 6E and Figure S4G, inhibition of γ -secretase resulted in a significant inhibition of tumor growth as compared to untreated controls. This inhibition of tumor growth was accompanied by the induction of p21, p27, and p53 and a downregulation of cyclin E expression in the primary tumor tissues (Figure 6F). Histologic examination of these tumors revealed, in accordance with the results we had obtained using CCC cell lines, that treatment with DAPT resulted in the induction of apoptosis in the xenotransplanted tumors as shown by TUNEL staining of the primary tissues (Figure S4H).

DISCUSSION

The pathogenesis of CCC is only incompletely understood. A number of genetic and epigenetic changes as well as alterations

in growth factor signaling have been described. Nevertheless, treatment options are still sparse and given the lack of a detailed understanding of the underlying pathogenesis, targeted therapies are difficult to implement. In this study, we used a transgenic mouse line that expresses the intracellular domain of the Notch 1 receptor in liver cells starting at day 9.5. Our phenotypic and molecular analysis of the *Notch1^{Cre}::Alb^{Cre}* mice revealed opposite roles for Notch signaling in the hepatic and cholangiocytic compartments. We found that NICD-overexpressing hepatocytes undergo endoreduplication cycles that result in the formation of polyploid liver cells. This defect in mitotic cell division is also apparent in liver regeneration experiments that show that NICD-expressing hepatocytes fail to re-enter the cell cycle after a partial hepatectomy. In line with our findings Croquelois and colleagues showed that loss of Notch 1 in hepatocytes led to the overproliferation of hepatocytes, which caused the formation of regenerative nodules (Croquelois et al., 2005). Together, these results suggest that Notch signaling in hepatocytes is primarily antiproliferative and prevents uncontrolled proliferation of liver cells.

We found that overexpression of NICD results in the formation of CCCs, implicating this signaling pathway in the pathogenesis of this tumor. Zong and colleagues convincingly showed that ectopic Notch expression led to the formation of biliary epithelial cells in the hepatic lobule (Zong et al., 2009). Moreover, expression of Notch in livers of 6-day-old mice led to the formation of ectopic biliary structures within the liver. Their experiments

therefore argue for the ability of Notch signaling to induce a fate decision in hepatoblasts or even terminally differentiated hepatocytes that allows them to differentiate toward the biliary lineage. The ability of hepatocytes to change their fate decision under the influence of AKT and Notch signaling or under conditions of chemically induced carcinogenesis has been shown recently (Fan et al., 2012; Sekiya and Suzuki, 2012). These studies provided evidence that hepatocytes localized around the central vein can be transformed into biliary cancers. While a growing body of evidence supports the hypothesis that human CCC is derived from intrahepatic stem cell compartments (Cardinale et al., 2012; Nakanuma et al., 2010), it needs to be shown whether a change in cellular differentiation can contribute to human CCC pathogenesis. Recent data in other systems indicate that Notch signaling drives intestinal cell fate determination of progenitor cells, for example, those lining the intestinal crypts, and blockade of Notch signaling via gamma secretase inhibition forces intestinal progenitor cells to differentiate into goblet cells (van Es et al., 2005; Zecchini et al., 2005). This pathologic profile is reminiscent of that seen in *Hes-1* deficient mice, a downstream Notch target gene (Kodama et al., 2004). Our analysis showed that expression of NICD in mouse liver cells results in the formation of CCCs, which in addition to cholangiocytic features, also express surface markers associated with stem cells thereby indicating that NICD expression in undifferentiated liver progenitor cells might have transformed those cells into tumor cells. It is not known how the expression of Notch ICD in differentiated cholangiocytes may also result in the formation of cancers.

The finding that NICD expression in hepatic progenitors results in the formation of CCCs was further substantiated by the fact that cells isolated from these primary tumors led to the formation of CCC after transplantation into nude mice. Given the high plasticity of these cells, we cannot exclude that Notch signaling might lead to the formation of tumors that resemble features of hepatocellular carcinoma or even mixed phenotypes (Villanueva et al., 2012). We therefore set out to directly prove that aberrant Notch signaling in bipotential liver progenitor cells causes the formation of CCC. To this end, we created progenitor cell lines that stably express NICD and found that these cells did indeed start to form tumors that show all characteristics of CCCs after transplantation into mice. These tumors also showed elevated levels of cyclin E expression and a high degree of genetic instability. We therefore concluded that liver progenitor cells can act as the cells of origin in the formation of CCCs in response to Notch signaling.

A central question that arose out of these findings is how the expression of NICD can lead to the formation of CCC. In this work, we found that cyclin E protein levels are greatly increased not only in CCCs derived from *Notch1^{Cre}::Alb^{Cre}* mice, but also in primary human CCC tissues. Several mouse models have demonstrated that deregulated cyclin E expression is causally associated with tumorigenesis in vivo. Overexpression of human cyclin E in mammary or thymic tissues, or prevention of cyclin E degradation through mutation of the T380 phosphorylation site in mouse cyclin E, resulted in the formation of tumors (Hwang and Clurman, 2005; Loeb et al., 2005). The oncogenic function of cyclin E is coupled to its ability to induce double-strand breaks that ultimately result in the formation of genetically unstable cells. Using γ H2AX as a marker for double-strand breaks, we

showed that the tumors derived from *Notch1^{Cre}::Alb^{Cre}* mice as well as tumors derived from NICD-expressing bipotential progenitors show high levels of DNA double-strand breaks and that reduction of cyclin E expression ameliorates this phenotype. Interestingly the dysregulation of cyclin E expression is caused by an increased transcription of the cyclin E promoter in response to NICD expression a finding that defines cyclin E as a direct transcriptional target of the Notch signaling pathway. Given that suppression of cyclin E expression by shRNA treatment results in a complete suppression of tumor formation in NICD-expressing liver progenitors, we conclude that cyclin E is indeed a critical downstream effector of Notch signaling-induced tumor formation.

Our observations together with the data provided by Zong and Stanger therefore suggest that Notch signaling can induce a biliary differentiation program in hepatocytes or hepatic progenitor cells, which together with the aberrant expression of the cyclin E protein results in the formation of intrahepatic CCCs. It is currently unknown why the Notch 1 and 3 receptors are up-regulated in CCC cells. T cell acute lymphoblastic leukemia, breast cancer, and other tumors or cell lines derived from such cancers show genetic alterations that affect the expression of different components of the Notch signaling pathway (Koch and Radtke, 2007).

Recently, Fbw7, the F-Box protein that controls the turnover of Notch 1 as part of a SCF^{Fbw7} ubiquitin ligase, was shown to be mutated in up to 35% of all CCCs examined (Akhoondi et al., 2007). This result points to a defect in Notch turnover that might contribute to the increase in protein levels. Interestingly the SCF^{Fbw7} complex also ubiquitylates the cyclin E1 and E2 proteins and loss or mutation of the Fbw7 protein results in increased cyclin E expression (Koepp et al., 2001; Welcker et al., 2003). We have shown that overexpression of the Notch ICD in mouse livers leads to an increase in cyclin E expression and that Notch ICD can directly transactivate the cyclin E1 promoter. Loss of Fbw7 might therefore cause an increase in cyclin E levels not only through a reduction of cyclin E ubiquitylation and turnover, but also through an increased transcription of the Cyclin E gene through the Notch signaling pathway.

CCCs frequently arise under conditions of chronic inflammation. The interleukin-6 (IL-6)/gp130 signaling system constitutes an important component of the inflammatory response in the liver and was shown to be involved in the pathogenesis of CCCs. This aberrant overexpression of IL-6 is a consequence of the epigenetic silencing of the suppressor of cytokine signaling 3 (SOCS-3) (Isomoto et al., 2007). Intriguingly IL-6 is able to induce a Notch-3-dependent transcriptional activation of the jagged gene in breast cancer cells (Sansone et al., 2007). Dysregulation of Notch signaling might therefore be a result of alterations in its proteolytic turnover and exogenous factors like the stimulation of jagged transcription by IL-6. While this hypothesis awaits experimental proof, our experiments using isolated NICD-expressing progenitors show that transformation of these cells does not require additional inflammation.

To date, no specific treatment exists for patients with CCCs that are not eligible for surgery. We therefore set out to test whether inhibition of Notch signaling would interfere with the proliferation and survival of CCC cells. Loss of Notch signaling either by inhibition of γ -secretase or by suppressing Notch

activity through siRNA-mediated ablation of Notch 1 and 3 expression resulted in the induction of cell cycle arrest and apoptosis. Notch inhibition also led to the regression of established xenotransplant tumors derived from CCC cell lines in vivo. Inhibition of γ -secretase activity might therefore constitute a molecular target that interferes with the dysregulated expression of cyclin E.

In this study we found that *Notch1C::AlbCre* mice not only formed ectopic biliary structures, but also intrahepatic CCCs. Together with the observation that Notch can induce a biliary cell fate in bipotential progenitors lead to the idea that the pathogenesis of intrahepatic CCCs might differ significantly from the formation of biliary tumors that arise primarily from the bile ducts (i.e., Klatskin carcinoma). Our data suggest that intrahepatic CCC might constitute a tumor that forms as a result of aberrant Notch signaling in hepatic progenitors that transform into tumor cells. Moreover we show that inhibition of Notch signaling constitutes an attractive target for future clinical trials in patients with intrahepatic CCCs.

EXPERIMENTAL PROCEDURES

Animals and Partial Hepatectomy Procedures

ROSA26 NICD mice (Murtaugh et al., 2003) were crossed with *AlbCre* mice (Kellendonk et al., 2000) to generate mice with a liver-specific overexpression of the activated form of the Notch 1 receptor. All genotyping was performed as described (Murtaugh et al., 2003). In all experiments, 8- to 10-week-old wild-type and double transgenic littermates were used. Mice were killed at the indicated time points after surgery, and the number of mice analyzed ranged from five to six per time point. Partial hepatectomy was performed as described (Satyanarayana et al., 2003). All animal experiments were performed after review and approval by the Niedersächsische Landesamt für Verbraucherschutz und Lebensmittelsicherheit, Lower Saxony, Germany.

Immunohistochemical Staining of Mouse and Human Tissues

Immunohistochemical staining of mouse and human tissue was performed as described previously (Kossatz et al., 2004). Surgical specimens were taken for diagnostic and scientific purposes permitted by the Ethics Committee of the University of Bern, Switzerland. Informed consent was obtained from all patients.

Feulgen Staining

To determine the DNA content, 3 μ m sections were Feulgen-stained using the Feulgen Staining Kit (Merck). Ploidy analysis was performed with the Ahrens ICM, Cytometric System. Statistical analysis was done using the Dunnett t test (DNA ploidy) and the mixed models analysis of variance (nuclear size analysis).

RT-PCR

RNA extraction was done as described (Satyanarayana et al., 2003). For cDNA synthesis, 2 μ g of RNA were used. The RT reaction was carried out using SuperScript-II RNase H reverse transcriptase (Invitrogen). For semiquantitative RT-PCR, 1 μ l cDNA was amplified using the following cycles: denaturation 94°C for 30 s, annealing 57°C for 1 min, and extension 72°C for 45 s using RedTaq (Sigma) for 35 cycles. Actin was used as a control.

siRNA

siRNA knockdown was performed using FuGene6 transfection reagent. Transfections were performed using siRNA at a concentration of 20 nM for Notch 1 siRNA; sc-36095 and Notch 3 siRNA; sc-37135 from Santa Cruz. siRNA at a concentration of 40 nM was used for cyclin E1 and cyclin E2 knockdown.

DAPT Treatment In Vitro

Five milligrams of DAPT were dissolved in 1 ml dimethyl sulfoxide. Cells were plated in six-well plates. When the cells reached 60% confluency, they were

treated with 38.7 μ M DAPT. Cells were collected after 12, 24, 36, and 48 hr for protein extraction and analyzed by western blot.

Western Blot

Antibodies included cleaved Notch 1 (Val1744, Cell signaling); Hes-1 (Santa Cruz Biotechnology); Notch 1: C-20; sc 6014 (Santa Cruz), Notch 3: (M-134); sc5593 (Santa Cruz); Jagged 1: C-20, sc-6011 (Santa Cruz); p27: Cat 610242 (BD Transduction), p21 C-19; sc397 (Santa Cruz), p53 FL-393, sc6243 (Santa Cruz); and cyclin E: C19 (Delta Biolabs). Western blots were performed as described (Malek et al., 2001).

Generation of Immortalized Bipotential Liver Progenitor Cells, Retroviral Transduction, and Subcutaneous Injection of Cells

Bipotential liver progenitor cells were isolated from C57Bl6 embryonic mouse livers as described recently (Zender et al., 2006). For additional information, please refer to the Supplemental Experimental Procedures.

Statistical Analysis

Statistical analysis was carried out using Microsoft Excel software. Unless stated otherwise, all data are presented as mean \pm SD; error bars represent SD in all figures. Intergroup comparisons were performed by two-tailed Student's t test. A p value <0.05 was considered to be statistically significant.

Caspase 3/7 Assay and TUNEL Staining

For detection of apoptosis, we used the Caspase-Glo 3/7 Assay from Promega that measures caspase-3 and -7 activities because these members of the caspase family play important roles in apoptosis in mammalian cells. The measurements were done as described in the manufacturer manual. We used the In Situ Cell Death Detection Kit (Roche) according to the manufacturer's manual for TUNEL staining.

Luciferase Assay

MzChA1 cells were transiently transfected with a cyclin E promoter luciferase reporter construct, a NICD expression construct, and pRL-TK (Promega) for normalization using FUGENE. After 48 hr, luciferase activity was measured using the "dual-luciferase reporter assay system" (Promega) following the manufacturer's instructions. In brief, cells were lysed in 1 \times passive lysis buffer; after 10 min, cells were scraped off the dishes and incubated for 5 min on ice. After centrifugation, 20 μ l of cleared lysates were used for analysis of luciferase activity. The 96-well plate reader "Glomax-integrated luciferase technologies" (TURNER Biosystems) was used to quantify luciferase activity. Firefly luciferase activity was normalized to cotransfected Renilla luciferase activity (pRLTK).

SUPPLEMENTAL INFORMATION

Supplemental Information includes four figures, one table, and Supplemental Experimental Procedures and can be found with this article online at <http://dx.doi.org/10.1016/j.ccr.2013.04.019>.

ACKNOWLEDGMENTS

We thank Dr. Holly Sundberg Malek for critical advice. This work was supported by the DFG (Cluster of excellence, REBIRTH), SFB 738 and TR77, as well as the Emmy Noether Programme (ZE 545/2-1). We thank Warren S. Pear for dnMAML expression plasmid.

Received: October 31, 2010

Revised: June 11, 2012

Accepted: April 20, 2013

Published: May 30, 2013

REFERENCES

Akhoondi, S., Sun, D., von der Lehr, N., Apostolidou, S., Klotz, K., Maljukova, A., Cepeda, D., Fiegl, H., Dafou, D., Marth, C., et al. (2007). FBXW7/hCDC4 is a general tumor suppressor in human cancer. *Cancer Res.* 67, 9006–9012.

- Benhamouche, S., Curto, M., Saotome, I., Gladden, A.B., Liu, C.H., Giovannini, M., and McClatchey, A.I. (2010). Nf2/Merlin controls progenitor homeostasis and tumorigenesis in the liver. *Genes Dev.* 24, 1718–1730.
- Cardinale, V., Carpino, G., Reid, L., Gaudio, E., and Alvaro, D. (2012). Multiple cells of origin in cholangiocarcinoma underlie biological, epidemiological and clinical heterogeneity. *World J. Gastrointest. Oncol.* 4, 94–102.
- Croquelois, A., Blindenbacher, A., Terracciano, L., Wang, X., Langer, I., Radtke, F., and Heim, M.H. (2005). Inducible inactivation of Notch1 causes nodular regenerative hyperplasia in mice. *Hepatology* 41, 487–496.
- El-Serag, H.B., Engels, E.A., Landgren, O., Chiao, E., Henderson, L., Amaratunge, H.C., and Giordano, T.P. (2009). Risk of hepatobiliary and pancreatic cancers after hepatitis C virus infection: A population-based study of U.S. veterans. *Hepatology* 49, 116–123.
- Fan, B., Malato, Y., Calvisi, D.F., Naqvi, S., Razumilava, N., Ribback, S., Gores, G.J., Dombrowski, F., Evert, M., Chen, X., and Willenbring, H. (2012). Cholangiocarcinomas can originate from hepatocytes in mice. *J. Clin. Invest.* 122, 2911–2915.
- Geisler, F., Nagl, F., Mazur, P.K., Lee, M., Zimmer-Strobl, U., Strobl, L.J., Radtke, F., Schmid, R.M., and Siveke, J.T. (2008). Liver-specific inactivation of Notch2, but not Notch1, compromises intrahepatic bile duct development in mice. *Hepatology* 48, 607–616.
- Geng, Y., Eaton, E.N., Picón, M., Roberts, J.M., Lundberg, A.S., Gifford, A., Sardet, C., and Weinberg, R.A. (1996). Regulation of cyclin E transcription by E2Fs and retinoblastoma protein. *Oncogene* 12, 1173–1180.
- Hwang, H.C., and Clurman, B.E. (2005). Cyclin E in normal and neoplastic cell cycles. *Oncogene* 24, 2776–2786.
- Isomoto, H., Mott, J.L., Kobayashi, S., Werneburg, N.W., Bronk, S.F., Haan, S., and Gores, G.J. (2007). Sustained IL-6/STAT-3 signaling in cholangiocarcinoma cells due to SOCS-3 epigenetic silencing. *Gastroenterology* 132, 384–396.
- Kellendonk, C., Opherck, C., Anlag, K., Schütz, G., and Tronche, F. (2000). Hepatocyte-specific expression of Cre recombinase. *Genesis* 26, 151–153.
- Kim, H., Park, C., Han, K.H., Choi, J., Kim, Y.B., Kim, J.K., and Park, Y.N. (2004). Primary liver carcinoma of intermediate (hepatocyte-cholangiocyte) phenotype. *J. Hepatol.* 40, 298–304.
- Koch, U., and Radtke, F. (2007). Notch and cancer: a double-edged sword. *Cell. Mol. Life Sci.* 64, 2746–2762.
- Kodama, Y., Hijikata, M., Kageyama, R., Shimotohno, K., and Chiba, T. (2004). The role of notch signaling in the development of intrahepatic bile ducts. *Gastroenterology* 127, 1775–1786.
- Koepf, D.M., Schaefer, L.K., Ye, X., Keyomarsi, K., Chu, C., Harper, J.W., and Elledge, S.J. (2001). Phosphorylation-dependent ubiquitination of cyclin E by the SCFFbw7 ubiquitin ligase. *Science* 294, 173–177.
- Kossatz, U., Dietrich, N., Zender, L., Buer, J., Manns, M.P., and Malek, N.P. (2004). Skp2-dependent degradation of p27kip1 is essential for cell cycle progression. *Genes Dev.* 18, 2602–2607.
- Kossatz, U., Breuhahn, K., Wolf, B., Hardtke-Wolenski, M., Wilkens, L., Steinemann, D., Singer, S., Brass, F., Kubicka, S., Schlegelberger, B., et al. (2010). The cyclin E regulator cullin 3 prevents mouse hepatic progenitor cells from becoming tumor-initiating cells. *J. Clin. Invest.* 120, 3820–3833.
- Loeb, K.R., Kostner, H., Firpo, E., Norwood, T., Tsuchiya, K., Clurman, B.E., and Roberts, J.M. (2005). A mouse model for cyclin E-dependent genetic instability and tumorigenesis. *Cancer Cell* 8, 35–47.
- Lorent, K., Yeo, S.Y., Oda, T., Chandrasekharappa, S., Chitnis, A., Matthews, R.P., and Pack, M. (2004). Inhibition of Jagged-mediated Notch signaling disrupts zebrafish biliary development and generates multi-organ defects compatible with an Alagille syndrome phenocopy. *Development* 131, 5753–5766.
- Malek, N.P., Sundberg, H., McGrew, S., Nakayama, K., Kyriakides, T.R., and Roberts, J.M. (2001). A mouse knock-in model exposes sequential proteolytic pathways that regulate p27Kip1 in G1 and S phase. *Nature* 413, 323–327.
- Murtaugh, L.C., Stanger, B.Z., Kwan, K.M., and Melton, D.A. (2003). Notch signaling controls multiple steps of pancreatic differentiation. *Proc. Natl. Acad. Sci. USA* 100, 14920–14925.
- Nakanuma, Y., Sato, Y., Harada, K., Sasaki, M., Xu, J., and Ikeda, H. (2010). Pathological classification of intrahepatic cholangiocarcinoma based on a new concept. *World J. Hepatol.* 2, 419–427.
- Patel, T. (2006). Cholangiocarcinoma. *Nat. Clin. Pract. Gastroenterol. Hepatol.* 3, 33–42.
- Ryan, M.J., Bales, C., Nelson, A., Gonzalez, D.M., Underkoffler, L., Segalov, M., Wilson-Rawls, J., Cole, S.E., Moran, J.L., Russo, P., et al. (2008). Bile duct proliferation in Jag1/fringe heterozygous mice identifies candidate modifiers of the Alagille syndrome hepatic phenotype. *Hepatology* 48, 1989–1997.
- Sansone, P., Storci, G., Tavoroli, S., Guarnieri, T., Giovannini, C., Taffurelli, M., Ceccarelli, C., Santini, D., Paterini, P., Marcu, K.B., et al. (2007). IL-6 triggers malignant features in mammospheres from human ductal breast carcinoma and normal mammary gland. *J. Clin. Invest.* 117, 3988–4002.
- Satyanarayana, A., Wiemann, S.U., Buer, J., Lauber, J., Dittmar, K.E., Wüstefeld, T., Blasco, M.A., Manns, M.P., and Rudolph, K.L. (2003). Telomere shortening impairs organ regeneration by inhibiting cell cycle re-entry of a subpopulation of cells. *EMBO J.* 22, 4003–4013.
- Sekiya, S., and Suzuki, A. (2012). Intrahepatic cholangiocarcinoma can arise from Notch-mediated conversion of hepatocytes. *J. Clin. Invest.* 122, 3914–3918.
- Spruck, C.H., Won, K.A., and Reed, S.I. (1999). Deregulated cyclin E induces chromosome instability. *Nature* 401, 297–300.
- van Es, J.H., van Gijn, M.E., Riccio, O., van den Born, M., Vooijs, M., Begthel, H., Cozijnsen, M., Robine, S., Winton, D.J., Radtke, F., and Clevers, H. (2005). Notch/gamma-secretase inhibition turns proliferative cells in intestinal crypts and adenomas into goblet cells. *Nature* 435, 959–963.
- Villanueva, A., Alsinet, C., Yanger, K., Hoshida, Y., Zong, Y., Toffanin, S., Rodriguez-Carunchio, L., Sole, M., Thung, S., Stanger, B.Z., and Llovet, J.M. (2012). Notch signaling is activated in human hepatocellular carcinoma and induces tumor formation in mice. *Gastroenterology* 143, 1660–1669.e7.
- von Hahn, T., Ciesek, S., Wegener, G., Plentz, R.R., Weismüller, T.J., Wedemeyer, H., Manns, M.P., Greten, T.F., and Malek, N.P. (2011). Epidemiological trends in incidence and mortality of hepatobiliary cancers in Germany. *Scand. J. Gastroenterol.* 46, 1092–1098.
- Welcker, M., and Clurman, B.E. (2008). FBW7 ubiquitin ligase: a tumour suppressor at the crossroads of cell division, growth and differentiation. *Nat. Rev. Cancer* 8, 83–93.
- Welcker, M., Singer, J., Loeb, K.R., Grim, J., Bloecher, A., Gurién-West, M., Clurman, B.E., and Roberts, J.M. (2003). Multisite phosphorylation by Cdk2 and GSK3 controls cyclin E degradation. *Mol. Cell* 12, 381–392.
- West, J., Wood, H., Logan, R.F., Quinn, M., and Aithal, G.P. (2006). Trends in the incidence of primary liver and biliary tract cancers in England and Wales 1971–2001. *Br. J. Cancer* 94, 1751–1758.
- Xu, X., Kobayashi, S., Qiao, W., Li, C., Xiao, C., Radaeva, S., Stiles, B., Wang, R.H., Ohara, N., Yoshino, T., et al. (2006). Induction of intrahepatic cholangiocellular carcinoma by liver-specific disruption of Smad4 and Pten in mice. *J. Clin. Invest.* 116, 1843–1852.
- Zecchini, V., Domasch, R., Winton, D., and Jones, P. (2005). Notch signaling regulates the differentiation of post-mitotic intestinal epithelial cells. *Genes Dev.* 19, 1686–1691.
- Zender, L., Spector, M.S., Xue, W., Flemming, P., Cordon-Cardo, C., Silke, J., Fan, S.T., Luk, J.M., Wigler, M., Hannon, G.J., et al. (2006). Identification and validation of oncogenes in liver cancer using an integrative oncogenomic approach. *Cell* 125, 1253–1267.
- Zong, Y., Panikkar, A., Xu, J., Antoniou, A., Raynaud, P., Lemaigre, F., and Stanger, B.Z. (2009). Notch signaling controls liver development by regulating biliary differentiation. *Development* 136, 1727–1739.

Epidermal Growth Factor Receptor Potentiates MCM7-Mediated DNA Replication through Tyrosine Phosphorylation of Lyn Kinase in Human Cancers

Tzu-Hsuan Huang,^{1,7,8} Longfei Huo,^{1,7} Ying-Nai Wang,^{1,5,6} Weiya Xia,¹ Yongkun Wei,¹ Shih-Shin Chang,^{1,3} Wei-Chao Chang,^{4,5} Yueh-Fu Fang,¹ Chun-Te Chen,¹ Jing-Yu Lang,¹ Chun Tu,¹ Yan Wang,¹ Ming-Chuan Hsu,¹ Hsu-Ping Kuo,¹ How-Wen Ko,¹ Jia Shen,^{1,3} Heng-Huan Lee,^{1,3} Pei-Chih Lee,¹ Yun Wu,² Chung-Hsuan Chen,⁴ and Mien-Chie Hung^{1,3,5,6,*}

¹Department of Molecular and Cellular Oncology, MD Anderson Cancer Center

²Department of Pathology, MD Anderson Cancer Center

³Graduate School of Biomedical Sciences at Houston

The University of Texas, Houston, TX 77030, USA

⁴The Genomics Research Center, Academia Sinica, 128 Academia Road, Section 2, Nankang, Taipei 115, Taiwan

⁵Center for Molecular Medicine and Graduate Institute of Cancer Biology, China Medical University, Taichung 404, Taiwan

⁶Asia University, Taichung 413, Taiwan

⁷These authors contributed equally to this work

⁸Present address: Therapeutic Innovation Unit, Amgen Inc., 360 Binney Street, AMA 7-F-12, Cambridge, MA 02142, USA

*Correspondence: mhung@mdanderson.org

<http://dx.doi.org/10.1016/j.ccr.2013.04.027>

SUMMARY

Epidermal growth factor receptor (EGFR) initiates a signaling cascade that leads to DNA synthesis and cell proliferation, but its role in regulating DNA replication licensing is unclear. Here, we show that activated EGFR phosphorylates the p56 isoform of Lyn, p56^{Lyn}, at Y32, which then phosphorylates MCM7, a licensing factor critical for DNA replication, at Y600 to increase its association with other minichromosome maintenance complex proteins, thereby promoting DNA synthesis complex assembly and cell proliferation. Both p56^{Lyn} Y32 and MCM7 Y600 phosphorylation are enhanced in proliferating cells and correlated with poor survival of breast cancer patients. These results establish a signaling cascade in which EGFR enhances MCM7 phosphorylation and DNA replication through Lyn phosphorylation in human cancer cells.

INTRODUCTION

MCM7 is a member of the minichromosome maintenance (MCM) proteins, which were originally identified through a yeast genetic screen aimed to identify mutants defective in MCM (Maine et al., 1984). The MCM proteins were subsequently found to be expressed in all eukaryotic organisms and are critical for licensing DNA replication in proliferating cells (Tye, 1999). MCM proteins 2–7 are highly conserved from yeast to humans and form a hexameric complex during the G1 phase, which is then loaded onto the replication origin to form a prereplication complex (pre-RC) that is indispensable for initiation of DNA repli-

cation (Lei and Tye, 2001). Assembly of the MCM protein complex is essential for cell survival and proliferation, and suppressing expression of individual MCM proteins resulted in compromised DNA replication (Shi et al., 2010; Tsuji et al., 2006), possibly due to lack of stable hexameric MCM complex. In addition to its role in initiation of replication, the MCM complex has been shown to serve as a putative replication fork helicase, melting DNA origins in preparation for replication (Ishimi, 1997; Labib et al., 2000; Lee and Hurwitz, 2001; Yan et al., 1993). Recent studies suggest that MCM2–MCM7 complex interacts with cell division cycle 45 (CDC45) and GINS to form the CDC45–MCM–GINS complex (Moyer et al., 2006), which is

Significance

Overexpression of MCM7 is associated with various human cancers and correlated with poor prognosis; however, the mechanisms that regulate its function remain unclear. Here, we showed that EGFR enhances p56^{Lyn} activity through Y32 phosphorylation, which potentiates the downstream MCM7 Y600 phosphorylation and positively modulates minichromosome maintenance complex assembly and cancer cell proliferation. We thus identified a tyrosine phosphorylation cascade, namely EGFR → phospho-p56^{Lyn} Y32 → phospho-MCM7 Y600, that links EGFR and Lyn in MCM7-mediated DNA replication licensing in human cancers. This finding links a cell-surface receptor, EGFR, and a nonreceptor tyrosine kinase, Lyn, to DNA replication licensing, which is an important step for initiating cell proliferation.

required for the activation of DNA helicase (Dang and Li, 2011; Kang et al., 2012). MCM2–MCM7 also forms a double-hexameric complex during pre-RC formation, which may be potentially required for the initiation of bidirectional replication forks in S phase (Evrin et al., 2009; Gambus et al., 2011).

Deregulation of DNA replication machinery components causes chromosome instability and tumorigenesis (Bergoglio et al., 2002; Rajagopalan et al., 2004), and the oncogenic potential of MCM7 deregulation has been well described (Luo, 2011). A transgenic mouse model demonstrates that expression of exogenous MCM7 in the epidermis accelerates squamous cell carcinoma development upon carcinogen challenge (Honeycutt et al., 2006). Additionally, increased MCM7 copy number and protein level are associated with prostate cancer relapse and metastasis, and a prostate cancer cell line ectopically expressing MCM7 exhibits increased proliferation and invasiveness (Ren et al., 2006). Similarly, MCM7 serves as a proliferation marker and is associated with tumorigenesis in various human cancers, including oral squamous cell carcinoma, colorectal cancer, ovarian cancer, glioblastoma, and esophageal carcinoma (Facchetti et al., 2006; Feng et al., 2008; Kan et al., 2009; Nishihara et al., 2008; Ota et al., 2011). MCM7 has recently been demonstrated as a prognostic marker that predicts poor cancer patient survival and a therapeutic target of non-small cell lung carcinomas (Toyokawa et al., 2011). Interestingly, MCM7 protein is a critical target of some oncogenic (e.g., androgen receptor; Shi et al., 2008) and tumor suppressor (e.g., integrin $\alpha 7$ and retinoblastoma; Han et al., 2010; Sterner et al., 1998) signaling pathways, implying that multiple layers of regulation may be involved in MCM7 biology and its oncogenic properties.

Epidermal growth factor receptor (EGFR) initiates a signaling cascade that leads to DNA synthesis and cell proliferation upon activation, and EGFR pathways are frequently deregulated in human cancers (Paez et al., 2004; Yarden, 2001). Previously, our mass spectrum analysis detected members of MCM hexameric ring complex in the EGFR immunoprecipitates from A431 cancer cells (Huo et al., 2010), thereby raising the possibility that EGFR signaling is functionally involved in DNA replication licensing. Since MCM7 is critical in DNA replication and involved in oncogenic signaling pathways, we set out to determine whether MCM7 is a downstream target of EGFR signaling.

RESULTS

MCM7 Is Tyr Phosphorylated by Lyn Kinase

We first validated the interaction between EGFR and MCM proteins by immunoprecipitation (IP)-western analysis and detected MCM5 and MCM7 in the EGFR immunoprecipitates (Figure S1A available online). Interestingly, the amount of MCM7 but not MCM5 in the EGFR immunoprecipitates was increased with EGF stimulation and decreased with the Tyr kinase inhibitor gefitinib treatment (Figure S1B), suggesting that the association between EGFR and MCM7 was dependent on EGFR kinase activity and MCM7 might be a kinase substrate of EGFR or EGFR downstream kinases.

Because Tyr phosphorylation carries significant biological functions and it is unclear whether Tyr phosphorylation is involved in MCM7 function in DNA replication licensing, we investigated whether MCM7 is regulated by this posttransla-

tional modification in proliferating cells. We examined MCM7 Tyr phosphorylation in a panel of cancer cell lines stimulated with EGF using an anti-phosphoTyr antibody (4G10) and found that MCM7 was Tyr phosphorylated to various degrees in all of them except in MDA-MB-231 cells (Figures 1A and S1C). The weaker MCM7 Tyr phosphorylation observed in Du145 compared with H266 cells is likely due to their lower EGFR expression level (Figure S1C). Since MCM7 is functionally involved in DNA synthesis and cell proliferation, the failure to observe EGF-induced MCM7 Tyr phosphorylation in MDA-MB-231 cells is consistent with the literature that MDA-MB-231 cells lack proliferative response to EGF (Price et al., 1999). We then asked whether MCM7's phosphorylation status affects its ability to associate with other MCM proteins. Interestingly, the kinetics between MCM7 Tyr phosphorylation and its association with MCM2 and MCM3 but not MCM4 were positively correlated upon EGF stimulation (Figure 1B). In the absence of EGF, we did not observe MCM7 Tyr phosphorylation or increased MCM2 and MCM3 association (Figure S1D). These data suggest that EGF-mediated Tyr phosphorylation of MCM7 regulates its association with other MCM members.

Although MCM7 was detected in the EGFR immunoprecipitates, MCM7 failed to be Tyr phosphorylated by recombinant EGFR in an in vitro kinase assay (data not shown). To identify the kinase that phosphorylates MCM7, we immunoprecipitated MCM7 and subjected the complex to mass spectrometry analysis. Among 94 MCM7-interacting proteins identified, Lyn was the only Tyr kinase (Table S1). The interaction between Lyn and MCM7 was validated by reciprocal immunoprecipitation, and Lyn was able to Tyr phosphorylate MCM7 when both proteins are ectopically expressed (Figure 1C). EGF stimulation increased the amount of endogenous MCM7 detected in Lyn immunoprecipitates, which could be reduced by the Lyn kinase inhibitor PP2, suggesting that the kinase activity of Lyn enhances its interaction with MCM7 (Figure 1D, top). Furthermore, EGF-stimulated MCM7 Tyr phosphorylation was then abolished by PP2 (Figure 1D, bottom), supporting Lyn as the Tyr kinase for MCM7. Indeed, purified recombinant Lyn kinase phosphorylated glutathione S-transferase (GST)-fused MCM7 in vitro (Figure 1E). To verify whether Lyn phosphorylates MCM7 in vivo, we knocked down Lyn expression using short interfering RNAs (siRNAs) and examined MCM7 Tyr phosphorylation in response to EGF. Upon EGF stimulation, siRNA targeting the 3' UTR of Lyn but not other members of Src family kinases (Src, Yes, and Fyn) diminished MCM7 Tyr phosphorylation, which was rescued by reintroduction of a siRNA-resistant Flag-p56^{Lyn} (Figure 1F). Small hairpin RNA targeting the protein coding region of Lyn also diminished the MCM7 Tyr phosphorylation (Figure S1E), and MCM7 was detected in the Lyn but not Src, Fyn, or Yes immunoprecipitates (Figure S1F). Lyn exists as two isoforms, p53^{Lyn} and p56^{Lyn} (Yamanashi et al., 1991). Although both p56^{Lyn} and p53^{Lyn} interacted with MCM7 (Figure S1G), the kinase activity of p56^{Lyn} but not p53^{Lyn} toward MCM7 was potentiated upon EGF stimulation (Figure S1H), suggesting p56^{Lyn} is the likely physiological Tyr kinase for MCM7 in response to EGF treatment in vivo. Taken together, these results demonstrate that Lyn Tyr phosphorylates MCM7 in vivo and that this event is EGF dependent.

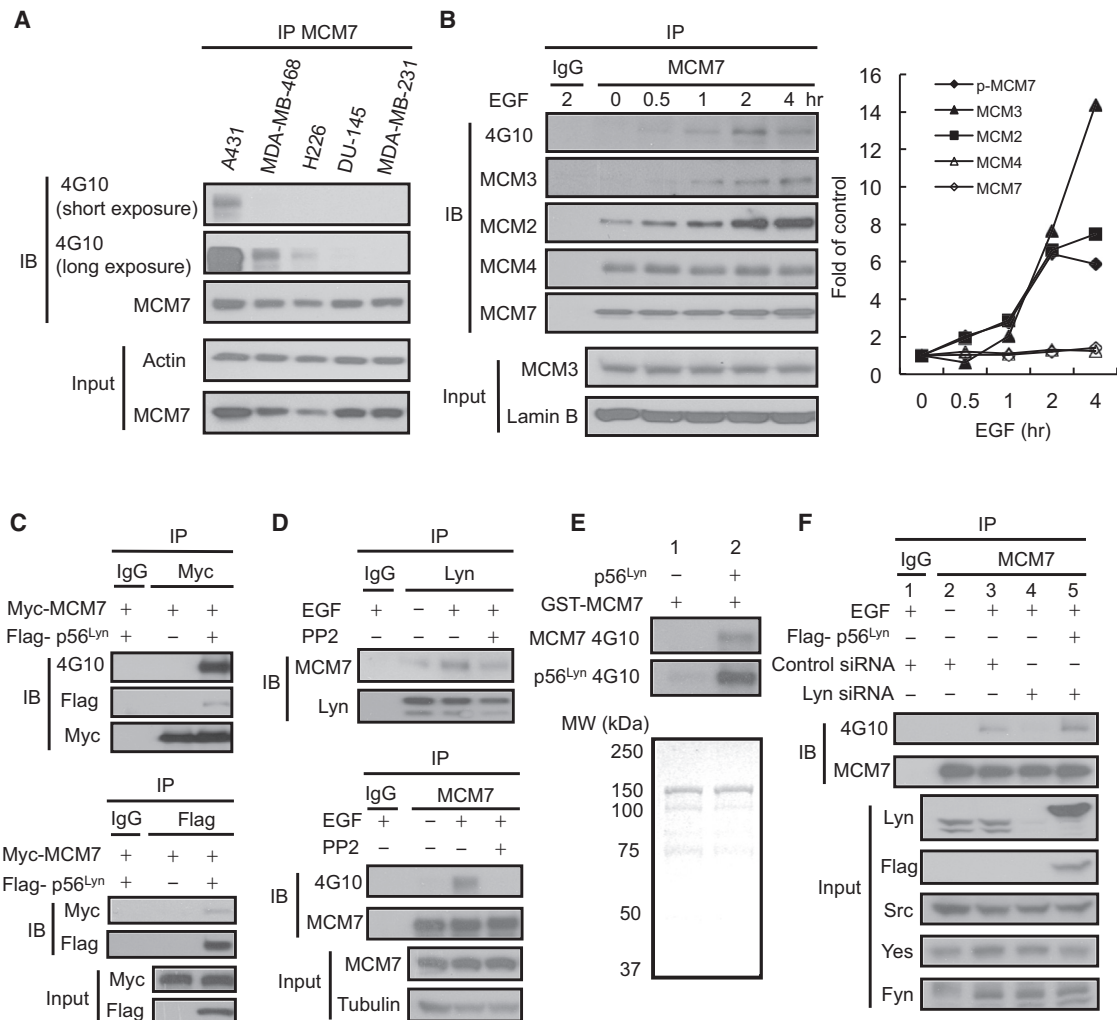


Figure 1. MCM7 Is Tyr phosphorylated by Lyn Kinase

(A) Immunoprecipitates of endogenous MCM7 were analyzed by western blotting using 4G10 antibody for detecting Tyr phosphorylation in various cancer cell lines stimulated with EGF for 1 hr.

(B) Western blot of endogenous MCM2, MCM3, and MCM4 in anti-MCM7 immunoprecipitates from A431 cells stimulated with EGF at various time points. The cell lysate from A431 cells treated with EGF for 2 hr was used for both the anti-MCM7 and control immunoglobulin G (IgG) immunoprecipitation. The right graph shows quantified densities of bands at different time points, and the band's density in control lane (i.e., EGF 0 hr) was set as 1.

(C) Cell lysates from 293T cells expressing exogenous Myc-MCM7 and Flag-p56^{Lyn} were subjected to immunoprecipitation and immunoblotting with indicated antibodies.

(D) A431 cell lysates with different treatments were subjected to immunoprecipitation and immunoblotting with indicated antibodies to detect the association of endogenous MCM7 with Lyn and MCM7 Tyr phosphorylation.

(E) Western blot of Tyr phosphorylation of GST-MCM7 by recombinant p56^{Lyn} (top) and phosphorylation of p56^{Lyn} itself (middle) using 4G10 antibody. Bottom: Coomassie Blue staining of the GST-MCM7 input.

(F) Western blot of endogenous MCM7 Tyr phosphorylation in A431 cells with or without EGF stimulation (lanes 3 and 2). Endogenous Lyn was knocked down by siRNA (targeting 3' UTR; lane 4) and rescued with a siRNA-resistant Flag-Lyn (lane 5).

See also Figure S1 and Table S1.

Lyn Phosphorylates MCM7 at Y600

To further validate the MCM7 Tyr phosphorylation and identify corresponding site(s), we used mass spectrometry to analyze endogenous MCM7 immunopurified from EGF-stimulated A431 cells and identified a peptide containing phosphorylated Y600 of MCM7 (Figure 2A). The MCM7 Y600 sequence matched the consensus sequence phosphorylated by Src family kinases (Olsen et al., 2006), and Lyn was predicted as the putative kinase

that phosphorylates MCM7 at Y600 (NetworkIN). Indeed, an in vivo Tyr phosphorylation assay demonstrated that it was not EGFR but Lyn that enhanced Tyr phosphorylation of MCM7 (Figure 2B, lanes 1–3). In the presence of EGFR, p56^{Lyn}-mediated MCM7 phosphorylation was significantly augmented, suggesting that EGFR signaling potentiates p56^{Lyn} kinase activity for MCM7 phosphorylation. Importantly, a kinase-dead (KD) p56^{Lyn} mutant (Kasahara et al., 2004) was unable to

phosphorylate MCM7 (lane 4 versus lane 6) and p56^{Lyn} did not phosphorylate the MCM7 Y600F mutant (lane 4 versus lane 5). Similarly, purified recombinant p56^{Lyn} kinase phosphorylated GST-MCM7 but not the GST-MCM7 Y600F (Figure 2C), indicating that Lyn phosphorylates MCM7 at Y600.

To facilitate the detection of MCM7 Y600 phosphorylation, we generated a polyclonal antibody that recognized Y600-phosphorylated MCM7. This antibody recognized ectopic MCM7 coexpressed with p56^{Lyn} but not MCM7 alone or MCM7 Y600F coexpressed with p56^{Lyn} in 293T cells (Figure S2A) and was used to verify MCM7 Y600 phosphorylation in vivo. In A431 cells, EGF induced phosphorylation of MCM7 Y600 (Figure 2D, lane 3 versus lane 2). Knockdown of endogenous Lyn protein by siRNA diminished MCM7 Y600 phosphorylation (lane 4), which was rescued by reintroduction of a siRNA-resistant Flag-p56^{Lyn} (lane 5), supporting that Lyn phosphorylates MCM7 at Y600 upon EGF stimulation. We also observed EGF-induced MCM7 Y600 phosphorylation in six other cancer cell lines (Figure S2B).

Because MCM7 is important for licensing DNA replication and Lyn phosphorylates MCM7 upon EGF stimulation, we examined whether Lyn regulated MCM7 function in DNA replication licensing upon EGF stimulation. Indeed, knockdown of the endogenous Lyn protein by two different siRNAs compromised the EGF-induced loading of MCM2, MCM3, and MCM7 onto the chromatin (Figures 2E and S2C) and the replication origins in the *LMNB2* (lamin B2) and *MCM4* locus measured by chromatin IP (ChIP)-quantitative PCR (qPCR) analysis (Figures 2F and S2D). These evidences suggest that Lyn-mediated Y600 phosphorylation may regulate MCM7 function in DNA replication licensing.

MCM7 Y600 Phosphorylation Enhances MCM Complex Assembly and Cancer Cell Proliferation

We then examined if MCM7 Y600 was also involved in cancer cell proliferation and generated MDA-MB-468 breast cancer cells expressing Myc-tagged MCM7 (468-MCM7), MCM7 Y600F (468-Y600F), or control vector (468-vector) for functional studies. MDA-MB-468 cells were chosen because Lyn was required for MCM7 phosphorylation (Figure S1E) and Lyn knockdown significantly compromised their proliferation (Figure S3A). Consistent with a previous study (Ren et al., 2006), ectopic expression of MCM7 enhanced cell proliferation and DNA synthesis rate of MDA-MB-468 cells (Figures 3A and 3B, lane 2 versus lane 1). Compared with 468-MCM7 cells, 468-Y600F cells showed decreased cell proliferation and DNA synthesis rate (Figure 3A and 3B, lane 3 versus lane 2). In addition, cell proliferation (Figure 3A, lane 4 versus lane 2) and DNA synthesis rate (Figure 3B, lane 4 versus lane 2) were decreased in 468-MCM7 cells treated with PP2. Furthermore, in an orthotopic breast cancer mouse model, 468-Y600F mammary tumor grew slower than did 468-MCM7 tumors (Figure 3C). MCM7 also enhanced the proliferation of H226 and A431 cells more significantly than did MCM7 Y600F (Figure S3B). Collectively, these results suggest that Y600 phosphorylation is involved in the MCM7-mediated DNA replication and cancer cell proliferation.

We further examined whether phosphorylation of Y600 enhances MCM7 interaction with other MCM members. Indeed, EGF stimulation enhanced association of Myc-MCM7 with MCM2, MCM3, and MCM5, which was decreased in cells

treated with PP2 (Figures 3D and S3C). In contrast, Myc-MCM7 Y600F exhibited a much weaker interaction with other MCM proteins (Figure 3D). It should be mentioned that, similar to the endogenous MCM7 (Figure 1B), Myc-MCM7 interacted with MCM2 without EGF (Figure S3D). We in addition used a phosphomimetic mutant MCM7 Y600E to determine whether the requirement of Lyn in MCM7 interaction with other MCM members could be bypassed. Indeed, in cells cultured in a low-serum medium to prevent EGFR activation, MCM7 Y600E interacted with other MCM members stronger than did MCM7 and MCM7 Y600F (Figure S3E). Furthermore, ectopic expression of MCM7 Y600E but not MCM7 Y600F rescued the EGF-induced DNA synthesis compromised by Lyn knockdown (Figure S3F). These data suggest that MCM7 Y600 phosphorylation is critical for the MCM complex assembly and DNA synthesis initiated by the EGFR-Lyn signaling axis.

Assembled MCM complex loads onto the replication origins on the chromatin to license DNA replication. Therefore, we examined whether the association of MCM members on the chromatin was enhanced upon EGF stimulation. Indeed, EGF stimulation increased chromatin loading of MCM7 together with MCM2, MCM3, and MCM5; however, EGF-induced chromatin loading of MCM7 Y600F was barely detectable (Figure 3E). We then performed ChIP-qPCR analysis of MCM7 or MCM7 Y600F binding to the DNA replication origins in the *MCM4* and *LMNB2* loci upon EGF stimulation to determine the functional important of MCM7 Y600 in DNA replication licensing. Indeed, Y600 phosphorylation enhanced MCM7-mediated DNA replication licensing, where EGF induced the loading of the Myc-MCM7 but not Myc-MCM7 Y600F onto the DNA replication origins (Figure 3F). Neither MCM7 nor MCM7 Y600F mutant exhibited increased binding to a control locus that did not contain a replication origin (2 kb downstream of *LMNB2* locus) upon EGF stimulation (Figure 3F). Consistently, EGF induced the loading of the endogenous MCM2, MCM3, and MCM7 onto the DNA replication origins much more significantly in cells expressing Myc-MCM7 than those expressing MCM7 Y600F (Figure S3G), suggesting that Y600 phosphorylation aids in complex assembly at the DNA replication origins upon EGF stimulation.

To determine whether Y600 phosphorylation is critical for EGF-induced DNA synthesis, we used a siRNA to knockdown endogenous MCM7 in cells expressing the siRNA-resistant Myc-MCM7 or Myc-MCM7 Y600F and examined their responses to EGF-induced DNA synthesis and cell cycle progression. Consistently, EGF-induced DNA synthesis was higher in cells expressing Myc-MCM7 than in cells expressing Myc-MCM7 Y600F (Figure 3G). Furthermore, 12 hr of EGF treatment allowed 20% (45%–25%) of Myc-MCM7-expressing cells but only 8% (34%–26%) of Myc-MCM7 Y600F-expressing cells to progress through G1 phase (Figure 3H). We also used untagged MCM7 and MCM7 Y600F to perform the DNA synthesis assay in cells with endogenous MCM7 knockdown, and consistently, the EGF-induced DNA synthesis was much more significant in cells expressing MCM7 than cells expressing MCM7 Y600F (Figure S3H). A bromodeoxyuridine (BrdU) pulse-chase approach was also used to evaluate the cell cycle progression of MCM7 and MCM7 Y600F cells. After BrdU labeling in S phase, the number of BrdU⁺ cells in G1 phase for MCM7 cells was increased more significantly than MCM7 Y600F cells at 9 hr and 12 hr chase

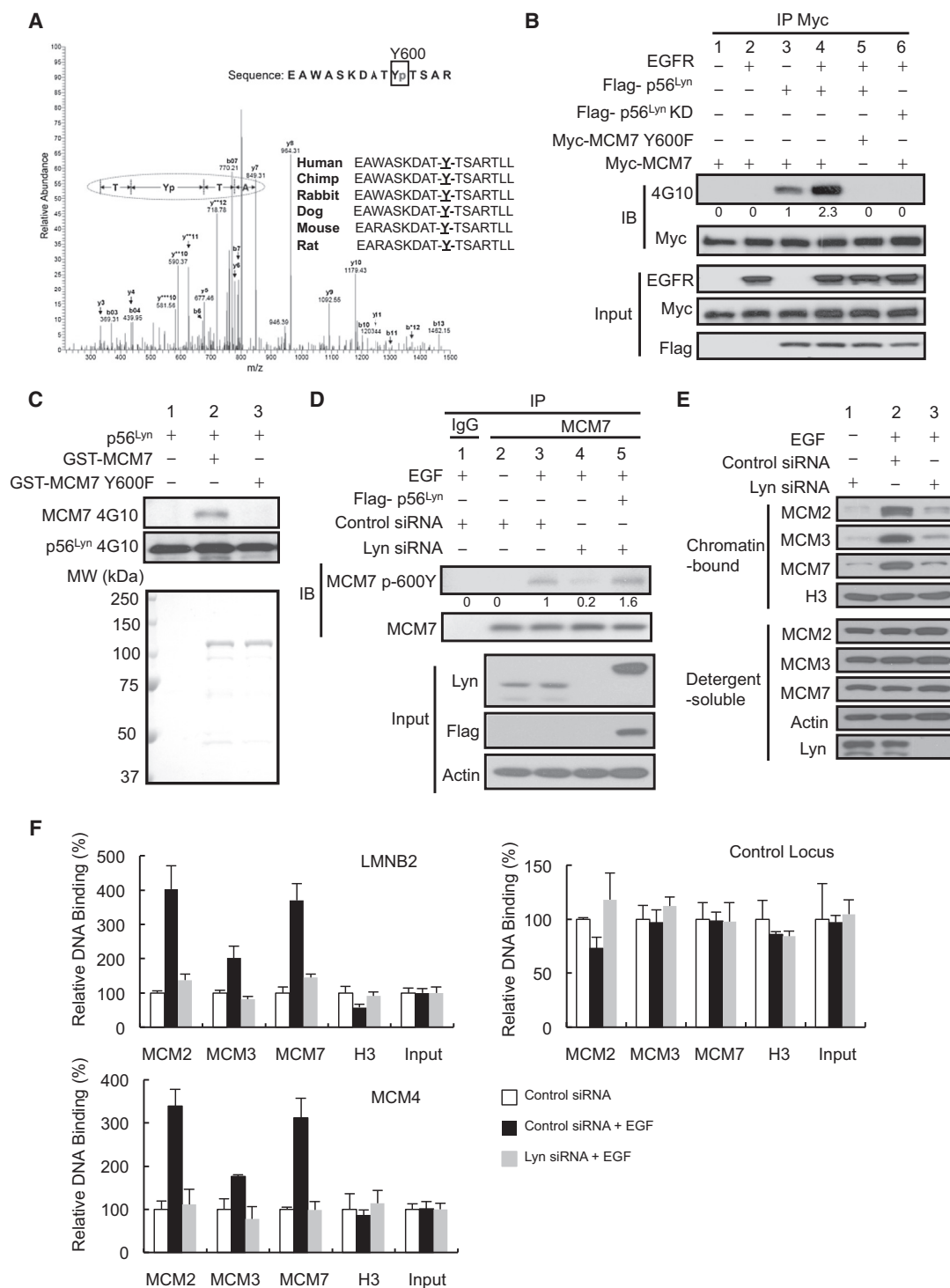


Figure 2. Lyn Phosphorylates MCM7 at Y600

(A) Mass spectrometry analysis of endogenous MCM7 immunopurified from A431 cells.

(B) Western blot of Tyr phosphorylation of MCM7 or MCM7 Y600F from 293T cells transfected with EGFR, Flag-p56^{Lyn}, and Myc-MCM7, as indicated. The number under each band is quantified relative density, with lane 3 being set as 1.

(C) Western blot analysis of Tyr phosphorylation of GST-MCM7 and GST-MCM7 Y600F by recombinant p56^{Lyn} kinase (top) and phosphorylation of p56^{Lyn} using 4G10 antibody (middle). Bottom: Coomassie Blue staining of the GST fusion protein input.

(D) Western blot of phosphorylation of the endogenous MCM7 Y600 in A431 cells with or without EGF stimulation (lanes 3 and 2). Endogenous Lyn was knocked down by siRNA (targeting 3' UTR; lane 4) and rescued with a siRNA-resistant Flag-p56^{Lyn} (lane 5). The number under each band is quantified relative density, with lane 3 being set as 1.

(legend continued on next page)

time points, suggesting that MCM7 cells have a shorter cell cycle time than MCM7 Y600F cells (Figures S3I and S3J). Taken together, these observations suggest a pathway in which phosphorylation of MCM7 Y600 by Lyn kinase enhances MCM complex assembly and DNA replication licensing in proliferating cells.

EGFR Phosphorylates p56^{Lyn} at Y32

To identify potential regulators of Lyn activation after EGF stimulation, endogenous Lyn was immunoprecipitated and the 4G10 antibody was used to detect Tyr-phosphorylated Lyn-associated proteins. A single 175 kDa Lyn-interacting protein, for which the Tyr phosphorylation relied on EGF stimulation, was detected (starred, Figure 4A). Since EGFR itself is 175 kDa, we examined whether EGFR interacts with Lyn in response to EGF stimulation. Indeed, coimmunoprecipitation analyses in A431 cells detected EGFR in the Lyn immunoprecipitates, which increased with EGF and decreased with two different EGFR kinase inhibitors, AG1478 and gefitinib (Figure 4B), suggesting that Lyn interacted with activated EGFR.

To further investigate how EGFR regulates Lyn, EGFR was immunoprecipitated and both p56^{Lyn} and p53^{Lyn} were detected. Moreover, EGF stimulation significantly increased the amount of p56^{Lyn} (Figure 4C). Interestingly, EGFR kinase inhibitors diminished the amount of p56^{Lyn} but not p53^{Lyn} in the EGFR immunoprecipitates (Figure 4C). The interaction between EGFR and p56^{Lyn} but not p53^{Lyn} was dependent on EGFR kinase activity, suggesting that p56^{Lyn} is a kinase substrate for EGFR. Indeed, purified recombinant EGFR phosphorylated a GST fusion of the domain unique to p56^{Lyn} that contained only one Tyr residue, Y32 (Figure 4D, lower left panel), and substitution of Y32 with Phe abolished the EGFR-mediated phosphorylation (Figure 4D, lower right panel). Furthermore, recombinant EGFR phosphorylated kinase-dead GST-p56^{Lyn} but not kinase-dead GST-p56^{Lyn} Y32F (Figure 4E). Since Y32 does not exist in p53^{Lyn} (Figure 4D, upper panel; Yamanashi et al., 1991), this result is consistent with our observation that EGFR kinase inhibitors diminished the association of EGFR with p56^{Lyn} but not p53^{Lyn} (Figure 4C). To facilitate detection of p56^{Lyn} Y32 phosphorylation, we generated a polyclonal antibody that specifically recognizes Y32-phosphorylated p56^{Lyn}. This antibody recognized ectopic p56^{Lyn} coexpressed with EGFR but not p56^{Lyn} alone or p56^{Lyn} Y32F coexpressed with EGFR in 293T cells (Figure S4). Thus, we used this antibody to detect p56^{Lyn} Y32 phosphorylation in vivo. Phosphorylation of p56^{Lyn} Y32 was significantly increased upon EGF stimulation but diminished by EGFR kinase inhibitors (Figure 4F). These results indicate that EGFR phosphorylates p56^{Lyn} at Y32 in response to EGF stimulation.

Phosphorylation of Y32 Enhances p56^{Lyn}-Mediated MCM7 Tyr Phosphorylation and Cell Proliferation

Next, we investigated whether phosphorylation at p56^{Lyn} Y32 is important for DNA synthesis and cancer cell proliferation. MDA-

MB-468 cells stably expressing p56^{Lyn} Y32F (468-Y32F) exhibited decreased cell proliferation (Figure 5A) and DNA synthesis rate (Figure 5B) compared with those expressing p56^{Lyn} (468-Lyn), and these results are similar to MDA-MB-468 cells expressing MCM7 Y600F (Figures 3A and 3B). When treated with gefitinib or AG1478, which abolished the Lyn Y32 phosphorylation (Figure 4F), 468-Lyn cells exhibited compromised cell growth and DNA synthesis similar to 468-Y32F cells (Figures 5A and 5B). In an orthotopic breast cancer mouse model, 468-Y32F-induced mammary tumor grew slower than did 468-Lyn cells (Figure 5C), which is comparable to the 468-MCM7 Y600F cells (Figure 3C). These results collectively suggest that Y32 phosphorylation is critical for the p56^{Lyn} function. In support of this notion, EGF-induced Lyn Y397 phosphorylation, which has been shown to enhance Lyn's kinase activity (Ingle, 2012; Figure 5D, top), and MCM7 Y600 phosphorylation (Figure 5D, middle) were clearly observed after 60 min EGF stimulation in p56^{Lyn} cells, while barely detectable in p56^{Lyn} Y32F mutant cells. Similarly, immunofluorescence analysis using confocal microscopy demonstrated that p56^{Lyn} is associated with more robust Lyn Y397 phosphorylation compared with p56^{Lyn} Y32F mutant (Figure S5A).

To show that Y32 phosphorylation is critical for p56^{Lyn} function in MCM7 phosphorylation, we used a phosphomimetic mutant p56^{Lyn} Y32E to determine whether the requirement of EGFR activation in Lyn-dependent MCM7 phosphorylation could be bypassed. Indeed, in cells cultured with a low-serum medium to prevent EGFR activation (Figure S5B, right), ectopic expression of p56^{Lyn} Y32E but not p56^{Lyn} significantly induced MCM7 Tyr phosphorylation that was associated with increased interaction with other MCM members (Figure S5B, left). Interestingly, p56^{Lyn} Y32E interacted with MCM7 much more significantly than p56^{Lyn} (Figure S5B, left). Collectively, these data suggest a cascade in which EGFR-mediated p56^{Lyn} Y32 phosphorylation regulates the downstream MCM7 Y600 phosphorylation and DNA synthesis.

p56^{Lyn} Y32 and MCM7 Y600 Phosphorylation Correlates with Physiological Proliferation

To investigate the biological importance of the EGFR → p56^{Lyn} → MCM7 → DNA replication licensing cascade in cells with physiological EGFR level, we first examined these events in regenerating liver. Liver regeneration is a well-established physiological model for DNA synthesis and cell proliferation and requires EGFR (Bucher, 1991; Natarajan et al., 2007). After a partial hepatectomy, robust DNA replication indicated by increased proliferating cell nuclear antigen and MCM7 protein expression ensued within 24 hr (Figure 6A, bottom). The increase in the MCM7 level was associated with prominent Y600 Tyr phosphorylation, suggesting that Lyn was activated in regenerating liver. Similarly, phosphorylation of p56^{Lyn} Y32 as well as association of p56^{Lyn} with MCM7 was increased in the regenerating liver

(E) Cell lysates from A431 cells transfected with the indicated siRNA with or without EGF stimulation were subjected to western blot analysis of endogenous MCM2, MCM3, and MCM7 in the soluble fraction or chromatin fraction.

(F) ChIP analysis of endogenous MCM2, MCM3, and MCM7 binding to the DNA replication origins in *LMNB2* (lamin B2), *MCM4*, and control locus (2 kb downstream of *LMNB2* locus) in A431 cells transfected with the indicated siRNA and stimulated with or without EGF for 7 hr. Results are normalized to levels in cells without EGF stimulation (n = 3). Error bars show ±SD.

See also Figure S2.

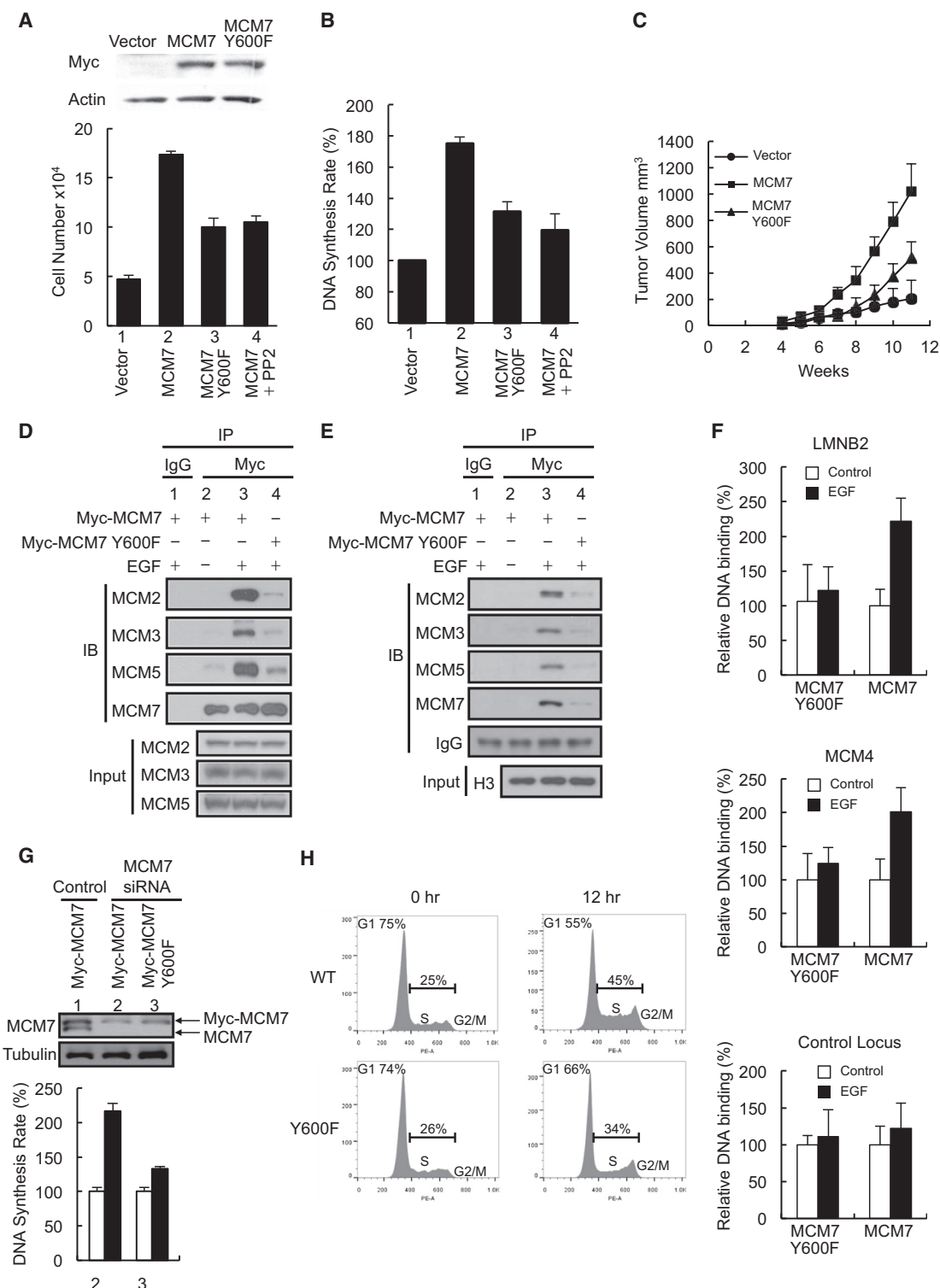


Figure 3. MCM7 Y600 Phosphorylation Enhances MCM Complex Assembly and Cancer Cell Proliferation

(A) MDA-MB-468 (1×10^4) cells carrying the indicated constructs were seeded in the presence or absence of $1 \mu\text{M}$ PP2, and cell number was determined at day 7 ($n = 3$).

(B) MDA-MB-468 cells were treated as (A), and DNA synthesis rate was assayed at day 5 by detection of BrdU incorporation ($n = 3$).

(C) In vivo tumor growth of orthotopically transplanted MDA-MB-468 cells ($n = 5$).

(D) Western blot of endogenous MCM2, MCM3, and MCM5 in the anti-Myc-MCM7 immunoprecipitates from the soluble fraction of A431 cells with or without EGF stimulation.

(legend continued on next page)

(Figure 6A, top). We in addition examined whether this cascade is associated with proliferation of normal mammary epithelial cells expressing physiological level of EGF, using MCF-10A cells as a model. It is well established that the survival and proliferation of MCF-10A cells relies on EGF and that EGF induces cell cycle progression of MCF-10A cells synchronized at G0 phase (LeVeau et al., 2004; Figure S6A). Upon EGF stimulation, phosphorylation of EGFR Y1173, p56^{Lyn} Y32, and MCM7 Y600 were simultaneously induced and the level of p56^{Lyn} Y32 and MCM7 Y600 phosphorylation persisted from 8 to 24 hr (Figure 6B). Since MCM7 Y600 phosphorylation is involved in its association with other MCM members, these results are consistent with the current model that MCM complex assembly begins during the G1 phase (Lei and Tye, 2001). As expected, we found that Lyn and MCM7 associate upon EGF stimulation (Figure 6C) and EGFR or Lyn kinase activity is required for the EGF-induced MCF-10A cell proliferation (Figure 6D). EGF also induced proliferation of human cancer cell line NCI-H226 and triggered p56^{Lyn} Y32 and MCM7 Y600 phosphorylation (Figure 6E). It has been shown that, when A431 cells are seeded at low density, lower concentrations (3–100 pM) rather than higher concentrations of EGF induce their proliferation (Kawamoto et al., 1983). Consistently, we found 100 pM EGF enhanced A431 cell proliferation and triggered Lyn Y32 and MCM7 Y600 phosphorylation (Figure S6B). Taken together, our findings demonstrate a biological importance for phosphorylation of p56^{Lyn} Y32 and MCM7 Y600 in cell proliferation.

p56^{Lyn} Y32 and MCM7 Y600 Phosphorylation Correlate with EGFR Status in Human Tumor Samples and Poor Survival of Breast Cancer Patients

To determine the pathological relevance of this signal pathway in human cancers, we analyzed the relationship between EGFR, phosphorylation of p56^{Lyn} Y32, and MCM7 Y600 in human breast tumor samples using immunohistochemistry (IHC) staining. Specificity of the antiphosphorylation antibodies for IHC staining was verified by demonstrating that the anti-phospho p56^{Lyn} Y32 or anti-phospho MCM7 Y600 staining can be neutralized with the corresponding tyrosine-phosphorylated peptide but not with the nonphosphorylated peptide (Figure S7A). Significantly, EGFR expression level was associated with Tyr phosphorylation level of p56^{Lyn} Y32 and MCM7 Y600 (Figures 7A and 7B). Additionally, Tyr phosphorylation level of MCM7 Y600 was correlated with the level of proliferation marker Ki-67. In the tumors with low (–/+) p-MCM7 level, only 44% (35/79) of them were identified as having the highest Ki-67 level (+++). In the tumors with higher p-MCM7 level (++ and +++), the samples identified as the highest Ki-67 level (+++) were significantly increased to 71% (10/14) and 75% (6/8), respectively (Figures

7C and 7D). These data suggested that MCM7 Y600 phosphorylation was pathologically associated with cancer cell proliferation. We also observed that Lyn and MCM7 protein levels were correlated with Ki-67 expression, suggesting their potential contributions to cell proliferation in breast tumors (Figure S7B).

To determine the pathological relevance of p56^{Lyn} activation and MCM7 Y600 phosphorylation, we analyzed the relationship between phosphorylation of p56^{Lyn} Y32 and MCM7 Y600 in human breast tumor samples and lung cancer tissue arrays using IHC staining. Significantly, phosphorylation of p56^{Lyn} Y32 was correlated with phosphorylation of MCM7 Y600 in human breast ($p < 0.02$) (Table S2) and lung cancers ($p = 0.003$) (Table S3). To verify Lyn is the Tyr kinase that phosphorylates MCM7 at Y600 in human tumor samples, we performed IHC staining in tissue microarrays of human lung and breast cancers. Expression of Lyn but not other Src family kinases (Src, Yes, Fyn, and Lck) was significantly correlated with the phosphorylation level of MCM7 Y600 in both human lung tumor tissues ($p < 0.001$) (Table S4; Figure S7C) and breast tumor tissues ($p = 0.002$) (Table S5).

We next sought to determine whether the levels of phospho-Lyn Y32 and phospho-MCM7 Y600 expression correlated with survival of breast cancer patients. We found that the overall survival of breast cancer patients whose cancers had high level of phospho-Lyn Y32 was worse than patients whose cancers had low level of phospho-Lyn Y32 ($p = 0.037$; Figure 7E). Similarly, overall survival of breast cancer patients whose cancers had high level of phospho-MCM7 Y600 was worse than patients whose cancers had low level of phospho-MCM7 Y600 ($p = 0.035$; Figure 7F). Multivariate survival analysis using Cox's regression model suggested that both phospho-Lyn Y32 and phospho-MCM7 Y600 were independently correlated with overall survival in the breast cancer patients (Figure S7D). Additionally, overall survival of the breast cancer patients whose cancers had high levels of both phospho-Lyn Y32 and phospho-MCM7 Y600 was much worse than patients in all other categories ($p = 0.003$; Figure S7E). Taken together, these findings provide a significant pathological relevance for phosphorylation of p56^{Lyn} Y32 and MCM7 Y600 in human cancers.

DISCUSSION

Deregulated MCM7 expression can increase cancer cell proliferation and contribute to tumorigenesis; however, how specific oncogenic pathways regulate MCM7 functions is not well understood. Here, we show that Lyn-mediated MCM7 Y600 phosphorylation increases MCM7's association with other MCM members, consequently enhancing DNA synthesis and cell

(E) Same as (D), except binding of MCM7 with other MCM members in chromatin fraction was assessed.

(F) ChIP analysis of Myc-MCM7 or Myc-MCM7 Y600F binding to the DNA replication origins in *LMNB2* (lamin B2), *MCM4*, and control locus (2 kb downstream of *LMNB2* locus) in A431 cells stimulated with EGF for 7 hr. Results are normalized to levels in cells without EGF stimulation ($n = 5$).

(G) Top: HeLa cells expressing siRNA-resistant Myc-MCM7 or Myc-MCM7 Y600F were transfected with a control siRNA or a siRNA targeting 3' UTR of MCM7, as indicated. After 3 days, cells were lysed and subjected to western blot analysis using the indicated antibodies. Bottom: after siRNA transfection, 1×10^4 cells were seeded in the presence or absence of 10 ng/ml EGF, and DNA synthesis rate was assayed at day 3 by detection of BrdU incorporation ($n = 3$).

(H) HeLa cells expressing siRNA-resistant Myc-MCM7 or Myc-MCM7 Y600F were transfected with siRNA targeting MCM7 3' UTR. Cells were synchronized by 48 hr of serum starvation and then stimulated with EGF for 12 hr. Cell cycle progression was analyzed by PI staining using fluorescence-activated cell sorting. Error bars show \pm SD.

See also Figure S3.

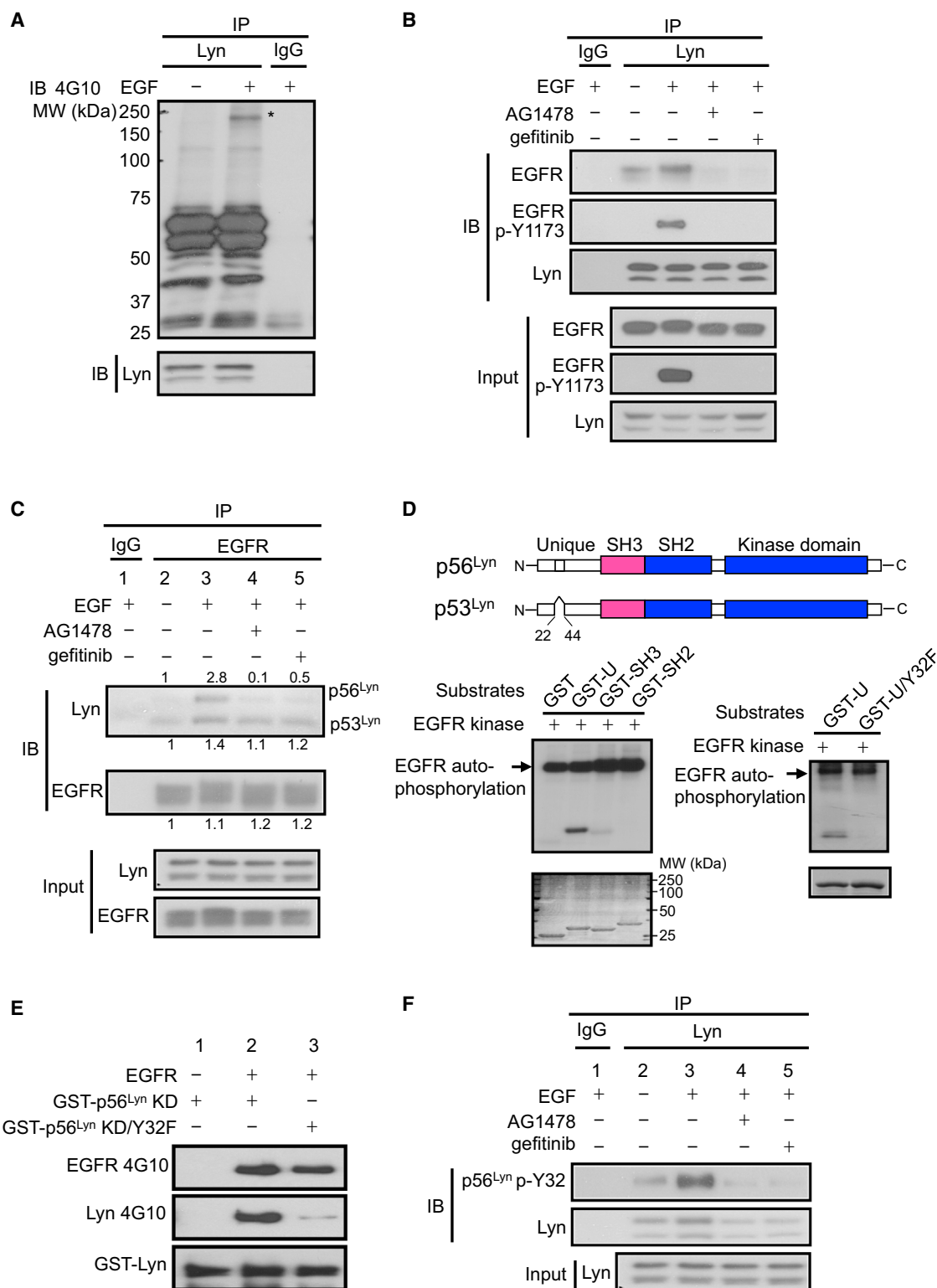


Figure 4. EGFR Phosphorylates p56^{Lyn} Y32

(A) Anti-Lyn immunoprecipitates from A431 cells with or without EGF stimulation were analyzed by western blotting using 4G10 antibody. The asterisk indicates the protein phosphorylated by EGF stimulation in the anti-Lyn immunoprecipitates.

(B) Western blot of endogenous EGFR and phospho-EGFR Y1173 (EGFR p-Y1173) in the anti-Lyn immunoprecipitates from A431 cells with indicated treatments.

(C) Western blot of endogenous Lyn in the anti-EGFR immunoprecipitates from A431 cells with different treatments. The number above (for p56^{Lyn}) or under (for p53^{Lyn} and EGFR) each band is quantified relative density, with lane 2 being set as 1.

(legend continued on next page)

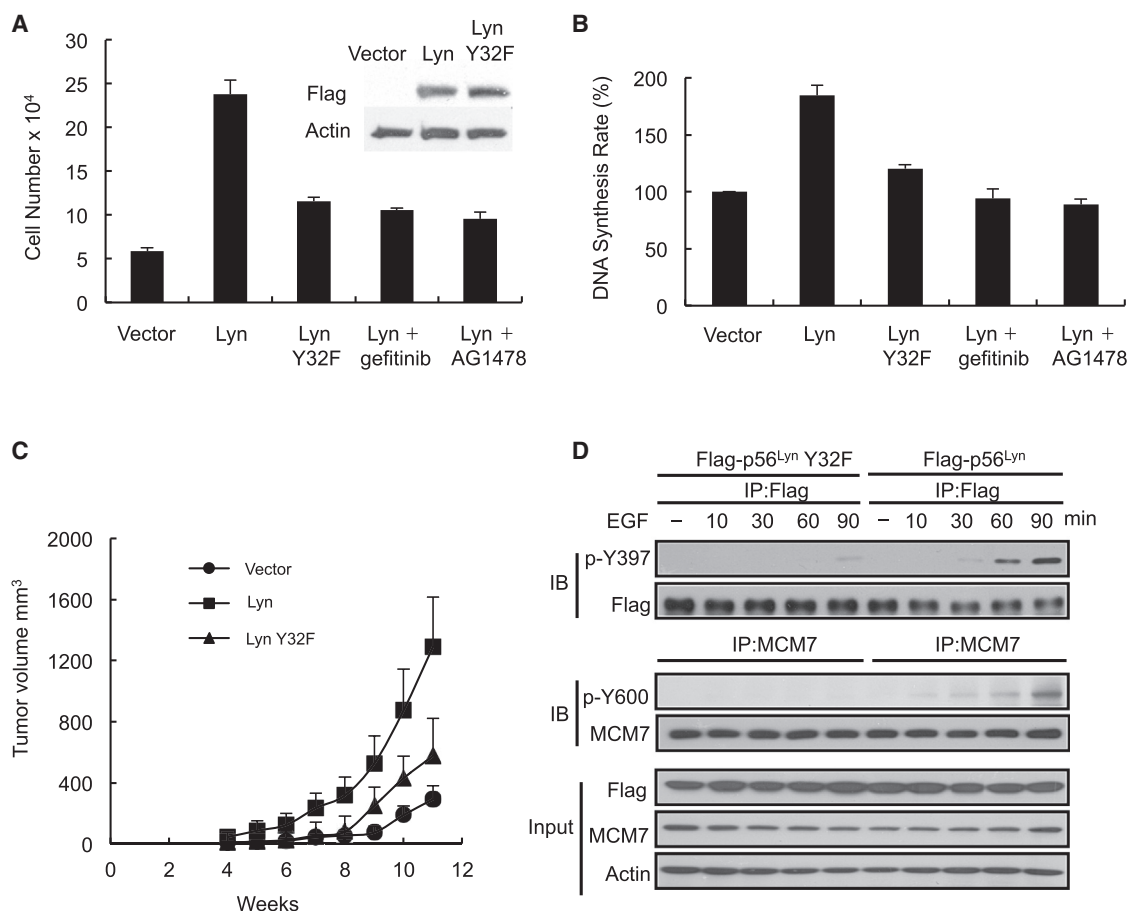


Figure 5. Phosphorylation of Y32 Enhances p56^{Lyn}-Mediated MCM7 Tyr Phosphorylation and Cancer Cell Proliferation

(A) MDA-MB-468 cells (1×10^4) carrying indicated constructs were seeded in the presence or absence of 500 nM inhibitors. Cell number was determined at day 7 ($n = 3$).

(B) DNA synthesis rate of MDA-MB-468 cells treated as (A) was assayed at day 5 by detection of BrdU incorporation ($n = 3$).

(C) In vivo tumor growth of orthotopically transplanted MDA-MB-468 cells ($n = 5$).

(D) Western blot of p56^{Lyn} Y397 and MCM7 Y600 phosphorylation in Lyn knockdown A431 cells expressing Flag-p56^{Lyn} Y32F or Flag-p56^{Lyn} stimulated with EGF at indicated time point. Error bars show \pm SD.

See also Figure S5.

proliferation. Furthermore, the activity of p56^{Lyn} is upregulated via Y32 phosphorylation by EGFR, resulting in potentiation of MCM7 Y600 phosphorylation. In human breast cancer, phosphorylation of both p56^{Lyn} Y32 and MCM7 Y600 correlate with EGFR expression level in tumor samples and with poor survival of patients. Thus, we propose a Tyr phosphorylation cascade triggered by EGFR for licensing DNA replication in proliferating cells, which is augmented in cancer cells with deregulated EGFR activity. These findings suggest that Lyn may be a critical EGFR downstream mediator in licensing DNA replication and

therefore may be a promising therapeutic target in treating EGFR-activated cancers.

Although the therapeutic efficacy of pan-Src family kinase inhibitors is currently being evaluated in the clinic, the Lyn-specific inhibitor is not yet available for treatment of human cancers. Together with the previous reports in prostate cancer (Goldberg-Furmanov et al., 2004; Park et al., 2008), this study further identifies Lyn as a therapeutic target in breast and lung cancers. It is worthwhile to mention that EGFR Tyr kinase inhibitors (TKIs), such as erlotinib and gefitinib, are well-established therapeutics

(D) Western blot detection of Tyr phosphorylation of GST fused various domains of p56^{Lyn} by recombinant EGFR in vitro. Coomassie blue staining is shown below each blot. A schematic representation of Lyn isoforms with the 21-amino acid presented in p56^{Lyn} but not in p53^{Lyn} indicated is shown at the top. U, the unique domain; U/Y32F, the U domain with Y32F mutation.

(E) Western blot of Tyr phosphorylation of GST-p56^{Lyn} KD and GST-p56^{Lyn} KD/Y32F by recombinant EGFR (middle) and phosphorylation of EGFR itself (top) using 4G10 antibody. Bottom: GST-p56^{Lyn} KD and GST-p56^{Lyn} KD/Y32F detected by western blot using an anti-GST antibody.

(F) Cell lysates of A431 cells with different treatments were subjected to anti-Lyn immunoprecipitation and then immunoblotted with the phospho-p56^{Lyn} Y32 (p56^{Lyn} p-Y32) antibody.

See also Figure S4.

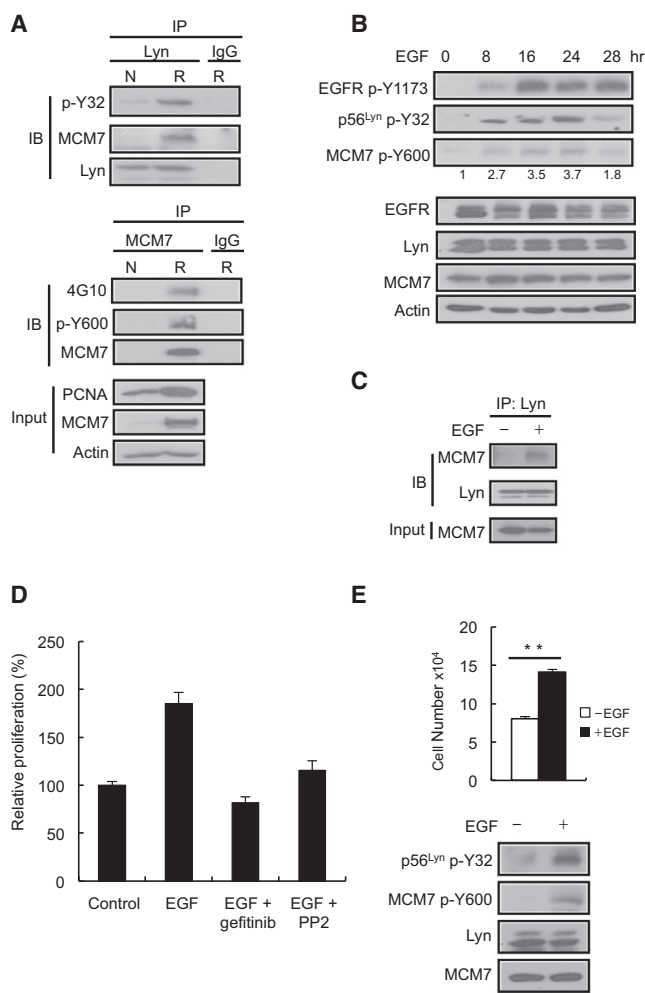


Figure 6. Phosphorylation of p56^{Lyn} Y32 and MCM7 Y600 Correlate Physiological Proliferation

(A) Tyr phosphorylation of p56^{Lyn} Y32 and MCM7 Y600 in regenerating liver. N, normal liver; R, regenerating liver 24 hr after partial hepatectomy.

(B) MCF-10A cells were serum starved for 48 hr and then stimulated with EGF at the indicated time points. Lysates were immunoblotted with indicated antibodies. The number under each band of anti-phospho MCM7 Y600 (MCM7 p-Y600) blot is quantified relative density, with the lane 1 (0 hr) being set as 1.

(C) Lysates of MCF-10A cell treated with EGF for 8 hr were subjected to Lyn immunoprecipitation and immunoblotting with indicated antibodies.

(D) MCF-10A cells were serum starving for 48 hr and then stimulated with EGF in the presence of indicated inhibitors. Cell number was determined 48 hr after EGF stimulation (n = 3).

(E) In the top panel, 1×10^4 NCI-H226 cells were seeded in the presence or absence of 50 ng/ml EGF in medium with 0.5% calf serum, and cell number was determined at day 5 (n = 3). In the bottom panel, NCI-H226 cells were untreated or treated with 50 ng/ml EGF for 4 hr, and the lysates were immunoblotted with the indicated antibodies. Error bars show \pm SD; **, p < 0.01.

See also Figure S6.

for treating human cancers with deregulated EGFR, yet patients frequently develop resistance (Balak et al., 2006). Several oncogenic pathways have been shown to be involved in TKI resistance, but the detailed mechanisms are not yet completed. The current study also raises an interesting possibility that the

identified Lyn \rightarrow MCM7 \rightarrow DNA replication licensing pathway is one of the underlying mechanisms contributing to the TKIs resistance, and therefore, the Lyn-specific inhibitor may be effective against the EGFR activating human cancers that have developed TKI resistance and is worthy of further development.

Several posttranslational modifications have been identified in other MCM family members and shown to be functionally important in initiating DNA replication. Specifically, phosphorylation of MCM2 at Ser27, Ser41, and Ser139 by CDC7/DBF4 kinase during G1/S phase enhances the ATPase activity of MCM complex and is essential for initiating DNA replication (Tsuji et al., 2006), whereas phosphorylation of MCM2 at Ser5 by CDC7/DBF4 kinase promotes chromatin loading of MCM2 and MCM complex assembly (Chuang et al., 2009). Additionally, cyclin-dependent kinase 1 (CDK1)-dependent MCM3 phosphorylation at Ser112 regulates its incorporation into the MCM2-MCM7 complex (Lin et al., 2008) and CDK2-dependent MCM3 phosphorylation at Thr722 regulates its loading onto chromatin in mammalian cells (Li et al., 2011). While Y600 phosphorylation that enhances MCM7 interaction with other MCM members contributes to the cancer cell proliferation triggered by the EGFR-Lyn signaling axis, the nonphosphorylatable mutant MCM7 Y600F still maintains its basal interaction with other MCM members, suggesting that MCM7 Y600F is a mutant insensitive to EGF stimulation rather than a dominant negative mutant. Thus, the EGFR/Lyn-mediated-MCM7 Y600 phosphorylation plays a positive regulatory role but not an indispensable role in the MCM7 functions. Besides, MCM7 regulates other biological processes independent of its DNA replication licensing function (Hubbi et al., 2011) and other posttranslational modifications of MCM7 could also regulate MCM7 functions in response to different mitogenic stimuli. Further investigation would be necessary to elucidate their biological functions.

Lyn is overexpressed in prostate cancer cells, and inhibition of Lyn expression suppresses prostate cancer cell proliferation (Goldenberg-Furmanov et al., 2004; Park et al., 2008). Intriguingly, while siRNA-mediated inhibition of Lyn suppresses cellular proliferation, siRNA inhibition of Src suppresses primarily cell migration in prostate cancer cells (Park et al., 2008). These observations indicate that Lyn and Src may not be functionally redundant and may regulate a different subset of substrates in cancer cells. In the present study, we found that Lyn is necessary for the MCM7 Y600 phosphorylation, and the expression of Lyn but not other Src family kinases correlated significantly with the phosphorylation level of MCM7 Y600 in both human lung tumor tissues and breast tumor tissues, suggesting that Lyn is the predominant Src family kinase to phosphorylate MCM7 Y600. The identification of Lyn-specific substrate, MCM7, provides rationale for the Lyn-associated cell proliferation and implies the existence of other Lyn kinase substrates involved in cancer cell proliferation. We predict that further elucidation of the Lyn kinase substrates and their Tyr phosphorylation status would help us to understand the oncogenic functions of Lyn.

An important observation in our current study is that the activity of Lyn in MCM7 phosphorylation and cancer cell proliferation is directly regulated by EGFR-mediated Tyr phosphorylation, which suggests that Lyn may be indispensable for the cancer cells that rely on EGFR signaling to proliferate. In support of this notion, we and others have shown that Lyn

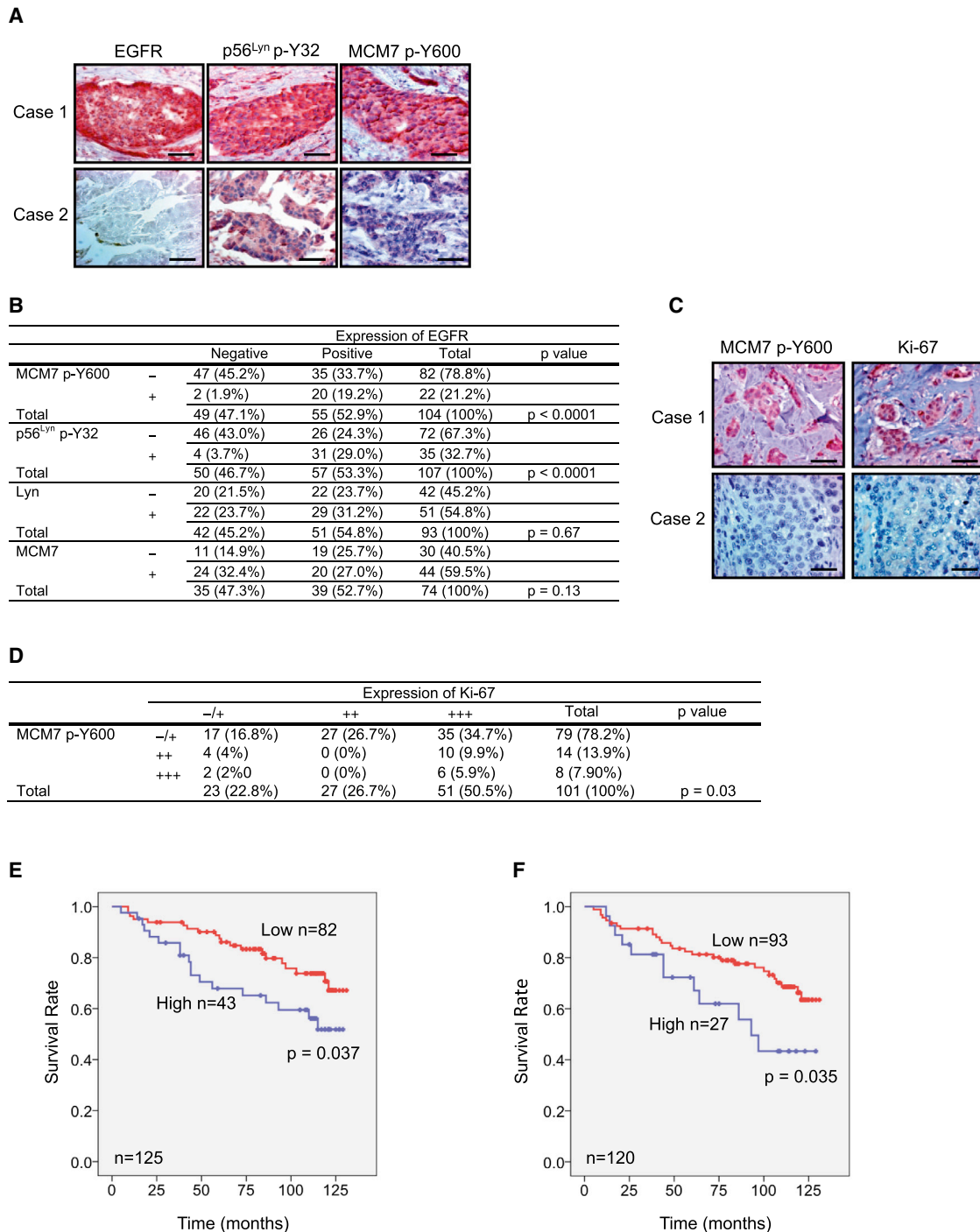


Figure 7. Phosphorylation of p56^{Lyn} Y32 and MCM7 Y600 Correlate with the EGFR Protein Level of Human Tumor Samples and Poor Survival of Breast Cancer Patients

(A) IHC staining of EGFR level and Tyr phosphorylation of p56^{Lyn} Y32 and MCM7 Y600 of representative human breast tumor samples with high and low EGFR. Scale bar, 25 μ m.

(B) Relationship between expression of EGFR, phospho-p56^{Lyn} Y32 (p56^{Lyn} p-Y32), phospho-MCM7 Y600 (MCM7 p-Y600), Lyn, and MCM7 in human breast cancer tissues.

(C) IHC staining of phospho-MCM7 Y600 and Ki-67 of representative human breast tumor samples. Scale bar, 25 μ m.

(D) Relationship between expression of phospho-MCM7 Y600 and Ki-67 in human breast cancer samples.

(E) The Kaplan-Meier analysis of overall survival of breast cancer patients according to the phospho-Lyn Y32 level in their breast cancer.

(F) The Kaplan-Meier analysis of overall survival of breast cancer patients according to the phospho-MCM7 Y600 level in their breast cancer.

See also Figure S7 and Tables S2–S5.

knockdown significantly compromised the proliferation of Du145 and MDA-MB-468 cells (Goldenberg-Furmanov et al., 2004), both of which rely on EGFR signaling to proliferate (Matar et al., 2004). In contrast, Lyn knockdown had no growth inhibitory effect on certain cancer cell lines, including HCC1954, BT-549, and MDA-MB-231 (Hochgräfe et al., 2010), that are less dependent on EGFR signaling for their proliferation (Hochgräfe et al., 2010; Krol et al., 2007; Sahin et al., 2009). Taken together, the oncogenic activity of Lyn in DNA synthesis and cell proliferation is potentiated in cancer cells that depend on EGFR signaling for their survival and targeting Lyn may demonstrate synergistic efficacy with EGFR TKIs for treatment of this subset of cancer cells. Given that MCM7 deregulation is frequently associated with human cancers and tumorigenesis, these observations also provide clinical implications for the treatment of human cancers with deregulated MCM7 status using EGFR and Lyn kinase inhibitors.

EXPERIMENTAL PROCEDURES

Cell Lysates and Immunoprecipitation

Cells were collected at the indicated time, washed with ice-cold PBS, and solubilized in lysis buffer containing 1% NP-40, 25 mM NaF, 2 mM Na₃VO₄, 5 mM phenylmethylsulfonyl fluoride, and 0.15 U/ml aprotinin followed by sonication. Cell lysates were clarified by centrifugation at 16,000 × *g* for 20 min at 4°C, and total protein concentration was determined by Bio-Rad protein assay kit using BSA as a standard. The chromatin fraction of cell lysates was isolated following a protocol described previously (Méndez and Stillman, 2000). For each immunoprecipitation assay, 2 mg cell lysates were used and 2 μg antibody was added for each reaction. The reaction was rotating at 4°C overnight followed by addition of 50 μl of 50% protein A or G sepharose slurry and rotating for 4 hr. Beads were collected and washed with PBS buffer containing 1% NP-40 three times. Immunoprecipitates were resolved by SDS-PAGE and analyzed by immunoblotting. Free software ImageJ was used for quantification analysis of the band density of target proteins in western blot assays.

DNA Synthesis Assay

The DNA synthesis rate was measured using the BrdU (colorimetric) ELISA kit obtained from Roche following the manufacturer's instructions.

Mouse Model for Tumorigenesis

In vivo cell growth was analyzed using an orthotopic breast cancer mouse model that has been described previously (Chang et al., 1997). Briefly, 2 × 10⁶ MDA-MB-468 cells infected with lentivirus carrying the wild-type or mutant constructs were mixed with the Matrigel (BD Biosciences) and PBS and injected into the mammary fat pads of female nude mice. The length (L) and width (W) of each tumor mass were measured by calipers once a week. Tumor volume (TV) was calculated by the formula (TV = 0.5 × L × W²) (Yaguchi et al., 2006). All animal procedures were conducted under regulations of Division of Laboratory Animal Medicine at The University of Texas MD Anderson Cancer Center. Animal protocols (number 06-87-06139) were reviewed and approved by the Institutional Animal Care and Use Committee at The University of Texas MD Anderson Cancer Center.

Human Tissues

The 150 cases of surgically resected human breast cancer specimens for immunohistochemistry and survival analysis were obtained retrospectively from patients undergoing surgical resection of breast cancer as primary treatment at The University of Texas MD Anderson Cancer Center (MDACC) between 2000 and 2006. The specimen collection and use of human tissue samples were conducted in accordance with the protocols approved by the Institutional Review Board at MDACC. Written informed consent was obtained from patients in all cases at time of enrollment. Tissue microarrays of 228 cases of breast cancer (BRC2281) and tissue microarrays of 228 cases of lung cancer

(LUC2281) were obtained from Pantomics. Tissue microarrays of 98 cases of lung cancer (TMA IMH-305 and IMH-358) were obtained from Imgenex.

Liver Regeneration Assay

The experiment was performed using male Fisher 344 rats according to the procedure described previously (Marti and Hug, 1995). In brief, 2/3 of rats' livers were removed by hepatectomy under anesthesia and were sacrificed 24 hr after the operation. Both regenerated and normal liver tissues were washed with PBS, and tissues were homogenized. The homogenized tissue was then lysed with radioimmunoprecipitation assay buffer, and the protein was extracted by centrifuge and used for western blot assay.

Statistical Analyses

Data were analyzed by the Student's *t* test, Pearson chi-square analysis, and Cox's regression analysis, except Kaplan-Meier analyses on survival rates. A *p* value <0.05 was considered statistically significant.

The remaining experimental procedures can be found in [Supplemental Information](#).

SUPPLEMENTAL INFORMATION

Supplemental Information includes Supplemental Experimental Procedures, seven figures, and five tables and can be found with this article online at <http://dx.doi.org/10.1016/j.ccr.2013.04.027>.

ACKNOWLEDGMENTS

We thank Dr. Yekaterina Khotskaya, Dr. Jennifer L. Hsu, and Dr. Stephanie A. Miller for editing this manuscript and the Center for Biological Pathways at MD Anderson Cancer Center for support. This study was funded in part by National Institutes of Health (CA109311, CA099031, and CCSG CA16672); Susan G. Komen Foundation (SAC100016); National Breast Cancer Foundation, Patel Memorial Breast Cancer Research Fund; The University of Texas MD Anderson-China Medical University and Hospital Sister Institution Fund (to M.-C.H.); Cancer Research Center of Excellence (DOH102-TD-C-111-005, Taiwan); Private University grant (NSC99-2632-B-039-001-MY3, Taiwan); Program for Stem Cell and Regenerative Medicine Frontier Research (NSC101-2321-B-039-001, Taiwan); International Research-Intensive Centers of Excellence in Taiwan (NSC102-2911-I-002-303, Taiwan); and National Science Council Taiwan Merit Postdoctoral Scholarship (TMS-94-2B-001 to Y.-N.W.).

Received: March 27, 2012

Revised: November 17, 2012

Accepted: April 26, 2013

Published: June 10, 2013

REFERENCES

- Balak, M.N., Gong, Y., Riely, G.J., Somwar, R., Li, A.R., Zakowski, M.F., Chiang, A., Yang, G., Ouerfelli, O., Kris, M.G., et al. (2006). Novel D761Y and common secondary T790M mutations in epidermal growth factor receptor-mutant lung adenocarcinomas with acquired resistance to kinase inhibitors. *Clin. Cancer Res.* 12, 6494–6501.
- Bergoglio, V., Pillaire, M.J., Lacroix-Triki, M., Raynaud-Messina, B., Canitrot, Y., Bieth, A., Garès, M., Wright, M., Delsol, G., Loeb, L.A., et al. (2002). Deregulated DNA polymerase beta induces chromosome instability and tumorigenesis. *Cancer Res.* 62, 3511–3514.
- Bucher, N.L. (1991). Liver regeneration: an overview. *J. Gastroenterol. Hepatol.* 6, 615–624.
- Chang, J.Y., Xia, W., Shao, R., Sorgi, F., Hortobagyi, G.N., Huang, L., and Hung, M.C. (1997). The tumor suppression activity of E1A in HER-2/neu-over-expressing breast cancer. *Oncogene* 14, 561–568.
- Chuang, L.C., Teixeira, L.K., Wohlschlegel, J.A., Henze, M., Yates, J.R., Méndez, J., and Reed, S.I. (2009). Phosphorylation of Mcm2 by Cdc7 promotes pre-replication complex assembly during cell-cycle re-entry. *Mol. Cell* 35, 206–216.

- Dang, H.Q., and Li, Z. (2011). The Cdc45-Mcm2-7-GINS protein complex in trypanosomes regulates DNA replication and interacts with two Orc1-like proteins in the origin recognition complex. *J. Biol. Chem.* 286, 32424–32435.
- Evrin, C., Clarke, P., Zech, J., Lurz, R., Sun, J., Uhle, S., Li, H., Stillman, B., and Speck, C. (2009). A double-hexameric MCM2-7 complex is loaded onto origin DNA during licensing of eukaryotic DNA replication. *Proc. Natl. Acad. Sci. USA* 106, 20240–20245.
- Facoetti, A., Ranza, E., Benericetti, E., Ceroni, M., Tedeschi, F., and Nano, R. (2006). Minichromosome maintenance protein 7: a reliable tool for glioblastoma proliferation index. *Anticancer Res.* 26(2A), 1071–1075.
- Feng, C.J., Li, H.J., Li, J.N., Lu, Y.J., and Liao, G.Q. (2008). Expression of Mcm7 and Cdc6 in oral squamous cell carcinoma and precancerous lesions. *Anticancer Res.* 28(6A), 3763–3769.
- Gambus, A., Khoudoli, G.A., Jones, R.C., and Blow, J.J. (2011). MCM2-7 form double hexamers at licensed origins in *Xenopus* egg extract. *J. Biol. Chem.* 286, 11855–11864.
- Goldenberg-Furmanov, M., Stein, I., Pikarsky, E., Rubin, H., Kasem, S., Wygoda, M., Weinstein, I., Reuveni, H., and Ben-Sasson, S.A. (2004). Lyn is a target gene for prostate cancer: sequence-based inhibition induces regression of human tumor xenografts. *Cancer Res.* 64, 1058–1066.
- Han, Y.C., Yu, Y.P., Nelson, J., Wu, C., Wang, H., Michalopoulos, G.K., and Luo, J.H. (2010). Interaction of integrin-linked kinase and miniature chromosome maintenance 7-mediating integrin $\alpha 7$ induced cell growth suppression. *Cancer Res.* 70, 4375–4384.
- Hochgräfe, F., Zhang, L., O'Toole, S.A., Browne, B.C., Pinese, M., Porta Cubas, A., Lehrbach, G.M., Croucher, D.R., Rickwood, D., Boulghourjian, A., et al. (2010). Tyrosine phosphorylation profiling reveals the signaling network characteristics of Basal breast cancer cells. *Cancer Res.* 70, 9391–9401.
- Honeycutt, K.A., Chen, Z., Koster, M.I., Miers, M., Nuchtern, J., Hicks, J., Roop, D.R., and Shohet, J.M. (2006). Deregulated minichromosomal maintenance protein MCM7 contributes to oncogene driven tumorigenesis. *Oncogene* 25, 4027–4032.
- Hubbi, M.E., Luo, W., Baek, J.H., and Semenza, G.L. (2011). MCM proteins are negative regulators of hypoxia-inducible factor 1. *Mol. Cell* 42, 700–712.
- Huo, L., Wang, Y.N., Xia, W., Hsu, S.C., Lai, C.C., Li, L.Y., Chang, W.C., Wang, Y., Hsu, M.C., Yu, Y.L., et al. (2010). RNA helicase A is a DNA-binding partner for EGFR-mediated transcriptional activation in the nucleus. *Proc. Natl. Acad. Sci. USA* 107, 16125–16130.
- Ingle, E. (2012). Functions of the Lyn tyrosine kinase in health and disease. *Cell Commun. Signal.* 10, 21.
- Ishimi, Y. (1997). A DNA helicase activity is associated with an MCM4, -6, and -7 protein complex. *J. Biol. Chem.* 272, 24508–24513.
- Kan, T., Sato, F., Ito, T., Matsumura, N., David, S., Cheng, Y., Agarwal, R., Paun, B.C., Jin, Z., Olaru, A.V., et al. (2009). The miR-106b-25 polycistron, activated by genomic amplification, functions as an oncogene by suppressing p21 and Bim. *Gastroenterology* 136, 1689–1700.
- Kang, Y.H., Galal, W.C., Farina, A., Tappin, I., and Hurwitz, J. (2012). Properties of the human Cdc45/Mcm2-7/GINS helicase complex and its action with DNA polymerase epsilon in rolling circle DNA synthesis. *Proc. Natl. Acad. Sci. USA* 109, 6042–6047.
- Kasahara, K., Nakayama, Y., Ikeda, K., Fukushima, Y., Matsuda, D., Horimoto, S., and Yamaguchi, N. (2004). Trafficking of Lyn through the Golgi caveolin involves the charged residues on α E and α F helices in the kinase domain. *J. Cell Biol.* 165, 641–652.
- Kawamoto, T., Sato, J.D., Le, A., Polikoff, J., Sato, G.H., and Mendelsohn, J. (1983). Growth stimulation of A431 cells by epidermal growth factor: identification of high-affinity receptors for epidermal growth factor by an anti-receptor monoclonal antibody. *Proc. Natl. Acad. Sci. USA* 80, 1337–1341.
- Krol, J., Francis, R.E., Albergaria, A., Sunter, A., Polychronis, A., Coombes, R.C., and Lam, E.W. (2007). The transcription factor FOXO3a is a crucial cellular target of gefitinib (Iressa) in breast cancer cells. *Mol. Cancer Ther.* 6, 3169–3179.
- Labib, K., Tercero, J.A., and Diffley, J.F. (2000). Uninterrupted MCM2-7 function required for DNA replication fork progression. *Science* 288, 1643–1647.
- Lee, J.K., and Hurwitz, J. (2001). Processive DNA helicase activity of the minichromosome maintenance proteins 4, 6, and 7 complex requires forked DNA structures. *Proc. Natl. Acad. Sci. USA* 98, 54–59.
- Lei, M., and Tye, B.K. (2001). Initiating DNA synthesis: from recruiting to activating the MCM complex. *J. Cell Sci.* 114, 1447–1454.
- LeVe, C.M., Reeder, J.E., and Mooney, R.A. (2004). EGF-dependent cell cycle progression is controlled by density-dependent regulation of Akt activation. *Exp. Cell Res.* 297, 272–284.
- Li, J., Deng, M., Wei, Q., Liu, T., Tong, X., and Ye, X. (2011). Phosphorylation of MCM3 protein by cyclin E/cyclin-dependent kinase 2 (Cdk2) regulates its function in cell cycle. *J. Biol. Chem.* 286, 39776–39785.
- Lin, D.I., Aggarwal, P., and Diehl, J.A. (2008). Phosphorylation of MCM3 on Ser-112 regulates its incorporation into the MCM2-7 complex. *Proc. Natl. Acad. Sci. USA* 105, 8079–8084.
- Luo, J.H. (2011). Oncogenic activity of MCM7 transforming cluster. *World J. Clin. Oncol.* 2, 120–124.
- Maine, G.T., Sinha, P., and Tye, B.K. (1984). Mutants of *S. cerevisiae* defective in the maintenance of minichromosomes. *Genetics* 106, 365–385.
- Marti, U., and Hug, M. (1995). Acinar and cellular distribution and mRNA expression of the epidermal growth factor receptor are changed during liver regeneration. *J. Hepatol.* 23, 318–327.
- Matar, P., Rojo, F., Cassia, R., Moreno-Bueno, G., Di Cosimo, S., Tabernero, J., Guzmán, M., Rodríguez, S., Arribas, J., Palacios, J., and Baselga, J. (2004). Combined epidermal growth factor receptor targeting with the tyrosine kinase inhibitor gefitinib (ZD1839) and the monoclonal antibody cetuximab (IMC-C225): superiority over single-agent receptor targeting. *Clin. Cancer Res.* 10, 6487–6501.
- Méndez, J., and Stillman, B. (2000). Chromatin association of human origin recognition complex, cdc6, and minichromosome maintenance proteins during the cell cycle: assembly of prereplication complexes in late mitosis. *Mol. Cell Biol.* 20, 8602–8612.
- Moyer, S.E., Lewis, P.W., and Botchan, M.R. (2006). Isolation of the Cdc45/Mcm2-7/GINS (CMG) complex, a candidate for the eukaryotic DNA replication fork helicase. *Proc. Natl. Acad. Sci. USA* 103, 10236–10241.
- Natarajan, A., Wagner, B., and Sibilia, M. (2007). The EGF receptor is required for efficient liver regeneration. *Proc. Natl. Acad. Sci. USA* 104, 17081–17086.
- Nishihara, K., Shomori, K., Fujioka, S., Tokuyasu, N., Inaba, A., Osaki, M., Ogawa, T., and Ito, H. (2008). Minichromosome maintenance protein 7 in colorectal cancer: implication of prognostic significance. *Int. J. Oncol.* 33, 245–251.
- Olsen, J.V., Blagoev, B., Gnäd, F., Macek, B., Kumar, C., Mortensen, P., and Mann, M. (2006). Global, in vivo, and site-specific phosphorylation dynamics in signaling networks. *Cell* 127, 635–648.
- Ota, T., Clayton, A.C., Minot, D.M., Shridhar, V., Hartmann, L.C., Gilks, C.B., and Chien, J.R. (2011). Minichromosome maintenance protein 7 as a potential prognostic factor for progression-free survival in high-grade serous carcinomas of the ovary. *Mod. Pathol.* 24, 277–287.
- Paez, J.G., Jänne, P.A., Lee, J.C., Tracy, S., Greulich, H., Gabriel, S., Herman, P., Kaye, F.J., Lindeman, N., Boggon, T.J., et al. (2004). EGFR mutations in lung cancer: correlation with clinical response to gefitinib therapy. *Science* 304, 1497–1500.
- Park, S.I., Zhang, J., Phillips, K.A., Araujo, J.C., Najjar, A.M., Volgin, A.Y., Gelovani, J.G., Kim, S.J., Wang, Z., and Gallick, G.E. (2008). Targeting SRC family kinases inhibits growth and lymph node metastases of prostate cancer in an orthotopic nude mouse model. *Cancer Res.* 68, 3323–3333.
- Price, J.T., Tiganis, T., Agarwal, A., Djakiew, D., and Thompson, E.W. (1999). Epidermal growth factor promotes MDA-MB-231 breast cancer cell migration through a phosphatidylinositol 3'-kinase and phospholipase C-dependent mechanism. *Cancer Res.* 59, 5475–5478.
- Rajagopalan, H., Jallepalli, P.V., Rago, C., Velculescu, V.E., Kinzler, K.W., Vogelstein, B., and Lengauer, C. (2004). Inactivation of hCDC4 can cause chromosomal instability. *Nature* 428, 77–81.

- Ren, B., Yu, G., Tseng, G.C., Cieply, K., Gavel, T., Nelson, J., Michalopoulos, G., Yu, Y.P., and Luo, J.H. (2006). MCM7 amplification and overexpression are associated with prostate cancer progression. *Oncogene* 25, 1090–1098.
- Sahin, O., Fröhlich, H., Löbke, C., Korf, U., Burmester, S., Majety, M., Mattern, J., Schupp, I., Chaouiya, C., Thieffry, D., et al. (2009). Modeling ERBB receptor-regulated G1/S transition to find novel targets for de novo trastuzumab resistance. *BMC Syst. Biol.* 3, 1.
- Shi, Y.K., Yu, Y.P., Zhu, Z.H., Han, Y.C., Ren, B., Nelson, J.B., and Luo, J.H. (2008). MCM7 interacts with androgen receptor. *Am. J. Pathol.* 173, 1758–1767.
- Shi, Y.K., Yu, Y.P., Tseng, G.C., and Luo, J.H. (2010). Inhibition of prostate cancer growth and metastasis using small interference RNA specific for minichromosome complex maintenance component 7. *Cancer Gene Ther.* 17, 694–699.
- Stern, J.M., Dew-Knight, S., Musahl, C., Kornbluth, S., and Horowitz, J.M. (1998). Negative regulation of DNA replication by the retinoblastoma protein is mediated by its association with MCM7. *Mol. Cell. Biol.* 18, 2748–2757.
- Toyokawa, G., Masuda, K., Daigo, Y., Cho, H.S., Yoshimatsu, M., Takawa, M., Hayami, S., Maejima, K., Chino, M., Field, H.I., et al. (2011). Minichromosome Maintenance Protein 7 is a potential therapeutic target in human cancer and a novel prognostic marker of non-small cell lung cancer. *Mol. Cancer* 10, 65.
- Tsuji, T., Ficarro, S.B., and Jiang, W. (2006). Essential role of phosphorylation of MCM2 by Cdc7/Dbp4 in the initiation of DNA replication in mammalian cells. *Mol. Biol. Cell* 17, 4459–4472.
- Tye, B.K. (1999). MCM proteins in DNA replication. *Annu. Rev. Biochem.* 68, 649–686.
- Yaguchi, S., Fukui, Y., Koshimizu, I., Yoshimi, H., Matsuno, T., Gouda, H., Hirano, S., Yamazaki, K., and Yamori, T. (2006). Antitumor activity of ZSTK474, a new phosphatidylinositol 3-kinase inhibitor. *J. Natl. Cancer Inst.* 98, 545–556.
- Yamanashi, Y., Miyasaka, M., Takeuchi, M., Ilic, D., Mizuguchi, J., and Yamamoto, T. (1991). Differential responses of p56lyn and p53lyn, products of alternatively spliced lyn mRNA, on stimulation of B-cell antigen receptor. *Cell Regul.* 2, 979–987.
- Yan, H., Merchant, A.M., and Tye, B.K. (1993). Cell cycle-regulated nuclear localization of MCM2 and MCM3, which are required for the initiation of DNA synthesis at chromosomal replication origins in yeast. *Genes Dev.* 7, 2149–2160.
- Yarden, Y. (2001). The EGFR family and its ligands in human cancer: signalling mechanisms and therapeutic opportunities. *Eur. J. Cancer* 37(Suppl 4), S3–S8.

Overcoming Intrinsic Multidrug Resistance in Melanoma by Blocking the Mitochondrial Respiratory Chain of Slow-Cycling JARID1B^{high} Cells

Alexander Roesch,^{1,2,*} Adina Vultur,² Ivan Bogeski,³ Huan Wang,² Katharina M. Zimmermann,^{1,3} David Speicher,² Christina Körbel,⁴ Matthias W. Laschke,⁴ Phyllis A. Gimotty,⁷ Stephan E. Philipp,⁵ Elmar Krause,⁶ Sylvie Pätzold,⁸ Jessie Villanueva,² Clemens Krepler,² Mizuho Fukunaga-Kalabis,² Markus Hoth,³ Boris C. Bastian,⁹ Thomas Vogt,¹ and Meenhard Herlyn^{2,*}

¹Department of Dermatology, The Saarland University Hospital, D-66421 Homburg/Saar, Germany

²The Wistar Institute, 3601 Spruce Street, Philadelphia, PA 19104, USA

³Department of Biophysics

⁴Institute for Clinical and Experimental Surgery

⁵Department of Experimental and Clinical Pharmacology and Toxicology

⁶Department of Physiology

The Saarland University, D-66421 Homburg/Saar, Germany

⁷Department of Biostatistics and Epidemiology, University of Pennsylvania School of Medicine, 631 Blockley Hall, 423 Guardian Drive, Philadelphia, PA 19104, USA

⁸Department of Dermatology, Venereology, and Allergology, The University of Frankfurt, D-60590 Frankfurt, Germany

⁹Cardiovascular Research Institute, The University of California, San Francisco, 555 Mission Bay, Boulevard South, San Francisco, CA 94159, USA

*Correspondence: alexander.roesch@uks.eu (A.R.), herlynm@wistar.org (M.H.)

<http://dx.doi.org/10.1016/j.ccr.2013.05.003>

SUMMARY

Despite success with BRAFV600E inhibitors, therapeutic responses in patients with metastatic melanoma are short-lived because of the acquisition of drug resistance. We identified a mechanism of intrinsic multidrug resistance based on the survival of a tumor cell subpopulation. Treatment with various drugs, including cisplatin and vemurafenib, uniformly leads to enrichment of slow-cycling, long-term tumor-maintaining melanoma cells expressing the H3K4-demethylase JARID1B/KDM5B/PLU-1. Proteome-profiling revealed an upregulation in enzymes of mitochondrial oxidative-ATP-synthesis (oxidative phosphorylation) in this subpopulation. Inhibition of mitochondrial respiration blocked the emergence of the JARID1B^{high} subpopulation and sensitized melanoma cells to therapy, independent of their genotype. Our findings support a two-tiered approach combining anticancer agents that eliminate rapidly proliferating melanoma cells with inhibitors of the drug-resistant slow-cycling subpopulation.

INTRODUCTION

Malignant melanoma is a heterogeneous tumor of neuroectodermal origin that can be cured if excised at an early stage; however, once disseminated to distant organs, the median survival of patients drops below 9 months. All major cancer therapies

have failed to persistently increase melanoma patients' survival rates. This failure is attributed to different resistance mechanisms, including increased DNA repair and overexpression of antiapoptotic proteins, such as BCL-2, and drug efflux pumps, such as ABCB5 (Chen et al., 2009). Despite encouraging response rates seen with the BRAF inhibitor vemurafenib in

Significance

Metastatic melanoma is a heterogeneous tumor of neuroectodermal origin with a median survival less than 9 months. All chemotherapies, immunotherapies, and radiotherapies have failed to persistently increase survival. Despite the encouraging response rates following BRAFV600E targeting, relapses occur after a median duration of ~5 months, because melanoma cells acquire multiple resistance mechanisms. However, even among functionally and genetically heterogeneous tumors, common and intrinsic mechanisms exist that support the immediate survival of certain cells against the attack of cytotoxic agents. We have identified a subpopulation of slow-cycling, tumor-maintaining melanoma cells with intrinsic phenotypic resistance to various therapies, irrespective of their mode of action. Targeting the slow-cycling subpopulation could increase the efficacy of current treatment regimens and reduce relapses.

BRAFV600E-positive individuals, relapses occur after a median duration of ~5 months following initial tumor shrinkage (Sosman et al., 2012). Several groups have identified various mechanisms of acquired therapy resistance in BRAF-targeted melanomas. Surviving melanomas reactivate pivotal networks, such as the mitogen-activated protein kinase (MAPK) and phosphoinositide 3-kinase (PI3K) pathways (e.g., through activation of platelet-derived growth factor receptor β , CRAF-1 kinase, and insulin growth factor receptor 1 [Nazarian et al., 2010; Villanueva et al., 2010], dimerization of aberrantly spliced BRAF isoforms [Poulidakos et al., 2011], or by secondary genetic events, such as genomic amplification of *COT*, *NRAS* mutations, or the *MEK1C121S* mutation [Johannessen et al., 2010; Wagle et al., 2011]). However, even among functionally and genetically heterogeneous tumors, common and intrinsic survival mechanisms exist. Cytotoxic agents, including conventional chemotherapy, targeted therapy, or radiation, most effectively eliminate rapidly dividing cells (Blagosklonny, 2005). This concept is gaining prominence in the field of cancer research, with several studies reporting the enrichment of quiescent cancer stem cells after chemotherapy. For example, slow-cycling glioblastoma cells survive temozolomide treatment (Chen et al., 2012). Accordingly, if cell subpopulations can act as major drivers for tumor maintenance and mediate universal therapeutic resistance, approaches that target this phenotype could increase the efficacy of treatment regimens and reduce the risk of melanoma relapses.

We have recently demonstrated that, even within highly proliferative melanomas, there is a slow-cycling cell subpopulation that is identifiable by the expression of the histone 3 K4 demethylase JARID1B (Roesch et al., 2005, 2010). JARID1B (KDM5B/PLU-1/RBP2-H1) is a member of the highly conserved family of jumoni/ARID1 H3K4 demethylases, which are involved in tissue development, cancer, and stem cell biology (Christensen et al., 2007; Dey et al., 2008; Yamane et al., 2007). The JARID1B^{high} slow-cycling subpopulation is required for the continuous tumor growth of melanoma; however, it does not follow a unidirectional cancer stem cell hierarchy. The JARID1B^{high} phenotype is temporarily distinct, dynamic, and can be acquired depending on the microenvironmental context (Roesch et al., 2010). In this respect, another study indicates that other types of cancers, such as breast or lung cancer, also harbor populations of quiescent cells that are drug resistant and whose phenotypes can switch dynamically (Sharma et al., 2010). Interestingly, in the latter study, slow-cycling cells were characterized by the expression of the chromatin-remodeling factor JARID1A, a homolog of JARID1B.

Considering JARID1B's role in continuous tumor maintenance (Roesch et al., 2010), we asked (1) whether the subpopulation of JARID1B^{high} slow-cycling melanoma cells displays lower drug susceptibility compared to the bulk of tumor cells and (2) whether this resistant phenotype can be pharmacologically eradicated.

RESULTS

Cytotoxic Treatment of Melanoma Cells Results in the Enrichment of a Surviving JARID1B^{high} Slow-Cycling Subpopulation

To assess whether slow-cycling melanoma cells show differences in the therapeutic response compared to the rapidly proliferating bulk, we treated melanoma cultures with various anticancer drugs. To discriminate between slowly and rapidly cycling subpopulations, we used a JARID1B-promoter-EGFP-reporter construct, as previously described (Roesch et al., 2010). This fluorescence-based model allows both the detection of slow-cycling melanoma cells based on their expression of JARID1B and monitoring of the dynamic nature of the JARID1B phenotype while cells are alive and interacting with their microenvironment. Prior in vitro and in vivo expression studies confirmed the correlation between the endogenous expression of JARID1B and the JARID1B promoter-induced expression of EGFP (J/EGFP) using an analytical threshold set to the maximum 5% of the fluorescence signal (Figure S1A available online; Roesch et al., 2010). Cells with an EGFP signal above this threshold show the highest endogenous JARID1B levels and, thus, can be reliably selected and analyzed. Two genetically different melanoma cell lines, WM3734 and 1205Lu, were stably transduced with this reporter construct and named WM3734^{JARID1Bprom-EGFP} and 1205Lu^{JARID1Bprom-EGFP}.

When the cell lines were treated with cisplatin at a highly toxic concentration (20 μ M) for 24, 48, and 72 hr, a gradual separation of the total population emerged into live, 7-aminoactinomycin (7AAD)⁻ and dead, 7AAD⁺ subpopulations (Figure 1A). With increasing incubation time, 7AAD⁻ cells were incrementally enriched for J/EGFP^{high} cells, whereas 7AAD⁺ cells were relatively J/EGFP^{low}. Control cells stably expressing a cytomegalovirus (CMV)-promoter-EGFP-reporter construct failed to show such a separation/enrichment pattern. While the total number of cells was constantly decreasing with rising cisplatin doses, the relative number of J/EGFP^{high} cells was significantly increasing in the drug-resistant population (Figures 1B and S1B). For example, up to 30.2% J/EGFP^{high} cells were seen following 20 μ M of cisplatin addition, compared to the 5% seen in vehicle controls. Immunoblotting confirmed an ~3-fold enrichment for endogenous JARID1B protein after densitometric normalization to glyceraldehyde 3-phosphate dehydrogenase (GAPDH) (Figure 1C). Vemurafenib also failed to eradicate all melanoma cells and enriched for J/EGFP^{high} cells, however, to a lesser extent than seen for cisplatin (Figure 1D). Interestingly, even when high concentrations of vemurafenib were applied, a distinct subpopulation of cells remained alive (7AAD⁻) and displayed an ~3-fold higher fluorescence intensity for J/EGFP (GMean = 25.55) than the population of vemurafenib-sensitive (7AAD⁺) cells (GMean = 8.54; Figure 1D). The surviving melanoma cells did not change in their mutational status of BRAF, as confirmed by DNA sequencing before and after treatment (data not shown). In a previous publication, we excluded the acquisition of secondary mutations for a large panel of diverse melanoma cell lines rendered resistant to BRAF inhibitors. We have tested 451Lu, Mel1617, WM983B, WM902B, and SKMel28 (parental and resistant pairs; several passages) for mutations in *BRAF*, *NRAS*, *TP53*, *PTEN*, *KIT*, *MEK1*, *MEK2*, *AKT1*, *CDKN2A*, and *CDK4* (Villanueva et al., 2010).

Interestingly, similar results were observed for other anticancer drugs, such as bortezomib and temozolomide (Figure 2A). We also note that a number of cells with relatively low J/EGFP expression can survive various drug treatments, indicating other potential operating mechanisms of phenotypic resistance. In contrast to its proposed effect on cancer stem

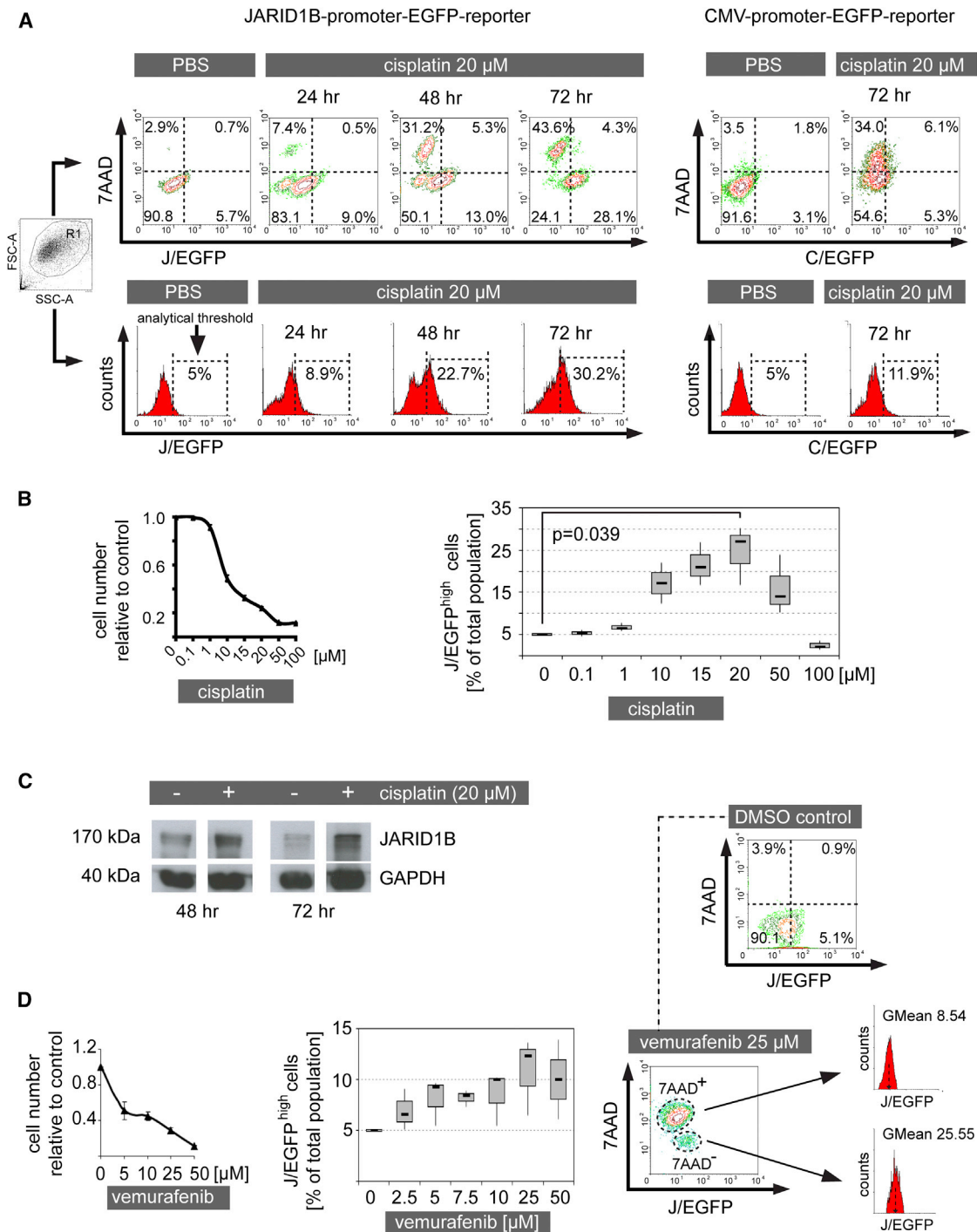


Figure 1. Cytotoxic Treatment Results in the Relative Enrichment of Therapy-Resistant JARID1B^{high} Melanoma Cells

(A) WM3734 melanoma cells were persistently treated with cisplatin and analyzed for J/EGFP expression by flow cytometry at the indicated time points (left). Dead cells were detected by 7AAD staining. Control cells were analyzed for C/EGFP expression (right). Depicted is one representative of at least three independently performed experiments.

(B) MTT cytotoxicity assay of WM3734 cells treated with increasing concentrations of cisplatin (left). Relative percentage of the J/EGFP^{high} subpopulation under escalating cisplatin treatment (right). Both panels show results from 72 hr of treatment.

(C) Immunoblot of JARID1B protein expression in pre- and postcisplatin-treated WM3734 cells at the indicated time points.

(D) Cytotoxicity assay and quantitation of the J/EGFP^{high} subpopulation after treatment of WM3734 cells for 72 hr with escalating vemurafenib concentrations (left and middle). Comparison of the J/EGFP expression levels of 7AAD⁺ and 7AAD⁻ cells (right). Error bars in the cytotoxicity assays represent SD. See also Figure S1.

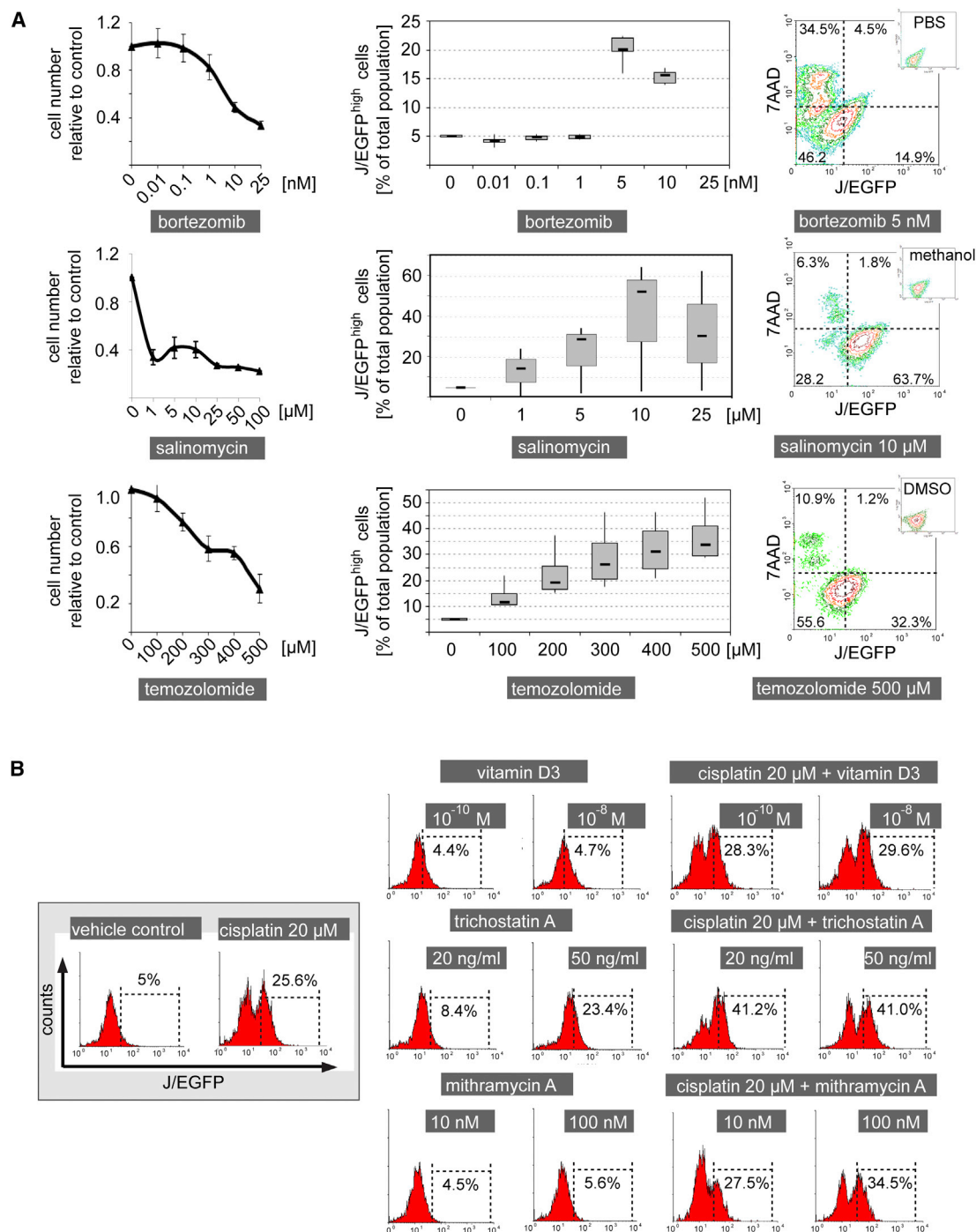


Figure 2. The JARID1B^{high} Subpopulation of Melanoma Cells Is Resistant to a Broad Panel of Anticancer Drugs

(A) Cytotoxicity assays of WM3734 cells after 72 hr of treatment with the indicated anticancer drugs (left). Flow cytometric determination of the relative percentage of the J/EGFP^{high} subpopulation under these treatments (middle). Typical examples for the corresponding drug-associated distribution of 7AAD and J/EGFP signals (right).

(B) Frequency of J/EGFP^{high} WM3734 cells as measured by flow cytometry after incubation with the indicated compounds over 72 hr. Error bars represent SD. See also Figure S2.

cells (Gupta et al., 2009), the potassium ionophore salinomycin also showed a strong enrichment of J/EGFP^{high} cells. To rule out an unspecific bias in our model, we tested vitamin D3 as

a compound with a different anticancer mechanism (prodifferentiation; Figure 2B). Here, no significant change in J/EGFP^{high} cells was seen. Next, we tested compounds that are expected

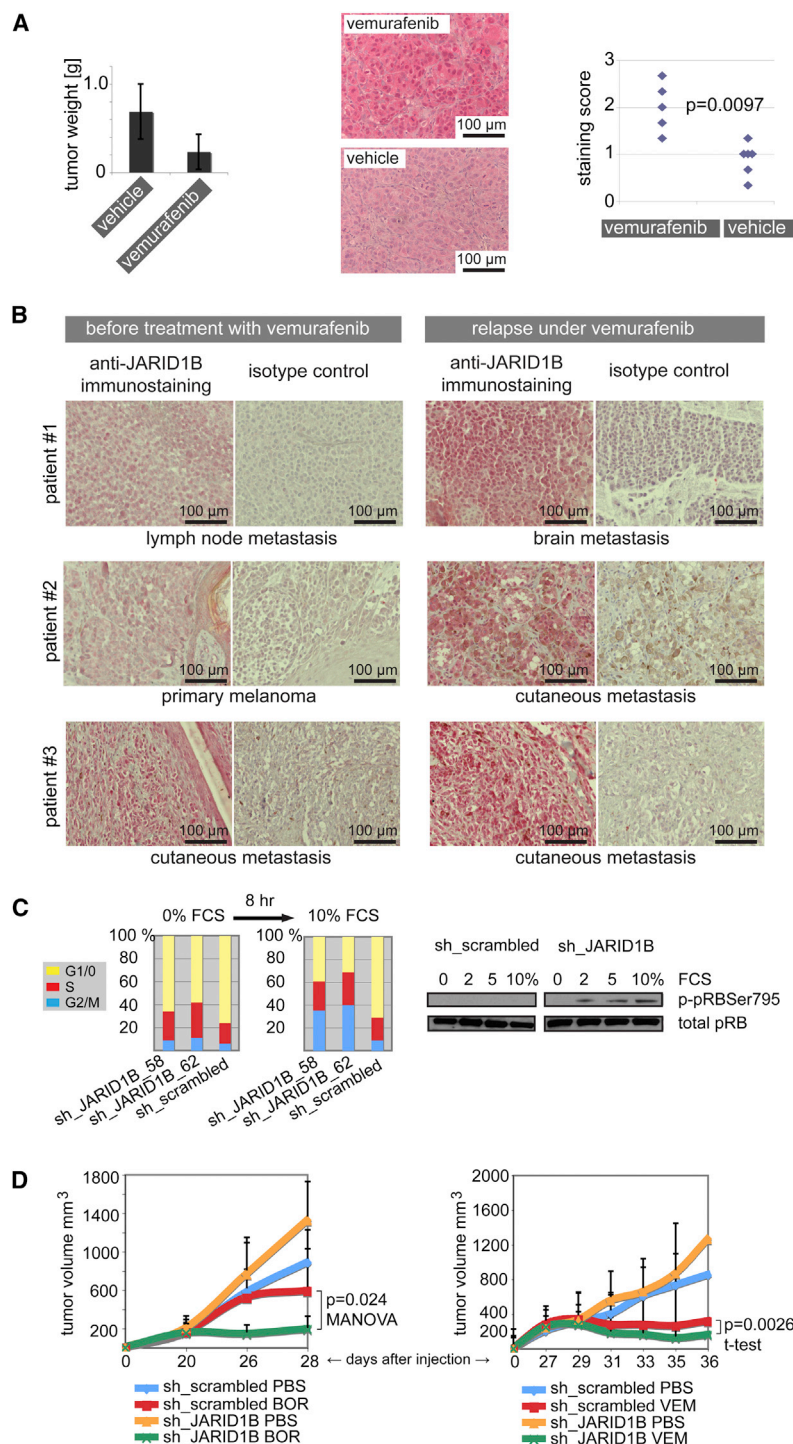


Figure 3. The JARID1B^{high} Subpopulation Is Enriched in Melanomas Resisting Therapy, and Knockdown of JARID1B Leads to Increased Drug Sensitivity

(A) NSG mice xenografted with WM3734 melanoma cells were treated with vemurafenib or vehicle (n = 7). Tumor weights were assessed after 11 days of treatment (left). Tumor residues were immunostained for JARID1B expression (middle), and nuclear-staining signals of each tumor were scored at 40X magnification in three representative fields of vision (right, two-sided Wilcoxon two-sample test). (B) Immunostaining of JARID1B in matched pairs of melanoma samples before and relapse under vemurafenib treatment from three melanoma patients.

(C) Two different JARID1B knockdown clones (sh_JARID1B_58 and 62) of WM35 melanoma cells and the sh_scrambled control were starved for 4 days at 0% FCS and subsequently stimulated by 10% FCS for 8 hr. The bar graph shows one example of five independent experiments of propidium iodide-based cell cycle analysis (left). The immunoblot shows pRB phosphorylation (right).

(D) NSG mice were xenotransplanted with WM3734 melanoma cells stably knocked down for JARID1B (sh_JARID1B) or with control cells (sh_scrambled). Each mouse received 10⁴ cells (n = 8). After tumors reached an average volume of ~200 mm³, mice were treated with bortezomib (left, BOR), vemurafenib (right, VEM), or vehicle (PBS). Tumor volumes were measured at the indicated time points. Error bars represent SD.

See also Figure S3.

2011), did not reduce the J/EGFP^{high} subpopulation in our model (Figure S2).

The in vivo relevance of our observations was confirmed in WM3734 cells xenografted to NOD/LtSscidIL2R γ^{null} (NSG) mice and treated with vemurafenib (Figure 3A). While tumors decreased in size due to treatment, the number and staining intensity of resistant JARID1B^{high} cells significantly increased. Importantly, a clear increase in JARID1B-expressing cells could be observed in three out of four matched pairs of patients' melanomas that relapsed under vemurafenib (Figure 3B). Together, these data indicate a universal resistance of the slow-cycling JARID1B^{high} melanoma subpopulation against various anticancer agents.

Knockdown of JARID1B Leads to Increased In Vivo Sensitivity to Antimelanoma Treatment

Previous studies suggested that the abrogation of the slow-cycling phenotype by JARID1B-

specific knockdown leads in vitro and in vivo to increased cell proliferation followed by melanoma exhaustion (Roesch et al., 2010). To quantify the shifts in cell-cycle progression, depending on the presence or absence of JARID1B, we performed cell-cycle experiments in WM35 melanoma cells stably knocked down for JARID1B (Figures 3C and S3). WM35 was chosen because changes in cell cycle of this low tumorigenic cell line could be better assessed compared to lines with high doubling

to diminish the slow-cycling phenotype, such as the histone deacetylase inhibitor trichostatin A (Sharma et al., 2010) or the Sp1 inhibitor mithramycin A (Sp1-binding sites within the JARID1B promoter are indicative of a possible regulatory potential); however, both compounds failed to reduce the J/EGFP^{high} subpopulation (Figure 2B). Similarly, leflunomide, which was suggested to interfere with developmental processes in melanocytes and melanoma growth (White et al.,

rate. Influences of cell densities and growth factors were considered. Cells were seeded at different densities and serum-starved at 0% fetal calf serum (FCS) for 4 days to synchronize the cell cycles. Under these conditions, knockdown of JARID1B led to an increase in S phase cells when compared to the control. Following stimulation with 2%, 5%, and 10% FCS over 4, 8, 16, and 24 hr, JARID1B knockdown cells shifted to G2/M. The most consistent changes in the cell cycle were seen after 8 hr of 10% FCS stimulation. Across five independently performed experiments, we saw an average decrease in G1 phase cells in JARID1B knocked down cells by ~20% (ranging from ~5% to 40%; the latter experiment is depicted in Figure 3C), while S phase cells increased by ~6% (~2%–12%), and G2/M phase cells by ~14% (~1%–31%). As predicted by previous studies showing JARID1B/retinoblastoma protein (pRB)-dependent cell cycle control (Roesch et al., 2006), JARID1B knockdown was accompanied by an increase in pRB phosphorylation at the JARID1B-specific phosphorylation site Ser795 (Figure 3C). Consequently, we asked if the inhibition of JARID1B could affect the therapeutic responsiveness of melanoma cells to anticancer drugs while releasing them from their slow-cycling phenotype. Indeed, stable knockdown of JARID1B in WM3734 melanoma cells xenografted to NSG mice led to increased cell proliferation accompanied by a significant sensitization to different treatments (Figure 3D). JARID1B knockdown plus bortezomib showed an additive effect, improving the moderate antimelanoma effect of bortezomib to an almost complete stasis of tumor growth. When we combined JARID1B knockdown with vemurafenib, which by itself dramatically prevents melanoma growth, we still observed a decrease in the average tumor volume below that of the treatment-starting volume. Because of the biological variability of tumor sizes, this effect was not significant in the multivariate analysis of variance (MANOVA), but an analysis of the change in the logarithm of volume per unit time by t test had significantly different rates. In sum, these results support the hypothesis that targeting the slow-cycling cell phenotype can sensitize melanoma to anticancer approaches, including chemotherapeutics and molecular-targeted drugs.

Dynamics of the Therapy-Resistant JARID1B^{high} Phenotype

According to our previous observations, the progeny of both J/EGFP^{high} and J/EGFP^{low} cells can dynamically interconvert into the opposing phenotype, indicating a flexible system that is dependent on the microenvironmental context (Roesch et al., 2010). Thus, we asked (1) if the newly developing progenies of initially sorted J/EGFP^{high} or J/EGFP^{low} cells show a differential drug response and (2) if the observed enrichment of J/EGFP^{high} cells after anticancer treatment results from selection of J/EGFP^{high} cells or induction of J/EGFP^{high} expression. In regular culture, spontaneous phenotype interconversion usually becomes visible within a few days after fluorescence-activated cell sorting (FACS) of the two populations. For example, 69.9% of FACS-sorted J/EGFP^{high} cells turned negative 72 hr after separation (Figure 4Ac, upper left plus lower left quadrant), while in total, 3.5% of the progeny of sorted J/EGFP^{low} cells became J/EGFP^{high} (Figure 4Ae). When sorted cells were treated with 20 μ M cisplatin for 72 hr, we saw no substantial enrichment for J/EGFP^{high} cells in the progeny of initially J/EGFP^{high} cells, indi-

cating that no additional JARID1B-expression cells were induced (summarized upper and lower right quadrants; Figure 4Ac versus Figure 4Ad). Interestingly, most newly developed J/EGFP^{low} cells became 7AAD⁺ under cisplatin treatment (Figure 4Ac versus Figure 4Ad, upper and lower left quadrants). The apparent preference for JARID1B induction in the progeny of J/EGFP^{low} cells (Figure 4Ae versus Figure 4Af) was counteracted by an increased rate of cisplatin-induced cell death in cells derived from the J/EGFP^{low} population. Manual counts revealed a significantly lower number of surviving cells in the progeny of sorted J/EGFP^{low} cells compared to the progeny of J/EGFP^{high} cells ($p < 0.05$ for 5 μ M and 10 μ M cisplatin; data not shown). Together with the results from consecutive measurements of JARID1B messenger RNA (mRNA) under cisplatin treatment that did not show transcriptional upregulation (Figure 4A), we concluded that the major mechanism for the enrichment of J/EGFP^{high} cells following therapy is a selection of pre-existent JARID1B^{high} slow-cycling cells. However, to a lesser extent, JARID1B induction may also occur (e.g., shifting cells with intermediate JARID1B expression to higher levels).

When cells were long-term challenged with cisplatin, the J/EGFP^{high} subpopulation remained constantly elevated over several weeks in a dose-dependent manner. The cisplatin-induced elevation of J/EGFP^{high} cells was fully reversible following drug withdrawal (Figure 4B). In line with the concept of dynamic phenotype switching (Roesch et al., 2010), drug-resistant cells that are enriched for JARID1B can regain the original cell distribution and J/EGFP ratios after drug removal. Moreover, cisplatin-surviving JARID1B-enriched cells gave rise to fewer but significantly larger (i.e., rapidly growing) three-dimensional (3D) colonies in soft agar compared to untreated cells (Figure 4C). This observation is reminiscent of earlier clonogenicity and single-cell dilution assays showing that untreated FACS-isolated J/EGFP^{high} cells give rise to a rapidly proliferating progeny with elevated repopulation capacity when compared to JARID1B^{low} cells (Roesch et al., 2010).

Bioenergetic Metabolism Plays an Important Role in the Survival of Slow-Cycling Melanoma Cells

We next designed experiments to unravel druggable targets that are specifically activated in slow-cycling melanoma cells. Since global gene expression screening with complementary DNA microarrays did not provide significant hit candidates in FACS-sorted J/EGFP^{high} versus J/EGFP^{low} or JARID1B knockdown versus control cells (data not shown), we performed quantitative proteome profiling. Following our established protocols for isolation of slow-cycling melanoma cells (Roesch et al., 2010), we costained WM3734^{JARID1B^{prom}-EGFP} cells with the PKH26 dye and then FACS-isolated the label-retaining and J/EGFP^{high} subpopulation versus nonlabel-retaining J/EGFP^{low} cells after a period of 4 weeks of cell divisions. Prior to sorting, the cells were grown as melanospheres to attain a more stringent J/EGFP phenotype, as previously reported (Roesch et al., 2010). Tryptic digests of the cell lysates were analyzed by liquid chromatography-mass spectrometry/mass spectrometry. Label-free computational quantitation identified 423 proteins with significant expression changes between label-retaining J/EGFP^{high} cells and nonlabel-retaining J/EGFP^{low} cells with a p value < 0.001 . Unexpectedly, neither common cancer target

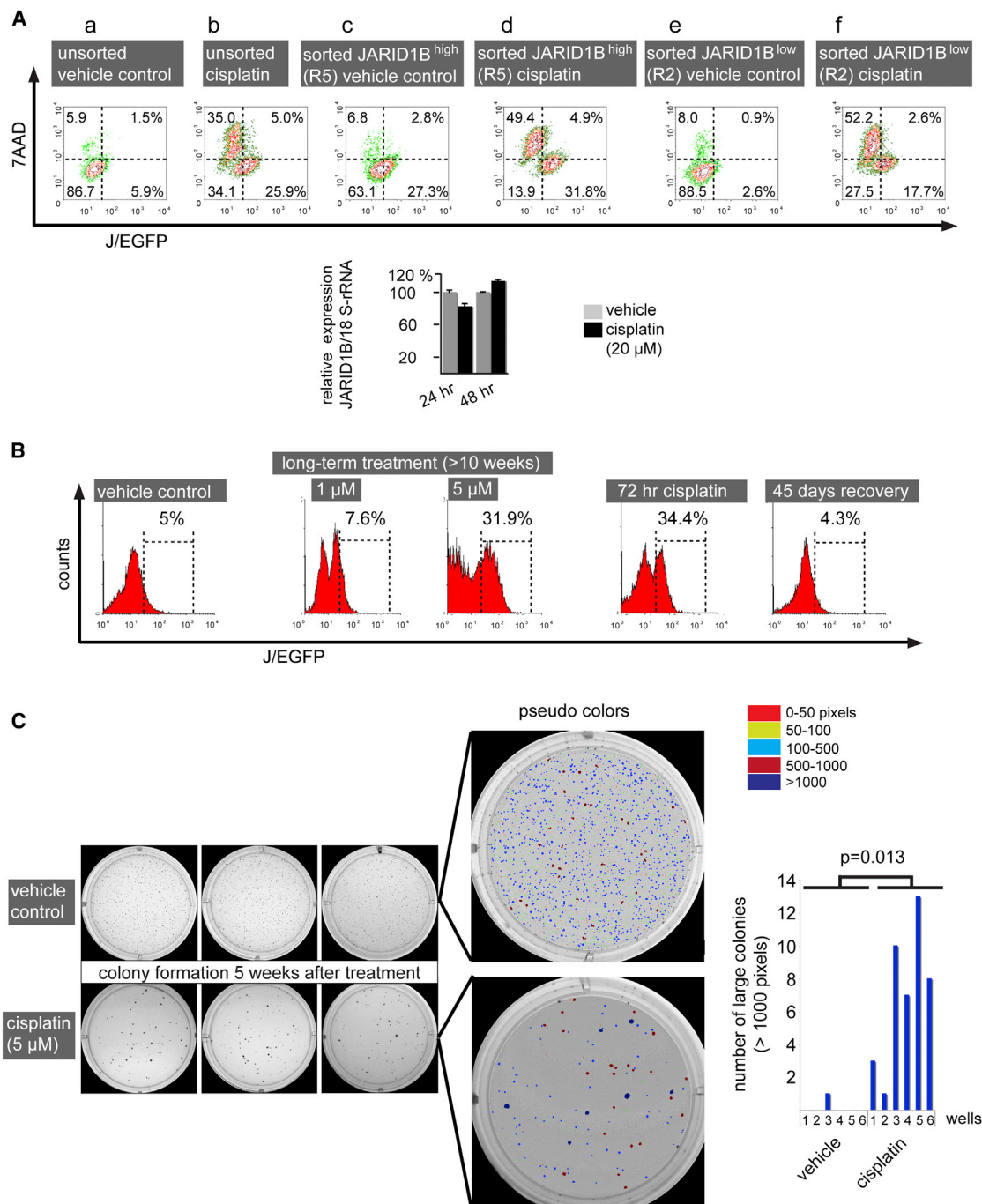


Figure 4. Dynamics of the Therapy-Resistant JARID1B^{high} Phenotype

(A) WM3734^{JARID1B^{prom}-EGFP} cells were FACS-sorted according to their J/EGFP expression, and the isolated subfractions were cultured as adherent monolayers overnight. After subsequent treatment for 72 hr, the frequencies of J/EGFP^{high} and J/EGFP^{low} cells were again quantified by flow cytometry. Dead cells were detected by 7AAD staining. JARID1B mRNA expression was quantified by quantitative PCR.

(B) Flow cytometric detection of J/EGFP^{high} WM3734 cells after prolonged incubation with different concentrations of cisplatin and after drug recovery.

(C) Colony-forming assay of WM3734 cells that underwent cytotoxic pulse treatment prior to seeding. Cells were treated for 72 hr with cisplatin or vehicle. Surviving cells were subsequently embedded into soft agar (2,000 cells/well). Colony sizes and numbers were digitally quantified and color-coded, with dark blue colonies representing large colonies above 1,000 pixels. Shown are results from two independent experiments, each performed in triplicate. Error bars represent SD.

nor drug resistance-related protein could be detected by this approach. Instead, we found a differential regulation of a number of mitochondrial proteins with particular functions in bioener-

getic metabolism (Table S1). Many of the upregulated proteins play a major role in cell respiratory electron transport (oxidative phosphorylation [OXPHOS]), such as nicotinamide adenine

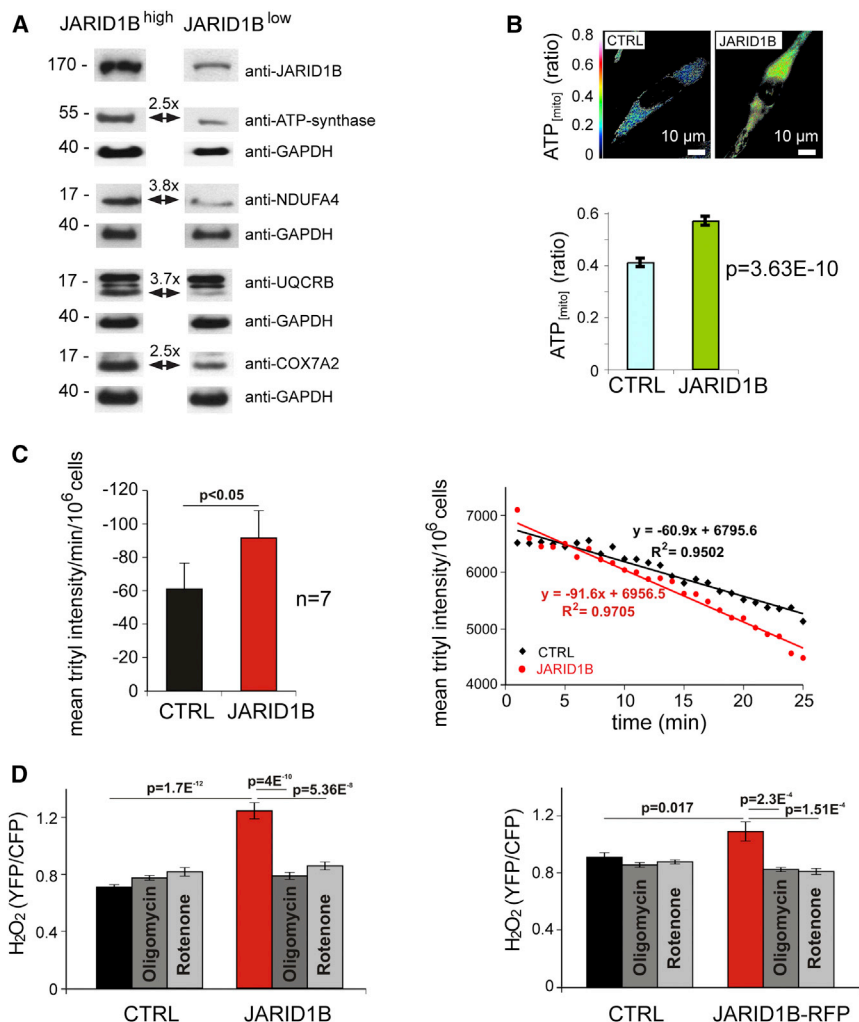


Figure 5. Elevated Mitochondrial Bioenergy Metabolism in the JARID1B^{high} Subpopulation

(A) Immunoblotting of mitochondrial respiratory enzymes in FACS-sorted J/EGFP^{high} and J/EGFP^{low} WM3734 cells. Fold changes were normalized to GAPDH.

(B) Relative mitochondrial ATP levels in control (CTRL) or JARID1B-transfected WM3734 cells were measured using the ATP sensor protein A_{TEAM}. Representative A_{TEAM} ratio images (top) and summarized A_{TEAM} ratio values in control (n = 72) and JARID1B-transfected (n = 47) cells (bottom).

(C) Mean oxygen consumption of control- (black) or JARID1B-transfected (red) WM3734 cells presented as decline of trityl radical intensity per minute per 10⁶ cells (left). Mean oxygen concentration in presence of control or JARID1B-transfected WM3734 cells presented as trityl intensity per 10⁶ cells. Each data point is an average of seven independent experiments.

(D) Relative H₂O₂ levels were measured in JARID1B-transfected WM3734 cells using the H₂O₂ sensor protein Hyper. Columns represent averaged Hyper ratio values of control- (black, n = 71) or JARID1B-transfected cells (red, n = 48). To test the role of mitochondria as source of H₂O₂, cells were treated with 1 μM oligomycin (dark gray) or 1 μM rotenone (light gray). Numbers of cells averaged were: CTRL plus oligomycin (n = 50), CTRL plus rotenone (n = 42), JARID1B plus oligomycin (n = 45), and JARID1B plus rotenone (n = 52). In a confirmation experiment with WM3734 cells transfected with pCAGGS-JARID1B-IRES-RFP (right), positively transfected cells were selected for analysis based on the expression of red fluorescent protein (RFP). Error bars represent SEM.

See also Table S1.

dinucleotide (NADH) dehydrogenase (complex I of the mitochondrial electron transport chain), ubiquinol cytochrome c reductase (complex III), cytochrome c oxidase (complex IV), and ATP synthase. In contrast, glycolytic hexokinase I and II were down-regulated. Immunoblotting of lysates from J/EGFP-sorted cells confirmed upregulation of ATP synthase, NADH dehydrogenase, ubiquinol-cytochrome C reductase-binding protein, and cytochrome c oxidase in J/EGFP^{high} cells (Figure 5A). WM3734 cells transiently overexpressing JARID1B had a higher mitochondrial energy production compared to the mock control (Figure 5B). Accordingly, JARID1B-overexpressing WM3734 cells consumed ~50% more oxygen than control cells (Figure 5C). Treatment with different concentrations of oligomycin and rotenone severely reduced the oxygen consumption by up to 94%, indicating a major role for mitochondria in this process (data not shown). Because high mitochondrial electron transfer activity can lead to increase in superoxide and hydrogen peroxide (H₂O₂) production, we analyzed the H₂O₂ level. JARID1B-overexpressing cells generated 76% more H₂O₂ than control cells 60–72 hr after transfection (Figure 5D). The H₂O₂ increase was completely abolished by treatment with oligomycin or rotenone. These results suggest that redox signaling may play an important role

for JARID1B^{high} cells. Furthermore, high oxygen consumption can ultimately lead to hypoxic conditions, which is known to favor the JARID1B^{high} slow-cycling phenotype (Xia et al., 2009; Roesch et al., 2010).

Targeting the Mitochondrial Respiratory Chain Inhibits the JARID1B^{high} Subpopulation and Reveals Long-Term Effects against Melanoma Cells

Inhibition of the mitochondrial respiratory chain has been reported to exert tumor-suppressive effects in different types of cancers, including neuroectodermal glioblastoma cells (Hao et al., 2010). Since enzymes of almost all respiratory chain complexes were found differentially regulated in slow-cycling J/EGFP^{high} cells (Table S1), we explored representative inhibitory tool compounds, such as (1) the ATP-synthase inhibitors oligomycin and Bz-423, (2) the NADH dehydrogenase (complex I) inhibitors rotenone and phenformin, and (3) antimycin A, which inhibits the ubiquinol cytochrome c reductase in a series of preliminary cytotoxicity assays (data not shown). Here, ATP-synthase and complex I inhibitors revealed the most prominent results; thus, these were selected for subsequent studies. High concentrations of oligomycin were reported

to exert unspecific effects in eukaryotes, due to the uncoupling of the respiratory chain (Charton et al., 2004). Therefore, MTT assays were used to estimate the minimal concentration of oligomycin that could cause mitochondrial uncoupling in our cell lines, since reduction of the tetrazolium compound MTT is dependent on intact mitochondrial electron transport (Grazette et al., 2004). We observed an abrupt decrease in MTT reduction above an oligomycin concentration of 2.5–5 $\mu\text{g/ml}$, independent of the incubation time and the genetic background of all cell lines tested (Figure 6A; depicted are WM3734 as an example). These results are in line with oligomycin concentrations that were reported by others to specifically block oxidative phosphorylation (Hao et al., 2010). Thus, we considered oligomycin concentrations less than 2.5 $\mu\text{g/ml}$ to work through the specific inhibition of the ATP-synthase and not through mitochondrial uncoupling.

We next asserted that low-dose oligomycin still leads to functional and significantly measurable effects, such as a decrease in ATP production or increase in lactate secretion in WM3734 cells (Figure 6B), and subsequently confirmed this for a panel of genetically different melanoma lines under normoxic and hypoxic conditions (Figure 6C). The detected changes in ATP and lactate were comparable to those measured by others for a number of different cell types (Hao et al., 2010). Interestingly, ATP-synthase inhibition was accompanied by a complete loss of endogenously expressed JARID1B protein after 72 hr of oligomycin treatment (Figure 6D). Also, the enrichment of JARID1B^{high} cells usually seen after hypoxic treatment was inhibited by low-dose oligomycin.

Due to the evolutionary link between nonproliferative and OXPHOS-dependent cell phenotypes (Berridge et al., 2010; Jose et al., 2011; Vander Heiden et al., 2009), we next asked if inhibition of mitochondrial ATP production also influences the cell cycle of melanoma cells. In fact, even very low doses of oligomycin (0.01 $\mu\text{g/ml}$) caused a measurable decrease in the percentage of cells in G1/S phase and an increase in the percentage of cells in S- and G2/M-phase compared to vehicle controls. To optimize the readout, cells were serum-starved for 4 days and subsequently stimulated with FCS for 8 and 16 hr (Figure 6E). After 24 hr, cell cycle phases were again equal in oligomycin and vehicle control-treated cell groups (data not shown). Despite the increase in proliferative cell cycle phases, we found a relative decrease in overall cell numbers after oligomycin treatment compared to controls (Figure 6F). A likely explanation for this paradox is that simultaneously to (or after) the acceleration of the cell cycle, a considerable portion of the cells is undergoing cell death, as indicated by independently performed 7AAD staining and subsequent flow cytometric analysis (e.g., ~20% dead cells after 72 hr of 0.1 $\mu\text{g/ml}$ oligomycin; Figure S4A). Short-term analysis of oligomycin's effect on total cell numbers showed that the cell population slightly expands at low doses (Figure 6F, left panel), whereas high doses starting from 5 $\mu\text{g/ml}$ caused persisting or decreasing cell numbers, possibly due to highly toxic mitochondrial uncoupling. The full effect of the antitumor potential of low-dose oligomycin became visible in long-term colony formation assays. Here, a significant reduction in colony growth was seen after 3 weeks of treatment (Figure 6F, right panel), which is reminiscent of the results previously reported for JARID1B knockdown (Roesch et al., 2010). Short-term treatment of WM3734 cells with the ATP-synthase inhibitor

Bz-423 and the complex I inhibitors rotenone and phenformin confirmed these findings (Figures S4B–S4D). In conclusion, this suggests that pharmacological targeting of the mitochondrial respiratory chain can inhibit the JARID1B^{high} slow-cycling subpopulation and reveal long-term suppressive effects in melanoma cells.

Inhibition of the Mitochondrial Respiratory Chain Overcomes Intrinsic Multidrug Resistance of Melanoma

We asked if inhibition of the mitochondrial respiration could counteract the intrinsic multidrug resistance mediated by slow-cycling melanoma cells. Flow cytometric quantitation of J/EGFP levels in WM3734 cells (Figure 7A) and 1205LU cells (Figure S5A) revealed a significant blockade of the JARID1B^{high} subpopulation when cells were treated with the combination of cisplatin plus oligomycin. Similar results were seen for Bz-423, which also acts as an ATP-synthase inhibitor (Figure S5B). Even treatment with extremely low doses of oligomycin (0.001 $\mu\text{g/ml}$; Figure S5C) still blocked the enrichment of J/EGFP^{high} cells. At 0.001 $\mu\text{g/ml}$, single-agent oligomycin did not induce substantial cell death, as measured by 7AAD flow cytometry in WM3734 cells (Figure S4A); however, when combined with cisplatin, the overall number of dead cells strongly increased (Figure S5C). Immunoblots revealed a complete loss of endogenous JARID1B under oligomycin cotreatment, overcoming the cisplatin-induced enrichment of JARID1B protein after 24, 48, and 72 hr (Figure 7A). Cytotoxicity assays confirmed that the combination with oligomycin sensitizes melanoma cells to cisplatin treatment, but depending on the cell line used, the contribution of single-agent oligomycin to cell killing can vary (Figure 7B). MeWo cells, the melanoma cell line with the lowest oligomycin response in lactate secretion (Figure 6C), were not sensitized to cisplatin, indicating that the combination with oligomycin is not universally cytotoxic, but instead, responses match our mitochondrial activity-based hypothesis. The tumor suppressive potential of combinatorial ATP-synthase inhibition was further demonstrated in 3D collagen-embedded spheroids of 1205Lu cells, a model which more readily mimics the melanoma microenvironment. The combination of oligomycin plus vemurafenib more potently inhibited cell invasion into collagen than each drug alone (Figure 7C; $p < 0.0003$). Notably, treatment of WM3734 cells with a single pulse of low-dose oligomycin plus cisplatin over 72 hr substantially reduced long-term growth in soft agar and the number of 3D colonies remained at almost undetectable levels, even after 5 weeks of culture in drug-free medium (Figure 7D). This effect reached statistical significance with $p < 0.02$ when large colonies above a diameter of 10 μm were counted. Consistent with the observation that significantly larger colonies grew from cisplatin pretreated cells (that were enriched for the J/EGFP^{high} subpopulation; Figure 4C), these results indicate that (1) adding mitochondrial inhibitors to common anticancer treatment significantly diminishes the number of cells with high repopulation and invasion potential and (2) that even a relatively short-term treatment can yield a sustained antitumor effect.

Mitochondrial inhibition as a combinatorial strategy against cancer drug-induced enrichment of slow-cycling JARID1B^{high} melanoma cells was further confirmed for the complex I inhibitors rotenone and phenformin. Phenformin is used in the clinics

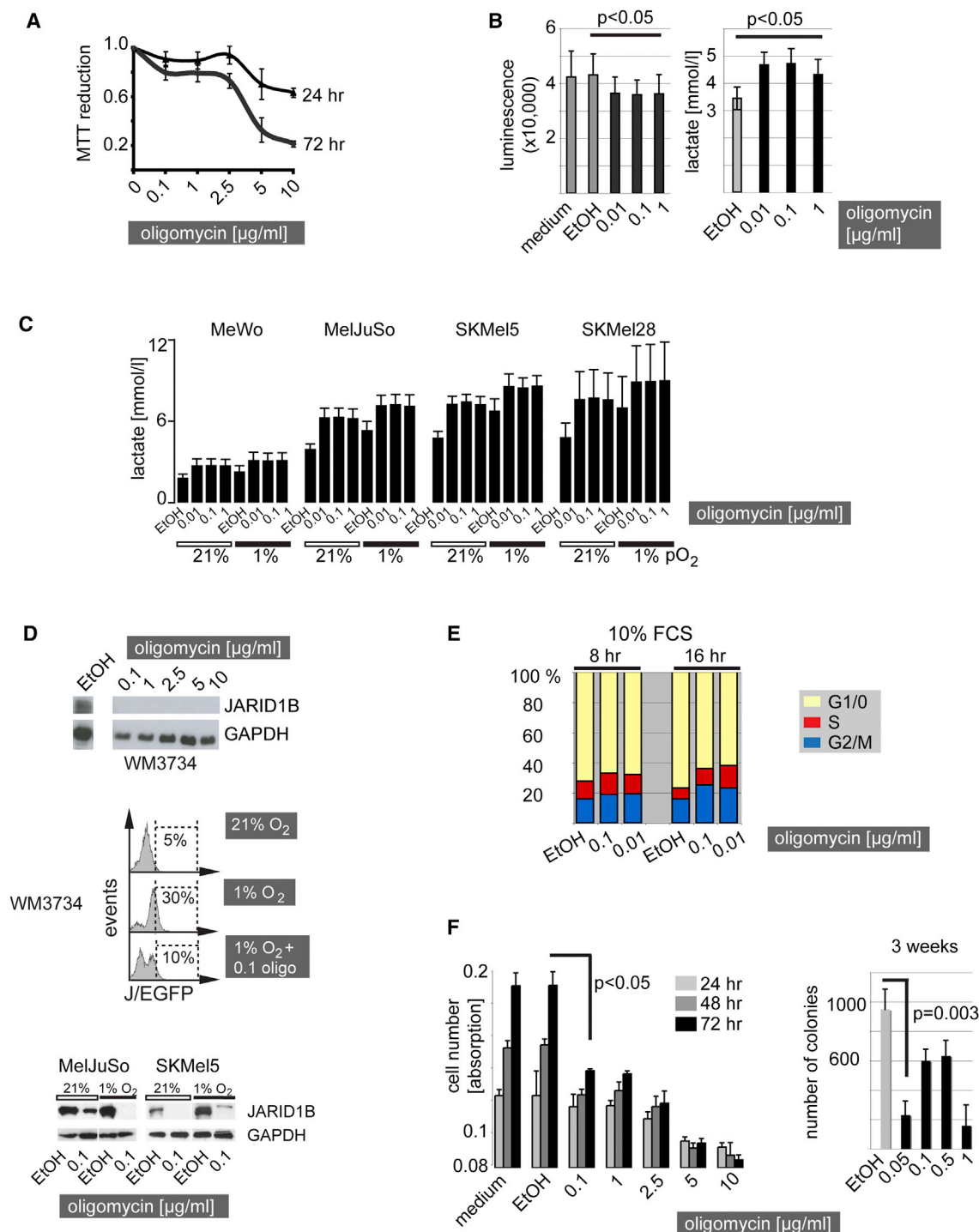


Figure 6. Inhibition of the Mitochondrial ATP Synthase Inhibits the JARID1B^{high} Subpopulation and Reveals Long-Term Melanoma Cell-Suppressive Effects

(A) MTT reduction curve of regularly cultured WM3734 melanoma cells after oligomycin treatment.
 (B) Total cellular ATP levels were luminometrically determined in WM3734 cells after 24 hr of treatment with oligomycin at the indicated concentrations (left). Lactate production was measured in WM3734 cell culture supernatants after 24 hr of oligomycin. Ethanol (EtOH, diluted 1:1000) was used as vehicle control. Shown are means of three independently performed experiments.
 (C) Lactate measurement in a panel of genetically diverse melanoma cell lines under normoxic versus hypoxic culture conditions after 24 hr of treatment.
 (D) Immunoblot of JARID1B protein expression in WM3734 cells treated with oligomycin for 72 hr at the indicated concentrations (top). Frequency of J/EGFP^{high} WM3734 cells under 72 hr of hypoxia versus hypoxia plus oligomycin (oligo) treatment as determined by flow cytometry (middle). Immunoblots of endogenous JARID1B expression in MelJuSo and SKMel5 melanoma cells under hypoxia and hypoxia plus oligomycin treatment (bottom).

(legend continued on next page)

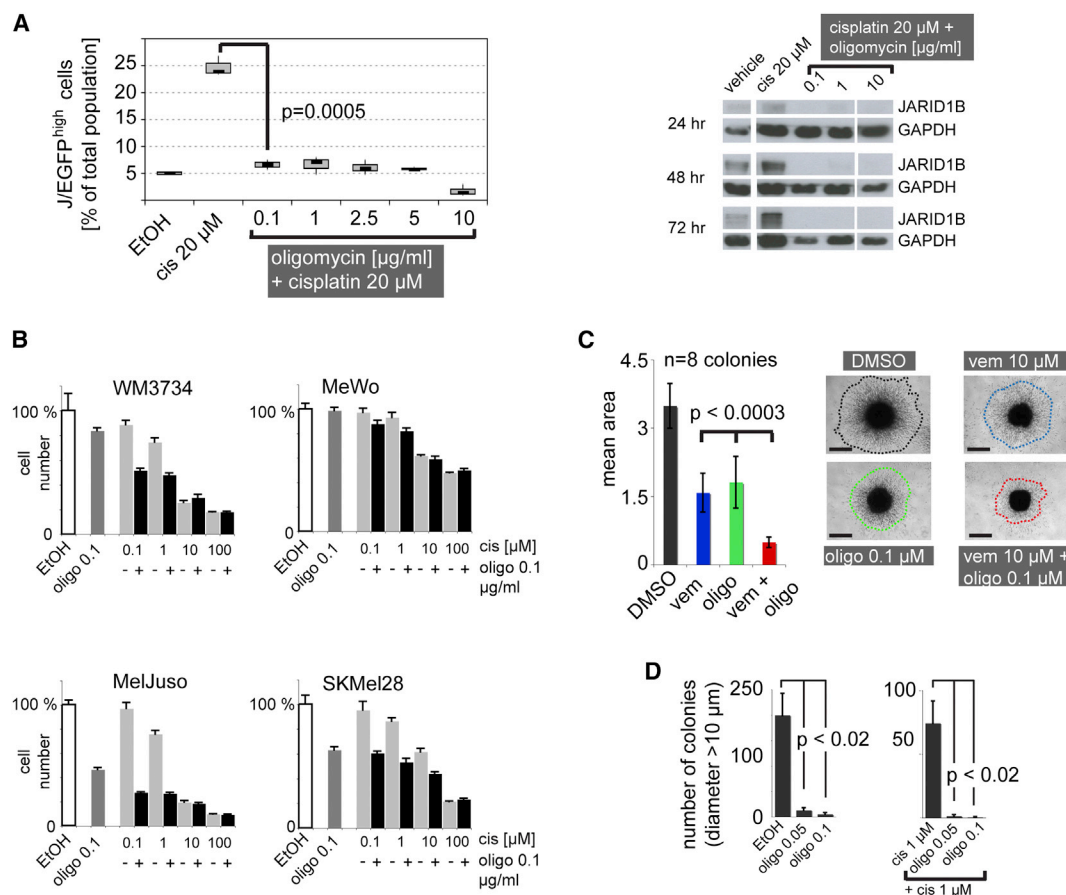


Figure 7. The Combination of Anticancer Agents plus Inhibition of the Mitochondrial ATP-Synthase Overcomes the Enrichment of the JARID1B^{high} Subpopulation In Vitro

(A) Relative percentage of the J/EGFP^{high} subpopulation under combinatorial treatment of WM3734 cells for 72 hr with cisplatin (cis) and oligomycin as determined by flow cytometry (left). Ethanol (EtOH) was used as vehicle control. Immunoblots of the endogenous JARID1B protein expression of WM3734 cells under cotreatment with oligomycin at the indicated time points (right).

(B) Cytotoxicity assays of melanoma cell lines after 72 hr of cotreatment with cisplatin (cis) and oligomycin (oligo).

(C) Three-dimensional growth/invasion/survival assay of 1205Lu cells treated with vemurafenib (vem) and oligomycin (oligo) for 96 hr. Colony sizes were quantified digitally based on the relative number of pixels. Scale bar represents 500 μ m.

(D) Soft agar colony-forming assay of WM3734 cells after 72 hr pulse treatment with oligomycin (left) and oligomycin plus cisplatin (right). Colonies were counted manually after 5 weeks of growth. Results shown are from one of two independent experiments. Error bars represent SD.

See also Figure S5.

as an antidiabetic drug. Both compounds potently blocked the emergence of JARID1B^{high} cells during antimelanoma treatment (Figures 8A and S6A–S6D). Immunoblots and immunohistochemistry of phenformin-treated cells confirmed that complex I inhibition affects the endogenous JARID1B phenotype in vitro and in vivo (Figures S6C and S6D). Similar to the combinations of bortezomib or vemurafenib with JARID1B gene knockdown shown in Figure 3D, the mitochondrial inhibition by phenformin improved the tumor-suppressive potential of vemurafenib in xenotransplanted melanomas in vivo (Figures 8B and S6D). Sta-

tistical overall significance was shown by MANOVA ($p = 0.0263$). Significant differences between the combination and single treatments were seen after adjusting for multiple hypothesis testing (combination versus vemurafenib was $p = 0.022$, versus phenformin $p = 0.010$, and versus control $p = 0.010$). Altogether, these findings suggest that multiresistant, slow-cycling melanoma cells are susceptible to the inhibition of the mitochondrial respiratory chain and that the oxidative energy metabolism could be a prime target to overcome intrinsic drug resistance in melanoma.

(E) WM3734 cells were starved at 0% FCS and then released by 10% FCS for 8 and 16 hr. The bar graph shows one example of three independent experiments of propidium iodide-based cell cycle analysis. Dead cells (SubG1) were gated out.

(F) Short-term effects of increasing concentrations of oligomycin on total WM3734 cell numbers as determined by crystal violet assays (left). Long-term growth reduction as measured by 3D soft agar colony formation assays (bidaily treatment, right). Error bars represent SD.

See also Figure S4.

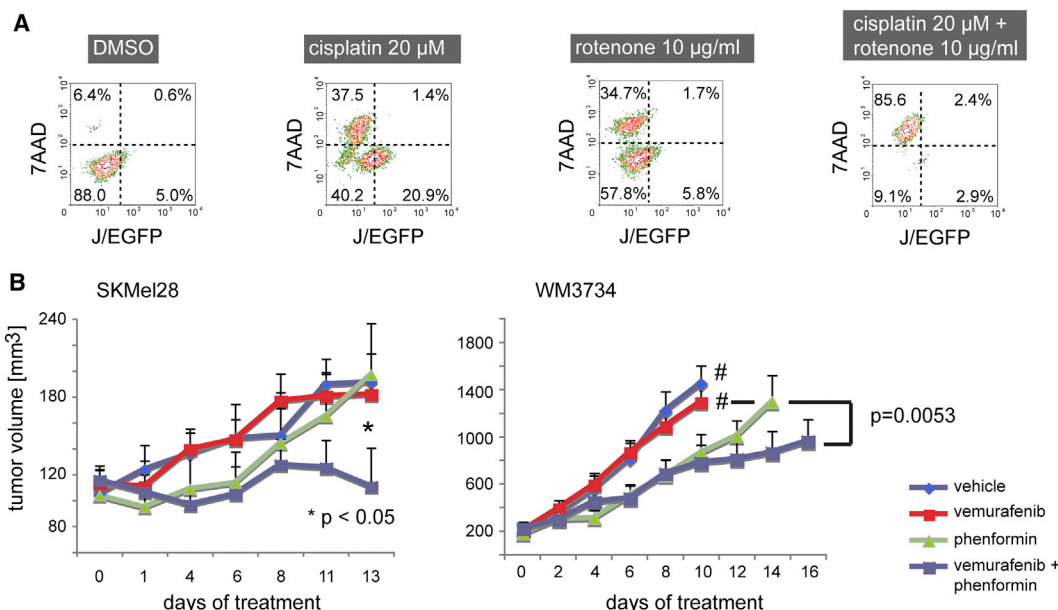


Figure 8. The Effect of Anticancer Agents Is Increased In Vitro and In Vivo by the Combination with Complex I Inhibitors

(A) Flow cytometric pattern of 7AAD and J/EGFP signals in cultured WM3734 cells after 72 hr of treatment with cisplatin and rotenone.

(B) SCID beige mice were xenotransplanted with 10^5 SKMel28 human melanoma cells (left, $n = 7$ per treatment group, $n = 6$ in vehicle group), NSG mice with 5×10^4 WM3734 cells (right, $n = 8$ per group). SKMel28 tumors were treated when an average volume of ~ 120 mm³ was reached, WM3734 tumors at an average volume of 200 mm³. Tumor volumes were assessed every other day. Groups marked with # were terminated earlier due to excessive tumor growth. Error bars represent SEM.

See also Figure S6.

DISCUSSION

Despite recent discoveries in the area of therapy resistance in melanoma, we do not fully know how therapeutic escape arises and if it is the result of an evolutionary process under treatment, from the selection of pre-existing resistant subpopulations, or a combination of both. Likely, even among functionally and genetically heterogeneous tumors, common mechanisms may exist that allow cells to survive in harsh conditions in general. Based on our experience with vemurafenib-resistant clones in vitro, we observed that functionally resistant resistance in cell lines that are initially vemurafenib-sensitive takes time to develop but eventually leads to reactivation of the MAPK and PI3K pathways (Villanueva et al., 2010). Intrinsic resistance conferred by the slow-cycling cell phenotype could represent an additional and universal protection mechanism that helps cells survive the very first contact with various cytotoxic agents and provides cells with added survival time to establish longer-lasting secondary resistance mechanisms. A major challenge for successful therapy is that these slow-cycling cells can be present at any stage of the disease and that this phenotype can be dynamically acquired by other melanoma cells, depending on the microenvironmental context, thus representing a “moving target” (Roesch et al., 2005, 2010).

Our findings indicate that the slow-cycling phenotype reflects a metabolic state that is characterized by high expression of mitochondrial bioenergetic enzymes relative to the rapidly proliferating tumor bulk population. Otto Warburg predicted that cancer cells generally rely on an increase in glucose uptake,

the enhancement of glycolysis and lactate production, along with the absence of oxidative respiration, despite the presence of sufficient oxygen concentrations (Warburg et al., 1924). He erroneously suggested defective mitochondria as a possible cause. However, it is becoming clear now that mitochondria in cancer cells are mostly intact and may play an important role in tumor growth (Caro et al., 2012; Weinberg et al., 2010). The cells’ decision to employ glycolysis or oxidative phosphorylation for their energy supply depends on multiple factors, including the cancer type and stage, the sequence of oncogenes activated, which can directly influence mitochondrial metabolism, the current microenvironmental context, and also the rate of cell proliferation (Berridge et al., 2010; Jose et al., 2011; Vander Heiden et al., 2009). Our results support the general hypothesis that slow-cycling cells rely more on oxidative phosphorylation, whereas rapidly growing cells are characterized by high glycolysis (Berridge et al., 2010; Jose et al., 2011; Vander Heiden et al., 2009). As previously shown by others, the blockage of glycolysis by bromopyruvate treatment is only efficient on rapidly growing cells and barely useful to decrease the growth rate of tumor cells with slow proliferation (Jose et al., 2011). This observation together with ours indicates that cell cycling and energy metabolism represent interwoven biologic processes that holistically contribute to the phenotype of tumor cell subpopulations. With regard to intrinsic drug susceptibility, we found that the JARID1B^{high} slow-cycling phenotype is not responding to exogenous cell cycle influences, such as serum starvation (data not shown). Since depletion of JARID1B does affect cell cycle phases, we would consider JARID1B expression to be a “driver”

of the slow-cycling phenotype rather than a “passenger.” Treatment with the multi-cyclin-dependent kinase (CDK) inhibitor dinaciclib resulted in massive cell death rather than in proliferation arrest and thus passively selected for JARID1B^{high} cells, as seen before for other anticancer agents (data not shown). We further suggest that consideration of single biologic features, such as cell cycling, without the metabolic contribution may not be sufficient to predict therapeutic response. For example, MeWo cells, which are known to have a high ability to metabolize glutamine in the (reversed) tricarboxylic acid (TCA) cycle as an alternative energy source (Scott et al., 2011), responded least to cytotoxic killing and mitochondrial inhibition, although having a rather high proliferation rate (and low endogenous JARID1B expression; data not shown).

We cannot exclude the possibility that our initial proteome profiling strategy may have missed additional important factors contributing to the biology of slow-cycling cells. Therefore, we analyzed common molecular players of melanoma tumorigenesis by immunoblotting of sorted J/EGFP^{high} versus J/EGFP^{low} cells. We found no difference in MAPK activation (measured by pMEK and pERK levels) nor in the expression of the apoptosis markers BCL-2, MCL-1, and BIM or the cell-cycle regulators CDK2, CDK4, and CDK9 (data not shown). Interestingly, we found an increase in pAKT in J/EGFP^{high} cells that correlates well with our previous finding that reactivation of PI3K signaling can overcome vemurafenib's cytotoxicity in melanoma cells (Vilanova et al., 2010). The relevance of this finding with regard to therapeutic strategies comprising combinatorial inhibition of PI3K in slow-cycling cells will be the subject of future studies. Considering the heterogeneity of melanoma, we are currently delineating additional molecular mechanisms underlying resistance of the JARID1B^{high} slow-cycling phenotype. However, non-JARID1B-related phenotypic resistance is likely to occur, and all potential resistance mechanisms could contribute to melanoma recurrence.

Our data confirm that slow-cycling melanoma cells of different genetic backgrounds are intrinsically resistant to various anticancer drugs and are characterized by the presence of several key enzymes of oxidative energy metabolism. Depletion of the JARID1B^{high} slow-cycling phenotype either by gene knockdown or by targeting of its bioenergetic metabolism sensitizes melanoma for a more pronounced and long-lasting therapeutic effect. Selective targeting of the slow-cycling subpopulation in combination with conventional tumor “debulking” strategies could help to eliminate a dramatically higher percentage of melanoma cells and significantly prolong the therapeutic response in patients with malignant melanoma.

EXPERIMENTAL PROCEDURES

Melanoma Cell Lines, Tissue, and Vector Constructs

Establishment and studying of noncommercial melanoma cell lines from human tumor samples was approved by the Internal Review Boards of the University of Pennsylvania School of Medicine and The Wistar Institute. Immunohistochemical staining of human melanoma samples was approved by the ethics committees of the University of Frankfurt and the Saarland University. Informed consents were obtained from all participating subjects. For details on cell culture techniques, see [Supplemental Experimental Procedures](#). The consistency of cellular genotypes was confirmed by DNA fingerprinting at the Department of Human Genetics of The Saarland University Hospital. The lenti-

viral vector constructs for stable knockdown of JARID1B were purchased from Sigma. Details on lentiviral pLU-JARID1Bprom-EGFP-Blast, pLU-CMVprom-EGFP-Blast, and transient transfection with pBIND-RBP2H1(JARID1B) were previously described (Roesch et al., 2008, 2010).

Detection of JARID1B and Flow Cytometry of J/EGFP Signals

For immunoblotting and immunostaining, rabbit polyclonal anti-JARID1B antibodies (Novus NB100-97821 and 22260002) were used, following established protocols (Roesch et al., 2010). Quantitative real time RT-PCR was performed on a StepOnePlus instrument (Applied Biosystems) using self-designed primers or primers from the Harvard primer bank as described earlier (Roesch et al., 2010). Flow cytometric detection of JARID1B promoter-driven EGFP signals was performed using a FACSCanto II (BD Biosciences) as described in the supplements. Dead cells were excluded by staining for 7AAD. Fluorescence-activated cell sorting was done on a Cytomation MoFlo (DakoCytomation) or a FACSARIAIII (BD Biosciences) instrument.

Cell Proliferation and Three-Dimensional Growth/Invasion/Survival Assays

Cell proliferation was quantified by MTT and crystal violet assays according to standard protocols. Anchorage-independent colony formation was measured in 0.35% soft agar assays and quantified manually or digitally as described before using Image Pro Plus 7.0 (Roesch et al., 2010). Collagen-embedded, three-dimensional melanoma spheroids were prepared and treated with inhibitors at the designated concentrations for 72 hr, as previously described (Smalley et al., 2006). Following treatment, spheroids were imaged using a Nikon-300 inverted fluorescence microscope. To quantitate invasion into the matrix, borders were established around the invasive edge based on an ImageJ-defined cell density parameter, and the same parameters were applied to all images.

Measurement of ATP and Lactate

Total cellular ATP was measured using the ATP-based CellTiter-Glo kit (Promega) according to the manufacturer's instructions. Each well on a 96 well plate was seeded with 2,000 cells, which were incubated with compounds at designated concentrations over varying time points (1, 2, 4, and 24 hr). Luminescence was measured on a Tecan M200 Infinite plate reader. Mitochondrial ATP levels were determined using the mitochondrial ATP sensor protein A_{TEAM} as reported (Imamura et al., 2009) and described in the [Supplemental Information](#). For lactate measurement, 10⁵ cells were plated per well on a six well plate and treated with compounds over 6, 24, or 72 hr. Cell culture supernatant (500 μ l) was collected and centrifuged to remove any cellular debris. Subsequently, an aliquot of 100 μ l was analyzed using Roche's automated Modular Analytics system.

In Vivo Melanoma Models

All animal experiments were performed in accordance with institutional and national guidelines and regulations. The protocols have been approved by the Wistar IACUC or the Saarland Veterinary Administration. NSG and severe combined immunodeficiency (SCID) beige mice were used for xenotransplantation. WM3734 or SKMel28 human melanoma cells were subcutaneously injected at a Matrigel/culture medium ratio of 1:1. Mice were treated with (1) bortezomib every other day (20 μ g per intraperitoneal injection), (2) with vemurafenib every 12 hr (100 mg/kg per oral gavage), or (3) for combination studies with vemurafenib (15 mg/kg) plus phenformin (150 mg/kg; Appleyard et al., 2012) every 12 hr. Buffered saline or 0.1% Tween 80/0.5% methylcellulose served as vehicle controls. Treatment started at an average tumor volume of \sim 120–200 mm³. Tumor growth was measured every 2 or 3 days using a caliper. Tumor volumes were calculated according to the formula $V = W \times D \times H$ [mm³].

Statistics

MANOVA was used to evaluate differences between treatment groups; the change in the natural logarithm of volume over time was estimated for each animal from a linear regression, and mean slopes were compared using a t test. For the SKMel28 animal study, p values were adjusted according to Hochberg (1988). The two-sided Wilcoxon two-sample test was used when assumptions for the t test were violated (Figure 3A); otherwise, the Student's

t test was used. Box plots show the sample minimum (lower whisker), the lower quartile (bottom of the box), the median (line inside the box), the upper quartile (top of the box), and the sample maximum (upper whisker). A p value of less than 0.05 was considered significant. As software tools, SAS version 9.2 using Proc GLM and Microsoft Excel were used.

SUPPLEMENTAL INFORMATION

Supplemental Information includes Supplemental Experimental Procedures, six figures, and one table and can be found with this article online at <http://dx.doi.org/10.1016/j.ccr.2013.05.003>.

ACKNOWLEDGMENTS

We thank K. Speicher and T. Beer (Wistar Proteomics Facility), J. Hayden and F. Keeney (Wistar Microscopy Facility), J.S. Faust (Wistar Flow Cytometry Facility), R. DelGiaccio (Wistar Histology Facility), C. Junker and R. Kappl (Department of Biophysics, The Saarland University), and A. Liu (Department of Neurology, The Saarland University Hospital) for technical support and S. Kugler, H. Palm, A. Stark, A. Kerber, R. Koerner (Department of Dermatology, The Saarland University Hospital), and G. Rajan (Wistar Melanoma Research Center) for technical assistance. The animals were housed at Wistar's Animal Facility and the Institute for Clinical and Experimental Surgery, The Saarland University. Lactate measurement was done at the Department of Clinical Chemistry of The Saarland University Hospital. We also thank N. Demaurex, H. Imamura, and H. Noji for providing the A_{TEAM} probe, V. Belousov for Hyper, and B. Niemeyer for the JARID1B pCAGGS-IRES-RFP construct. The research was funded by NIH grants CA25874, CA047159, and CA10815, the Dr. Miriam and Scheldon G. Adelson Medical Research Foundation, and DFG grants SFB1027 project C4, SFB 894 (A1), R3577/2-1, and R3577/3-1.

Received: May 31, 2012

Revised: November 28, 2012

Accepted: May 1, 2013

Published: June 10, 2013

REFERENCES

- Appleyard, M.V., Murray, K.E., Coates, P.J., Wullschlegel, S., Bray, S.E., Kernohan, N.M., Fleming, S., Alessi, D.R., and Thompson, A.M. (2012). Phenformin as prophylaxis and therapy in breast cancer xenografts. *Br. J. Cancer* **106**, 1117–1122.
- Berridge, M.V., Herst, P.M., and Tan, A.S. (2010). Metabolic flexibility and cell hierarchy in metastatic cancer. *Mitochondrion* **10**, 584–588.
- Blagosklonny, M.V. (2005). Why therapeutic response may not prolong the life of a cancer patient: selection for oncogenic resistance. *Cell Cycle* **4**, 1693–1698.
- Caro, P., Kishan, A.U., Norberg, E., Stanley, I.A., Chapuy, B., Ficarro, S.B., Polak, K., Tondera, D., Gounarides, J., Yin, H., et al. (2012). Metabolic signatures uncover distinct targets in molecular subsets of diffuse large B cell lymphoma. *Cancer Cell* **22**, 547–560.
- Charton, C., Ulaszewski, S., da Silva Vieira, M.R., Henoux, V., and Claisse, M.L. (2004). Effects of oligomycins on adenosine triphosphatase activity of mitochondria isolated from the yeasts *Saccharomyces cerevisiae* and *Schwanniomyces castellii*. *Biochem. Biophys. Res. Commun.* **318**, 67–72.
- Chen, K.G., Valencia, J.C., Gillet, J.P., Hearing, V.J., and Gottesman, M.M. (2009). Involvement of ABC transporters in melanogenesis and the development of multidrug resistance of melanoma. *Pigment Cell Melanoma Res.* **22**, 740–749.
- Chen, J., Li, Y., Yu, T.S., McKay, R.M., Burns, D.K., Kernie, S.G., and Parada, L.F. (2012). A restricted cell population propagates glioblastoma growth after chemotherapy. *Nature* **488**, 522–526.
- Christensen, J., Agger, K., Cloos, P.A., Pasini, D., Rose, S., Sennels, L., Rappsilber, J., Hansen, K.H., Salcini, A.E., and Helin, K. (2007). RBP2 belongs to a family of demethylases, specific for tri- and dimethylated lysine 4 on histone 3. *Cell* **128**, 1063–1076.
- Dey, B.K., Stalker, L., Schnerch, A., Bhatia, M., Taylor-Papadimitriou, J., and Wynder, C. (2008). The histone demethylase KDM5b/JARID1b plays a role in cell fate decisions by blocking terminal differentiation. *Mol. Cell. Biol.* **28**, 5312–5327.
- Grazette, L.P., Boecker, W., Matsui, T., Semigran, M., Force, T.L., Hajjar, R.J., and Rosenzweig, A. (2004). Inhibition of ErbB2 causes mitochondrial dysfunction in cardiomyocytes: implications for herceptin-induced cardiomyopathy. *J. Am. Coll. Cardiol.* **44**, 2231–2238.
- Gupta, P.B., Onder, T.T., Jiang, G., Tao, K., Kuperwasser, C., Weinberg, R.A., and Lander, E.S. (2009). Identification of selective inhibitors of cancer stem cells by high-throughput screening. *Cell* **138**, 645–659.
- Hao, W., Chang, C.P., Tsao, C.C., and Xu, J. (2010). Oligomycin-induced bioenergetic adaptation in cancer cells with heterogeneous bioenergetic organization. *J. Biol. Chem.* **285**, 12647–12654.
- Hochberg, Y. (1988). A sharper Bonferroni procedure for multiple tests of significance. *Biometrika* **75**, 800–802.
- Imamura, H., Nhat, K.P., Togawa, H., Saito, K., Iino, R., Kato-Yamada, Y., Nagai, T., and Noji, H. (2009). Visualization of ATP levels inside single living cells with fluorescence resonance energy transfer-based genetically encoded indicators. *Proc. Natl. Acad. Sci. USA* **106**, 15651–15656.
- Johannessen, C.M., Boehm, J.S., Kim, S.Y., Thomas, S.R., Wardwell, L., Johnson, L.A., Emery, C.M., Stransky, N., Cogdill, A.P., Barretina, J., et al. (2010). COT drives resistance to RAF inhibition through MAP kinase pathway reactivation. *Nature* **468**, 968–972.
- Jose, C., Bellance, N., and Rossignol, R. (2011). Choosing between glycolysis and oxidative phosphorylation: a tumor's dilemma? *Biochim. Biophys. Acta* **1807**, 552–561.
- Nazarian, R., Shi, H., Wang, Q., Kong, X., Koya, R.C., Lee, H., Chen, Z., Lee, M.K., Attar, N., Sazegar, H., et al. (2010). Melanomas acquire resistance to B-RAF(V600E) inhibition by RTK or N-RAS upregulation. *Nature* **468**, 973–977.
- Poulikakos, P.I., Persaud, Y., Janakiraman, M., Kong, X., Ng, C., Moriceau, G., Shi, H., Atefi, M., Titz, B., Gabay, M.T., et al. (2011). RAF inhibitor resistance is mediated by dimerization of aberrantly spliced BRAF(V600E). *Nature* **480**, 387–390.
- Roesch, A., Becker, B., Meyer, S., Wild, P., Hafner, C., Landthaler, M., and Vogt, T. (2005). Retinoblastoma-binding protein 2-homolog 1: a retinoblastoma-binding protein downregulated in malignant melanomas. *Mod. Pathol.* **18**, 1249–1257.
- Roesch, A., Becker, B., Schneider-Brachert, W., Hagen, I., Landthaler, M., and Vogt, T. (2006). Re-expression of the retinoblastoma-binding protein 2-homolog 1 reveals tumor-suppressive functions in highly metastatic melanoma cells. *J. Invest. Dermatol.* **126**, 1850–1859.
- Roesch, A., Mueller, A.M., Stempf, T., Moehle, C., Landthaler, M., and Vogt, T. (2008). RBP2-H1/JARID1B is a transcriptional regulator with a tumor suppressive potential in melanoma cells. *Int. J. Cancer* **122**, 1047–1057.
- Roesch, A., Fukunaga-Kalabis, M., Schmidt, E.C., Zabierowski, S.E., Brafford, P.A., Vultur, A., Basu, D., Gimotty, P., Vogt, T., and Herlyn, M. (2010). A temporally distinct subpopulation of slow-cycling melanoma cells is required for continuous tumor growth. *Cell* **141**, 583–594.
- Scott, D.A., Richardson, A.D., Filipp, F.V., Knutzen, C.A., Chiang, G.G., Ronai, Z.A., Osterman, A.L., and Smith, J.W. (2011). Comparative metabolic flux profiling of melanoma cell lines: beyond the Warburg effect. *J. Biol. Chem.* **286**, 42626–42634.
- Sharma, S.V., Lee, D.Y., Li, B., Quinlan, M.P., Takahashi, F., Maheswaran, S., McDermott, U., Azizian, N., Zou, L., Fischbach, M.A., et al. (2010). A chromatin-mediated reversible drug-tolerant state in cancer cell subpopulations. *Cell* **141**, 69–80.
- Smalley, K.S., Haass, N.K., Brafford, P.A., Lioni, M., Flaherty, K.T., and Herlyn, M. (2006). Multiple signaling pathways must be targeted to overcome drug resistance in cell lines derived from melanoma metastases. *Mol. Cancer Ther.* **5**, 1136–1144.
- Sosman, J.A., Kim, K.B., Schuchter, L., Gonzalez, R., Pavlick, A.C., Weber, J.S., McArthur, G.A., Hutson, T.E., Moschos, S.J., Flaherty, K.T., et al.

- (2012). Survival in BRAF V600-mutant advanced melanoma treated with vemurafenib. *N. Engl. J. Med.* 366, 707–714.
- Vander Heiden, M.G., Cantley, L.C., and Thompson, C.B. (2009). Understanding the Warburg effect: the metabolic requirements of cell proliferation. *Science* 324, 1029–1033.
- Villanueva, J., Vultur, A., Lee, J.T., Somasundaram, R., Fukunaga-Kalabis, M., Cipolla, A.K., Wubbenhorst, B., Xu, X., Gimotty, P.A., Kee, D., et al. (2010). Acquired resistance to BRAF inhibitors mediated by a RAF kinase switch in melanoma can be overcome by cotargeting MEK and IGF-1R/PI3K. *Cancer Cell* 18, 683–695.
- Wagle, N., Emery, C., Berger, M.F., Davis, M.J., Sawyer, A., Pochanard, P., Kehoe, S.M., Johannessen, C.M., Macconail, L.E., Hahn, W.C., et al. (2011). Dissecting therapeutic resistance to RAF inhibition in melanoma by tumor genomic profiling. *J. Clin. Oncol.* 29, 3085–3096.
- Warburg, O., Posener, K., and Negelein, E. (1924). Ueber den stoffwechsel der tumoren. *Biochem. Z.* 152, 319–344.
- Weinberg, F., Hamanaka, R., Wheaton, W.W., Weinberg, S., Joseph, J., Lopez, M., Kalyanaraman, B., Mutlu, G.M., Budinger, G.R., and Chandel, N.S. (2010). Mitochondrial metabolism and ROS generation are essential for Kras-mediated tumorigenicity. *Proc. Natl. Acad. Sci. USA* 107, 8788–8793.
- White, R.M., Cech, J., Ratanasirintrao, S., Lin, C.Y., Rahl, P.B., Burke, C.J., Langdon, E., Tomlinson, M.L., Mosher, J., Kaufman, C., et al. (2011). DHODH modulates transcriptional elongation in the neural crest and melanoma. *Nature* 471, 518–522.
- Xia, X., Lemieux, M.E., Li, W., Carroll, J.S., Brown, M., Liu, X.S., and Kung, A.L. (2009). Integrative analysis of HIF binding and transactivation reveals its role in maintaining histone methylation homeostasis. *Proc. Natl. Acad. Sci. USA* 106, 4260–4265.
- Yamane, K., Tateishi, K., Klose, R.J., Fang, J., Fabrizio, L.A., Erdjument-Bromage, H., Taylor-Papadimitriou, J., Tempst, P., and Zhang, Y. (2007). PLU-1 is an H3K4 demethylase involved in transcriptional repression and breast cancer cell proliferation. *Mol. Cell* 25, 801–812.

SYK Inhibition Modulates Distinct PI3K/AKT-Dependent Survival Pathways and Cholesterol Biosynthesis in Diffuse Large B Cell Lymphomas

Linfeng Chen,¹ Stefano Monti,^{3,7} Przemyslaw Juszczynski,^{1,8} Jing Ouyang,¹ Bjoern Chapuy,¹ Donna Neuberg,² John G. Doench,³ Agata M. Bogusz,^{4,9} Thomas M. Habermann,⁵ Ahmet Dogan,⁶ Thomas E. Witzig,⁵ Jeffery L. Kutok,^{4,10} Scott J. Rodig,⁴ Todd Golub,³ and Margaret A. Shipp^{1,*}

¹Department of Medical Oncology

²Department of Biostatistics

Dana Farber Cancer Institute, Boston, MA 02215, USA

³Cancer Program, Broad Institute of MIT and Harvard, Cambridge, MA 02142, USA

⁴Department of Pathology, Brigham and Women's Hospital, Boston, MA 02115, USA

⁵Department of Medicine

⁶Department of Pathology

Mayo Clinic, Rochester, MN 55905, USA

⁷Current address: Section of Computational Biomedicine, Boston University School of Medicine, Boston, MA 02118, USA

⁸Current address: Instytut Hematologii i Transfuzjologii, Poland, Warszawa 02-776

⁹Current address: Department of Pathology, Beth Israel and Deaconess Medical Center, Boston, MA 02215, USA

¹⁰Current address: Infinity Pharmaceuticals, Cambridge, MA 02139, USA

*Correspondence: margaret_shipp@dfci.harvard.edu

<http://dx.doi.org/10.1016/j.ccr.2013.05.002>

SUMMARY

B cell receptor (BCR) signaling pathway components represent promising treatment targets in diffuse large B cell lymphoma (DLBCL) and additional B cell tumors. BCR signaling activates spleen tyrosine kinase (SYK) and downstream pathways including PI3K/AKT and NF- κ B. In previous studies, chemical SYK blockade selectively decreased BCR signaling and induced apoptosis of BCR-dependent DLBCLs. Herein, we characterize distinct SYK/PI3K-dependent survival pathways in DLBCLs with high or low baseline NF- κ B activity including selective repression of the pro-apoptotic HRK protein in NF- κ B-low tumors. We also define SYK/PI3K-dependent cholesterol biosynthesis as a feed-forward mechanism of maintaining the integrity of BCRs in lipid rafts in DLBCLs with low or high NF- κ B. In addition, SYK amplification and *PTEN* deletion are identified as selective genetic alterations in primary “BCR”-type DLBCLs.

INTRODUCTION

Several lines of evidence support the role of B cell receptor (BCR)-mediated survival signals in certain B cell malignancies (Chen et al., 2008; Gupta and DeFranco, 2007; Küppers, 2005; Young et al., 2009). The BCR complex includes membrane-bound immunoglobulin and the disulfide-linked heterodimer, immunoglobulin- α (Ig α) and Ig β (also termed CD79A and CD79B, respectively). BCR signaling induces receptor oligomer-

ization and phosphorylation of Ig α and Ig β immunoreceptor tyrosine-based activation motifs (ITAMS) by Src family kinases. Following ITAM phosphorylation, the spleen tyrosine kinase (SYK) is recruited and activated, engaging additional adaptor proteins and initiating downstream signaling through phosphatidylinositol-3-kinase (PI3K), NF- κ B, extracellular signal-related kinase (ERK)-mitogen-activated protein kinase (MAPK), and NFAT pathways. After ligand binding, BCRs cluster and rapidly associate with cholesterol-enriched membrane microdomains

Significance

Chemical inhibitors of SYK and additional proximal BCR pathway components are in clinical trials in patients with DLBCL and additional B cell malignancies. However, the BCR-dependent survival pathways and respective roles of proximal components such as SYK and PI3K and distal NF- κ B signaling remain to be defined. We delineate the downstream signaling, apoptotic, and metabolic pathways perturbed by chemical inhibition or molecular depletion of SYK/PI3K and identify additional genetic bases for enhanced BCR signaling in DLBCLs. These functional and genetic studies further define BCR-dependent DLBCLs and provide a framework for analyzing targeted inhibition of SYK, PI3K, and additional proximal components of the BCR signaling pathway in these tumors.

termed lipid rafts (Dykstra et al., 2003; Gupta and DeFranco, 2007). SYK is recruited to BCR clusters associated with lipid rafts and protein tyrosine phosphorylation is enhanced in these regions (Gupta and DeFranco, 2007).

In addition to ligand-induced receptor aggregation and activation, normal mature B cells rely upon “tonic” BCR-dependent survival signals (Kraus et al., 2004; Monroe, 2006; Srinivasan et al., 2009; Torres et al., 1996). Tonic BCR signaling was initially defined in murine models in which BCR ablation or Ig α mutation triggered the apoptosis of normal mature B cells (Kraus et al., 2004; Lam et al., 1997). In follow-up studies, BCR ablation was combined with activation of specific BCR-dependent signaling cascades to delineate the nature of tonic BCR survival signals (Srinivasan et al., 2009). PI3K/AKT signaling, but not NF- κ B or MAPK kinase activation, rescued the survival of BCR-deficient B cells (Srinivasan et al., 2009). These studies defined important differences between PI3K/AKT-dependent tonic BCR survival signals and those resulting from activation of additional downstream pathways following BCR engagement (Srinivasan et al., 2009).

Diffuse large B cell lymphomas (DLBCLs) are clinically and genetically heterogeneous disorders in which subsets of tumors share certain molecular features. In the cell-of-origin (COO) classification, groups of DLBCLs share components of their transcriptional profiles with normal B cell subtypes, including germinal center B cells (GC) and activated B cells (ABC) (Wright et al., 2003). In comparison to GC DLBCLs, ABC tumors more frequently exhibit constitutive activation of NF- κ B and genetic alterations of several NF- κ B pathway components (Compagno et al., 2009; Davis et al., 2001; Rosenwald et al., 2002). This group of DLBCLs is also reported to have more frequent somatic mutations of the Ig α or Ig β subunits and altered BCR surface expression, a process termed “chronic active BCR signaling” (Davis et al., 2010). Certain BCR-dependent “ABC” DLBCL cell lines also exhibit constitutive PI3K activation, which modulates downstream NF- κ B signaling (Kloo et al., 2011).

Using an alternative approach to define DLBCLs with shared molecular features, we previously applied consensus clustering methods to the transcriptional profiles of primary DLBCLs and identified three highly reproducible tumor groups: BCR, OxPhos (oxidative phosphorylation), and HR (host response) (Monti et al., 2005). “BCR” DLBCLs had increased expression of multiple components of the BCR signaling pathway including SYK (Monti et al., 2005) prompting speculation that these lymphomas relied upon SYK/BCR-mediated survival signals (Chen et al., 2008). This hypothesis was of additional interest given the known role of SYK in tonic BCR signaling (Monroe, 2006) and malignant B cell survival (Chen et al., 2006).

For these reasons, we previously assessed the *in vitro* efficacy of an ATP-competitive inhibitor of SYK525/526 phosphorylation and activation, R406, in DLBCL cell lines and primary tumors (Chen et al., 2008). Chemical SYK blockade selectively decreased the proliferation and induced apoptosis of surface slg $^{+}$ DLBCL cell lines with intact BCR signaling (Chen et al., 2008). In R406-sensitive DLBCL cell lines, the compound specifically inhibited both baseline- and ligand-induced autophosphorylation of SYK525/526 and SYK-dependent phosphorylation of BCR signaling components such as B cell linker protein BLNK (Chen et al., 2008). The majority of examined slg $^{+}$ primary

DLBCLs also exhibited baseline and ligand-induced BCR activity. In these primary tumors, BCR signaling, as reflected by intracellular phospho-BLNK (p-BLNK) expression, was also inhibited by R406 (Chen et al., 2008).

We subsequently performed a clinical trial of the oral SYK inhibitor, fostamatinib (R788), of which R406 is a prodrug, in patients with recurrent B cell non-Hodgkin lymphoma (B-NHL) and found that 22% of patients with DLBCL and 50% of patients with small lymphocytic lymphoma/chronic lymphocytic leukemia responded to treatment (Friedberg et al., 2010). Other investigators also demonstrated the efficacy of chemical inhibition or molecular depletion of SYK in BCR-dependent DLBCL cell lines and *in vivo* murine lymphoma models (Cheng et al., 2011; Rinaldi et al., 2011; Young et al., 2009). We also recently defined distinct fuel utilization programs in BCR-dependent and BCR-independent/OxPhos DLBCLs (Caro et al., 2012).

Although BCR signaling is an attractive rational therapeutic target and chemical inhibitors of SYK and additional proximal BCR-pathway components have demonstrated efficacy in early clinical trials (Friedberg et al., 2010; Hendriks, 2011; Herman et al., 2011; Lannutti et al., 2011; Robertson et al., 2007), subtype-specific effector pathways and underlying genetic mechanisms are incompletely understood. In addition, the consequences of inhibiting BCR signaling in tumors assigned to different transcriptional subtypes require further definition. Herein, we characterize the downstream signaling, apoptotic, and metabolic pathways altered by chemical or molecular SYK inhibition and identify additional genetic bases for enhanced BCR signaling in DLBCLs.

RESULTS

SYK Depletion Selectively Inhibits the Proliferation of BCR-Dependent DLBCL Cell Lines

To further characterize SYK as a potential target, we depleted SYK with multiple independent shRNAs, then assessed cellular proliferation in a panel of DLBCL cell lines that captured known functional distinctions: BCR dependence versus independence and ABC versus GC transcriptional subtype. The panel included BCR-dependent/GC lines (DHL4 and LY7), BCR-dependent/ABC lines (HBL-1 and U-2932), and BCR-independent lines (K422 and LY4, otherwise classified as “OxPhos”) (Caro et al., 2012; Chen et al., 2008; Figures S1A–S1E available online). SYK knockdown significantly decreased the proliferation of all BCR-dependent lines but had little effect on the growth of BCR-independent lines (Figures 1A and 1B; Figure S1F). The selectivity of molecular SYK depletion for BCR-dependent DLBCLs closely mirrors that of the chemical SYK inhibitor, R406 (Figure 1B; Figures S1D–S1F; Chen et al., 2008).

SYK- and PI3K-Dependent BCR Signaling in DLBCLs with High Baseline NF- κ B

A subset of DLBCL primary tumors and cell lines exhibits high baseline NF- κ B activity and multiple genetic alterations of NF- κ B pathway components (Compagno et al., 2009; Davis et al., 2001; Lenz et al., 2008). We therefore characterized signaling pathways affected by SYK inhibition in DLBCLs with high versus low baseline NF- κ B activity. First, we assessed the baseline NF- κ B activity in a panel of eight DLBCL cell lines,

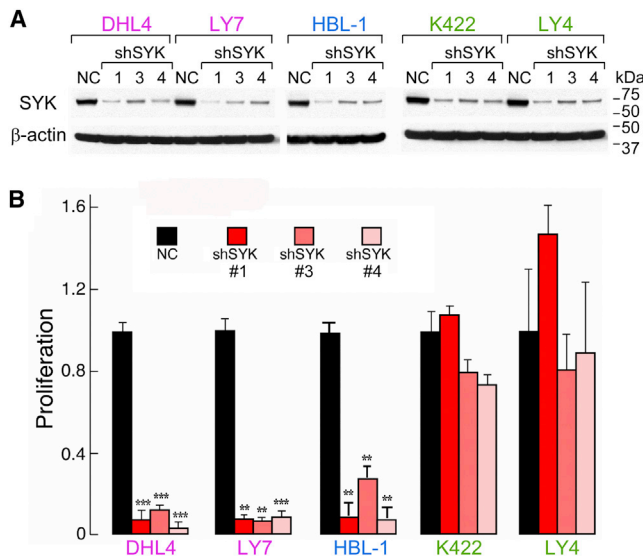


Figure 1. Cellular Proliferation of DLBCL Cell Lines following SYK Depletion

(A) The SYK protein level in cell lysates prepared from the indicated cell lines transduced with a negative control (NC) shRNA or the indicated SYK shRNAs was assessed by immunoblotting. β -actin, loading control.

(B) Cellular proliferation of SYK-depleted DLBCL cell lines was measured 72 hr after puromycin selection by MTS assay. The proliferation of SYK-depleted cells is relative to that of NC cells. Error bars represent SD of three independent assays from a representative experiment. The p values for NC versus each SYK shRNA were determined with a one-sided Welch t test. ***p \leq 0.0001; **p \leq 0.001. See also Figure S1.

including the six used above and an additional BCR-dependent/GC line (DHL6) and another BCR-independent (Toledo) line (Chen et al., 2008; Caro et al., 2012). As expected, baseline NF- κ B activity was higher in the BCR-dependent/ABC lines than in the BCR-dependent/GC lines (Figure 2A; Davis et al., 2001). R406 treatment significantly decreased the high baseline NF- κ B activity in HBL-1 and U-2932 and also reduced the low baseline activity in DHL4, DHL6, and LY7, but had no effect on the BCR-independent lines (Figure 2A).

To further characterize the consequences of chemical SYK inhibition in the BCR-dependent DLBCL cell lines with high or low baseline NF- κ B activity, we performed transcriptional profiling of all five lines at baseline and following 6 and 24 hr treatment with R406 or DMSO (vehicle). At each time point, the genes that were differentially expressed between the vehicle and R406-treated samples (FDR-corrected q-values \leq 0.01 and fold changes \geq 1.5 \times) were analyzed for pathway enrichment (Figures S2A–S2C; Table S1).

In contrast to the NF- κ B-low lines, NF- κ B-high lines exhibited significant downregulation of TNF, TNFR2, NF- κ B, CD40, and RELA pathway components including multiple common NF- κ B target genes (Figures S2B and S2C; Table S1). Independently, we also performed gene set enrichment analysis (GSEA) of vehicle- versus R406-treated cell lines using functionally defined series of NF- κ B target genes (Davis et al., 2010; Schreiber et al., 2006). With this approach, we identified statistically significant, concordant downregulation of multiple functionally validated

NF- κ B target genes in the NF- κ B-high DLBCL cell lines following R406 treatment (Figures 2B and 2C). In contrast, GSEA revealed no significant modulation of NF- κ B target gene sets in the NF- κ B-low DLBCL cell lines (data not shown). We further assessed the transcript abundance of 4 of these NF- κ B targets (BCL2A1 [also known as BFL-1/A1], TNF, CD40, and TRAF1; Figure 2C) in the full series of eight DLBCL lines treated with vehicle or R406 using qRT-PCR. All four NF- κ B targets were selectively and significantly downregulated in the BCR-dependent NF- κ B-high DLBCL cell lines (Figure 2D; Figure S2D).

Given the demonstrated role of the NF- κ B target, BCL2A1, in B cell survival and resistance to apoptosis (Lee et al., 1999; Ottina et al., 2012; Zong et al., 1999), we also evaluated BCL2A1 protein expression in DLBCLs treated with vehicle or R406. The two BCR-dependent NF- κ B-high lines, HBL-1 and U-2932, had abundant baseline BCL2A1 protein expression that decreased following R406 treatment whereas BCR-dependent NF- κ B-low lines (DHL4, DHL6, and LY7) and BCR-independent lines (K422, Toledo, and LY4) had much lower BCL2A1 expression (Figure 2E). We also depleted SYK with multiple independent shRNAs and evaluated BCL2A1 transcript abundance in two BCR-dependent NF- κ B-high DLBCL lines (HBL-1 and U-2932) and a BCR-dependent NF- κ B-low line (DHL4). SYK knockdown significantly decreased BCL2A1 transcript abundance in the NF- κ B-high lines and also reduced the modest BCL2A1 expression in the NF- κ B-low line (Figure 2F).

Given the recently described role of PI3K signaling in modulating NF- κ B activity in certain DLBCL cell lines (Kloo et al., 2011), we next treated BCR-dependent lines with PI3K inhibitor, LY294002, and evaluated NF- κ B activity and BCL2A1 expression. In DLBCL cell lines with high baseline NF- κ B (HBL-1 and U-2932), PI3K inhibition significantly decreased NF- κ B activity and BCL2A1 abundance (Figures 2G and 2H). Together, these data confirm that NF- κ B activity is modulated by BCR-dependent SYK and PI3K signaling in certain “ABC” DLBCL cell lines.

SYK- and PI3K-Dependent BCR Signaling in DLBCLs with Low Baseline NF- κ B

Previous murine models of tonic BCR signaling implicated PI3K/AKT activation and FOXO1 modulation in normal B cell survival, independent of NF- κ B (Srinivasan et al., 2009). These data prompted us to evaluate the role of PI3K/AKT in BCR-dependent DLBCLs with low baseline NF- κ B activity.

Representative BCR-dependent DLBCL cell lines with low baseline NF- κ B activity, DHL4, DHL6 and LY7, were infected with either a pMIG empty vector or the pMIG-mAKT1-IRES-GFP (mAKT) vector which encodes constitutively active AKT1. GFP⁺ cells were sorted by flow cytometry, treated with R406 or vehicle control and analyzed for p-AKT expression and cellular proliferation. All three BCR-dependent DLBCL cell lines infected with the control pMIG vector exhibited baseline AKT phosphorylation that was inhibited by R406 (Figure 3A). As expected, expression of mAKT increased the level of p-AKT, which was not significantly affected by R406 (Figure 3A). Expression of mAKT largely protected these BCR-dependent DLBCLs from chemical SYK inhibition (Figure 3B). Although mAKT may signal to a larger series of targets than endogenous AKT, these studies nonetheless highlight the role of PI3K/AKT in SYK-dependent survival signals.

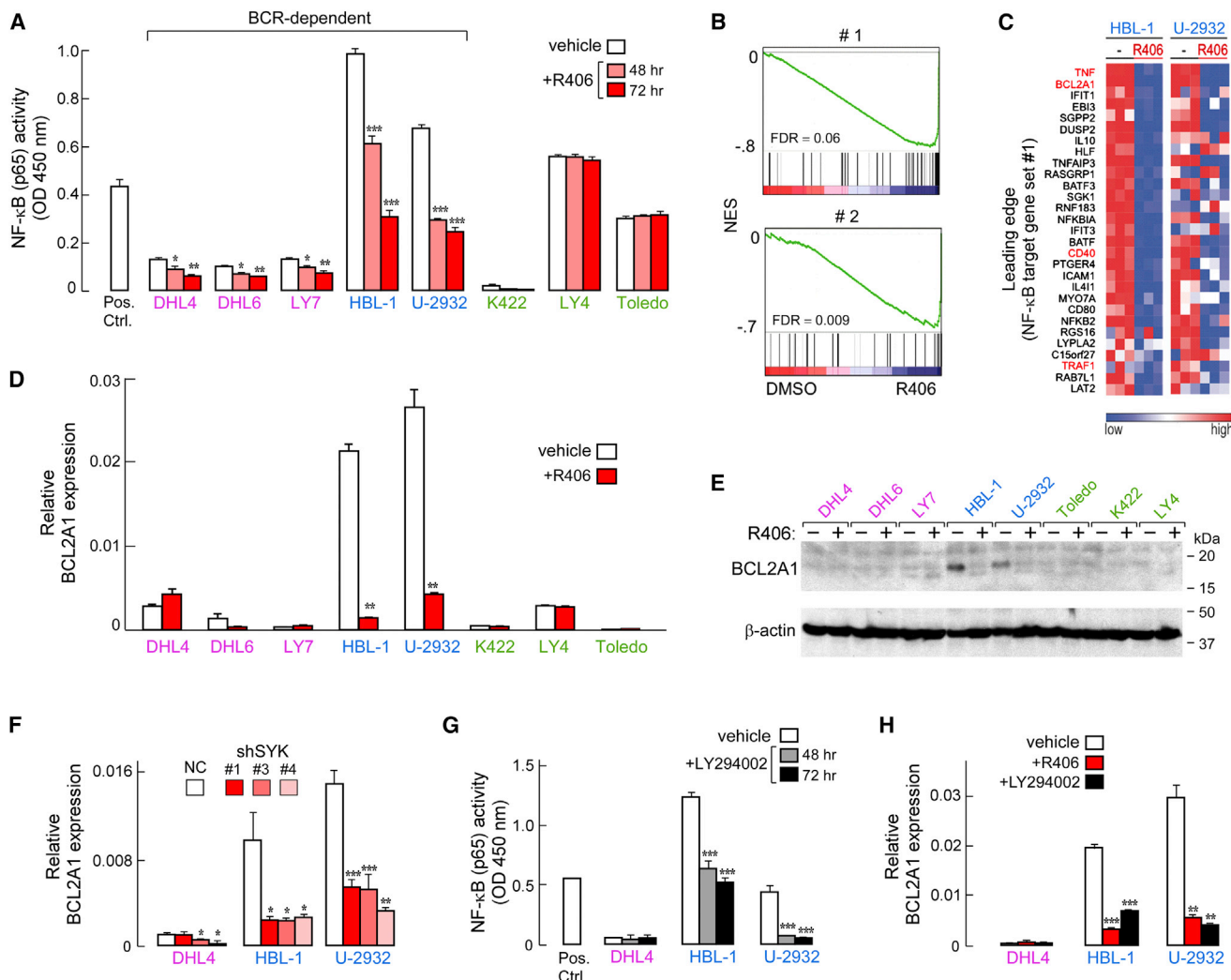


Figure 2. SYK- and PI3K-Dependent BCR Signaling in DLBCLs with High Baseline NF- κ B

(A) NF- κ B (p65) activity was determined in vehicle and R406-treated DLBCL cell lines. Pos. Ctrl., manufacturer's positive control. BCR-dependent NF- κ B-low lines, purple; BCR-dependent NF- κ B-high lines, blue; BCR-independent OxPhos lines, green.

(B) GSEA of NF- κ B targets was performed in vehicle- versus R406-treated DLBCL cell lines with high-baseline NF- κ B activity (HBL-1 and U-2932). The 19K genes in the genome were sorted from highest (left, red) to lowest (right, blue) relative expression in vehicle- versus R406-treated lines (horizontal axis). Note that the positions of the NF- κ B targets (set #1, Davis et al., 2010; and set #2, Schreiber et al., 2006) were significantly skewed toward the right end of the sorted list, reflecting their statistically significant downregulation in R406-treated lines.

(C) Relative abundance of NF- κ B target genes in vehicle- versus R406-treated DLBCL cell lines with high baseline NF- κ B activity was displayed with a colometric scale. NF- κ B target genes derived from the GSEA leading edge, set #1 (Davis et al., 2010).

(D) BCL2A1 transcript abundance in DLBCL cell lines treated with vehicle or R406 (24 hr) was determined by qRT-PCR relative to PPIA.

(E) BCL2A1 protein abundance in vehicle- and R406-treated DLBCL cell lines was assessed by immunoblotting. β -actin, loading control.

(F) BCL2A1 transcript abundance in SYK-depleted DLBCL cell lines (72 hr following completion of puromycin selection) was determined by qRT-PCR relative to PPIA.

(G) NF- κ B (p65) activity was determined in DLBCL cell lines treated with the PI3K inhibitor LY294002 or vehicle.

(H) BCL2A1 transcript abundance in DLBCL cell lines treated with LY294002, R406, or vehicle (24 hr) was assessed by qRT-PCR relative to PPIA.

In (A), (D), and (F)–(H), p values for control versus treated were determined with a one-sided Welch t test. ***p < 0.0001; **p < 0.001; *p < 0.01. Error bars represent the SD of three independent assays in a representative experiment.

See also Figure S2 and Table S1.

PI3K/AKT signaling phosphorylates the FOXO1 transcription factor resulting in its nuclear exclusion and degradation and decreased FOXO1 activity (Fu and Tindall, 2008; Srinivasan et al., 2009). Given the role of PI3K/AKT in mediating SYK/BCR survival signals, we assessed nuclear FOXO1 expression in

R406-treated BCR-dependent DLBCLs. In addition to directly visualizing FOXO1 by immunofluorescence (Figure 3C, left), nuclear FOXO1 staining was quantified (Figure 3C, right). In each of the BCR-dependent DLBCL cell lines, chemical SYK/BCR inhibition significantly increased the nuclear localization of

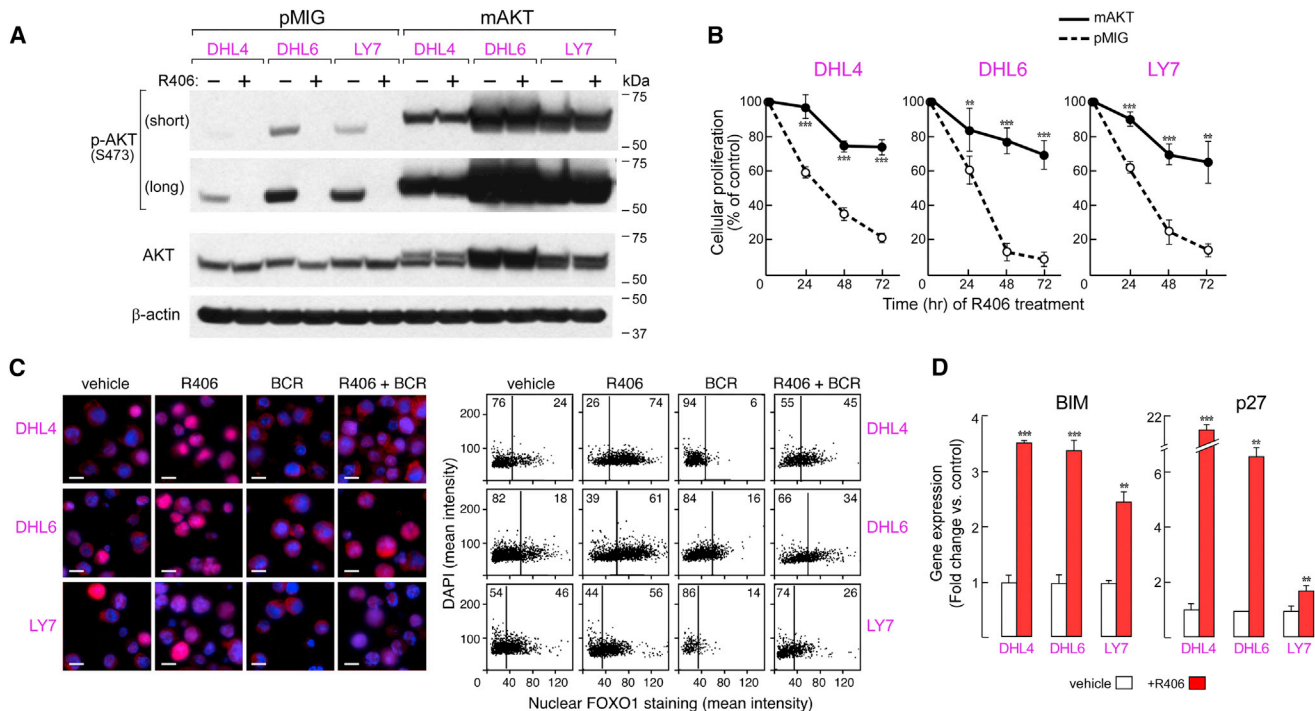


Figure 3. SYK and PI3K-Dependent Signaling in DLBCLs with Low Baseline NF- κ B

(A and B) DHL4, DHL6, and LY7 cell lines were retrovirally transduced with mAKT or pMIG vector, FACS-sorted for GFP expression, treated for 24 hr with R406 or vehicle, then analyzed for p-AKT(S473) and total AKT by immunoblotting (A) and for proliferation (B).

(C) DLBCL cell lines were incubated with R406 or vehicle for 1 hr, BCR cross-linked (BCR) or left untreated, fixed, then stained with DAPI (blue) and with Cy3-conjugated anti-FOXO1 antibody (red) (left). Scale bar represents 10 μ m. The mean nuclear staining intensity of Cy3-conjugated-FOXO1 was quantified for each cell and plotted against its mean DAPI staining intensity (right).

(D) The transcript abundance of FOXO1 target genes, p27 and BIM, in DLBCL cell lines treated with R406 or vehicle for 24 hr was assessed by qRT-PCR relative to PPIA. The p values for mAKT versus pMIG (control) at each time point (B) and for vehicle versus R406 (D) were determined with a one-sided Welch t test. ***p \leq 0.0001; **p \leq 0.001. Error bars represent the SD of three independent assays in a representative experiment.

See also Figure S3.

FOXO1 at baseline and following BCR crosslinking (Figure 3C). Similar results were obtained in additional BCR-dependent, but not BCR-independent, DLBCL cell lines (Figures S3A and S3B). Consistent with these observations, R406 treatment selectively induced expression of the FOXO1 target genes, BIM and p27, in BCR-dependent, but not BCR-independent, DLBCL cell lines (Figure 3D; Figure S3C).

SYK Inhibition Induces the Pro-Apoptotic BCL2 Family Member, HRK

We next assessed the transcriptional profiles of R406-treated BCR-dependent NF- κ B-low DLBCLs for potential selective apoptotic mechanisms. Differential analysis revealed selective upregulation of the pro-apoptotic BCL2 family member, HRK, in NF- κ B-low DLBCLs following chemical SYK inhibition (Figure S4A). Although little is known about the role of HRK in lymphoid cells, this BH3-only protein is specifically induced by growth factor withdrawal in hematopoietic progenitors, leading to cell death (Nakamura et al., 2008; Sanz et al., 2000). For this reason, HRK induction was also evaluated by qRT-PCR in the full panel of BCR-dependent and -independent DLBCL cell lines treated with R406. Chemical SYK inhibition selectively induced HRK in BCR-dependent NF- κ B-low cell lines (DHL4, DHL6,

and LY7); in contrast, HRK was not comparably upregulated in BCR-dependent NF- κ B-high cell lines (HBL-1 and U-2932) or BCR-independent cell lines (K422, LY4, Toledo) (Figure 4A). SYK depletion also selectively induced HRK expression in BCR-dependent DLBCL cell lines with low baseline NF- κ B activity (Figure 4B).

Given the role of PI3K/AKT in mediating SYK/BCR survival signals in these DLBCLs (Figure 3B), we asked whether PI3K/AKT also modulated HRK expression. In the BCR-dependent NF- κ B-low DLBCL lines, DHL4, DHL6, and LY7, chemical PI3K inhibition (LY294002) was as effective as R406 treatment in inducing HRK (Figure 4C). In each of these lines, expression of mAKT abrogated HRK induction by R406 (Figure 4D). Therefore, BCR signaling actively represses HRK expression via a SYK- and PI3K/AKT-mediated mechanism in BCR-dependent DLBCLs with low baseline NF- κ B.

We next assessed the role of HRK in the apoptosis of BCR-dependent NF- κ B-low DLBCLs using stable HRK knockdown clones. In these HRK-depleted cells, R406 still inhibited proximal components of the BCR signaling cascade (Figure S4B), but failed to induce HRK (Figure 4E; Figure S4C). Most importantly, R406 did not trigger the apoptosis of HRK-depleted DLBCLs (Figure 4F; Figure S4D). These data directly implicate this

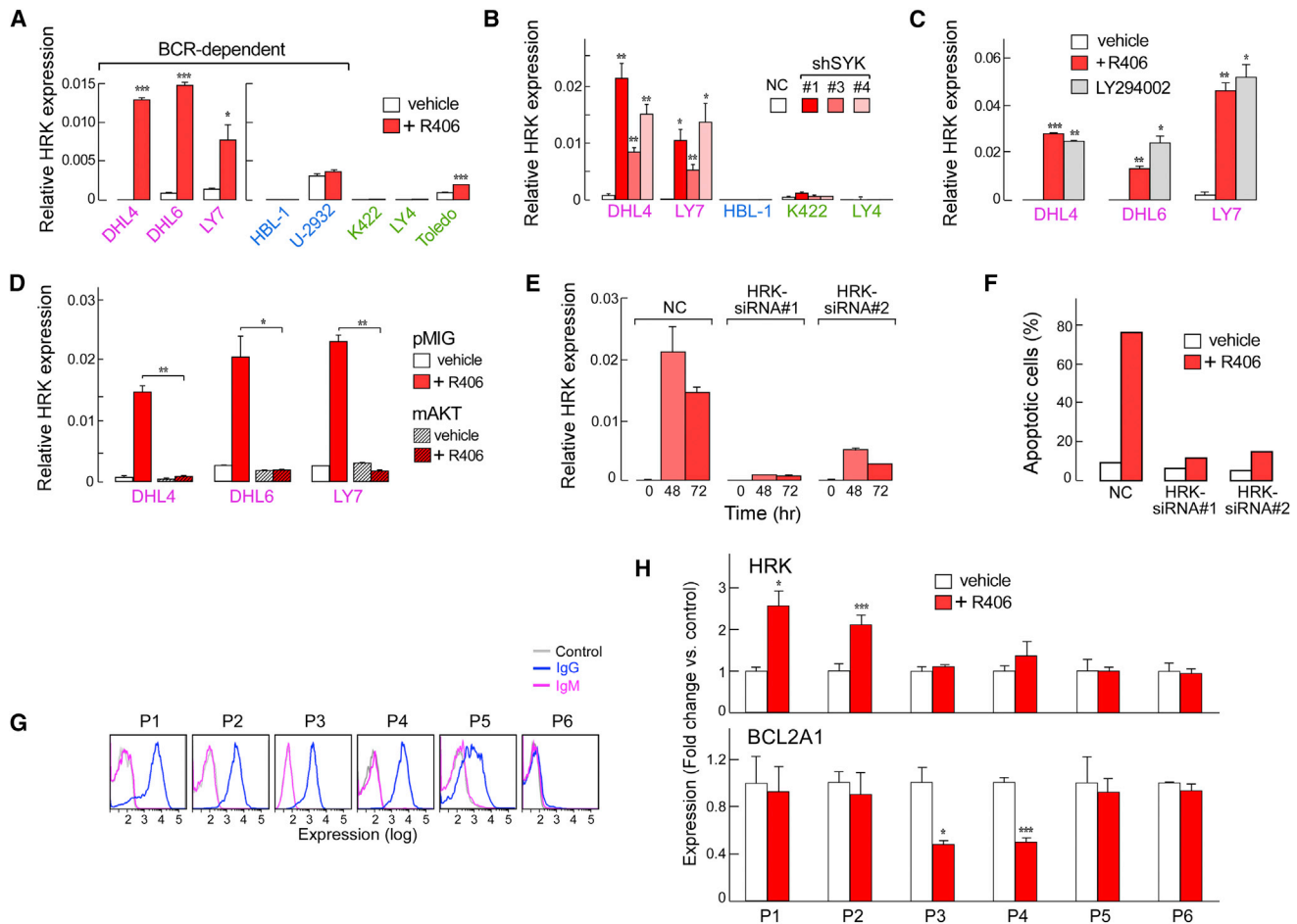


Figure 4. HRK Induction in DLBCL Cell Lines following SYK or PI3K Inhibition

(A) HRK transcript abundance in DLBCL cell lines following R406 treatment (24 hr) was determined by qRT-PCR.

(B) HRK expression in SYK-depleted DLBCL cell lines was assessed by qRT-PCR.

(C) HRK expression in the indicated cell lines following treatment with R406, LY294002, or vehicle for 24 hr assessed by qRT-PCR.

(D) HRK transcript abundance in DLBCL lines transduced with mAKT or pMIG, FACS-sorted, then treated with R406 or vehicle for 24 hr was analyzed by qRT-PCR.

(E) DHL4 cells stably transduced with the indicated HRK siRNA or negative control siRNA (NC) were treated with R406 or vehicle for 24 hr and analyzed for HRK transcript abundance by qRT-PCR.

(F) Apoptosis of DHL4 cells transduced with HRK siRNA or negative control siRNA (NC) and treated with vehicle or R406 for 72 hr was assessed by Annexin V/PI staining.

(G and H) Viable DLBCL tumor cells isolated from cryopreserved primary patient samples were analyzed for cell surface Ig expression (G) or for HRK and BCL2A1 transcript abundance after treatment with R406 or vehicle for 24 hr by qRT-PCR (H). The p values for vehicle versus R406 (A and H), vehicle versus R406 or LY294002 (C), NC versus shSYK (B), and pMIG +R406 versus mAKT +R406 (D) were determined with a one-sided Welch t test. ***p < 0.0001; **p < 0.001; *p < 0.01. Error bars represent the SD of three independent assays in a representative experiment.

See also Figure S4.

BH3-only protein in R406-induced apoptosis of NF- κ B-low DLBCLs and indicate that BCR-dependent survival signals include active HRK repression.

Modulation of Survival Pathways in Primary DLBCLs

After defining distinct viability pathways in BCR-dependent DLBCL cell lines with low or high baseline NF- κ B activity, we evaluated the same parameters in primary DLBCLs. Viable primary tumor cell suspensions were prepared and aliquots were evaluated for cell-surface Ig or treated with vehicle or R406 and harvested for qRT-PCR analysis of HRK and BCL2A1 tran-

scripts. We identified primary DLBCLs with high surface Ig (P1–P4) or lower/undetectable surface Ig (P5 and P6) (Figure 4G), as previously described (Chen et al., 2008), and assessed p65 nuclear staining in the associated P1–P4 fixed biopsy specimens. Primary tumors P3 and P4 had significantly higher p65 nuclear staining than P1 and P2, indicating that P3 and P4 had higher baseline NF- κ B activity (Figures S4E and S2F). In primary DLBCLs with higher baseline NF- κ B activity (P3 and P4), R406 treatment significantly decreased BCL2A1 abundance; in contrast, chemical SYK inhibition significantly increased HRK abundance in DLBCLs with lower baseline p65 NF- κ B activity

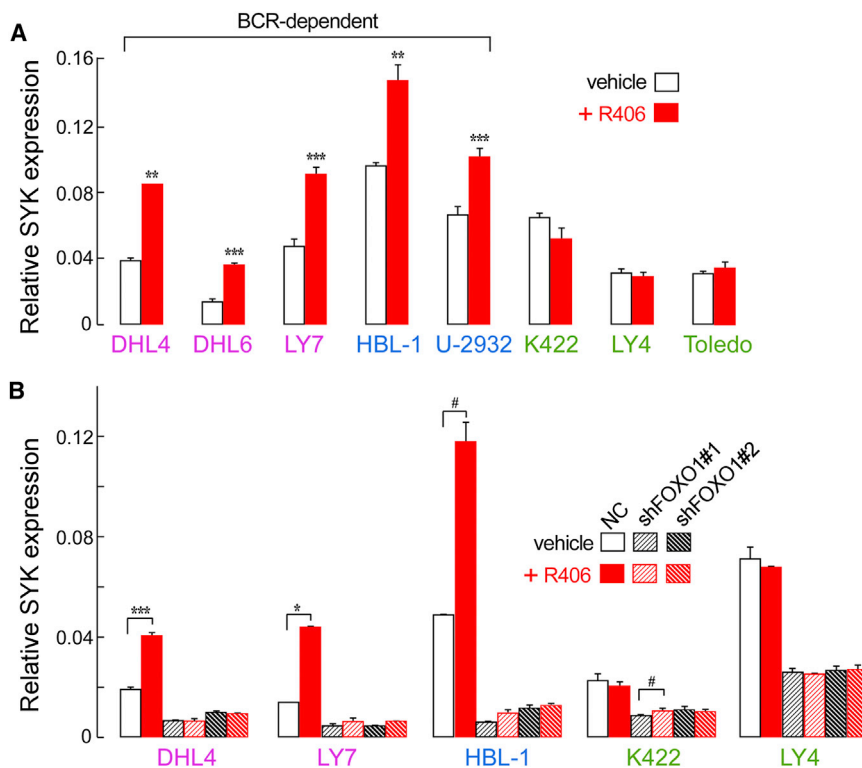


Figure 5. SYK Expression following Chemical SYK Inhibition and FOXO1 Depletion

(A) SYK transcript abundance in DLBCL cell lines was assessed by qRT-PCR following 24 hr of treatment with R406 or vehicle.

(B) SYK transcript abundance in DLBCL cell lines treated with R406 or vehicle for 24 hr following transduction with indicated shRNA was analyzed by qRT-PCR. The p values for vehicle versus R406 were determined with a one-sided Welch t test. ***p ≤ 0.0001; **p ≤ 0.001; *p ≤ 0.01, #, p ≤ 0.05. Error bars represent the SD of three independent assays in a representative experiment. See also Figure S5.

(Ochiai et al., 2012). For these reasons, we assessed the role of FOXO1 in SYK expression. FOXO1 was depleted with two independent shRNAs (Figure S5C) and SYK transcript abundance was assessed by qRT-PCR following vehicle or R406 treatment. In the BCR-dependent DLBCL lines (DHL4, LY7, and HBL-1), the R406-associated induction of SYK was abrogated by FOXO1 knockdown (Figure 5B). Therefore, in BCR-dependent DLBCLs, the attempted compensatory response to chemical

(P1 and P2) (Figure 4H). R406 treatment did not alter HRK or BCL2A1 levels in primary DLBCLs with low or no surface Ig (P5 and P6; Figure 4H). Similar results were obtained in additional viable primary tumor cell suspensions (Figures S4G and S4H). Therefore, the distinct survival pathways defined in representative BCR-dependent DLBCL cell lines—SYK- and PI3K-modulated NF-κB signaling or HRK repression—were also operative in primary tumors.

Chemical SYK Inhibition Induces the FOXO1-Dependent Transcriptional Upregulation of SYK

After characterizing distinct viability pathways in BCR-dependent DLBCLs with low- or high-baseline NF-κB, we evaluated the transcription profiles of all five R406-treated BCR-dependent cell lines for potential common features. Pathway analyses revealed transcriptional upregulation of proximal BCR signaling pathway components including CD79B and SYK itself following chemical SYK inhibition (Table S1; Figure S5A). We confirmed the selective upregulation of SYK transcripts and protein in BCR-dependent DLBCLs using the full panel of R406-treated cell lines, qRT-PCR, and intracellular flow cytometry (Figure 5A; Figure S5B). Although R406 treatment increased SYK transcript and total protein abundance, phosphorylation of the downstream BCR signaling component BLNK was inhibited (Figure 5A; Figure S5B). The data suggest that the transcriptional upregulation of certain proximal BCR signaling components may be an attempted, but ineffective, compensatory response to chemical SYK inhibition.

Chemical SYK inhibition increases the nuclear localization of FOXO1 and FOXO1 activity (Figures 3C and 3D; Figures S3A–S3C) and SYK is a recently described FOXO1 target

SYK inhibition includes FOXO1-mediated transcriptional upregulation of SYK.

SYK/BCR Inhibition Decreases the Abundance of Cholesterol Biosynthesis Pathway Components

Pathway analyses of the five profiled BCR-dependent DLBCL cell lines suggested that chemical SYK inhibition also had important metabolic consequences. R406 treatment downregulated multiple components of the cholesterol biosynthesis pathway, including HMGCS1 (Figure 6A; Table S1; Reed et al., 2008). In the full DLBCL cell line panel, chemical SYK inhibition selectively decreased HMGCS1 protein abundance in BCR-dependent DLBCLs but had no effect on BCR-independent tumors (Figure 6B). SYK depletion similarly decreased HMGCS1 expression in representative BCR-dependent DLBCL cell lines with low or high baseline NF-κB (Figure 6C).

Because cholesterol biosynthesis can be regulated by growth factor- and hormone-induced PI3K/AKT signaling (Krycer et al., 2010; Liu et al., 2009), we assessed the role of PI3K/AKT in R406-mediated downregulation of HMGCS1. In a representative BCR-dependent DLBCL cell line (DHL4), R406 and LY294002 treatment similarly decreased HMGCS1 expression (Figure 6D). In addition, expression of mAKT completely abrogated R406-mediated downregulation of HMGCS1 (Figure 6E). Together, these data indicate that SYK/BCR inhibition modulates sterol biosynthesis via PI3K/AKT.

Each of the SYK/BCR-responsive cholesterol pathway components (Figure 6A) is a known target of SREBP, a PI3K/AKT-dependent transcription factor and master regulator of cholesterol biosynthesis (Krycer et al., 2010; Reed et al., 2008). PI3K/AKT regulation of SREBP occurs at multiple levels, including

FOXO1-mediated repression of SREBP transcripts (Liu et al., 2009; Zhang et al., 2006) and mTORC1 and S6K1-dependent processing of SREBP1 to its active nuclear form (Düvel et al., 2010). In BCR-dependent DLBCLs, R406 treatment also decreased the processing of SREBP1 (Figure S6A).

SYK Blockade Decreases Membrane Cholesterol Content and Inhibits BCR Capping

To assess the functional consequences of SYK/PI3K-dependent cholesterol biosynthesis in DLBCLs, we treated the full panel of DLBCL cell lines with R406 and evaluated cholesterol membrane content. Following R406 or vehicle treatment, DLBCL cell lines were stained with filipin, which forms a fluorescent complex with cholesterol (Gimpl and Gehrig-Burger, 2007; Karnell et al., 2005). Then, filipin flow cytometry was used to quantify and visualize the cellular distribution of cholesterol. SYK/BCR inhibition clearly decreased cholesterol membrane content in BCR-dependent DLBCLs but had no effect on BCR-independent DLBCLs (Figure 6F).

To determine the functional consequences of decreased cholesterol membrane content, we characterized ligand (anti-IgG)-induced BCR redistribution in filipin-stained DLBCLs (Karnell et al., 2005). In BCR-dependent NF- κ B-low DLBCLs, filipin-stained cholesterol-enriched membrane domains colocalized with the BCR following anti-Ig induced capping (Figure 6G, +BCR). In contrast, BCR capping and the colocalization of BCR and filipin/cholesterol were markedly decreased following R406 treatment (Figure 6G, +R406/+BCR). Similar results were obtained in two high-NF- κ B cell lines, HBL-1 and U-2932 (Figure S6B). These studies indicate that in BCR-dependent DLBCLs, chemical SYK inhibition perturbs the integrity of cholesterol-rich lipid rafts and the association of BCR clusters with these regions.

Genetic Bases for Enhanced BCR Signaling in BCR-Dependent DLBCLs

After defining a role for SYK and PI3K/AKT in the survival of BCR-dependent DLBCL cell lines and primary tumors, we assessed potential genetic bases for the enhanced BCR signaling. Using a well-annotated series of primary DLBCLs with available transcription profiles and high-resolution copy number data (Monti et al., 2012), we evaluated proximal BCR signaling components including SYK and the negative regulator of PI3K/AKT signaling, PTEN. In this primary DLBCL series, there were recurrent single copy gains of SYK and monoallelic chromosome 10q23/PTEN deletions with associated highly significant changes in transcript abundance (Figure 7A; Figures S7A and S7B; Table S2). These genetic alterations were largely mutually exclusive and significantly more abundant in primary DLBCLs defined as “BCR-type” by transcriptional profiling (Figure 7B; Figures S7A and S7B). Consistent with these findings, PTEN depletion protected one of the three BCR-dependent DLBCL cell lines from chemical SYK inhibition (Figures S7C and S7D).

DISCUSSION

In this study, we characterize distinct SYK/PI3K/AKT-dependent BCR viability pathways in DLBCL cell lines and primary tumors with high- and low-baseline NF- κ B activity and define

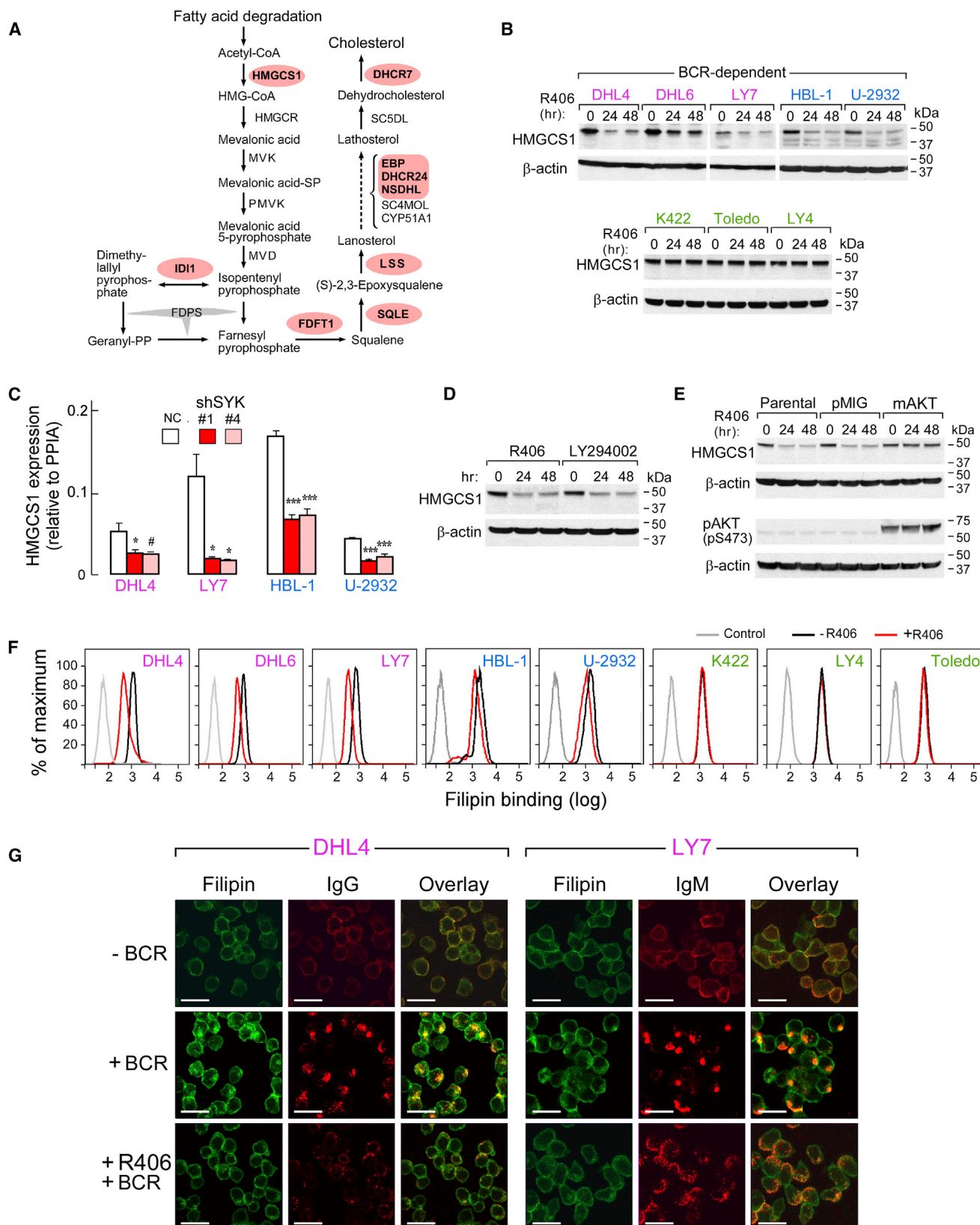
SYK/PI3K/AKT-dependent repression of the pro-apoptotic HRK protein as an important survival mechanism in BCR-dependent NF- κ B low DLBCLs (Figure 8A). In addition, we identify SYK/PI3K/AKT-dependent cholesterol biosynthesis as a feed-forward mechanism of preserving the integrity of BCRs in lipid rafts in DLBCLs with low- or high-baseline NF- κ B (Figure 8B). Consistent with the roles of SYK and PI3K/AKT as important mediators of BCR survival signals in primary DLBCLs, we also identify SYK amplification and PTEN deletion as selective and largely mutually exclusive genetic alterations in “BCR”-type tumors.

Our studies highlight the important role of PI3K/AKT in the BCR-dependent survival of DLBCLs with high- or low-baseline NF- κ B activity. In DLBCLs with high-baseline NF- κ B activity, genetic alterations of multiple NF- κ B pathway components have been described (Compagno et al., 2009; Lenz et al., 2008; Ngo et al., 2011) and additional CD79A and CD79B mutations have been reported (Davis et al., 2010). However, the sensitivity of DLBCLs with high baseline NF- κ B activity to inhibition of upstream BCR signals was incompletely defined. In this study, chemical SYK blockade and molecular SYK depletion decreased NF- κ B activity and target gene expression in DLBCL primary tumors and cell lines with high-baseline NF- κ B, including lines with wild-type CARD11 and either wild-type CD79B (U-2932) or CD79B missense mutations (HBL-1) (Davis et al., 2010). Chemical PI3K inhibition had similar effects. Taken together, these studies indicate that DLBCLs with high-baseline NF- κ B activity remain sensitive to inhibition of proximal SYK/PI3K signals.

In BCR-dependent DLBCL cell lines and primary tumors with low-baseline NF- κ B activity, both the chemical inhibition and molecular depletion of SYK induced the pro-apoptotic HRK protein via a PI3K/AKT-dependent mechanism. HRK depletion abrogated R406-induced cytotoxicity in these cells. These data highlight the previously unappreciated role of this BH3-only protein in DLBCL apoptosis and indicate that BCR-dependent survival signals include active HRK repression. These observations are consistent with earlier studies in which HRK was actively repressed at baseline and specifically induced following growth factor withdrawal in hematopoietic progenitors and neuronal cells (Nakamura et al., 2008; Sanz et al., 2001; Towers et al., 2009). In these experimental settings, HRK induction led to rapid cell death, as in our study. Additional genetic bases of HRK repression, such as hypermethylation and allelic loss, have been described in certain cancers including primary central nervous system lymphomas (Nakamura et al., 2008).

In our studies, molecular SYK depletion phenocopies chemical SYK inhibition in a panel of BCR-dependent and -independent DLBCL cell lines. Similar results were recently described in an overlapping series of DLBCL cell lines (Cheng et al., 2011). In BCR-dependent DLBCLs, R406 treatment induces FOXO1-mediated transcriptional upregulation of SYK, indicating that SYK is a tightly regulated component of the BCR signaling and survival pathway.

Chemical SYK inhibition also selectively decreased multiple components of the cholesterol biosynthesis pathway. SYK/BCR inhibition modulated cholesterol biosynthesis via PI3K/AKT and implicated the PI3K/AKT-dependent transcription factor and master regulator of cholesterol biosynthesis, SREBP



(legend on next page)

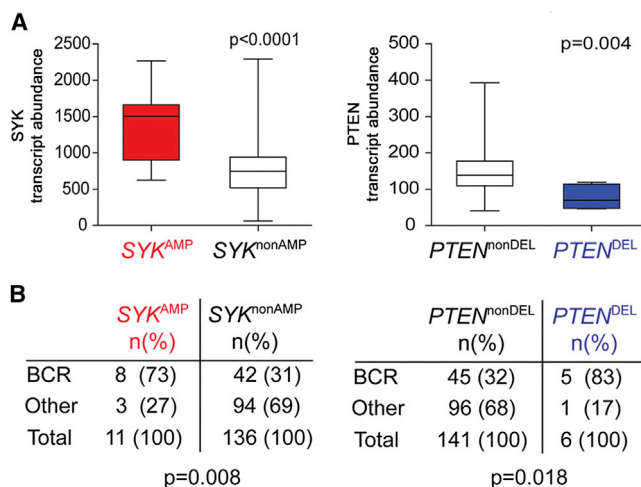


Figure 7. SYK and PTEN Copy Number Alterations in Primary DLBCLs

(A) SYK and PTEN copy numbers were assessed and associated with SYK and PTEN transcript levels in primary DLBCLs (n = 169). SYK and PTEN copy numbers and transcript abundance were derived from (Monti et al., 2012). The p values were determined with a one-sided t test. Box plot (median, line; 25% and 75% quartile, box; whiskers, maximum to minimum).

(B) Relative frequency of SYK^{AMP} and PTEN^{DEL} was assessed in transcriptionally defined “BCR” type versus other primary DLBCLs (n = 147; tumors with high confidence classification into CCC categories) (Monti et al., 2012). The p values were determined with a two-sided Fisher exact test.

See also Figure S7 and Table S2.

(Bengoechea-Alonso and Ericsson, 2007; Krycer et al., 2010; Porstmann et al., 2008). In BCR-dependent DLBCLs, R406-treatment also decreased cholesterol membrane content and perturbed the integrity of cholesterol-rich lipid rafts and the association of BCR clusters with these membrane domains (Gupta and DeFranco, 2007). Therefore, in addition to directly modulating downstream apoptotic pathways, chemical SYK inhibition alters cholesterol biosynthesis, with associated adverse consequences for cell membrane integrity and the assembly of BCR clusters.

The modulation of cholesterol biosynthesis by SYK is of additional interest given the recently described distinct metabolic profiles in BCR-dependent and BCR-independent/OxPhos DLBCLs (Caro et al., 2012). In BCR-dependent DLBCLs, SYK signaling limits the mitochondrial oxidation of fatty acids (Caro

et al., 2012), which likely ensures the availability of metabolic intermediates such as acetyl CoA for HMGCS1-mediated cholesterol biosynthesis. In comparison, acetyl-CoA derived from fatty acid enters the tricarboxylic acid cycle in BCR-independent/OxPhos DLBCLs that exhibit increased mitochondrial fatty acid oxidation (Caro et al., 2012). These findings further define molecular subsets of DLBCLs with distinct metabolic features that are linked to the functional state of upstream BCR signaling components.

We previously found that BCR-dependent DLBCL cell lines and primary tumors with low baseline NF- κ B activity also responded to SYK/BCR inhibition (Chen et al., 2008). However, it was unclear whether these DLBCLs had uncharacterized genetic alterations of BCR signaling pathway components or preserved reliance on physiologic “tonic” BCR survival signals. In the current analysis of an extensive series of newly diagnosed primary DLBCLs, SYK amplification and PTEN deletion were identified as largely mutually exclusive genetic alterations in transcriptionally-defined “BCR-type” DLBCLs. Given the role of PI3K/AKT in SYK/BCR-dependent survival signals in DLBCLs, these data suggest additional genetic bases for increased BCR pathway activity in these tumors.

Taken together, these functional and genetic studies provide a framework for analyzing targeted inhibition of SYK, PI3K and additional proximal components of the BCR signaling pathway in BCR-dependent DLBCLs and set the stage for further clinical analysis of promising candidate inhibitors.

EXPERIMENTAL PROCEDURES

Cell lines and culture conditions are in Supplemental Experimental Procedures. BCR crosslinking was performed as previously described (Chen et al., 2008).

Primary Tumor Specimens

Cryopreserved viable primary DLBCL samples were obtained according to Institutional Review Board (IRB)-approved protocols from Mayo Clinic, Brigham and Women’s Hospital and the Dana-Farber Cancer Institute. These anonymous primary tumor specimens were considered discarded tissues that did not require informed consent.

Chemical Inhibition with R406 or LY294002

For immediate inhibition, cells were incubated with 1 μ M R406 or vehicle alone (in PBS) in a 37°C water bath for 1 hr. For long-term inhibition, compounds (R406 [1 μ M or 4 μ M] or LY29004 [10 μ M]) were added to cell culture medium at the final indicated concentration and cells were maintained in a 37°C

Figure 6. Cholesterol Biosynthesis in DLBCLs following SYK or PI3K Inhibition

(A) Components of the cholesterol biosynthesis pathway modulated by R406 treatment (red) were identified by pathway analyses of the profiled cell lines.

(B) HMGCS1 protein abundance in R406- or vehicle-treated DLBCL cell lines was assessed by immunoblotting. β -actin, loading control.

(C) HMGCS1 transcript abundance in DLBCL cell lines transduced with indicated shRNA was assessed by qRT-PCR. The p values for NC versus shSYK were determined with a one-sided Welch t test. ***p \leq 0.0001; *p \leq 0.01; #, p \leq 0.02. Error bars represent the SD of three independent assays in a representative experiment.

(D) HMGCS1 protein abundance in DHL4 following treatment with R406 or LY294002 was assessed by immunoblotting. β -actin, loading control.

(E) HMGCS1 and p-AKT(S473) in parental DHL4 cells and DHL4 cells transduced with mAKT or pMIG and treated with R406 was determined by immunoblotting. β -actin, loading control.

(F) Membrane cholesterol content in DLBCL cell lines treated with vehicle (black) or R406 (red) for 2 days and fixed with 4% paraformaldehyde was assessed by filipin flow cytometry. Unstained controls in gray. (G) DHL4 and LY7 cells were incubated with vehicle or R406 for 48 hr and left untreated (–BCR) or stimulated with anti-Ig for 10 min (+BCR). The cells were fixed, stained with filipin (green) and the indicated Cy3-conjugated anti-Ig (red), and assessed with confocal microscopy. Scale bar represents 25 μ m.

See also Figure S6.

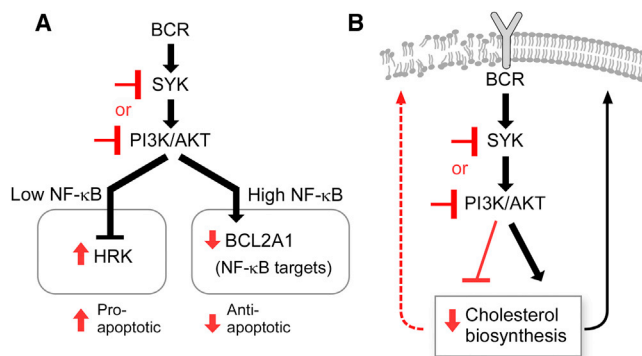


Figure 8. SYK and PI3K-Dependent Viability Pathways in DLBCLs

(A) SYK- and PI3K-dependent anti-apoptotic pathways in BCR-dependent DLBCLs. In BCR-dependent DLBCLs with low-baseline NF-κB activity, SYK or PI3K inhibition relieve BCR-dependent repression of the pro-apoptotic BH3 molecule, HRK. In BCR-dependent DLBCLs with high-baseline NF-κB activity, SYK or PI3K inhibition decreases the abundance of the anti-apoptotic NF-κB targets such as BCL2A1.

(B) SYK- and PI3K-dependent regulation of cholesterol biosynthesis and associated integrity of BCRs in lipid rafts in BCR-dependent DLBCLs.

incubator for 24 or 48 hr. Details are provided in the [Supplemental Experimental Procedures](#).

RNA Interference

Cells were infected with lentivirus containing either negative control (vector pLKO.1-emptyT, TRCN0000208001, Broad Institute, MA) or specific SYK, FOXO1, or PTEN shRNAs, puromycin-selected for 48 hr and analyzed for knockdown efficacy and cellular proliferation thereafter. HRK-specific oligonucleotides or negative control (NC) oligonucleotides were ligated into the linearized pSIREN-RetroQ retroviral vector (Clontech, Mountain View, CA). After retroviral infection and puromycin selection, cells were subcloned by limiting dilution. Selected subclones were treated with R406 or vehicle and efficient HRK knockdown (>75%) was confirmed by qRT-PCR. Details are provided in the [Supplemental Experimental Procedures](#).

Intracellular Flow

Intracellular flow cytometry for p-SYK352, p-BLNK84, total SYK, and PTEN (BD Biosciences, CA) was performed as previously described ([Chen et al., 2008](#)).

Immunofluorescence

DLBCL cell lines that were treated with vehicle or R406, with or without subsequent BCR crosslinking, were formalin-fixed, paraffin-embedded, and analyzed for FOXO1 expression and subcellular localization using a rabbit monoclonal anti-FOXO1 antibody (Cell Signaling Technology) and anti-rabbit Cy3-conjugated antibody solution (Invitrogen). The FOXO1-Cy3 stained slides were scanned with a digital FACS imaging system (TissueGnostics, Vienna, Austria) and analyzed with TissueQuest (TissueGnostics, Vienna, Austria). Details are provided in the [Supplemental Experimental Procedures](#).

Analyses of cellular proliferation and apoptosis, immunoblotting, qRT-PCR, transcriptional profiling and transduction with mAKT are provided in the [Supplemental Experimental Procedures](#).

NF-κB Activity Assay

DLBCL cell lines that were treated with vehicle, R406 or LY294002 were harvested, nuclear extracts were prepared and NF-κB activity was assessed using a TransAM NF-κB family kit and the manufacturer's positive control (Active Motif, Carlsbad, CA). This colorimetric assay detects binding of nuclear (activated) p65 (RELA) to immobilized NF-κB target consensus oligonucleotide sequences as described ([Feuerhake et al., 2005](#)).

Filipin Staining

After fixation in 4% paraformaldehyde (1 hr at room temperature) and washes in PBS, cells were incubated in 1 ml PBS-glycine (1.5 mg/ml; 10 min at room temperature) to quench the paraformaldehyde. Thereafter, cells were stained with 1 ml PBS containing 50 μg/ml filipin (1 hr at room temperature) and directly analyzed on a flow cytometer (FACS Canto II, BD Biosciences).

Confocal Microscopy

DLBCL lines (5×10^6 cells) treated with 1 μM R406 or vehicle were harvested and resuspended in 0.5 ml PBS and incubated at 37°C water bath for 20 min. Thereafter, cells were stimulated with Cy3-conjugated AffiniPure F(ab')₂ Fragment Goat anti-human IgG or IgM for 10 min, and the reaction was stopped by the addition of cold PBS/0.1% bovine serum albumin/0.02% azide. The cells were fixed in 4% paraformaldehyde/0.1% glutaraldehyde, followed by washing and resuspension in 0.5 mg/ml sodium borohydride to stop fixation. For untreated DLBCL lines that were not BCR crosslinked, cells were fixed with paraformaldehyde before staining with Cy3-conjugated AffiniPure F(ab')₂ fragment rabbit anti-goat IgG or IgM. Thereafter, all samples were incubated in PBS containing 50 μg/ml filipin for 1 hr. The cells were adhered to glass slides by centrifugation at 1,200 rpm using cytospin centrifuge (Shandon) and mounted with Prolong Gold anti-fade agent (Invitrogen, Oregon). The cells were visualized using Leica SP5x confocal microscope. Images were captured and analyzed using LAS AF software (Leica Microsystems CMS GmbH).

Analysis of SYK and PTEN Somatic Copy Number Changes and Transcript Abundance in Primary DLBCLs

SYK and PTEN loci copy numbers were assessed and associated with respective SYK and PTEN transcript levels in 169 newly diagnosed DLBCLs (HD-SNP array data and transcriptional profiles from [Monti et al., 2012](#); Gene Expression Omnibus accession number GSE34171). In tumors with SYK^{AMP} versus SYK^{nonAMP} or PTEN^{DEL} versus PTEN^{nonDEL}, respective SYK or PTEN transcript levels were visualized with a box plot and evaluated with a Fisher exact test ([Dawson-Saunders and Trapp, 1994](#)). The distribution of SYK and PTEN copy number alterations in BCR versus Other CCC categories was evaluated with a Fisher exact test. Visualization and statistical testing were performed using GraphPad Prism version 5.04 for Windows, GraphPad Software, San Diego, CA, <http://www.graphpad.com>.

ACCESSION NUMBER

The Gene Expression Omnibus accession number for the gene expression data reported in this paper is GSE43510.

SUPPLEMENTAL INFORMATION

Supplemental Information includes Supplemental Experimental Procedures, seven figures, and two tables and can be found with this article online at <http://dx.doi.org/10.1016/j.ccr.2013.05.002>.

ACKNOWLEDGMENTS

This work was supported by NIH grants P01CA092625, LLS SCOR 7391, and LLS SCOR 7009.

Received: December 9, 2011

Revised: January 23, 2013

Accepted: May 1, 2013

Published: June 10, 2013

REFERENCES

- Bengoechea-Alonso, M.T., and Ericsson, J. (2007). SREBP in signal transduction: cholesterol metabolism and beyond. *Curr. Opin. Cell Biol.* 19, 215–222.
- Caro, P., Kishan, A.U., Norberg, E., Stanley, I.A., Chapuy, B., Ficarro, S.B., Polak, K., Tondera, D., Gounarides, J., Yin, H., et al. (2012). Metabolic

signatures uncover distinct targets in molecular subsets of diffuse large B cell lymphoma. *Cancer Cell* 22, 547–560.

Chen, L., Juszczynski, P., Takeyama, K., Aguiar, R.C., and Shipp, M.A. (2006). Protein tyrosine phosphatase receptor-type O truncated (PTPROt) regulates SYK phosphorylation, proximal B-cell-receptor signaling, and cellular proliferation. *Blood* 108, 3428–3433.

Chen, L., Monti, S., Juszczynski, P., Daley, J., Chen, W., Witzig, T.E., Habermann, T.M., Kutok, J.L., and Shipp, M.A. (2008). SYK-dependent tonic B-cell receptor signaling is a rational treatment target in diffuse large B-cell lymphoma. *Blood* 111, 2230–2237.

Cheng, S., Coffey, G., Zhang, X.H., Shaknovich, R., Song, Z., Lu, P., Pandey, A., Melnick, A.M., Sinha, U., and Wang, Y.L. (2011). SYK inhibition and response prediction in diffuse large B-cell lymphoma. *Blood* 118, 6342–6352.

Compagno, M., Lim, W.K., Grunn, A., Nandula, S.V., Brahmachary, M., Shen, Q., Bertoni, F., Ponzoni, M., Scandurra, M., Califano, A., et al. (2009). Mutations of multiple genes cause deregulation of NF-kappaB in diffuse large B-cell lymphoma. *Nature* 459, 717–721.

Davis, R.E., Brown, K.D., Siebenlist, U., and Staudt, L.M. (2001). Constitutive nuclear factor kappaB activity is required for survival of activated B cell-like diffuse large B cell lymphoma cells. *J. Exp. Med.* 194, 1861–1874.

Davis, R.E., Ngo, V.N., Lenz, G., Tolar, P., Young, R.M., Romesser, P.B., Kohlhammer, H., Lamy, L., Zhao, H., Yang, Y., et al. (2010). Chronic active B-cell-receptor signalling in diffuse large B-cell lymphoma. *Nature* 463, 88–92.

Dawson-Saunders, B., and Trapp, R.G. (1994). Basic and clinical biostatistics (Norwalk, CT: Appleton & Lange).

Düvel, K., Yecies, J.L., Menon, S., Raman, P., Lipovsky, A.I., Souza, A.L., Triantafellow, E., Ma, Q., Gorski, R., Cleaver, S., et al. (2010). Activation of a metabolic gene regulatory network downstream of mTOR complex 1. *Mol. Cell* 39, 171–183.

Dykstra, M., Cherukuri, A., Sohn, H.W., Tzeng, S.J., and Pierce, S.K. (2003). Location is everything: lipid rafts and immune cell signaling. *Annu. Rev. Immunol.* 21, 457–481.

Feuerhake, F., Kutok, J.L., Monti, S., Chen, W., LaCasce, A.S., Cattoretto, G., Kurtin, P., Pinkus, G.S., de Leval, L., Harris, N.L., et al. (2005). NFkappaB activity, function, and target-gene signatures in primary mediastinal large B-cell lymphoma and diffuse large B-cell lymphoma subtypes. *Blood* 106, 1392–1399.

Friedberg, J.W., Sharman, J., Sweetenham, J., Johnston, P.B., Vose, J.M., Lacasce, A., Schaefer-Cuttillo, J., De Vos, S., Sinha, R., Leonard, J.P., et al. (2010). Inhibition of Syk with fostamatinib disodium has significant clinical activity in non-Hodgkin lymphoma and chronic lymphocytic leukemia. *Blood* 115, 2578–2585.

Fu, Z., and Tindall, D.J. (2008). FOXOs, cancer and regulation of apoptosis. *Oncogene* 27, 2312–2319.

Gimpl, G., and Gehrig-Burger, K. (2007). Cholesterol reporter molecules. *Biosci. Rep.* 27, 335–358.

Gupta, N., and DeFranco, A.L. (2007). Lipid rafts and B cell signaling. *Semin. Cell Dev. Biol.* 18, 616–626.

Hendriks, R.W. (2011). Drug discovery: New Btk inhibitor holds promise. *Nat. Chem. Biol.* 7, 4–5.

Herman, S.E., Gordon, A.L., Hertlein, E., Ramanunni, A., Zhang, X.D., Jaglowski, S., Flynn, J., Jones, J., Blum, K.A., Buggy, J.J., et al. (2011). Bruton tyrosine kinase represents a promising therapeutic target for treatment of chronic lymphocytic leukemia and is effectively targeted by PCI-32765. *Blood* 117, 6287–6296.

Karnell, F.G., Brezski, R.J., King, L.B., Silverman, M.A., and Monroe, J.G. (2005). Membrane cholesterol content accounts for developmental differences in surface B cell receptor compartmentalization and signaling. *J. Biol. Chem.* 280, 25621–25628.

Kloo, B., Nagel, D., Pfeifer, M., Grau, M., Düvel, M., Vincendeau, M., Dörken, B., Lenz, P., Lenz, G., and Krappmann, D. (2011). Critical role of PI3K signaling for NF-kappaB-dependent survival in a subset of activated B-cell-like diffuse large B-cell lymphoma cells. *Proc. Natl. Acad. Sci. USA* 108, 272–277.

Kraus, M., Alimzhanov, M.B., Rajewsky, N., and Rajewsky, K. (2004). Survival of resting mature B lymphocytes depends on BCR signaling via the Igalphabeta heterodimer. *Cell* 117, 787–800.

Krycer, J.R., Sharpe, L.J., Luu, W., and Brown, A.J. (2010). The Akt-SREBP nexus: cell signaling meets lipid metabolism. *Trends Endocrinol. Metab.* 21, 268–276.

Küppers, R. (2005). Mechanisms of B-cell lymphoma pathogenesis. *Nat. Rev. Cancer* 5, 251–262.

Lam, K.P., Kühn, R., and Rajewsky, K. (1997). In vivo ablation of surface immunoglobulin on mature B cells by inducible gene targeting results in rapid cell death. *Cell* 90, 1073–1083.

Lannutti, B.J., Meadows, S.A., Herman, S.E., Kashishian, A., Steiner, B., Johnson, A.J., Byrd, J.C., Tyner, J.W., Loriaux, M.M., Deininger, M., et al. (2011). CAL-101, a p110delta selective phosphatidylinositol-3-kinase inhibitor for the treatment of B-cell malignancies, inhibits PI3K signaling and cellular viability. *Blood* 117, 591–594.

Lee, H.H., Dadgostar, H., Cheng, Q., Shu, J., and Cheng, G. (1999). NF-kappaB-mediated up-regulation of Bcl-x and Bfl-1/A1 is required for CD40 survival signaling in B lymphocytes. *Proc. Natl. Acad. Sci. USA* 96, 9136–9141.

Lenz, G., Davis, R.E., Ngo, V.N., Lam, L., George, T.C., Wright, G.W., Dave, S.S., Zhao, H., Xu, W., Rosenwald, A., et al. (2008). Oncogenic CARD11 mutations in human diffuse large B cell lymphoma. *Science* 319, 1676–1679.

Liu, Z., Rudd, M.D., Hernandez-Gonzalez, I., Gonzalez-Robayna, I., Fan, H.-Y., Zeleznik, A.J., and Richards, J.S. (2009). FSH and FOXO1 regulate genes in the sterol/steroid and lipid biosynthetic pathways in granulosa cells. *Mol. Endocrinol.* 23, 649–661.

Monroe, J.G. (2006). ITAM-mediated tonic signalling through pre-BCR and BCR complexes. *Nat. Rev. Immunol.* 6, 283–294.

Monti, S., Savage, K.J., Kutok, J.L., Feuerhake, F., Kurtin, P., Mihm, M., Wu, B., Pasqualucci, L., Neuberger, D., Aguiar, R.C., et al. (2005). Molecular profiling of diffuse large B-cell lymphoma identifies robust subtypes including one characterized by host inflammatory response. *Blood* 105, 1851–1861.

Monti, S., Chapuy, B., Takeyama, K., Rodig, S.J., Hao, Y., Yeda, K.T., Inguiluzian, H., Mermel, C., Currie, T., Dogan, A., et al. (2012). Integrative analysis reveals an outcome-associated and targetable pattern of p53 and cell cycle deregulation in diffuse large B cell lymphoma. *Cancer Cell* 22, 359–372.

Nakamura, M., Shimada, K., and Konishi, N. (2008). The role of HRK gene in human cancer. *Oncogene* 27(Suppl 1), S105–S113.

Ngo, V.N., Young, R.M., Schmitz, R., Jhavar, S., Xiao, W., Lim, K.H., Kohlhammer, H., Xu, W., Yang, Y., Zhao, H., et al. (2011). Oncogenically active MYD88 mutations in human lymphoma. *Nature* 470, 115–119.

Ochiai, K., Maienschein-Cline, M., Mandal, M., Triggs, J.R., Bertolino, E., Sciammas, R., Dinner, A.R., Clark, M.R., and Singh, H. (2012). A self-reinforcing regulatory network triggered by limiting IL-7 activates pre-BCR signaling and differentiation. *Nat. Immunol.* 13, 300–307.

Ottina, E., Grespi, F., Tischner, D., Soratroi, C., Geley, S., Ploner, A., Reichardt, H.M., Villunger, A., and Herold, M.J. (2012). Targeting antiapoptotic A1/Bfl-1 by in vivo RNAi reveals multiple roles in leukocyte development in mice. *Blood* 119, 6032–6042.

Porstmann, T., Santos, C.R., Griffiths, B., Cully, M., Wu, M., Leever, S., Griffiths, J.R., Chung, Y.-L., and Schulze, A. (2008). SREBP activity is regulated by mTORC1 and contributes to Akt-dependent cell growth. *Cell Metab.* 8, 224–236.

Reed, B.D., Charos, A.E., Szekeley, A.M., Weissman, S.M., and Snyder, M. (2008). Genome-wide occupancy of SREBP1 and its partners NFY and SP1 reveals novel functional roles and combinatorial regulation of distinct classes of genes. *PLoS Genet.* 4, e1000133.

Rinaldi, A., Ponzoni, M., Uccella, S., Rossi, D., Gaidano, G., Facchetti, F., Pruneri, G., Tibiletti, M.G., Capella, C., Zucca, E., et al. (2011). In vitro efficacy of tyrosine kinase inhibitors: SYK and BCR-ABL inhibitors in lymphomas. *Hematol. Oncol.* 29, 164–166.

Robertson, M.J., Kahl, B.S., Vose, J.M., de Vos, S., Laughlin, M., Flynn, P.J., Rowland, K., Cruz, J.C., Goldberg, S.L., Musib, L., et al. (2007). Phase II study

- p>of enzastaurin, a protein kinase C beta inhibitor, in patients with relapsed or refractory diffuse large B-cell lymphoma.
- J. Clin. Oncol.*
- 25**
- , 1741–1746.
- Rosenwald, A., Wright, G., Chan, W.C., Connors, J.M., Campo, E., Fisher, R.I., Gascoyne, R.D., Muller-Hermelink, H.K., Smeland, E.B., Giltner, J.M., et al.; Lymphoma/Leukemia Molecular Profiling Project. (2002). The use of molecular profiling to predict survival after chemotherapy for diffuse large-B-cell lymphoma. *N. Engl. J. Med.* **346**, 1937–1947.
- Sanz, C., Benito, A., Inohara, N., Ekhterae, D., Nunez, G., and Fernandez-Luna, J.L. (2000). Specific and rapid induction of the proapoptotic protein Bcl-2 after growth factor withdrawal in hematopoietic progenitor cells. *Blood* **95**, 2742–2747.
- Sanz, C., Mellstrom, B., Link, W.A., Naranjo, J.R., and Fernandez-Luna, J.L. (2001). Interleukin 3-dependent activation of DREAM is involved in transcriptional silencing of the apoptotic Bcl-2 gene in hematopoietic progenitor cells. *EMBO J.* **20**, 2286–2292.
- Schreiber, J., Jenner, R.G., Murray, H.L., Gerber, G.K., Gifford, D.K., and Young, R.A. (2006). Coordinated binding of NF- κ B family members in the response of human cells to lipopolysaccharide. *Proc. Natl. Acad. Sci. USA* **103**, 5899–5904.
- Srinivasan, L., Sasaki, Y., Calado, D.P., Zhang, B., Paik, J.H., DePinho, R.A., Kutok, J.L., Kearney, J.F., Otipoby, K.L., and Rajewsky, K. (2009). PI3 kinase signals BCR-dependent mature B cell survival. *Cell* **139**, 573–586.
- Torres, R.M., Flaswinkel, H., Reth, M., and Rajewsky, K. (1996). Aberrant B cell development and immune response in mice with a compromised BCR complex. *Science* **272**, 1804–1808.
- Towers, E., Gilley, J., Randall, R., Hughes, R., Kristiansen, M., and Ham, J. (2009). The proapoptotic Bcl-2 gene is a direct target of the MLK-JNK-c-Jun pathway in sympathetic neurons. *Nucleic Acids Res.* **37**, 3044–3060.
- Wright, G., Tan, B., Rosenwald, A., Hurt, E.H., Wiestner, A., and Staudt, L.M. (2003). A gene expression-based method to diagnose clinically distinct subgroups of diffuse large B cell lymphoma. *Proc. Natl. Acad. Sci. USA* **100**, 9991–9996.
- Young, R.M., Hardy, I.R., Clarke, R.L., Lundy, N., Pine, P., Turner, B.C., Potter, T.A., and Refaelli, Y. (2009). Mouse models of non-Hodgkin lymphoma reveal Bcl-2 as an important therapeutic target. *Blood* **113**, 2508–2516.
- Zhang, W., Patil, S., Chauhan, B., Guo, S., Powell, D.R., Le, J., Kotsas, A., Matika, R., Xiao, X., Franks, R., et al. (2006). FoxO1 regulates multiple metabolic pathways in the liver: effects on gluconeogenic, glycolytic, and lipogenic gene expression. *J. Biol. Chem.* **281**, 10105–10117.
- Zong, W.X., Edelstein, L.C., Chen, C., Bash, J., and Gélinas, C. (1999). The prosurvival Bcl-2 homolog Bcl-11/A1 is a direct transcriptional target of NF- κ B that blocks TNF α -induced apoptosis. *Genes Dev.* **13**, 382–387.

Phosphorylation of EZH2 Activates STAT3 Signaling via STAT3 Methylation and Promotes Tumorigenicity of Glioblastoma Stem-like Cells

Eunhee Kim,^{1,6} Misuk Kim,^{2,6} Dong-Hun Woo,^{1,6} Yongjae Shin,¹ Jihye Shin,³ Nakho Chang,² Young Taek Oh,² Hong Kim,¹ Jingeun Rhee,² Ichiro Nakano,⁴ Cheolju Lee,³ Kyeong Min Joo,⁵ Jeremy N. Rich,¹ Do-Hyun Nam,^{2,*} and Jeongwu Lee^{1,*}

¹Department of Stem Cell Biology and Regenerative Medicine, Lerner Research Institute, Cleveland Clinic, Cleveland, OH 44195, USA

²Department of Neurosurgery and Samsung Advanced Institute for Health Sciences and Technology, Samsung Medical Center, Sungkyunkwan University School of Medicine, Seoul, 135-710, Korea

³BRI, Life Sciences Division, Korea Institute of Science and Technology, Seoul 136-791, Korea

⁴Department of Neurological Surgery, Center for Neuro-oncology, James Cancer Hospital and The Ohio State University, Columbus, OH 43210, USA

⁵Department of Anatomy and Cell Biology, Sungkyunkwan University School of Medicine, Suwon, Gyeonggi-do, 440-746, Korea

⁶These authors contributed equally to this work

*Correspondence: nsnam@skku.edu (D.-H.N.), leej7@ccf.org (J.L.)

<http://dx.doi.org/10.1016/j.ccr.2013.04.008>

SUMMARY

Glioblastoma multiforme (GBM) displays cellular hierarchies harboring a subpopulation of stem-like cells (GSCs). Enhancer of Zeste Homolog 2 (EZH2), the lysine methyltransferase of Polycomb repressive complex 2, mediates transcriptional repression of prodifferentiation genes in both normal and neoplastic stem cells. An oncogenic role of EZH2 as a transcriptional silencer is well established; however, additional functions of EZH2 are incompletely understood. Here, we show that EZH2 binds to and methylates STAT3, leading to enhanced STAT3 activity by increased tyrosine phosphorylation of STAT3. The EZH2-STAT3 interaction preferentially occurs in GSCs relative to non-stem bulk tumor cells, and it requires a specific phosphorylation of EZH2. Inhibition of EZH2 reverses the silencing of Polycomb target genes and diminishes STAT3 activity, suggesting therapeutic strategies.

INTRODUCTION

Glioblastoma multiforme (GBM) is the most common and most lethal primary brain cancer (Louis et al., 2007). The current standard of care for patients with GBM provides only palliation with a median survival of about 15 months (Furnari et al., 2007; Stupp et al., 2005).

Cancer stem/propagating cells (CSCs) are functionally defined by the enriched capacity to propagate tumors in vivo, and have characteristics of normal stem cells such as self-renewal and differentiation potential to establish cellular hierarchy and heterogeneity (Dirks, 2010; Reya et al., 2001). While some cancers may not follow the CSC model, numerous studies support that

GBMs harbor a subpopulation of highly tumorigenic, stem-like cells (GSCs) (Dirks, 2010; Hemmati et al., 2003; Singh et al., 2004), and that GSCs are responsible for glioma propagation, resistance to conventional therapy, and tumor recurrence (Bao et al., 2006; Chen et al., 2012; Gilbert and Ross, 2009; Zhou et al., 2009). Therefore, it may be crucial to identify the mechanisms involved in GSC maintenance.

Polycomb group (PcG) proteins are important epigenetic regulators of embryonic development and cell fate decision (Maugueron and Reinberg, 2011; Richly et al., 2011; Sparmann and van Lohuizen, 2006). They execute transcriptional repression in two multiprotein complexes named Polycomb repressive complexes 1 and 2 (PRC1 and PRC2). Core components of PRC2

Significance

Elucidation of the regulatory pathways operating in stem-like cancer cells will be critical to understand the pathogenesis of primary human tumors and may help lead to better therapies. We demonstrate that EZH2 not only mediates transcriptional silencing but also contributes to the activation of STAT3, a key GSC signaling node. Phosphorylation of EZH2 at serine 21 (pS21 EZH2) by AKT signaling facilitates STAT3 methylation by EZH2 and enhances STAT3 activity. Selective blocking of histone methylation-independent EZH2-STAT3 signaling decreases tumor growth in an orthotopic animal model. Together, these data suggest that the AKT-EZH2-STAT3 axis is a positive regulator of GSC self-renewal and tumor malignancy, and a promising therapeutic target for GBM.

include EZH2 (enhancer of Zeste homolog 2), Suz12 (suppressor of Zeste 12), and EED (embryonic ectoderm development) (Sparmann and van Lohuizen, 2006). EZH2 functions as a lysine methyl transferase and EZH2-containing PRC2 catalyzes trimethylation of histone 3 at lysine 27 (H3K27me3) (Cao et al., 2002). PRC1 in turn recognizes the H3K27me3 mark and maintains gene silencing (Shao et al., 1999; Sparmann and van Lohuizen, 2006).

Many of the PRC2 target genes in embryonic and tissue-specific stem cells are lineage-committed prodifferentiation genes, supporting Polycomb-mediated maintenance of stem cells (Boyer et al., 2006; Lee et al., 2006b; Mikkelsen et al., 2007). Several genome-wide integrative studies have revealed that a significant subset of PRC2 target genes is repressed in various tumors, some of which are further silenced by promoter hypermethylation, implying crucial roles of the Polycomb pathway in cancer initiation and progression (Schlesinger et al., 2007; Viré et al., 2006; Widschwendter et al., 2007). In a wide range of cancers including GBM, EZH2 is highly expressed and its expression positively correlates with tumor malignancy and invasiveness (Crea et al., 2010; Kleer et al., 2003; Varambally et al., 2002). We and others have previously shown that EZH2 is a critical regulator for GSC maintenance and GBM propagation (Abdouh et al., 2009; Lee et al., 2008; Suvà et al., 2009).

The reported roles of EZH2 have been attributed to its ability to drive transcriptional repression via a repressive histone mark, especially H3K27 trimethylation (Esteller, 2008; Morey and Helin, 2010; Simon and Kingston, 2009; Simon and Lange, 2008). However, emerging evidence suggests the presence of additional downstream effectors of EZH2 signaling (Cha et al., 2005; He et al., 2012; Lee et al., 2011; Wei et al., 2008; Xu et al., 2012). Consistent with this hypothesis, recent studies reported that EZH2 interacts with various transcription factors including androgen receptor (AR), GATA4, and ROR α (He et al., 2012; Lee et al., 2012; Xu et al., 2012). A series of reports showed that histone methyltransferases such as SET7/9 can regulate signaling pathways through direct methylation of p53, NF- κ B, and STAT3 (Huang et al., 2006; Lu et al., 2010; Stark et al., 2011; Yang et al., 2010), raising the possibility that EZH2 might have such a property. Based on this background, we investigated the histone methylation-independent role of EZH2 in GSC self-renewal and GBM propagation.

RESULTS

EZH2 Interacts with STAT3 in GSCs

To identify proteins that interact with EZH2, we performed co-immunoprecipitation (IP) experiments using an anti-EZH2 antibody and characterized proteins that coprecipitate with EZH2 by mass spectrometry (data not shown). GBM cells prospectively enriched by the putative GSC enrichment markers CD133 and/or CD15 (Singh et al., 2004; Son et al., 2009) were isolated from surgical specimens of GBM patients or their derivative xenograft tumors and functionally validated in assays of self-renewal and tumor propagation (Joo et al., 2013; Lee et al., 2008; Pastrana et al., 2011; Pollard et al., 2009). We found that EZH2 coprecipitated with STAT3 in protein lysates isolated from CD133 and/or CD15-enriched GSCs (Figure 1A). Co-IP experiments using an anti-STAT3 antibody in the same lysates

revealed that STAT3 coprecipitated with EZH2 as well as SUZ12 and EED, other core components of PRC2, suggesting that STAT3 and PRC2 may interact in GSCs (Figure 1B).

Because EZH2 is implicated in the maintenance of normal and neoplastic stem cells, we assessed whether the EZH2-STAT3 interaction is affected by the differentiation states of these cells. The addition of serum or the removal of epidermal growth factor (EGF) and fibroblast growth factor 2 (FGF2) in culture media decreased expression of stem-cell-associated markers such as SOX2 and concurrently increased an astroglial marker expression (e.g., GFAP), consistent with a “differentiated” phenotype (Galli et al., 2004; Lee et al., 2006a; Piccirillo et al., 2006; Zheng et al., 2010). We determined the relative abundance of the EZH2-STAT3 complex in two pairs of GSCs and their differentiated progenies by co-IP assays. An association between EZH2 and STAT3 was prominent in GSCs, but lost in the cells cultured in the presence of serum or the absence of growth factors (Figure 1C; Figure S1 available online), providing an initial link between the EZH2-STAT3 interaction and GSC maintenance. Because GSCs share many characteristics with normal human neural stem/progenitor cells (NPCs), we assessed whether the EZH2-STAT3 association is present in NPCs derived from fetal brain tissues. Similar to GSCs, EZH2 and STAT3 were co-immunoprecipitated in NPCs but not in differentiated cells (Figure 1C). Collectively, these data demonstrate an interaction between EZH2 and STAT3 in GSCs.

We performed additional co-IP experiments to determine the EZH2-STAT3 interaction in GSC-derived GBM xenografts or other glioma cell lines. U87 and U251 are two most widely used, established glioma cell lines. EZH2 and STAT3 proteins were expressed in these cells at comparable levels. While the EZH2-STAT3 coprecipitation was abundant in GSCs and GBM xenografts, it was barely detectable in lysates isolated from U87 and U251 (Figure 1D).

EZH2 Targeting Decreases STAT3 Activation in GSCs

Because an association between EZH2 and STAT3 is abundant in GSCs, and STAT3 is a key signaling node in GSCs (Cao et al., 2010; Sherry et al., 2009; Yang et al., 2012), we hypothesized that EZH2 may positively regulate STAT3 signaling in GSCs. To investigate the role of EZH2 in STAT3 activation, we targeted EZH2 expression by lentiviral-mediated short hairpin RNA (shRNA) directed against *EZH2* (shEZH2) and measured STAT3 activation in GSCs (Figure 2A). Some GSCs appear to have a constitutively active STAT3 signaling, evidenced by a high basal level of tyrosine phosphorylated STAT3 at the 705 residue (pY-STAT3) (Cao et al., 2010). As expected, EZH2 knockdown greatly decreased global levels of H3K27 trimethylation in GSCs. EZH2 knockdown in two different GSCs also reduced the levels of pY-STAT3 to ~30% of those in nontargeting shRNA-transduced GSCs (Figures 2A and 2B). We complemented these findings using a prototype EZH2 inhibitor (3-deazaneplanocin A, DZNep) (Tan et al., 2007) and a highly selective EZH2 inhibitor GSK126 (McCabe et al., 2012). pY-STAT3 in GSCs was rapidly decreased by treatment with either DZNep or GSK126 (Figure 2C). In contrast, the levels of phosphorylated AKT and ERK in GSCs were not changed within 4 hr of drug treatment (Figure 2C).

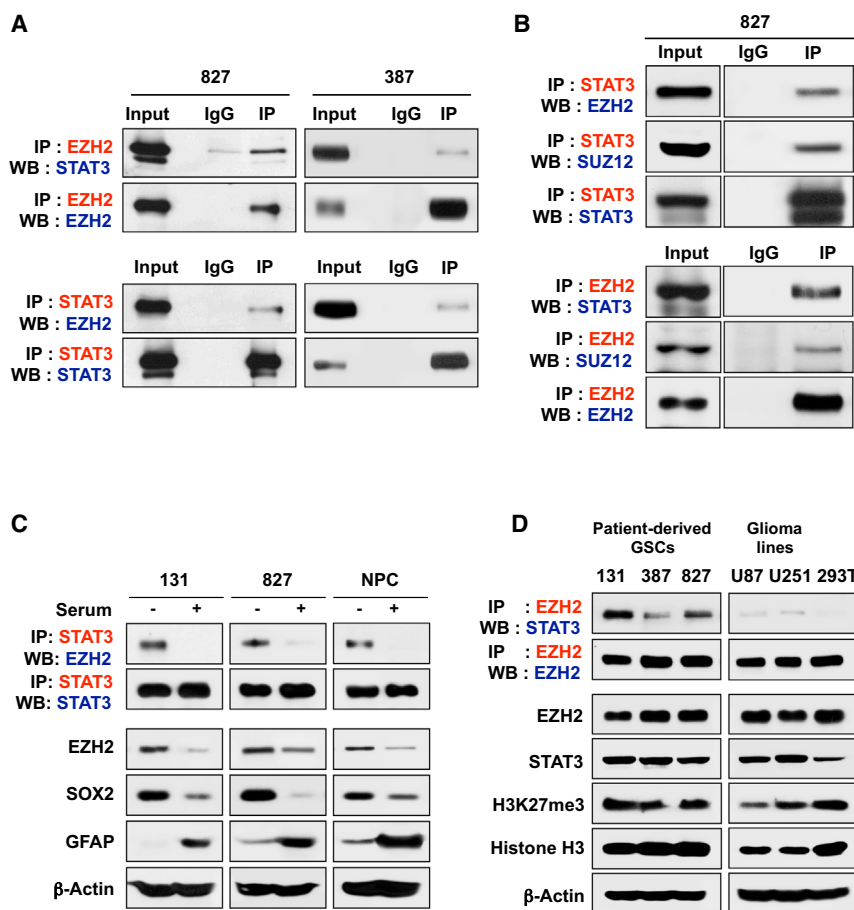


Figure 1. EZH2 Protein Interacts with STAT3 in GSCs

(A and B) Co-immunoprecipitation (Co-IP) of EZH2 and STAT3 in GSCs (827 and 387). IgG represents a control antibody used for IPs. For IP-immunoblotting data, antibodies used for IP and western blotting were labeled as red and blue, respectively. Two hundred micrograms of lysates were used for each IP reaction and total lysates (20 μ g) were used as input controls.

(C) Co-IP and immunoblot analysis of EZH2 and STAT3 in GSCs and NPCs versus differentiated progenies. Differentiation was induced by culturing these cells in serum (10%)-containing media for 3 days. The EZH2-STAT3 complex was analyzed by co-IP, followed by immunoblot analysis. Protein levels of EZH2, SOX2 (a GSC-specific transcription factor), and GFAP (an astroglial differentiation marker) were examined. β -actin was used as a loading control.

(D) Co-IP and immunoblots of the EZH2-STAT3 complexes in various cells. A 293T cell line (derived from human embryonic kidney cells) was used as a reference.

See also Figure S1.

Because STAT3 functions as a transcription factor, we determined the functional effects of decreased STAT3 activity in GSCs after EZH2 inhibition. We performed real-time RT-PCR analysis to measure mRNA expression of validated STAT3 transcriptional target genes including *STAT3*, *SOCS3*, and *c-MYC* (Figure 2D) in EZH2-inhibited cells (Frank, 2007). Messenger RNA levels of these genes were significantly decreased in GSCs treated with DZNep or EZH2 knockdown cells compared to the control (Figure 2D and data not shown). In addition, we determined STAT3 transcriptional activity by STAT3 responsive promoter reporter assays in which a luciferase reporter was driven by a STAT3 DNA-binding sequence-containing promoter. STAT3 transcriptional activity was substantially lower in cells treated with DZNep or EZH2 knockdown cells than in the controls (Figure 2E and data not shown). Together, these data support that EZH2 may directly regulate STAT3 activity in GSCs.

STAT3 Is Methylated by EZH2 in GSCs

Because EZH2 methylates specific lysine residues of histone proteins and EZH2 interacts with STAT3, we hypothesized that EZH2 methylates STAT3. By immunoprecipitation with an anti-STAT3 antibody followed by immunoblotting using a pan-methyl lysine antibody, we found that STAT3 is methylated in GSCs (Figure 3A). To interrogate the role of EZH2 in STAT3 methylation, we targeted EZH2 genetically (shRNA-mediated knockdown) or pharmacologically (with DZNep), and then assessed the methylation status

of STAT3 protein in GSCs. In both cases, STAT3 methylation was markedly decreased (Figures 3A and 3B). To determine whether a methyltransferase activity of EZH2 is required for STAT3 methylation, we overexpressed a methyltransferase-inactive EZH2 H689A mutant (Kuzmichev et al., 2002) in GSCs via lentiviral transduction and assessed the level of STAT3 methylation (Figure 3C). Ectopic expression of EZH2 H689A mutant decreased H3K27 trimethylation and reversed transcriptional repression of *Dickkopf-1* (*Dkk1*), a Wnt antagonist and Polycomb target gene (Götze et al., 2010; Hussain et al., 2009), suggesting that this mutant functions as a dominant-negative form (Figures 3C and 3D). Compared to the GFP-transduced cells or the wild-type EZH2-transduced cells, EZH2 H689A mutant-transduced cells showed decreased STAT3 methylation (Figure 3C). Collectively, these data support that STAT3 methylation in GSCs is mediated by EZH2.

EZH2 Inhibition Decreases STAT3 Methylation and Activity in GBM Xenografts

Because EZH2-STAT3 interaction is prominent in GSCs in vitro, we determined STAT3 methylation status in GBM xenografts. Protein lysates of GBM xenograft tumors derived from four different GSCs were interrogated by reciprocal co-IP experiments using anti-STAT3 and methylated lysine-specific antibodies. Methylated STAT3 was present in lysates from all tumors tested (Figure 3E). Next, we determined whether EZH2 inhibition could affect STAT3 methylation and STAT3 activity in GBM in vivo by using two complementary approaches. First, we implanted GSCs expressing either EZH2 shRNA or control shRNA into the brains of immunocompromised mice. Second, we generated GSC-derived xenograft tumors and treated the animals with DZNep after tumors were established. EZH2

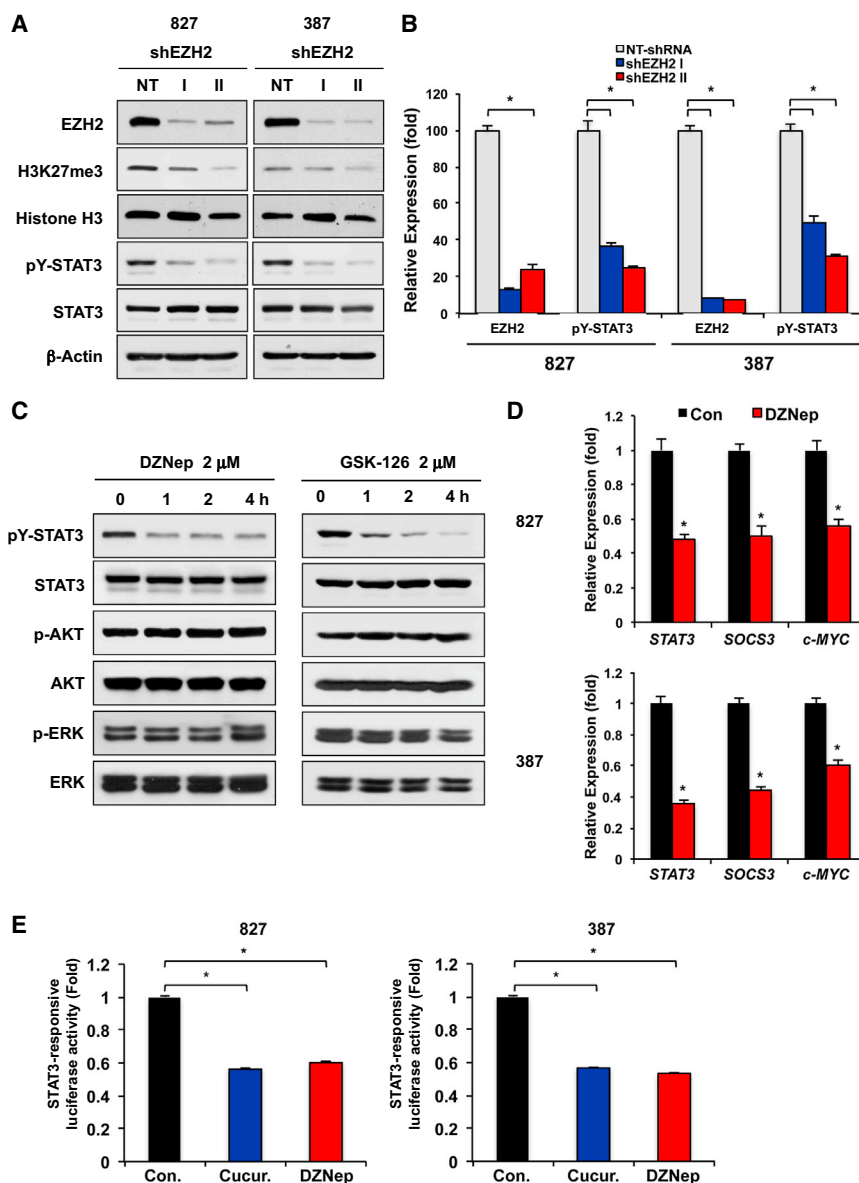


Figure 2. EZH2 Targeting Decreases STAT3 Activation in GSCs

(A) Immunoblots of EZH2, H3K27me3, pY-STAT3 (Y705) and total STAT3 in GSCs transduced with shEZH2-I, shEZH2-II, or nontargeting (NT) control shRNA.

(B) Quantification of protein intensities in immunoblots including the one shown in (A) was performed by densitometry.

(C) Immunoblots of pY-STAT3 and total STAT3 in GSCs treated with EZH2 inhibitors DZNep (2 μ M) or GSK-126 (2 μ M) for the indicated times (0 hr to 4 hr). Representative blots using 827 cells were shown.

(D) Semiquantitative real-time RT-PCR analysis to determine mRNA expression of STAT3 target genes in GSCs (827 and 387) treated with DZNep for 1 day. Expression levels of these genes were normalized and compared to those of the untreated control cells. Data are means \pm SD (n = 3).

(E) Determination of STAT3 transcription activity by STAT3-responsive luciferase reporter assays. Luciferase activities in GSCs treated with DZNep were compared to those of the untreated control. Cells treated with cucurbitacin (a STAT3 inhibitor) were used as a positive control. Error bar represents SD. *p < 0.01.

ated xenograft tumors using these cells. The tagged STAT3 was phosphorylated normally in response to EGF and interleukin-6 (IL-6), potent inducers for pY-STAT3 (Zhong et al., 1994). Flag-STAT3 protein was purified from GSC-derived xenograft tumors and analyzed by mass spectrometry (MS). A mass shift of +42 was observed for a STAT3 peptide, consistent with trimethyl modifications (Figure S2A). The previously reported lysine 140 methylation of STAT3 was not detected in these tumors with MS analysis (Yang et al., 2010) (data not shown). Because the methylation was in a peptide that includes residues 178 to 197, and

knockdown (Figures 3F and 3G) or DZNep treatment (Figures 3H and 3I) decreased the growth of xenograft tumors. Tumors obtained from both experiments were dissected and processed for western blot analysis and co-IP experiments. Compared to the controls, tumors treated with DZNep or tumors expressing EZH2 shRNA showed low levels of STAT3 methylation and pY-STAT3 (Figures 3F–3J). Furthermore, immunohistochemical analyses on tumor sections showed the decreased number of pY-STAT3 positive cells in tumors treated with DZNep compared to the control (Figure 3K). Taken together, these data demonstrate that targeting EZH2 effectively inhibits H3K27 methylation, STAT3 methylation, and STAT3 activation in GBM xenografts.

STAT3 Methylation Positively Regulates STAT3 Activity in GSCs

To analyze the methylation status of STAT3 protein, we overexpressed Flag-tagged STAT3 (Flag-STAT3) in GSCs and gener-

tandem MS analysis localized the site to lysine 180 (K180) (Figure S2A), we generated lentiviruses expressing STAT3 mutants in which a K180 residue of STAT3 protein was replaced by alanine (A) or arginine (R). We overexpressed these STAT3 mutants in GSCs and performed co-IP experiments to assess the methylation status of these proteins and the interaction with EZH2 (Figure 4). While exogenous wild-type STAT3 was methylated, both K180A and K180R mutants showed little or no methylation (Figure 4A). Similarly, STAT3 K180 mutants were unable to immunoprecipitate with EZH2 in contrast to the wild-type STAT3 (Figure 4A). These data support K180 of STAT3 as a key residue required for the EZH2-STAT3 interaction and EZH2-mediated STAT3 methylation.

Because pY-STAT3 is an important indicator of STAT3 activity, we performed IP experiments to determine the phosphorylation status of exogenous STAT3 proteins. While wild-type STAT3 was phosphorylated at tyrosine 705, both K180A and K180R

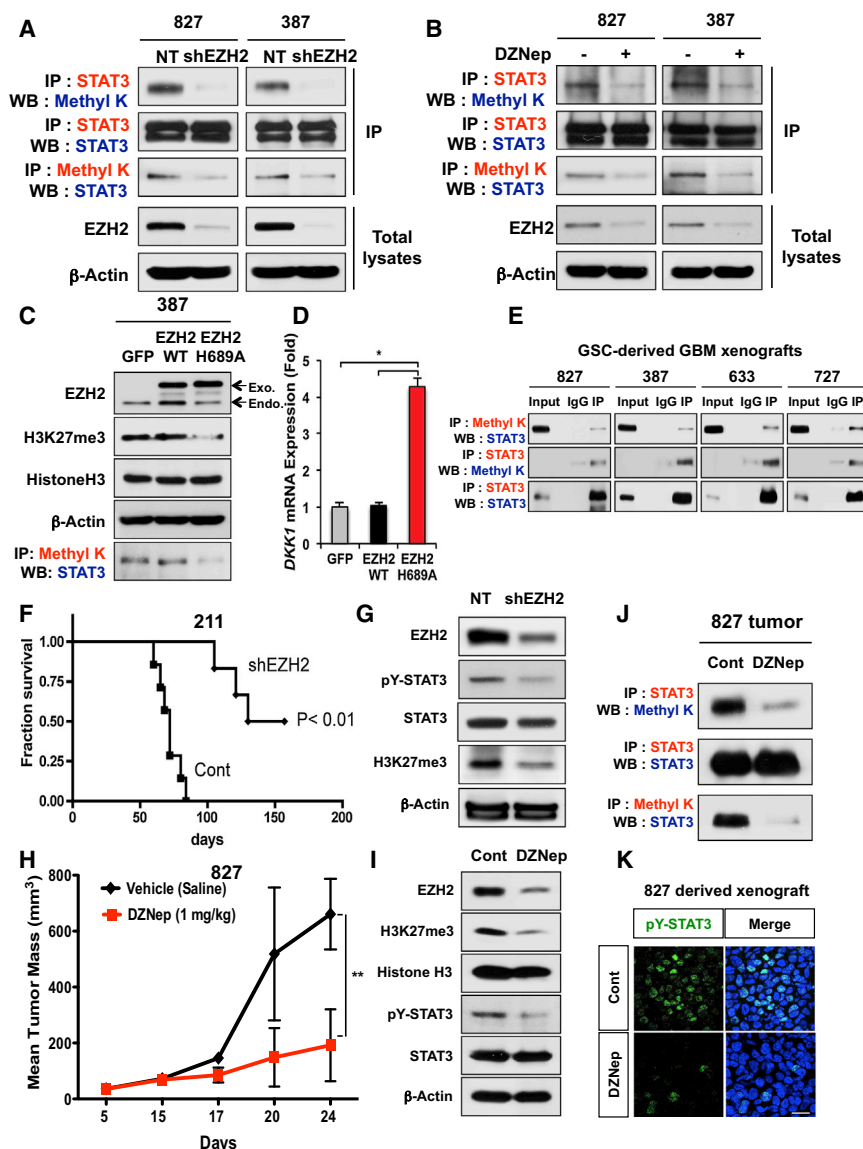


Figure 3. EZH2 Methylates STAT3 Protein in GSCs

(A and B) Co-IP and immunoblots of the methylated STAT3 in GSCs. Either *EZH2* knockdown (A) or treatment with DZNep (B) decreased methylated STAT3 in GSCs. Methyl K represents an antibody recognizing the methylated lysine.

(C) Co-IP and immunoblots of the methylated STAT3 in GSCs that express GFP, wild-type *EZH2*, and *EZH2* H689A. Arrows indicate protein bands of endogenous *EZH2* (endo) and exogenous *EZH2* transgenes (exo).

(D) Expression levels of *DKK1*, a PRC2 target gene, in GSCs expressing *EZH2* transgenes were determined by real-time RT-PCR analysis. Data are means \pm SD ($n = 3$). * $p < 0.01$.

(E) IP and immunoblots of methylated STAT3 in various GSC-derived GBM tumors.

(F) Kaplan-Meier survival curves of mice orthotopically implanted with 211 GSCs transduced with either control or *EZH2* shRNA expressing lentivirus ($n = 7$). $p < 0.01$.

(G) Immunoblots of pY-STAT3 and H3K27me3 in xenograft tumors (F). Human tumor cells were harvested 3 months after intracranial implantation and processed for immunoblot analysis.

(H–J) Measurement of subcutaneous xenograft tumor size after treatment with DZNep. Error bar represents SD ($n = 5$). ** $p < 0.01$. GSC-derived xenograft tumors were treated with DZNep (1 mg/kg body weight twice a week via intraperitoneal injection) for 2 weeks, harvested, and processed for immunoblots and co-IP analysis (I) and (J) and IF staining (K).

(K) IF staining of pY-STAT3 (green) on the frozen sections of GBM xenografts treated with vehicle or DZNep. Nuclei were stained with DAPI. Bar represents 10 microns.

mutants showed little or no phosphorylation (Figure 4A). To further investigate the effects of K180 mutation on STAT3 function, we overexpressed wild-type STAT3 and STAT3 K180 mutants in PC3, a STAT3 null prostate cancer cell line. After treatment with IL-6, activating tyrosine phosphorylation of STAT3 was evident in the wild-type STAT3-PC3 cells but not in STAT3 K180 mutant-PC3 cells (Figures S2B and S2C). Consistent with this, overexpression of K180 STAT3 mutant in PC3 failed to increase STAT3 transcriptional activity responding to IL-6. To interrogate the role of these STAT3 mutants in GSCs, we performed similar experiments in GSCs in which endogenous STAT3 signaling is active. Luciferase reporter assays to monitor STAT3 transcriptional activation revealed that STAT3 K180 mutant-expressing cells were impaired in the ability to activate STAT3, in contrast to the wild-type STAT3-expressing GSCs (Figure 4B). Unlike wild-type STAT3, overexpression of STAT3 K180A in GSCs did not increase transcription of STAT3 target genes, such as *SOCS3* and *c-MYC* (Figure 4C). Because nuclear

accumulation of pY-STAT3 is another indicator of STAT3 activation, we assessed the levels of nuclear pY-STAT3 in STAT3 mutant-expressing GSCs. pY-STAT3 was highly accumulated after IL-6 challenge in empty vector control GSCs or the wild-type STAT3-expressing GSCs but not in STAT3 K180 mutant-expressing cells (Figure 4D and data not shown). In GSCs, STAT3 signaling promotes activation of stem cell-associated transcriptional factors including *Olig2*, *Sox2*, and *Nanog* (Guryanova et al., 2011). Overexpression of wild-type STAT3 but not STAT3 K180A mutant induced transcription of these genes (Figure 4E). We then assessed the effect of STAT3 mutants on the growth of GSCs. Compared to the wild-type STAT3-expressing cells, STAT3 K180 mutant-expressing cells were less proliferative (Figures 4F–4H). Clonogenic growth as a form of sphere is an in vitro indicator of GSC self-renewal. To determine the role of STAT3 K180 mutants on clonogenic growth of GSCs, we performed neurosphere formation limiting dilution assays. Tumor cells were plated into 96-well plates with various seeding densities and allowed to grow. Compared to the empty vector control and the wild-type STAT3, ectopic expression of STAT3 K180 mutants reduced the efficiency of sphere formation (Figure 4I).

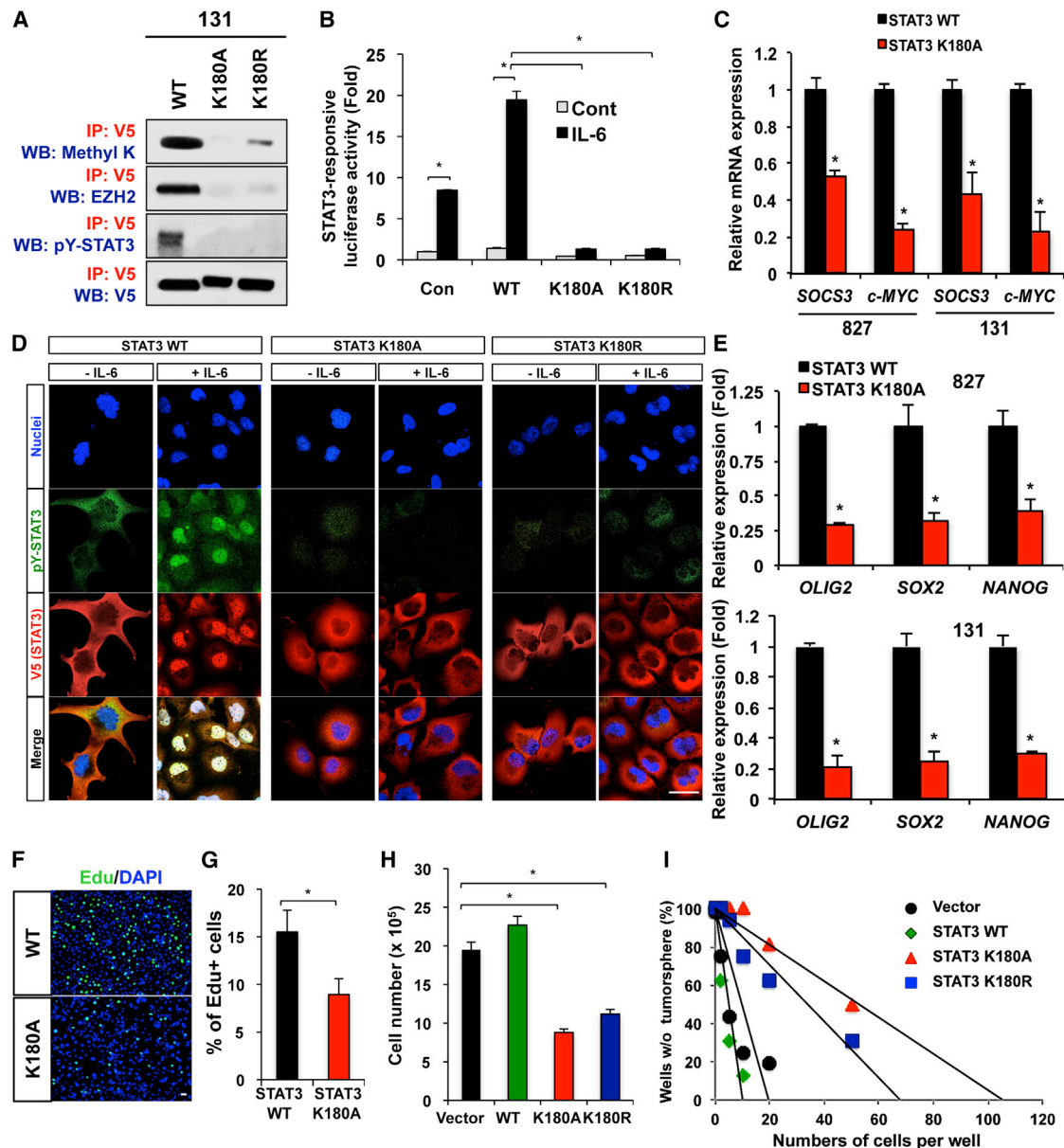


Figure 4. Effects of STAT3 Methylation on STAT3 Activity and GSC Self-Renewal

(A) Co-IP analyses of methylated STAT3, pY-STAT3 and the EZH2-STAT3 complex in 131 GSCs expressing STAT3 K180 mutants. V5 is a protein tag fused with STAT3. Methyl K denotes an antibody recognizing either di- or trimethylated lysine.

(B) STAT3 transcriptional activity in response to IL-6 in 131 GSCs expressing the empty vector control, wild-type STAT3, or the STAT3 K180 mutants. * $p < 0.01$.

(C) Real-time RT-PCR analysis to determine mRNA levels of *SOCS3* and *c-MYC* in GSCs (827 and 131) expressing either wild-type or STAT3 K180A mutant. Messenger RNA levels of *SOCS3* and *c-MYC* in STAT3 K180 expressing cells were compared to those in wild-type STAT3 expressing cells (set to 1). Data are means \pm SD ($n = 3$). * $p < 0.01$.

(D) IF staining of pY-STAT3 (green) on GSCs expressing the wild-type STAT3 and STAT3 K180 mutants in response to IL-6 (50ng/ml). V5 (red) was used to stain exogenous STAT3 and DAPI (blue) was used to stain nuclei.

(E) Real-time RT-PCR analysis to determine mRNA expression of stem cell associated transcription factors (*OLIG2*, *SOX2*, and *NANOG*) in GSCs (827 and 131) expressing STAT3 mutants. Data are means \pm SD ($n = 3$). * $p < 0.01$.

(F–I) Effects of STAT3 K180 mutant overexpression on proliferation and clonogenic growth of GSCs. 5'-ethynyl-2'-deoxyuridine (EdU)-positive cells (stained green) were counted in three random fields and plotted (in F and G). * $p < 0.01$. Cell counts of STAT3 mutant-expressing GSCs after 6 days of culture (H) and limiting dilution assay results (I) were shown. Error bars represent SD. Bars (in D and F) represent 10 microns. See also Figure S2.

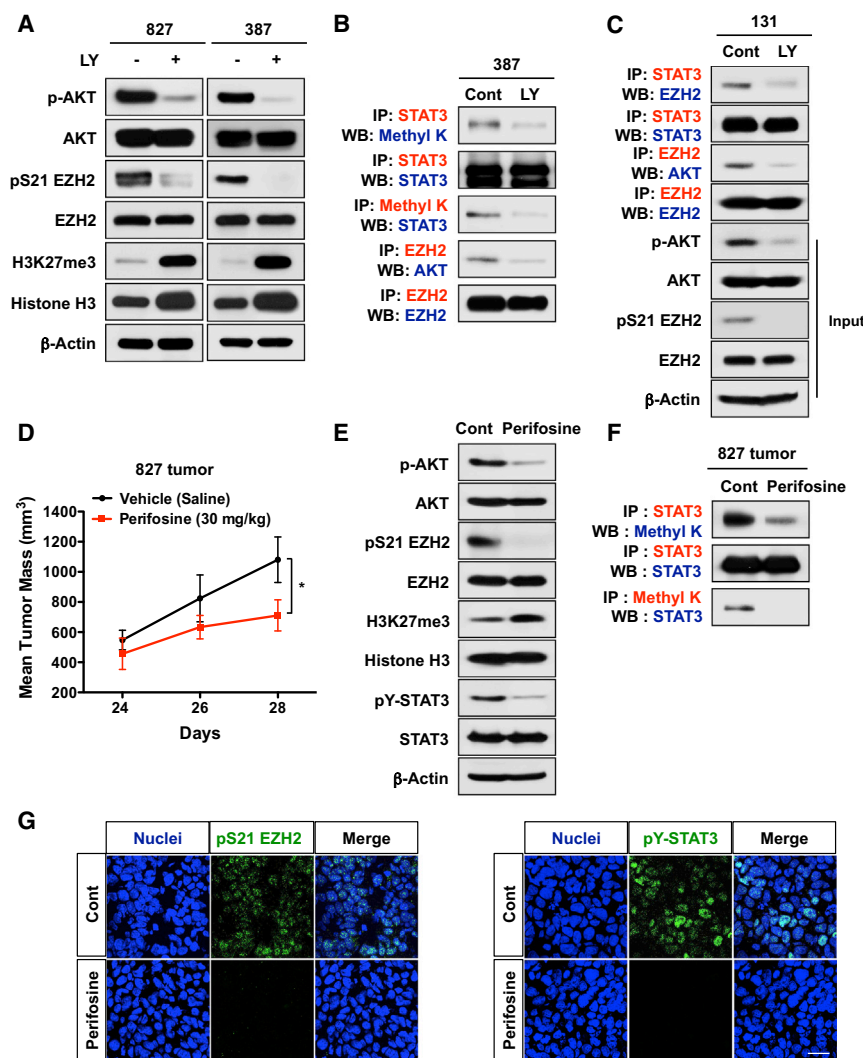


Figure 5. AKT Signaling Is Essential for the EZH2-STAT3 Interaction in GSCs and AKT Inhibition Decreases STAT3 Activity in GBM Xenografts

(A) Immunoblot analysis of AKT, pS473 AKT, EZH2, pS21 EZH2, and trimethylated H3K27 in GSCs treated with a PI3K/AKT pathway inhibitor LY294002.

(B and C) Co-IP analysis of methylated STAT3 and the EZH2-STAT3 complex in GSCs treated with LY294002 for 1 day.

(D) Tumor growth of 827 GSC-derived xenografts treated with an AKT inhibitor perifosine (30 mg/kg body weight). Twenty-three days after tumor implantation in mice, perifosine was administered by intraperitoneal injection (daily for 5 days). Error bars represent SD. Five mice per group, **p* < 0.01.

(E) Immunoblot analysis of pY-STAT3, EZH2, AKT, and trimethylated H3K27 in lysates from xenograft tumors in (D).

(F) Co-IP analysis of methylated STAT3 in GBM xenograft tumors treated with perifosine.

(G) IF staining of pS21 EZH2 and pY-STAT3 on the frozen sections of GBM xenografts treated with vehicle or perifosine. Nuclei were stained with DAPI. Bar represents 10 microns.

Together, these data are consistent with the possibility that EZH2 methylates STAT3 at K180 and this methylation enhances STAT3 activation and promotes clonogenic growth of GSCs.

AKT Signaling Is Essential for the EZH2-STAT3 Interaction in GSCs

Because our data indicate that the EZH2-STAT3 interaction leads to STAT3 activation, we investigated a potential upstream effector(s) to facilitate this interaction. An initial clue came from a previous study in which the authors reported that EZH2 is phosphorylated at serine residue 21 (pS21 EZH2) by AKT (Cha et al., 2005). Cha et al. showed that phosphorylation of EZH2 at S21 significantly decreased H3K27 trimethylation leading to the derepression of PRC2 target genes (Cha et al., 2005). However, breast cancer cells overexpressing EZH2 S21D (phosphorylation mimetic mutant of pS21 EZH2) showed increased proliferation and invasiveness. H3K27 trimethylation and PRC2-mediated transcriptional repression are generally associated with tumor malignancy, thus an oncogenic role of EZH2 phosphorylation appears to be counterintuitive. A potential explanation for this discrepancy is that S21 phosphorylation of EZH2 may exert pro-

tumorigenic functions in H3K27 in a trimethylation-independent manner, as suggested in a recent report (Xu et al., 2012).

Because EZH2 interacts with and methylates STAT3, we hypothesized that STAT3 is one such molecule to exert pro-tumorigenic functions in GSCs. PI3K/AKT signaling is highly active in about 90% of GBM specimens (Fan et al., 2006; Fan and Weiss, 2010; Cancer Genome Atlas Research Network, 2008; Verhaak et al., 2010) and all of GSCs we tested have a

high level of activating phosphorylation of AKT (Figure 2C and data not shown). In agreement with the previous reports (Cha et al., 2005; Costa et al., 2010), treatment with LY294002 (a PI3K-AKT inhibitor) or perifosine (an AKT inhibitor) blocked S21 phosphorylation of EZH2 but increased global levels of H3K27 trimethylation in GSCs (Figure 5A). In GSCs treated with these inhibitors, levels of EZH2-STAT3 complexes and methylated STAT3 were markedly reduced compared to controls (Figures 5B and 5C). Overexpression of a dominant-negative AKT in GSCs showed similar results (data not shown). Together, these data suggest that AKT signaling is required for the EZH2-STAT3 interaction and STAT3 methylation in GSCs.

AKT Inhibition Decreases Methylation and Activation of STAT3 in GBM Xenografts

To address the relevance of the above findings in vivo, we established GSC-derived xenograft tumors and evaluated the effects of AKT inhibition on STAT3 activity and tumor growth (Figure 5). Animals treated with perifosine for 5 days displayed reduced tumor size relative to those treated with vehicle control (Figure 5D). One day after the final injection of perifosine, we dissected

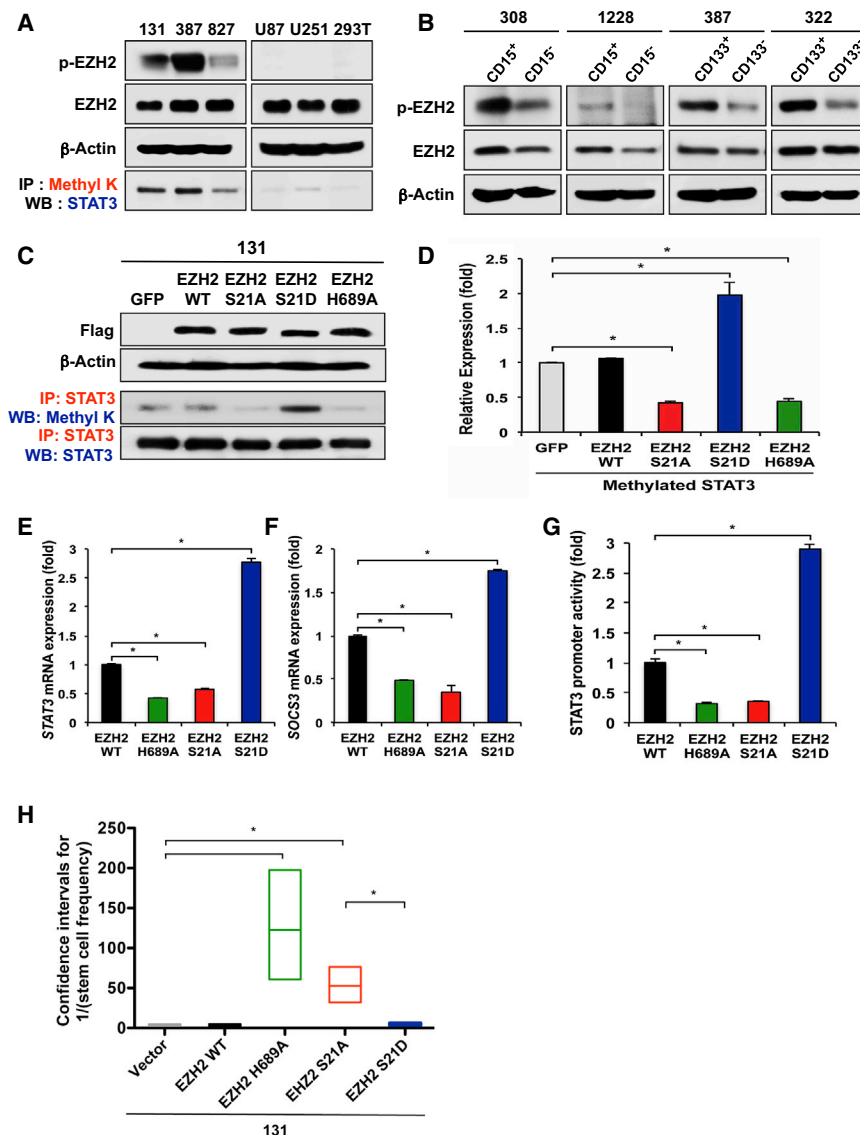


Figure 6. Phosphorylation of EZH2 at Serine 21 Is Critical for STAT3 Methylation and STAT3 Activity in GSCs

(A) Co-IP and Immunoblot analysis of pS21 EZH2 and methylated STAT3.

(B) Immunoblot analysis of pS21 EZH2 in GSC-enriched or GSC-depleted GBM cells (CD133+ or – and CD15+ or –).

(C) Co-IP and immunoblot analyses of methylated STAT3 in GSCs transduced with various EZH2 mutants. EZH2 transgenes were detected by Flag tag.

(D) Quantification of methylated STAT3 shown in (C). Protein amounts were estimated by densitometry of immunoblots. Error bars represent SD. * $p < 0.01$.

(E and F) Real-time RT-PCR analysis to determine mRNA expression of STAT3 and SOCS3 in 131 GSCs expressing various EZH2 mutants. Data are means \pm SD ($n = 3$). * $p < 0.01$.

(G) Determination of STAT3 transcription activity by reporter promoter assays. Luciferase activity in GSCs expressing various EZH2 constructs was compared to that of the GFP-expressing control cells. Error bars represent SD. * $p < 0.01$.

(H) Effects of ectopic expression of various EZH2 constructs on GSC tumorsphere formation. GSC cells (131) transduced with lentivirus expressing various EZH2 transgenes were cultured for limiting dilution assays. Frequency of stem-like clonogenic cells was determined by a web-based tool “ELDA” (extreme limiting dilution analysis, available on <http://bioinf.wehi.edu.au/software/elda/>) and represented as a box plot. Boxes indicate the upper and lower confidence intervals, and the lines denote the estimated values. * $p < 0.01$. See also Figure S3.

tumors for immunoblot analysis and co-IP experiments. Compared to the control, tumors treated with perifosine showed low levels of phosphorylated AKT and EZH2 phosphorylation (Figure 5E). Consistent with in vitro results, AKT inhibition in vivo decreased STAT3 methylation and pY-STAT3, but increased global levels of H3K27 trimethylation (Figures 5E and 5F). Immunofluorescence analyses on tumor sections further confirmed that perifosine treatment decreased pS21 EZH2 and nuclear PY-STAT3 (Figure 5G). Together, these data suggest that AKT regulates STAT3 signaling in part via EZH2 phosphorylation and STAT3 methylation.

GSCs Have a High Level of EZH2 Phosphorylation at Serine 21

Because phosphorylation of EZH2 at S21 appears to be an important signal node between AKT signaling and STAT3 methylation in GSCs, we determined the levels of pS21 EZH2 and STAT3 methylation in various GBM cells. Immunoblot anal-

ysis showed that pS21 EZH2 is highly expressed in GSCs but not in U87 and U251 glioma cell lines (Figure 6A). Similarly, STAT3 methylation was abundant in GSCs but much lower in glioma cell lines (Figure 6A). This trend is entirely consistent with the level of the EZH2-STAT3 complex in these cells (Figure 1D). To further examine preferential expression of pS21 EZH2 in GSCs, we used four additional GBM cells with prospective sorting for CD133 and/or CD15. CD133- and/or CD15-positive GSCs have higher level of pS21 EZH2 compared to CD133- and/or CD15-negative cells (Figure 6B). Together, these data show that pS21 EZH2 is preferentially expressed in GSCs and suggest that pS21 EZH2 is required for the EZH2-STAT3 interaction and STAT3 methylation in GSCs.

EZH2 Phosphorylation at Serine 21 Enhances STAT3 Methylation and Activation

To interrogate the role of pS21 EZH2 in regulating STAT3, we overexpressed a phosphorylation-defective or phosphorylation mimetic EZH2 mutant in GSCs and examined the effects on STAT3 methylation and STAT3 activity (Figures 6C–6G). Expression of the EZH2 S21A mutant markedly decreased STAT3 methylation similar to a catalytic activity-dead EZH2 H689A

mutant. In sharp contrast, expression of EZH2 S21D mutant significantly increased STAT3 methylation (Figures 6C and 6D). These data prompted us to test whether a low level of STAT3 methylation in U87 glioma cells is due to the low expression of pS21 EZH2. Exogenous expression of EZH2 S21D mutant significantly increased STAT3 methylation and STAT3 activity in U87 cells and NPCs, similar to GSCs (Figure S3 and data not shown). Furthermore, STAT3 target gene expression (e.g., *STAT3* and *SOCS3*) and luciferase-based STAT3 transcriptional activity were significantly high in EZH2 S21D mutant-expressing cells but low in EZH2 S21A mutant-expressing cells compared to the control (Figures 6E–6G). Together, these data support the notion that STAT3 methylation and activation are mediated by pS21 EZH2.

To interrogate the role of pS21 EZH2 in GSC growth, we overexpressed various EZH2 constructs in GSCs via lentiviral transduction and determined the effects on clonogenic growth of GSCs (Figure 6H). Limiting dilution assays were performed and the frequencies of sphere-forming clonogenic cells were estimated. The frequencies of sphere-forming clonogenic cells were approximately one out of five cells in the control or wild-type EZH2 expressing cells. In contrast, most of EZH2 H689A-expressing cells failed to generate colonies. Ectopic expression of EZH2 S21A also significantly reduced the number of clonogenic cells to less than 10% of the controls (Figure 6H).

STAT3 Signaling Is a Crucial Downstream Effector of EZH2 Signaling in GBM

To interrogate the role of pS21 EZH2, we further analyzed the effects of EZH2 S21A overexpression in GSCs. Ectopic expression of a catalytic activity-dead EZH2 H689A mutant in GSCs decreased methylation of both H3K27 and STAT3 (Figure 3C). In contrast, expression of EZH2 S21A mutant significantly decreased STAT3 methylation but increased global levels of H3K27 trimethylation in GSCs (Figure 7A). Overexpression of EZH2 S21A mutant in GSCs did not change the level of *Dkk1* mRNA expression, suggesting that PRC2-mediated silencing is unaffected by EZH2 S21A (data not shown). However, EZH2 S21A mutant was unable to immunoprecipitate with STAT3 in contrast to the wild-type EZH2 (Figure 7B) and pY-STAT3 was significantly low in EZH2 S21A-expressing cells compared to the controls (Figure 7A). Because EZH2 S21A mutant-expressing cells show the decreased STAT3 activity, we then determined whether forced activation of STAT3 could rescue the reduced clonogenic growth in these cells (Figures 7C–7E). We overexpressed a constitutively active STAT3 mutant (STAT3C) in EZH2 S21A-expressing GSCs and determined their clonogenic growth by limiting dilution assays. In the control and STAT3C-expressing cells, the numbers of clonogenic cells are similar. Expression of STAT3C in EZH2 S21A mutant cells significantly increased the number of clonogenic cells (Figure 7E), suggesting that STAT3 signaling is a crucial downstream effector of EZH2 signaling in GBM.

To interrogate the role of EZH2 in tumor growth in vivo, we overexpressed EZH2 H689A or EZH2 S21A proteins in GSCs and implanted these cells into the brains of SCID mice (50,000 cells per mouse, $n = 10$ per each group). While animals bearing control cells died within 2 months (median survival: 47 days), animals injected with EZH2 H689A-expressing cells survived

significantly longer (median survival: 75 days; $p < 0.001$). Median survival of the mice bearing EZH2 S21A-expressing cells was 67 days ($p < 0.001$), which is significantly longer than that of the controls (Figure 7F). Kaplan-Meier curves showed the increase in survival of mice bearing EZH2 S21A- and EZH2 H689A-expressing tumor ($p < 0.001$ compared to the control). These in vivo data demonstrate that the selective blocking of a STAT3-related arm of EZH2 function can increase the survival of tumor-bearing mice. Our findings, therefore, support that EZH2 contributes to GBM tumor growth by both H3K27 trimethylation-dependent and STAT3-dependent pathways.

Our data obtained in the models of various patient-derived GSCs and GBM xenografts in vitro and in vivo suggest that EZH2 phosphorylation has protumorigenic roles in part via STAT3 activation. To assess the in vivo relevance of the EZH2-STAT3 axis, we determined the expression of pS21 EZH2 and pY-STAT3 in protein lysates from the patient-derived GBM specimens (Figure S4). The correlation between the expression of EZH2 and pS21 EZH2 is not always linear; however, there appears to be a potentially positive correlation between pS21 EZH2 and pY-STAT3 (Figure S4). To determine whether pS21 EZH2 is associated with survival in patients with GBM, we performed immunohistochemical analysis using the tissue microarray (TMA) sections containing 87 GBM specimens from the patients (Figure S4). Expression of pS21 EZH2 displayed inter- and intratumoral heterogeneity. A high frequency of cells positive for pS21 EZH2 in GBM specimens was positively correlated with the shorter overall survival of the patients ($p < 0.001$ by log rank analysis).

Collectively, these data support a model in which EZH2 not only mediates transcriptional silencing, but also contributes to the activation of STAT3 signaling in GBM (Figure 7G). We propose that the molecular mechanism through which EZH2 activates STAT3 involves a specific EZH2 phosphorylation and STAT3 methylation.

DISCUSSION

Altered profile of histone modification is a major epigenetic mechanism, deregulation of which leads to tumor initiation and propagation (Margueron and Reinberg, 2011; Schlesinger et al., 2007; Widschwendter et al., 2007). Polycomb-mediated transcriptional silencing plays a critical role in the maintenance of the stem cell status in both normal and malignant stem cells. In this study, we demonstrate that EZH2 methylates STAT3 leading to the enhanced STAT3 activity.

Our data indicate that EZH2 not only mediates transcriptional silencing, but also contributes to the activation of STAT3 signaling in stem-like GBM cells. As supporting evidence, we found that the EZH2-STAT3 interaction and EZH2 S21 phosphorylation preferentially occur in GSCs relative to non-stem tumor cells. Overexpression of EZH2 S21D induced STAT3 methylation and enhanced STAT3 activity, suggesting that EZH2 S21 phosphorylation is a molecular switch that facilitates STAT3 methylation. We do not know the underlying molecular mechanism by which the EZH2 S21 phosphorylation is more prominent in stem-like cells. One possibility is that a cofactor of PRC2 component preferentially expressed in stem cell population (Simon and Kingston, 2009) might facilitate the AKT-EZH2

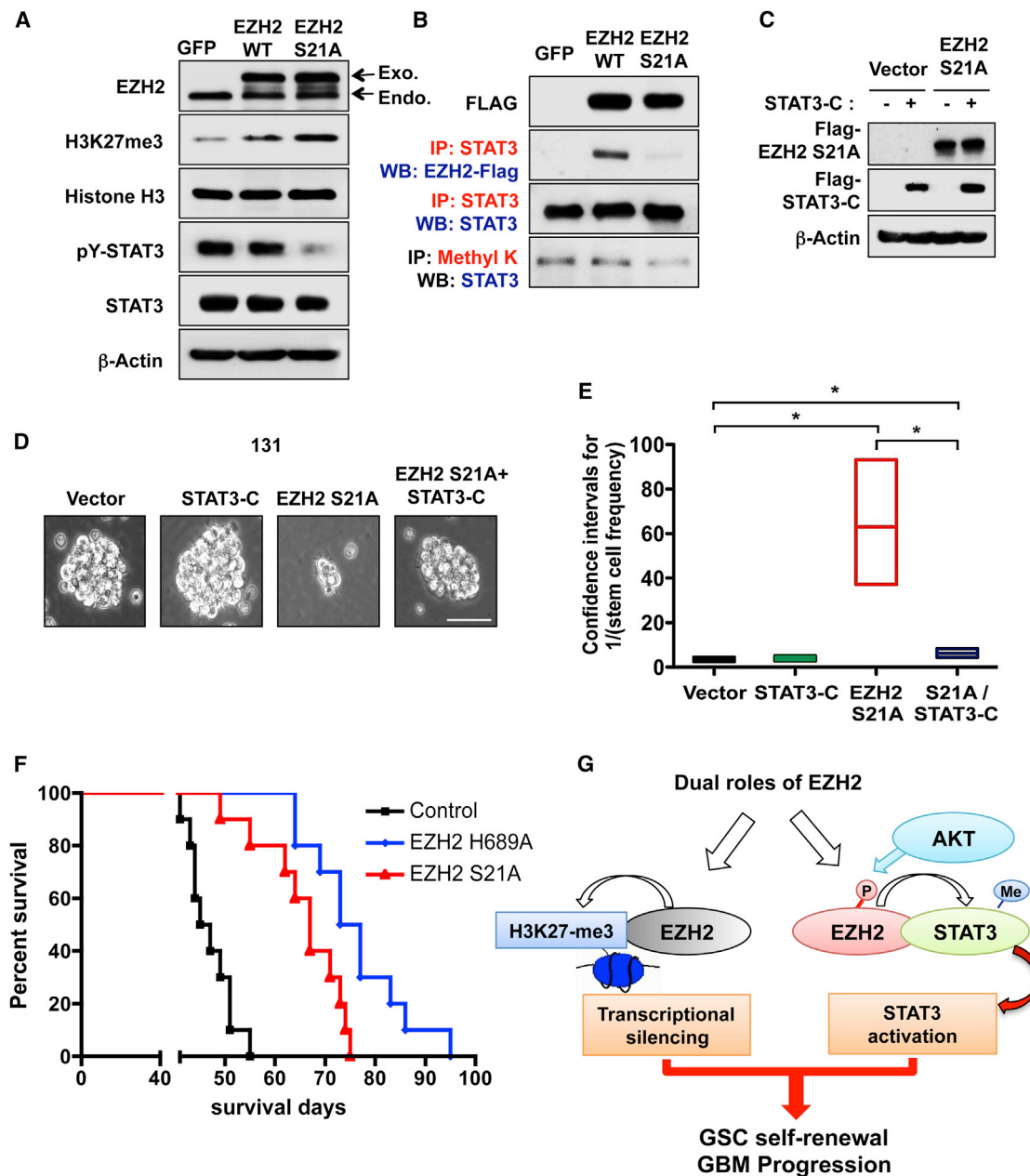


Figure 7. EZH2 Contributes to GBM Tumor Growth by both H3K27 Trimethylation-Dependent and STAT3-Dependent Pathways

(A and B) Immunoblot and Co-IP analysis of methylated STAT3 and H3K27me3 in GSCs that express GFP, wild-type EZH2, or EZH2 S21A.

(C) Immunoblots of exogenous EZH2 S21A and STAT3-C proteins in 131 GSCs.

(D) Representative images of 131 GSCs expressing EZH2 S21A and STAT3-C protein. Bar represent 50 microns.

(E) Effects of ectopic expression of EZH2 S21A and STAT3-C protein on GSC tumorsphere formation. From limiting dilution assays, frequencies of stem-like clonogenic cells were calculated using ELDA and presented as a box plot. * $p < 0.01$.

(F) Kaplan-Meier survival curves of mice ($n = 10$ for each group) intracranially implanted with 131 GSCs expressing control, EZH2 689A, or EZH2 S21A proteins (control versus EZH2 H689A, $p < 0.0001$; control versus EZH2 S21A, $p < 0.0001$; EZH2 H689A versus EZH2 S21A, $p = 0.015$ by log rank analysis).

(G) A schematic model that illustrates two functional arms of EZH2. P and Me represent phosphorylation and methylation, respectively.

See also Figure S4.

interaction and subsequent interaction with STAT3. It is also possible that EZH2 S21 phosphorylation is regulated by differential AKT or AKT-related downstream effects which may not be directly associated with stem-like characteristics. Further

studies to decipher underlying molecular mechanisms are warranted as a recent study reported EZH2 S21 phosphorylation as a critical modification for EZH2 to function as a transcriptional co-activator with androgen receptor (Xu et al., 2012).

Our data support that EZH2-mediated STAT3 methylation is a critical modification that leads to STAT3 activation, although the precise molecular events that link STAT3 methylation to STAT3 activation are unknown. STAT3 activation involves a series of sequential events including tyrosine phosphorylation, dimerization, nuclear import, DNA binding, serine phosphorylation, nuclear retention, and binding to protein partners (Akira et al., 1994; Yang and Stark, 2008; Zhong et al., 1994). It is possible that K180 methylation of STAT3 enhances its tyrosine phosphorylation by protecting it from dephosphorylation, as supported by K180 STAT3 mutant data. It has been proposed that K140 methylation of STAT3 destabilizes STAT3 tyrosine phosphorylation, thereby negatively affecting STAT3-dependent transcription (Yang et al., 2010). In contrast to K180 STAT3 methylation by EZH2, K140 methylation can be viewed as a negative event for STAT3 signaling cascade. By analogy with the cases in P53 and NF- κ B, specific lysine site and the degree of methylation will likely determine STAT3 activity. Although K140 methylation of STAT3 was not detected in our studies, these findings may suggest a critical role of methylation in STAT3 signaling cascade in various cancers. In addition to K180 methylation, we also found K709 dimethylation of STAT3 by MS analysis (data not shown), suggesting that there might be additional lysine residues of STAT3 that could be methylated by EZH2. Further studies are required to precisely define when lysine methylation of STAT3 occurs during the STAT3 signaling cascade and interrogate the role of STAT3 methylation in STAT3 activation.

Despite these caveats, there are important biological and clinical implications derived from our findings. First, the EZH2 and STAT3 signaling pathways are critical therapeutic targets for GBMs, and our findings suggest that EZH2 targeting may effectively inhibit oncogenic activities of both pathways. Significant research efforts have been aimed at developing therapeutic agents targeted for EZH2 because highly specific EZH2 inhibitors have been reported recently (Knutson et al., 2012; McCabe et al., 2012; Qi et al., 2012). Our findings may lead to accelerated development of Polycomb/EZH2 targeting agents and provide a potential biomarker for evaluating therapeutic efficacy.

Second, STAT3 signaling is hyperactive in various cancers including GBMs and is an important therapeutic target; however, the specific inactivation of STAT3 has been challenging (Guryanova et al., 2011; Yue and Turkson, 2009). Our finding adds EZH2 to a growing list of upstream pathways leading to the STAT3 activation in GSCs, including IL-6, Notch, PI3K, LIF, BMX, and various receptor tyrosine kinases (epidermal growth factor receptor, platelet-derived growth factor, and MET) (Bromberg et al., 1999; Fan et al., 2010; Guryanova et al., 2011). It will be highly desirable if EZH2 targeting achieves the effective inhibition of both transcriptional silencing and STAT3 activity in a clinical setting.

A recent study reported that STAT3 signaling is a master regulator of mesenchymal transformation of gliomas, and that STAT3 downstream genes are highly expressed in the mesenchymal GBM subtype (Carro et al., 2010; Verhaak et al., 2010). Further studies aim to identify the subset of tumors in which the EZH2-STAT3 axis is particularly active, and to demonstrate the mechanistic correlations between these pathways. It is enticing to propose that EZH2 targeting agents may be particularly useful for patients harboring high levels of phosphorylated EZH2.

Inhibition of AKT signaling decreases STAT3 activity via EZH2 phosphorylation, implying that PI3K/AKT signaling is an upstream mediator of the EZH2-STAT3 interaction in GSCs. Activation of the PI3K/AKT pathway in glioma is associated with an adverse clinical outcome and various PI3K/AKT inhibitors are being tested in clinical trials (Fan et al., 2006; Fan and Weiss, 2010; Cancer Genome Atlas Research Network, 2008; Verhaak et al., 2010). Our data indicate that EZH2 S21 phosphorylation is required for the EZH2-STAT3 interaction and the enhanced STAT3 activity, and AKT inhibition in vivo effectively abolished pS21 EZH2. Therefore, it would be interesting to examine pS21 EZH2 expression as a biomarker to predict therapeutic responses to PI3K/AKT targeted therapies.

In conclusion, we demonstrate that EZH2 binds to and methylates STAT3, thereby enhancing STAT3 activity in GSCs. EZH2 phosphorylation by AKT is critical for the EZH2-STAT3 interaction. By utilizing EZH2 constructs that allow the dissection of two distinct functions of EZH2, we showed the role of STAT3-dependent EZH2 function in GBMs. We propose that two arms of EZH2 function, namely a histone methylation-dependent transcriptional silencing and STAT3 activation by direct protein-protein interaction, can cooperatively contribute to GSC self-renewal and GBM malignancy. These data suggest that functional disruption of EZH2 may attenuate multiple key signals involved in GSC self-renewal and survival, and further support that EZH2 is a promising therapeutic target for GBM.

EXPERIMENTAL PROCEDURES

Human GBM Specimens and Derivative GSCs

Following informed consent, glioblastoma specimens were obtained from patients undergoing surgery at the Samsung Medical Center in accordance with the Institutional Review Boards. Within hours after surgical removal, tumor specimens were enzymatically dissociated into single cells, following the procedures previously reported (Lee et al., 2006a; Son et al., 2009). For short-term in vitro expansion of GSCs, tumor cells were cultured in Neurobasal media with N2 and B27 supplements (0.5 \times each; Invitrogen), human recombinant basic fibroblast growth factor and epidermal growth factor (25 ng/ml each; R&D systems). Human NPCs were purchased from Lonza and cultured similar to GSCs. For differentiation of GSCs and NPCs, cells were cultured in the absence of growth factors or in the presence of 10% fetal bovine serum (Cellgro).

Intracranial Tumor Cell Injection

All mice experiments were performed according to the guidelines of the Animal Use and Care Committees at Samsung Medical Center. GBM cells were dissociated, resuspended in 2 μ l of HBSS, and injected intracranially into the striatum of adult nude mice by using a stereotactic device (Kopf instruments) (coordinates: 2 mm anterior, 2 mm lateral, 2.5 mm depth from the dura). Mice with neurologic signs were killed for the analysis of tumor histology and immunohistochemistry. Brains were perfused with 4% paraformaldehyde by cardiac perfusion and further fixed at 4°C overnight.

Chemicals and Antibodies

3-Deazaneplanocin A (DZNep) was kindly provided from Dr. Victor Marquez (National Cancer Institute). GSK126 was purchased from Xcessbio. Cucurbitacin and perifosine were purchased from Tocris and Selleckchem, respectively. The following antibodies were used as primary antibodies: EZH2 (BD Transduction Laboratories; 1:4,000); phospho-EZH2 (Bethyl Laboratories; 1:500); methylated lysine (Enzo Life Science and Abcam; 1:500); STAT3, phospho-STAT3 (Y705), histone H3, AKT, and phospho-AKT (S473) (Cell Signaling; 1:2,000); SOX2 and OLIG2 (R&D Systems; 1:2000 for western blotting and 1:400 for IF); trimethylated histone H3K27 and SUZ12 (Millipore; 1:1,000); GFAP (Dako; 1:1,000); β -actin (Sigma-Aldrich; 1:5,000).

Immunoprecipitation

Cells were collected and lysed in lysis buffer supplemented with protease inhibitors, incubated on ice for 15 min, and cleared by centrifugation at 13,200 rpm at 4°C for 15 min. Total protein lysate (500 µg) was subjected to immunoprecipitation with the agarose-immobilized antibody (1 µg of anti-STAT3, EZH2, methylated lysine antibody, or isotype control antibodies) for overnight at 4°C.

SUPPLEMENTAL INFORMATION

Supplemental Information includes four figures and Supplemental Experimental Procedures and can be found with this article online at <http://dx.doi.org/10.1016/j.ccr.2013.04.008>.

ACKNOWLEDGMENTS

We thank Drs. George Stark and Bingcheng Wang for critical reading of the manuscript. This work was supported by R01 NS082312 (to J.L.), the Case Comprehensive Cancer Center pilot grant P30CA043703 (to J.L.), the Korea Healthcare Technology R&D Project, Ministry for Health & Welfare Affairs, Republic of Korea, A092255 (to D.-H.N.), and Samsung Medical Center grant GFO1130011 (to D.-H.N.).

Received: July 16, 2012

Revised: February 2, 2013

Accepted: April 8, 2013

Published: May 16, 2013

REFERENCES

- Abdouh, M., Facchino, S., Chato, W., Balasingam, V., Ferreira, J., and Bernier, G. (2009). BMI1 sustains human glioblastoma multiforme stem cell renewal. *J. Neurosci.* 29, 8884–8896.
- Akira, S., Nishio, Y., Inoue, M., Wang, X.J., Wei, S., Matsusaka, T., Yoshida, K., Sudo, T., Naruto, M., and Kishimoto, T. (1994). Molecular cloning of APRF, a novel IFN-stimulated gene factor 3 p91-related transcription factor involved in the gp130-mediated signaling pathway. *Cell* 77, 63–71.
- Bao, S., Wu, Q., McLendon, R.E., Hao, Y., Shi, Q., Hjelmeland, A.B., Dewhirst, M.W., Bigner, D.D., and Rich, J.N. (2006). Glioma stem cells promote radioresistance by preferential activation of the DNA damage response. *Nature* 444, 756–760.
- Boyer, L.A., Plath, K., Zeitlinger, J., Brambrink, T., Medeiros, L.A., Lee, T.I., Levine, S.S., Wernig, M., Tajonar, A., Ray, M.K., et al. (2006). Polycomb complexes repress developmental regulators in murine embryonic stem cells. *Nature* 441, 349–353.
- Bromberg, J.F., Wrzeszczynska, M.H., Devgan, G., Zhao, Y., Pestell, R.G., Albanese, C., and Darnell, J.E., Jr. (1999). Stat3 as an oncogene. *Cell* 98, 295–303.
- Cancer Genome Atlas Research Network. (2008). Comprehensive genomic characterization defines human glioblastoma genes and core pathways. *Nature* 455, 1061–1068.
- Cao, R., Wang, L., Wang, H., Xia, L., Erdjument-Bromage, H., Tempst, P., Jones, R.S., and Zhang, Y. (2002). Role of histone H3 lysine 27 methylation in Polycomb-group silencing. *Science* 298, 1039–1043.
- Cao, Y., Lathia, J.D., Eyler, C.E., Wu, Q., Li, Z., Wang, H., McLendon, R.E., Hjelmeland, A.B., and Rich, J.N. (2010). Erythropoietin Receptor Signaling Through STAT3 Is Required For Glioma Stem Cell Maintenance. *Genes Cancer* 1, 50–61.
- Carro, M.S., Lim, W.K., Alvarez, M.J., Bollo, R.J., Zhao, X., Snyder, E.Y., Sulman, E.P., Anne, S.L., Doetsch, F., Colman, H., et al. (2010). The transcriptional network for mesenchymal transformation of brain tumours. *Nature* 463, 318–325.
- Cha, T.L., Zhou, B.P., Xia, W., Wu, Y., Yang, C.C., Chen, C.T., Ping, B., Otte, A.P., and Hung, M.C. (2005). Akt-mediated phosphorylation of EZH2 suppresses methylation of lysine 27 in histone H3. *Science* 310, 306–310.
- Chen, J., Li, Y., Yu, T.S., McKay, R.M., Burns, D.K., Kernie, S.G., and Parada, L.F. (2012). A restricted cell population propagates glioblastoma growth after chemotherapy. *Nature* 488, 522–526.
- Costa, B.M., Smith, J.S., Chen, Y., Chen, J., Phillips, H.S., Aldape, K.D., Zardo, G., Nigro, J., James, C.D., Fridlyand, J., et al. (2010). Reversing HOXA9 oncogene activation by PI3K inhibition: epigenetic mechanism and prognostic significance in human glioblastoma. *Cancer Res.* 70, 453–462.
- Crea, F., Hurt, E.M., and Farrar, W.L. (2010). Clinical significance of Polycomb gene expression in brain tumors. *Mol. Cancer* 9, 265.
- Dirks, P.B. (2010). Brain tumor stem cells: the cancer stem cell hypothesis writ large. *Mol. Oncol.* 4, 420–430.
- Esteller, M. (2008). Epigenetics in cancer. *N. Engl. J. Med.* 358, 1148–1159.
- Fan, Q.W., and Weiss, W.A. (2010). Targeting the RTK-PI3K-mTOR axis in malignant glioma: overcoming resistance. *Curr. Top. Microbiol. Immunol.* 347, 279–296.
- Fan, Q.W., Knight, Z.A., Goldenberg, D.D., Yu, W., Mostov, K.E., Stokoe, D., Shokat, K.M., and Weiss, W.A. (2006). A dual PI3 kinase/mTOR inhibitor reveals emergent efficacy in glioma. *Cancer Cell* 9, 341–349.
- Fan, X., Khaki, L., Zhu, T.S., Soules, M.E., Talsma, C.E., Gul, N., Koh, C., Zhang, J., Li, Y.M., Maciarczyk, J., et al. (2010). NOTCH pathway blockade depletes CD133-positive glioblastoma cells and inhibits growth of tumor neurospheres and xenografts. *Stem Cells* 28, 5–16.
- Frank, D.A. (2007). STAT3 as a central mediator of neoplastic cellular transformation. *Cancer Lett.* 251, 199–210.
- Furnari, F.B., Fenton, T., Bachoo, R.M., Mukasa, A., Stommel, J.M., Stegh, A., Hahn, W.C., Ligon, K.L., Louis, D.N., Brennan, C., et al. (2007). Malignant astrocytic glioma: genetics, biology, and paths to treatment. *Genes Dev.* 21, 2683–2710.
- Galli, R., Binda, E., Orfanelli, U., Cipelletti, B., Gritti, A., De Vitis, S., Fiocco, R., Foroni, C., Dimeco, F., and Vescovi, A. (2004). Isolation and characterization of tumorigenic, stem-like neural precursors from human glioblastoma. *Cancer Res.* 64, 7011–7021.
- Gilbert, C.A., and Ross, A.H. (2009). Cancer stem cells: cell culture, markers, and targets for new therapies. *J. Cell. Biochem.* 108, 1031–1038.
- Götze, S., Wolter, M., Reifenberger, G., Müller, O., and Sievers, S. (2010). Frequent promoter hypermethylation of Wnt pathway inhibitor genes in malignant astrocytic gliomas. *Int. J. Cancer* 126, 2584–2593.
- Guryanova, O.A., Wu, Q., Cheng, L., Lathia, J.D., Huang, Z., Yang, J., MacSwords, J., Eyler, C.E., McLendon, R.E., Hedderston, J.M., et al. (2011). Nonreceptor tyrosine kinase BMX maintains self-renewal and tumorigenic potential of glioblastoma stem cells by activating STAT3. *Cancer Cell* 19, 498–511.
- He, A., Shen, X., Ma, Q., Cao, J., von Gise, A., Zhou, P., Wang, G., Marquez, V.E., Orkin, S.H., and Pu, W.T. (2012). PRC2 directly methylates GATA4 and represses its transcriptional activity. *Genes Dev.* 26, 37–42.
- Hemmati, H.D., Nakano, I., Lazareff, J.A., Mesterman-Smith, M., Geschwind, D.H., Bronner-Fraser, M., and Kornblum, H.I. (2003). Cancerous stem cells can arise from pediatric brain tumors. *Proc. Natl. Acad. Sci. USA* 100, 15178–15183.
- Huang, J., Perez-Burgos, L., Placek, B.J., Sengupta, R., Richter, M., Dorsey, J.A., Kubicek, S., Opravil, S., Jenuwein, T., and Berger, S.L. (2006). Repression of p53 activity by Smdy2-mediated methylation. *Nature* 444, 629–632.
- Hussain, M., Rao, M., Humphries, A.E., Hong, J.A., Liu, F., Yang, M., Caragacianu, D., and Schrupp, D.S. (2009). Tobacco smoke induces polycomb-mediated repression of Dickkopf-1 in lung cancer cells. *Cancer Res.* 69, 3570–3578.
- Joo, K.M., Kim, J., Jin, J., Kim, M., Seol, H.J., Muradov, J., Yang, H., Choi, Y.L., Park, W.Y., Kong, D.S., et al. (2013). Patient-specific orthotopic glioblastoma xenograft models recapitulate the histopathology and biology of human glioblastomas in situ. *Cell Rep.* 3, 260–273.
- Kleer, C.G., Cao, Q., Varambally, S., Shen, R., Ota, I., Tomlins, S.A., Ghosh, D., Sewalt, R.G., Otte, A.P., Hayes, D.F., et al. (2003). EZH2 is a marker of

aggressive breast cancer and promotes neoplastic transformation of breast epithelial cells. *Proc. Natl. Acad. Sci. USA* 100, 11606–11611.

Knutson, S.K., Wigle, T.J., Warholik, N.M., Sneeringer, C.J., Allain, C.J., Klaus, C.R., Sacks, J.D., Raimondi, A., Majer, C.R., Song, J., et al. (2012). A selective inhibitor of EZH2 blocks H3K27 methylation and kills mutant lymphoma cells. *Nat. Chem. Biol.* 8, 890–896.

Kuzmichev, A., Nishioka, K., Erdjument-Bromage, H., Tempst, P., and Reinberg, D. (2002). Histone methyltransferase activity associated with a human multiprotein complex containing the Enhancer of Zeste protein. *Genes Dev.* 16, 2893–2905.

Lee, J., Kotliarova, S., Kotliarov, Y., Li, A., Su, Q., Donin, N.M., Pastorino, S., Purow, B.W., Christopher, N., Zhang, W., et al. (2006a). Tumor stem cells derived from glioblastomas cultured in bFGF and EGF more closely mirror the phenotype and genotype of primary tumors than do serum-cultured cell lines. *Cancer Cell* 9, 391–403.

Lee, T.I., Jenner, R.G., Boyer, L.A., Guenther, M.G., Levine, S.S., Kumar, R.M., Chevalier, B., Johnstone, S.E., Cole, M.F., Isono, K., et al. (2006b). Control of developmental regulators by Polycomb in human embryonic stem cells. *Cell* 125, 301–313.

Lee, J., Son, M.J., Woolard, K., Donin, N.M., Li, A., Cheng, C.H., Kotliarova, S., Kotliarov, Y., Walling, J., Ahn, S., et al. (2008). Epigenetic-mediated dysfunction of the bone morphogenetic protein pathway inhibits differentiation of glioblastoma-initiating cells. *Cancer Cell* 13, 69–80.

Lee, S.T., Li, Z., Wu, Z., Aau, M., Guan, P., Karuturi, R.K., Liou, Y.C., and Yu, Q. (2011). Context-specific regulation of NF- κ B target gene expression by EZH2 in breast cancers. *Mol. Cell* 43, 798–810.

Lee, J.M., Lee, J.S., Kim, H., Kim, K., Park, H., Kim, J.Y., Lee, S.H., Kim, I.S., Kim, J., Lee, M., et al. (2012). EZH2 generates a methyl degron that is recognized by the DCAF1/DDB1/CUL4 E3 ubiquitin ligase complex. *Mol. Cell* 48, 572–586.

Louis, D.N., Ohgaki, H., Wiestler, O.D., Cavenee, W.K., Burger, P.C., Jouvet, A., Scheithauer, B.W., and Kleihues, P. (2007). The 2007 WHO classification of tumours of the central nervous system. *Acta Neuropathol.* 114, 97–109.

Lu, T., Jackson, M.W., Wang, B., Yang, M., Chance, M.R., Miyagi, M., Gudkov, A.V., and Stark, G.R. (2010). Regulation of NF- κ B by NSD1/FBXL11-dependent reversible lysine methylation of p65. *Proc. Natl. Acad. Sci. USA* 107, 46–51.

Margueron, R., and Reinberg, D. (2011). The Polycomb complex PRC2 and its mark in life. *Nature* 469, 343–349.

McCabe, M.T., Ott, H.M., Ganji, G., Korenchuk, S., Thompson, C., Van Aller, G.S., Liu, Y., Graves, A.P., Della Pietra, A., 3rd, Diaz, E., et al. (2012). EZH2 inhibition as a therapeutic strategy for lymphoma with EZH2-activating mutations. *Nature* 492, 108–112.

Mikkelsen, T.S., Ku, M., Jaffe, D.B., Issac, B., Lieberman, E., Giannoukos, G., Alvarez, P., Brockman, W., Kim, T.K., Koche, R.P., et al. (2007). Genome-wide maps of chromatin state in pluripotent and lineage-committed cells. *Nature* 448, 553–560.

Morey, L., and Helin, K. (2010). Polycomb group protein-mediated repression of transcription. *Trends Biochem. Sci.* 35, 323–332.

Pastrana, E., Silva-Vargas, V., and Doetsch, F. (2011). Eyes wide open: a critical review of sphere-formation as an assay for stem cells. *Cell Stem Cell* 8, 486–498.

Piccirillo, S.G., Reynolds, B.A., Zanetti, N., Lamorte, G., Binda, E., Broggi, G., Brem, H., Olivi, A., Dimeco, F., and Vescovi, A.L. (2006). Bone morphogenetic proteins inhibit the tumorigenic potential of human brain tumour-initiating cells. *Nature* 444, 761–765.

Pollard, S.M., Yoshikawa, K., Clarke, I.D., Danovi, D., Stricker, S., Russell, R., Bayani, J., Head, R., Lee, M., Bernstein, M., et al. (2009). Glioma stem cell lines expanded in adherent culture have tumor-specific phenotypes and are suitable for chemical and genetic screens. *Cell Stem Cell* 4, 568–580.

Qi, W., Chan, H., Teng, L., Li, L., Chuai, S., Zhang, R., Zeng, J., Li, M., Fan, H., Lin, Y., et al. (2012). Selective inhibition of Ezh2 by a small molecule inhibitor blocks tumor cells proliferation. *Proc. Natl. Acad. Sci. USA* 109, 21360–21365.

Reya, T., Morrison, S.J., Clarke, M.F., and Weissman, I.L. (2001). Stem cells, cancer, and cancer stem cells. *Nature* 414, 105–111.

Richly, H., Aloia, L., and Di Croce, L. (2011). Roles of the Polycomb group proteins in stem cells and cancer. *Cell Death Dis* 2, e204.

Schlesinger, Y., Straussman, R., Keshet, I., Farkash, S., Hecht, M., Zimmerman, J., Eden, E., Yakhini, Z., Ben-Shushan, E., Reubinf, B.E., et al. (2007). Polycomb-mediated methylation on Lys27 of histone H3 pre-marks genes for de novo methylation in cancer. *Nat. Genet.* 39, 232–236.

Shao, Z., Raible, F., Mollaaghababa, R., Guyon, J.R., Wu, C.T., Bender, W., and Kingston, R.E. (1999). Stabilization of chromatin structure by PRC1, a Polycomb complex. *Cell* 98, 37–46.

Sherry, M.M., Reeves, A., Wu, J.K., and Cochran, B.H. (2009). STAT3 is required for proliferation and maintenance of multipotency in glioblastoma stem cells. *Stem Cells* 27, 2383–2392.

Simon, J.A., and Lange, C.A. (2008). Roles of the EZH2 histone methyltransferase in cancer epigenetics. *Mutat. Res.* 647, 21–29.

Simon, J.A., and Kingston, R.E. (2009). Mechanisms of polycomb gene silencing: knowns and unknowns. *Nat. Rev. Mol. Cell Biol.* 10, 697–708.

Singh, S.K., Hawkins, C., Clarke, I.D., Squire, J.A., Bayani, J., Hide, T., Henkelman, R.M., Cusimano, M.D., and Dirks, P.B. (2004). Identification of human brain tumour initiating cells. *Nature* 432, 396–401.

Son, M.J., Woolard, K., Nam, D.H., Lee, J., and Fine, H.A. (2009). SSEA-1 is an enrichment marker for tumor-initiating cells in human glioblastoma. *Cell Stem Cell* 4, 440–452.

Sparmann, A., and van Lohuizen, M. (2006). Polycomb silencers control cell fate, development and cancer. *Nat. Rev. Cancer* 6, 846–856.

Stark, G.R., Wang, Y., and Lu, T. (2011). Lysine methylation of promoter-bound transcription factors and relevance to cancer. *Cell Res.* 21, 375–380.

Stupp, R., Mason, W.P., van den Bent, M.J., Weller, M., Fisher, B., Taphoorn, M.J., Belanger, K., Brandes, A.A., Marosi, C., Bogdahn, U., et al.; European Organisation for Research and Treatment of Cancer Brain Tumor and Radiotherapy Groups; National Cancer Institute of Canada Clinical Trials Group. (2005). Radiotherapy plus concomitant and adjuvant temozolomide for glioblastoma. *N. Engl. J. Med.* 352, 987–996.

Suvà, M.L., Riggi, N., Janiszewska, M., Radovanovic, I., Provero, P., Stehle, J.C., Baumer, K., Le Bitoux, M.A., Marino, D., Cironi, L., et al. (2009). EZH2 is essential for glioblastoma cancer stem cell maintenance. *Cancer Res.* 69, 9211–9218.

Tan, J., Yang, X., Zhuang, L., Jiang, X., Chen, W., Lee, P.L., Karuturi, R.K., Tan, P.B., Liu, E.T., and Yu, Q. (2007). Pharmacologic disruption of Polycomb-repressive complex 2-mediated gene repression selectively induces apoptosis in cancer cells. *Genes Dev.* 21, 1050–1063.

Varambally, S., Dhanasekaran, S.M., Zhou, M., Barrette, T.R., Kumar-Sinha, C., Sanda, M.G., Ghosh, D., Pienta, K.J., Sewalt, R.G., Otte, A.P., et al. (2002). The polycomb group protein EZH2 is involved in progression of prostate cancer. *Nature* 419, 624–629.

Verhaak, R.G., Hoadley, K.A., Purdom, E., Wang, V., Qi, Y., Wilkerson, M.D., Miller, C.R., Ding, L., Golub, T., Mesirov, J.P., et al.; Cancer Genome Atlas Research Network. (2010). Integrated genomic analysis identifies clinically relevant subtypes of glioblastoma characterized by abnormalities in PDGFRA, IDH1, EGFR, and NF1. *Cancer Cell* 17, 98–110.

Viré, E., Brenner, C., Deplus, R., Blanchon, L., Fraga, M., Didelot, C., Morey, L., Van Eynde, A., Bernard, D., Vanderwinden, J.M., et al. (2006). The Polycomb group protein EZH2 directly controls DNA methylation. *Nature* 439, 871–874.

Wei, Y., Xia, W., Zhang, Z., Liu, J., Wang, H., Adsay, N.V., Albarracín, C., Yu, D., Abbruzzese, J.L., Mills, G.B., et al. (2008). Loss of trimethylation at lysine 27 of histone H3 is a predictor of poor outcome in breast, ovarian, and pancreatic cancers. *Mol. Carcinog.* 47, 701–706.

Widschwendter, M., Fiegl, H., Egle, D., Mueller-Holzner, E., Spizzo, G., Marth, C., Weisenberger, D.J., Campan, M., Young, J., Jacobs, I., and Laird, P.W. (2007). Epigenetic stem cell signature in cancer. *Nat. Genet.* 39, 157–158.

Xu, K., Wu, Z.J., Groner, A.C., He, H.H., Cai, C., Lis, R.T., Wu, X., Stack, E.C., Loda, M., Liu, T., et al. (2012). EZH2 oncogenic activity in castration-resistant prostate cancer cells is Polycomb-independent. *Science* 338, 1465–1469.

- Yang, J., and Stark, G.R. (2008). Roles of unphosphorylated STATs in signaling. *Cell Res.* 18, 443–451.
- Yang, J., Huang, J., Dasgupta, M., Sears, N., Miyagi, M., Wang, B., Chance, M.R., Chen, X., Du, Y., Wang, Y., et al. (2010). Reversible methylation of promoter-bound STAT3 by histone-modifying enzymes. *Proc. Natl. Acad. Sci. USA* 107, 21499–21504.
- Yang, Y.P., Chang, Y.L., Huang, P.I., Chiou, G.Y., Tseng, L.M., Chiou, S.H., Chen, M.H., Chen, M.T., Shih, Y.H., Chang, C.H., et al. (2012). Resveratrol suppresses tumorigenicity and enhances radiosensitivity in primary glioblastoma tumor initiating cells by inhibiting the STAT3 axis. *J. Cell. Physiol.* 227, 976–993.
- Yue, P., and Turkson, J. (2009). Targeting STAT3 in cancer: how successful are we? *Expert Opin. Investig. Drugs* 18, 45–56.
- Zheng, H., Ying, H., Wiedemeyer, R., Yan, H., Quayle, S.N., Ivanova, E.V., Paik, J.H., Zhang, H., Xiao, Y., Perry, S.R., et al. (2010). PLAGL2 regulates Wnt signaling to impede differentiation in neural stem cells and gliomas. *Cancer Cell* 17, 497–509.
- Zhong, Z., Wen, Z., and Darnell, J.E., Jr. (1994). Stat3: a STAT family member activated by tyrosine phosphorylation in response to epidermal growth factor and interleukin-6. *Science* 264, 95–98.
- Zhou, B.B., Zhang, H., Damelin, M., Geles, K.G., Grindley, J.C., and Dirks, P.B. (2009). Tumour-initiating cells: challenges and opportunities for anticancer drug discovery. *Nat. Rev. Drug Discov.* 8, 806–823.

The E3 Ubiquitin Ligase Siah2 Contributes to Castration-Resistant Prostate Cancer by Regulation of Androgen Receptor Transcriptional Activity

Jianfei Qi,^{*} Manisha Tripathi, Rajeev Mishra, Natasha Sahgal, Ladan Fazli, Susan Ettinger, William J. Placzek, Giuseppina Claps, Leland W.K. Chung, David Bowtell, Martin Gleave, Neil Bhowmick, and Ze'ev A. Ronai^{*}

^{*}Correspondence: [jqf@sbmri.org](mailto:jfq@sbmri.org) (J.Q.), ronai@sbmri.org (Z.A.R.)

<http://dx.doi.org/10.1016/j.ccr.2013.05.018>

(Cancer Cell 23, 332–346; March 18, 2013)

Dr. Ladan Fazli's name was spelled incorrectly as "Fazil" in the original article. It appears correctly in this erratum.